CIPM MRA
Comparison reports

# CCPR-K2.b.2016

# Spectral responsitivity

KEY COMPARISON

**© 2026, J.-M. Coutin *et al***

**This report is published by the BIPM.**

Original content from this Report may be used under the terms of the Creative Commons Attribution 4.0 International (CC BY 4.0) Licence.

**Any further distribution of this Report must be cited as:**
J.-M. Coutin *et al* 2026 *CIPM MRA Comparison reports* **02004**

**https://doi.org/10.59161/CXMJ7668**

The CIPM MRA Comparison reports are made available under the Creative Commons Attribution International licence:
**Attribution 4.0 International (CC BY 4.0)**

By using this Report, you accept to be bound by the terms of this licence
**(https://creativecommons.org/licenses/by/4.0/).**

**Distribution** – you may distribute the Report according to the stipulations below.

**Attribution** – you must cite the Report.

**Adaptations** – you must cite the original Report, identify changes to the original and add the following text: This is an adaptation of an original Report by the Author(s). The opinions expressed and arguments employed in this adaptation should not be reported as representing the views of the Authors.

**Translations** – you must cite the original Report, identify changes to the original and add the following text: In the event of any discrepancy between the original work and the translation, only the text of the original Report should be considered valid.

**Third-party material** – the licence does not apply to third-party material in the Report. If using such material, you are responsible for obtaining permission from the third-party and of any claims of infringement.

# CCPR-K2.b.2016

# Spectral Responsivity 300 nm to 1000 nm

# Final Report

01 July 2026

Dong-Hoon Lee, Seongchong Park

*Korea Research Institute of Standards and Science (KRISS), Korea*

Joaquin Campos, Alicia Pons

*Instituto de Óptica "Daza de Valdés" (IO-CSIC), Spain*

Jeanne-Marie Coutin, Fatima Chandoul, Gaël Obein

*LNE-CNAM, France*

Francois Shindo, Neil Swift

*Measurement Standards Laboratory (MSL), Callaghan Innovation, New Zealand*

Jeanne Houston, Howard Yoon, Cameron Miller

*National Institute of Standards and Technology (NIST), USA*

Jing Zhang

*National Metrology Centre (NMC), A*STAR, Singapore*

Kenichi Kinoshita, Yoshiro Ichino

*National Metrology Institute of Japan (NMIJ), AIST, Japan*

Angela Gamouras

*National Research Council Canada (NRC), Canada*

Teresa Goodman, Subrena Harris

*National Physical Laboratory (NPL), UK*

Lutz Werner, Peter Meindl

*Physikalisch-Technische Bundesanstalt (PTB), Germany*

Özcan Bazkir

*TUBITAK UME, Turkiye*

Boris Khlevnoy

*VNIIOFI, Russia*

# Table of Contents

# 1. INTRODUCTION

Under the Mutual Recognition Arrangement (MRA), the metrological equivalence of national measurement standards is determined by a set of key comparisons chosen and organized by the consultative committees of CIPM working closely with regional metrology organizations (RMOs). At its meeting in June 2007, the Consultative Committee for Photometry and Radiometry (CCPR) instigated a new series of key comparisons in the field of optical radiation metrology. In particular, it was decided that a key comparison of spectral responsivity from 300 nm to 1000 nm would be carried out with KRISS of Rep. Korea as the pilot laboratory.

A call for participants was circulated to the member institutes of CCPR in November 2011, and the 12 participants were selected according to the CCPR-G4 guidelines and agreed upon by the CCPR WG-KC in October 2012. The technical protocol was agreed by all the participants and approved by the CCPR WG-KC in November 2015. The comparison was then registered to KCDB in February 2016 with the identification code of CCPR-K2.b.2016.

The comparison was carried out by measuring two types of transfer detectors: reflection-type three-element Si trap detector and single-element Si photodiode. Measurements of the transfer detectors were carried out in the period from June 2016 to July 2018. This report summarizes the procedure of the comparison, the measurement results of each participant, and the data analysis details according to the CCPR-G2 guidelines [1]. The resulting degrees of equivalence (DoEs) of each participant are tabulated in Appendix A. The technical capabilities and uncertainty budgets of each participant are described in Appendix B. Appendix C provides the report on the stability test of the transfer detectors, which was performed during the pre-draft A procedure by NIST.

# 2. ORGANIZATION OF COMPARISON

## 2.1. Participants

Table 2-1 shows the list of the participants at the time of the report preparation. Among the participants, the following participants have formed a task group (TG) to draw up the technical protocol: KRISS (Korea), MSL (New Zealand), NMIJ (Japan), NIST (USA), LNE-CNAM (France), NPL (UK), and PTB (Germany).

**Table 2-1.** List of participants, status Oct 2023.

| No | NMI/RMO | country /RMO | contact person | email address |
|---|---|---|---|---|
| 1 | KRISS (pilot) | Korea /APMP | Lee, Dong-Hoon<br>Park, Seongchong | dh.lee@kriss.re.kr<br>spark@kriss.re.kr |
| 2 | IO-CSIC | Spain /EURAMET | Campos, Joaquin<br>Pons, Alicia | Joaquin.campos@csic.es<br>alicia.pons@csic.es |
| 3 | LNE-CNAM | France /EURAMET | Coutin, Jeanne-Marie<br>Chandoul, Fatima<br>Obein, Gaël | jeanne-marie.coutin@cnam.fr<br>fatima.chandoul@cnam.fr<br>gael.obein@cnam.fr |
| 4 | MSL | New Zealand /APMP | Shindo, Francois<br>Swift, Neil | francois.shindo@callaghaninnovation.govt.nz<br>neil.swift@callaghaninnovation.govt.nz |
| 5 | NIST | USA /SIM | Houston, Jeanne<br>Yoon, Howard | jeanne.houston@nist.gov<br>howard.yoon@nist.gov |

| | | | | |
|---|---|---|---|---|
| | | | Miller, Cameron | c.miller@nist.gov |
| 6 | NMC-ASTAR | Singapore<br>/APMP | Zhang, Jing | zhang_jing@nmc.a-star.edu.sg |
| 7 | NMIJ | Japan<br>/APMP | Kinoshita, Kenichi<br>Ichino, Yoshiro | kenichi.kinoshita@aist.go.jp<br>y.ichino@aist.go.jp |
| 8 | NRC | Canada<br>/SIM | Gamouras, Angela | angela.gamouras@nrc-cnrc.gc.ca |
| 9 | NPL | UK<br>/EURAMET | Goodman, Teresa<br>Harris, Subrena | Teresa.Goodman@npl.co.uk<br>Subrena.Harris@npl.co.uk |
| 10 | PTB | Germany<br>/EURAMET | Werner, Lutz<br>Meindl, Peter | lutz.werner@ptb.de<br>peter.meindl@ptb.de |
| 11 | UME | Turkiye<br>/EURAMET | Bazkir, Özcan | ozcan.bazkir@tubitak.gov.tr |
| 12 | VNIIOFI | Russia<br>/COOMET | Khlevnoy, Boris | Khlevnoy-m4@vniiofi.ru |

### 2.2. Form of Comparison

The comparison was carried out by distributing six sets of transfer detectors prepared and provided by the pilot, which were designated as set A, B, C, D, E, and F. Each set contained 3 pieces of single-element silicon photodiodes, numbered as #1, #2, and #3, and 2 pieces of reflection-type three-element Si trap detectors, numbered as #4 and #5. The specifications and characteristics of the transfer detectors are described in Section 3.

The comparison had the form of a star comparison with a sequence of the measurements "Pilot – Participant – Pilot" so that the drifts of the detectors were monitored by the repeated measurements by the pilot. All the sets of the transfer detectors except set C were measured by two participants in two phases with a sequence "Pilot – Participant (1) – Pilot – Participant (2) – Pilot."

### 2.3. Measurement Schedule

The measurement schedule was planned through a survey among the participants to form three groups according to the three selected measurement periods:

- The first-round group: NMC-ASTAR, IO-CSIC for measurement in March ~ May 2016
- The second-round group: NMIJ, LNE-CNAM, NRC, UME, MSL for measurement in Oct. 2016 ~ Jan. 2017
- The third-round group: NIST, VNIIOFI, NPL, PTB for measurement in May ~ August 2017

The initial schedule plan in the technical protocol had to be modified in practice. The records of the actions performed by the pilot and participants for each set of transfer detectors are summarized in Table 2-2.

**Table 2-2.** Records of the actions for each set of transfer detectors.

| action | set A | set B | set C | set D | set E | set F |
|---|---|---|---|---|---|---|
| Pilot measurement | May 2016 | May 2016 | Sept 2016 | Sept 2016 | Sept 2016 | Sept 2016 |
| Participant measurement (first phase) | July ~ Oct. 2016<br>by NMC-ASTAR | Jan. ~ Mar. 2017<br>by IO-CSIC | Nov 2016<br>by NMIJ[1] | Dec. 2016 ~ Feb. 2017<br>by LNE-CNAM | Feb. 2017<br>by NRC | Nov. 2016 ~ Jan. 2017<br>by UME |
| Result reporting (first phase) | Nov. 2016 | Sept. 2017 | April 2017 | July 2017 | May 2018 | Feb. 2017 |
| Pilot measurement | May 2017 | May 2017 | April 2018 (traps) / Sept 2019 (singles) | May 2017 | May ~ June 2017 | May ~ June 2017 |
| Participant measurement (second phase) | Sept. ~ Oct. 2017<br>by NIST | Nov. ~ Dec. 2017<br>by VNIIOFI | June 2018<br>by NMIJ<br>(only for trap detectors) | June ~ July 2017<br>by PTB | Nov 2017<br>by MSL | Feb. ~ March 2018<br>by NPL |
| Result reporting (second phase) | June 2019 | April 2019 | July 2018 (traps) | Nov. 2018 | April 2018 | Nov. 2019 |
| Pilot measurement | March 2020 | March 2020 | March 2020 (traps) | Feb. ~ March 2020 | Feb. ~ March 2020 | Feb. ~ March 2020 |

# 3. TRANSFER DETECTORS

## 3.1. Construction

A set of transfer detectors consisted of three single-element silicon photodiodes of the type Hamamatsu S1337-1010BQ (with quartz window) and two three-element reflection-type Si trap detectors containing Hamamatsu S1337-11 (windowless).

Figure 3-1 shows the construction of the single-element detector where the photodiode is mounted in a housing designed by MSL, New Zealand. Each detector housing was fitted with a BNC connector for reading photocurrent and a 4-pin LEMO connector for 4-wire reading the resistance of a PT100 temperature sensor attached to the photodiode. Figure 3-2 shows the connection diagram of the detectors. The cable to the LEMO connector for reading the temperature sensor was included in each set of transfer detectors.

[1] During the measurement of the set C by NMIJ in Nov. 2016, contact failures of the trap detectors were identified. After return of the detectors, the pilot repaired the trap detectors of the set C and re-sent them to NMIJ. Consequently, set C was measured only by one participant NMIJ, but the single-element and trap detectors were measured separately.

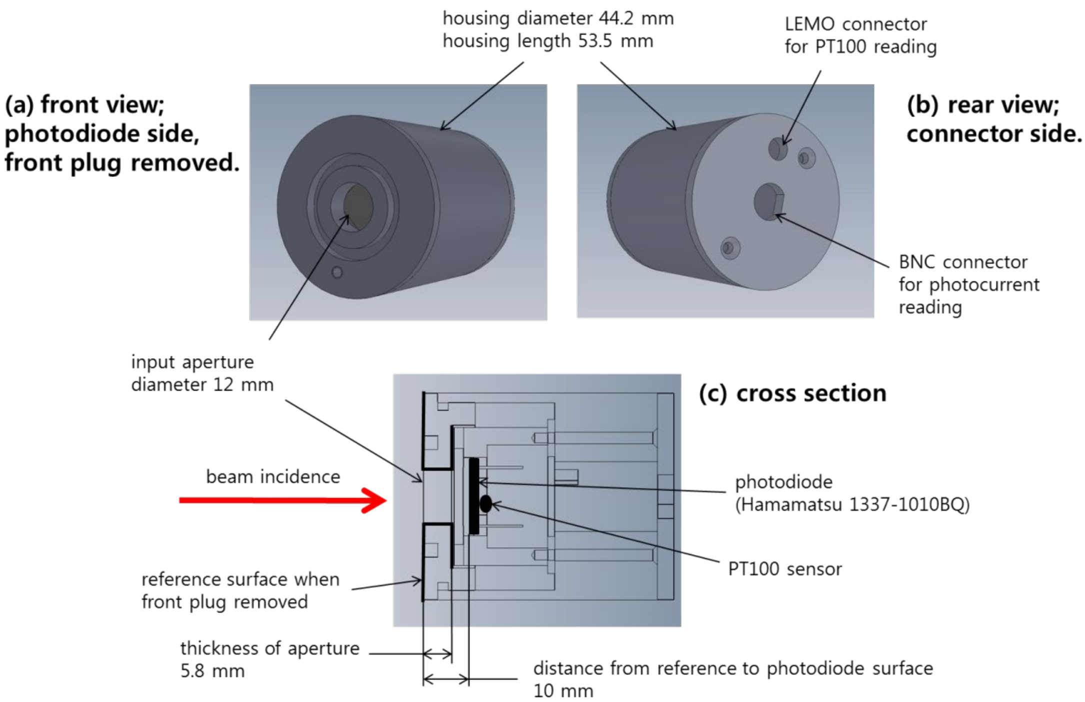


**Figure 3-1.** Schematic drawing of the single-element transfer detectors.

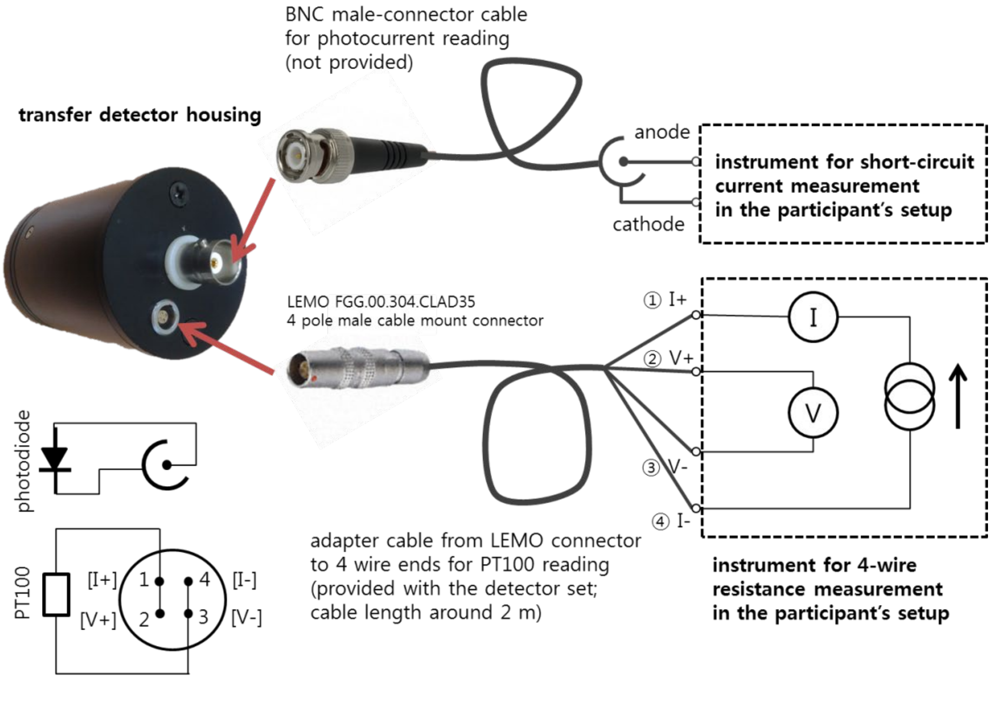


**Figure 3-2.** Connection diagram of the single-element transfer detectors.

Figure 3-3 shows the construction of the trap detector, which were provided by the BIPM. The housing was modified by the pilot laboratory to enable the temperature monitoring. Similar to the single-element photodiodes, each trap detector was fitted with a BNC connector for reading the photocurrent and a 4-pin LEMO connector for 4-wire reading the resistance of a PT100 temperature sensor attached to the detector housing.

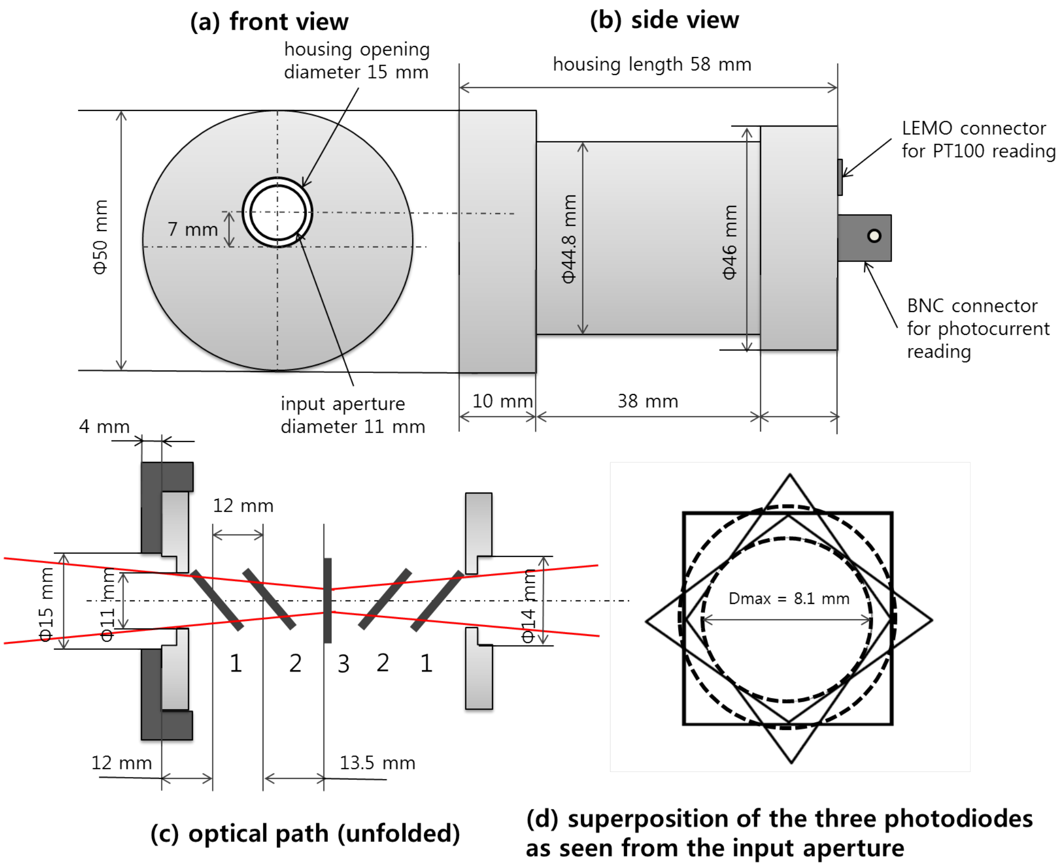


**Figure 3-3.** Schematic drawing of the trap transfer detectors.

### *3.2. Stability*

The stability of the transfer detectors during the transport and measurement by each participant was evaluated by comparing the results of each detector measured by the pilot laboratory before and after the measurement of each participant at the same temperature. The relative changes of responsivity between two pilot measurements for all the transfer detectors are shown in Figure 3-4 as a function of wavelength. For comparison, the expanded uncertainty ($k = 2$) due to the long-term reproducibility of the pilot laboratory is also plotted as red dashed lines. The evaluation of the long-term reproducibility of the pilot laboratory is provided in Appendix B, Section 1.

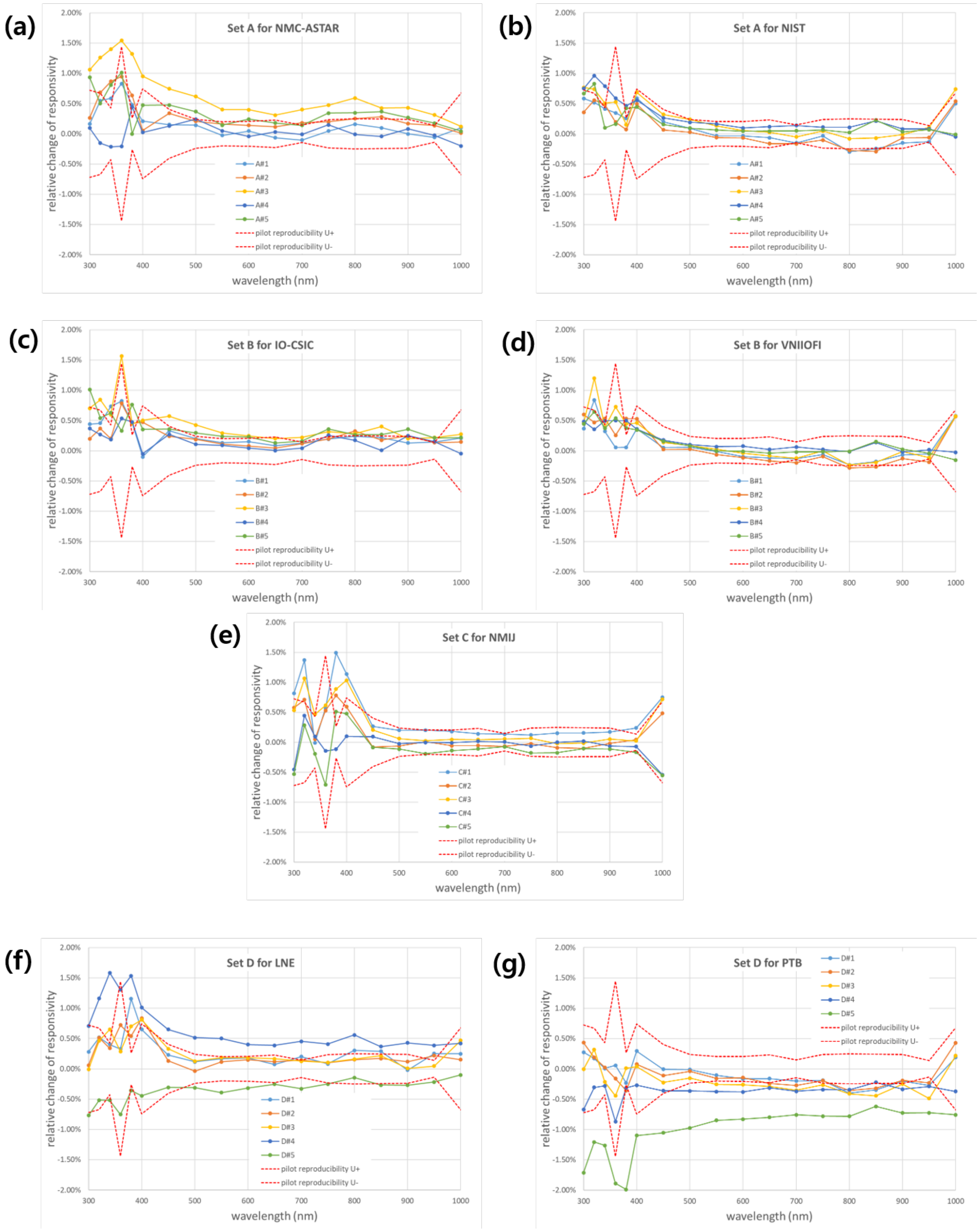
(a)
Set A for NMC-ASTAR
(b)
Set A for NIST
(c)
Set B for IO-CSIC
(d)
Set B for VNIIOFI
(e)
Set C for NMIJ
(f)
Set D for LNE
(g)
Set D for PTB
relative change of responsivity
wavelength (nm)
2.00%
1.50%
1.00%
0.50%
0.00%
-0.50%
-1.00%
-1.50%
-2.00%
300
400
500
600
700
800
900
1000
A#1
A#2
A#3
A#4
A#5
B#1
B#2
B#3
B#4
B#5
C#1
C#2
C#3
C#4
C#5
D#1
D#2
D#3
D#4
D#5
pilot reproducibility U+
pilot reproducibility U-

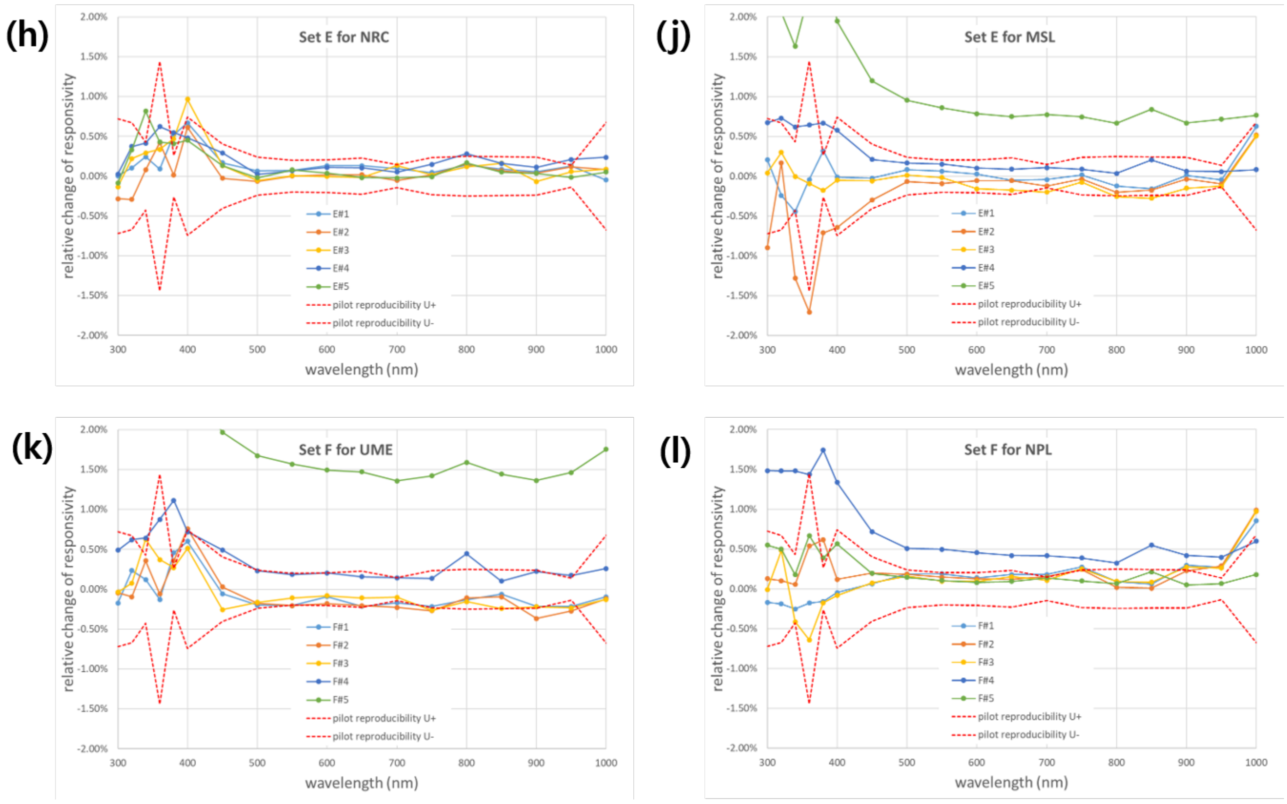


**Figure 3-4.** Results of the stability evaluation of the transfer detectors: (a) difference of set A before and after measurement of NMC-ASTAR, (b) difference of set A before and after measurement of NIST, (c) difference of set B before and after measurement of IO-CSIC, (d) difference of set B before and after measurement of VNIIOFI, (e) difference of set C before and after measurement of NMIJ, (f) difference of set D before and after measurement of LNE-CNAM, (g) difference of set D before and after measurement of PTB, (h) difference of set E before and after measurement of NRC, (j) difference of set E before and after measurement of MSL, (k) difference of set F before and after measurement of UME, (l) difference of set F before and after measurement of NPL. The symbols are the measured data, while the connecting lines are only for better visibility. The red dashed lines show the long-term reproducibility uncertainty ($k = 2$) of the pilot laboratory.

We see in Figure 3-4 that the changes of the responsivity are, in the most cases, comparable with the reproducibility uncertainty of the measurement setup of the pilot. This indicates that the stability of the transfer detectors could not be accurately evaluated as the reproducibility of the pilot was probably the main cause of the responsivity changes observed in the comparison. Nevertheless, there are several detectors showing an obviously high drift beyond the reproducibility. These detectors with poor stability were identified in the review of relative data during the pre-draft A process and excluded from the data analysis (see Section 5).

The uncertainty of each detector representing its stability during the measurement phase at each participant was evaluated by taking the maximum of the measured differences in the wavelength range from 500 nm to 900 nm, where the reproducibility of the pilot was relatively small. The stability of each transfer detectors is summarized in Table 3-1, where $\Delta_{\max}$ and $u_{\text{stability}}$ indicate the maximum relative difference of responsivity and the relative standard uncertainty, respectively. The standard uncertainty related to the stability of the transfer detectors $u_{\text{stability}}$ was calculated from $\Delta_{\max}$ by assuming the rectangular probability distribution:

$$u_{\text{stability}} = \Delta_{\max} \big/ \sqrt{3} \qquad (3\text{-}1)$$

We note that the stability uncertainties in Table 3-1 are over-estimated due to the reproducibility of the pilot laboratory. To verify this, an additional test of detector stability was performed after the measurement rounds were completed by using the highly stable setup of NIST with the transfer detector set A. The results of this test confirmed a long-term stability of almost all the detectors of set A lower than 0.05% over the wavelength range from 500 nm to 1000 nm during the period from 2017 to 2021. The procedure and results of this more accurate stability test are reported in Appendix C.

**Table 3-1.** Stability uncertainty of each transfer detector evaluated from the differences of responsivity between two measurements by the pilot laboratory before and after the measurement of each participant. $\Delta_{max}$ indicates the maximum relative difference of responsivity in a range from 500 nm to 900 nm, and $u_{stability}$ is the relative standard uncertainty calculated from $\Delta_{max}$ with Eq. (3-1). Note that the detectors with an extraordinary instability ($u_{stability}$ > 0.3%) are indicated in red letters.

| single-element detectors | | | | | | |
|---|---|---|---|---|---|---|
| detector | participant | $\Delta_{max}$ | $u_{stability}$ | participant | $\Delta_{max}$ | $u_{stability}$ |
| A#1 | NMC-ASTAR | 0.16% | 0.09% | NIST | 0.30% | 0.17% |
| A#2 | NMC-ASTAR | 0.28% | 0.16% | NIST | 0.29% | 0.17% |
| A#3 | NMC-ASTAR | 0.62% | 0.36% | NIST | 0.24% | 0.14% |
| B#1 | IO-CSIC | 0.24% | 0.14% | VNIIOFI | 0.23% | 0.13% |
| B#2 | IO-CSIC | 0.33% | 0.19% | VNIIOFI | 0.28% | 0.16% |
| B#3 | IO-CSIC | 0.42% | 0.25% | VNIIOFI | 0.24% | 0.14% |
| C#1 | NMIJ | 0.20% | 0.12% | | | |
| C#2 | NMIJ | 0.10% | 0.06% | | | |
| C#3 | NMIJ | 0.07% | 0.04% | | | |
| D#1 | LNE | 0.30% | 0.18% | PTB | 0.40% | 0.23% |
| D#2 | LNE | 0.17% | 0.10% | PTB | 0.35% | 0.20% |
| D#3 | LNE | 0.21% | 0.12% | PTB | 0.44% | 0.26% |
| E#1 | NRC | 0.14% | 0.08% | MSL | 0.16% | 0.09% |
| E#2 | NRC | 0.16% | 0.09% | MSL | 0.20% | 0.12% |
| E#3 | NRC | 0.16% | 0.09% | MSL | 0.28% | 0.16% |
| F#1 | UME | 0.22% | 0.13% | NPL | 0.30% | 0.17% |
| F#2 | UME | 0.37% | 0.21% | NPL | 0.24% | 0.14% |
| F#3 | UME | 0.27% | 0.15% | NPL | 0.27% | 0.16% |
| trap detectors | | | | | | |
| detector | participant | $\Delta_{max}$ | $u_{stability}$ | participant | $\Delta_{max}$ | $u_{stability}$ |
| A#4 | NMC-ASTAR | 0.24% | 0.14% | NIST | 0.21% | 0.12% |
| A#5 | NMC-ASTAR | 0.37% | 0.21% | NIST | 0.23% | 0.13% |
| B#4 | IO-CSIC | 0.26% | 0.15% | VNIIOFI | 0.14% | 0.08% |
| B#5 | IO-CSIC | 0.36% | 0.21% | VNIIOFI | 0.15% | 0.09% |
| C#4 | NMIJ | 0.06% | 0.04% | | | |
| C#5 | NMIJ | 0.19% | 0.11% | | | |
| D#4 | LNE | 0.56% | 0.32% | PTB | 0.38% | 0.22% |
| D#5 | LNE | 0.39% | 0.23% | PTB | 0.97% | 0.56% |
| E#4 | NRC | 0.28% | 0.16% | MSL | 0.20% | 0.12% |
| E#5 | NRC | 0.17% | 0.10% | MSL | 0.95% | 0.55% |
| F#4 | UME | 0.45% | 0.26% | NPL | 0.55% | 0.32% |
| F#5 | UME | 1.67% | 0.97% | NPL | 0.21% | 0.12% |

## 3.3. Uniformity

For testing the spatial uniformity of the transfer detectors, the variation of photocurrent signal was recorded by scanning a monochromatic beam at 550 nm around the centre position in an area of 10 mm × 10 mm with a step of 1 mm. A separate comparator setup was used for this test, in which the detector could be mounted on a motorized X-Y translation stage. A monochromatic beam with a spectral bandwidth of approximately 5 nm was provided from a double-grating monochromator illuminated with a laser-driven Xe light source. The light output from the monochromator was propagated in free space to form a nearly collimated beam with a spot size of 2 mm × 1 mm at the detector position. A power-monitoring unit consisting of a beam splitter and a temperature-stabilized photodiode was installed to compensate the temporal instability of radiant power of the monochromatic beam. The temporal power instability of the monochromatic beam could be kept less than 0.01% when the compensation via the power-monitoring unit was applied. Figure 3-5 shows the results of the spatial uniformity for each single-element transfer detector.

The obtained data at the 11 × 11 positions were normalized with respect to the maximum value among them, and the relative differences from 1 were calculated at each position. In a selected area corresponding to a diameter of 6 mm around the centre position, the largest difference $\Delta_{max}$ was selected as the maximum error due to spatial non-uniformity of the tested transfer detector. The standard uncertainty $u_{uniformity}$ related to the spatial uniformity of the transfer detector was then estimated by assuming the rectangular probability distribution:

$$u_{uniformity} = \Delta_{max} / \sqrt{3} \qquad (3\text{-}2)$$

The results of the spatial uniformity uncertainty of the single-element detectors are summarized in Table 3-2.

It should be noted that the surface of the transfer detectors was never cleaned or contacted at the pilot laboratory during the whole comparison process. The uniformity test was performed once at the end of the comparison measurements so that the change of the uniformity during the comparison could not be verified. The uniformity test was performed only for the single-element transfer detectors, but not performed for the trap detectors as the clear aperture of the trap detectors was very small and the normal incidence could not be precisely verified in the setup used by the pilot. For the set A, the spatial uniformity of trap detectors was also tested at NIST, which is reported in Appendix C.

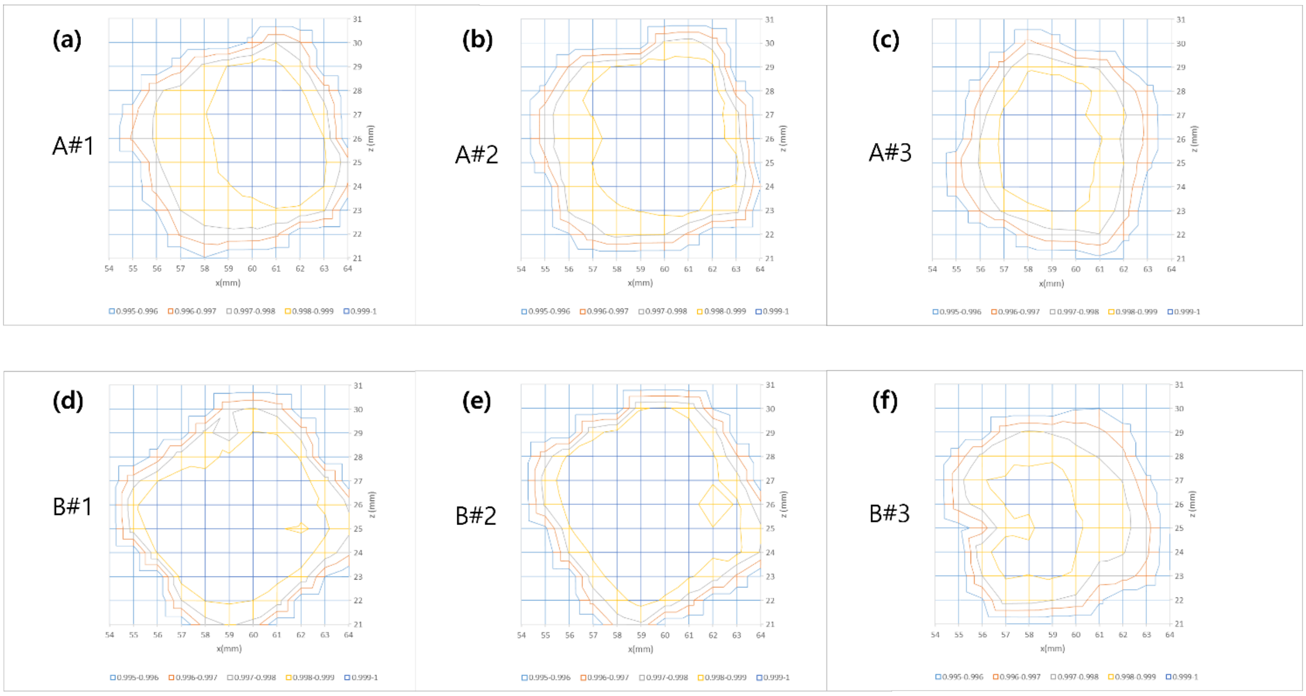


**Figure 3-5.** Results of the spatial uniformity of the single-element transfer detectors. The relative change of responsivity was measured at a wavelength of 550 nm in an area of 5 mm × 5 mm at the centre of the active area by scanning a beam spot of a size 2 mm × 1 mm with a step of 1 mm.

**Table 3-2.** Uniformity uncertainty of each single-element transfer detector evaluated for an area of 6 mm diameter at the centre at a wavelength of 550 nm. $\Delta_{max}$ indicates the maximum relative difference of responsivity in the evaluated area, and $u_{uniformity}$ is the relative standard uncertainty calculated from $\Delta_{max}$ with

Eq. (3-2). Note that the detectors with an extraordinary non-uniformity ($u_{\text{uniformity}}$ > 0.3%) are indicated in red letters.

| detector | $\Delta_{\text{max}}$ | $u_{\text{uniformity}}$ | detector | $\Delta_{\text{max}}$ | $u_{\text{uniformity}}$ |
|---|---|---|---|---|---|
| A#1 | 0.21% | 0.12% | D#1 | 0.41% | 0.24% |
| A#2 | 0.15% | 0.08% | D#2 | 0.20% | 0.12% |
| A#3 | 0.24% | 0.14% | D#3 | 0.19% | 0.11% |
| B#1 | 0.26% | 0.15% | E#1 | 0.78% | 0.45% |
| B#2 | 0.19% | 0.11% | E#2 | 0.24% | 0.14% |
| B#3 | 0.36% | 0.21% | E#3 | 0.43% | 0.25% |
| C#1 | 1.07% | 0.62% | F#1 | 0.34% | 0.20% |
| C#2 | 0.47% | 0.27% | F#2 | 0.30% | 0.18% |
| C#3 | 0.17% | 0.10% | F#3 | 0.38% | 0.22% |

### *3.4. Temperature Dependence*

The temperature dependence of the transfer detectors was evaluated by measuring the spectral responsivity of each detector at two different housing temperatures of $T_1$ = 23 °C and $T_2$ = 26 °C. The housing temperature was controlled by using a water-circulated mount and determined via the resistance reading of the PT100 temperature sensor of each transfer detector. From the measurements, the relative temperature sensitivity coefficient $C_T(\lambda)$ of each detector against the PT100 resistance reading $R$ at each wavelength $\lambda$ was determined, which is defined as

$$C_T(\lambda) \equiv \frac{S(\lambda,T_2)-S(\lambda,T_1)}{S(\lambda,T_1)\left[R(T_2)-R(T_1)\right]} = \frac{dS(\lambda)}{S(\lambda)\cdot dR}. \quad \text{(3-3)}$$

Here, $S(\lambda, T)$ and $R(T)$ denote the spectral responsivity and the PT100 resistance reading at the temperature of $T$. The coefficient $C_T(\lambda)$ corresponds to the relative sensitivity of the responsivity against the resistance reading of the PT100 sensor near the ambient temperature of 23 °C, at which the detectors should be compared. The resulting values of $C_T(\lambda)$ for all the transfer detectors are plotted in Figure 3-6. For comparison, the expanded uncertainty ($k$ = 2) due to the long-term reproducibility of the pilot laboratory is also plotted as red dashed lines.

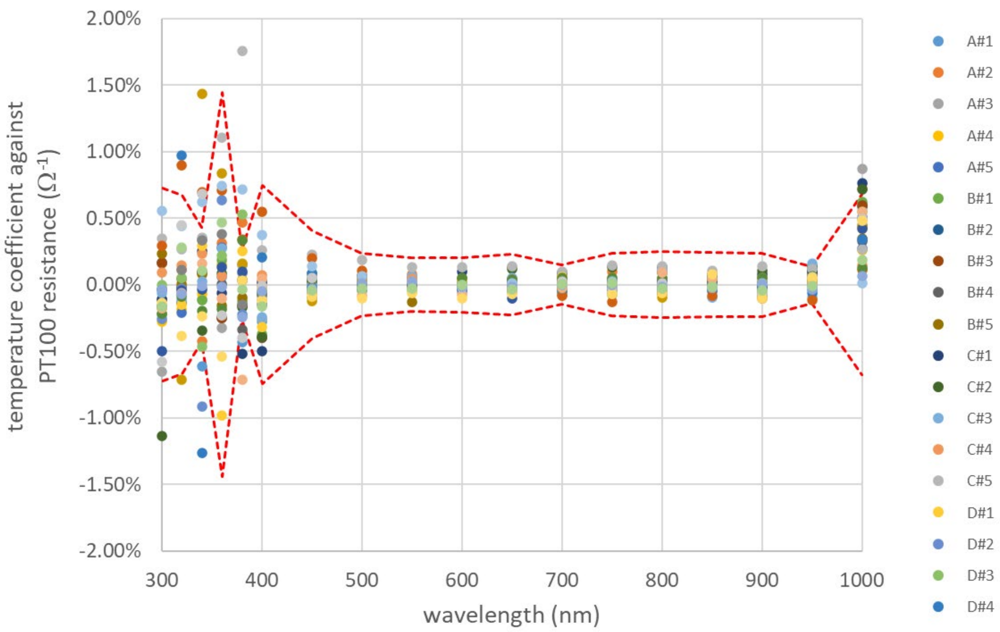


**Figure 3-6.** Temperature sensitivity of the transfer detector responsivity measured in a range from 23 °C to 26 °C. The dot symbols are the measured data of the relative temperature sensitivity coefficients defined in Eq. (3-3). The red dashed lines show the long-term reproducibility uncertainty ($k = 2$) of the pilot laboratory.

Figure 3-6 shows that, in the wavelength range from 450 nm to 950 nm, the temperature dependence of all the transfer detectors was as small as the typical random uncertainty of 0.2% of the pilot measurement setup. At the wavelength of 1000 nm, all the detectors had the temperature coefficients significantly larger than those in the visible range as expected from the property of the Si photodiodes with a bandgap edge near 1000 nm. In the short wavelength range below 400 nm, the poor reproducibility of the pilot laboratory disturbed the determination of the temperature coefficients. We also note that some of the trap detectors showed an anomalous temperature dependence, which were probably caused by a poor thermal and/or electric contact of the PT100 sensor.[2]

In the technical protocol, it was proposed to perform a temperature correction to the target value of 109.0 Ω of the PT100 reading. The participants reported the PT100 readings together with the spectral responsivity data for this purpose, which are summarized in Table 3-3. The maximum deviation of the reported values among the participants for the same detector was mostly less than 1 Ω, at maximum 2 Ω for two participants. This means that the effect of the temperature correction was less than the reproducibility uncertainty in the visible wavelength range. Only at the wavelength range of 1000 nm, the temperature correction could result a meaningful difference, but the uncertainty of the temperature coefficient itself would increase the uncertainty of the DoEs due to the large reproducibility uncertainty of the pilot. In addition, one participant did not have reported the PT100 readings. With these considerations, the quantitative results of the comparison were calculated without temperature correction. The results at a wavelength 1000 nm showed a consistent result without temperature correction.

**Table 3-3.** Resistance reading values of PT100 reported by the participants during the measurement. The resistance values were averaged over the wavelengths for each detector.

| *R* in Ω | KRISS | NMC-ASTAR | NIST | *R* in Ω | KRISS | NMIJ | | *R* in Ω | KRISS | NRC | MSL |
|---|---|---|---|---|---|---|---|---|---|---|---|

[2] IO-CSIC and NMIJ reported a reading failure of PT100 for B#4 and C#4, respectively.

| | | | | | | | | | | | |
|---|---|---|---|---|---|---|---|---|---|---|---|
| A#1 | 108.62 | 109.27 | 109.18 | C#1 | 108.64 | 108.88 | | E#1 | 109.66 | 110.02 | 109.90 |
| A#2 | 108.62 | 109.31 | 109.08 | C#2 | 108.62 | 108.90 | | E#2 | 108.68 | 109.34 | 109.14 |
| A#3 | 108.63 | 109.33 | 109.33 | C#3 | 108.58 | 108.85 | | E#3 | 109.53 | 110.12 | 109.95 |
| A#4 | 108.68 | 109.78 | 109.91 | C#4 | 115.93 | failed | | E#4 | 108.67 | 109.20 | 109.18 |
| A#5 | 108.67 | 109.78 | 109.31 | C#5 | 108.60 | 109.01 | | E#5 | 108.68 | 109.20 | 109.12 |
| *R* in Ω | KRISS | IO-CSIC | VNIIOFI | *R* in Ω | KRISS | LNE-CNAM | PTB | *R* in Ω | KRISS | UME | NPL |
| B#1 | 108.62 | 111.06 | N.A. | D#1 | 108.51 | 109.52 | 109.01 | F#1 | 108.68 | 110.16 | 109.11 |
| B#2 | 108.62 | 111.02 | N.A. | D#2 | 108.55 | 109.41 | 109.05 | F#2 | 108.56 | 110.88 | 109.00 |
| B#3 | 108.63 | 111.02 | N.A. | D#3 | 108.56 | 109.51 | 109.07 | F#3 | 108.63 | 110.16 | 108.98 |
| B#4 | 108.65 | failed | N.A. | D#4 | 108.72 | 109.19 | 109.01 | F#4 | 108.63 | 110.06 | 109.02 |
| B#5 | 108.65 | 111.11 | N.A. | D#5 | 108.70 | 109.27 | 108.97 | F#5 | 108.69 | 110.26 | 108.94 |

# 4. MEASUREMENT DATA

The measurement data of spectral responsivity submitted from the participants are summarized from Table 4-1 through Table 4-12. The detailed technical information of each participant including the uncertainty budgets is reported in Appendix B.

For the results of the pilot in Table 4-12, the measurement data of each detector are determined by averaging the multiple measurements of the same detector during the comparison. The reproducibility of the pilot is not included in the uncertainty of the pilot in Table 4-12. Instead, it is added as a separate uncertainty component $u_{PR}$ corresponding to the stability of the pilot scale during the comparison in Eq. (6-2). More information on the long-term stability of the pilot setup, which was evaluated from the comparison, is summarized in Appendix B, Section 1.

**Table 4-1.** Spectral responsivity and its standard uncertainty measured and submitted by NMC-ASTAR.

| | A#1 | | A#2 | | A#3 | | A#4 | | A#5 | |
|---|---|---|---|---|---|---|---|---|---|---|
| WL (nm) | *S* (A/W) | *u*(*S*) | *S* (A/W) | *u*(*S*) | *S* (A/W) | *u*(*S*) | *S* (A/W) | *u*(*S*) | *S* (A/W) | *u*(*S*) |
| 300 | 0.131 | 0.90% | 0.129 | 0.90% | 0.132 | 0.90% | 0.249 | 0.99% | 0.246 | 0.99% |
| 320 | 0.143 | 0.85% | 0.142 | 0.85% | 0.145 | 0.85% | 0.252 | 1.01% | 0.254 | 1.01% |
| 340 | 0.151 | 0.90% | 0.150 | 0.90% | 0.152 | 0.90% | 0.268 | 0.98% | 0.270 | 0.98% |
| 360 | 0.147 | 0.90% | 0.146 | 0.90% | 0.148 | 0.90% | 0.279 | 0.98% | 0.280 | 0.98% |
| 380 | 0.158 | 0.85% | 0.157 | 0.85% | 0.159 | 0.85% | 0.296 | 0.96% | 0.297 | 0.96% |
| 400 | 0.1834 | 0.15% | 0.1823 | 0.15% | 0.1844 | 0.15% | 0.3193 | 0.14% | 0.3193 | 0.14% |
| 450 | 0.2220 | 0.14% | 0.2210 | 0.14% | 0.2228 | 0.14% | 0.3599 | 0.13% | 0.3599 | 0.13% |
| 500 | 0.2540 | 0.12% | 0.2531 | 0.12% | 0.2547 | 0.12% | 0.4005 | 0.11% | 0.4005 | 0.11% |
| 550 | 0.2839 | 0.11% | 0.2831 | 0.11% | 0.2845 | 0.11% | 0.4411 | 0.10% | 0.4411 | 0.10% |
| 600 | 0.3129 | 0.11% | 0.3121 | 0.11% | 0.3134 | 0.11% | 0.4817 | 0.094% | 0.4817 | 0.094% |
| 650 | 0.3413 | 0.10% | 0.3406 | 0.10% | 0.3418 | 0.10% | 0.5223 | 0.087% | 0.5224 | 0.087% |
| 700 | 0.3693 | 0.09% | 0.3687 | 0.09% | 0.3698 | 0.09% | 0.5629 | 0.081% | 0.5630 | 0.081% |
| 750 | 0.3972 | 0.09% | 0.3967 | 0.09% | 0.3977 | 0.09% | 0.6035 | 0.076% | 0.6036 | 0.076% |
| 800 | 0.4250 | 0.09% | 0.4244 | 0.09% | 0.4253 | 0.09% | 0.6441 | 0.071% | 0.6442 | 0.071% |
| 850 | 0.4526 | 0.08% | 0.4520 | 0.08% | 0.4529 | 0.08% | 0.6847 | 0.067% | 0.6848 | 0.067% |

| | | | | | | | | | | |
|---|---|---|---|---|---|---|---|---|---|---|
| 900 | 0.4800 | 0.08% | 0.4793 | 0.08% | 0.4802 | 0.08% | 0.7253 | 0.064% | 0.7254 | 0.064% |
| 950 | 0.5048 | 0.74% | 0.5041 | 0.74% | 0.5049 | 0.74% | 0.7657 | 0.72% | 0.7654 | 0.72% |
| 1000 | 0.4777 | 0.74% | 0.4770 | 0.74% | 0.4781 | 0.74% | 0.7632 | 0.72% | 0.7639 | 0.72% |

**Table 4-2.** Spectral responsivity and its standard uncertainty measured and submitted by NIST.

| | A#1 | | A#2 | | A#3 | | A#4 | | A#5 | |
|---|---|---|---|---|---|---|---|---|---|---|
| WL (nm) | *S* (A/W) | *u*(*S*) | *S* (A/W) | *u*(*S*) | *S* (A/W) | *u*(*S*) | *S* (A/W) | *u*(*S*) | *S* (A/W) | *u*(*S*) |
| 300 | 0.12900 | 0.130% | 0.12753 | 0.110% | 0.13069 | 0.110% | 0.24344 | 0.111% | 0.24284 | 0.111% |
| 320 | 0.14136 | 0.110% | 0.13989 | 0.110% | 0.14297 | 0.100% | 0.25058 | 0.108% | 0.25003 | 0.108% |
| 340 | 0.14734 | 0.095% | 0.14592 | 0.092% | 0.14891 | 0.088% | 0.26293 | 0.090% | 0.26234 | 0.090% |
| 360 | 0.14463 | 0.086% | 0.14329 | 0.082% | 0.14610 | 0.081% | 0.27529 | 0.081% | 0.27455 | 0.081% |
| 380 | 0.15569 | 0.054% | 0.15448 | 0.046% | 0.15705 | 0.046% | 0.29248 | 0.046% | 0.29182 | 0.046% |
| 400 | 0.17979 | 0.035% | 0.17864 | 0.030% | 0.18112 | 0.028% | 0.31282 | 0.029% | 0.31238 | 0.029% |
| 450 | 0.22070 | 0.075% | 0.21968 | 0.074% | 0.22191 | 0.073% | 0.35765 | 0.073% | 0.35747 | 0.073% |
| 500 | 0.25369 | 0.040% | 0.25278 | 0.038% | 0.25479 | 0.037% | 0.39991 | 0.037% | 0.39983 | 0.037% |
| 550 | 0.28407 | 0.039% | 0.28324 | 0.038% | 0.28506 | 0.036% | 0.44120 | 0.037% | 0.44118 | 0.037% |
| 600 | 0.31314 | 0.038% | 0.31238 | 0.037% | 0.31404 | 0.035% | 0.48198 | 0.035% | 0.48200 | 0.035% |
| 650 | 0.34148 | 0.037% | 0.34079 | 0.035% | 0.34231 | 0.034% | 0.52249 | 0.034% | 0.52253 | 0.034% |
| 700 | 0.36949 | 0.036% | 0.36884 | 0.035% | 0.37026 | 0.034% | 0.56300 | 0.034% | 0.56306 | 0.034% |
| 750 | 0.39712 | 0.035% | 0.39651 | 0.035% | 0.39784 | 0.034% | 0.60322 | 0.034% | 0.60331 | 0.034% |
| 800 | 0.42450 | 0.036% | 0.42391 | 0.035% | 0.42517 | 0.035% | 0.64333 | 0.035% | 0.64343 | 0.035% |
| 850 | 0.45171 | 0.034% | 0.45111 | 0.033% | 0.45232 | 0.033% | 0.68344 | 0.033% | 0.68356 | 0.033% |
| 900 | 0.47873 | 0.036% | 0.47801 | 0.035% | 0.47926 | 0.035% | 0.72351 | 0.035% | 0.72365 | 0.035% |
| 950 | 0.50263 | 0.054% | 0.50176 | 0.052% | 0.50303 | 0.052% | 0.76267 | 0.052% | 0.76283 | 0.052% |
| 1000 | 0.47313 | 0.170% | 0.47217 | 0.170% | 0.47393 | 0.170% | 0.75934 | 0.175% | 0.75940 | 0.175% |

**Table 4-3.** Spectral responsivity and its standard uncertainty measured and submitted by IO-CSIC.

| | B#1 | | B#2 | | B#3 | | B#4 | | B#5 | |
|---|---|---|---|---|---|---|---|---|---|---|
| WL (nm) | *S* (A/W) | *u*(*S*) | *S* (A/W) | *u*(*S*) | *S* (A/W) | *u*(*S*) | *S* (A/W) | *u*(*S*) | *S* (A/W) | *u*(*S*) |
| 300 | 0.1362 | 0.64% | 0.1343 | 0.64% | 0.1368 | 0.64% | 0.2545 | 0.66% | 0.2558 | 0.84% |
| 320 | 0.1493 | 0.62% | 0.1476 | 0.62% | 0.1500 | 0.62% | 0.2630 | 0.64% | 0.2640 | 0.70% |
| 340 | 0.1559 | 0.62% | 0.1544 | 0.62% | 0.1566 | 0.63% | 0.2770 | 0.63% | 0.2780 | 0.65% |
| 360 | 0.1526 | 0.59% | 0.1509 | 0.60% | 0.1531 | 0.59% | 0.2891 | 0.62% | 0.2907 | 0.66% |
| 380 | 0.1637 | 0.56% | 0.1623 | 0.58% | 0.1641 | 0.57% | 0.3054 | 0.58% | 0.3070 | 0.64% |
| 400 | 0.1863 | 0.57% | 0.1849 | 0.57% | 0.1868 | 0.57% | 0.3221 | 0.59% | 0.3230 | 0.59% |
| 450 | 0.2219 | 0.32% | 0.2209 | 0.32% | 0.2222 | 0.33% | 0.3591 | 0.34% | 0.3595 | 0.60% |
| 500 | 0.2538 | 0.24% | 0.2527 | 0.24% | 0.2540 | 0.24% | 0.3997 | 0.25% | 0.4000 | 0.34% |
| 550 | 0.2796 | 0.24% | 0.2785 | 0.25% | 0.2799 | 0.25% | 0.4333 | 0.25% | 0.4337 | 0.25% |
| 600 | 0.3082 | 0.24% | 0.3074 | 0.24% | 0.3085 | 0.24% | 0.4738 | 0.25% | 0.4740 | 0.25% |
| 650 | 0.3363 | 0.24% | 0.3353 | 0.24% | 0.3364 | 0.24% | 0.5141 | 0.24% | 0.5142 | 0.25% |
| 700 | 0.3641 | 0.24% | 0.3632 | 0.24% | 0.3641 | 0.24% | 0.5540 | 0.24% | 0.5541 | 0.24% |
| 750 | 0.3983 | 0.23% | 0.3975 | 0.23% | 0.3983 | 0.23% | 0.6044 | 0.24% | 0.6048 | 0.24% |
| 800 | 0.4269 | 0.25% | 0.4262 | 0.26% | 0.4267 | 0.25% | 0.6464 | 0.26% | 0.6466 | 0.24% |

| | | | | | | | | | | |
|---|---|---|---|---|---|---|---|---|---|---|
| 850 | 0.4540 | 0.37% | 0.4534 | 0.37% | 0.4537 | 0.37% | 0.6863 | 0.37% | 0.6868 | 0.26% |
| 900 | 0.4811 | 0.36% | 0.4805 | 0.36% | 0.4808 | 0.36% | 0.7263 | 0.37% | 0.7268 | 0.37% |
| 950 | 0.5062 | 0.39% | 0.5056 | 0.39% | 0.5058 | 0.39% | 0.7672 | 0.40% | 0.7676 | 0.37% |
| 1000 | 0.4799 | 0.36% | 0.4786 | 0.36% | 0.4786 | 0.36% | 0.7685 | 0.37% | 0.7692 | 0.40% |

**Table 4-4.** Spectral responsivity and its standard uncertainty measured and submitted by VNIIOFI.

| | B#1 | | B#2 | | B#3 | | B#4 | | B#5 | |
|---|---|---|---|---|---|---|---|---|---|---|
| WL (nm) | *S* (A/W) | *u*(*S*) | *S* (A/W) | *u*(*S*) | *S* (A/W) | *u*(*S*) | *S* (A/W) | *u*(*S*) | *S* (A/W) | *u*(*S*) |
| 300 | 0.1286 | 0.38% | 0.1265 | 0.38% | 0.1284 | 0.38% | 0.2485 | 0.38% | 0.2497 | 0.38% |
| 320 | 0.1429 | 0.32% | 0.1413 | 0.32% | 0.1435 | 0.33% | 0.2550 | 0.32% | 0.2558 | 0.32% |
| 340 | 0.1500 | 0.26% | 0.1484 | 0.26% | 0.1506 | 0.26% | 0.2672 | 0.26% | 0.2683 | 0.26% |
| 360 | 0.1491 | 0.26% | 0.1475 | 0.26% | 0.1498 | 0.26% | 0.2796 | 0.26% | 0.2806 | 0.26% |
| 380 | 0.1542 | 0.21% | 0.1530 | 0.21% | 0.1549 | 0.21% | 0.2945 | 0.21% | 0.2957 | 0.21% |
| 400 | 0.1794 | 0.21% | 0.1784 | 0.21% | 0.1801 | 0.21% | 0.3147 | 0.21% | 0.3153 | 0.21% |
| 450 | 0.2208 | 0.16% | 0.2196 | 0.16% | 0.2213 | 0.16% | 0.3587 | 0.16% | 0.3590 | 0.16% |
| 500 | 0.2538 | 0.16% | 0.2529 | 0.16% | 0.2542 | 0.16% | 0.4004 | 0.16% | 0.4008 | 0.16% |
| 550 | 0.2843 | 0.16% | 0.2833 | 0.16% | 0.2847 | 0.16% | 0.4417 | 0.16% | 0.4419 | 0.16% |
| 600 | 0.3133 | 0.11% | 0.3125 | 0.11% | 0.3137 | 0.11% | 0.4826 | 0.11% | 0.4826 | 0.11% |
| 650 | 0.3418 | 0.11% | 0.3409 | 0.11% | 0.3420 | 0.11% | 0.5228 | 0.11% | 0.5229 | 0.11% |
| 700 | 0.3697 | 0.11% | 0.3690 | 0.11% | 0.3699 | 0.11% | 0.5631 | 0.11% | 0.5632 | 0.11% |
| 750 | 0.3976 | 0.11% | 0.3969 | 0.11% | 0.3978 | 0.11% | 0.6034 | 0.11% | 0.6035 | 0.11% |
| 800 | 0.4251 | 0.11% | 0.4245 | 0.11% | 0.4252 | 0.11% | 0.6439 | 0.11% | 0.6437 | 0.11% |
| 850 | 0.4525 | 0.11% | 0.4519 | 0.11% | 0.4525 | 0.11% | 0.6838 | 0.11% | 0.6838 | 0.11% |
| 900 | 0.4796 | 0.11% | 0.4792 | 0.11% | 0.4796 | 0.11% | 0.7238 | 0.11% | 0.7239 | 0.11% |
| 950 | 0.5027 | 0.21% | 0.5022 | 0.21% | 0.5026 | 0.21% | 0.7602 | 0.21% | 0.7602 | 0.21% |
| 1000 | 0.4829 | 0.26% | 0.4820 | 0.26% | 0.4822 | 0.26% | 0.7618 | 0.26% | 0.7627 | 0.26% |

**Table 4-5.** Spectral responsivity and its standard uncertainty measured and submitted by NMIJ.

| | C#1 | | C#2 | | C#3 | | C#4 | | C#5 | |
|---|---|---|---|---|---|---|---|---|---|---|
| WL (nm) | *S* (A/W) | *u*(*S*) | *S* (A/W) | *u*(*S*) | *S* (A/W) | *u*(*S*) | *S* (A/W) | *u*(*S*) | *S* (A/W) | *u*(*S*) |
| 300 | 0.12860 | 0.85% | 0.13064 | 0.85% | 0.13001 | 0.85% | 0.24547 | 0.85% | 0.24656 | 0.85% |
| 320 | 0.14188 | 0.85% | 0.14386 | 0.85% | 0.14328 | 0.85% | 0.25400 | 0.85% | 0.25510 | 0.85% |
| 340 | 0.14817 | 0.85% | 0.15005 | 0.85% | 0.14951 | 0.85% | 0.26679 | 0.85% | 0.26799 | 0.85% |
| 360 | 0.14513 | 0.85% | 0.14688 | 0.85% | 0.14637 | 0.85% | 0.27920 | 0.85% | 0.28054 | 0.85% |
| 380 | 0.15692 | 0.55% | 0.15848 | 0.55% | 0.15801 | 0.55% | 0.29600 | 0.55% | 0.29730 | 0.55% |
| 400 | 0.18067 | 0.53% | 0.18209 | 0.53% | 0.18166 | 0.53% | 0.31565 | 0.53% | 0.31675 | 0.53% |
| 450 | 0.22046 | 0.47% | 0.22164 | 0.47% | 0.22131 | 0.47% | 0.35868 | 0.47% | 0.35944 | 0.47% |
| 500 | 0.25283 | 0.41% | 0.25381 | 0.41% | 0.25358 | 0.41% | 0.39993 | 0.41% | 0.40024 | 0.41% |
| 550 | 0.28293 | 0.35% | 0.28377 | 0.35% | 0.28358 | 0.35% | 0.44089 | 0.35% | 0.44118 | 0.35% |
| 600 | 0.31200 | 0.30% | 0.31270 | 0.30% | 0.31258 | 0.30% | 0.48111 | 0.30% | 0.48191 | 0.30% |
| 650 | 0.34028 | 0.24% | 0.34088 | 0.24% | 0.34079 | 0.24% | 0.52137 | 0.24% | 0.52178 | 0.24% |
| 700 | 0.36825 | 0.25% | 0.36876 | 0.25% | 0.36871 | 0.25% | 0.56204 | 0.25% | 0.56191 | 0.25% |
| 750 | 0.39562 | 0.27% | 0.39607 | 0.27% | 0.39603 | 0.27% | 0.60198 | 0.27% | 0.60189 | 0.27% |

| | | | | | | | | | | |
|---|---|---|---|---|---|---|---|---|---|---|
| 800 | 0.42272 | 0.28% | 0.42312 | 0.28% | 0.42312 | 0.28% | 0.64115 | 0.28% | 0.64150 | 0.28% |
| 850 | 0.44988 | 0.29% | 0.45028 | 0.29% | 0.45030 | 0.29% | 0.68108 | 0.29% | 0.68133 | 0.29% |
| 900 | 0.47701 | 0.30% | 0.47744 | 0.30% | 0.47745 | 0.30% | 0.72071 | 0.30% | 0.72101 | 0.30% |
| 950 | 0.50140 | 0.44% | 0.50191 | 0.44% | 0.50187 | 0.44% | 0.76066 | 0.44% | 0.76111 | 0.44% |
| 1000 | 0.47588 | 0.77% | 0.47640 | 0.77% | 0.47583 | 0.77% | 0.76327 | 0.77% | 0.76404 | 0.77% |

**Table 4-6.** Spectral responsivity and its standard uncertainty measured and submitted by LNE-CNAM.

| | D#1 | | D#2 | | D#3 | | D#4 | | D#5 | |
|---|---|---|---|---|---|---|---|---|---|---|
| WL (nm) | *S* (A/W) | *u*(*S*) | *S* (A/W) | *u*(*S*) | *S* (A/W) | *u*(*S*) | *S* (A/W) | *u*(*S*) | *S* (A/W) | *u*(*S*) |
| 300 | 0.1294 | 0.30% | 0.1282 | 0.23% | 0.1306 | 0.20% | 0.2415 | 0.44% | 0.2419 | 0.35% |
| 320 | 0.1421 | 0.26% | 0.1407 | 0.28% | 0.1430 | 0.25% | 0.2507 | 0.36% | 0.2508 | 0.31% |
| 340 | 0.1480 | 0.24% | 0.1466 | 0.24% | 0.1489 | 0.25% | 0.2635 | 0.28% | 0.2634 | 0.26% |
| 360 | 0.1447 | 0.26% | 0.1432 | 0.25% | 0.1454 | 0.31% | 0.2754 | 0.24% | 0.2754 | 0.21% |
| 380 | 0.1564 | 0.27% | 0.1553 | 0.24% | 0.1572 | 0.20% | 0.2921 | 0.25% | 0.2920 | 0.20% |
| 400 | 0.1801 | 0.12% | 0.1792 | 0.12% | 0.1810 | 0.12% | 0.3124 | 0.14% | 0.3125 | 0.17% |
| 450 | 0.2210 | 0.12% | 0.2201 | 0.12% | 0.2219 | 0.11% | 0.3576 | 0.12% | 0.3574 | 0.11% |
| 500 | 0.2541 | 0.16% | 0.2533 | 0.16% | 0.2549 | 0.16% | 0.3999 | 0.17% | 0.3998 | 0.17% |
| 550 | 0.2847 | 0.15% | 0.2840 | 0.15% | 0.2854 | 0.15% | 0.4409 | 0.16% | 0.4407 | 0.15% |
| 600 | 0.3134 | 0.20% | 0.3128 | 0.20% | 0.3141 | 0.20% | 0.4818 | 0.21% | 0.4817 | 0.20% |
| 650 | 0.3421 | 0.15% | 0.3416 | 0.15% | 0.3427 | 0.15% | 0.5231 | 0.16% | 0.5230 | 0.16% |
| 700 | 0.3699 | 0.12% | 0.3695 | 0.12% | 0.3705 | 0.12% | 0.5634 | 0.12% | 0.5631 | 0.12% |
| 750 | 0.3979 | 0.13% | 0.3975 | 0.13% | 0.3985 | 0.13% | 0.6038 | 0.14% | 0.6038 | 0.13% |
| 800 | 0.4249 | 0.15% | 0.4246 | 0.15% | 0.4255 | 0.15% | 0.6435 | 0.16% | 0.6433 | 0.15% |
| 850 | 0.4524 | 0.13% | 0.4523 | 0.13% | 0.4530 | 0.13% | 0.6842 | 0.14% | 0.6838 | 0.13% |
| 900 | 0.4788 | 0.11% | 0.4790 | 0.11% | 0.4797 | 0.11% | 0.7233 | 0.12% | 0.7229 | 0.12% |
| 950 | 0.5033 | 0.19% | 0.5037 | 0.17% | 0.5046 | 0.21% | 0.7625 | 0.29% | 0.7622 | 0.29% |
| 1000 | 0.4769 | 0.32% | 0.4774 | 0.29% | 0.4774 | 0.30% | 0.7630 | 0.45% | 0.7632 | 0.41% |

**Table 4-7.** Spectral responsivity and its standard uncertainty measured and submitted by PTB.

| | D#1 | | D#2 | | D#3 | | D#4 | | D#5 | |
|---|---|---|---|---|---|---|---|---|---|---|
| WL (nm) | *S* (A/W) | *u*(*S*) | *S* (A/W) | *u*(*S*) | *S* (A/W) | *u*(*S*) | *S* (A/W) | *u*(*S*) | *S* (A/W) | *u*(*S*) |
| 300 | 0.12894 | 0.117% | 0.12752 | 0.118% | 0.12996 | 0.117% | 0.24167 | 0.095% | 0.24192 | 0.095% |
| 320 | 0.14184 | 0.098% | 0.14038 | 0.098% | 0.14270 | 0.099% | 0.25050 | 0.098% | 0.25056 | 0.098% |
| 340 | 0.14793 | 0.089% | 0.14649 | 0.089% | 0.14870 | 0.089% | 0.26337 | 0.088% | 0.26334 | 0.088% |
| 360 | 0.14499 | 0.109% | 0.14358 | 0.109% | 0.14561 | 0.109% | 0.27584 | 0.099% | 0.27577 | 0.099% |
| 380 | 0.15620 | 0.105% | 0.15495 | 0.106% | 0.15681 | 0.105% | 0.29242 | 0.097% | 0.29227 | 0.097% |
| 400 | 0.179978 | 0.051% | 0.178808 | 0.051% | 0.180623 | 0.051% | 0.31258 | 0.044% | 0.31240 | 0.044% |
| 450 | 0.220735 | 0.034% | 0.219710 | 0.034% | 0.221324 | 0.034% | 0.35737 | 0.032% | 0.35720 | 0.032% |
| 500 | 0.253595 | 0.024% | 0.252692 | 0.023% | 0.254133 | 0.023% | 0.399471 | 0.022% | 0.399302 | 0.022% |
| 550 | 0.283837 | 0.020% | 0.283048 | 0.020% | 0.284339 | 0.020% | 0.440634 | 0.019% | 0.440460 | 0.019% |
| 600 | 0.312850 | 0.019% | 0.312151 | 0.019% | 0.313303 | 0.019% | 0.481365 | 0.017% | 0.481180 | 0.018% |
| 650 | 0.341149 | 0.019% | 0.340522 | 0.019% | 0.341532 | 0.019% | 0.521866 | 0.018% | 0.521664 | 0.018% |
| 700 | 0.369050 | 0.017% | 0.368510 | 0.017% | 0.369420 | 0.018% | 0.562252 | 0.016% | 0.562046 | 0.016% |

| | | | | | | | | | | |
|---|---|---|---|---|---|---|---|---|---|---|
| 750 | 0.396725 | 0.017% | 0.396263 | 0.017% | 0.397163 | 0.017% | 0.602587 | 0.016% | 0.602383 | 0.016% |
| 800 | 0.424205 | 0.018% | 0.423835 | 0.018% | 0.424697 | 0.018% | 0.64287 | 0.016% | 0.64265 | 0.016% |
| 850 | 0.451487 | 0.018% | 0.451263 | 0.018% | 0.452019 | 0.018% | 0.68311 | 0.017% | 0.68288 | 0.017% |
| 900 | 0.478461 | 0.018% | 0.478480 | 0.018% | 0.479148 | 0.018% | 0.72324 | 0.017% | 0.72299 | 0.017% |
| 950 | 0.50226 | 0.026% | 0.50262 | 0.026% | 0.50331 | 0.027% | 0.76226 | 0.025% | 0.76202 | 0.025% |
| 1000 | 0.47608 | 0.070% | 0.47595 | 0.070% | 0.47620 | 0.070% | 0.76260 | 0.060% | 0.76301 | 0.059% |

**Table 4-8.** Spectral responsivity and its standard uncertainty measured and submitted by NRC.

| | E#1 | | E#2 | | E#3 | | E#4 | | E#5 | |
|---|---|---|---|---|---|---|---|---|---|---|
| WL (nm) | *S* (A/W) | *u*(*S*) | *S* (A/W) | *u*(*S*) | *S* (A/W) | *u*(*S*) | *S* (A/W) | *u*(*S*) | *S* (A/W) | *u*(*S*) |
| 300 | 0.127472 | 0.125% | 0.129621 | 0.126% | 0.128137 | 0.127% | 0.241682 | 0.141% | 0.241197 | 0.139% |
| 320 | 0.140307 | 0.052% | 0.142166 | 0.064% | 0.141071 | 0.055% | 0.250449 | 0.057% | 0.250178 | 0.060% |
| 340 | 0.146539 | 0.052% | 0.148165 | 0.064% | 0.147252 | 0.059% | 0.263502 | 0.068% | 0.263198 | 0.071% |
| 360 | 0.144085 | 0.131% | 0.145568 | 0.135% | 0.144790 | 0.130% | 0.276190 | 0.135% | 0.275871 | 0.144% |
| 380 | 0.154578 | 0.083% | 0.155918 | 0.087% | 0.155240 | 0.082% | 0.292292 | 0.095% | 0.292140 | 0.102% |
| 400 | 0.178648 | 0.044% | 0.180055 | 0.046% | 0.179331 | 0.043% | 0.312096 | 0.058% | 0.311996 | 0.060% |
| 450 | 0.220353 | 0.130% | 0.222167 | 0.130% | 0.220960 | 0.129% | 0.358117 | 0.130% | 0.357927 | 0.131% |
| 500 | 0.253391 | 0.056% | 0.255274 | 0.056% | 0.253935 | 0.055% | 0.400305 | 0.056% | 0.400049 | 0.059% |
| 550 | 0.283781 | 0.060% | 0.285619 | 0.061% | 0.284283 | 0.060% | 0.441539 | 0.060% | 0.441212 | 0.064% |
| 600 | 0.312779 | 0.047% | 0.314536 | 0.048% | 0.313252 | 0.047% | 0.482124 | 0.047% | 0.481743 | 0.052% |
| 650 | 0.341301 | 0.045% | 0.342970 | 0.046% | 0.341746 | 0.044% | 0.522824 | 0.045% | 0.522452 | 0.050% |
| 700 | 0.369293 | 0.051% | 0.370897 | 0.051% | 0.369729 | 0.050% | 0.563203 | 0.050% | 0.562889 | 0.053% |
| 750 | 0.397150 | 0.081% | 0.398685 | 0.081% | 0.397559 | 0.081% | 0.602287 | 0.086% | 0.601496 | 0.083% |
| 800 | 0.424893 | 0.099% | 0.426367 | 0.099% | 0.425296 | 0.099% | 0.642751 | 0.103% | 0.641945 | 0.100% |
| 850 | 0.452733 | 0.134% | 0.454170 | 0.135% | 0.453134 | 0.134% | 0.683438 | 0.138% | 0.682575 | 0.135% |
| 900 | 0.479576 | 0.084% | 0.480975 | 0.085% | 0.479976 | 0.084% | 0.722642 | 0.091% | 0.721665 | 0.087% |
| 950 | 0.503181 | 0.058% | 0.504534 | 0.058% | 0.503577 | 0.058% | 0.760725 | 0.069% | 0.759689 | 0.061% |
| 1000 | 0.475004 | 0.117% | 0.475792 | 0.117% | 0.475522 | 0.117% | 0.758181 | 0.125% | 0.758120 | 0.121% |

**Table 4-9.** Spectral responsivity and its standard uncertainty measured and submitted by MSL.

| | E#1 | | E#2 | | E#3 | | E#4 | | E#5 | |
|---|---|---|---|---|---|---|---|---|---|---|
| WL (nm) | *S* (A/W) | *u*(*S*) | *S* (A/W) | *u*(*S*) | *S* (A/W) | *u*(*S*) | *S* (A/W) | *u*(*S*) | *S* (A/W) | *u*(*S*) |
| 300 | 0.12867 | 0.50% | 0.13172 | 0.50% | 0.13032 | 0.50% | 0.2457 | 0.50% | 0.2451 | 0.50% |
| 320 | 0.14131 | 0.50% | 0.14386 | 0.50% | 0.14288 | 0.50% | 0.2537 | 0.50% | 0.2533 | 0.50% |
| 340 | 0.14690 | 0.52% | 0.14908 | 0.52% | 0.14833 | 0.52% | 0.2654 | 0.52% | 0.2650 | 0.52% |
| 360 | 0.14415 | 0.50% | 0.14595 | 0.50% | 0.14541 | 0.50% | 0.2780 | 0.50% | 0.2777 | 0.50% |
| 380 | 0.15574 | 0.50% | 0.15721 | 0.50% | 0.15683 | 0.50% | 0.2944 | 0.50% | 0.2942 | 0.50% |
| 400 | 0.17960 | 0.41% | 0.18127 | 0.40% | 0.18060 | 0.41% | 0.3142 | 0.40% | 0.3139 | 0.40% |
| 450 | 0.22048 | 0.24% | 0.22246 | 0.24% | 0.22123 | 0.24% | 0.35855 | 0.23% | 0.35825 | 0.23% |
| 500 | 0.25331 | 0.14% | 0.25532 | 0.14% | 0.25395 | 0.14% | 0.40029 | 0.13% | 0.39994 | 0.13% |
| 550 | 0.28355 | 0.10% | 0.28549 | 0.10% | 0.28412 | 0.11% | 0.44123 | 0.10% | 0.44079 | 0.10% |
| 600 | 0.31259 | 0.11% | 0.31446 | 0.10% | 0.31317 | 0.11% | 0.48191 | 0.10% | 0.48138 | 0.10% |
| 650 | 0.34095 | 0.10% | 0.34269 | 0.10% | 0.34146 | 0.11% | 0.52236 | 0.10% | 0.52181 | 0.10% |

| | | | | | | | | | | |
|---|---|---|---|---|---|---|---|---|---|---|
| 700 | 0.36897 | 0.11% | 0.37064 | 0.11% | 0.36946 | 0.11% | 0.56281 | 0.10% | 0.56233 | 0.10% |
| 750 | 0.39678 | 0.11% | 0.39821 | 0.11% | 0.39713 | 0.12% | 0.60302 | 0.11% | 0.60253 | 0.11% |
| 800 | 0.42433 | 0.12% | 0.42581 | 0.12% | 0.42485 | 0.12% | 0.64347 | 0.12% | 0.64295 | 0.12% |
| 850 | 0.45180 | 0.13% | 0.45324 | 0.13% | 0.45234 | 0.13% | 0.68381 | 0.13% | 0.68323 | 0.13% |
| 900 | 0.47901 | 0.14% | 0.48055 | 0.14% | 0.47947 | 0.15% | 0.7241 | 0.14% | 0.7235 | 0.14% |
| 950 | 0.50260 | 0.18% | 0.50419 | 0.18% | 0.50392 | 0.18% | 0.7634 | 0.18% | 0.7629 | 0.18% |
| 1000 | 0.4764 | 0.23% | 0.4770 | 0.23% | 0.4768 | 0.23% | 0.7640 | 0.23% | 0.7643 | 0.23% |

**Table 4-10.** Spectral responsivity and its standard uncertainty measured and submitted by UME.

| | F#1 | | F#2 | | F#3 | | F#4 | | F#5 | |
|---|---|---|---|---|---|---|---|---|---|---|
| WL (nm) | *S* (A/W) | *u*(*S*) | *S* (A/W) | *u*(*S*) | *S* (A/W) | *u*(*S*) | *S* (A/W) | *u*(*S*) | *S* (A/W) | *u*(*S*) |
| 300 | 0.1216 | 0.57% | 0.1212 | 0.57% | 0.1230 | 0.58% | 0.2233 | 0.56% | 0.2230 | 0.56% |
| 320 | 0.1358 | 0.56% | 0.1351 | 0.57% | 0.1376 | 0.59% | 0.2435 | 0.56% | 0.2429 | 0.56% |
| 340 | 0.1437 | 0.56% | 0.1430 | 0.56% | 0.1457 | 0.58% | 0.2614 | 0.56% | 0.2609 | 0.56% |
| 360 | 0.1409 | 0.56% | 0.1401 | 0.56% | 0.1427 | 0.57% | 0.2740 | 0.56% | 0.2735 | 0.56% |
| 380 | 0.1538 | 0.26% | 0.1529 | 0.26% | 0.1555 | 0.27% | 0.2918 | 0.25% | 0.2912 | 0.25% |
| 400 | 0.1777 | 0.26% | 0.1770 | 0.26% | 0.1795 | 0.27% | 0.3127 | 0.25% | 0.3121 | 0.25% |
| 450 | 0.2192 | 0.26% | 0.2188 | 0.26% | 0.2209 | 0.27% | 0.3580 | 0.25% | 0.3576 | 0.25% |
| 500 | 0.2526 | 0.26% | 0.2523 | 0.26% | 0.2541 | 0.26% | 0.4001 | 0.25% | 0.3998 | 0.25% |
| 550 | 0.2831 | 0.26% | 0.2829 | 0.26% | 0.2846 | 0.26% | 0.4413 | 0.25% | 0.4411 | 0.25% |
| 600 | 0.3122 | 0.26% | 0.3120 | 0.26% | 0.3137 | 0.26% | 0.4820 | 0.25% | 0.4819 | 0.25% |
| 650 | 0.3407 | 0.26% | 0.3405 | 0.26% | 0.3421 | 0.26% | 0.5228 | 0.25% | 0.5228 | 0.25% |
| 700 | 0.3685 | 0.26% | 0.3684 | 0.26% | 0.3699 | 0.26% | 0.5631 | 0.25% | 0.5631 | 0.25% |
| 750 | 0.3963 | 0.26% | 0.3962 | 0.26% | 0.3976 | 0.26% | 0.6033 | 0.25% | 0.6034 | 0.25% |
| 800 | 0.4239 | 0.26% | 0.4238 | 0.26% | 0.4252 | 0.26% | 0.6437 | 0.25% | 0.6439 | 0.25% |
| 850 | 0.4513 | 0.26% | 0.4513 | 0.26% | 0.4526 | 0.26% | 0.6840 | 0.25% | 0.6842 | 0.25% |
| 900 | 0.4785 | 0.56% | 0.4785 | 0.56% | 0.4797 | 0.56% | 0.7242 | 0.56% | 0.7242 | 0.56% |
| 950 | 0.5024 | 0.56% | 0.5024 | 0.56% | 0.5034 | 0.56% | 0.7629 | 0.56% | 0.7627 | 0.56% |
| 1000 | 0.4759 | 0.56% | 0.4766 | 0.57% | 0.4776 | 0.57% | 0.7654 | 0.56% | 0.7643 | 0.56% |

**Table 4-11.** Spectral responsivity and its standard uncertainty measured and submitted by NPL.

| | F#1 | | F#2 | | F#3 | | F#4 | | F#5 | |
|---|---|---|---|---|---|---|---|---|---|---|
| WL (nm) | *S* (A/W) | *u*(*S*) | *S* (A/W) | *u*(*S*) | *S* (A/W) | *u*(*S*) | *S* (A/W) | *u*(*S*) | *S* (A/W) | *u*(*S*) |
| 300 | 0.1255 | 0.38% | 0.1247 | 0.38% | 0.1271 | 0.37% | 0.2434 | 0.40% | 0.2432 | 0.42% |
| 320 | 0.1383 | 0.37% | 0.1374 | 0.37% | 0.1398 | 0.37% | 0.2521 | 0.38% | 0.2518 | 0.41% |
| 340 | 0.1442 | 0.37% | 0.1433 | 0.37% | 0.1457 | 0.37% | 0.2647 | 0.39% | 0.2643 | 0.41% |
| 360 | 0.1412 | 0.37% | 0.1404 | 0.37% | 0.1427 | 0.37% | 0.2767 | 0.39% | 0.2763 | 0.42% |
| 380 | 0.1535 | 0.22% | 0.1528 | 0.22% | 0.1549 | 0.22% | 0.2952 | 0.22% | 0.2948 | 0.22% |
| 400 | 0.1766 | 0.14% | 0.1759 | 0.14% | 0.1779 | 0.13% | 0.3128 | 0.14% | 0.3125 | 0.13% |
| 450 | 0.2186 | 0.08% | 0.2180 | 0.08% | 0.2197 | 0.08% | 0.3577 | 0.08% | 0.3575 | 0.07% |
| 500 | 0.2521 | 0.06% | 0.2516 | 0.06% | 0.2531 | 0.06% | 0.3997 | 0.06% | 0.3997 | 0.05% |
| 550 | 0.2827 | 0.05% | 0.2822 | 0.05% | 0.2836 | 0.05% | 0.4408 | 0.06% | 0.4408 | 0.05% |
| 600 | 0.3119 | 0.05% | 0.3114 | 0.05% | 0.3127 | 0.05% | 0.4813 | 0.05% | 0.4814 | 0.04% |

| | | | | | | | | | | |
|---|---|---|---|---|---|---|---|---|---|---|
| 650 | 0.3403 | 0.05% | 0.3399 | 0.05% | 0.3411 | 0.05% | 0.5218 | 0.05% | 0.5219 | 0.04% |
| 700 | 0.3684 | 0.05% | 0.3680 | 0.05% | 0.3692 | 0.05% | 0.5621 | 0.05% | 0.5622 | 0.05% |
| 750 | 0.3963 | 0.05% | 0.3959 | 0.05% | 0.3970 | 0.05% | 0.6024 | 0.05% | 0.6025 | 0.04% |
| 800 | 0.4240 | 0.05% | 0.4236 | 0.05% | 0.4246 | 0.05% | 0.6427 | 0.05% | 0.6428 | 0.04% |
| 850 | 0.4515 | 0.05% | 0.4511 | 0.05% | 0.4520 | 0.05% | 0.6829 | 0.05% | 0.6831 | 0.04% |
| 900 | 0.4788 | 0.05% | 0.4784 | 0.05% | 0.4793 | 0.05% | 0.7232 | 0.05% | 0.7233 | 0.05% |
| 950 | 0.5028 | 0.17% | 0.5025 | 0.17% | 0.5033 | 0.17% | 0.7625 | 0.17% | 0.7626 | 0.18% |
| 1000 | 0.4750 | 0.15% | 0.4751 | 0.15% | 0.4756 | 0.15% | 0.7631 | 0.16% | 0.7640 | 0.17% |

**Table 4-12.** Spectral responsivity and its standard uncertainty measured and submitted by KRISS.

| | A#1 | | A#2 | | A#3 | | A#4 | | A#5 | |
|---|---|---|---|---|---|---|---|---|---|---|
| WL (nm) | *S* (A/W) | *u*(*S*) | *S* (A/W) | *u*(*S*) | *S* (A/W) | *u*(*S*) | *S* (A/W) | *u*(*S*) | *S* (A/W) | *u*(*S*) |
| 300 | 0.1286 | 0.23% | 0.1270 | 0.25% | 0.1304 | 0.25% | 0.2414 | 0.48% | 0.2401 | 0.21% |
| 320 | 0.1413 | 0.22% | 0.1398 | 0.20% | 0.1431 | 0.21% | 0.2497 | 0.39% | 0.2494 | 0.22% |
| 340 | 0.1471 | 0.25% | 0.1461 | 0.32% | 0.1489 | 0.23% | 0.2615 | 0.21% | 0.2598 | 0.44% |
| 360 | 0.1439 | 0.24% | 0.1426 | 0.22% | 0.1458 | 0.23% | 0.2733 | 0.54% | 0.2726 | 0.29% |
| 380 | 0.1549 | 0.27% | 0.1536 | 0.30% | 0.1561 | 0.35% | 0.2891 | 0.31% | 0.2888 | 0.23% |
| 400 | 0.1794 | 0.30% | 0.1783 | 0.29% | 0.1812 | 0.36% | 0.3106 | 0.21% | 0.3105 | 0.21% |
| 450 | 0.2209 | 0.20% | 0.2199 | 0.21% | 0.2224 | 0.21% | 0.3568 | 0.19% | 0.3568 | 0.19% |
| 500 | 0.2535 | 0.20% | 0.2527 | 0.20% | 0.2551 | 0.20% | 0.3990 | 0.20% | 0.3989 | 0.20% |
| 550 | 0.2839 | 0.20% | 0.2832 | 0.20% | 0.2853 | 0.20% | 0.4402 | 0.20% | 0.4402 | 0.20% |
| 600 | 0.3125 | 0.19% | 0.3119 | 0.20% | 0.3138 | 0.19% | 0.4800 | 0.19% | 0.4802 | 0.19% |
| 650 | 0.3412 | 0.21% | 0.3406 | 0.21% | 0.3424 | 0.21% | 0.5211 | 0.21% | 0.5212 | 0.21% |
| 700 | 0.3690 | 0.21% | 0.3686 | 0.21% | 0.3703 | 0.21% | 0.5616 | 0.21% | 0.5616 | 0.21% |
| 750 | 0.3966 | 0.23% | 0.3961 | 0.23% | 0.3978 | 0.23% | 0.6014 | 0.23% | 0.6016 | 0.23% |
| 800 | 0.4247 | 0.32% | 0.4243 | 0.32% | 0.4258 | 0.32% | 0.6420 | 0.31% | 0.6422 | 0.31% |
| 850 | 0.4516 | 0.28% | 0.4512 | 0.28% | 0.4527 | 0.29% | 0.6818 | 0.28% | 0.6821 | 0.28% |
| 900 | 0.4770 | 0.20% | 0.4766 | 0.20% | 0.4784 | 0.20% | 0.7198 | 0.20% | 0.7199 | 0.20% |
| 950 | 0.5015 | 0.21% | 0.5009 | 0.21% | 0.5030 | 0.21% | 0.7601 | 0.21% | 0.7606 | 0.21% |
| 1000 | 0.4749 | 0.22% | 0.4733 | 0.22% | 0.4747 | 0.22% | 0.7612 | 0.21% | 0.7609 | 0.22% |
| | B#1 | | B#2 | | B#3 | | B#4 | | B#5 | |
| WL (nm) | *S* (A/W) | *u*(*S*) | *S* (A/W) | *u*(*S*) | *S* (A/W) | *u*(*S*) | *S* (A/W) | *u*(*S*) | *S* (A/W) | *u*(*S*) |
| 300 | 0.1281 | 0.40% | 0.1268 | 0.23% | 0.1288 | 0.23% | 0.2400 | 0.21% | 0.2411 | 0.23% |
| 320 | 0.1408 | 0.50% | 0.1394 | 0.21% | 0.1425 | 0.47% | 0.2484 | 0.34% | 0.2500 | 0.21% |
| 340 | 0.1462 | 0.23% | 0.1454 | 0.23% | 0.1474 | 0.24% | 0.2609 | 0.22% | 0.2618 | 0.23% |
| 360 | 0.1431 | 0.34% | 0.1422 | 0.29% | 0.1448 | 0.47% | 0.2732 | 0.21% | 0.2745 | 0.21% |
| 380 | 0.1544 | 0.26% | 0.1535 | 0.24% | 0.1552 | 0.25% | 0.2889 | 0.23% | 0.2900 | 0.23% |
| 400 | 0.1792 | 0.32% | 0.1782 | 0.29% | 0.1800 | 0.30% | 0.3103 | 0.21% | 0.3110 | 0.21% |
| 450 | 0.2207 | 0.21% | 0.2195 | 0.20% | 0.2213 | 0.21% | 0.3569 | 0.19% | 0.3570 | 0.20% |
| 500 | 0.2535 | 0.20% | 0.2523 | 0.20% | 0.2539 | 0.20% | 0.3988 | 0.20% | 0.3989 | 0.20% |
| 550 | 0.2840 | 0.20% | 0.2828 | 0.20% | 0.2842 | 0.20% | 0.4401 | 0.20% | 0.4401 | 0.20% |
| 600 | 0.3125 | 0.19% | 0.3113 | 0.19% | 0.3127 | 0.19% | 0.4802 | 0.19% | 0.4800 | 0.19% |
| 650 | 0.3412 | 0.21% | 0.3402 | 0.21% | 0.3414 | 0.21% | 0.5211 | 0.21% | 0.5209 | 0.21% |
| 700 | 0.3691 | 0.21% | 0.3680 | 0.21% | 0.3693 | 0.21% | 0.5614 | 0.21% | 0.5613 | 0.21% |

| | | | | | | | | | | |
|---|---|---|---|---|---|---|---|---|---|---|
| 750 | 0.3967 | 0.23% | 0.3958 | 0.23% | 0.3968 | 0.23% | 0.6013 | 0.23% | 0.6014 | 0.23% |
| 800 | 0.4250 | 0.32% | 0.4239 | 0.32% | 0.4250 | 0.32% | 0.6418 | 0.31% | 0.6419 | 0.31% |
| 850 | 0.4519 | 0.29% | 0.4509 | 0.28% | 0.4519 | 0.29% | 0.6817 | 0.28% | 0.6817 | 0.28% |
| 900 | 0.4771 | 0.20% | 0.4762 | 0.20% | 0.4770 | 0.20% | 0.7196 | 0.20% | 0.7198 | 0.20% |
| 950 | 0.5015 | 0.21% | 0.5005 | 0.21% | 0.5014 | 0.21% | 0.7601 | 0.21% | 0.7601 | 0.21% |
| 1000 | 0.4749 | 0.22% | 0.4731 | 0.22% | 0.4742 | 0.23% | 0.7609 | 0.21% | 0.7610 | 0.21% |
| | C#1 | | C#2 | | C#3 | | C#4 | | C#5 | |
| WL (nm) | *S* (A/W) | *u*(*S*) | *S* (A/W) | *u*(*S*) | *S* (A/W) | *u*(*S*) | *S* (A/W) | *u*(*S*) | *S* (A/W) | *u*(*S*) |
| 300 | 0.1261 | 0.22% | 0.1278 | 0.27% | 0.1274 | 0.22% | 0.2388 | 0.25% | 0.2386 | 0.23% |
| 320 | 0.1386 | 0.19% | 0.1402 | 0.19% | 0.1401 | 0.21% | 0.2475 | 0.21% | 0.2478 | 0.21% |
| 340 | 0.1443 | 0.21% | 0.1457 | 0.21% | 0.1457 | 0.21% | 0.2592 | 0.23% | 0.2594 | 0.23% |
| 360 | 0.1414 | 0.21% | 0.1429 | 0.23% | 0.1424 | 0.21% | 0.2721 | 0.26% | 0.2711 | 0.22% |
| 380 | 0.1524 | 0.23% | 0.1541 | 0.24% | 0.1535 | 0.28% | 0.2871 | 0.23% | 0.2869 | 0.23% |
| 400 | 0.1767 | 0.21% | 0.1777 | 0.21% | 0.1776 | 0.21% | 0.3091 | 0.20% | 0.3089 | 0.21% |
| 450 | 0.2192 | 0.19% | 0.2200 | 0.20% | 0.2199 | 0.19% | 0.3559 | 0.20% | 0.3556 | 0.20% |
| 500 | 0.2521 | 0.20% | 0.2528 | 0.20% | 0.2527 | 0.20% | 0.3982 | 0.20% | 0.3978 | 0.20% |
| 550 | 0.2825 | 0.20% | 0.2832 | 0.20% | 0.2830 | 0.21% | 0.4397 | 0.20% | 0.4391 | 0.20% |
| 600 | 0.3112 | 0.19% | 0.3118 | 0.19% | 0.3117 | 0.19% | 0.4795 | 0.19% | 0.4791 | 0.19% |
| 650 | 0.3400 | 0.21% | 0.3405 | 0.21% | 0.3405 | 0.21% | 0.5206 | 0.21% | 0.5200 | 0.21% |
| 700 | 0.3680 | 0.20% | 0.3686 | 0.21% | 0.3686 | 0.21% | 0.5610 | 0.21% | 0.5602 | 0.21% |
| 750 | 0.3956 | 0.22% | 0.3959 | 0.22% | 0.3960 | 0.23% | 0.6009 | 0.23% | 0.6001 | 0.23% |
| 800 | 0.4239 | 0.31% | 0.4242 | 0.31% | 0.4238 | 0.31% | 0.6417 | 0.31% | 0.6407 | 0.31% |
| 850 | 0.4509 | 0.28% | 0.4513 | 0.28% | 0.4516 | 0.28% | 0.6812 | 0.28% | 0.6804 | 0.28% |
| 900 | 0.4762 | 0.20% | 0.4767 | 0.20% | 0.4767 | 0.21% | 0.7193 | 0.20% | 0.7184 | 0.20% |
| 950 | 0.5007 | 0.20% | 0.5016 | 0.21% | 0.5009 | 0.21% | 0.7598 | 0.21% | 0.7589 | 0.21% |
| 1000 | 0.4739 | 0.22% | 0.4751 | 0.22% | 0.4758 | 0.22% | 0.7617 | 0.21% | 0.7621 | 0.22% |
| | D#1 | | D#2 | | D#3 | | D#4 | | D#5 | |
| WL (nm) | *S* (A/W) | *u*(*S*) | *S* (A/W) | *u*(*S*) | *S* (A/W) | *u*(*S*) | *S* (A/W) | *u*(*S*) | *S* (A/W) | *u*(*S*) |
| 300 | 0.1290 | 0.22% | 0.1276 | 0.36% | 0.1295 | 0.22% | 0.2375 | 0.28% | 0.2334 | 0.30% |
| 320 | 0.1415 | 0.25% | 0.1398 | 0.21% | 0.1424 | 0.34% | 0.2466 | 0.21% | 0.2427 | 0.21% |
| 340 | 0.1472 | 0.26% | 0.1455 | 0.23% | 0.1476 | 0.23% | 0.2598 | 0.52% | 0.2547 | 0.24% |
| 360 | 0.1442 | 0.31% | 0.1423 | 0.25% | 0.1441 | 0.38% | 0.2701 | 0.22% | 0.2646 | 0.21% |
| 380 | 0.1547 | 0.39% | 0.1530 | 0.31% | 0.1555 | 0.26% | 0.2870 | 0.32% | 0.2798 | 0.32% |
| 400 | 0.1800 | 0.29% | 0.1778 | 0.30% | 0.1794 | 0.29% | 0.3083 | 0.21% | 0.3038 | 0.21% |
| 450 | 0.2212 | 0.20% | 0.2200 | 0.21% | 0.2216 | 0.21% | 0.3550 | 0.19% | 0.3510 | 0.19% |
| 500 | 0.2538 | 0.20% | 0.2527 | 0.20% | 0.2542 | 0.20% | 0.3971 | 0.20% | 0.3933 | 0.20% |
| 550 | 0.2842 | 0.20% | 0.2831 | 0.20% | 0.2845 | 0.21% | 0.4383 | 0.20% | 0.4347 | 0.20% |
| 600 | 0.3127 | 0.19% | 0.3119 | 0.20% | 0.3131 | 0.20% | 0.4780 | 0.19% | 0.4743 | 0.19% |
| 650 | 0.3413 | 0.21% | 0.3406 | 0.21% | 0.3416 | 0.21% | 0.5192 | 0.21% | 0.5151 | 0.21% |
| 700 | 0.3692 | 0.21% | 0.3686 | 0.21% | 0.3697 | 0.21% | 0.5592 | 0.21% | 0.5551 | 0.21% |
| 750 | 0.3968 | 0.23% | 0.3963 | 0.23% | 0.3972 | 0.23% | 0.5991 | 0.23% | 0.5947 | 0.23% |
| 800 | 0.4249 | 0.32% | 0.4243 | 0.32% | 0.4252 | 0.32% | 0.6395 | 0.31% | 0.6349 | 0.31% |
| 850 | 0.4519 | 0.29% | 0.4513 | 0.29% | 0.4525 | 0.29% | 0.6791 | 0.28% | 0.6742 | 0.28% |
| 900 | 0.4770 | 0.20% | 0.4771 | 0.21% | 0.4780 | 0.21% | 0.7171 | 0.20% | 0.7120 | 0.20% |

| | | | | | | | | | | |
|---|---|---|---|---|---|---|---|---|---|---|
| 950 | 0.5014 | 0.21% | 0.5022 | 0.21% | 0.5028 | 0.21% | 0.7574 | 0.21% | 0.7521 | 0.21% |
| 1000 | 0.4752 | 0.22% | 0.4757 | 0.22% | 0.4757 | 0.22% | 0.7578 | 0.21% | 0.7541 | 0.21% |

| | E#1 | | E#2 | | E#3 | | E#4 | | E#5 | |
|---|---|---|---|---|---|---|---|---|---|---|
| WL (nm) | *S* (A/W) | *u*(*S*) | *S* (A/W) | *u*(*S*) | *S* (A/W) | *u*(*S*) | *S* (A/W) | *u*(*S*) | *S* (A/W) | *u*(*S*) |
| 300 | 0.1271 | 0.25% | 0.1281 | 0.24% | 0.1281 | 0.22% | 0.2413 | 0.22% | 0.2402 | 0.23% |
| 320 | 0.1392 | 0.27% | 0.1415 | 0.43% | 0.1408 | 0.21% | 0.2497 | 0.21% | 0.2490 | 0.21% |
| 340 | 0.1447 | 0.37% | 0.1453 | 0.34% | 0.1466 | 0.22% | 0.2618 | 0.24% | 0.2606 | 0.28% |
| 360 | 0.1424 | 0.42% | 0.1417 | 0.33% | 0.1432 | 0.22% | 0.2743 | 0.23% | 0.2732 | 0.23% |
| 380 | 0.1536 | 0.37% | 0.1532 | 0.35% | 0.1542 | 0.24% | 0.2898 | 0.25% | 0.2904 | 0.44% |
| 400 | 0.1773 | 0.31% | 0.1777 | 0.30% | 0.1784 | 0.30% | 0.3112 | 0.21% | 0.3104 | 0.21% |
| 450 | 0.2197 | 0.21% | 0.2212 | 0.20% | 0.2206 | 0.20% | 0.3570 | 0.19% | 0.3565 | 0.19% |
| 500 | 0.2526 | 0.20% | 0.2542 | 0.20% | 0.2534 | 0.20% | 0.3991 | 0.20% | 0.3984 | 0.20% |
| 550 | 0.2830 | 0.20% | 0.2847 | 0.20% | 0.2838 | 0.20% | 0.4405 | 0.20% | 0.4397 | 0.20% |
| 600 | 0.3117 | 0.20% | 0.3134 | 0.20% | 0.3123 | 0.19% | 0.4802 | 0.19% | 0.4796 | 0.19% |
| 650 | 0.3404 | 0.21% | 0.3422 | 0.21% | 0.3412 | 0.21% | 0.5213 | 0.21% | 0.5205 | 0.21% |
| 700 | 0.3683 | 0.21% | 0.3699 | 0.21% | 0.3689 | 0.21% | 0.5616 | 0.21% | 0.5608 | 0.21% |
| 750 | 0.3961 | 0.23% | 0.3974 | 0.23% | 0.3965 | 0.23% | 0.6017 | 0.23% | 0.6008 | 0.23% |
| 800 | 0.4242 | 0.32% | 0.4259 | 0.32% | 0.4247 | 0.32% | 0.6421 | 0.31% | 0.6412 | 0.31% |
| 850 | 0.4511 | 0.29% | 0.4526 | 0.29% | 0.4518 | 0.29% | 0.6820 | 0.28% | 0.6810 | 0.28% |
| 900 | 0.4767 | 0.21% | 0.4781 | 0.21% | 0.4773 | 0.21% | 0.7200 | 0.20% | 0.7190 | 0.20% |
| 950 | 0.5016 | 0.21% | 0.5030 | 0.21% | 0.5020 | 0.21% | 0.7602 | 0.21% | 0.7594 | 0.21% |
| 1000 | 0.4751 | 0.22% | 0.4762 | 0.22% | 0.4757 | 0.22% | 0.7607 | 0.21% | 0.7604 | 0.21% |

| | F#1 | | F#2 | | F#3 | | F#4 | | F#5 | |
|---|---|---|---|---|---|---|---|---|---|---|
| WL (nm) | *S* (A/W) | *u*(*S*) | *S* (A/W) | *u*(*S*) | *S* (A/W) | *u*(*S*) | *S* (A/W) | *u*(*S*) | *S* (A/W) | *u*(*S*) |
| 300 | 0.1246 | 0.22% | 0.1238 | 0.23% | 0.1263 | 0.25% | 0.2408 | 0.23% | 0.2405 | 0.23% |
| 320 | 0.1368 | 0.21% | 0.1359 | 0.23% | 0.1390 | 0.21% | 0.2496 | 0.22% | 0.2487 | 0.22% |
| 340 | 0.1423 | 0.28% | 0.1417 | 0.22% | 0.1439 | 0.26% | 0.2615 | 0.26% | 0.2606 | 0.30% |
| 360 | 0.1396 | 0.35% | 0.1393 | 0.30% | 0.1401 | 0.49% | 0.2735 | 0.27% | 0.2736 | 0.23% |
| 380 | 0.1507 | 0.25% | 0.1506 | 0.52% | 0.1518 | 0.28% | 0.2900 | 0.37% | 0.2891 | 0.28% |
| 400 | 0.1750 | 0.33% | 0.1745 | 0.28% | 0.1765 | 0.28% | 0.3110 | 0.21% | 0.3108 | 0.22% |
| 450 | 0.2184 | 0.21% | 0.2178 | 0.21% | 0.2197 | 0.20% | 0.3570 | 0.19% | 0.3568 | 0.20% |
| 500 | 0.2518 | 0.20% | 0.2512 | 0.20% | 0.2529 | 0.20% | 0.3988 | 0.20% | 0.3989 | 0.20% |
| 550 | 0.2823 | 0.20% | 0.2820 | 0.20% | 0.2835 | 0.20% | 0.4401 | 0.20% | 0.4403 | 0.20% |
| 600 | 0.3111 | 0.19% | 0.3106 | 0.20% | 0.3122 | 0.19% | 0.4801 | 0.19% | 0.4800 | 0.19% |
| 650 | 0.3401 | 0.21% | 0.3395 | 0.21% | 0.3410 | 0.21% | 0.5210 | 0.21% | 0.5212 | 0.21% |
| 700 | 0.3681 | 0.21% | 0.3675 | 0.21% | 0.3688 | 0.21% | 0.5613 | 0.21% | 0.5614 | 0.21% |
| 750 | 0.3957 | 0.23% | 0.3954 | 0.23% | 0.3966 | 0.23% | 0.6013 | 0.23% | 0.6015 | 0.23% |
| 800 | 0.4239 | 0.32% | 0.4235 | 0.32% | 0.4247 | 0.32% | 0.6418 | 0.31% | 0.6422 | 0.31% |
| 850 | 0.4510 | 0.29% | 0.4505 | 0.29% | 0.4516 | 0.29% | 0.6818 | 0.28% | 0.6818 | 0.28% |
| 900 | 0.4769 | 0.21% | 0.4763 | 0.21% | 0.4776 | 0.21% | 0.7198 | 0.20% | 0.7198 | 0.20% |
| 950 | 0.5015 | 0.21% | 0.5010 | 0.21% | 0.5018 | 0.21% | 0.7602 | 0.21% | 0.7603 | 0.21% |
| 1000 | 0.4741 | 0.22% | 0.4742 | 0.22% | 0.4749 | 0.22% | 0.7625 | 0.22% | 0.7624 | 0.22% |

# 5. PRE-DRAFT-A PROCESS

After the results and technical reports from all the participants were submitted, the pre-draft A process according to the CCPR-G2 guidelines started in January 2020. Verification of the reported results was completed in March 2020.

The pilot calculated the relative data according to Appendix A of CCPR-G2 [1]. During the review of relative data in July – September 2020, an issue of a common drift of all the single-element detectors was raised. This was also reported and consulted to the CCPR WG-KC in its meeting on 25 November 2020. The pilot investigated this issue and reported in January 2021 to the participants that the pilot made a mistake in the final control measurements performed in February – March 2020 by applying a different incident angle condition for the single-element detectors. Therefore, the measurements of stability control of all the single-element detectors had to be repeated in January – April 2021. A summary report of the re-measurement was sent to the participants on 15 April 2021.

On 2 June 2021, an online participants meeting was held to discuss the further steps:

- The pilot reported the re-measurement results of the single-element detectors, in which the common drift problem of all the single-element detectors seems to be disappeared.
- The long-term reproducibility of the pilot laboratory was identified to be poorer than anticipated, especially in the range shorter than 400 nm. Its impact on the comparison (no accurate information on detector stability, lower accuracy of the comparison results, etc.) as well as the proposals to overcome this problem were discussed.
- It was decided to conduct two actions before resuming the data analysis: (1) stability test of a set of transfer detectors by NIST, (2) calculation of DoEs without showing the participants identities to check the impact of an improved reproducibility.

From June 2021 to January 2022, KRISS and NIST conducted a stability test by exchanging the transfer detector set A. The stability of the detectors could be confirmed by using the NIST setup with a high reproducibility, which is reported in Appendix C. In parallel, KRISS conducted the data analysis to calculate the preliminary and anonymous DoEs of all the participants.

The second online participants meeting was held on 16 March 2022. The results of the detector stability test and the results of the anonymous DoE results were shared in the meeting, and it was decided that the data analysis should be continued without re-measuring any transfer detector.

Resuming the process, relative data based on the re-measured final control measurement from January – April 2021 was sent to the participants and reviewed. In parallel, the uncertainty budgets of all the participants were also shared and reviewed. No change in the uncertainty budget was proposed from the review. The review of relative data and uncertainty budgets was closed on 4 November 2022.

As the results of review of relative data, the following data will be excluded from data analysis:

- D#5 used for PTB
- E#5 used for MSL
- F#5 used for UME
- F#4 used for NPL

Identification of outliers and consistency check was started on 28 November 2022 as the pilot sent to the participants the preliminary and anonymous results of DoEs with the proposals of outliers by the pilot based on the consistency criteria. The data set was revised (Rev. 1) by correcting errors in the Chi-square calculation and sent to the participants on 24 April 2023. On request of participants, the information on DoE/$U$(DoE) of the proposed outliers was added and this data set Rev. 2 was sent on 4 May 2023, where $U$(DoE) is the expanded uncertainty of DoE with $k = 2$. Through the discussions per email, a fixed criterion for outliers was suggested, and the pilot revised the data set by applying an outlier criteria of DoE/$U$(DoE) > 2 to the preliminary results (i.e., without outliers or Mandel Paule factor) at all the wavelengths. The data set Rev. 3 was sent to the participants on 14 June 2023. As no objection or further comments to the data set Rev. 3 was received, the outliers and the Mandel Paule factors proposed in the data set Rev. 3 were regarded as agreed by all the participants. The pre-draft A process was completed on 31 August 2023.

For documentation, the DoE/*U*(DoE) calculated without applying the outliers, as shared in the data set Rev. 3, were summarized in Table 5-1 and Table 5-2 for the single-element and trap detectors, respectively. Differently from the pre-draft A process, the names of the participants are revealed here.

**Table 5-1.** Preliminary results of DoE/*U*(DoE) for single-element detectors used for identification of outliers. The data with DoE/*U*(DoE) > 2 are identified in red letters.

| DoE/ *U*(DoE) | KRISS | NMC-ASTAR | NIST | IO-CSIC | VNIIOFI | NMIJ | LNE-CNAM | PTB | NRC | MSL | UME | NPL |
|---|---|---|---|---|---|---|---|---|---|---|---|---|
| 300 nm | 0.749 | 0.47 | 0.308 | 3.614 | 0.599 | 0.738 | 0.059 | 0.596 | 0.108 | 0.981 | 2.1 | 0.093 |
| 320 nm | 0.975 | 0.315 | 0.845 | 3.368 | 0.411 | 0.838 | 0.293 | 0.589 | 0.305 | 0.599 | 1.121 | 0.138 |
| 340 nm | 1.888 | 0.691 | 1.503 | 3.754 | 1.433 | 0.862 | 0.488 | 0.716 | 0.139 | 0.505 | 0.066 | 0.115 |
| 360 nm | 1.149 | 0.132 | 0.862 | 2.374 | 1.351 | 0.442 | 0.693 | 0.589 | 0.028 | 0.115 | 0.316 | 0.272 |
| 380 nm | 1.916 | 0.47 | 0.942 | 3.672 | 2.011 | 1.283 | 0.08 | 0.256 | 0.209 | 0.616 | 1.105 | 0.884 |
| 400 nm | 1.051 | 1.17 | 0.866 | 2.019 | 0.87 | 0.926 | 0.418 | 0.623 | 0.079 | 0.458 | 0.608 | 0.109 |
| 450 nm | 0.266 | 0.324 | 0.391 | 0.421 | 0.163 | 0.403 | 0.159 | 0.466 | 0.19 | 0.286 | 0.4 | 0.126 |
| 500 nm | 0.293 | 0.103 | 0.223 | 0.025 | 0.054 | 0.191 | 0.122 | 0.322 | 0.289 | 0.264 | 0.359 | 0.03 |
| 550 nm | 0.002 | 0.149 | 0.007 | 2.065 | 0.256 | 0.178 | 0.446 | 0.137 | 0.403 | 0.297 | 0.466 | 0.159 |
| 600 nm | 0.234 | 0.094 | 0.1 | 1.958 | 0.374 | 0.181 | 0.291 | 0.043 | 0.388 | 0.316 | 0.432 | 0.223 |
| 650 nm | 0.001 | 0.075 | 0.059 | 1.966 | 0.316 | 0.105 | 0.464 | 0.058 | 0.327 | 0.181 | 0.346 | 0.116 |
| 700 nm | 0.032 | 0.043 | 0.074 | 1.925 | 0.312 | 0.04 | 0.38 | 0.107 | 0.374 | 0.239 | 0.29 | 0.186 |
| 750 nm | 0.314 | 0.091 | 0.111 | 0.352 | 0.173 | 0.138 | 0.26 | 0.305 | 0.2 | 0.037 | 0.066 | 0.033 |
| 800 nm | 0.036 | 0.049 | 0.19 | 0.584 | 0.082 | 0.264 | 0.026 | 0.302 | 0.173 | 0.008 | 0.046 | 0.029 |
| 850 nm | 0.17 | 0.071 | 0.204 | 0.393 | 0.092 | 0.355 | 0.068 | 0.33 | 0.338 | 0.058 | 0.077 | 0.028 |
| 900 nm | 0.848 | 0.251 | 0.131 | 0.526 | 0.336 | 0.209 | 0.023 | 0.16 | 0.332 | 0.164 | 0.041 | 0.069 |
| 950 nm | 0.578 | 0.207 | 0.151 | 0.766 | 0.071 | 0.078 | 0.19 | 0.219 | 0.147 | 0.074 | 0.037 | 0.114 |
| 1000 nm | 0.458 | 0.205 | 0.637 | 0.655 | 1.467 | 0.06 | 0.016 | 0.278 | 0.428 | 0.122 | 0.105 | 0.186 |

**Table 5-2.** Preliminary results of DoE/*U*(DoE) for trap detectors used for identification of outliers. The data with DoE/*U*(DoE) > 2 are identified in red letters.

| DoE/ *U*(DoE) | KRISS | NMC-ASTAR | NIST | IO-CSIC | VNIIOFI | NMIJ | LNE-CNAM | PTB | NRC | MSL | UME | NPL |
|---|---|---|---|---|---|---|---|---|---|---|---|---|
| 300 nm | 1.535 | 0.737 | 0.242 | 2.886 | 2.182 | 1.012 | 0.962 | 0.56 | 0.885 | 0.482 | 5.441 | 0.044 |
| 320 nm | 1.641 | 0.075 | 1.057 | 2.995 | 1.347 | 0.873 | 0.919 | 0.428 | 0.836 | 0.307 | 2.367 | 0.017 |
| 340 nm | 2.287 | 0.844 | 0.989 | 3.424 | 1.354 | 0.95 | 0.767 | 0.101 | 0.751 | 0.069 | 1.025 | 0.025 |
| 360 nm | 1.231 | 0.256 | 0.708 | 2.158 | 0.348 | 0.58 | 0.701 | 0.241 | 0.588 | 0.251 | 0.805 | 0.3 |
| 380 nm | 2.74 | 0.527 | 0.73 | 3.281 | 0.66 | 1.611 | 1.295 | 0.508 | 1.045 | 0.035 | 0.915 | 0.196 |
| 400 nm | 1.636 | 1.637 | 0.691 | 1.79 | 0.125 | 0.809 | 0.617 | 0.102 | 0.853 | 0.293 | 0.596 | 0.33 |
| 450 nm | 0.921 | 0.56 | 0.362 | 0.179 | 0.109 | 0.45 | 0.705 | 0.276 | 0.117 | 0.041 | 0.183 | 0.128 |
| 500 nm | 0.786 | 0.106 | 0.147 | 0.105 | 0.208 | 0.236 | 0.756 | 0.427 | 0.044 | 0.072 | 0.004 | 0.063 |
| 550 nm | 0.278 | 0.142 | 0.183 | 2.479 | 0.509 | 0.344 | 0.79 | 0.662 | 0.239 | 0.131 | 0.156 | 0.004 |
| 600 nm | 0.628 | 0.145 | 0.251 | 2.345 | 0.583 | 0.336 | 0.808 | 0.698 | 0.233 | 0.223 | 0.134 | 0.018 |
| 650 nm | 0.333 | 0.136 | 0.19 | 2.231 | 0.433 | 0.187 | 0.887 | 0.551 | 0.247 | 0.133 | 0.183 | 0.003 |
| 700 nm | 0.357 | 0.165 | 0.193 | 2.303 | 0.397 | 0.191 | 0.88 | 0.643 | 0.251 | 0.179 | 0.174 | 0.002 |
| 750 nm | 0.653 | 0.048 | 0.029 | 0.364 | 0.092 | 0.109 | 0.761 | 0.413 | 0.252 | 0.16 | 0.032 | 0.069 |
| 800 nm | 0.451 | 0.048 | 0.147 | 0.647 | 0.021 | 0.425 | 0.611 | 0.358 | 0.222 | 0.137 | 0.001 | 0.094 |
| 850 nm | 0.556 | 0.158 | 0.14 | 0.509 | 0.019 | 0.41 | 0.693 | 0.41 | 0.112 | 0.097 | 0.002 | 0.059 |
| 900 nm | 1.204 | 0.421 | 0.024 | 0.516 | 0.14 | 0.345 | 0.626 | 0.528 | 0.169 | 0.133 | 0.075 | 0.012 |
| 950 nm | 0.765 | 0.258 | 0.054 | 0.784 | 0.482 | 0.089 | 0.591 | 0.558 | 0.31 | 0.246 | 0.043 | 0.009 |
| 1000 nm | 0.361 | 0.036 | 0.537 | 0.731 | 0.106 | 0.021 | 0.447 | 0.407 | 0.568 | 0.198 | 0.08 | 0.027 |

# 6. DATA ANALYSIS

As agreed in the technical protocol, the data analysis was separated for each type of transfer detectors to allow a linkage to the follow-up RMO key comparisons only by using a set of single-element detectors. The data analysis of the comparison was performed according to the step-by-step approach as described in Appendix B of CCPR-G2 [1]. As measurements at each wavelength are taken as each separate comparison, the equations in the following should be applied to the data at each wavelength.

For each participant with index $i$ for each detector with index $j$, the relative difference $\Delta_{i,j}$ between participant measurement $S_{i,j}$ and pilot measurement $S^{\mathrm{P}}_{i,j}$ is given by

$$\Delta_{i,j} = \frac{S_{i,j}}{S^{\mathrm{P}}_{i,j}} - 1 \tag{6-1}$$

with the data measured and reported from the participants and the pilot, which are summarized from Table 4-1 to Table 4-12. For each participant, the uncertainty of the relative difference is calculated by

$$u\left(\Delta_{\mathrm{i,j}}\right) = \sqrt{u^2_{\mathrm{rel}}\left(S_{i,j}\right) + u^2_{\mathrm{PR}} + u^2_{\mathrm{stability},j} + u^2_{\mathrm{uniformity},j}}, \tag{6-2}$$

where $u_{\mathrm{rel}}(S_{i,j})$ is the relative standard uncertainty as reported by the participant for each detector,

$u_{\mathrm{PR}}$ is the long-term reproducibility of the pilot expressed as a relative standard uncertainty,

$u_{\mathrm{stability},j}$ is the stability uncertainty of each detector as summarized in Table 3-1,

$u_{\mathrm{uniformity},j}$ is the uniformity uncertainty of each detector as summarized in Table 3-2.

The long-term reproducibility uncertainty of the pilot was evaluated from the long-term operation data collected by the setup and can be regarded as the stability of the pilot scale during the comparison (see Table 1-5 and Figure 1-5 of Appendix B). The stability uncertainty is an estimate for reproducibility of the pilot measurements when each detector is measured before and after the participant measurement. The uniformity uncertainty is an estimate for possible errors caused by different beam conditions among participants. Note that the uniformity uncertainty is only applied to the single-element detectors. The trap detectors are regarded as spatially uniform by setting $u_{\mathrm{uniformity},j} = 0$.

For each participant with index $i$, the relative differences are averaged over $X$ transfer detectors (usually $X = 3$ for the single-element detectors and $X = 2$ for the trap detectors but reduced where data has been excluded from the analysis):

$$\Delta_i = \frac{1}{X}\sum_{j=1}^{X} \Delta_{i,j} \tag{6-3}$$

The uncertainty of $\Delta_i$ is an average of the uncertainties of $\Delta_{i,j}$ assuming that the results from the multiple detectors measured by the same participant are nearly fully correlated:

$$u\left(\Delta_{\mathrm{i}}\right) = \frac{1}{X}\sum_{j=1}^{X} u\left(\Delta_{i,j}\right) \tag{6-4}$$

For the pilot, we use $i = 0$ and set $\Delta_0 = 0$. The uncertainty of $\Delta_0$ is calculated from the average total uncertainty of all measurements by the pilot laboratory and the long-term reproducibility by

$$u(\Delta_0) = \sqrt{\left(\frac{1}{YX}\sum_{i=1}^{Y}\sum_{j=1}^{X} u_{\mathrm{rel}}(S^{\mathrm{P}}_{i,j})\right)^2 + u^2_{\mathrm{PR}}}\ . \tag{6-5}$$

Here, $Y$ is the number of the transfer detector sets so that $YX$ corresponds to the total number of the transfer detectors. We have $Y = 6$ so that $YX = 18$ for the single-element detectors and $YX = 12$ for the trap detectors.

The calculated values of the relative differences $\Delta_i$ and their uncertainties are summarized in Table 6-1 and Table 6-2 for the single-element and trap detectors, respectively. Note that the data with poor stability, which were identified in the review of relative data, were excluded in this calculation: D#5 for PTB, E#5 for MSL, F#5 for UME, and F#4 for NPL.

**Table 6-1.** Values of the relative differences defined in Eq. (6-3) and their uncertainties for the single-element detectors.

| $\Delta_i$ | KRISS | NMC-ASTAR | NIST | IO-CSIC | VNIIOFI | NMIJ | LNE-CNAM | PTB | NRC | MSL | UME | NPL |
|---|---|---|---|---|---|---|---|---|---|---|---|---|
| 300 nm | 0 | 1.55E-02 | 3.12E-03 | 6.13E-02 | -7.25E-04 | 2.07E-02 | 5.48E-03 | 8.63E-04 | 5.00E-03 | 1.93E-02 | -2.36E-02 | 7.07E-03 |
| 320 nm | 0 | 1.37E-02 | 3.32E-05 | 5.73E-02 | 1.18E-02 | 2.41E-02 | 4.90E-03 | 2.82E-03 | 4.92E-03 | 1.56E-02 | -7.89E-03 | 9.12E-03 |
| 340 nm | 0 | 2.47E-02 | 1.98E-04 | 6.38E-02 | 2.30E-02 | 2.77E-02 | 7.50E-03 | 6.64E-03 | 1.23E-02 | 1.77E-02 | 1.04E-02 | 1.24E-02 |
| 360 nm | 0 | 2.01E-02 | 3.93E-03 | 6.16E-02 | 3.79E-02 | 2.72E-02 | 6.31E-03 | 8.36E-03 | 1.66E-02 | 1.91E-02 | 1.12E-02 | 1.26E-02 |
| 380 nm | 0 | 2.03E-02 | 5.66E-03 | 5.82E-02 | -2.22E-03 | 2.91E-02 | 1.22E-02 | 1.02E-02 | 1.03E-02 | 1.90E-02 | 1.99E-02 | 1.78E-02 |
| 400 nm | 0 | 2.08E-02 | 1.22E-03 | 3.83E-02 | 9.20E-04 | 2.31E-02 | 5.63E-03 | 3.97E-03 | 8.59E-03 | 1.50E-02 | 1.54E-02 | 8.35E-03 |
| 450 nm | 0 | 3.88E-03 | -1.42E-03 | 5.24E-03 | 2.45E-04 | 6.54E-03 | 3.66E-04 | -1.49E-03 | 2.86E-03 | 3.90E-03 | 4.66E-03 | 6.01E-04 |
| 500 nm | 0 | 5.44E-04 | -1.68E-04 | 1.05E-03 | 1.58E-03 | 3.42E-03 | 1.99E-03 | -4.81E-04 | 3.13E-03 | 3.10E-03 | 3.93E-03 | 1.07E-03 |
| 550 nm | 0 | -9.82E-04 | 3.67E-05 | -1.52E-02 | 1.61E-03 | 1.85E-03 | 2.66E-03 | -7.20E-04 | 2.59E-03 | 1.97E-03 | 3.45E-03 | 8.50E-04 |
| 600 nm | 0 | 3.13E-04 | 1.55E-03 | -1.33E-02 | 3.12E-03 | 2.70E-03 | 2.83E-03 | 7.04E-04 | 3.42E-03 | 3.05E-03 | 4.13E-03 | 2.13E-03 |
| 650 nm | 0 | -4.94E-04 | 3.64E-04 | -1.45E-02 | 1.88E-03 | 9.48E-04 | 2.81E-03 | -3.10E-04 | 2.12E-03 | 1.22E-03 | 2.59E-03 | 6.29E-04 |
| 700 nm | 0 | -1.42E-04 | 5.70E-04 | -1.36E-02 | 1.90E-03 | 4.92E-04 | 2.23E-03 | -4.08E-04 | 2.47E-03 | 1.70E-03 | 2.24E-03 | 1.10E-03 |
| 750 nm | 0 | 9.06E-04 | 7.96E-04 | 4.04E-03 | 2.53E-03 | 1.88E-04 | 3.03E-03 | -1.23E-04 | 2.82E-03 | 1.75E-03 | 1.99E-03 | 1.32E-03 |
| 800 nm | 0 | -8.47E-05 | -9.64E-04 | 4.65E-03 | 7.28E-04 | -2.30E-03 | 3.94E-04 | -1.38E-03 | 1.41E-03 | 1.78E-04 | 5.79E-04 | 7.79E-05 |
| 850 nm | 0 | 1.45E-03 | -2.90E-04 | 4.64E-03 | 1.54E-03 | -2.46E-03 | 1.40E-03 | -7.65E-04 | 3.36E-03 | 1.40E-03 | 1.58E-03 | 1.15E-03 |
| 900 nm | 0 | 5.29E-03 | 2.84E-03 | 8.47E-03 | 5.67E-03 | 1.60E-03 | 3.80E-03 | 2.82E-03 | 5.88E-03 | 4.83E-03 | 4.18E-03 | 4.05E-03 |
| 950 nm | 0 | 5.56E-03 | 1.32E-03 | 9.42E-03 | 2.70E-03 | 1.32E-03 | 3.40E-03 | 1.13E-03 | 3.14E-03 | 2.75E-03 | 2.67E-03 | 2.91E-03 |
| 1000 nm | 0 | 6.97E-03 | -2.57E-03 | 1.05E-02 | 1.76E-02 | 2.32E-03 | 3.59E-03 | 1.16E-03 | -5.06E-04 | 2.21E-03 | 4.89E-03 | 1.84E-03 |
| $u(\Delta_i)$ | KRISS | NMC-ASTAR | NIST | IO-CSIC | VNIIOFI | NMIJ | LNE-CNAM | PTB | NRC | MSL | UME | NPL |
| 300 nm | 4.4E-03 | 1.0E-02 | 4.3E-03 | 7.8E-03 | 5.7E-03 | 1.0E-02 | 4.9E-03 | 4.7E-03 | 4.9E-03 | 7.0E-03 | 7.3E-03 | 5.8E-03 |
| 320 nm | 4.3E-03 | 9.5E-03 | 4.0E-03 | 7.5E-03 | 5.1E-03 | 1.0E-02 | 4.8E-03 | 4.5E-03 | 4.6E-03 | 6.9E-03 | 7.1E-03 | 5.6E-03 |
| 340 nm | 3.3E-03 | 9.6E-03 | 3.1E-03 | 7.1E-03 | 4.0E-03 | 9.6E-03 | 3.9E-03 | 3.7E-03 | 3.8E-03 | 6.5E-03 | 6.6E-03 | 5.0E-03 |
| 360 nm | 7.8E-03 | 1.2E-02 | 7.5E-03 | 9.7E-03 | 8.0E-03 | 1.2E-02 | 8.0E-03 | 7.8E-03 | 8.0E-03 | 9.4E-03 | 9.5E-03 | 8.5E-03 |
| 380 nm | 3.3E-03 | 9.0E-03 | 2.4E-03 | 6.4E-03 | 3.3E-03 | 6.8E-03 | 3.4E-03 | 3.3E-03 | 3.4E-03 | 6.1E-03 | 3.9E-03 | 3.6E-03 |
| 400 nm | 4.7E-03 | 4.7E-03 | 4.2E-03 | 7.3E-03 | 4.8E-03 | 7.5E-03 | 4.5E-03 | 4.7E-03 | 4.9E-03 | 6.4E-03 | 5.3E-03 | 4.7E-03 |
| 450 nm | 2.9E-03 | 3.5E-03 | 2.9E-03 | 4.6E-03 | 3.4E-03 | 6.4E-03 | 3.1E-03 | 3.5E-03 | 3.9E-03 | 4.5E-03 | 4.2E-03 | 3.3E-03 |
| 500 nm | 2.3E-03 | 3.0E-03 | 2.3E-03 | 3.7E-03 | 2.9E-03 | 5.7E-03 | 2.9E-03 | 3.1E-03 | 3.3E-03 | 3.7E-03 | 3.9E-03 | 2.9E-03 |
| 550 nm | 2.3E-03 | 2.9E-03 | 2.3E-03 | 3.7E-03 | 2.9E-03 | 5.2E-03 | 2.8E-03 | 3.0E-03 | 3.2E-03 | 3.5E-03 | 3.8E-03 | 2.8E-03 |
| 600 nm | 2.2E-03 | 2.9E-03 | 2.3E-03 | 3.6E-03 | 2.6E-03 | 4.9E-03 | 3.1E-03 | 3.0E-03 | 3.2E-03 | 3.5E-03 | 3.8E-03 | 2.8E-03 |
| 650 nm | 2.4E-03 | 2.9E-03 | 2.3E-03 | 3.7E-03 | 2.7E-03 | 4.5E-03 | 2.8E-03 | 3.1E-03 | 3.2E-03 | 3.5E-03 | 3.9E-03 | 2.9E-03 |
| 700 nm | 2.2E-03 | 2.7E-03 | 2.1E-03 | 3.6E-03 | 2.5E-03 | 4.5E-03 | 2.5E-03 | 2.9E-03 | 3.1E-03 | 3.4E-03 | 3.8E-03 | 2.7E-03 |
| 750 nm | 2.6E-03 | 2.9E-03 | 2.3E-03 | 3.6E-03 | 2.7E-03 | 4.7E-03 | 2.7E-03 | 3.1E-03 | 3.3E-03 | 3.6E-03 | 3.9E-03 | 2.8E-03 |
| 800 nm | 3.4E-03 | 2.9E-03 | 2.4E-03 | 3.8E-03 | 2.7E-03 | 4.8E-03 | 2.9E-03 | 3.1E-03 | 3.4E-03 | 3.6E-03 | 3.9E-03 | 2.9E-03 |
| 850 nm | 3.1E-03 | 2.8E-03 | 2.3E-03 | 4.7E-03 | 2.7E-03 | 4.9E-03 | 2.8E-03 | 3.1E-03 | 3.5E-03 | 3.6E-03 | 3.9E-03 | 2.9E-03 |
| 900 nm | 2.4E-03 | 2.8E-03 | 2.3E-03 | 4.6E-03 | 2.7E-03 | 4.9E-03 | 2.7E-03 | 3.1E-03 | 3.3E-03 | 3.7E-03 | 6.3E-03 | 2.9E-03 |
| 950 nm | 2.2E-03 | 7.9E-03 | 2.2E-03 | 4.7E-03 | 3.1E-03 | 5.8E-03 | 2.9E-03 | 2.9E-03 | 3.1E-03 | 3.7E-03 | 6.2E-03 | 3.1E-03 |
| 1000 nm | 4.0E-03 | 8.5E-03 | 4.3E-03 | 5.6E-03 | 4.8E-03 | 9.3E-03 | 5.0E-03 | 4.5E-03 | 4.7E-03 | 5.2E-03 | 7.1E-03 | 4.5E-03 |

**Table 6-2.** Values of the relative differences defined in Eq. (6-3) and their uncertainties for the trap detectors.

| $\Delta_i$ | KRISS | NMC-ASTAR | NIST | IO-CSIC | VNIIOFI | NMIJ | LNE-CNAM | PTB | NRC | MSL | UME | NPL |
|---|---|---|---|---|---|---|---|---|---|---|---|---|
| 300 nm | 0 | 2.82E-02 | 1.01E-02 | 6.05E-02 | 3.54E-02 | 3.07E-02 | 2.67E-02 | 1.75E-02 | 2.98E-03 | 1.83E-02 | -7.26E-02 | 1.12E-02 |
| 320 nm | 0 | 1.37E-02 | 2.92E-03 | 5.74E-02 | 2.48E-02 | 2.78E-02 | 2.50E-02 | 1.59E-02 | 3.81E-03 | 1.58E-02 | -2.44E-02 | 1.25E-02 |
| 340 nm | 0 | 3.20E-02 | 7.62E-03 | 6.17E-02 | 2.44E-02 | 3.11E-02 | 2.42E-02 | 1.38E-02 | 8.21E-03 | 1.38E-02 | -4.24E-04 | 1.40E-02 |
| 360 nm | 0 | 2.40E-02 | 7.17E-03 | 5.87E-02 | 2.29E-02 | 3.03E-02 | 3.03E-02 | 2.13E-02 | 8.32E-03 | 1.34E-02 | 1.86E-03 | 9.80E-03 |
| 380 nm | 0 | 2.62E-02 | 1.11E-02 | 5.78E-02 | 1.95E-02 | 3.37E-02 | 3.08E-02 | 1.90E-02 | 7.34E-03 | 1.60E-02 | 6.20E-03 | 1.98E-02 |
| 400 nm | 0 | 2.82E-02 | 6.65E-03 | 3.83E-02 | 1.40E-02 | 2.32E-02 | 2.10E-02 | 1.38E-02 | 3.99E-03 | 9.58E-03 | 5.56E-03 | 5.55E-03 |

| | | | | | | | | | | | | |
|---|---|---|---|---|---|---|---|---|---|---|---|---|
| 450 nm | 0 | 8.71.E-03 | 2.16.E-03 | 6.59.E-03 | 5.33.E-03 | 9.26.E-03 | 1.27.E-02 | 6.66.E-03 | 3.64.E-03 | 4.37.E-03 | 2.69.E-03 | 1.93.E-03 |
| 500 nm | 0 | 3.92.E-03 | 2.35.E-03 | 2.48.E-03 | 4.36.E-03 | 5.27.E-03 | 1.18.E-02 | 6.04.E-03 | 3.58.E-03 | 2.87.E-03 | 3.28.E-03 | 1.90.E-03 |
| 550 nm | 0 | 2.02.E-03 | 2.22.E-03 | -1.50.E-02 | 3.81.E-03 | 3.68.E-03 | 9.95.E-03 | 5.40.E-03 | 2.97.E-03 | 1.74.E-03 | 2.74.E-03 | 1.22.E-03 |
| 600 nm | 0 | 3.36.E-03 | 3.97.E-03 | -1.29.E-02 | 5.22.E-03 | 4.64.E-03 | 1.18.E-02 | 6.97.E-03 | 4.25.E-03 | 3.51.E-03 | 3.84.E-03 | 2.83.E-03 |
| 650 nm | 0 | 2.29.E-03 | 2.60.E-03 | -1.32.E-02 | 3.54.E-03 | 2.47.E-03 | 1.14.E-02 | 5.04.E-03 | 3.35.E-03 | 2.08.E-03 | 3.34.E-03 | 1.38.E-03 |
| 700 nm | 0 | 2.41.E-03 | 2.55.E-03 | -1.30.E-02 | 3.22.E-03 | 2.46.E-03 | 1.10.E-02 | 5.49.E-03 | 3.31.E-03 | 2.23.E-03 | 3.20.E-03 | 1.37.E-03 |
| 750 nm | 0 | 3.36.E-03 | 2.89.E-03 | 5.42.E-03 | 3.51.E-03 | 2.40.E-03 | 1.15.E-02 | 5.77.E-03 | 1.07.E-03 | 2.27.E-03 | 3.39.E-03 | 1.60.E-03 |
| 800 nm | 0 | 3.19.E-03 | 1.99.E-03 | 7.19.E-03 | 2.99.E-03 | 2.31.E-04 | 9.76.E-03 | 5.24.E-03 | 1.11.E-03 | 2.20.E-03 | 2.90.E-03 | 9.18.E-04 |
| 850 nm | 0 | 4.14.E-03 | 2.30.E-03 | 7.10.E-03 | 3.07.E-03 | 5.36.E-04 | 1.09.E-02 | 5.85.E-03 | 2.24.E-03 | 2.66.E-03 | 3.18.E-03 | 1.93.E-03 |
| 900 nm | 0 | 7.68.E-03 | 5.22.E-03 | 9.50.E-03 | 5.75.E-03 | 2.80.E-03 | 1.20.E-02 | 8.53.E-03 | 3.73.E-03 | 5.76.E-03 | 6.15.E-03 | 4.83.E-03 |
| 950 nm | 0 | 6.85.E-03 | 3.17.E-03 | 9.60.E-03 | 1.28.E-04 | 2.06.E-03 | 1.00.E-02 | 6.35.E-03 | 5.28.E-04 | 4.15.E-03 | 3.47.E-03 | 3.05.E-03 |
| 1000 nm | 0 | 3.26.E-03 | -2.23.E-03 | 1.04.E-02 | 1.70.E-03 | 2.30.E-03 | 9.46.E-03 | 6.28.E-03 | -3.14.E-03 | 4.35.E-03 | 3.89.E-03 | 2.06.E-03 |
| $u(\Delta_i)$ | KRISS | NMC-ASTAR | NIST | IO-CSIC | VNIIOFI | NMIJ | LNE-CNAM | PTB | NRC | MSL | UME | NPL |
| 300 nm | 4.5.E-03 | 1.1.E-02 | 4.0.E-03 | 8.5.E-03 | 5.3.E-03 | 9.3.E-03 | 6.0.E-03 | 4.3.E-03 | 4.1.E-03 | 6.3.E-03 | 7.2.E-03 | 5.7.E-03 |
| 320 nm | 4.1.E-03 | 1.1.E-02 | 3.7.E-03 | 7.7.E-03 | 4.7.E-03 | 9.2.E-03 | 5.5.E-03 | 4.1.E-03 | 3.7.E-03 | 6.1.E-03 | 7.0.E-03 | 5.4.E-03 |
| 340 nm | 3.6.E-03 | 1.0.E-02 | 2.6.E-03 | 7.0.E-03 | 3.5.E-03 | 8.8.E-03 | 4.4.E-03 | 3.2.E-03 | 2.6.E-03 | 5.8.E-03 | 6.5.E-03 | 4.8.E-03 |
| 360 nm | 7.7.E-03 | 1.2.E-02 | 7.4.E-03 | 9.8.E-03 | 7.7.E-03 | 1.1.E-02 | 8.1.E-03 | 7.6.E-03 | 7.5.E-03 | 8.9.E-03 | 9.5.E-03 | 8.4.E-03 |
| 380 nm | 3.2.E-03 | 9.9.E-03 | 1.9.E-03 | 6.5.E-03 | 2.6.E-03 | 5.7.E-03 | 3.8.E-03 | 2.7.E-03 | 2.1.E-03 | 5.3.E-03 | 3.8.E-03 | 2.8.E-03 |
| 400 nm | 4.3.E-03 | 4.4.E-03 | 3.9.E-03 | 7.2.E-03 | 4.4.E-03 | 6.5.E-03 | 4.9.E-03 | 4.3.E-03 | 4.0.E-03 | 5.6.E-03 | 5.2.E-03 | 4.1.E-03 |
| 450 nm | 2.8.E-03 | 3.0.E-03 | 2.5.E-03 | 5.4.E-03 | 2.7.E-03 | 5.2.E-03 | 3.6.E-03 | 3.0.E-03 | 2.7.E-03 | 3.3.E-03 | 4.1.E-03 | 2.4.E-03 |
| 500 nm | 2.3.E-03 | 2.4.E-03 | 1.8.E-03 | 3.7.E-03 | 2.2.E-03 | 4.3.E-03 | 3.5.E-03 | 2.5.E-03 | 1.9.E-03 | 2.1.E-03 | 3.8.E-03 | 1.8.E-03 |
| 550 nm | 2.3.E-03 | 2.3.E-03 | 1.6.E-03 | 3.3.E-03 | 2.1.E-03 | 3.7.E-03 | 3.3.E-03 | 2.4.E-03 | 1.8.E-03 | 1.9.E-03 | 3.7.E-03 | 1.6.E-03 |
| 600 nm | 2.2.E-03 | 2.2.E-03 | 1.7.E-03 | 3.3.E-03 | 1.7.E-03 | 3.3.E-03 | 3.6.E-03 | 2.4.E-03 | 1.7.E-03 | 1.9.E-03 | 3.7.E-03 | 1.6.E-03 |
| 650 nm | 2.4.E-03 | 2.3.E-03 | 1.7.E-03 | 3.3.E-03 | 1.8.E-03 | 2.8.E-03 | 3.4.E-03 | 2.5.E-03 | 1.8.E-03 | 1.9.E-03 | 3.8.E-03 | 1.7.E-03 |
| 700 nm | 2.2.E-03 | 2.1.E-03 | 1.5.E-03 | 3.1.E-03 | 1.6.E-03 | 2.7.E-03 | 3.1.E-03 | 2.3.E-03 | 1.6.E-03 | 1.7.E-03 | 3.7.E-03 | 1.5.E-03 |
| 750 nm | 2.5.E-03 | 2.3.E-03 | 1.7.E-03 | 3.2.E-03 | 1.8.E-03 | 3.1.E-03 | 3.3.E-03 | 2.5.E-03 | 2.0.E-03 | 2.0.E-03 | 3.8.E-03 | 1.7.E-03 |
| 800 nm | 3.4.E-03 | 2.3.E-03 | 1.8.E-03 | 3.3.E-03 | 1.9.E-03 | 3.2.E-03 | 3.4.E-03 | 2.5.E-03 | 2.1.E-03 | 2.1.E-03 | 3.8.E-03 | 1.8.E-03 |
| 850 nm | 3.0.E-03 | 2.2.E-03 | 1.8.E-03 | 3.9.E-03 | 1.8.E-03 | 3.2.E-03 | 3.3.E-03 | 2.5.E-03 | 2.3.E-03 | 2.1.E-03 | 3.8.E-03 | 1.8.E-03 |
| 900 nm | 2.3.E-03 | 2.2.E-03 | 1.8.E-03 | 4.3.E-03 | 1.8.E-03 | 3.3.E-03 | 3.2.E-03 | 2.5.E-03 | 2.0.E-03 | 2.2.E-03 | 6.3.E-03 | 1.8.E-03 |
| 950 nm | 2.2.E-03 | 7.4.E-03 | 1.5.E-03 | 4.3.E-03 | 2.4.E-03 | 4.5.E-03 | 4.1.E-03 | 2.3.E-03 | 1.6.E-03 | 2.3.E-03 | 6.2.E-03 | 2.3.E-03 |
| 1000 nm | 4.0.E-03 | 8.2.E-03 | 4.0.E-03 | 5.4.E-03 | 4.4.E-03 | 8.5.E-03 | 6.1.E-03 | 4.1.E-03 | 3.8.E-03 | 4.3.E-03 | 7.0.E-03 | 4.0.E-03 |

The Key Comparison Reference Value (KCRV) is calculated using weighted mean with cut-off. The cut-off value $u_{\text{cut-off}}$ is calculated by

$$u_{\text{cut-off}} = \text{average}\{u_{\text{rel}}(S_i)\} \text{ for } u_{\text{rel}}(S_i) \le \text{median}\{u_{\text{rel}}(S_i)\}_{i=0 \text{ to } N}. \quad (6\text{-}6)$$

Here, the relative uncertainty of measurements of the participant $i$ is averaged for all the detectors:

$$u_{\text{rel}}(S_{\text{i}}) = \frac{1}{X}\sum_{j=1}^{X} u_{\text{rel}}(S_{i,j}). \quad (6\text{-}7)$$

For the pilot, we use $u(\Delta_0)$ for the relative uncertainty of measurements as given in Eq. (6-5):

$$u_{\text{rel}}(S_0) = u(\Delta_0). \quad (6\text{-}8)$$

The reported uncertainty $u_{\text{rel}}(S_i)$ of each participant $i$ is then adjusted by the cut-off as follows for $i$ = 0 to $N$:

$$\begin{aligned} u_{\text{rel, adj}}(S_i) &= u_{\text{rel}}(S_i) \quad \text{for } u_{\text{rel}}(S_i) \ge u_{\text{cut-off}} \\ u_{\text{rel, adj}}(S_i) &= u_{\text{cut-off}} \quad \text{for } u_{\text{rel}}(S_i) < u_{\text{cut-off}} \end{aligned} \quad (6\text{-}9)$$

After cut-off, the uncertainty of $\Delta_i$ is adjusted to

$$u_{\text{adj}}(\Delta_i) = \sqrt{u^2_{\text{rel, adj}}(S_i) + u^2_{\text{T}}(\Delta_i)} \quad (6\text{-}10)$$

with the transfer uncertainty component given by

$$u_{\mathrm{T}}(\Delta_i) = \sqrt{u^2(\Delta_i) - u_{\mathrm{rel}}^2(S_i)}\,. \tag{6-11}$$

The weights $w_i$ for each participant $i$ is determined by

$$w_i = \frac{u_{\mathrm{adj}}^{-2}(\Delta_i)}{\sum_{i=0}^{N} u_{\mathrm{adj}}^{-2}(\Delta_i)} \tag{6-12}$$

The index $i$ in Eq. (6-12) indicates each participant of the comparison. In this comparison, the total number of the participants was 12 so that the index $i$ runs from 0 (the pilot) up to $N = 11$.

The KCRV is determined by

$$\Delta_{KCRV} = \sum_{i=0}^{N} w_i \cdot \Delta_i \tag{6-13}$$

with the standard uncertainty given by

$$u(\Delta_{\mathrm{KCRV}}) = \sqrt{\sum_{i=0}^{N} \frac{u^2(\Delta_i)}{u_{\mathrm{adj}}^4(\Delta_i)}} \Bigg/ \sum_{i=0}^{N} u_{\mathrm{adj}}^{-2}(\Delta_i) \tag{6-14}$$

The unilateral DoE of the participant $i$ is given by

$$D_i = \Delta_i - \Delta_{KCRV} \tag{6-15}$$

with the standard uncertainty given by

$$u(D_i) = \sqrt{u^2(\Delta_i) + u^2(\Delta_{\mathrm{KCRV}}) - 2\left(\frac{u^2(\Delta_i)}{u_{\mathrm{adj}}^2(\Delta_i)} \Bigg/ \sum_{j=0}^{N} u_{\mathrm{adj}}^{-2}(\Delta_j)\right)} \tag{6-16}$$

To verify the consistency of the results, the Chi-square value $\chi^2_{\mathrm{obs}}$ are calculated by

$$\chi^2_{\mathrm{obs}} = \sum_{i=0}^{N} \frac{\left(\Delta_i - \Delta_{\mathrm{KCRV}}\right)^2}{u_{\mathrm{adj}}^2(\Delta_i)}. \tag{6-17}$$

The consistency check is failed if $\chi^2_{\mathrm{obs}} > \chi^2_{0.05}(\nu)$. The values of $\chi^2_{0.05}(\nu)$ are given in the table below with the degree of freedom $\nu$, where the maximum value of $\nu$ is $N = 11$ [1]:

| $\nu$ | 8 | 9 | 10 | 11 |
|---|---|---|---|---|
| $\chi^2_{0.05}$ | 15.507 | 16.919 | 18.307 | 19.675 |

The outliers identified under agreement of the participants are excluded from the data analysis. After excluding, the KCRV and the Chi-square are re-calculated with the modified value of $\nu$. In case that the consistency is not achieved even considering the outliers, the Mandel Paule factor $s$ is introduced to increase the uncertainties of Eq. (6-10) to

$$u_{\mathrm{adj}}(\Delta_i) = \sqrt{u_{\mathrm{rel,\,adj}}^2(S_i) + u_{\mathrm{T}}^2(\Delta_i) + s^2}. \tag{6-18}$$

Calculation of the KCRV and the Chi-square is again repeated with the increased uncertainties of Eq. (6-18). The value of $s$ is determined by iterative process until the consistency condition $\chi^2_{\mathrm{obs}} \leq \chi^2_{0.05}(\nu)$ is satisfied. For the participants identified as the outliers and excluded from the KCRV calculation, the uncertainty of the DoE is calculated by

$$u\left(D_i\right)=\sqrt{u^2\left(\Delta_i\right)+u^2\left(\Delta_{\mathrm{KCRV}}\right)} \tag{6-19}$$

The preliminary results of DoE/$U$(DoE), which are summarized in Table 5-1 and Table 5-2, were calculated according to Eqs. (6-15) and (6-16) without identifying any outlier. As agreed in the pre-draft A process described in Section 5, the participants with DoE/$U$(DoE) > 2 are identified as outliers, which are indicated by red letters in Table 5-1 and Table 5-2. The values of $\chi^2_{\mathrm{obs}}$ and the results of the consistency check without and with outliers are summarized in Table 6-3 and Table 6-4 for the single-element and trap detectors, respectively.

**Table 6-3.** Results of the consistency check without and with exclusion of outliers for the single-element detectors. A failed consistency is indicated in red letters.

| consistency check | Without exclusion of outliers | | | outliers identified | With exclusion of outliers | | |
|---|---|---|---|---|---|---|---|
| | $\Delta_{\mathrm{KCRV}}$ | $\chi^2_{\mathrm{obs}}$ | $\chi^2_{0.05}(\nu)$ | | $\Delta_{\mathrm{KCRV}}$ | $\chi^2_{\mathrm{obs}}$ | $\chi^2_{0.05}(\nu)$ |
| 300 nm | 0.0060 | 78.387 | 19.675 | IO-CSIC, UME | 0.0049 | 10.958 | 16.919 |
| 320 nm | 0.0075 | 61.622 | 19.675 | IO-CSIC | 0.0051 | 15.359 | 18.307 |
| 340 nm | 0.0110 | 94.002 | 19.675 | IO-CSIC | 0.0090 | 36.100 | 18.307 |
| 360 nm | 0.0170 | 40.068 | 19.675 | IO-CSIC | 0.0137 | 17.289 | 18.307 |
| 380 nm | 0.0110 | 104.554 | 19.675 | IO-CSIC, VNIIOFI | 0.0111 | 33.715 | 16.919 |
| 400 nm | 0.0092 | 39.828 | 19.675 | IO-CSIC | 0.0080 | 23.094 | 18.307 |
| 450 nm | 0.0013 | 4.955 | 19.675 | | | | |
| 500 nm | 0.0012 | 2.270 | 19.675 | | | | |
| 550 nm | 0.0000 | 20.496 | 19.675 | IO-CSIC | 0.0009 | 2.305 | 18.307 |
| 600 nm | 0.0010 | 18.709 | 19.675 | | | | |
| 650 nm | 0.0001 | 18.103 | 19.675 | | | | |
| 700 nm | 0.0002 | 17.398 | 19.675 | | | | |
| 750 nm | 0.0015 | 1.947 | 19.675 | | | | |
| 800 nm | 0.0002 | 2.315 | 19.675 | | | | |
| 850 nm | 0.0010 | 2.380 | 19.675 | | | | |
| 900 nm | 0.0038 | 5.288 | 19.675 | | | | |
| 950 nm | 0.0022 | 4.180 | 19.675 | | | | |
| 1000 nm | 0.0034 | 14.350 | 19.675 | | | | |

**Table 6-4.** Results of the consistency check without and with exclusion of outliers for the trap detectors. A failed consistency is indicated in red letters.

| consistency check | Without exclusion of outliers | | | outliers identified | With exclusion of outliers | | |
|---|---|---|---|---|---|---|---|
| | $\Delta_{\mathrm{KCRV}}$ | $\chi^2_{\mathrm{obs}}$ | $\chi^2_{0.05}(\nu)$ | | $\Delta_{\mathrm{KCRV}}$ | $\chi^2_{\mathrm{obs}}$ | $\chi^2_{0.05}(\nu)$ |
| 300 nm | 0.0116 | 217.261 | 19.675 | IO-CSIC, VNIIOFI, UME | 0.0118 | 26.618 | 15.507 |
| 320 nm | 0.0117 | 95.604 | 19.675 | IO-CSIC, UME | 0.0116 | 34.105 | 16.919 |
| 340 nm | 0.0141 | 95.696 | 19.675 | KRISS, IO-CSIC | 0.0140 | 34.663 | 16.919 |
| 360 nm | 0.0172 | 34.692 | 19.675 | IO-CSIC | 0.0144 | 15.647 | 18.307 |
| 380 nm | 0.0154 | 121.219 | 19.675 | KRISS, IO-CSIC | 0.0159 | 54.464 | 16.919 |
| 400 nm | 0.0120 | 51.664 | 19.675 | | | | |
| 450 nm | 0.0046 | 13.534 | 19.675 | | | | |
| 500 nm | 0.0034 | 10.709 | 19.675 | | | | |
| 550 nm | 0.0020 | 37.396 | 19.675 | IO-CSIC | 0.0026 | 8.944 | 18.307 |
| 600 nm | 0.0034 | 36.752 | 19.675 | IO-CSIC | 0.0040 | 10.704 | 18.307 |
| 650 nm | 0.0022 | 33.077 | 19.675 | IO-CSIC | 0.0029 | 9.790 | 18.307 |
| 700 nm | 0.0023 | 36.357 | 19.675 | IO-CSIC | 0.0028 | 11.182 | 18.307 |

| | | | | | | | |
|---|---|---|---|---|---|---|---|
| 750 nm | 0.0030 | 11.689 | 19.675 | | | | |
| 800 nm | 0.0026 | 10.155 | 19.675 | | | | |
| 850 nm | 0.0032 | 10.322 | 19.675 | | | | |
| 900 nm | 0.0055 | 14.404 | 19.675 | | | | |
| 950 nm | 0.0029 | 12.660 | 19.675 | | | | |
| 1000 nm | 0.0023 | 8.162 | 19.675 | | | | |

From Table 6-3 and Table 6-4, we see that there are comparisons at several wavelengths where an introduction of the Mandel Paule factor is necessary. The introduced Mandel Paule factors and their impact to the consistency are summarized in Table 6-5 and Table 6-6.

**Table 6-5.** Results of the consistency check without and with the Mandel Paule factor for the single-element detectors. A failed consistency is indicated in red letters.

| Mandel Paule method | Without Mandel Paule factor | | | $s$ | With Mandel Paule factor | | |
|---|---|---|---|---|---|---|---|
| | $\Delta_{KCRV}$ | $\chi^2_{obs}$ | $\chi^2_{0.05}(\nu)$ | | $\Delta_{KCRV}$ | $\chi^2_{obs}$ | $\chi^2_{0.05}(\nu)$ |
| 340 nm | 0.0090 | 36.100 | 18.307 | 0.00423 | 0.0103 | 18.269 | 18.307 |
| 380 nm | 0.0111 | 33.715 | 16.919 | 0.00395 | 0.0123 | 16.916 | 16.919 |
| 400 nm | 0.0080 | 23.094 | 18.307 | 0.00261 | 0.0082 | 18.303 | 18.307 |

**Table 6-6.** Results of the consistency check without and with the Mandel Paule factor for the trap detectors. A failed consistency is indicated in red letters.

| Mandel Paule method | Without Mandel Paule factor | | | $s$ | With Mandel Paule factor | | |
|---|---|---|---|---|---|---|---|
| | $\Delta_{KCRV}$ | $\chi^2_{obs}$ | $\chi^2_{0.05}(\nu)$ | | $\Delta_{KCRV}$ | $\chi^2_{obs}$ | $\chi^2_{0.05}(\nu)$ |
| 300 nm | 0.0118 | 26.618 | 15.507 | 0.00470 | 0.0132 | 15.489 | 15.507 |
| 320 nm | 0.0116 | 34.105 | 16.919 | 0.00483 | 0.0127 | 16.890 | 16.919 |
| 340 nm | 0.0140 | 34.663 | 16.919 | 0.00460 | 0.0151 | 16.889 | 16.919 |
| 380 nm | 0.0159 | 54.464 | 16.919 | 0.00525 | 0.0176 | 16.897 | 16.919 |
| 400 nm | 0.0120 | 51.664 | 19.675 | 0.00647 | 0.0132 | 19.665 | 16.919 |

After considering the outliers and the Mandel Paule factor as described above, the calculated values of weights $w_i$ of each participant are summarized in Table 6-7 and Table 6-8 for the single-element and trap detectors, respectively. Note that the weights for the outliers are set to zero. The values of the KCRV and their uncertainties are summarized in Table 6-9 together with the introduced Mandel Paule factors.

**Table 6-7.** Values of the weights defined in Eq. (6-12) for the single-element detectors.

| $w_i$ | KRISS | NMC-ASTAR | NIST | IO-CSIC | VNIIOFI | NMIJ | LNE-CNAM | PTB | NRC | MSL | UME | NPL |
|---|---|---|---|---|---|---|---|---|---|---|---|---|
| 300 nm | 0.1645 | 0.0316 | 0.1438 | 0 | 0.0989 | 0.0316 | 0.1349 | 0.1211 | 0.1142 | 0.0651 | 0 | 0.0943 |
| 320 nm | 0.1502 | 0.0304 | 0.1420 | 0 | 0.1039 | 0.0277 | 0.1202 | 0.1168 | 0.1097 | 0.0582 | 0.0538 | 0.0872 |
| 340 nm | 0.1327 | 0.0348 | 0.1295 | 0 | 0.1130 | 0.0348 | 0.1163 | 0.1136 | 0.1095 | 0.0636 | 0.0624 | 0.0899 |
| 360 nm | 0.1121 | 0.0492 | 0.1143 | 0 | 0.1083 | 0.0491 | 0.1070 | 0.1068 | 0.1038 | 0.0782 | 0.0759 | 0.0952 |
| 380 nm | 0.1256 | 0.0344 | 0.1429 | 0 | 0 | 0.0531 | 0.1211 | 0.1214 | 0.1168 | 0.0624 | 0.1067 | 0.1156 |
| 400 nm | 0.1004 | 0.0986 | 0.1141 | 0 | 0.0974 | 0.0454 | 0.1085 | 0.980 | 0.0931 | 0.0604 | 0.0842 | 0.0998 |
| 450 nm | 0.1324 | 0.0892 | 0.1225 | 0.0520 | 0.0967 | 0.0267 | 0.1101 | 0.0838 | 0.0761 | 0.0538 | 0.0613 | 0.0952 |
| 500 nm | 0.1475 | 0.0896 | 0.1356 | 0.0584 | 0.0921 | 0.0244 | 0.0943 | 0.0797 | 0.0724 | 0.0587 | 0.0530 | 0.0944 |
| 550 nm | 0.1532 | 0.0966 | 0.1453 | 0 | 0.0962 | 0.0291 | 0.1028 | 0.0830 | 0.0753 | 0.0652 | 0.0543 | 0.0990 |
| 600 nm | 0.1532 | 0.0896 | 0.1356 | 0.0557 | 0.1068 | 0.0310 | 0.0774 | 0.0774 | 0.0702 | 0.0603 | 0.0505 | 0.0923 |
| 650 nm | 0.1330 | 0.0906 | 0.1345 | 0.0556 | 0.1047 | 0.0367 | 0.0938 | 0.0776 | 0.0704 | 0.0602 | 0.0505 | 0.0924 |
| 700 nm | 0.1373 | 0.0928 | 0.1369 | 0.0527 | 0.1049 | 0.0333 | 0.1053 | 0.0746 | 0.0677 | 0.0569 | 0.0475 | 0.0900 |
| 750 nm | 0.1170 | 0.0947 | 0.1330 | 0.0590 | 0.1067 | 0.0347 | 0.1030 | 0.0780 | 0.0695 | 0.0604 | 0.0517 | 0.0924 |
| 800 nm | 0.0722 | 0.1013 | 0.1402 | 0.0586 | 0.1140 | 0.0366 | 0.1024 | 0.0834 | 0.0725 | 0.0643 | 0.0558 | 0.0985 |
| 850 nm | 0.0875 | 0.1043 | 0.1399 | 0.0389 | 0.1148 | 0.0357 | 0.1108 | 0.0832 | 0.0675 | 0.0632 | 0.0560 | 0.0983 |
| 900 nm | 0.1430 | 0.1004 | 0.1348 | 0.0386 | 0.1105 | 0.0333 | 0.1142 | 0.0799 | 0.0717 | 0.0589 | 0.0203 | 0.0945 |

| | | | | | | | | | | | | |
|---|---|---|---|---|---|---|---|---|---|---|---|---|
| 950 nm | 0.1915 | 0.0148 | 0.1614 | 0.0412 | 0.0958 | 0.0267 | 0.1069 | 0.0938 | 0.0857 | 0.0658 | 0.0236 | 0.0929 |
| 1000 nm | 0.1362 | 0.0306 | 0.1228 | 0.0721 | 0.0973 | 0.0259 | 0.0883 | 0.0999 | 0.0935 | 0.0815 | 0.0443 | 0.1076 |

**Table 6-8.** Values of the weights defined in Eq. (6-12) for the trap detectors.

| $w_i$ | KRISS | NMC-ASTAR | NIST | IO-CSIC | VNIIOFI | NMIJ | LNE-CNAM | PTB | NRC | MSL | UME | NPL |
|---|---|---|---|---|---|---|---|---|---|---|---|---|
| 300 nm | 0.1446 | 0.0445 | 0.1510 | 0 | 0 | 0.0561 | 0.1037 | 0.1396 | 0.1502 | 0.0985 | 0 | 0.1118 |
| 320 nm | 0.1317 | 0.0379 | 0.1295 | 0 | 0.1164 | 0.0493 | 0.0991 | 0.1199 | 0.1289 | 0.0869 | 0 | 0.1004 |
| 340 nm | 0 | 0.0353 | 0.1482 | 0 | 0.1326 | 0.0447 | 0.1083 | 0.1335 | 0.1472 | 0.0813 | 0.0690 | 0.1001 |
| 360 nm | 0.1114 | 0.0433 | 0.1135 | 0 | 0.1100 | 0.0524 | 0.1009 | 0.1074 | 0.1131 | 0.0834 | 0.0726 | 0.0920 |
| 380 nm | 0 | 0.0341 | 0.1286 | 0 | 0.1236 | 0.0707 | 0.1014 | 0.1170 | 0.1279 | 0.0764 | 0.1006 | 0.1196 |
| 400 nm | 0.0911 | 0.0898 | 0.0939 | 0.0582 | 0.0898 | 0.0647 | 0.0830 | 0.0889 | 0.0936 | 0.0747 | 0.0795 | 0.0928 |
| 450 nm | 0.1026 | 0.0907 | 0.1243 | 0.0272 | 0.1097 | 0.0301 | 0.0619 | 0.0826 | 0.1207 | 0.0747 | 0.0472 | 0.1282 |
| 500 nm | 0.0898 | 0.0830 | 0.1386 | 0.0355 | 0.1015 | 0.0251 | 0.0398 | 0.0708 | 0.1318 | 0.1050 | 0.0330 | 0.1461 |
| 550 nm | 0.0847 | 0.0840 | 0.1452 | 0 | 0.1002 | 0.0309 | 0.0391 | 0.0690 | 0.1373 | 0.1246 | 0.0307 | 0.1543 |
| 600 nm | 0.0857 | 0.0807 | 0.1386 | 0 | 0.1364 | 0.0379 | 0.0316 | 0.0655 | 0.1310 | 0.1166 | 0.0289 | 0.1470 |
| 650 nm | 0.0769 | 0.0828 | 0.1348 | 0 | 0.1321 | 0.0553 | 0.0373 | 0.0664 | 0.1279 | 0.1143 | 0.0299 | 0.1423 |
| 700 nm | 0.0717 | 0.0800 | 0.1426 | 0 | 0.1389 | 0.0459 | 0.0358 | 0.0603 | 0.1338 | 0.1153 | 0.0253 | 0.1504 |
| 750 nm | 0.0678 | 0.0865 | 0.1289 | 0.0420 | 0.1324 | 0.0469 | 0.0405 | 0.0656 | 0.1145 | 0.1089 | 0.0305 | 0.1355 |
| 800 nm | 0.0419 | 0.0921 | 0.1357 | 0.0426 | 0.1368 | 0.0472 | 0.0410 | 0.0700 | 0.1101 | 0.1075 | 0.0326 | 0.1425 |
| 850 nm | 0.0534 | 0.0947 | 0.1351 | 0.0328 | 0.1438 | 0.0463 | 0.0449 | 0.0709 | 0.0963 | 0.1064 | 0.0338 | 0.1416 |
| 900 nm | 0.0845 | 0.0941 | 0.1374 | 0.0250 | 0.1373 | 0.0416 | 0.0440 | 0.0695 | 0.1166 | 0.0956 | 0.0117 | 0.1426 |
| 950 nm | 0.1250 | 0.0105 | 0.1711 | 0.0314 | 0.1044 | 0.0285 | 0.0353 | 0.0874 | 0.1638 | 0.1137 | 0.0152 | 0.1137 |
| 1000 nm | 0.1193 | 0.0290 | 0.1211 | 0.0650 | 0.1015 | 0.0270 | 0.0511 | 0.1004 | 0.1195 | 0.1057 | 0.0388 | 0.1217 |

**Table 6-9.** Values of the KCRV and their uncertainties defined in Eqs. (6-13) and (6-14), respectively, for all the transfer detectors. The Mandel Paule factors introduced to make the comparison consistent are also listed.

| KCRV | single-element detectors | | | trap detectors | | |
|---|---|---|---|---|---|---|
| | $\Delta_{KCRV}$ | $u(\Delta_{KCRV})$ | $s$ | $\Delta_{KCRV}$ | $u(\Delta_{KCRV})$ | $s$ |
| 300 nm | 0.0049 | 0.0017 | | 0.0132 | 0.0018 | 0.00470 |
| 320 nm | 0.0051 | 0.0016 | | 0.0127 | 0.0016 | 0.00483 |
| 340 nm | 0.0103 | 0.0014 | 0.00423 | 0.0151 | 0.0014 | 0.00460 |
| 360 nm | 0.0137 | 0.0026 | | 0.0144 | 0.0025 | |
| 380 nm | 0.0123 | 0.0012 | 0.00395 | 0.0176 | 0.0011 | 0.00525 |
| 400 nm | 0.0082 | 0.0015 | 0.00261 | 0.0132 | 0.0014 | 0.00647 |
| 450 nm | 0.0013 | 0.0010 | | 0.0046 | 0.0009 | |
| 500 nm | 0.0012 | 0.0009 | | 0.0034 | 0.0007 | |
| 550 nm | 0.0009 | 0.0009 | | 0.0026 | 0.0006 | |
| 600 nm | 0.0010 | 0.0009 | | 0.0040 | 0.0006 | |
| 650 nm | 0.0001 | 0.0009 | | 0.0029 | 0.0006 | |
| 700 nm | 0.0002 | 0.0008 | | 0.0028 | 0.0006 | |
| 750 nm | 0.0015 | 0.0009 | | 0.0030 | 0.0007 | |
| 800 nm | 0.0002 | 0.0009 | | 0.0026 | 0.0007 | |
| 850 nm | 0.0010 | 0.0009 | | 0.0032 | 0.0007 | |
| 900 nm | 0.0038 | 0.0009 | | 0.0055 | 0.0007 | |
| 950 nm | 0.0022 | 0.0009 | | 0.0029 | 0.0007 | |
| 1000 nm | 0.0034 | 0.0015 | | 0.0023 | 0.0014 | |

# 7. COMPARISON RESULTS

The degrees of equivalences (DoEs) of all the participants for the single-element and trap detectors are summarized in Table 7-1 and Table 7-2, respectively, with their expanded uncertainties ($k$ = 2). The DoEs of each participant are separately tabulated and plotted in Appendix A.

**Table 7-1.** Values of degree of equivalence $D_i$ defined in Eq. (6-15) and their expanded uncertainties $U(D_i) = k \cdot u(D_i)$ with $k = 2$ calculated with Eqs. (6-16) and (6-19) for the single-element detectors.

| $D_i$ | KRISS | NMC-ASTAR | NIST | IO-CSIC | VNIIOFI | NMIJ | LNE-CNAM | PTB | NRC | MSL | UME | NPL |
|---|---|---|---|---|---|---|---|---|---|---|---|---|
| 300 nm | -0.0049 | 0.0107 | -0.0017 | 0.0564 | -0.0056 | 0.0158 | 0.0006 | -0.0040 | 0.0001 | 0.0144 | -0.0284 | 0.0022 |
| 320 nm | -0.0051 | 0.0086 | -0.0050 | 0.0522 | 0.0068 | 0.0191 | -0.0002 | -0.0022 | -0.0001 | 0.0105 | -0.0129 | 0.0041 |
| 340 nm | -0.0103 | 0.0144 | -0.0101 | 0.0535 | 0.0127 | 0.0174 | -0.0028 | -0.0037 | 0.0020 | 0.0074 | 0.0001 | 0.0021 |
| 360 nm | -0.0137 | 0.0064 | -0.0098 | 0.0479 | 0.0242 | 0.0135 | -0.0074 | -0.0054 | 0.0029 | 0.0054 | -0.0025 | -0.0011 |
| 380 nm | -0.0123 | 0.0079 | -0.0067 | 0.0459 | -0.0146 | 0.0168 | -0.0001 | -0.0021 | -0.0021 | 0.0067 | 0.0076 | 0.0054 |
| 400 nm | -0.0082 | 0.0126 | -0.0070 | 0.0301 | -0.0073 | 0.0150 | -0.0025 | -0.0042 | 0.0004 | 0.0069 | 0.0073 | 0.0002 |
| 450 nm | -0.0013 | 0.0025 | -0.0027 | 0.0039 | -0.0011 | 0.0052 | -0.0010 | -0.0028 | 0.0015 | 0.0026 | 0.0033 | -0.0007 |
| 500 nm | -0.0012 | -0.0006 | -0.0014 | -0.0001 | 0.0004 | 0.0022 | 0.0008 | -0.0017 | 0.0019 | 0.0019 | 0.0027 | -0.0001 |
| 550 nm | -0.0009 | -0.0019 | -0.0009 | -0.0161 | 0.0007 | 0.0009 | 0.0017 | -0.0016 | 0.0017 | 0.0010 | 0.0025 | -0.0001 |
| 600 nm | -0.0010 | -0.0007 | 0.0005 | -0.0143 | 0.0021 | 0.0017 | 0.0018 | -0.0003 | 0.0024 | 0.0020 | 0.0031 | 0.0011 |
| 650 nm | 0.0001 | -0.0006 | 0.0003 | -0.0145 | 0.0018 | 0.0009 | 0.0027 | -0.0004 | 0.0020 | 0.0011 | 0.0025 | 0.0005 |
| 700 nm | -0.0002 | -0.0003 | 0.0003 | -0.0139 | 0.0017 | 0.0003 | 0.0020 | -0.0006 | 0.0022 | 0.0015 | 0.0020 | 0.0009 |
| 750 nm | -0.0015 | -0.0006 | -0.0007 | 0.0025 | 0.0010 | -0.0013 | 0.0015 | -0.0017 | 0.0013 | 0.0002 | 0.0005 | -0.0002 |
| 800 nm | -0.0002 | -0.0003 | -0.0012 | 0.0044 | 0.0005 | -0.0025 | 0.0002 | -0.0016 | 0.0012 | 0.0000 | 0.0004 | -0.0001 |
| 850 nm | -0.0010 | 0.0005 | -0.0013 | 0.0037 | 0.0006 | -0.0034 | 0.0004 | -0.0018 | 0.0024 | 0.0004 | 0.0006 | 0.0002 |
| 900 nm | -0.0038 | 0.0015 | -0.0009 | 0.0047 | 0.0019 | -0.0021 | 0.0000 | -0.0009 | 0.0021 | 0.0011 | 0.0004 | 0.0003 |
| 950 nm | -0.0022 | 0.0033 | -0.0009 | 0.0072 | 0.0005 | -0.0009 | 0.0012 | -0.0011 | 0.0009 | 0.0005 | 0.0004 | 0.0007 |
| 1000 nm | -0.0034 | 0.0036 | -0.0060 | 0.0071 | 0.0142 | -0.0011 | 0.0002 | -0.0023 | -0.0039 | -0.0012 | 0.0015 | -0.0016 |
| $U(D_i)$ | KRISS | NMC-ASTAR | NIST | IO-CSIC | VNIIOFI | NMIJ | LNE-CNAM | PTB | NRC | MSL | UME | NPL |
| 300 nm | 0.0080 | 0.0197 | 0.0080 | 0.0159 | 0.0107 | 0.0198 | 0.0090 | 0.0090 | 0.0093 | 0.0135 | 0.0149 | 0.0110 |
| 320 nm | 0.0078 | 0.0187 | 0.0076 | 0.0153 | 0.0097 | 0.0196 | 0.0089 | 0.0085 | 0.0087 | 0.0133 | 0.0139 | 0.0107 |
| 340 nm | 0.0063 | 0.0187 | 0.0059 | 0.0144 | 0.0076 | 0.0187 | 0.0073 | 0.0070 | 0.0072 | 0.0125 | 0.0126 | 0.0094 |
| 360 nm | 0.0148 | 0.0231 | 0.0142 | 0.0201 | 0.0150 | 0.0231 | 0.0151 | 0.0148 | 0.0151 | 0.0180 | 0.0183 | 0.0162 |
| 380 nm | 0.0062 | 0.0175 | 0.0048 | 0.0130 | 0.0070 | 0.0132 | 0.0065 | 0.0062 | 0.0064 | 0.0117 | 0.0074 | 0.0068 |
| 400 nm | 0.0089 | 0.0090 | 0.0080 | 0.0148 | 0.0091 | 0.0147 | 0.0084 | 0.0090 | 0.0093 | 0.0124 | 0.0100 | 0.0089 |
| 450 nm | 0.0053 | 0.0067 | 0.0055 | 0.0089 | 0.0064 | 0.0126 | 0.0059 | 0.0067 | 0.0075 | 0.0088 | 0.0082 | 0.0064 |
| 500 nm | 0.0043 | 0.0057 | 0.0044 | 0.0071 | 0.0056 | 0.0113 | 0.0055 | 0.0059 | 0.0063 | 0.0071 | 0.0075 | 0.0055 |
| 550 nm | 0.0042 | 0.0054 | 0.0042 | 0.0076 | 0.0055 | 0.0103 | 0.0053 | 0.0058 | 0.0062 | 0.0067 | 0.0074 | 0.0053 |
| 600 nm | 0.0040 | 0.0055 | 0.0042 | 0.0071 | 0.0050 | 0.0096 | 0.0059 | 0.0058 | 0.0062 | 0.0068 | 0.0074 | 0.0053 |
| 650 nm | 0.0044 | 0.0055 | 0.0043 | 0.0071 | 0.0051 | 0.0089 | 0.0054 | 0.0059 | 0.0063 | 0.0068 | 0.0075 | 0.0054 |
| 700 nm | 0.0041 | 0.0051 | 0.0040 | 0.0069 | 0.0048 | 0.0088 | 0.0048 | 0.0056 | 0.0060 | 0.0067 | 0.0073 | 0.0051 |
| 750 nm | 0.0048 | 0.0054 | 0.0044 | 0.0070 | 0.0051 | 0.0093 | 0.0052 | 0.0059 | 0.0064 | 0.0069 | 0.0075 | 0.0054 |
| 800 nm | 0.0066 | 0.0055 | 0.0044 | 0.0074 | 0.0051 | 0.0094 | 0.0054 | 0.0059 | 0.0066 | 0.0070 | 0.0075 | 0.0055 |
| 850 nm | 0.0059 | 0.0054 | 0.0044 | 0.0091 | 0.0051 | 0.0095 | 0.0052 | 0.0059 | 0.0068 | 0.0071 | 0.0075 | 0.0054 |
| 900 nm | 0.0044 | 0.0054 | 0.0044 | 0.0090 | 0.0051 | 0.0097 | 0.0050 | 0.0059 | 0.0064 | 0.0072 | 0.0125 | 0.0054 |
| 950 nm | 0.0039 | 0.0156 | 0.0040 | 0.0092 | 0.0059 | 0.0115 | 0.0055 | 0.0056 | 0.0060 | 0.0072 | 0.0123 | 0.0060 |
| 1000 nm | 0.0075 | 0.0168 | 0.0080 | 0.0107 | 0.0091 | 0.0183 | 0.0096 | 0.0085 | 0.0091 | 0.0100 | 0.0139 | 0.0085 |

**Table 7-2.** Values of degree of equivalence $D_i$ defined in Eq. (6-15) and their expanded uncertainties $U(D_i) = k \cdot u(D_i)$ with $k = 2$ calculated with Eqs. (6-16) and (6-19) for the trap detectors.

| $D_i$ | KRISS | NMC-ASTAR | NIST | IO-CSIC | VNIIOFI | NMIJ | LNE-CNAM | PTB | NRC | MSL | UME | NPL |
|---|---|---|---|---|---|---|---|---|---|---|---|---|
| 300 nm | -0.0132 | 0.0150 | -0.0031 | 0.0473 | 0.0222 | 0.0175 | 0.0135 | 0.0043 | -0.0102 | 0.0051 | -0.0858 | -0.0020 |
| 320 nm | -0.0127 | 0.0010 | -0.0098 | 0.0447 | 0.0122 | 0.0152 | 0.0124 | 0.0032 | -0.0089 | 0.0032 | -0.0371 | 0.0002 |
| 340 nm | -0.0151 | 0.0170 | -0.0074 | 0.0467 | 0.0094 | 0.0161 | 0.0091 | -0.0012 | -0.0068 | -0.0013 | -0.0155 | -0.0010 |
| 360 nm | -0.0144 | 0.0096 | -0.0072 | 0.0443 | 0.0085 | 0.0159 | 0.0159 | 0.0069 | -0.0061 | -0.0010 | -0.0125 | -0.0046 |
| 380 nm | -0.0176 | 0.0086 | -0.0065 | 0.0402 | 0.0019 | 0.0161 | 0.0132 | 0.0014 | -0.0103 | -0.0016 | -0.0114 | 0.0022 |
| 400 nm | -0.0132 | 0.0151 | -0.0065 | 0.0251 | 0.0008 | 0.0100 | 0.0078 | 0.0007 | -0.0092 | -0.0036 | -0.0076 | -0.0076 |
| 450 nm | -0.0046 | 0.0041 | -0.0024 | 0.0020 | 0.0008 | 0.0047 | 0.0082 | 0.0021 | -0.0009 | -0.0002 | -0.0019 | -0.0026 |
| 500 nm | -0.0034 | 0.0006 | -0.0010 | -0.0009 | 0.0010 | 0.0019 | 0.0084 | 0.0027 | 0.0002 | -0.0005 | -0.0001 | -0.0015 |
| 550 nm | -0.0026 | -0.0006 | -0.0004 | -0.0177 | 0.0012 | 0.0010 | 0.0073 | 0.0028 | 0.0003 | -0.0009 | 0.0001 | -0.0014 |
| 600 nm | -0.0040 | -0.0007 | 0.0001 | -0.0169 | 0.0012 | 0.0006 | 0.0077 | 0.0029 | 0.0002 | -0.0005 | -0.0002 | -0.0012 |
| 650 nm | -0.0029 | -0.0006 | -0.0003 | -0.0160 | 0.0007 | -0.0004 | 0.0085 | 0.0022 | 0.0005 | -0.0008 | 0.0005 | -0.0015 |
| 700 nm | -0.0028 | -0.0004 | -0.0003 | -0.0158 | 0.0004 | -0.0004 | 0.0082 | 0.0027 | 0.0005 | -0.0006 | 0.0004 | -0.0015 |
| 750 nm | -0.0030 | 0.0004 | -0.0001 | 0.0024 | 0.0005 | -0.0006 | 0.0085 | 0.0028 | -0.0019 | -0.0007 | 0.0004 | -0.0014 |
| 800 nm | -0.0026 | 0.0005 | -0.0007 | 0.0046 | 0.0003 | -0.0024 | 0.0071 | 0.0026 | -0.0015 | -0.0004 | 0.0003 | -0.0017 |
| 850 nm | -0.0032 | 0.0010 | -0.0009 | 0.0039 | -0.0001 | -0.0026 | 0.0077 | 0.0027 | -0.0009 | -0.0005 | 0.0000 | -0.0013 |
| 900 nm | -0.0055 | 0.0022 | 0.0002 | 0.0041 | 0.0003 | -0.0026 | 0.0065 | 0.0031 | -0.0017 | 0.0003 | 0.0007 | -0.0006 |
| 950 nm | -0.0029 | 0.0040 | 0.0003 | 0.0067 | -0.0027 | -0.0008 | 0.0072 | 0.0035 | -0.0023 | 0.0013 | 0.0006 | 0.0002 |
| 1000 nm | -0.0023 | 0.0009 | -0.0046 | 0.0080 | -0.0006 | 0.0000 | 0.0071 | 0.0039 | -0.0055 | 0.0020 | 0.0016 | -0.0003 |

| $U(D_i)$ | KRISS | NMC-ASTAR | NIST | IO-CSIC | VNIIOFI | NMIJ | LNE-CNAM | PTB | NRC | MSL | UME | NPL |
|---|---|---|---|---|---|---|---|---|---|---|---|---|
| 300 nm | 0.0083 | 0.0207 | 0.0076 | 0.0174 | 0.0112 | 0.0178 | 0.0113 | 0.0082 | 0.0077 | 0.0118 | 0.0148 | 0.0106 |
| 320 nm | 0.0078 | 0.0210 | 0.0072 | 0.0157 | 0.0088 | 0.0177 | 0.0103 | 0.0079 | 0.0071 | 0.0116 | 0.0144 | 0.0102 |
| 340 nm | 0.0076 | 0.0198 | 0.0052 | 0.0142 | 0.0066 | 0.0170 | 0.0083 | 0.0061 | 0.0052 | 0.0109 | 0.0124 | 0.0090 |
| 360 nm | 0.0144 | 0.0241 | 0.0139 | 0.0203 | 0.0146 | 0.0218 | 0.0153 | 0.0144 | 0.0141 | 0.0170 | 0.0183 | 0.0161 |
| 380 nm | 0.0067 | 0.0191 | 0.0039 | 0.0132 | 0.0050 | 0.0108 | 0.0071 | 0.0053 | 0.0042 | 0.0100 | 0.0072 | 0.0054 |
| 400 nm | 0.0082 | 0.0084 | 0.0076 | 0.0138 | 0.0084 | 0.0125 | 0.0094 | 0.0083 | 0.0077 | 0.0107 | 0.0099 | 0.0079 |
| 450 nm | 0.0053 | 0.0057 | 0.0047 | 0.0107 | 0.0051 | 0.0102 | 0.0070 | 0.0058 | 0.0051 | 0.0063 | 0.0081 | 0.0046 |
| 500 nm | 0.0044 | 0.0046 | 0.0033 | 0.0072 | 0.0041 | 0.0086 | 0.0068 | 0.0048 | 0.0035 | 0.0040 | 0.0075 | 0.0033 |
| 550 nm | 0.0043 | 0.0043 | 0.0031 | 0.0066 | 0.0039 | 0.0074 | 0.0065 | 0.0047 | 0.0033 | 0.0035 | 0.0074 | 0.0030 |
| 600 nm | 0.0042 | 0.0043 | 0.0031 | 0.0066 | 0.0032 | 0.0064 | 0.0065 | 0.0047 | 0.0032 | 0.0035 | 0.0074 | 0.0030 |
| 650 nm | 0.0045 | 0.0044 | 0.0032 | 0.0066 | 0.0034 | 0.0054 | 0.0071 | 0.0048 | 0.0034 | 0.0036 | 0.0075 | 0.0032 |
| 700 nm | 0.0042 | 0.0040 | 0.0028 | 0.0063 | 0.0029 | 0.0053 | 0.0067 | 0.0045 | 0.0030 | 0.0032 | 0.0073 | 0.0027 |
| 750 nm | 0.0049 | 0.0043 | 0.0033 | 0.0063 | 0.0034 | 0.0060 | 0.0061 | 0.0048 | 0.0037 | 0.0038 | 0.0075 | 0.0032 |
| 800 nm | 0.0066 | 0.0043 | 0.0033 | 0.0065 | 0.0035 | 0.0062 | 0.0064 | 0.0049 | 0.0039 | 0.0040 | 0.0075 | 0.0033 |
| 850 nm | 0.0059 | 0.0043 | 0.0033 | 0.0076 | 0.0034 | 0.0063 | 0.0064 | 0.0049 | 0.0043 | 0.0040 | 0.0075 | 0.0033 |
| 900 nm | 0.0045 | 0.0042 | 0.0033 | 0.0085 | 0.0034 | 0.0065 | 0.0063 | 0.0048 | 0.0037 | 0.0042 | 0.0125 | 0.0033 |
| 950 nm | 0.0040 | 0.0148 | 0.0028 | 0.0085 | 0.0044 | 0.0089 | 0.0080 | 0.0044 | 0.0030 | 0.0042 | 0.0123 | 0.0042 |
| 1000 nm | 0.0075 | 0.0161 | 0.0075 | 0.0105 | 0.0083 | 0.0167 | 0.0120 | 0.0078 | 0.0072 | 0.0081 | 0.0138 | 0.0074 |

The results of DoEs of all the participants are plotted in Figure 7-1 to 7-18, with one figure for each wavelength. The expanded uncertainties of DoEs are indicated as error bars for each value. The plots for the single-element detectors and for the trap detectors are presented side-by-side for comparison. Finally, the summaries of all the results as a function of wavelength are presented in Figure 7-19 and Figure 7-20 for the single-element and trap detectors, respectively, from which the overall scattering of the DoE data can be visualized.

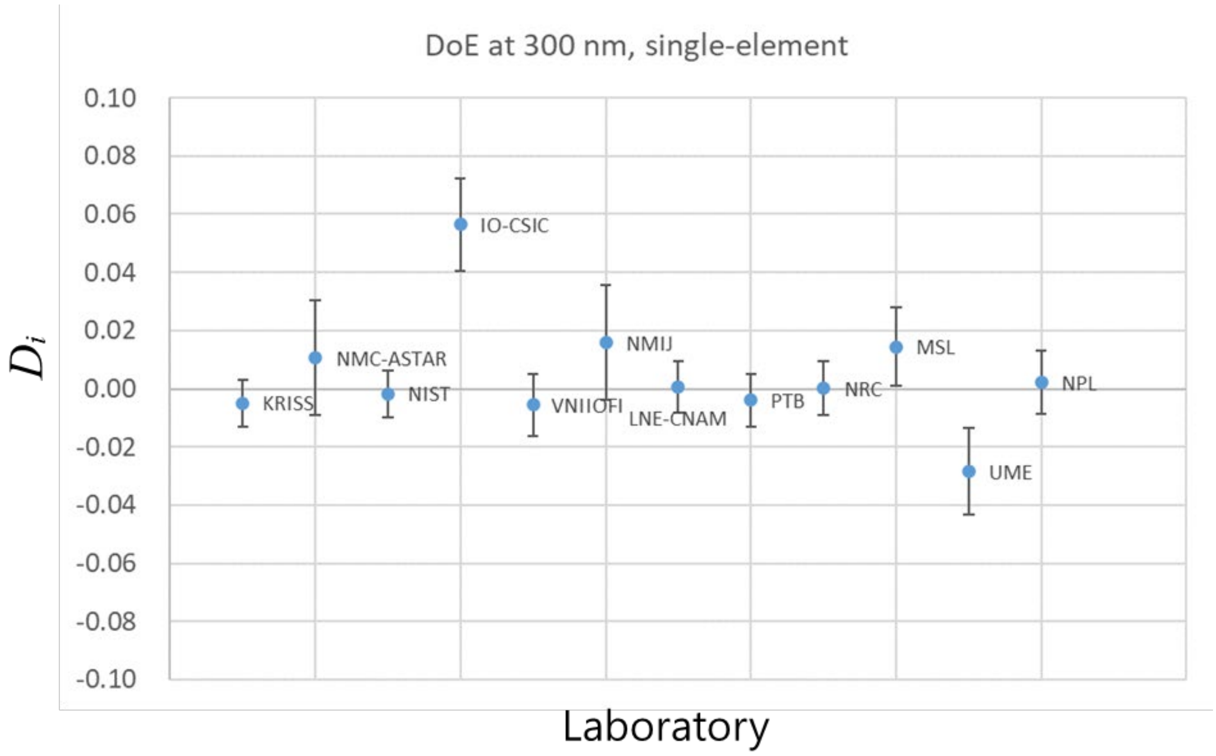


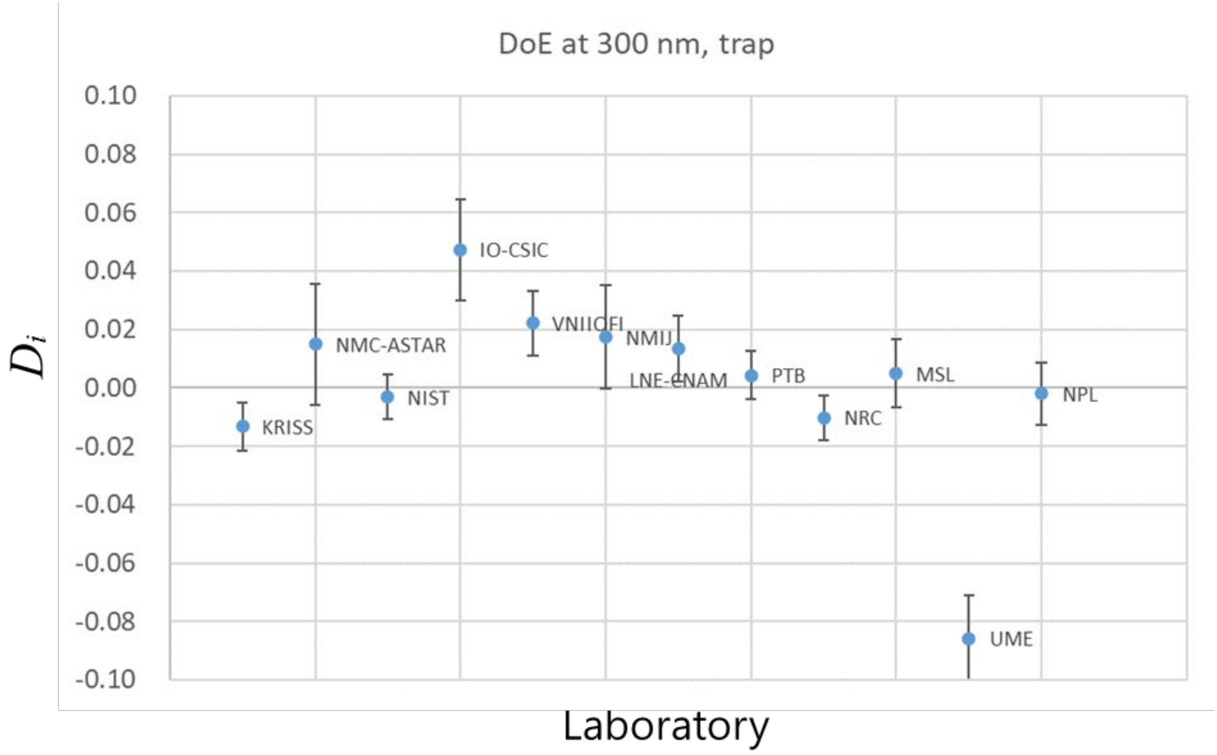


**Figure 7-1.** Results of the degree of equivalence (DoE) of all the participants at a wavelength of 300 nm for the single-element detectors (top) and the trap detectors (bottom). The error bars indicate the expanded uncertainties of DoEs ($k = 2$).

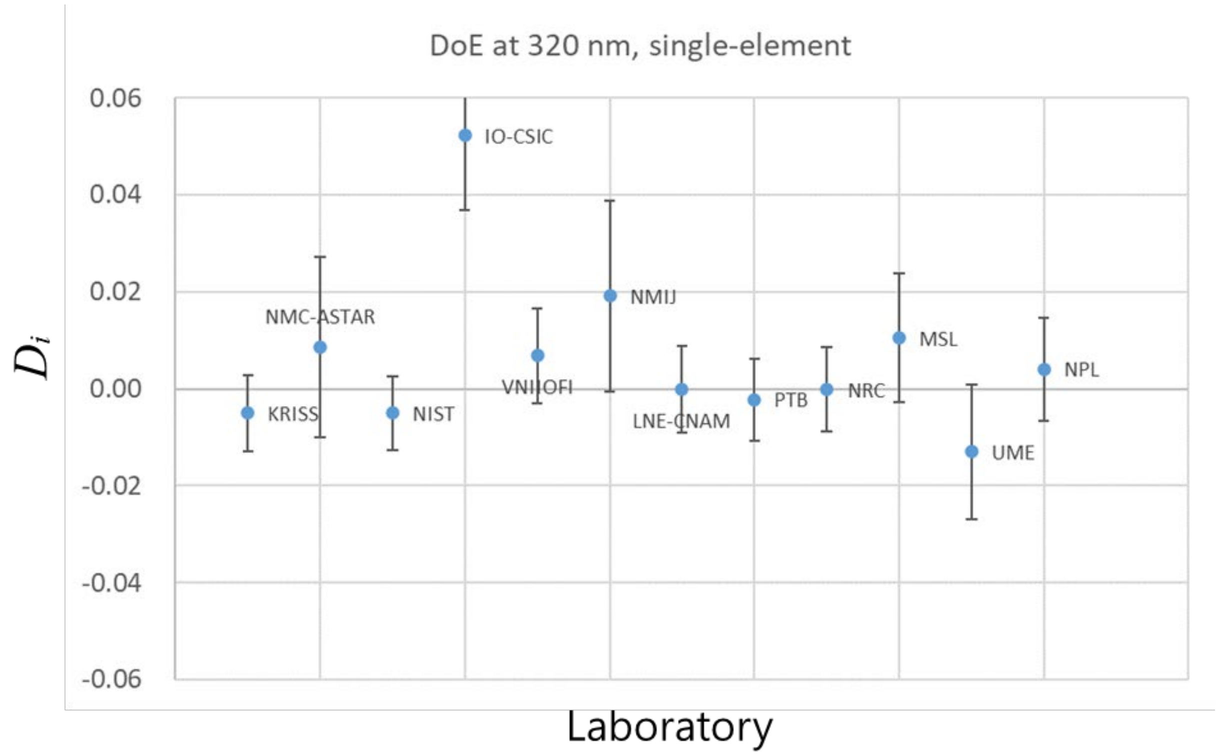


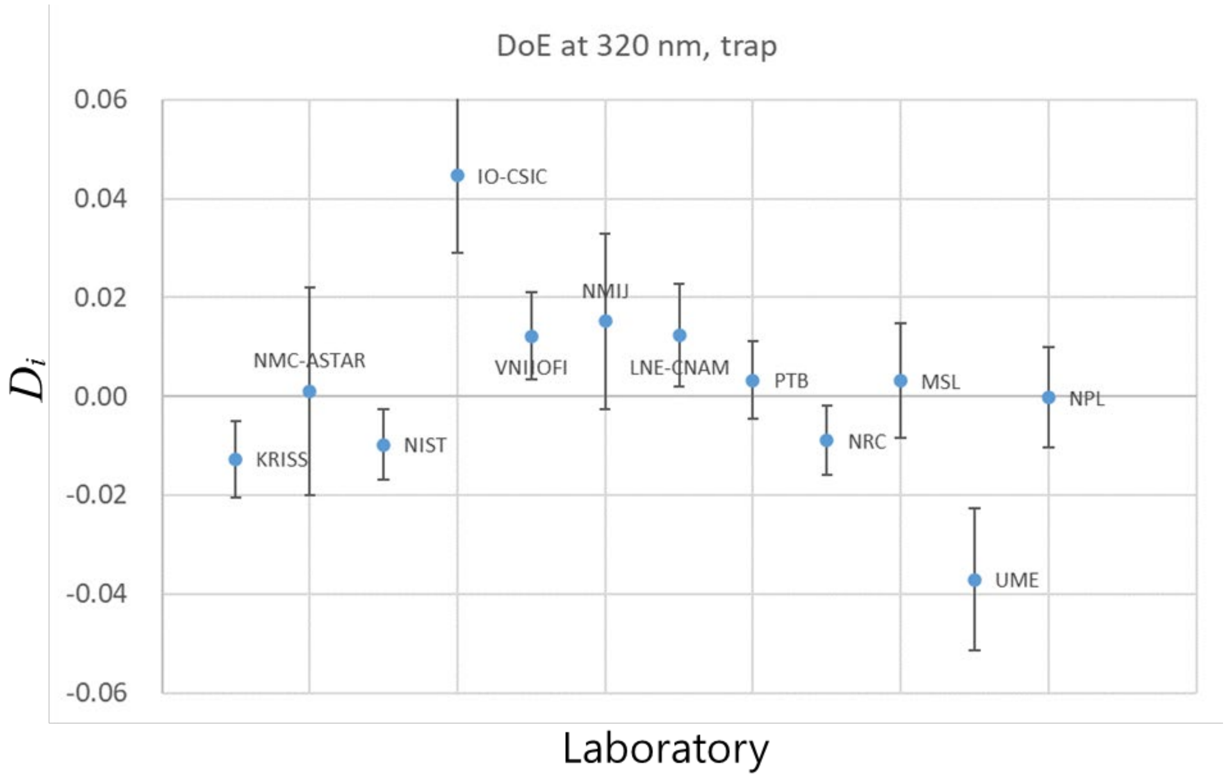


**Figure 7-2.** Results of the degree of equivalence (DoE) of all the participants at a wavelength of 320 nm for the single-element detectors (top) and the trap detectors (bottom). The error bars indicate the expanded uncertainties of DoEs ($k$ = 2).

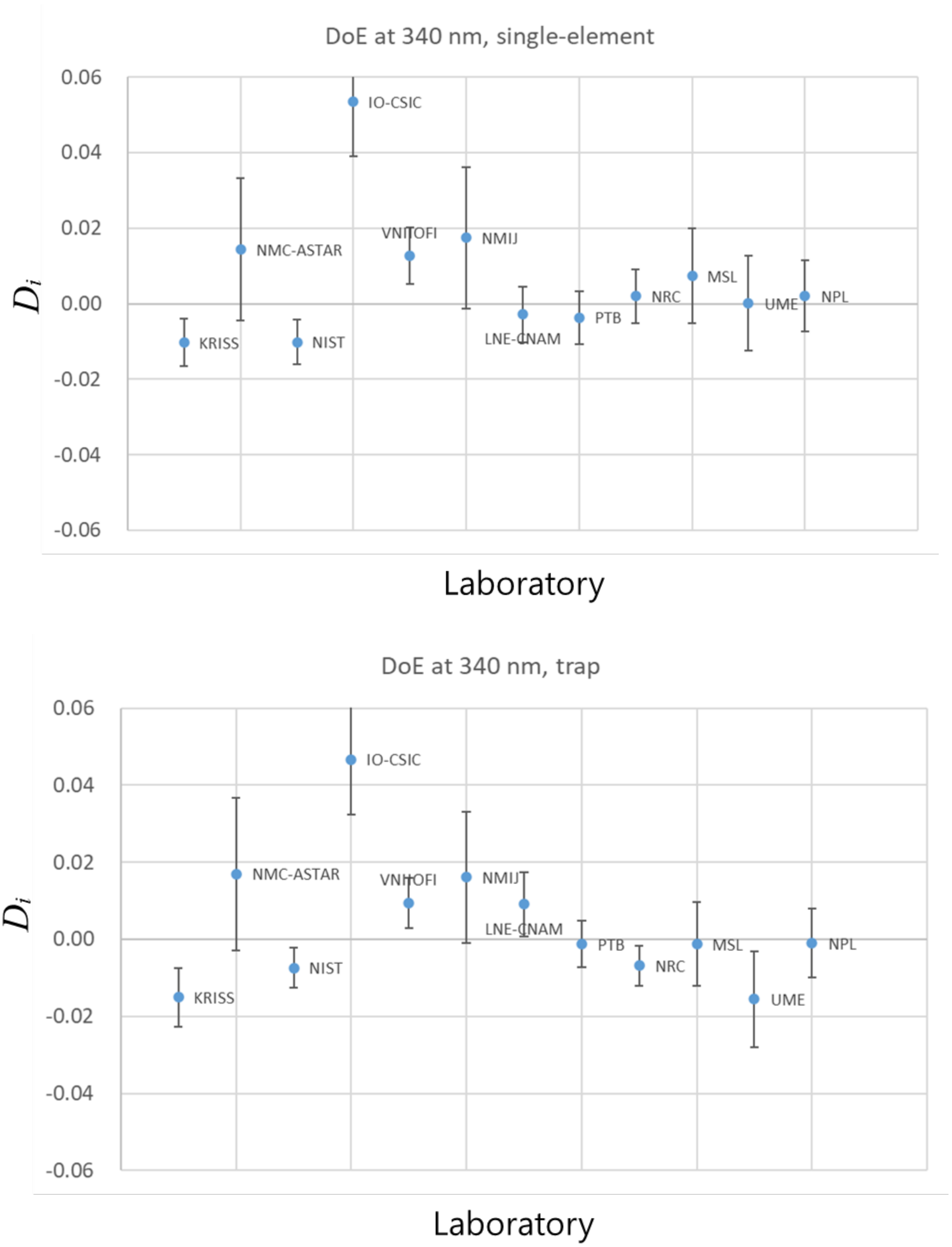


**Figure 7-3.** Results of the degree of equivalence (DoE) of all the participants at a wavelength of 340 nm for the single-element detectors (top) and the trap detectors (bottom). The error bars indicate the expanded uncertainties of DoEs ($k = 2$).

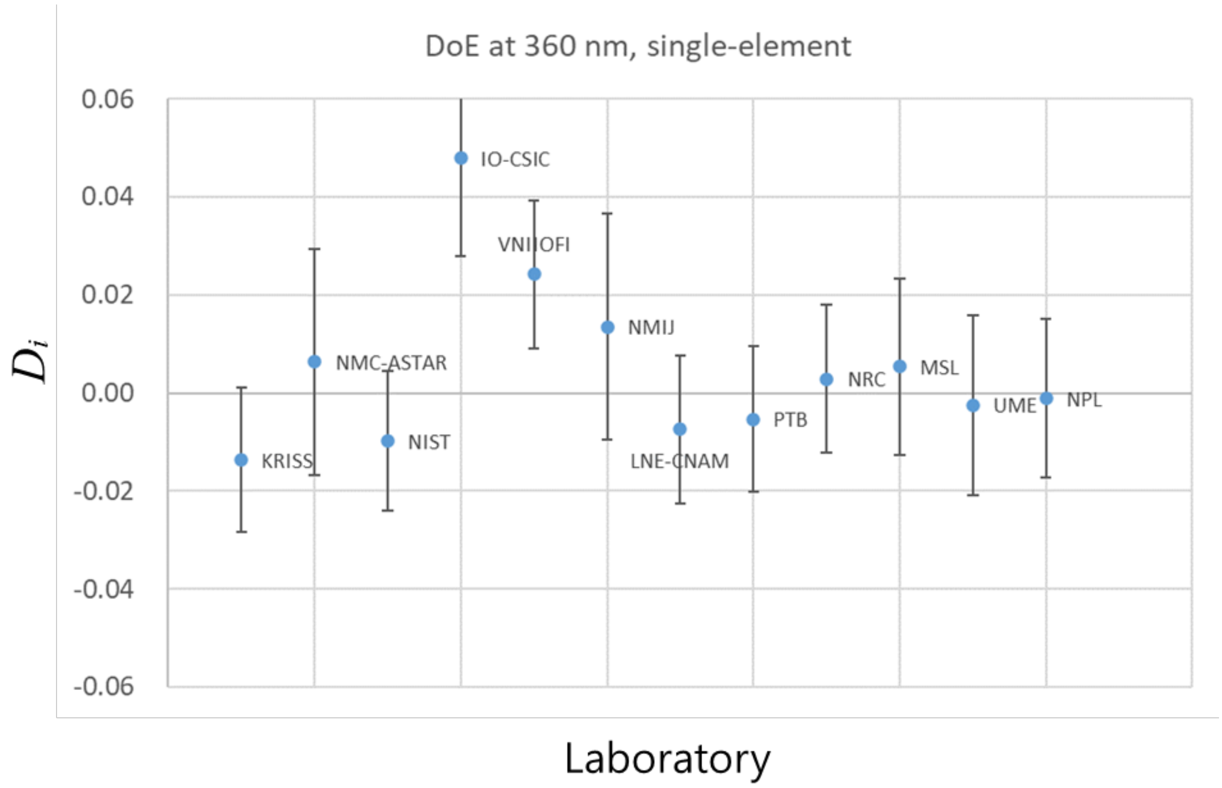


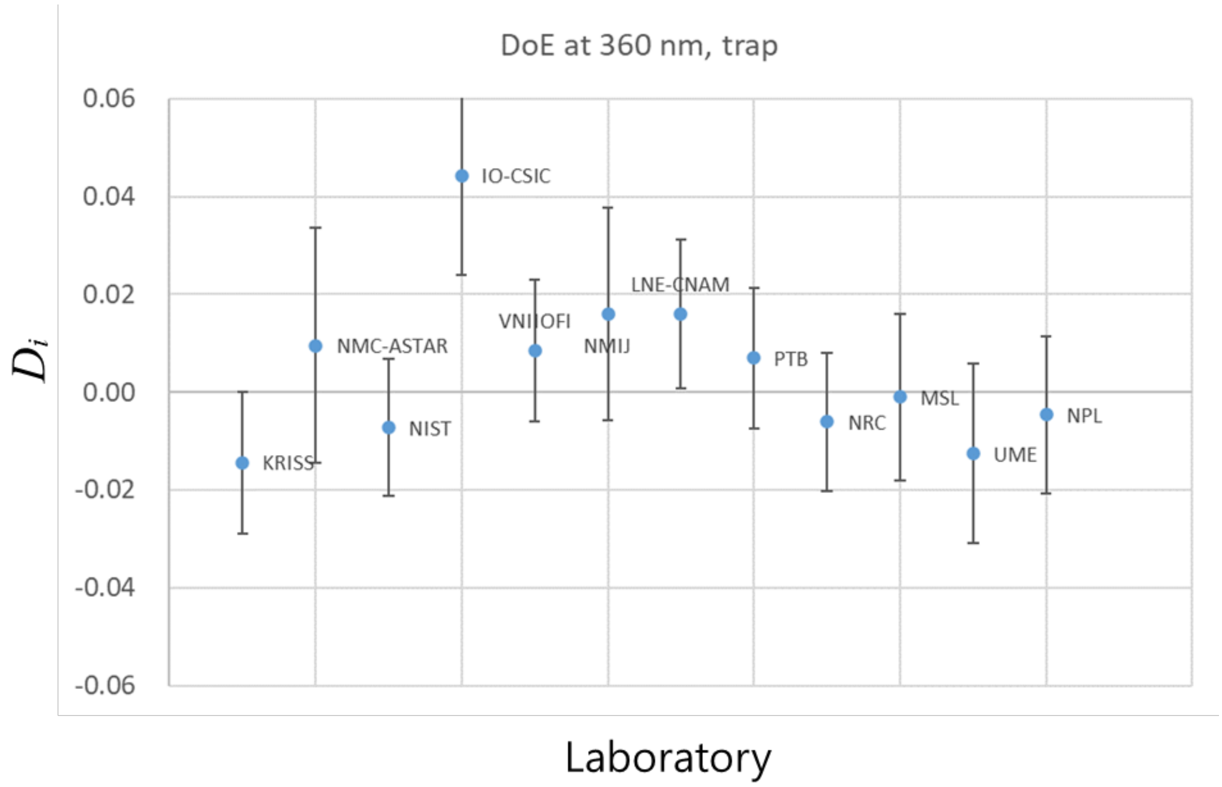


**Figure 7-4.** Results of the degree of equivalence (DoE) of all the participants at a wavelength of 360 nm for the single-element detectors (top) and the trap detectors (bottom). The error bars indicate the expanded uncertainties of DoEs ($k = 2$).

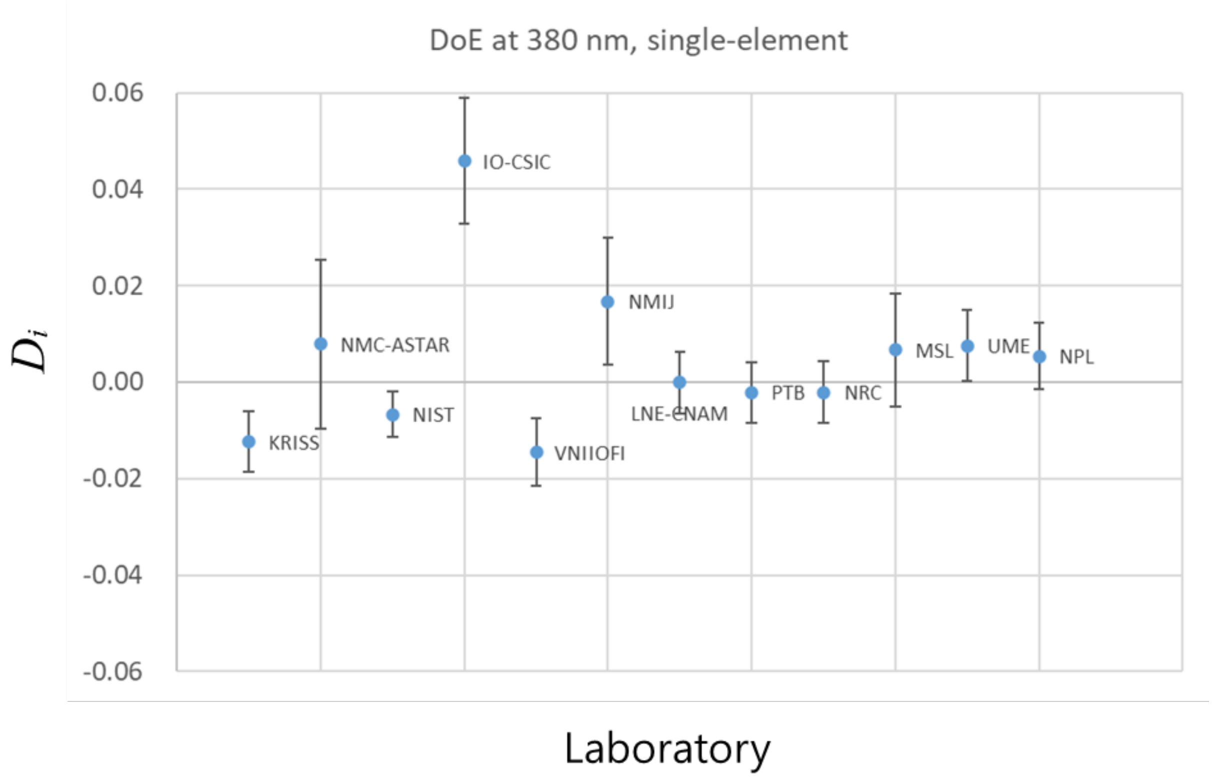


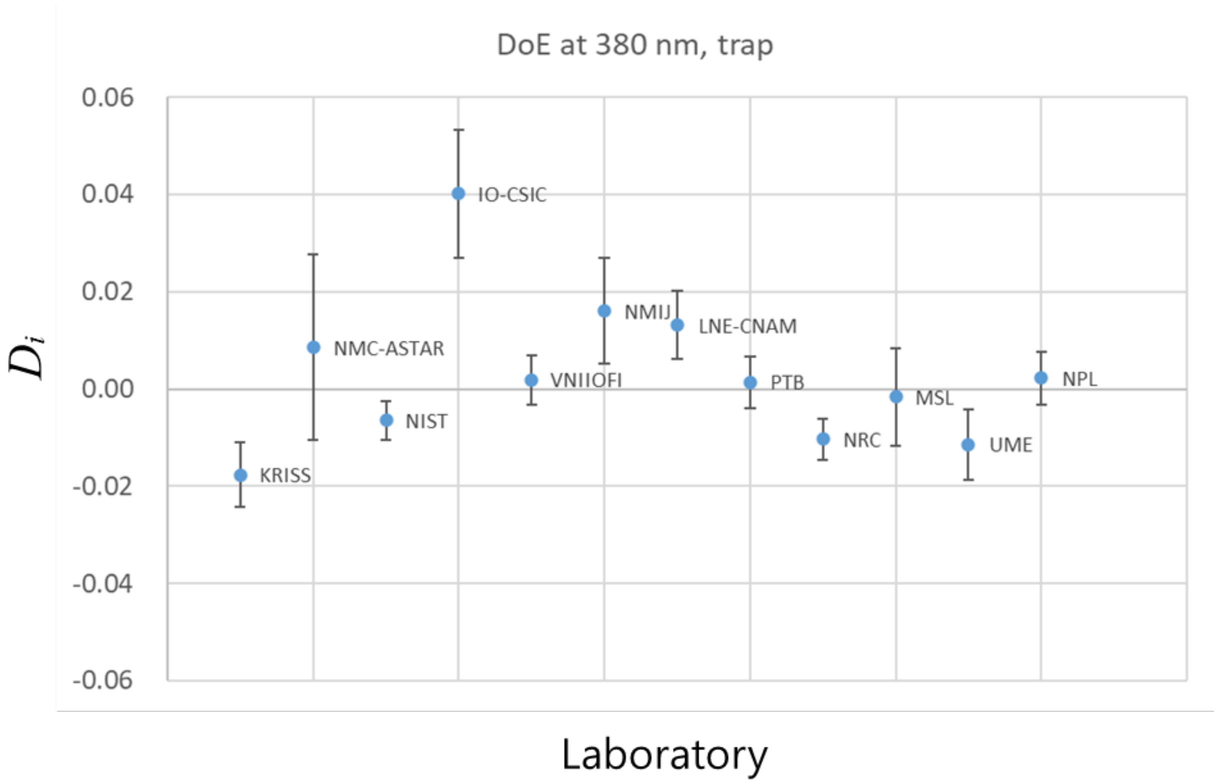


**Figure 7-5.** Results of the degree of equivalence (DoE) of all the participants at a wavelength of 380 nm for the single-element detectors (top) and the trap detectors (bottom). The error bars indicate the expanded uncertainties of DoEs ($k = 2$).

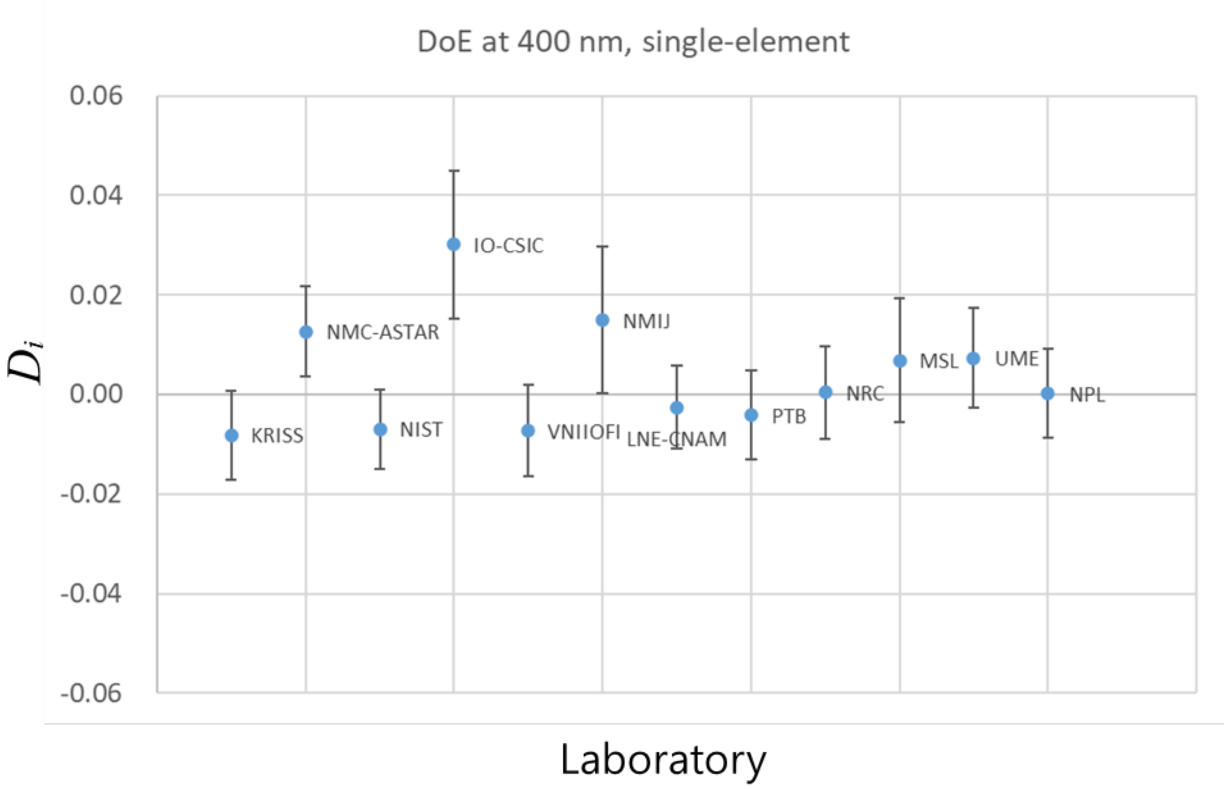


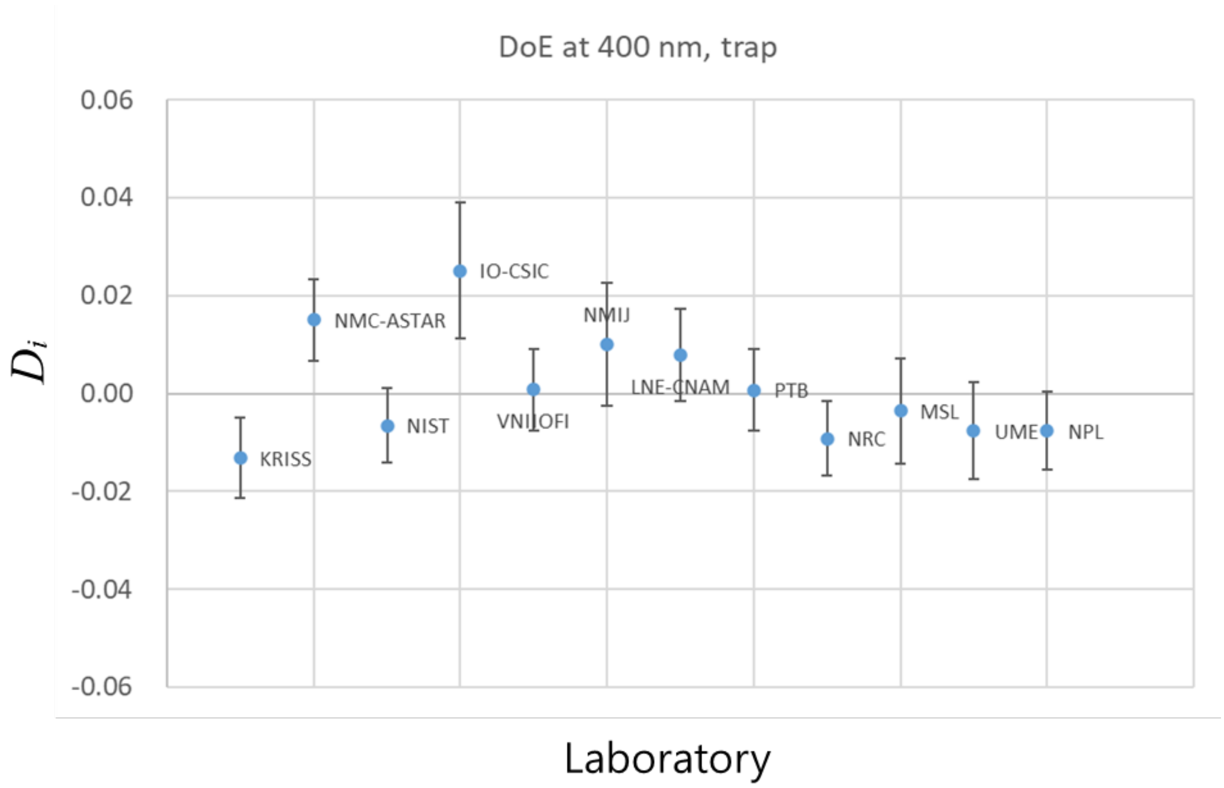


**Figure 7-6.** Results of the degree of equivalence (DoE) of all the participants at a wavelength of 400 nm for the single-element detectors (top) and the trap detectors (bottom). The error bars indicate the expanded uncertainties of DoEs ($k = 2$).

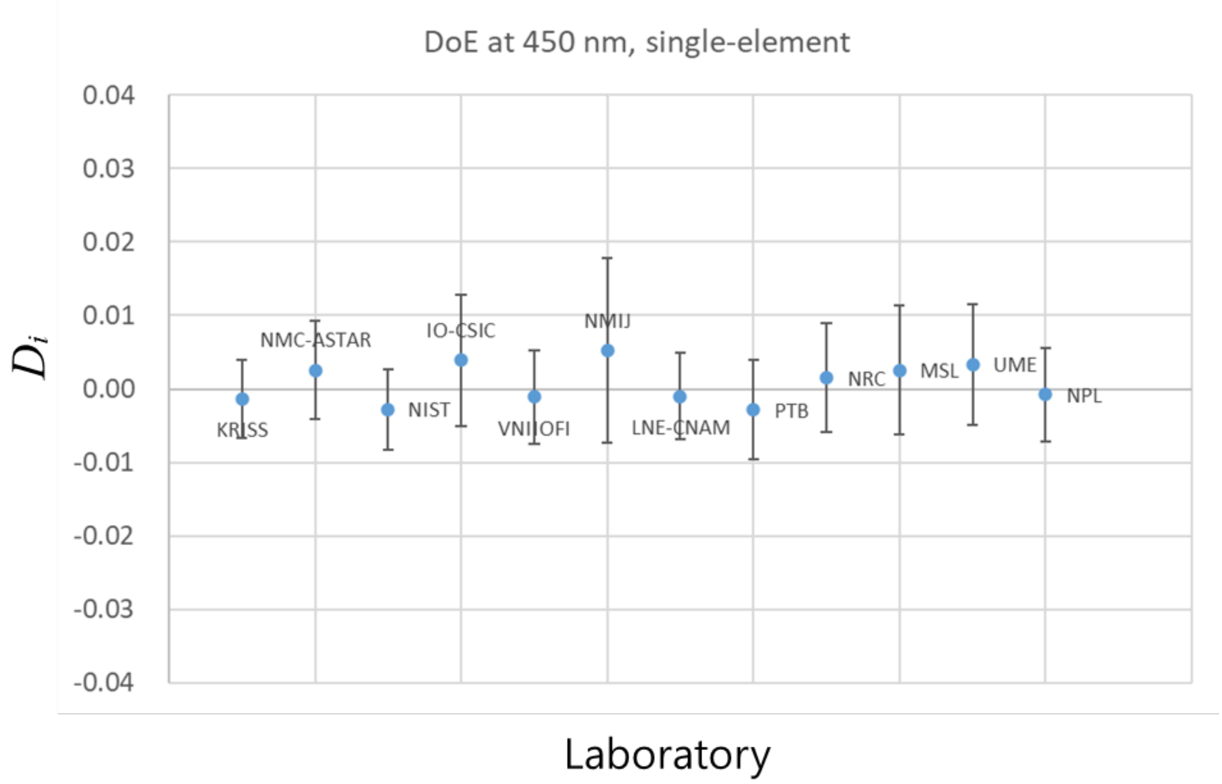


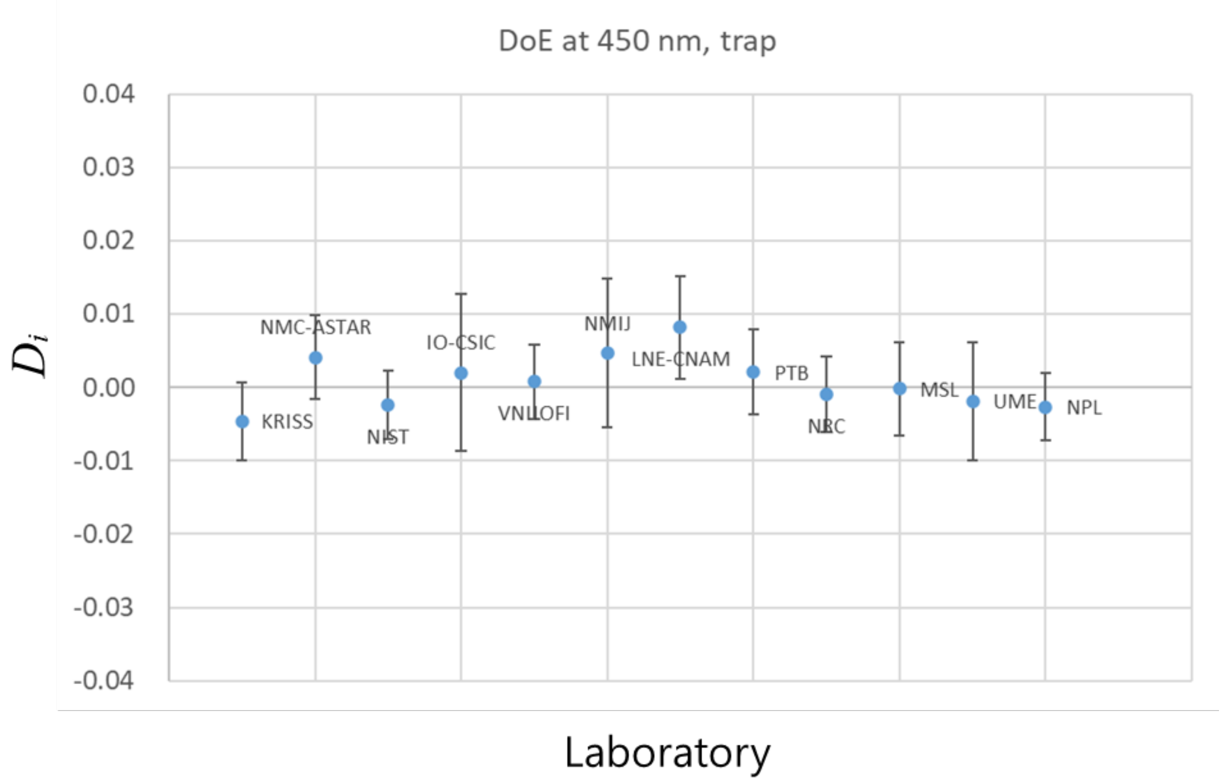


**Figure 7-7.** Results of the degree of equivalence (DoE) of all the participants at a wavelength of 450 nm for the single-element detectors (top) and the trap detectors (bottom). The error bars indicate the expanded uncertainties of DoEs ($k = 2$).

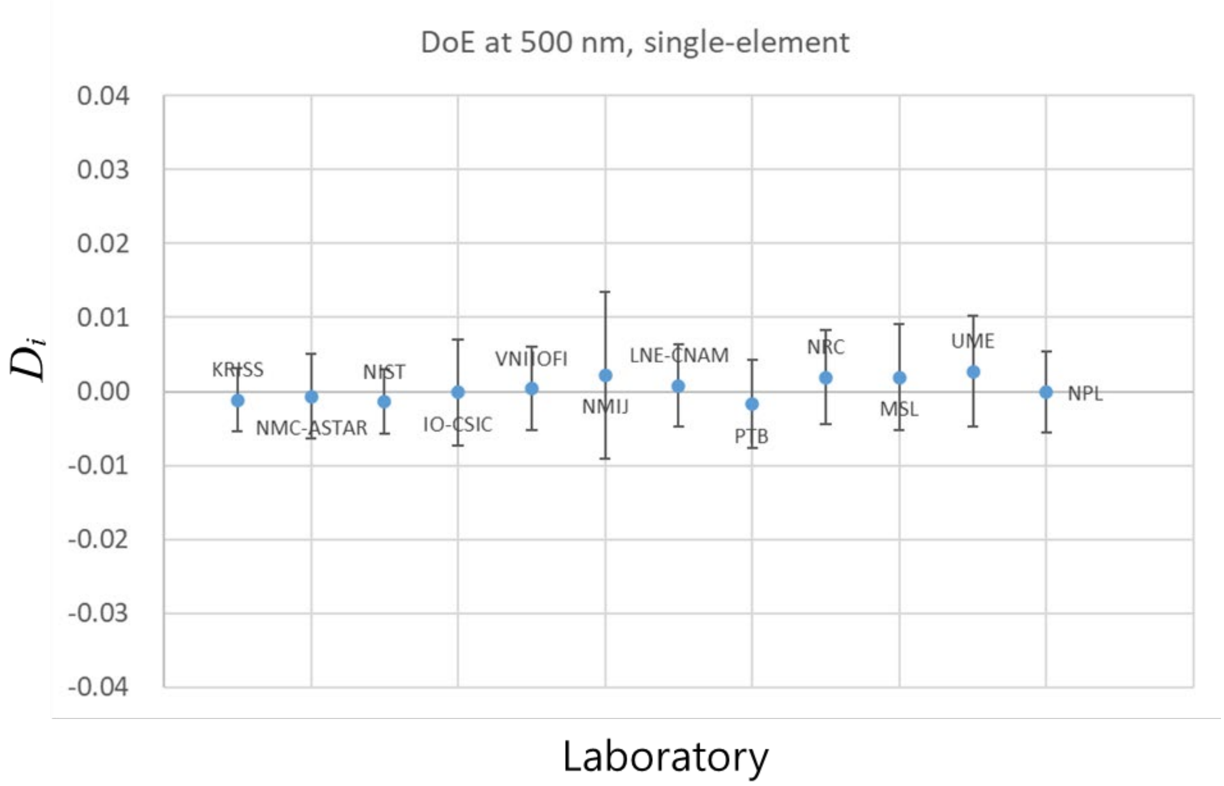


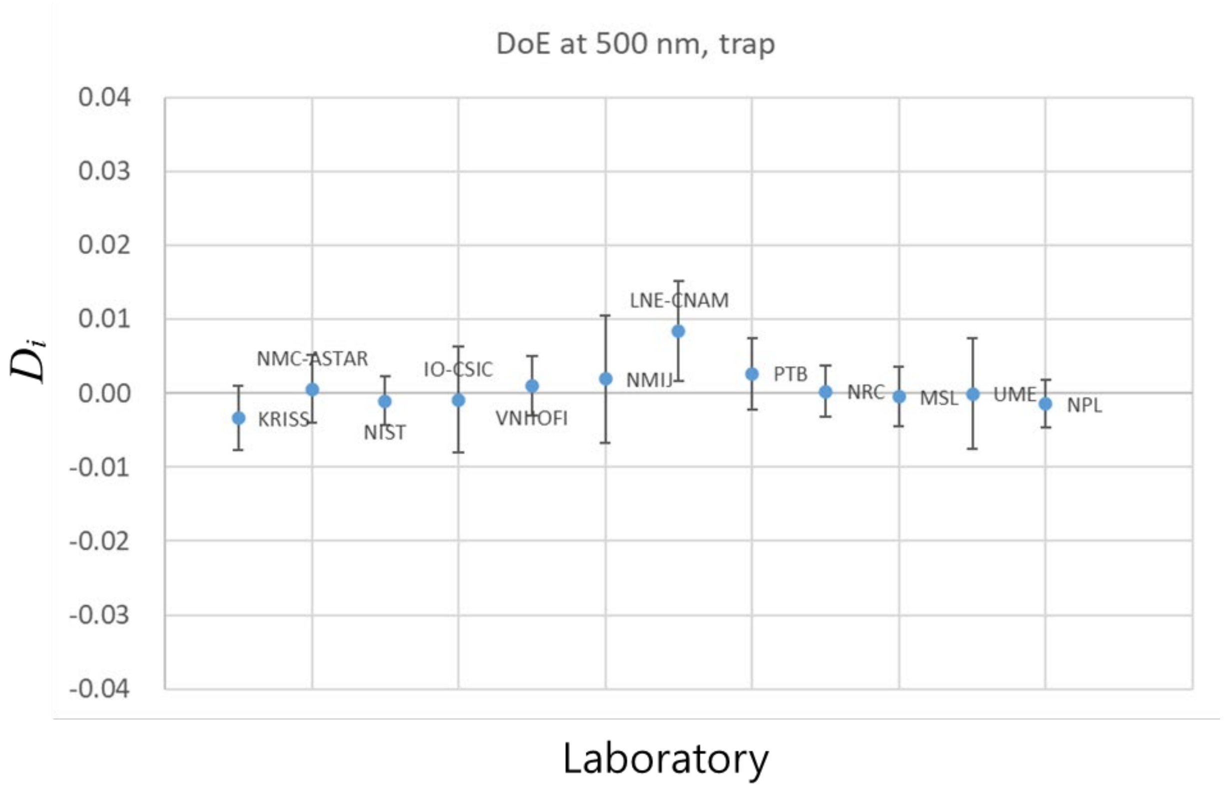


**Figure 7-8.** Results of the degree of equivalence (DoE) of all the participants at a wavelength of 500 nm for the single-element detectors (top) and the trap detectors (bottom). The error bars indicate the expanded uncertainties of DoEs ($k$ = 2).

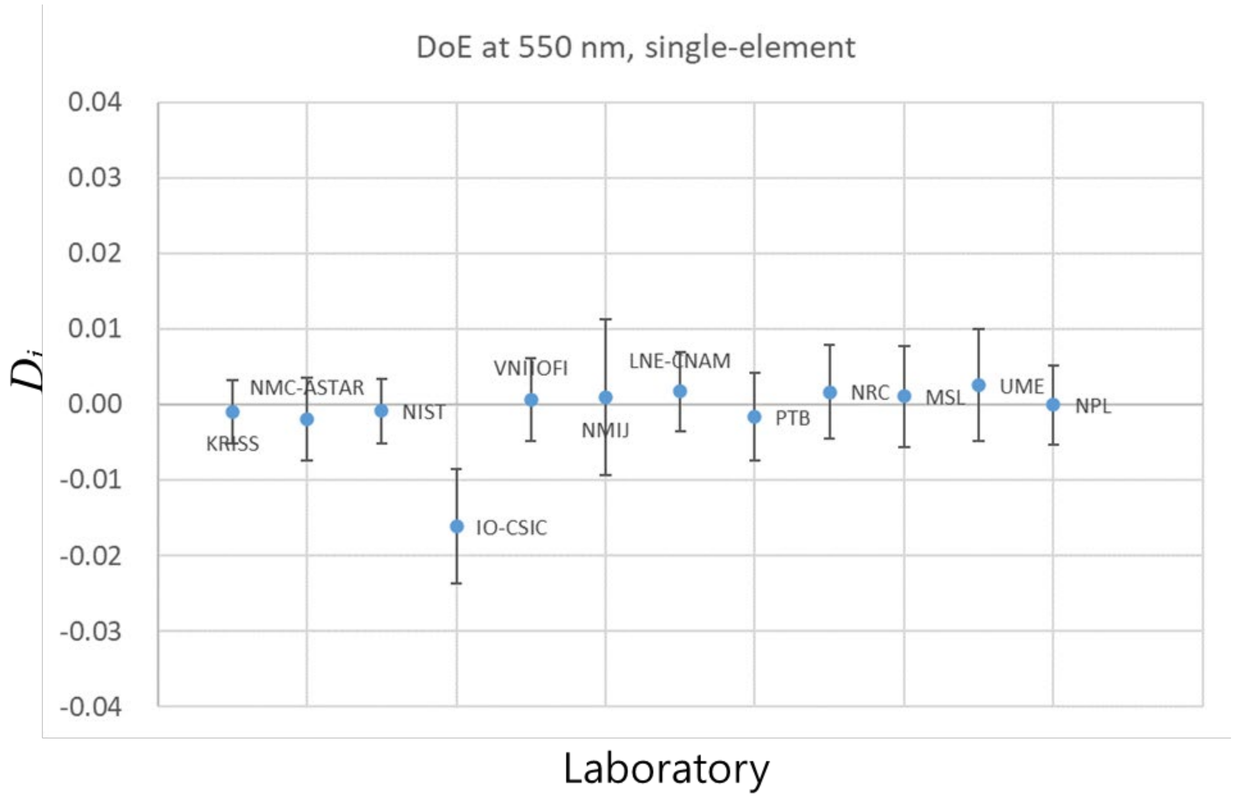


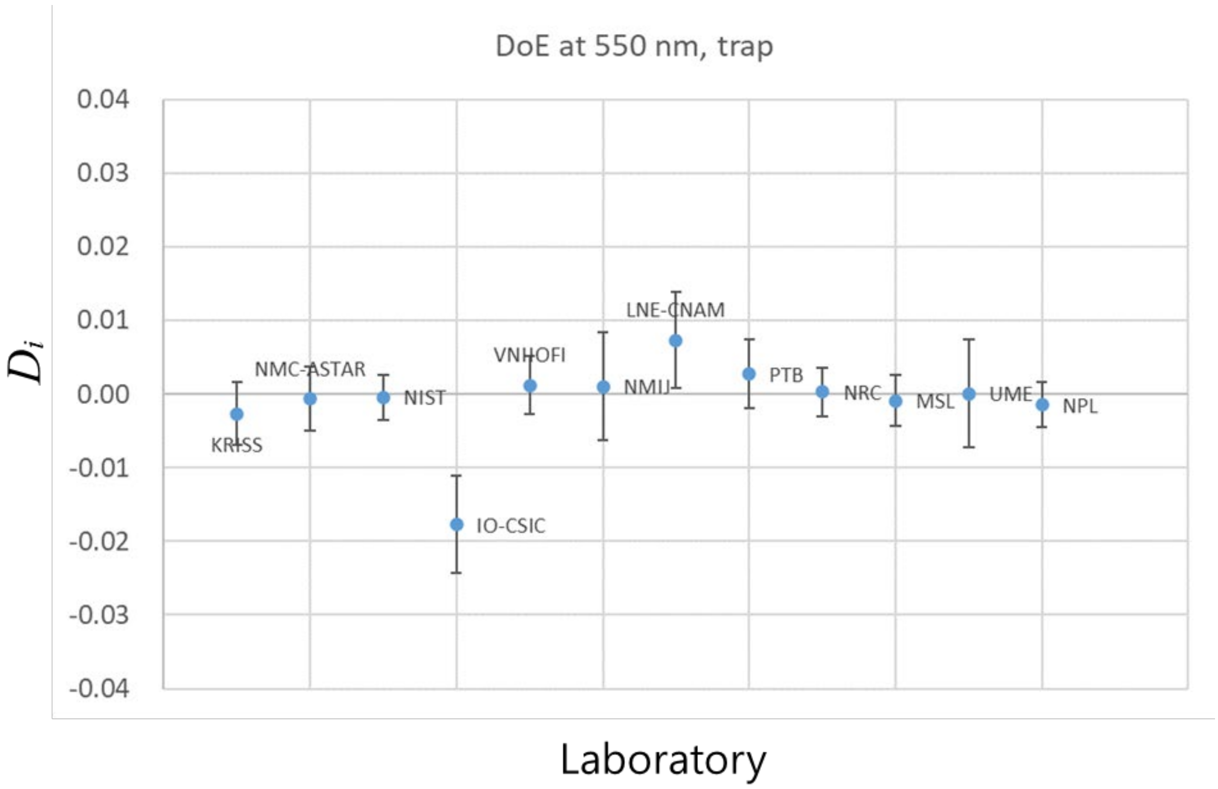


**Figure 7-9.** Results of the degree of equivalence (DoE) of all the participants at a wavelength of 550 nm for the single-element detectors (top) and the trap detectors (bottom). The error bars indicate the expanded uncertainties of DoEs ($k$ = 2).

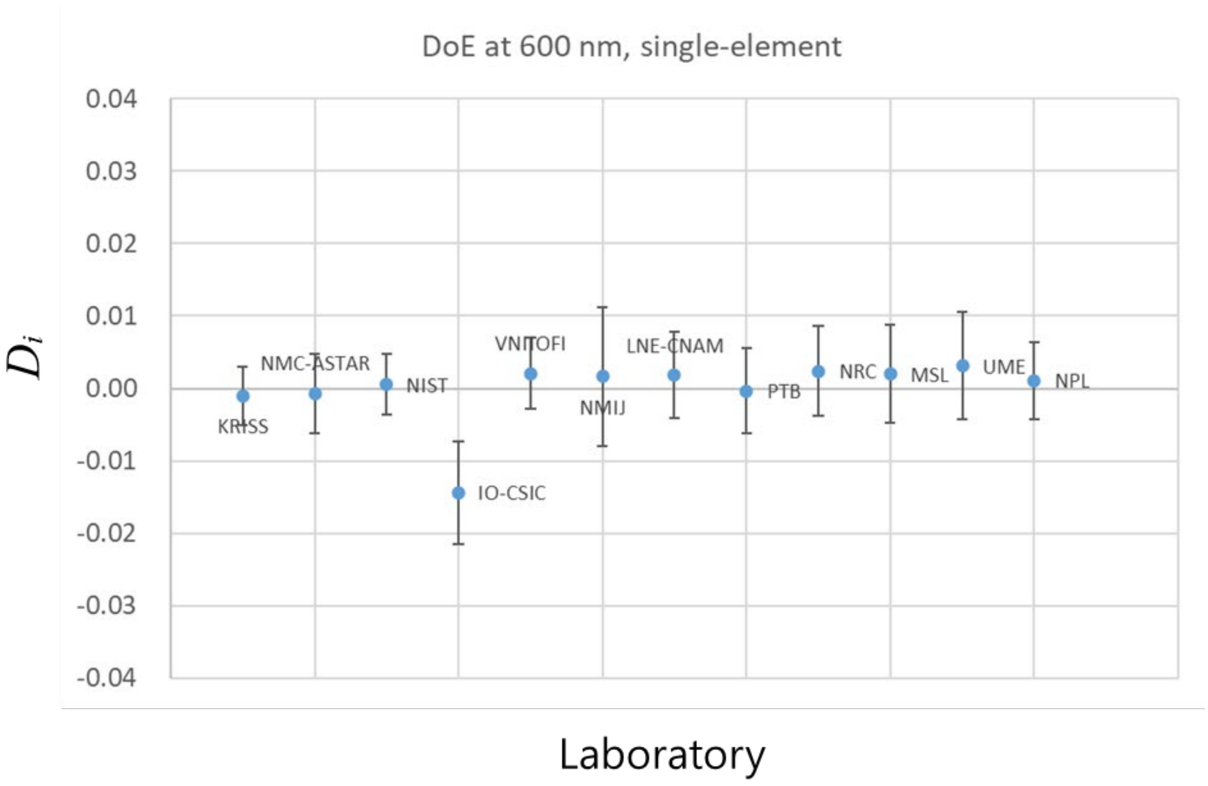


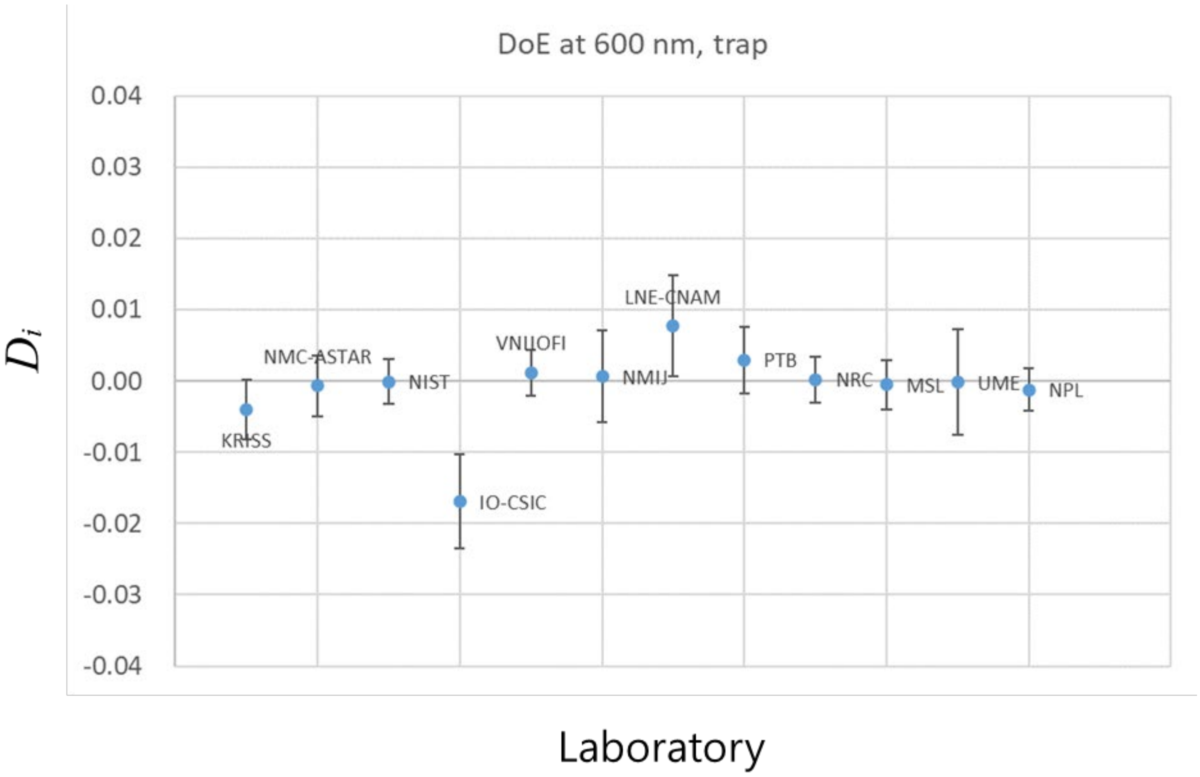


**Figure 7-10.** Results of the degree of equivalence (DoE) of all the participants at a wavelength of 600 nm for the single-element detectors (top) and the trap detectors (bottom). The error bars indicate the expanded uncertainties of DoEs ($k$ = 2).

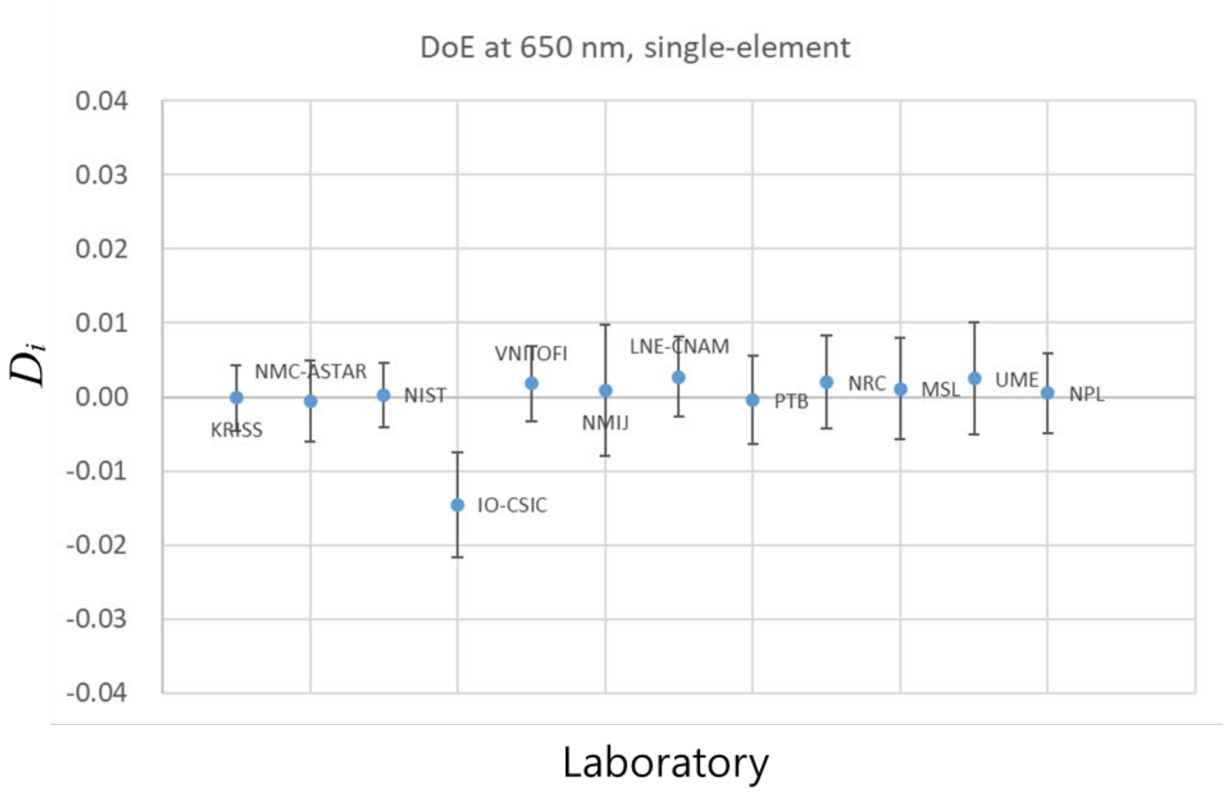


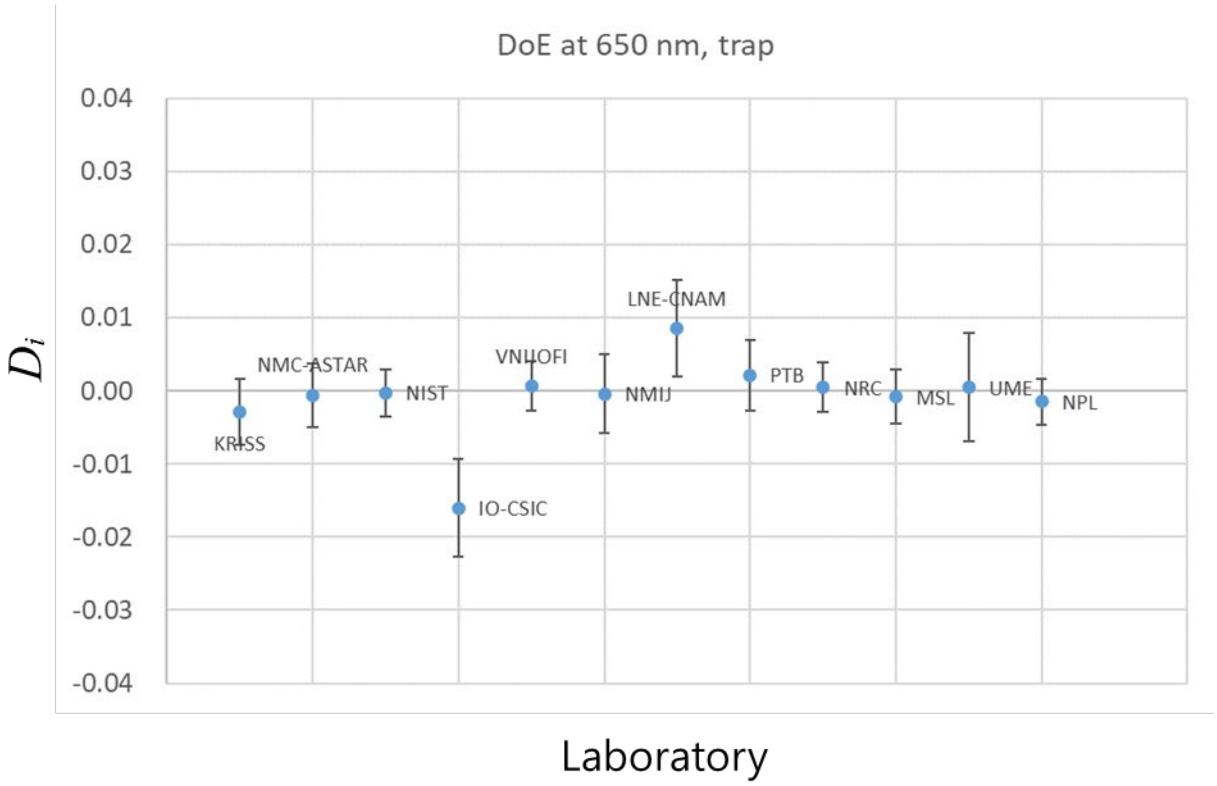


**Figure 7-11.** Results of the degree of equivalence (DoE) of all the participants at a wavelength of 650 nm for the single-element detectors (top) and the trap detectors (bottom). The error bars indicate the expanded uncertainties of DoEs ($k = 2$).

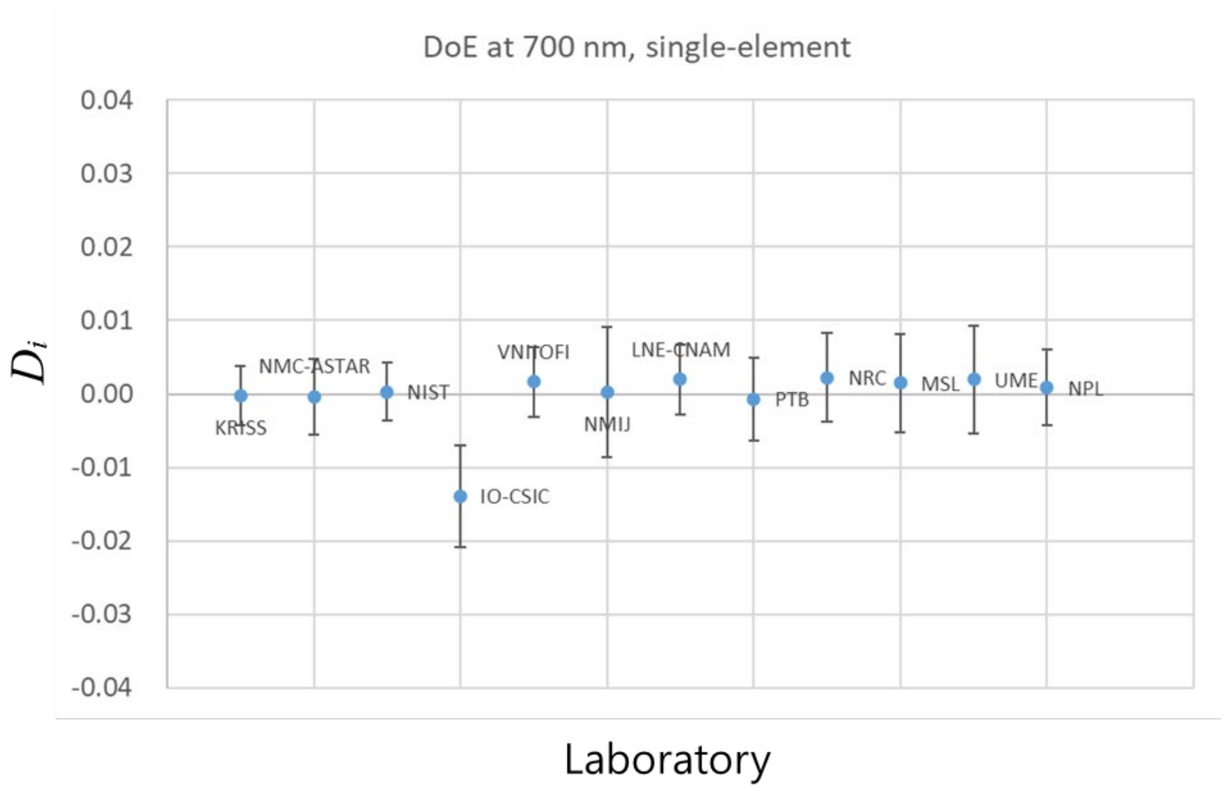


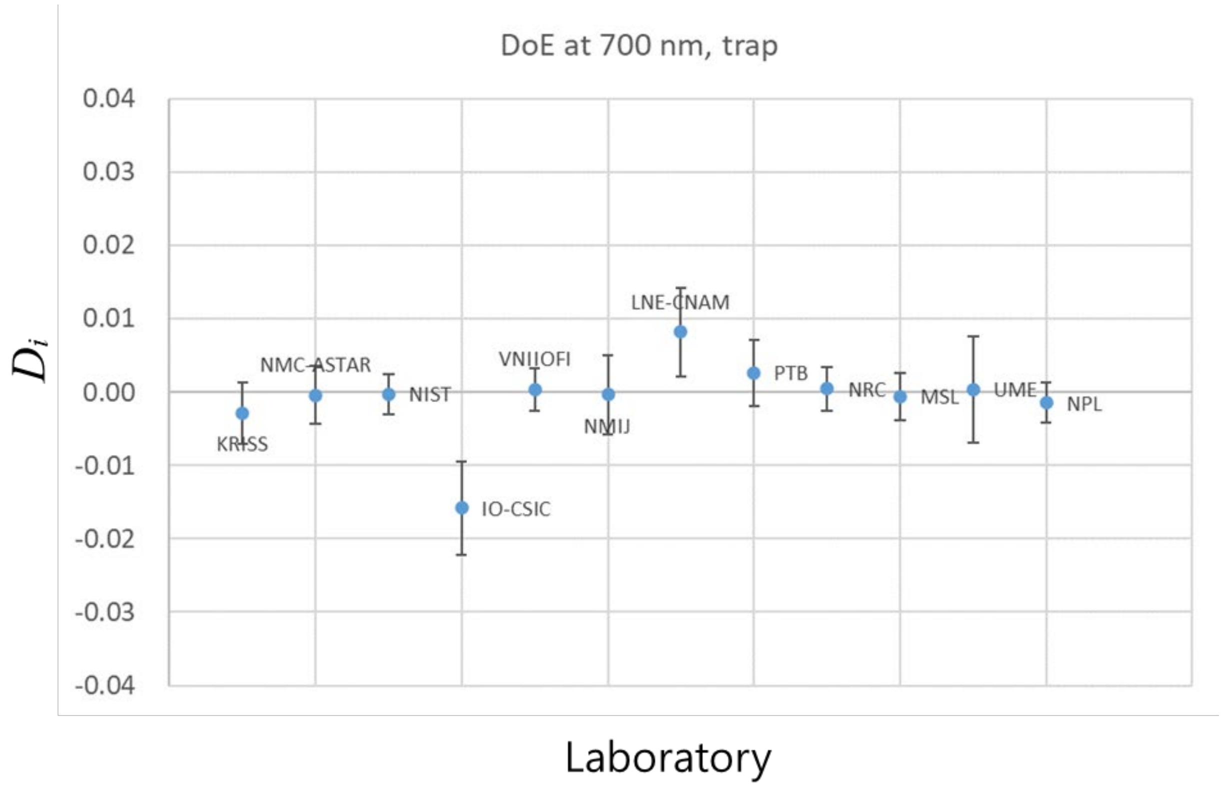


**Figure 7-12.** Results of the degree of equivalence (DoE) of all the participants at a wavelength of 700 nm for the single-element detectors (top) and the trap detectors (bottom). The error bars indicate the expanded uncertainties of DoEs ($k$ = 2).

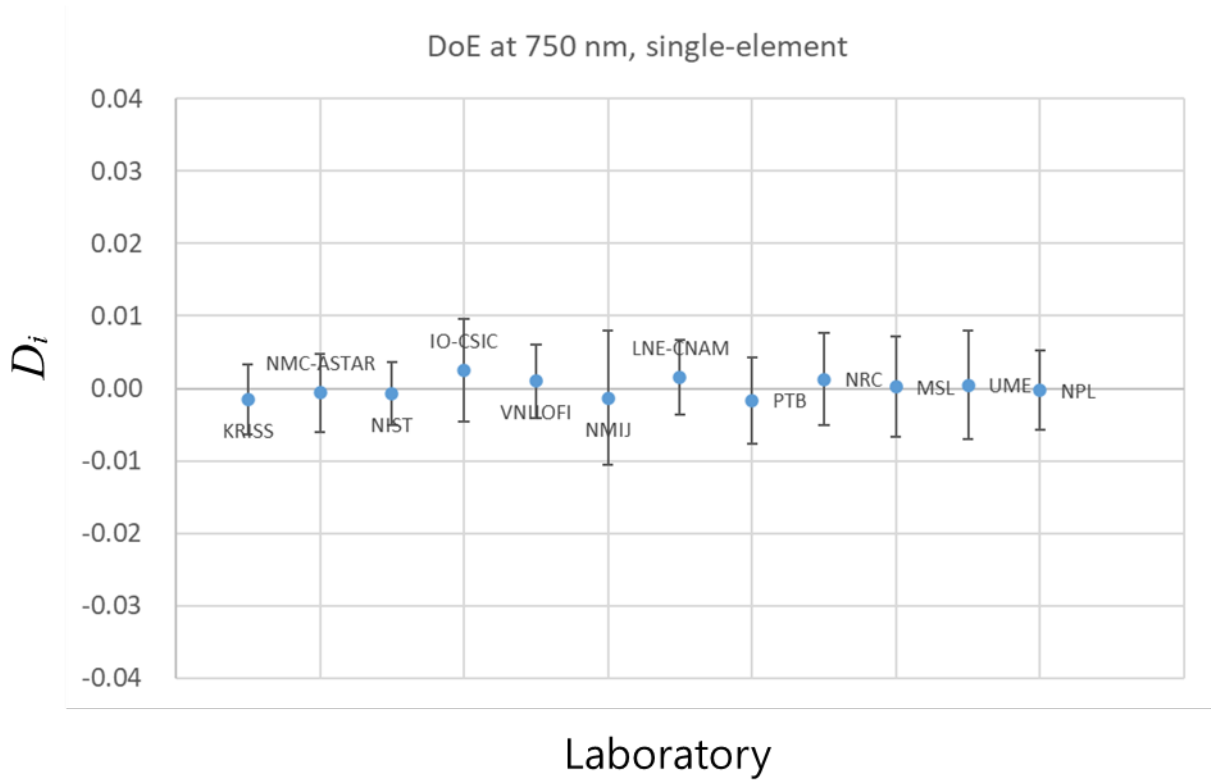


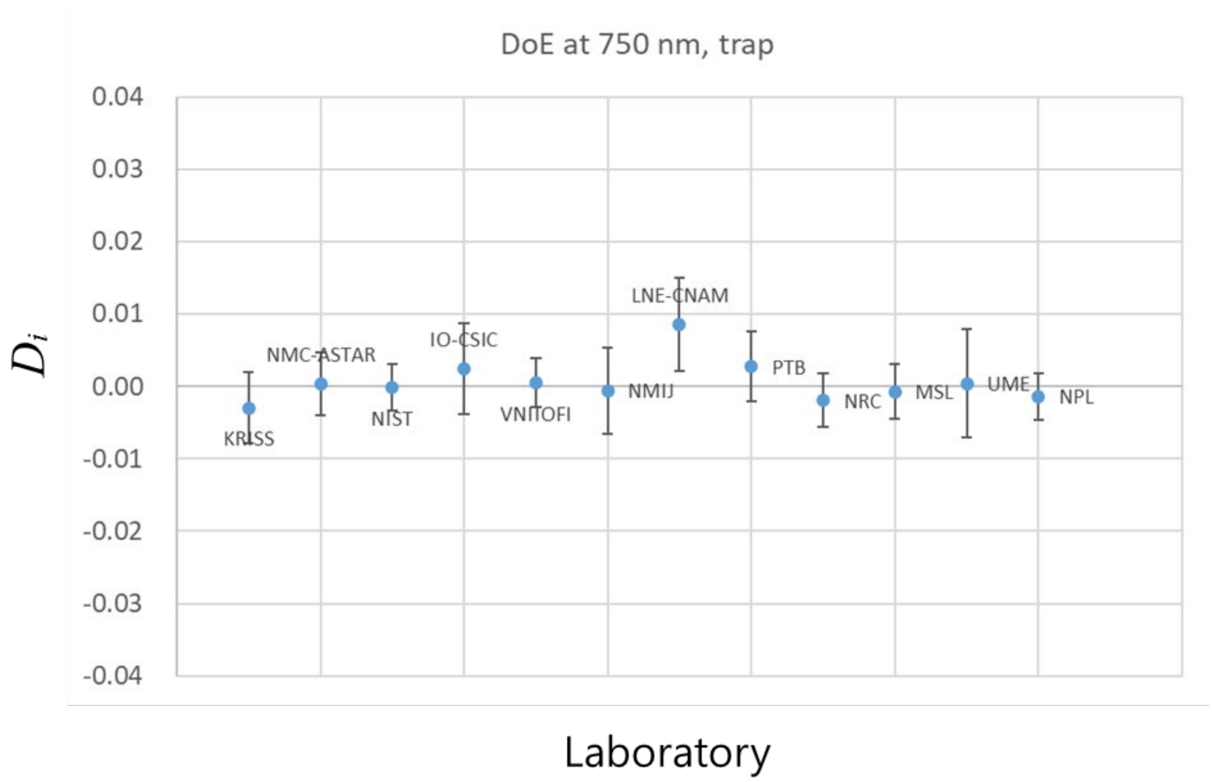


**Figure 7-13.** Results of the degree of equivalence (DoE) of all the participants at a wavelength of 750 nm for the single-element detectors (top) and the trap detectors (bottom). The error bars indicate the expanded uncertainties of DoEs ($k$ = 2).

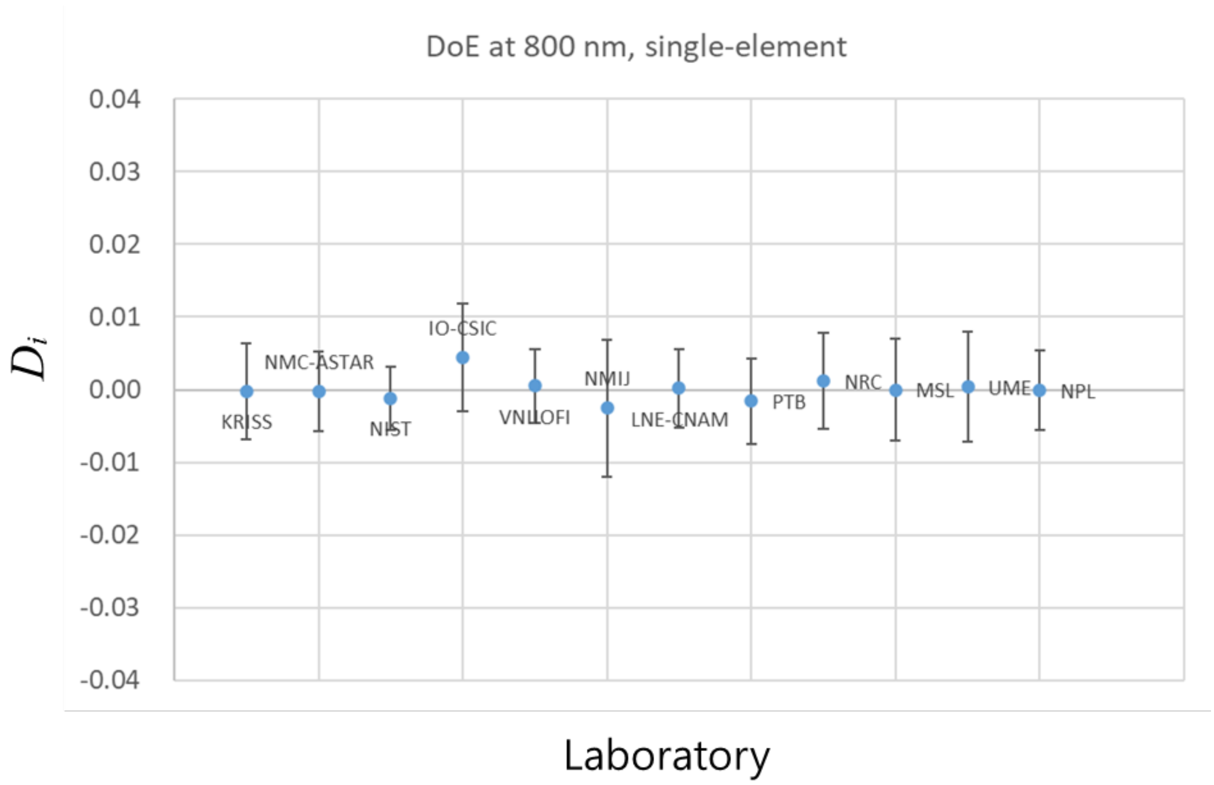


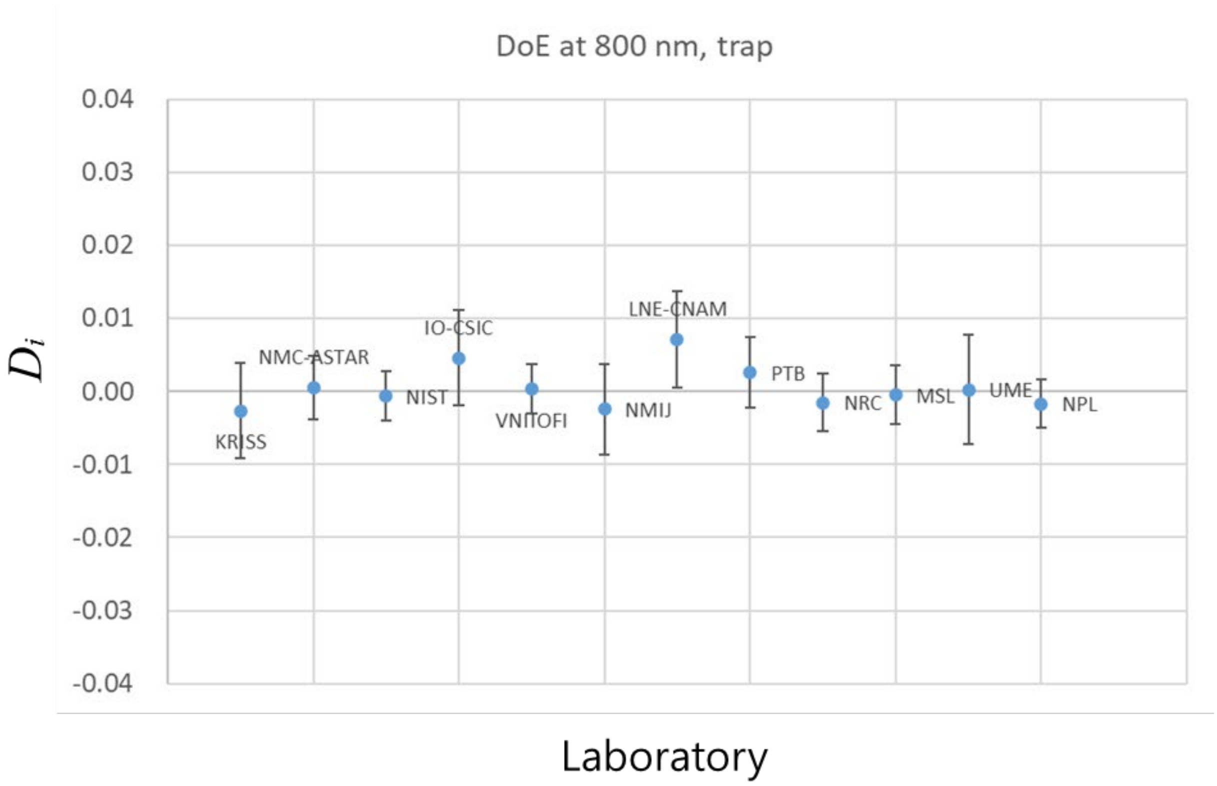


**Figure 7-14.** Results of the degree of equivalence (DoE) of all the participants at a wavelength of 800 nm for the single-element detectors (top) and the trap detectors (bottom). The error bars indicate the expanded uncertainties of DoEs ($k = 2$).

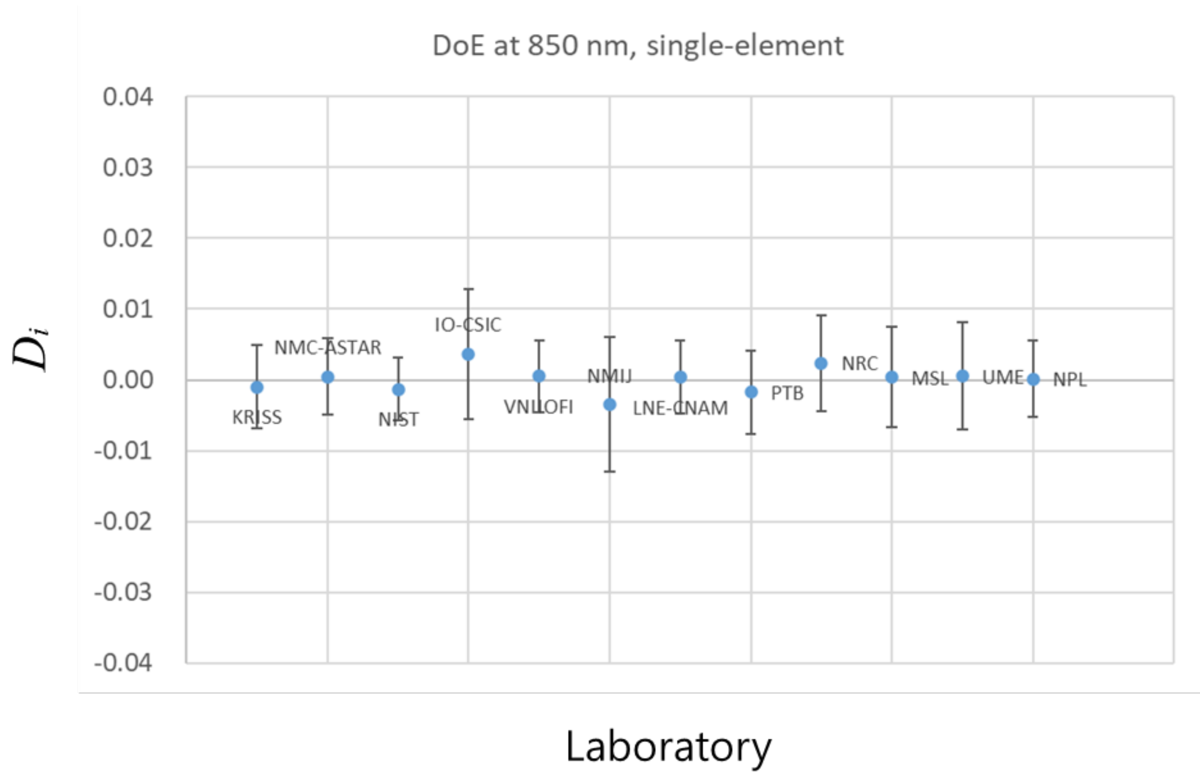


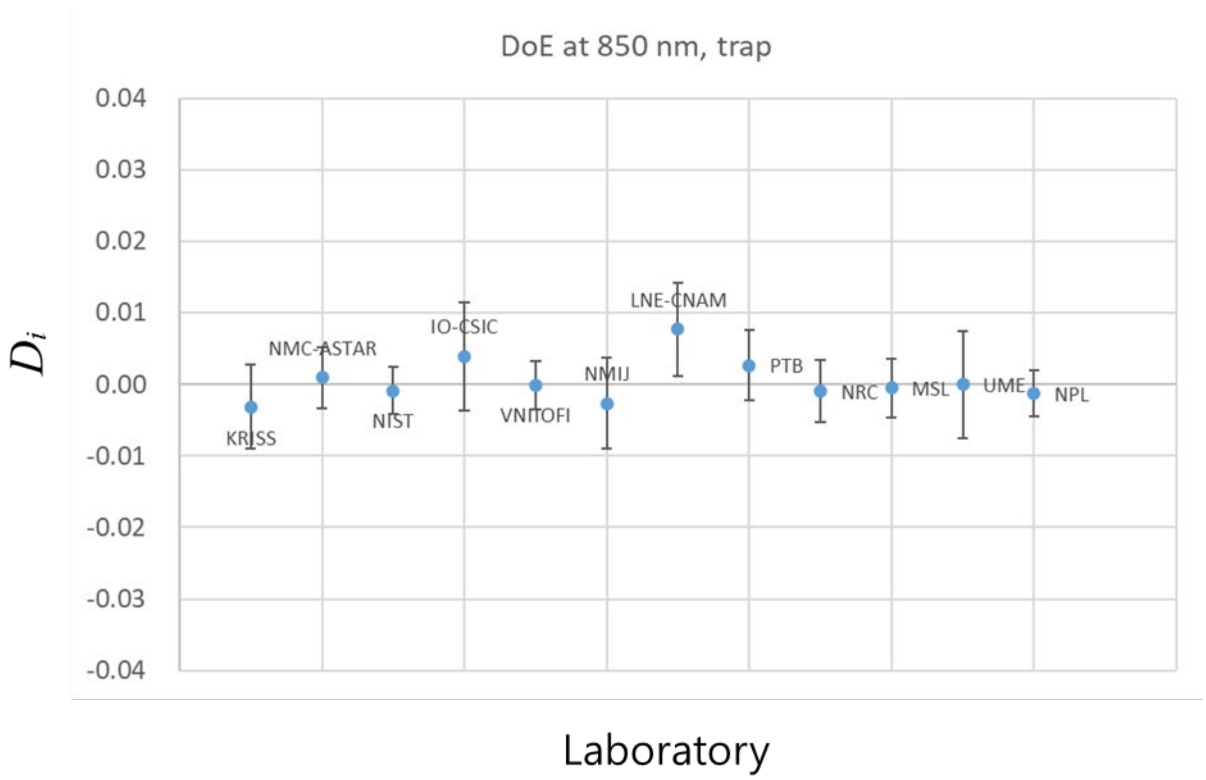


**Figure 7-15.** Results of the degree of equivalence (DoE) of all the participants at a wavelength of 850 nm for the single-element detectors (top) and the trap detectors (bottom). The error bars indicate the expanded uncertainties of DoEs ($k = 2$).

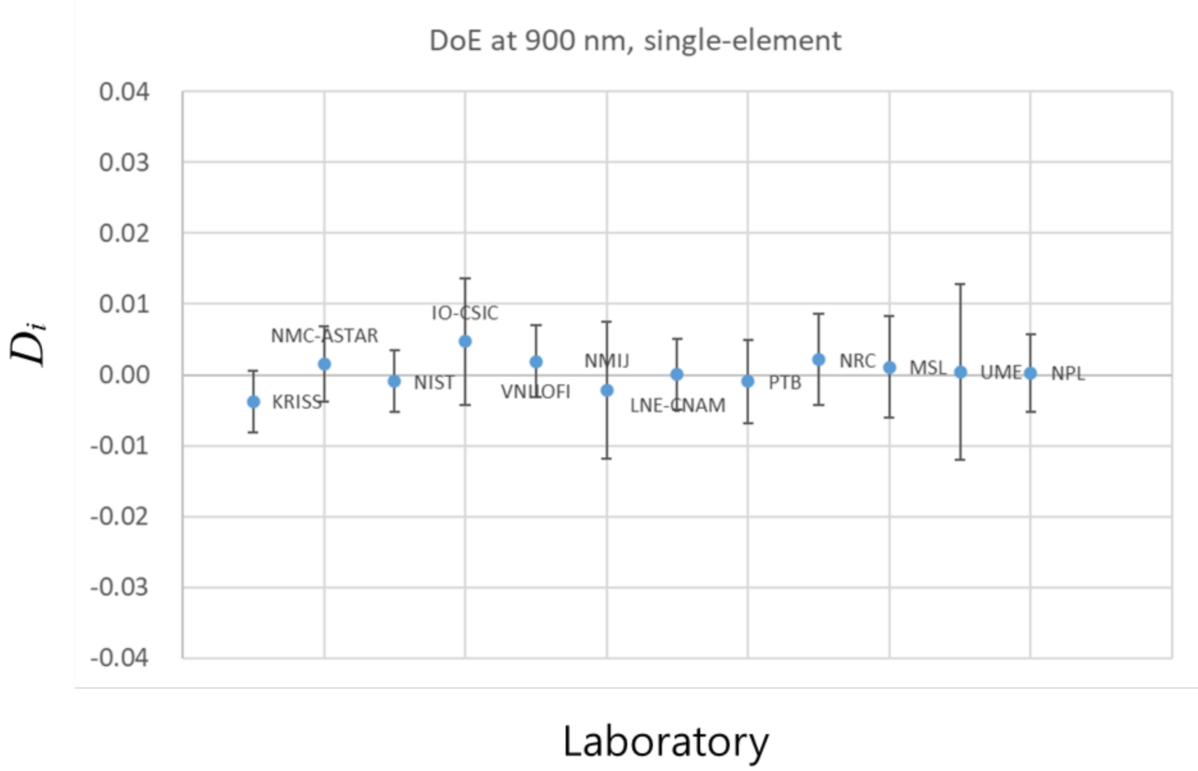


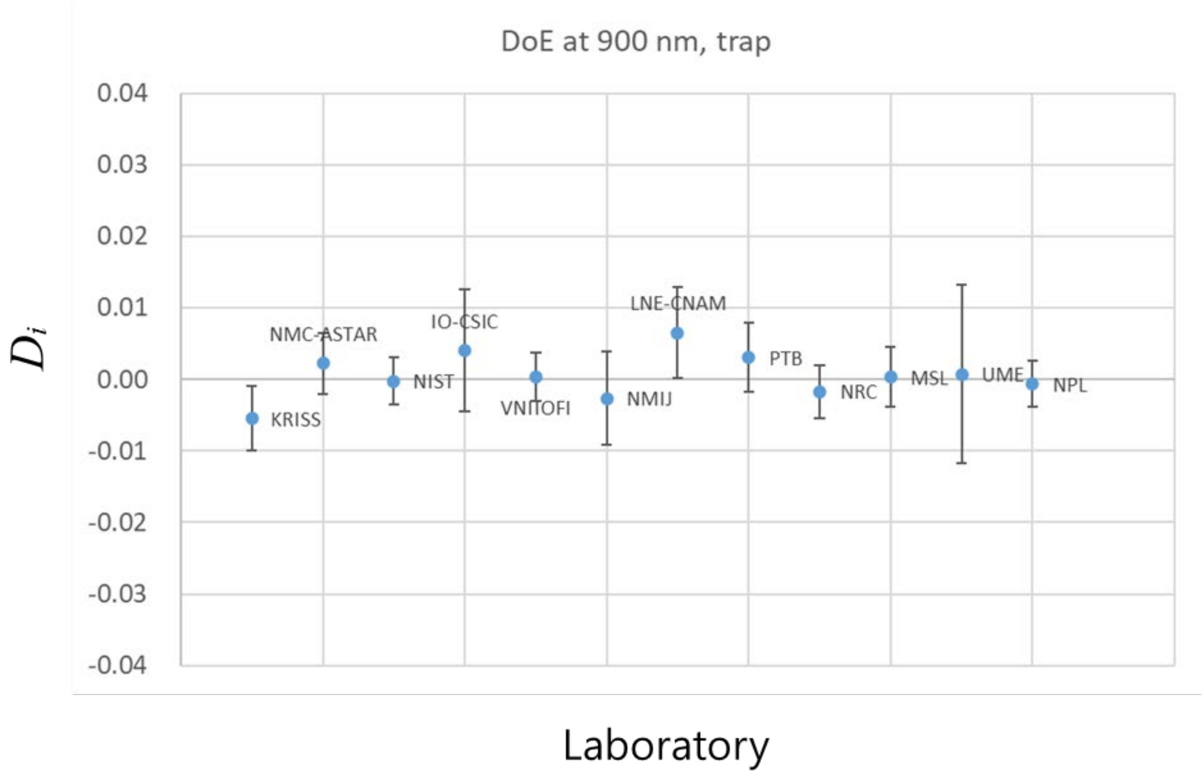


**Figure 7-16.** Results of the degree of equivalence (DoE) of all the participants at a wavelength of 900 nm for the single-element detectors (top) and the trap detectors (bottom). The error bars indicate the expanded uncertainties of DoEs ($k$ = 2).

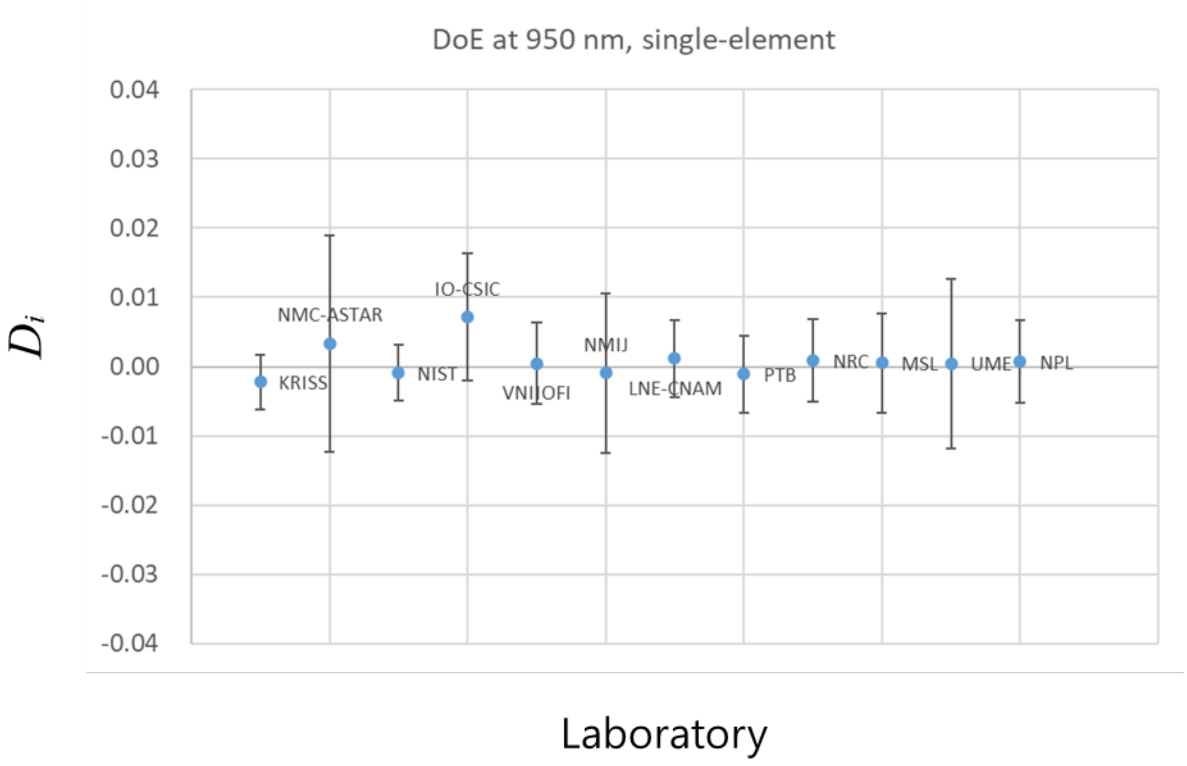


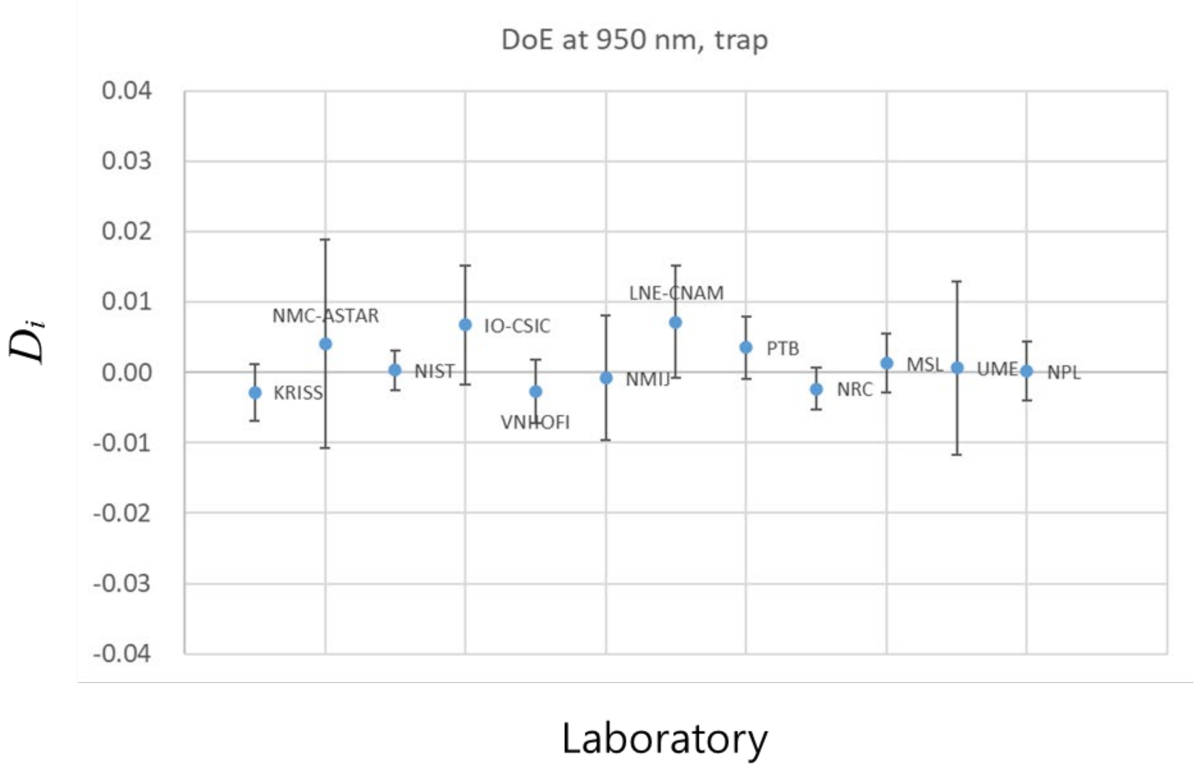


**Figure 7-17.** Results of the degree of equivalence (DoE) of all the participants at a wavelength of 950 nm for the single-element detectors (top) and the trap detectors (bottom). The error bars indicate the expanded uncertainties of DoEs ($k = 2$).

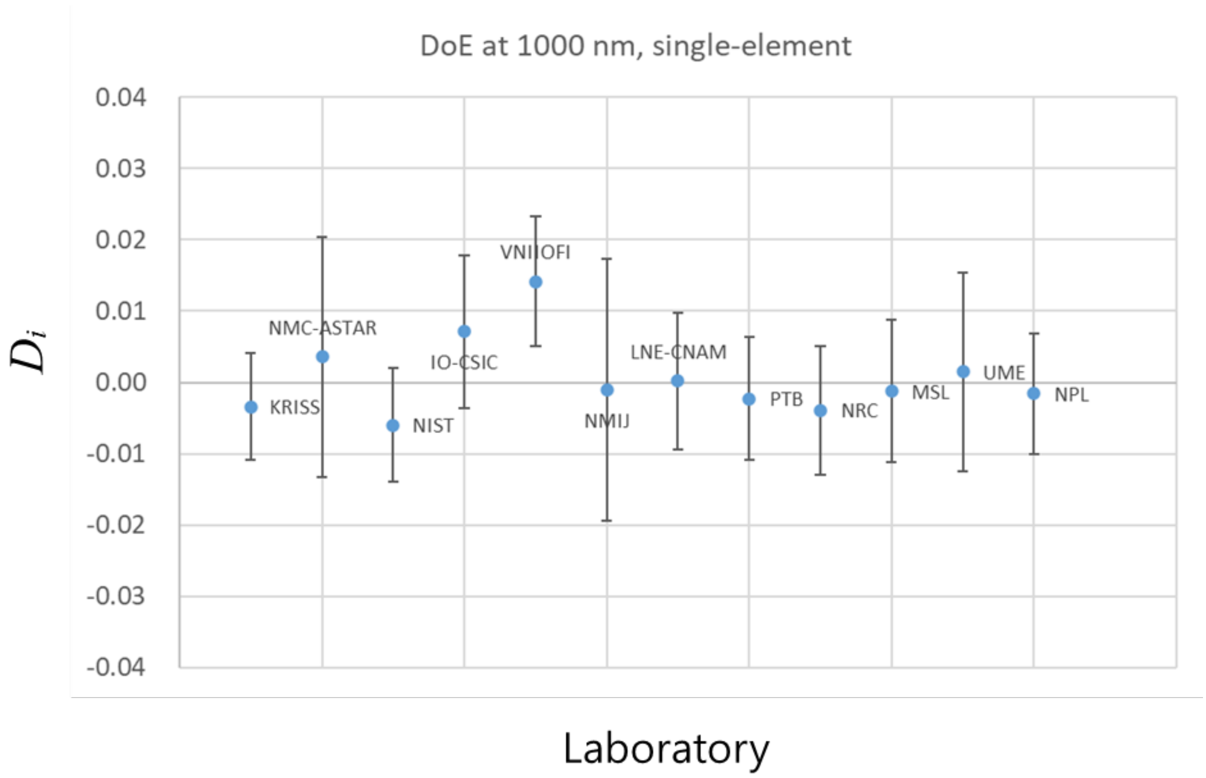


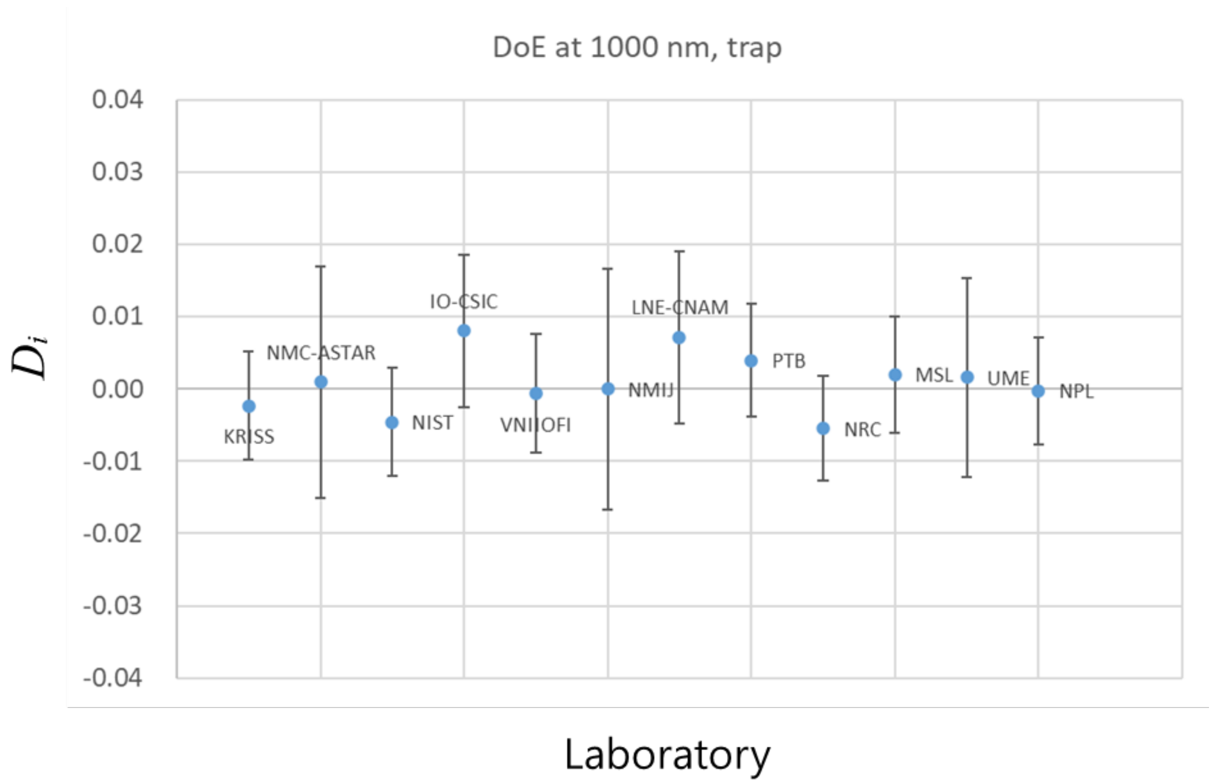


**Figure 7-18.** Results of the degree of equivalence (DoE) of all the participants at a wavelength of 1000 nm for the single-element detectors (top) and the trap detectors (bottom). The error bars indicate the expanded uncertainties of DoEs ($k = 2$). Temperature correction is not applied.

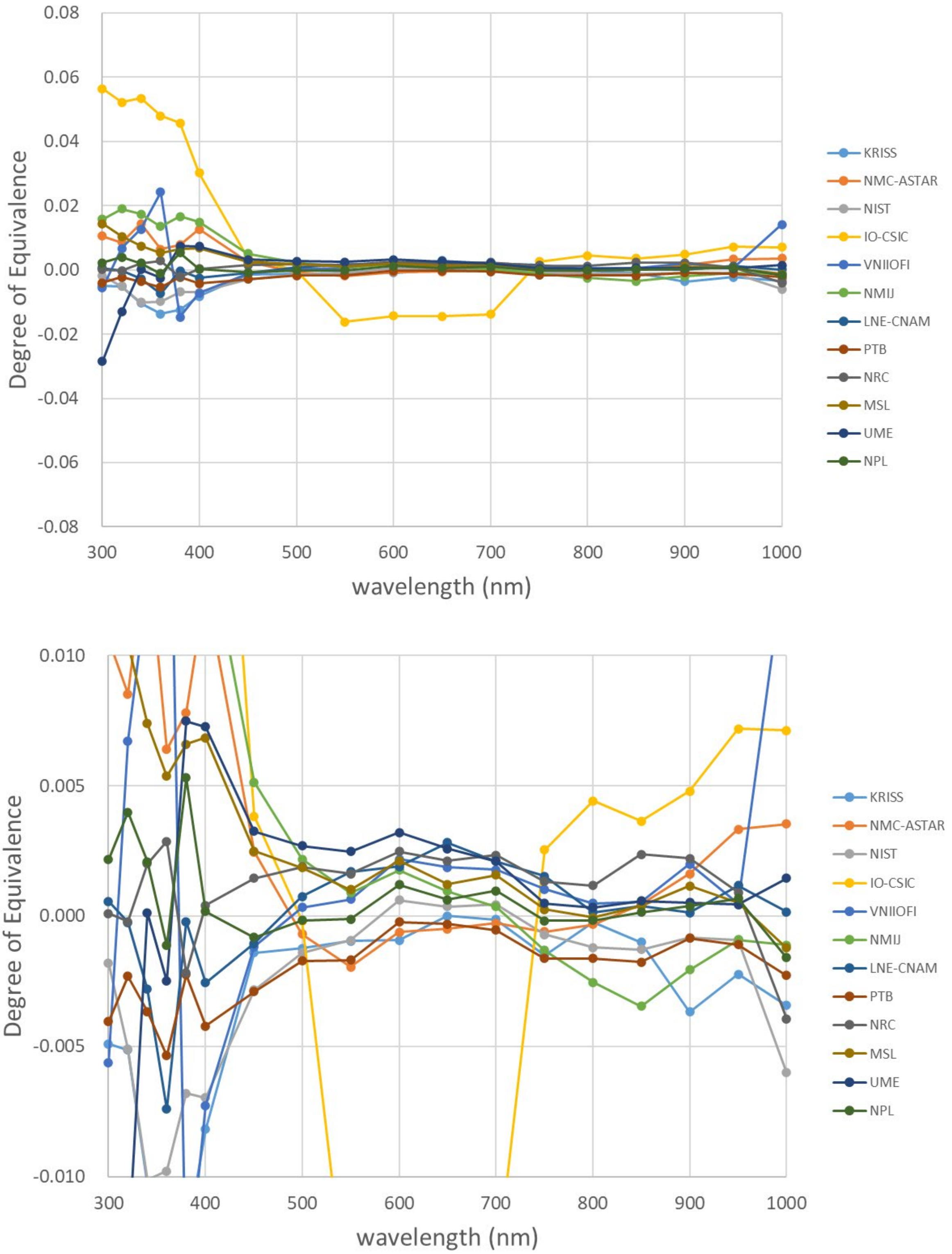


**Figure 7-19.** Values of degree of equivalence (DoE) of all the participants as a function of wavelength for the single-element detectors. One colour for the symbols and connecting lines is assigned to one participant. Two plots in the top and bottom have different scales in the Y-axis.

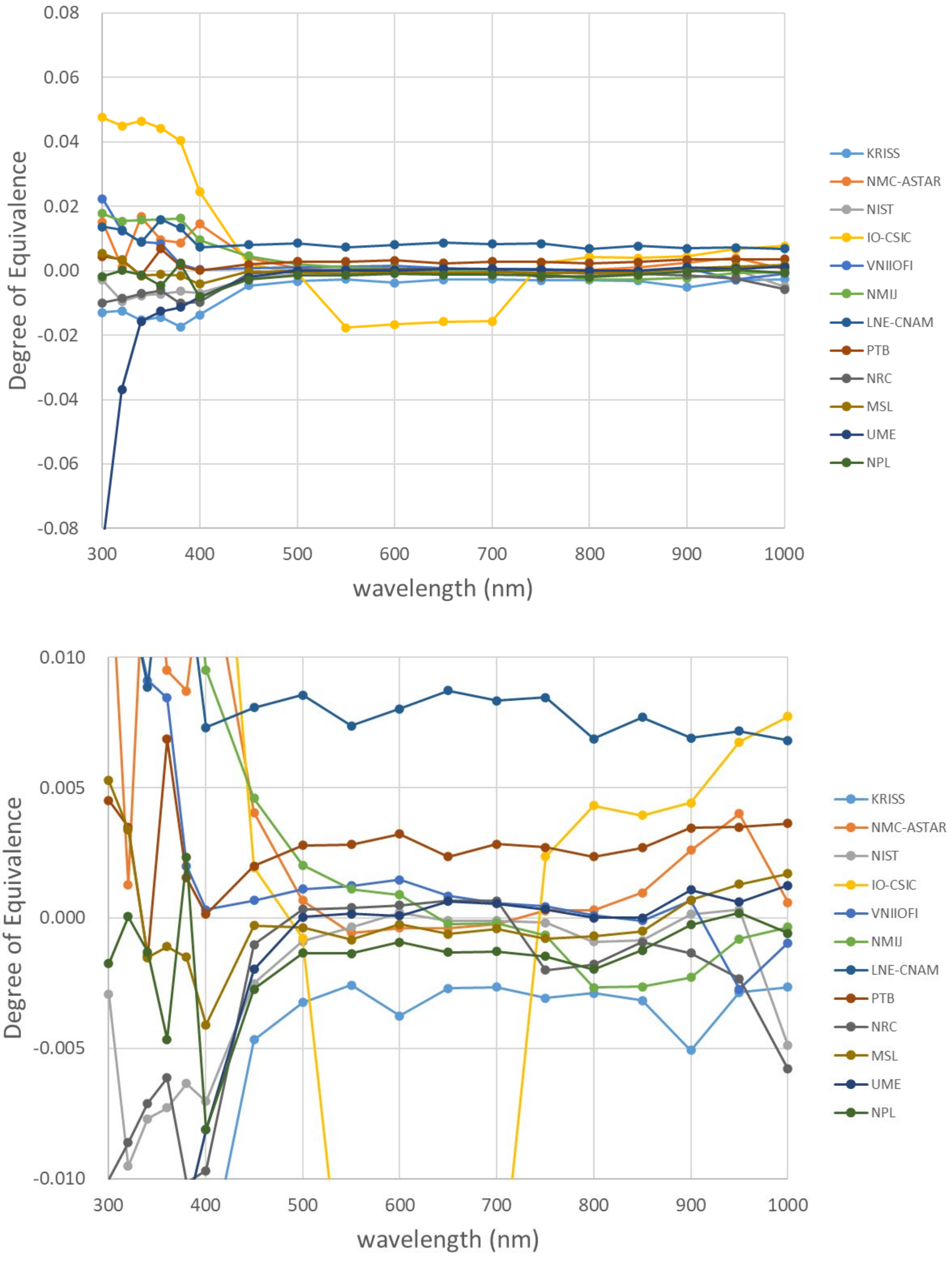


**Figure 7-20.** Values of degree of equivalence (DoE) of all the participants as a function of wavelength for the trap detectors. One colour for the symbols and connecting lines is assigned to one participant. Two plots in the top and bottom have different scales in the Y-axis.

# 8. Summary and Discussion

The comparison resulted in a consistent result in the visible wavelength range, while the consistency was poor in the short wavelength range below 450 nm. Outliers were identified with a criterion of DoE/$U$(DoE) > 2 from the preliminary results of data analysis and were agreed by all the participants. At several wavelengths, the Mandel Paule factors in a range from 0.2% up to 0.6% had to be introduced as "dark uncertainties" to make the comparison consistent.

The overall equivalence among the participants in the short wavelength range is also worse than in the visible range. Comparing the comparison results for the single-element detectors and trap detectors, the equivalence was in general better for the single-element detector.

The pilot laboratory has monitored the long-term stability of their setup during the whole measurement period and found that the reproducibility in the short wavelength range below 450 nm was very poor. In the visible range, the long-term reproducibility uncertainty of the pilot was around 0.2 % ($k$ = 2), while this exceeded 1% at several wavelengths below 450 nm. This has an impact to increase the overall uncertainty of the comparison as the reproducibility uncertainty of the pilot had to be added to the uncertainty of all the transfer detectors. The real stability or drift of the detectors could not be accurately evaluated due to the limited reproducibility of the pilot. After the completion of the measurement period, the pilot started to investigate the origin of the poor reproducibility and found that the trap detector used as the working standard for spectral responsivity has a significant wavelength-dependent non-uniformity. This means that the variation of the properties such as beam size, divergence, and direction of the monochromatic beam should be characterized as a function of wavelength. Considering that a trap detector is used in many other laboratories as a working standard for spectral responsivity, this could be also a possible origin of the stronger divergence of the DoEs in this comparison in the short wavelength range, especially for the trap detectors. More studies are encouraged to this issue.

The stability test performed in the pre-draft A process by NIST confirmed that the intrinsic stability of the most of the transfer detectors was better than 0.1% between 2017 and 2021. The spatial uniformity and its stability were also tested by NIST at different wavelengths. A change of spatial uniformity with wavelength was also confirmed in this test.

The temperature was monitored by using a PT100 sensor attached to each detector. Most of the participants reported the PT100 reading values close to 109 Ω. A temperature correction was not applied as the accuracy of the temperature coefficient was limited by the reproducibility uncertainty of the pilot. From the results, the impact of the temperature correction was also expected to be small in this comparison.

In conclusion, the following points should be improved in the next round comparison for spectral responsivity from 300 nm to 1000 nm.

- The long-term reproducibility of the pilot laboratory should be experimentally confirmed before starting the comparison.
- The spatial uniformity of the transfer detectors should be measured at different wavelengths and its change should be monitored before and after each measurement.
- The orientation of the detectors in the mounting should be specified to minimize the influence of the spatial non-uniformity.
- For trap detectors, the beam alignment method should be specified more precisely.

# References

[1] CCPR of CIPM, "Guidelines for CCPR Key comparison Report Preparation, CCPR-G2 Rev. 4," 2019.

# CCPR-K2.b.2016

# Spectral Responsivity 300 nm to 1000 nm

# Final Report

# Appendix A

# Degree of Equivalence for Each Participant

# 1. KRISS

**Table A-1.** Values of the degree of equivalence (DoE) and their expanded uncertainties ($k$ = 2) for the participant KRISS.

| wavelength | single-element detectors | | | trap detectors | | |
|---|---|---|---|---|---|---|
| | DoE | *U*(DoE) | DoE/*U*(DoE) | DoE | *U*(DoE) | DoE/*U*(DoE) |
| 300 nm | -0.0049 | 0.0080 | -0.607 | -0.0132 | 0.0083 | -1.588 |
| 320 nm | -0.0051 | 0.0078 | -0.645 | -0.0127 | 0.0078 | -1.635 |
| 340 nm | -0.0103 | 0.0063 | -1.635 | -0.0151 | 0.0076 | -1.972 |
| 360 nm | -0.0137 | 0.0148 | -0.930 | -0.0144 | 0.0144 | -0.997 |
| 380 nm | -0.0123 | 0.0062 | -1.996 | -0.0176 | 0.0067 | -2.640 |
| 400 nm | -0.0082 | 0.0089 | -0.918 | -0.0132 | 0.0082 | -1.610 |
| 450 nm | -0.0013 | 0.0053 | -0.249 | -0.0046 | 0.0053 | -0.862 |
| 500 nm | -0.0012 | 0.0043 | -0.277 | -0.0034 | 0.0044 | -0.770 |
| 550 nm | -0.0009 | 0.0042 | -0.222 | -0.0026 | 0.0043 | -0.613 |
| 600 nm | -0.0010 | 0.0040 | -0.252 | -0.0040 | 0.0042 | -0.969 |
| 650 nm | -0.0001 | 0.0044 | -0.019 | -0.0029 | 0.0045 | -0.632 |
| 700 nm | -0.0002 | 0.0041 | -0.058 | -0.0028 | 0.0042 | -0.672 |
| 750 nm | -0.0015 | 0.0048 | -0.318 | -0.0030 | 0.0049 | -0.612 |
| 800 nm | -0.0002 | 0.0066 | -0.031 | -0.0026 | 0.0066 | -0.401 |
| 850 nm | -0.0010 | 0.0059 | -0.167 | -0.0032 | 0.0059 | -0.541 |
| 900 nm | -0.0038 | 0.0044 | -0.856 | -0.0055 | 0.0045 | -1.220 |
| 950 nm | -0.0022 | 0.0039 | -0.571 | -0.0029 | 0.0040 | -0.711 |
| 1000 nm | -0.0034 | 0.0075 | -0.454 | -0.0023 | 0.0075 | -0.310 |

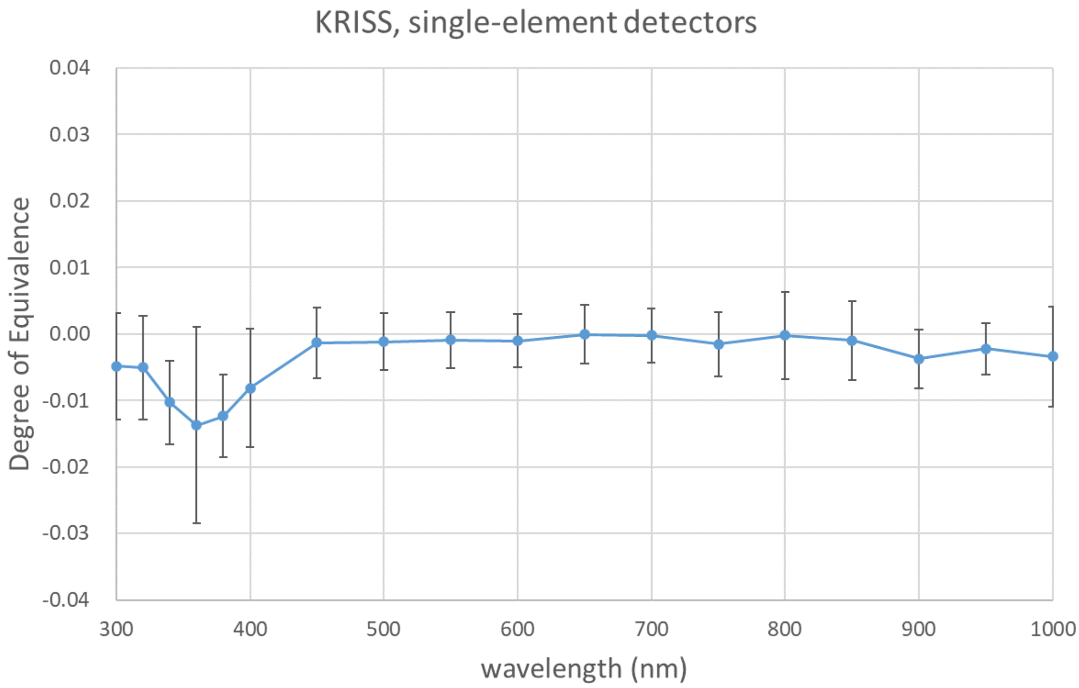


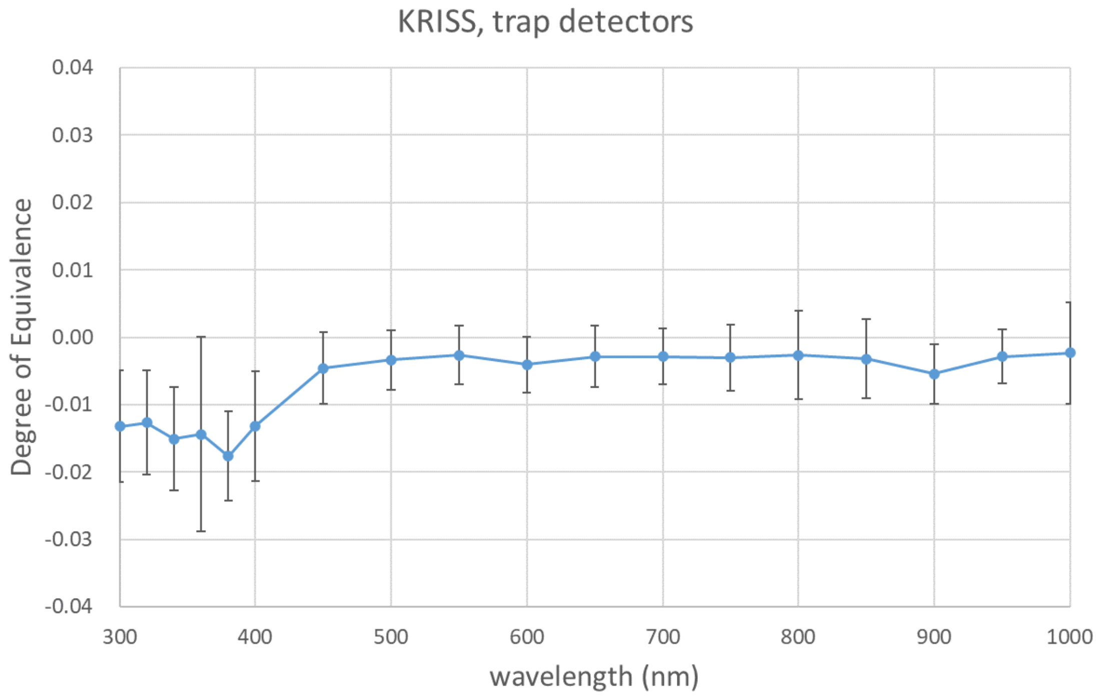


**Figure A-1.** Results of the degree of equivalence (DoE) of KRISS as a function of wavelength for the single-element detectors (top) and the trap detectors (bottom). The error bars indicate the expanded uncertainties of DoEs ($k = 2$).

## 2. NMC-ASTAR

**Table A-2.** Values of the degree of equivalence (DoE) and their expanded uncertainties ($k$ = 2) for the participant NMC-ASTAR.

| wavelength | single-element detectors | | | trap detectors | | |
|---|---|---|---|---|---|---|
| | DoE | $U$(DoE) | DoE/$U$(DoE) | DoE | $U$(DoE) | DoE/$U$(DoE) |
| 300 nm | 0.0107 | 0.0197 | 0.540 | 0.0150 | 0.0207 | 0.722 |
| 320 nm | 0.0086 | 0.0187 | 0.461 | 0.0010 | 0.0210 | 0.050 |
| 340 nm | 0.0144 | 0.0187 | 0.769 | 0.0170 | 0.0198 | 0.857 |
| 360 nm | 0.0064 | 0.0231 | 0.277 | 0.0096 | 0.0241 | 0.397 |
| 380 nm | 0.0079 | 0.0175 | 0.452 | 0.0086 | 0.0191 | 0.448 |
| 400 nm | 0.0126 | 0.0090 | 1.401 | 0.0151 | 0.0084 | 1.804 |
| 450 nm | 0.0025 | 0.0067 | 0.382 | 0.0041 | 0.0057 | 0.726 |
| 500 nm | -0.0006 | 0.0057 | -0.113 | 0.0006 | 0.0046 | 0.121 |
| 550 nm | -0.0019 | 0.0054 | -0.351 | -0.0006 | 0.0043 | -0.145 |
| 600 nm | -0.0007 | 0.0055 | -0.128 | -0.0007 | 0.0043 | -0.155 |
| 650 nm | -0.0006 | 0.0055 | -0.105 | -0.0006 | 0.0044 | -0.131 |
| 700 nm | -0.0004 | 0.0051 | -0.074 | -0.0004 | 0.0040 | -0.105 |
| 750 nm | -0.0006 | 0.0054 | -0.116 | 0.0004 | 0.0043 | 0.082 |
| 800 nm | -0.0003 | 0.0055 | -0.053 | 0.0005 | 0.0043 | 0.126 |
| 850 nm | 0.0005 | 0.0054 | 0.086 | 0.0010 | 0.0043 | 0.224 |
| 900 nm | 0.0015 | 0.0054 | 0.286 | 0.0022 | 0.0042 | 0.526 |
| 950 nm | 0.0033 | 0.0156 | 0.213 | 0.0040 | 0.0148 | 0.270 |
| 1000 nm | 0.0036 | 0.0168 | 0.211 | 0.0009 | 0.0161 | 0.057 |

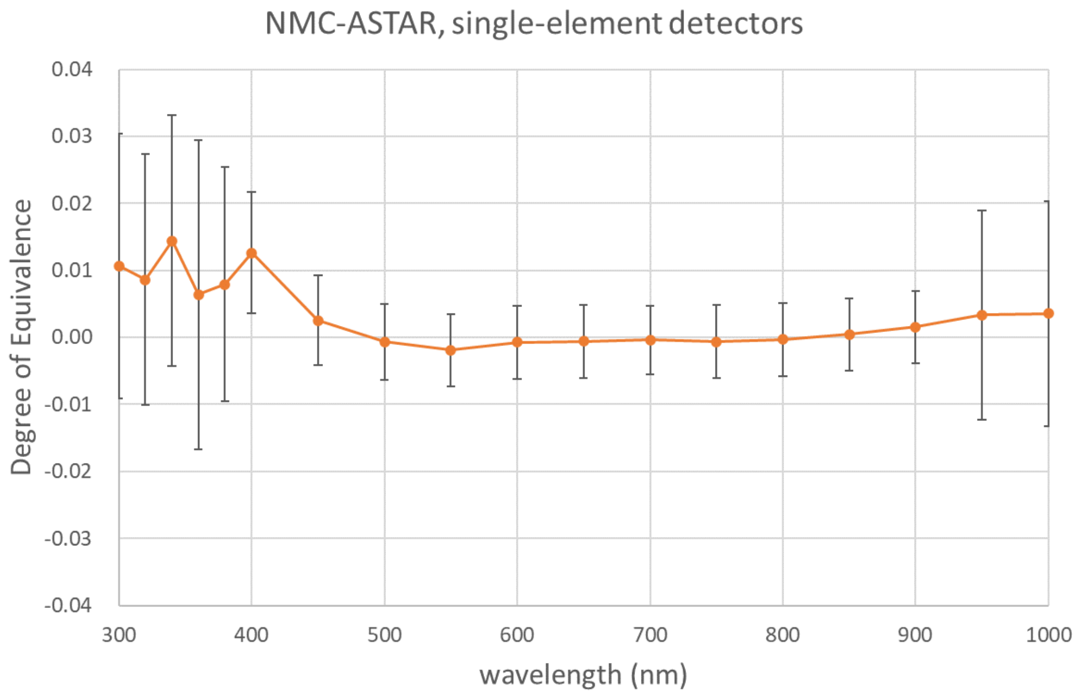


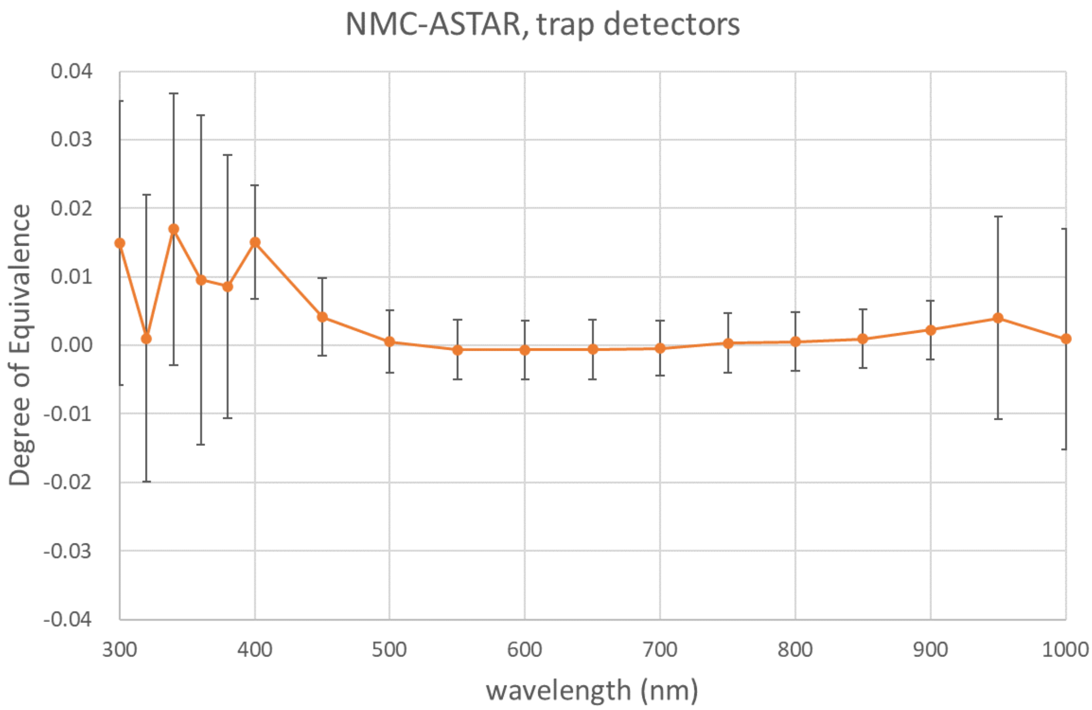


**Figure A-2.** Results of the degree of equivalence (DoE) of NMC-ASTAR as a function of wavelength for the single-element detectors (top) and the trap detectors (bottom). The error bars indicate the expanded uncertainties of DoEs ($k = 2$).

# 3. NIST

**Table A-3.** Values of the degree of equivalence (DoE) and their expanded uncertainties ($k$ = 2) for the participant NIST.

| wavelength | single-element detectors | | | trap detectors | | |
|---|---|---|---|---|---|---|
| | DoE | $U$(DoE) | DoE/$U$(DoE) | DoE | $U$(DoE) | DoE/$U$(DoE) |
| 300 nm | -0.0017 | 0.0080 | -0.216 | -0.0031 | 0.0076 | -0.414 |
| 320 nm | -0.0050 | 0.0076 | -0.665 | -0.0098 | 0.0072 | -1.359 |
| 340 nm | -0.0101 | 0.0059 | -1.704 | -0.0074 | 0.0052 | -1.430 |
| 360 nm | -0.0098 | 0.0142 | -0.688 | -0.0072 | 0.0139 | -0.519 |
| 380 nm | -0.0067 | 0.0048 | -1.400 | -0.0065 | 0.0039 | -1.668 |
| 400 nm | -0.0070 | 0.0080 | -0.869 | -0.0065 | 0.0076 | -0.856 |
| 450 nm | -0.0027 | 0.0055 | -0.501 | -0.0024 | 0.0047 | -0.520 |
| 500 nm | -0.0014 | 0.0044 | -0.310 | -0.0010 | 0.0033 | -0.312 |
| 550 nm | -0.0009 | 0.0042 | -0.213 | -0.0004 | 0.0031 | -0.137 |
| 600 nm | 0.0005 | 0.0042 | 0.127 | -0.0001 | 0.0031 | -0.021 |
| 650 nm | 0.0003 | 0.0043 | 0.065 | -0.0003 | 0.0032 | -0.083 |
| 700 nm | 0.0003 | 0.0040 | 0.084 | -0.0003 | 0.0028 | -0.101 |
| 750 nm | -0.0007 | 0.0044 | -0.170 | -0.0001 | 0.0033 | -0.036 |
| 800 nm | -0.0012 | 0.0044 | -0.266 | -0.0007 | 0.0033 | -0.195 |
| 850 nm | -0.0013 | 0.0044 | -0.292 | -0.0009 | 0.0033 | -0.265 |
| 900 nm | -0.0009 | 0.0044 | -0.208 | -0.0002 | 0.0033 | -0.070 |
| 950 nm | -0.0009 | 0.0040 | -0.226 | 0.0003 | 0.0028 | 0.110 |
| 1000 nm | -0.0060 | 0.0080 | -0.747 | -0.0046 | 0.0075 | -0.608 |

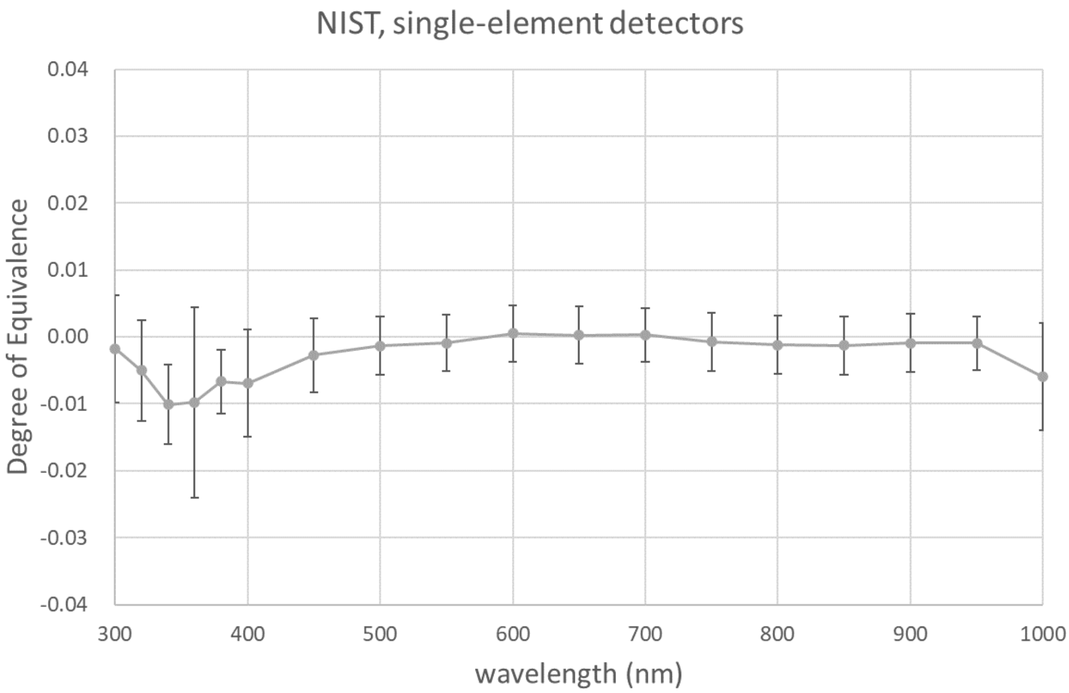


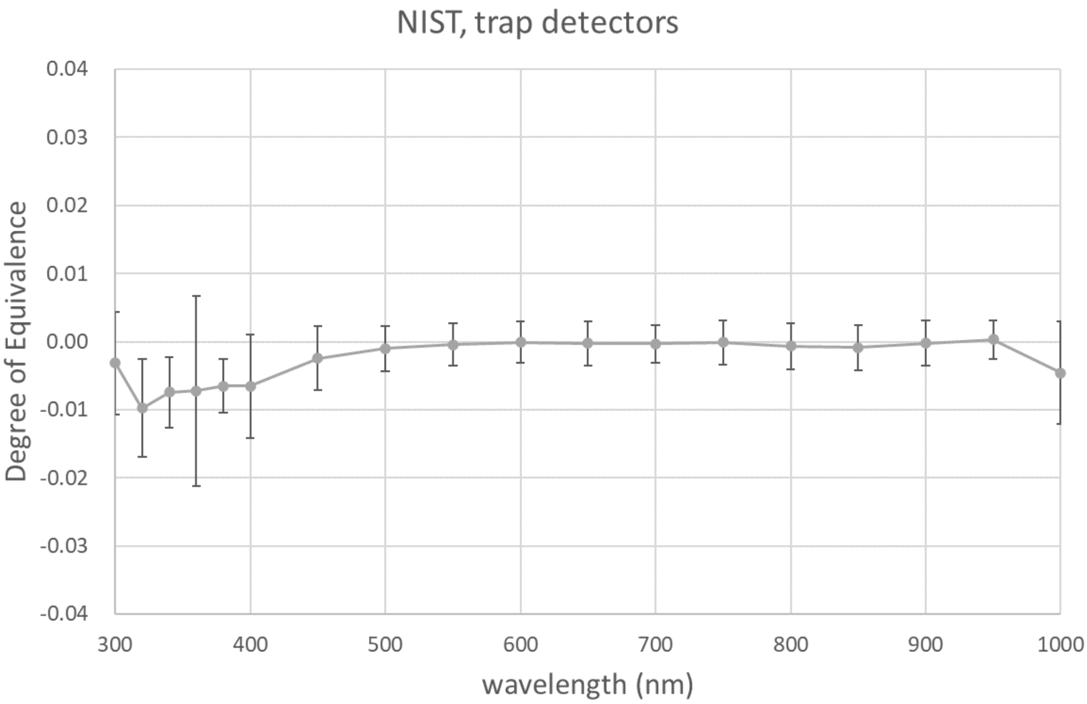


**Figure A-3.** Results of the degree of equivalence (DoE) of NIST as a function of wavelength for the single-element detectors (top) and the trap detectors (bottom). The error bars indicate the expanded uncertainties of DoEs ($k = 2$).

# 4. IO-CSIC

**Table A-4.** Values of the degree of equivalence (DoE) and their expanded uncertainties ($k = 2$) for the participant IO-CSIC.

| wavelength | single-element detectors | | | trap detectors | | |
|---|---|---|---|---|---|---|
| | DoE | *U*(DoE) | DoE/*U*(DoE) | DoE | *U*(DoE) | DoE/*U*(DoE) |
| 300 nm | 0.0564 | 0.0159 | 3.538 | 0.0473 | 0.0174 | 2.716 |
| 320 nm | 0.0522 | 0.0153 | 3.405 | 0.0447 | 0.0157 | 2.838 |
| 340 nm | 0.0535 | 0.0144 | 3.713 | 0.0467 | 0.0142 | 3.277 |
| 360 nm | 0.0479 | 0.0201 | 2.388 | 0.0443 | 0.0203 | 2.183 |
| 380 nm | 0.0459 | 0.0130 | 3.532 | 0.0402 | 0.0132 | 3.051 |
| 400 nm | 0.0301 | 0.0148 | 2.031 | 0.0251 | 0.0138 | 1.817 |
| 450 nm | 0.0039 | 0.0089 | 0.438 | 0.0020 | 0.0107 | 0.187 |
| 500 nm | -0.0001 | 0.0071 | -0.018 | -0.0009 | 0.0072 | -0.125 |
| 550 nm | -0.0161 | 0.0076 | -2.133 | -0.0177 | 0.0066 | -2.668 |
| 600 nm | -0.0143 | 0.0071 | -2.030 | -0.0169 | 0.0066 | -2.553 |
| 650 nm | -0.0145 | 0.0071 | -2.037 | -0.0160 | 0.0066 | -2.414 |
| 700 nm | -0.0139 | 0.0069 | -2.001 | -0.0158 | 0.0063 | -2.510 |
| 750 nm | 0.0025 | 0.0070 | 0.358 | 0.0024 | 0.0063 | 0.383 |
| 800 nm | 0.0044 | 0.0074 | 0.605 | 0.0046 | 0.0065 | 0.698 |
| 850 nm | 0.0037 | 0.0091 | 0.401 | 0.0039 | 0.0076 | 0.516 |
| 900 nm | 0.0047 | 0.0090 | 0.527 | 0.0041 | 0.0085 | 0.478 |
| 950 nm | 0.0072 | 0.0092 | 0.781 | 0.0067 | 0.0085 | 0.795 |
| 1000 nm | 0.0071 | 0.0107 | 0.666 | 0.0080 | 0.0105 | 0.764 |

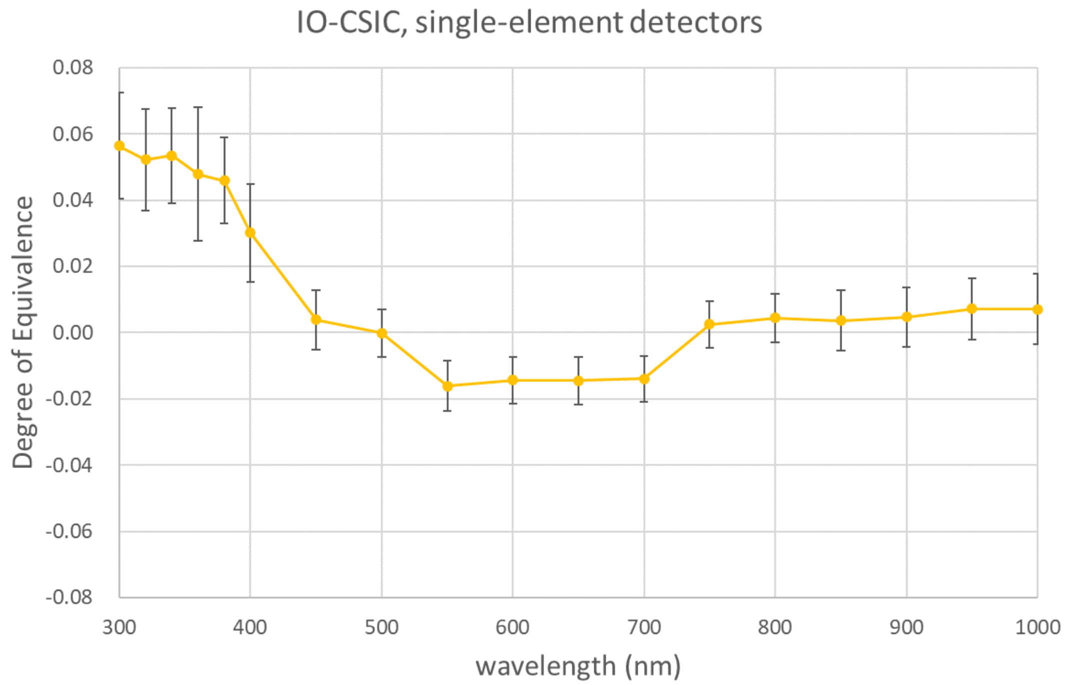


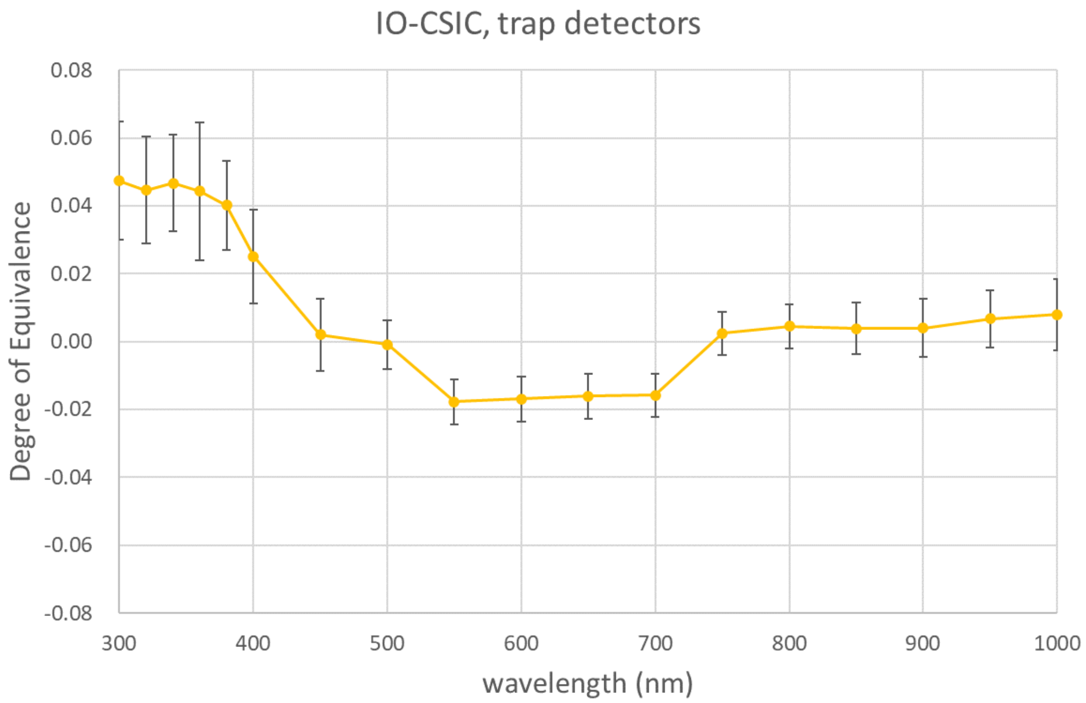


**Figure A-4.** Results of the degree of equivalence (DoE) of IO-CSIC as a function of wavelength for the single-element detectors (top) and the trap detectors (bottom). The error bars indicate the expanded uncertainties of DoEs ($k = 2$).

# 5. VNIIOFI

**Table A-5.** Values of the degree of equivalence (DoE) and their expanded uncertainties ($k = 2$) for the participant VNIIOFI.

| wavelength | single-element detectors | | | trap detectors | | |
|---|---|---|---|---|---|---|
| | DoE | *U*(DoE) | DoE/*U*(DoE) | DoE | *U*(DoE) | DoE/*U*(DoE) |
| 300 nm | -0.0056 | 0.0107 | -0.520 | 0.0222 | 0.0112 | 1.978 |
| 320 nm | 0.0068 | 0.0097 | 0.701 | 0.0122 | 0.0088 | 1.376 |
| 340 nm | 0.0127 | 0.0076 | 1.677 | 0.0094 | 0.0066 | 1.430 |
| 360 nm | 0.0242 | 0.0150 | 1.608 | 0.0085 | 0.0146 | 0.584 |
| 380 nm | -0.0146 | 0.0070 | -2.076 | 0.0019 | 0.0050 | 0.369 |
| 400 nm | -0.0073 | 0.0091 | -0.797 | 0.0008 | 0.0084 | 0.099 |
| 450 nm | -0.0011 | 0.0064 | -0.170 | 0.0008 | 0.0051 | 0.147 |
| 500 nm | 0.0004 | 0.0056 | 0.071 | 0.0010 | 0.0041 | 0.241 |
| 550 nm | 0.0007 | 0.0055 | 0.125 | 0.0012 | 0.0039 | 0.296 |
| 600 nm | 0.0021 | 0.0050 | 0.424 | 0.0012 | 0.0032 | 0.372 |
| 650 nm | 0.0018 | 0.0051 | 0.354 | 0.0007 | 0.0034 | 0.200 |
| 700 nm | 0.0017 | 0.0048 | 0.349 | 0.0004 | 0.0029 | 0.136 |
| 750 nm | 0.0010 | 0.0051 | 0.196 | 0.0005 | 0.0034 | 0.150 |
| 800 nm | 0.0005 | 0.0051 | 0.102 | 0.0003 | 0.0035 | 0.101 |
| 850 nm | 0.0006 | 0.0051 | 0.109 | -0.0001 | 0.0034 | -0.034 |
| 900 nm | 0.0019 | 0.0051 | 0.377 | 0.0003 | 0.0034 | 0.088 |
| 950 nm | 0.0005 | 0.0059 | 0.080 | -0.0027 | 0.0044 | -0.613 |
| 1000 nm | 0.0142 | 0.0091 | 1.559 | -0.0006 | 0.0083 | -0.077 |

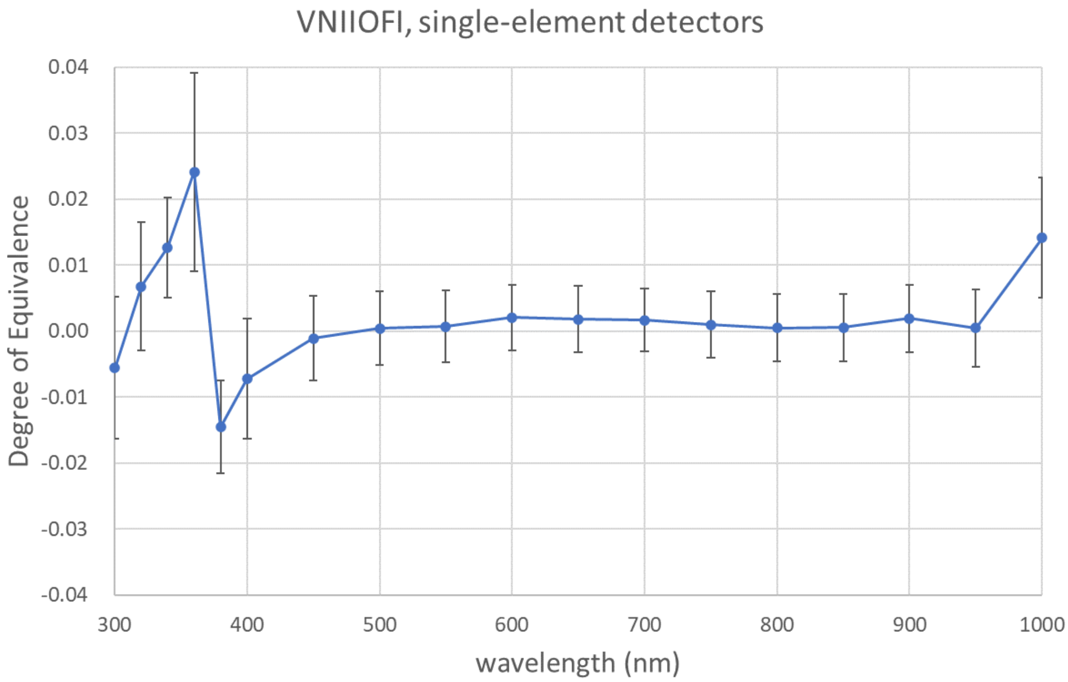


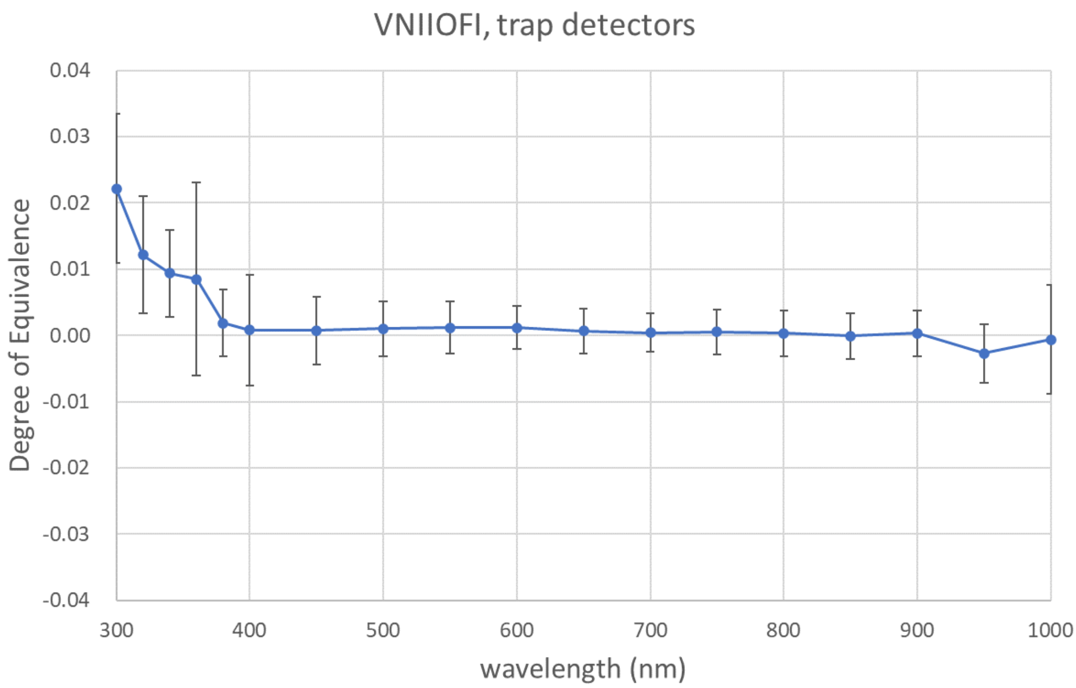


**Figure A-5.** Results of the degree of equivalence (DoE) of VNIIOFI as a function of wavelength for the single-element detectors (top) and the trap detectors (bottom). The error bars indicate the expanded uncertainties of DoEs ($k = 2$).

# 6. NMIJ

**Table A-6.** Values of the degree of equivalence (DoE) and their expanded uncertainties ($k$ = 2) for the participant NMIJ.

| wavelength | single-element detectors | | | trap detectors | | |
|---|---|---|---|---|---|---|
| | DoE | *U*(DoE) | DoE/*U*(DoE) | DoE | *U*(DoE) | DoE/*U*(DoE) |
| 300 nm | 0.0158 | 0.0198 | 0.801 | 0.0175 | 0.0178 | 0.981 |
| 320 nm | 0.0191 | 0.0196 | 0.974 | 0.0152 | 0.0177 | 0.857 |
| 340 nm | 0.0174 | 0.0187 | 0.930 | 0.0161 | 0.0170 | 0.944 |
| 360 nm | 0.0135 | 0.0231 | 0.587 | 0.0159 | 0.0218 | 0.732 |
| 380 nm | 0.0168 | 0.0132 | 1.274 | 0.0161 | 0.0108 | 1.488 |
| 400 nm | 0.0150 | 0.0147 | 1.018 | 0.0100 | 0.0125 | 0.804 |
| 450 nm | 0.0052 | 0.0126 | 0.414 | 0.0047 | 0.0102 | 0.459 |
| 500 nm | 0.0022 | 0.0113 | 0.198 | 0.0019 | 0.0086 | 0.222 |
| 550 nm | 0.0009 | 0.0103 | 0.090 | 0.0010 | 0.0074 | 0.141 |
| 600 nm | 0.0017 | 0.0096 | 0.176 | 0.0006 | 0.0064 | 0.095 |
| 650 nm | 0.0009 | 0.0089 | 0.098 | -0.0004 | 0.0054 | -0.073 |
| 700 nm | 0.0003 | 0.0088 | 0.029 | -0.0004 | 0.0053 | -0.069 |
| 750 nm | -0.0013 | 0.0093 | -0.145 | -0.0006 | 0.0060 | -0.101 |
| 800 nm | -0.0025 | 0.0094 | -0.266 | -0.0024 | 0.0062 | -0.390 |
| 850 nm | -0.0034 | 0.0095 | -0.361 | -0.0026 | 0.0063 | -0.418 |
| 900 nm | -0.0021 | 0.0097 | -0.222 | -0.0026 | 0.0065 | -0.406 |
| 950 nm | -0.0009 | 0.0115 | -0.079 | -0.0008 | 0.0089 | -0.089 |
| 1000 nm | -0.0011 | 0.0183 | -0.059 | 0.0000 | 0.0167 | -0.002 |

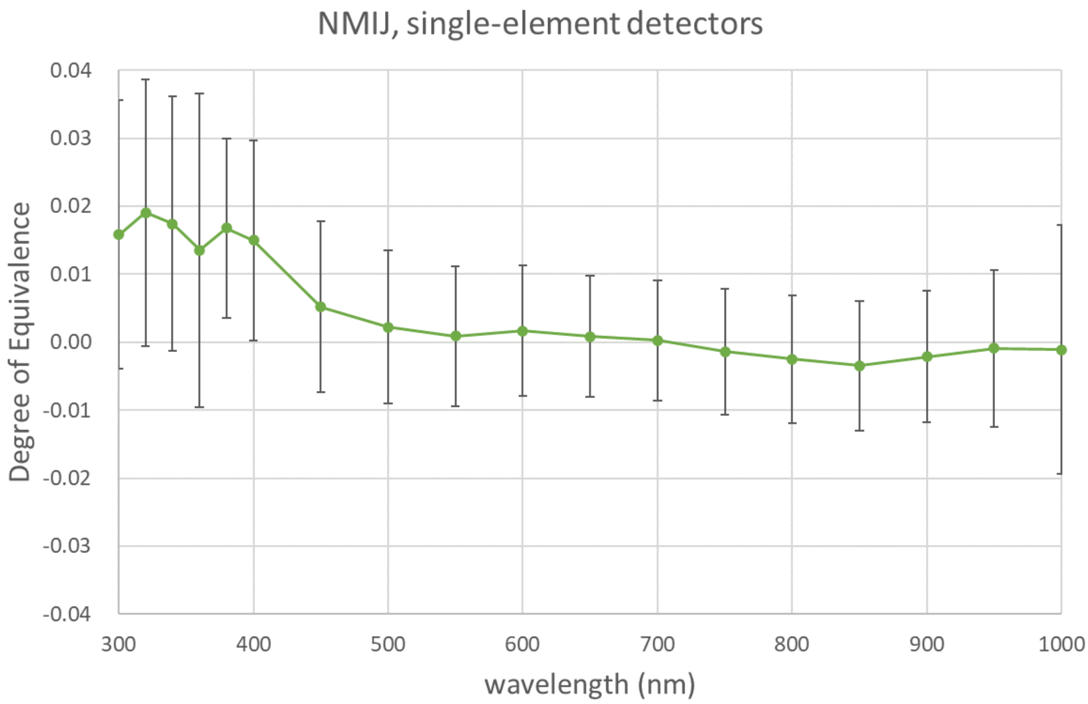


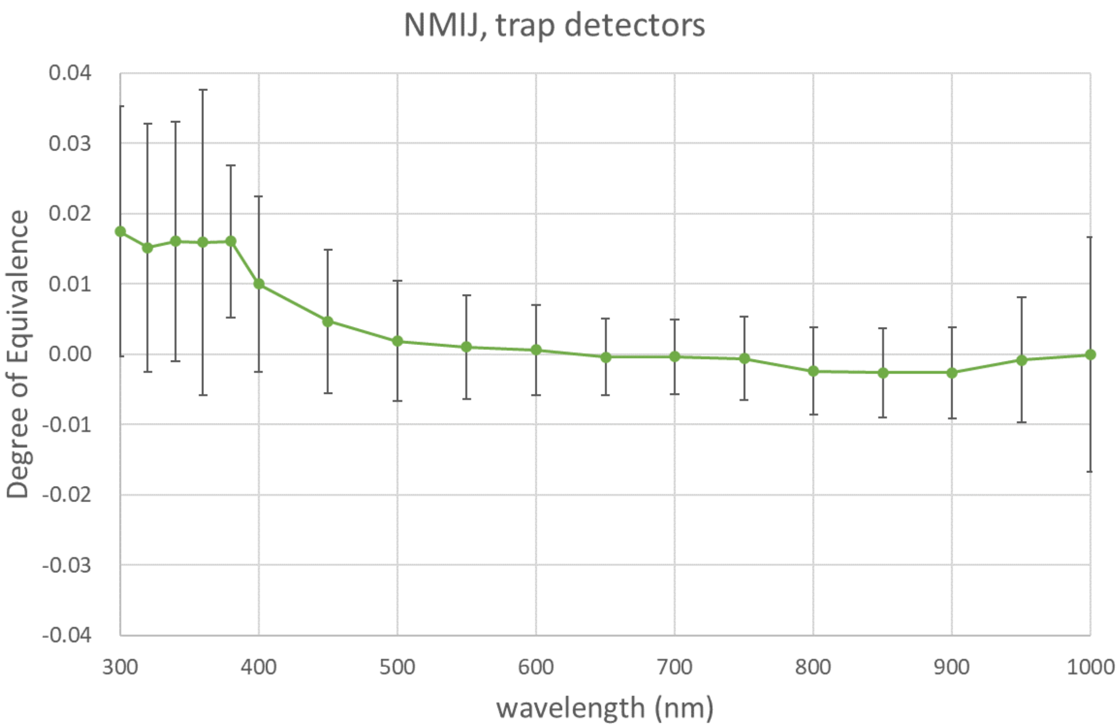


**Figure A-6.** Results of the degree of equivalence (DoE) of NMIJ as a function of wavelength for the single-element detectors (top) and the trap detectors (bottom). The error bars indicate the expanded uncertainties of DoEs ($k = 2$).

# 7. LNE-CNAM

**Table A-7.** Values of the degree of equivalence (DoE) and their expanded uncertainties ($k = 2$) for the participant LNE-CNAM.

| wavelength | single-element detectors | | | trap detectors | | |
|---|---|---|---|---|---|---|
| | DoE | *U*(DoE) | DoE/*U*(DoE) | DoE | *U*(DoE) | DoE/*U*(DoE) |
| 300 nm | 0.0006 | 0.0090 | 0.069 | 0.0135 | 0.0113 | 1.191 |
| 320 nm | -0.0002 | 0.0089 | -0.018 | 0.0124 | 0.0103 | 1.196 |
| 340 nm | -0.0028 | 0.0073 | -0.384 | 0.0091 | 0.0083 | 1.100 |
| 360 nm | -0.0074 | 0.0151 | -0.489 | 0.0159 | 0.0153 | 1.043 |
| 380 nm | -0.0001 | 0.0065 | -0.016 | 0.0132 | 0.0071 | 1.852 |
| 400 nm | -0.0025 | 0.0084 | -0.301 | 0.0078 | 0.0094 | 0.836 |
| 450 nm | -0.0010 | 0.0059 | -0.162 | 0.0082 | 0.0070 | 1.167 |
| 500 nm | 0.0008 | 0.0055 | 0.146 | 0.0084 | 0.0068 | 1.245 |
| 550 nm | 0.0017 | 0.0053 | 0.329 | 0.0073 | 0.0065 | 1.121 |
| 600 nm | 0.0018 | 0.0059 | 0.307 | 0.0077 | 0.0071 | 1.097 |
| 650 nm | 0.0027 | 0.0054 | 0.507 | 0.0085 | 0.0067 | 1.285 |
| 700 nm | 0.0020 | 0.0048 | 0.418 | 0.0082 | 0.0061 | 1.343 |
| 750 nm | 0.0015 | 0.0052 | 0.288 | 0.0085 | 0.0064 | 1.324 |
| 800 nm | 0.0002 | 0.0054 | 0.035 | 0.0071 | 0.0067 | 1.071 |
| 850 nm | 0.0004 | 0.0052 | 0.079 | 0.0077 | 0.0064 | 1.191 |
| 900 nm | 0.0000 | 0.0050 | 0.010 | 0.0065 | 0.0063 | 1.031 |
| 950 nm | 0.0012 | 0.0055 | 0.212 | 0.0072 | 0.0080 | 0.900 |
| 1000 nm | 0.0002 | 0.0096 | 0.019 | 0.0071 | 0.0120 | 0.597 |

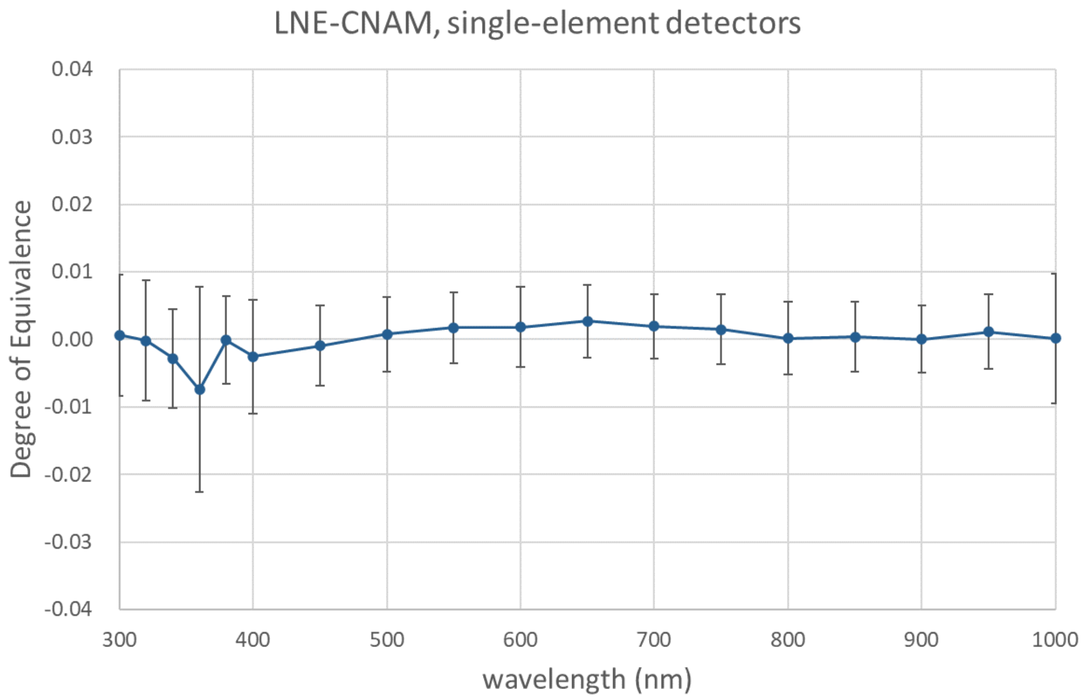


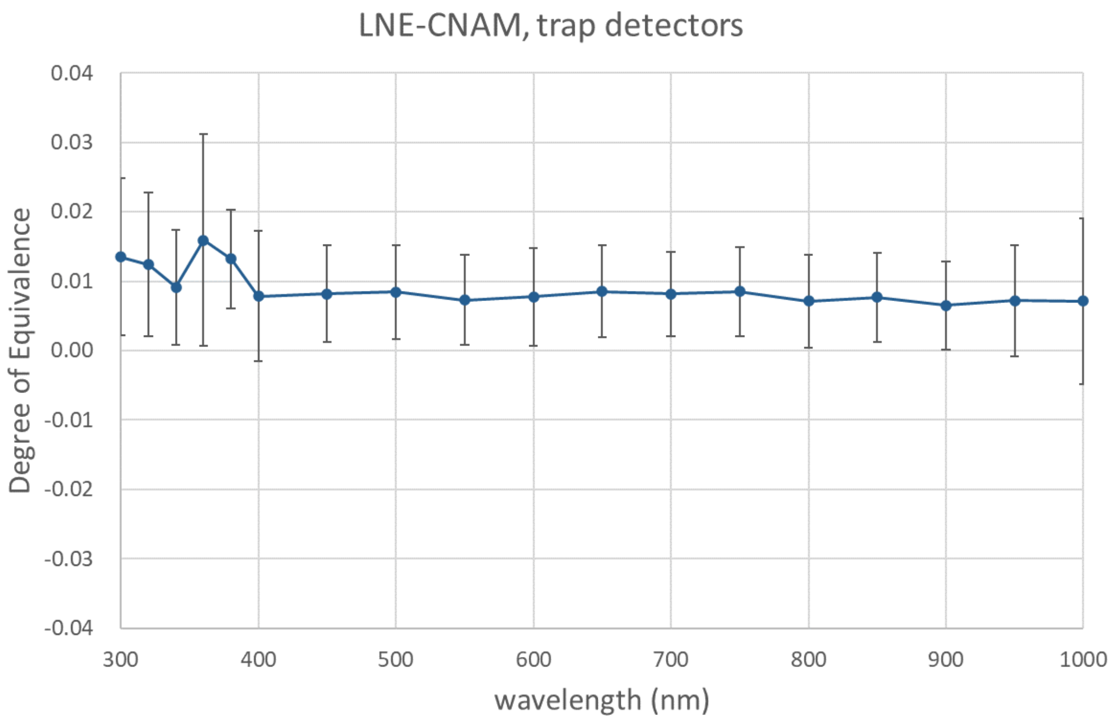


**Figure A-7.** Results of the degree of equivalence (DoE) of LNE-CNAM as a function of wavelength for the single-element detectors (top) and the trap detectors (bottom). The error bars indicate the expanded uncertainties of DoEs ($k = 2$).

# 8. PTB

**Table A-8.** Values of the degree of equivalence (DoE) and their expanded uncertainties ($k$ = 2) for the participant PTB.

| wavelength | single-element detectors | | | trap detectors | | |
|---|---|---|---|---|---|---|
| | DoE | *U*(DoE) | DoE/*U*(DoE) | DoE | *U*(DoE) | DoE/*U*(DoE) |
| 300 nm | -0.0040 | 0.0090 | -0.446 | 0.0043 | 0.0082 | 0.524 |
| 320 nm | -0.0022 | 0.0085 | -0.262 | 0.0032 | 0.0079 | 0.411 |
| 340 nm | -0.0037 | 0.0070 | -0.525 | -0.0012 | 0.0061 | -0.198 |
| 360 nm | -0.0054 | 0.0148 | -0.361 | 0.0069 | 0.0144 | 0.480 |
| 380 nm | -0.0021 | 0.0062 | -0.342 | 0.0014 | 0.0053 | 0.268 |
| 400 nm | -0.0042 | 0.0090 | -0.469 | 0.0007 | 0.0083 | 0.080 |
| 450 nm | -0.0028 | 0.0067 | -0.420 | 0.0021 | 0.0058 | 0.360 |
| 500 nm | -0.0017 | 0.0059 | -0.281 | 0.0027 | 0.0048 | 0.551 |
| 550 nm | -0.0016 | 0.0058 | -0.285 | 0.0028 | 0.0047 | 0.587 |
| 600 nm | -0.0003 | 0.0058 | -0.053 | 0.0029 | 0.0047 | 0.626 |
| 650 nm | -0.0004 | 0.0059 | -0.067 | 0.0022 | 0.0048 | 0.452 |
| 700 nm | -0.0006 | 0.0056 | -0.114 | 0.0027 | 0.0045 | 0.590 |
| 750 nm | -0.0017 | 0.0059 | -0.281 | 0.0028 | 0.0048 | 0.572 |
| 800 nm | -0.0016 | 0.0059 | -0.267 | 0.0026 | 0.0049 | 0.533 |
| 850 nm | -0.0018 | 0.0059 | -0.296 | 0.0027 | 0.0049 | 0.549 |
| 900 nm | -0.0009 | 0.0059 | -0.158 | 0.0031 | 0.0048 | 0.636 |
| 950 nm | -0.0011 | 0.0056 | -0.196 | 0.0035 | 0.0044 | 0.786 |
| 1000 nm | -0.0023 | 0.0085 | -0.264 | 0.0039 | 0.0078 | 0.506 |

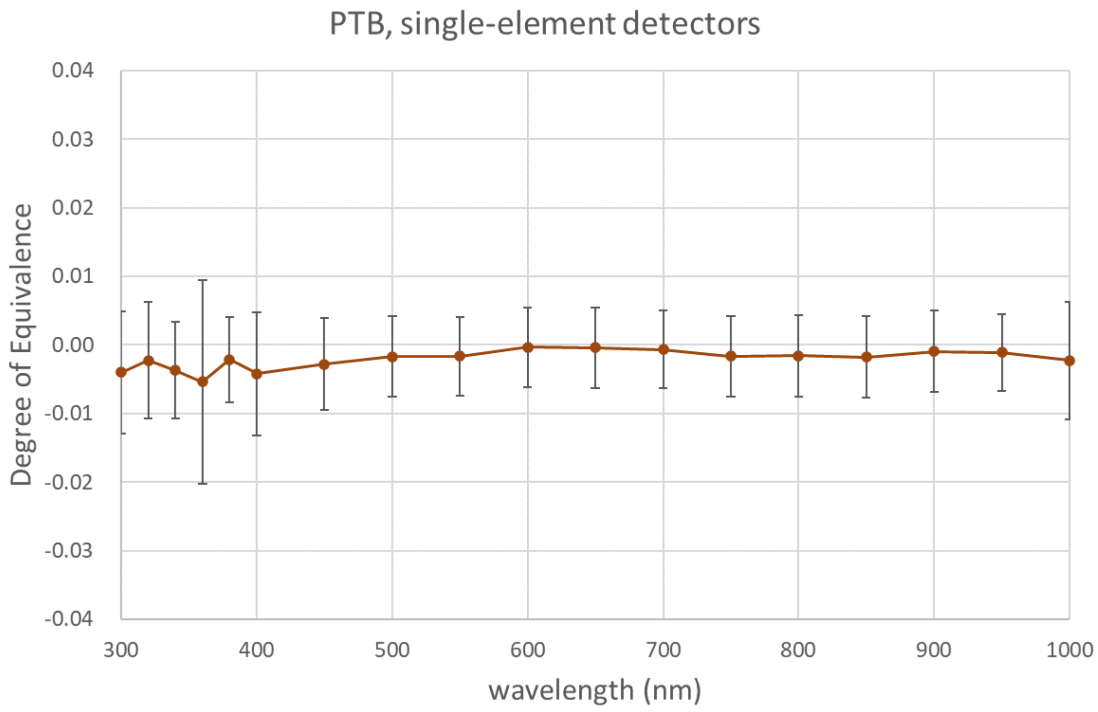


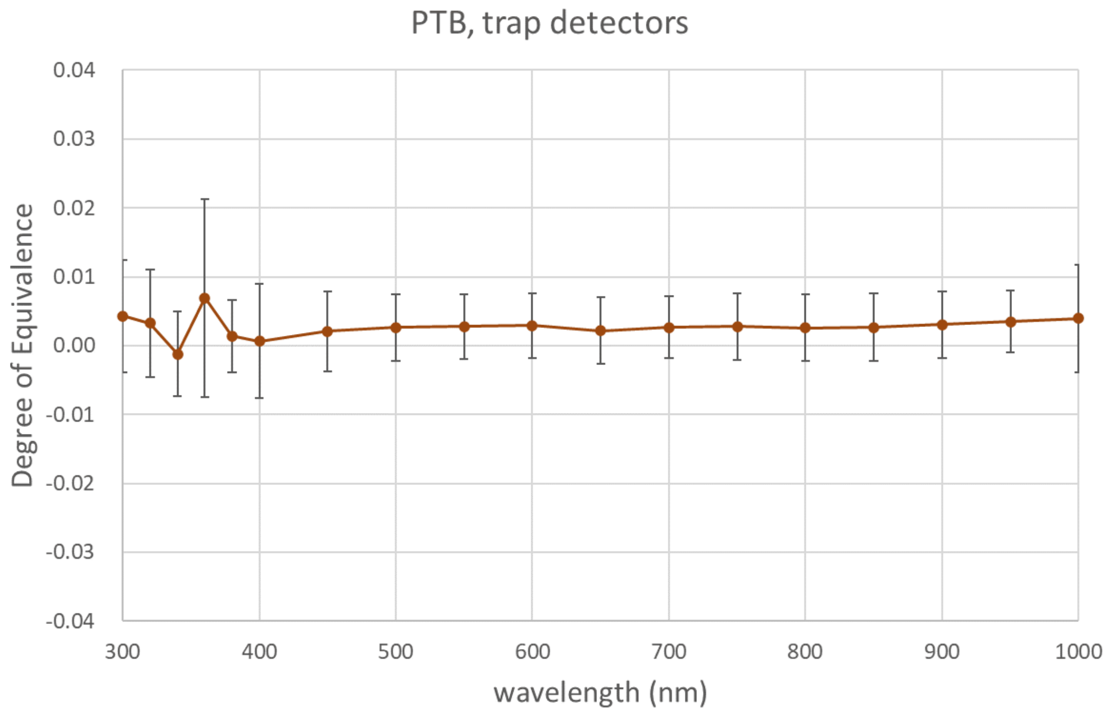


**Figure A-8.** Results of the degree of equivalence (DoE) of PTB as a function of wavelength for the single-element detectors (top) and the trap detectors (bottom). The error bars indicate the expanded uncertainties of DoEs ($k = 2$).

# 9. NRC

**Table A-9.** Values of the degree of equivalence (DoE) and their expanded uncertainties ($k = 2$) for the participant NRC.

| wavelength | single-element detectors | | | trap detectors | | |
|---|---|---|---|---|---|---|
| | DoE | *U*(DoE) | DoE/*U*(DoE) | DoE | *U*(DoE) | DoE/*U*(DoE) |
| 300 nm | 0.0001 | 0.0093 | 0.016 | -0.0102 | 0.0077 | -1.324 |
| 320 nm | -0.0001 | 0.0087 | -0.016 | -0.0089 | 0.0071 | -1.256 |
| 340 nm | 0.0020 | 0.0072 | 0.277 | -0.0068 | 0.0052 | -1.324 |
| 360 nm | 0.0029 | 0.0151 | 0.190 | -0.0061 | 0.0141 | -0.432 |
| 380 nm | -0.0021 | 0.0064 | -0.321 | -0.0103 | 0.0042 | -2.423 |
| 400 nm | 0.0004 | 0.0093 | 0.045 | -0.0092 | 0.0077 | -1.190 |
| 450 nm | 0.0015 | 0.0075 | 0.205 | -0.0009 | 0.0051 | -0.184 |
| 500 nm | 0.0019 | 0.0063 | 0.308 | 0.0002 | 0.0035 | 0.061 |
| 550 nm | 0.0017 | 0.0062 | 0.268 | 0.0003 | 0.0033 | 0.098 |
| 600 nm | 0.0024 | 0.0062 | 0.389 | 0.0002 | 0.0032 | 0.067 |
| 650 nm | 0.0020 | 0.0063 | 0.325 | 0.0005 | 0.0034 | 0.143 |
| 700 nm | 0.0022 | 0.0060 | 0.371 | 0.0005 | 0.0030 | 0.163 |
| 750 nm | 0.0013 | 0.0064 | 0.200 | -0.0019 | 0.0037 | -0.526 |
| 800 nm | 0.0012 | 0.0066 | 0.183 | -0.0015 | 0.0039 | -0.391 |
| 850 nm | 0.0024 | 0.0068 | 0.348 | -0.0009 | 0.0043 | -0.221 |
| 900 nm | 0.0021 | 0.0064 | 0.329 | -0.0017 | 0.0037 | -0.460 |
| 950 nm | 0.0009 | 0.0060 | 0.152 | -0.0023 | 0.0030 | -0.773 |
| 1000 nm | -0.0039 | 0.0091 | -0.433 | -0.0055 | 0.0072 | -0.756 |

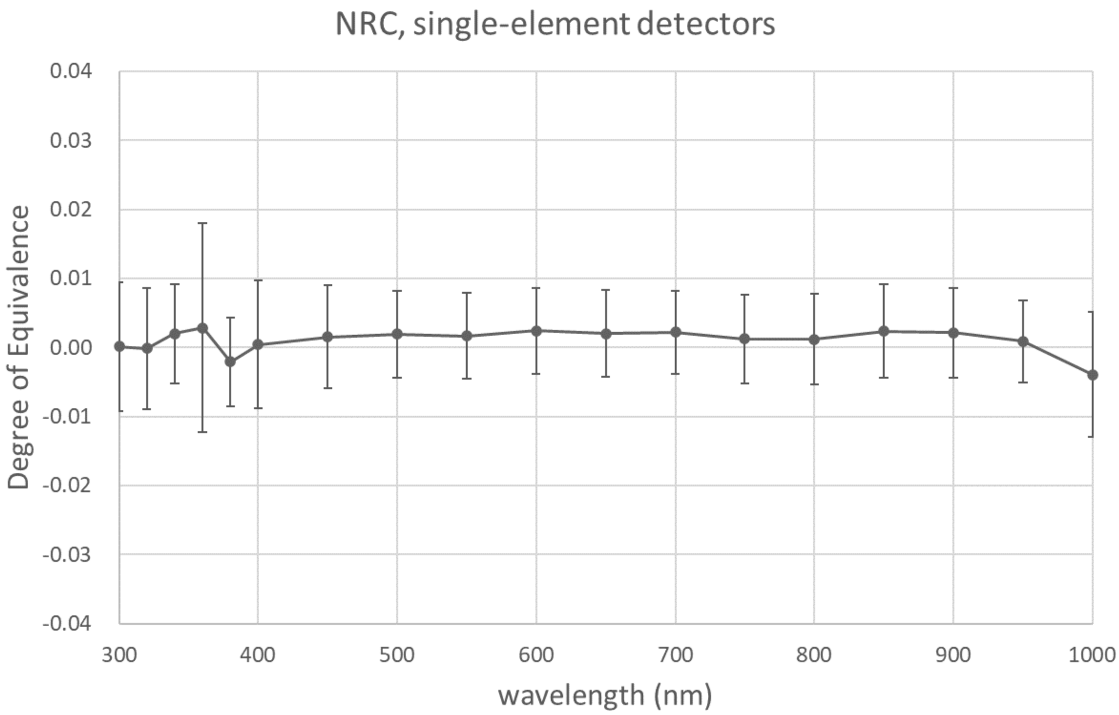


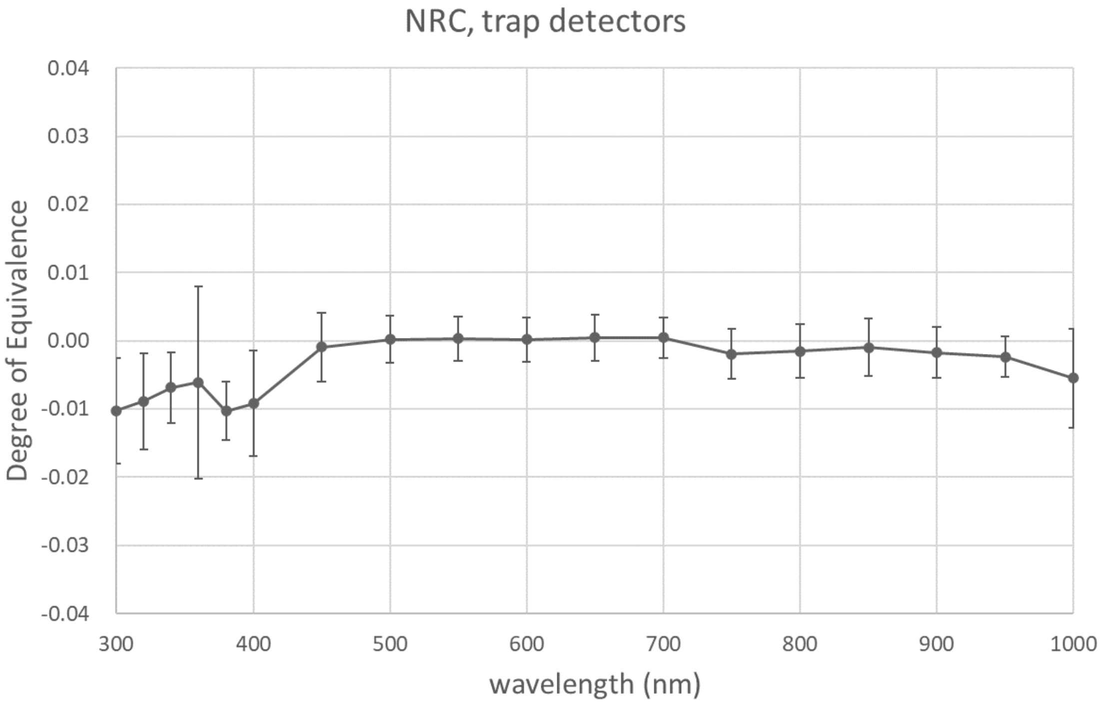


**Figure A-9.** Results of the degree of equivalence (DoE) of NRC as a function of wavelength for the single-element detectors (top) and the trap detectors (bottom). The error bars indicate the expanded uncertainties of DoEs ($k = 2$).

# 10. MSL

**Table A-10.** Values of the degree of equivalence (DoE) and their expanded uncertainties ($k$ = 2) for the participant MSL.

| wavelength | single-element detectors | | | trap detectors | | |
|---|---|---|---|---|---|---|
| | DoE | $U$(DoE) | DoE/$U$(DoE) | DoE | $U$(DoE) | DoE/$U$(DoE) |
| 300 nm | 0.0144 | 0.0135 | 1.069 | 0.0051 | 0.0118 | 0.428 |
| 320 nm | 0.0105 | 0.0133 | 0.793 | 0.0032 | 0.0116 | 0.272 |
| 340 nm | 0.0074 | 0.0125 | 0.592 | -0.0013 | 0.0109 | -0.116 |
| 360 nm | 0.0054 | 0.0180 | 0.298 | -0.0010 | 0.0170 | -0.061 |
| 380 nm | 0.0067 | 0.0117 | 0.573 | -0.0016 | 0.0100 | -0.164 |
| 400 nm | 0.0069 | 0.0124 | 0.553 | -0.0036 | 0.0107 | -0.335 |
| 450 nm | 0.0026 | 0.0088 | 0.293 | -0.0002 | 0.0063 | -0.033 |
| 500 nm | 0.0019 | 0.0071 | 0.269 | -0.0005 | 0.0040 | -0.124 |
| 550 nm | 0.0010 | 0.0067 | 0.156 | -0.0009 | 0.0035 | -0.260 |
| 600 nm | 0.0020 | 0.0068 | 0.300 | -0.0005 | 0.0035 | -0.149 |
| 650 nm | 0.0011 | 0.0068 | 0.167 | -0.0008 | 0.0036 | -0.217 |
| 700 nm | 0.0015 | 0.0067 | 0.220 | -0.0006 | 0.0032 | -0.185 |
| 750 nm | 0.0002 | 0.0069 | 0.031 | -0.0007 | 0.0038 | -0.193 |
| 800 nm | 0.0000 | 0.0070 | -0.004 | -0.0004 | 0.0040 | -0.112 |
| 850 nm | 0.0004 | 0.0071 | 0.059 | -0.0005 | 0.0040 | -0.129 |
| 900 nm | 0.0011 | 0.0072 | 0.151 | 0.0003 | 0.0042 | 0.075 |
| 950 nm | 0.0005 | 0.0072 | 0.073 | 0.0013 | 0.0042 | 0.305 |
| 1000 nm | -0.0012 | 0.0100 | -0.119 | 0.0020 | 0.0081 | 0.250 |

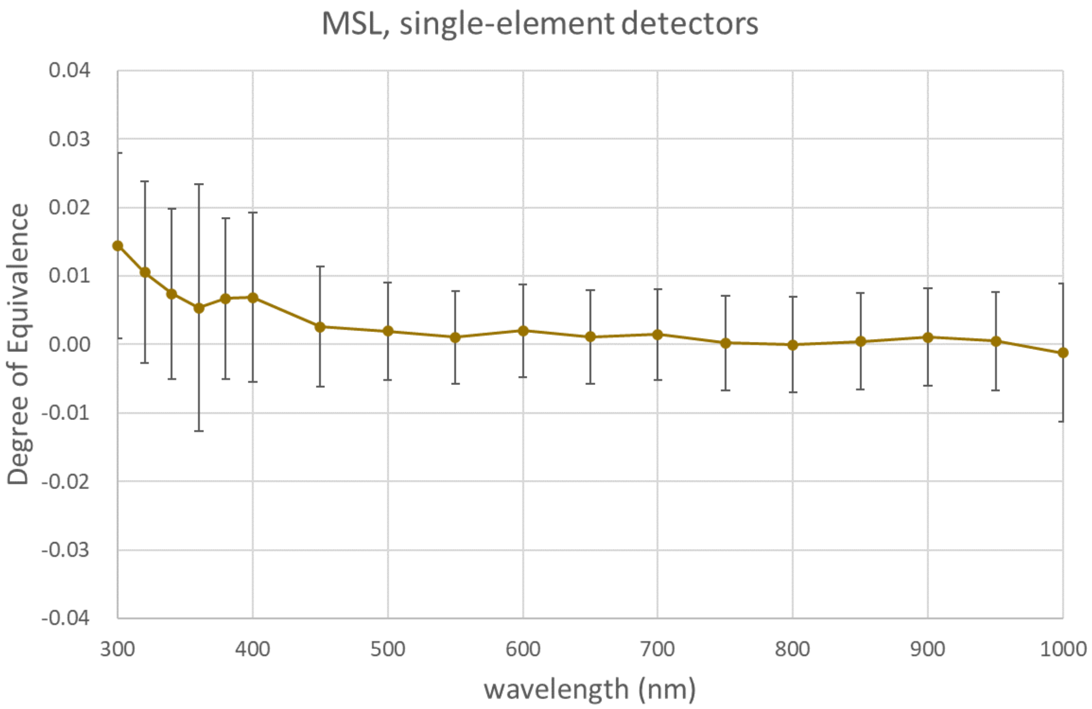


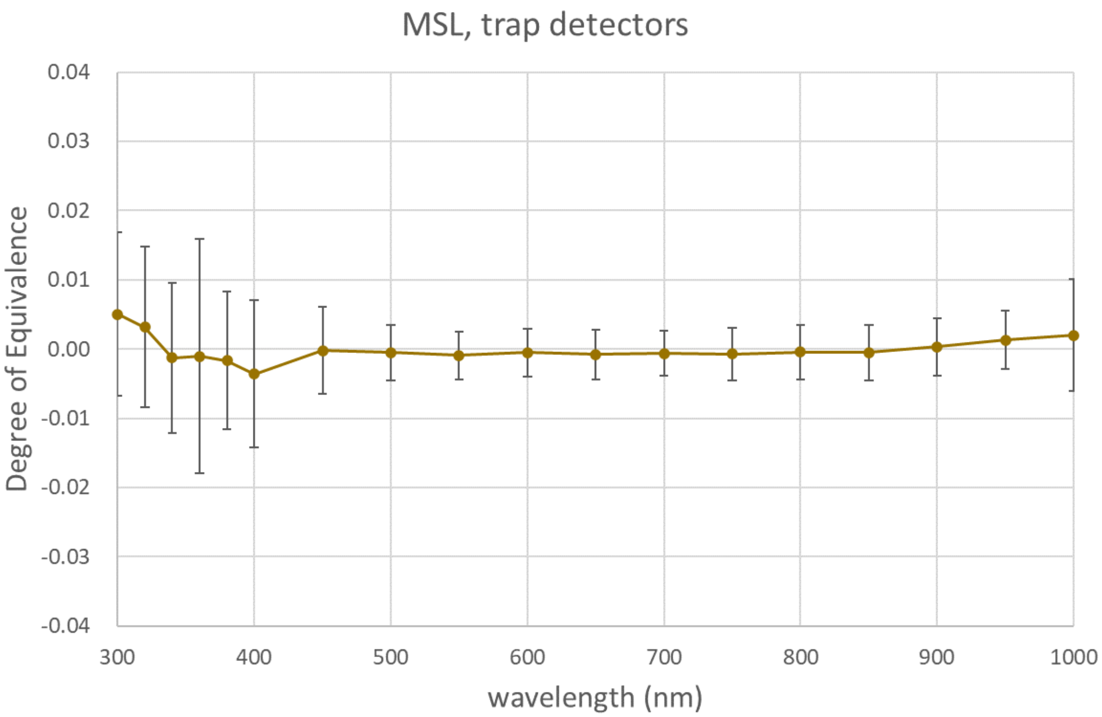


**Figure A-10.** Results of the degree of equivalence (DoE) of MSL as a function of wavelength for the single-element detectors (top) and the trap detectors (bottom). The error bars indicate the expanded uncertainties of DoEs ($k = 2$).

# 11. UME

**Table A-11.** Values of the degree of equivalence (DoE) and their expanded uncertainties ($k$ = 2) for the participant UME.

| wavelength | single-element detectors | | | trap detectors | | |
|---|---|---|---|---|---|---|
| | DoE | $U$(DoE) | DoE/$U$(DoE) | DoE | $U$(DoE) | DoE/$U$(DoE) |
| 300 nm | -0.0284 | 0.0149 | -1.903 | -0.0858 | 0.0148 | -5.817 |
| 320 nm | -0.0129 | 0.0139 | -0.934 | -0.0371 | 0.0144 | -2.574 |
| 340 nm | 0.0001 | 0.0126 | 0.010 | -0.0155 | 0.0124 | -1.245 |
| 360 nm | -0.0025 | 0.0183 | -0.136 | -0.0125 | 0.0183 | -0.686 |
| 380 nm | 0.0076 | 0.0074 | 1.027 | -0.0114 | 0.0072 | -1.586 |
| 400 nm | 0.0073 | 0.0100 | 0.725 | -0.0076 | 0.0099 | -0.768 |
| 450 nm | 0.0033 | 0.0082 | 0.408 | -0.0019 | 0.0081 | -0.234 |
| 500 nm | 0.0027 | 0.0075 | 0.365 | -0.0001 | 0.0075 | -0.012 |
| 550 nm | 0.0025 | 0.0074 | 0.340 | 0.0001 | 0.0074 | 0.013 |
| 600 nm | 0.0031 | 0.0074 | 0.419 | -0.0002 | 0.0074 | -0.026 |
| 650 nm | 0.0025 | 0.0075 | 0.333 | 0.0005 | 0.0075 | 0.064 |
| 700 nm | 0.0020 | 0.0073 | 0.274 | 0.0004 | 0.0073 | 0.051 |
| 750 nm | 0.0005 | 0.0075 | 0.061 | 0.0004 | 0.0075 | 0.052 |
| 800 nm | 0.0004 | 0.0075 | 0.049 | 0.0003 | 0.0075 | 0.034 |
| 850 nm | 0.0006 | 0.0075 | 0.078 | 0.0000 | 0.0075 | -0.001 |
| 900 nm | 0.0004 | 0.0125 | 0.035 | 0.0007 | 0.0125 | 0.056 |
| 950 nm | 0.0004 | 0.0123 | 0.036 | 0.0006 | 0.0123 | 0.050 |
| 1000 nm | 0.0015 | 0.0139 | 0.107 | 0.0016 | 0.0138 | 0.113 |

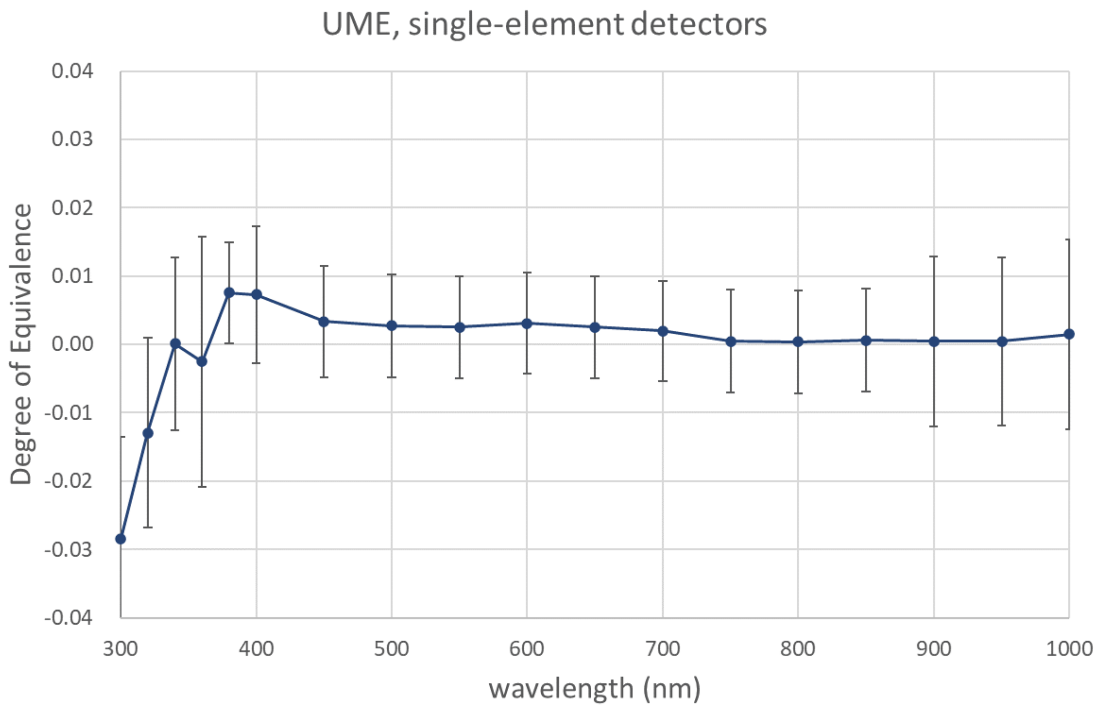


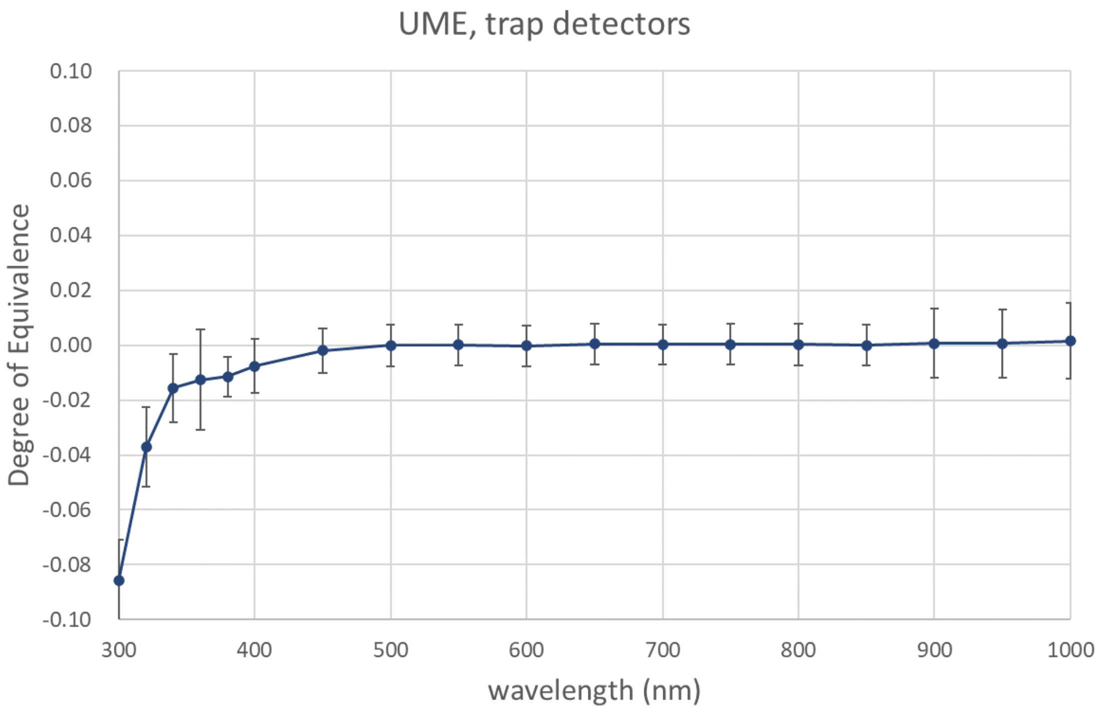


**Figure A-11.** Results of the degree of equivalence (DoE) of UME as a function of wavelength for the single-element detectors (top) and the trap detectors (bottom). The error bars indicate the expanded uncertainties of DoEs ($k = 2$).

# 12. NPL

**Table A-12.** Values of the degree of equivalence (DoE) and their expanded uncertainties ($k$ = 2) for the participant NPL.

| wavelength | single-element detectors | | | trap detectors | | |
|---|---|---|---|---|---|---|
| | DoE | *U*(DoE) | DoE/*U*(DoE) | DoE | *U*(DoE) | DoE/*U*(DoE) |
| 300 nm | 0.0022 | 0.0110 | 0.201 | -0.0020 | 0.0106 | -0.186 |
| 320 nm | 0.0041 | 0.0107 | 0.381 | -0.0002 | 0.0102 | -0.018 |
| 340 nm | 0.0021 | 0.0094 | 0.220 | -0.0010 | 0.0090 | -0.116 |
| 360 nm | -0.0011 | 0.0162 | -0.069 | -0.0046 | 0.0161 | -0.286 |
| 380 nm | 0.0054 | 0.0068 | 0.799 | 0.0022 | 0.0054 | 0.406 |
| 400 nm | 0.0002 | 0.0089 | 0.020 | -0.0076 | 0.0079 | -0.960 |
| 450 nm | -0.0007 | 0.0064 | -0.114 | -0.0026 | 0.0046 | -0.577 |
| 500 nm | -0.0001 | 0.0055 | -0.021 | -0.0015 | 0.0033 | -0.451 |
| 550 nm | -0.0001 | 0.0053 | -0.015 | -0.0014 | 0.0030 | -0.471 |
| 600 nm | 0.0011 | 0.0053 | 0.210 | -0.0012 | 0.0030 | -0.400 |
| 650 nm | 0.0005 | 0.0054 | 0.101 | -0.0015 | 0.0032 | -0.470 |
| 700 nm | 0.0009 | 0.0051 | 0.168 | -0.0015 | 0.0027 | -0.531 |
| 750 nm | -0.0002 | 0.0054 | -0.040 | -0.0014 | 0.0032 | -0.435 |
| 800 nm | -0.0001 | 0.0055 | -0.024 | -0.0017 | 0.0033 | -0.524 |
| 850 nm | 0.0002 | 0.0054 | 0.030 | -0.0013 | 0.0033 | -0.384 |
| 900 nm | 0.0003 | 0.0054 | 0.054 | -0.0006 | 0.0033 | -0.191 |
| 950 nm | 0.0007 | 0.0060 | 0.114 | 0.0002 | 0.0042 | 0.046 |
| 1000 nm | -0.0016 | 0.0085 | -0.185 | -0.0003 | 0.0074 | -0.036 |

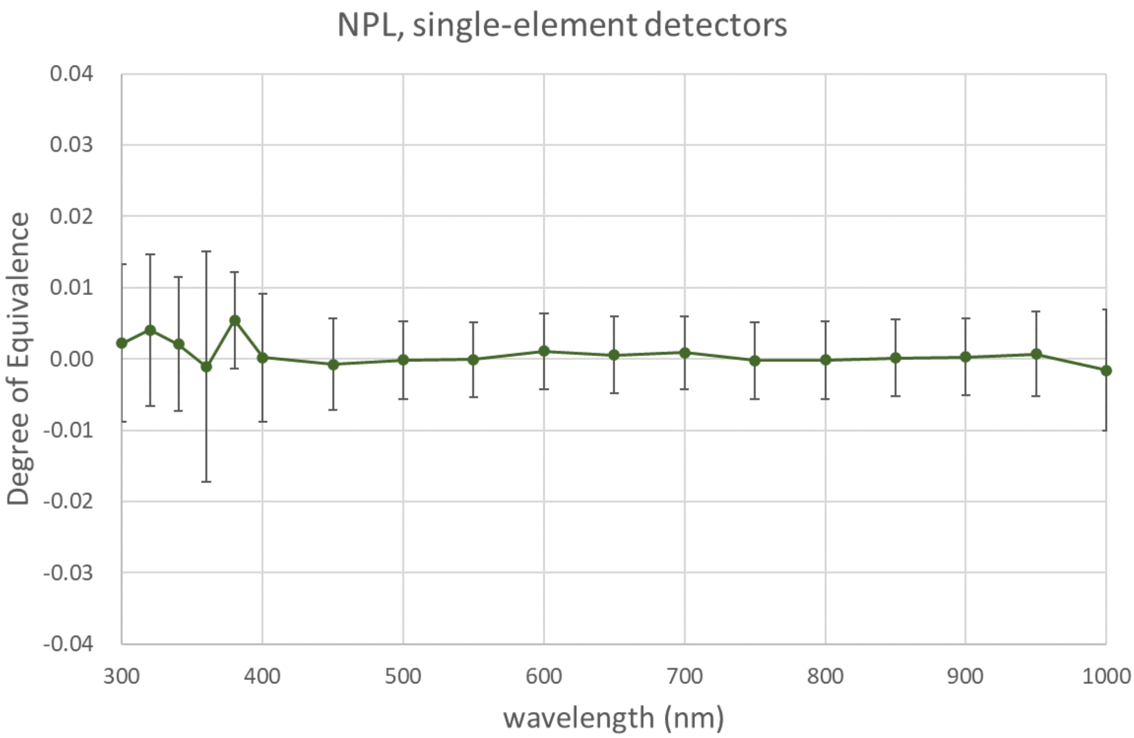


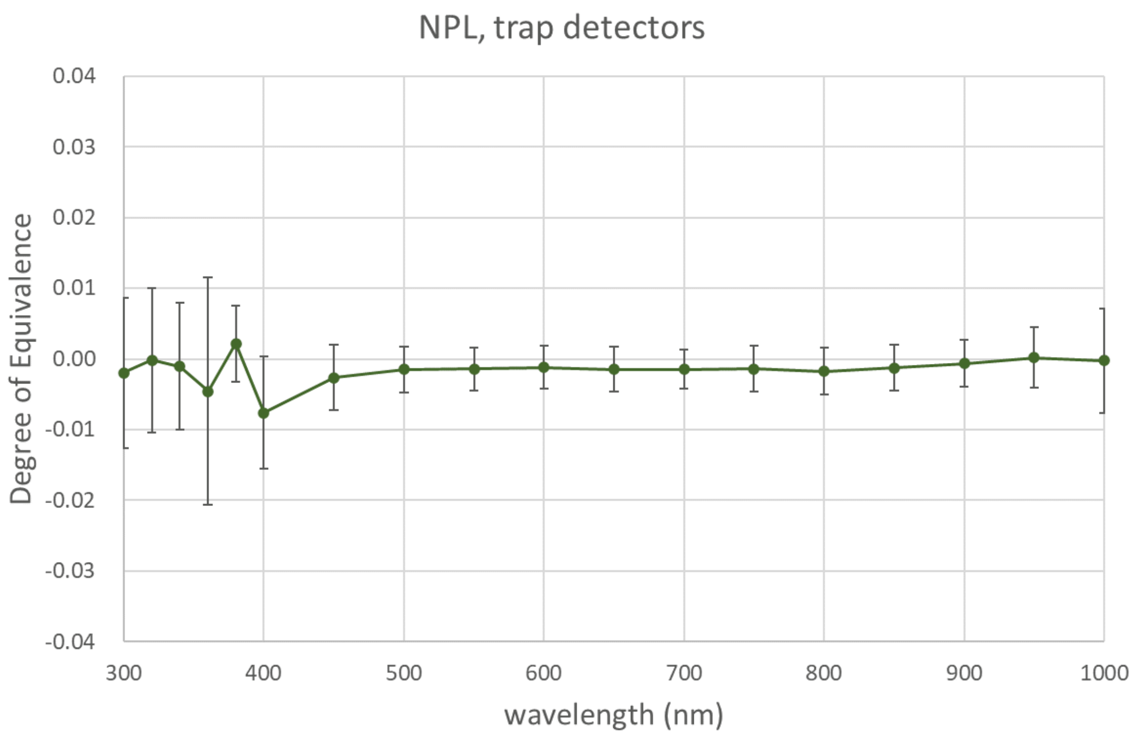


**Figure A-12.** Results of the degree of equivalence (DoE) of NPL as a function of wavelength for the single-element detectors (top) and the trap detectors (bottom). The error bars indicate the expanded uncertainties of DoEs ($k = 2$).

# CCPR-K2.b.2016
# Spectral Responsivity 300 nm to 1000 nm
# Final Report
# Appendix B
# Technical Report of Each Participant

# 1. KRISS

## 1.1. Measurement Setup and Instruments

Figure 1-1 shows the schematic setup of the spectral responsivity comparator at KRISS. The detector under test (DUT) is compared with the reference detector (REF) at a collimated, monochromatic beam with a variable diameter, which is delivered from a lamp-based wavelength-variable source via a fused-silica fibre bundle. The wavelength-variable source consists of a double-grating monochromator and a lamp that is selected by a flip mirror between a quartz-tungsten halogen (QTH) lamp (for wavelength longer than 400 nm) and a Hg(Xe) lamp (for wavelength shorter than 400 nm). The photocurrent output signals from the REF and from the DUT are measured with a pico-ammeter and an electrometer, respectively. By using a multi-channel switch, more than one DUT can be compared in this setup. In addition, a source-meter is used to measure the resistance of the temperature sensor mounted at the DUT for the comparison.

As the REF, a reflection-type trap detector consisting of three Si photodiodes (Hamamatsu S6337-01, active area 18 mm x 18 mm) is used. The DUT is mounted in a temperature-controlled holder. In addition to REF and DUT, another temperature-stabilized single-element photodiode (Hamamatsu S1337-1010BQ) was mounted as a monitoring (MON) detector for long-term stability and also for measurement of temperature coefficients of the transfer detectors. The position of the MON was fixed through all the comparison measurements. The photocurrent signals of three detectors are recorded in sequence by moving the translation stage.

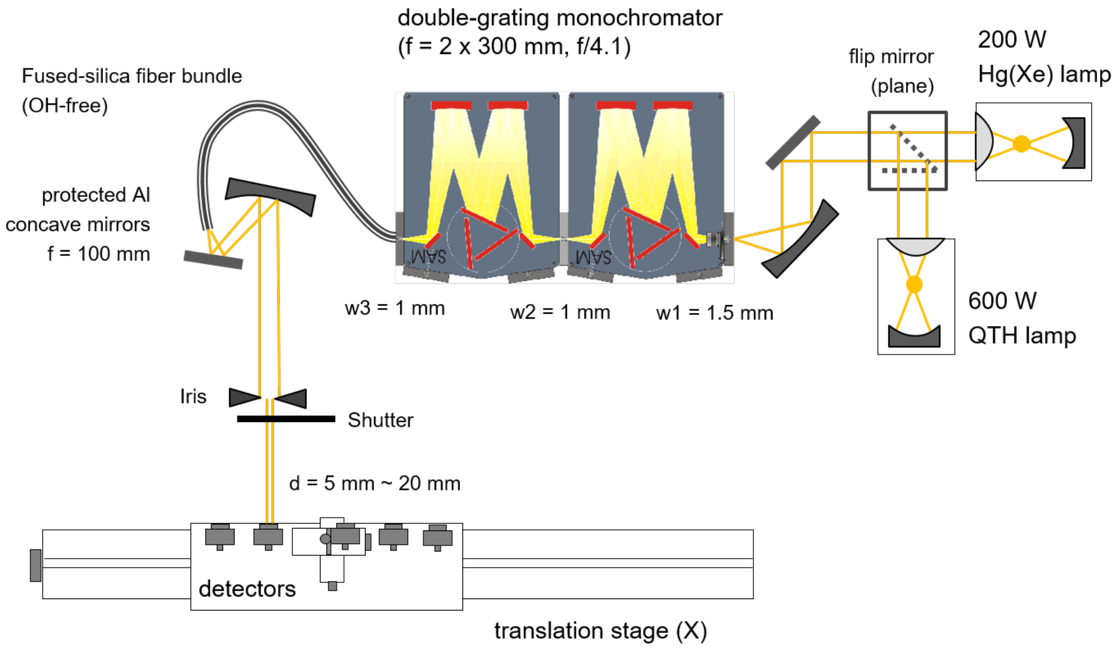


**Figure 1-1. Spectral responsivity comparator setup at KRISS.**

## 1.2. Measurement Conditions and Parameters

The setup is operated in the ambient conditions with temperature of (23.0 ± 3) °C and relative humidity of less than 55 %. The ambient conditions are monitored by using a calibrated temperature/humidity meter. In addition, the temperature of the detectors to be measured is kept constant by using a water-circulated mount. The temperature of the detector is monitored by measuring the resistance of the PT100 sensor inside the detector with a source-meter in the 4-wire configuration.

The monochromatic beam used for the spectral responsivity measurement is collimated and aligned at the centre of the clear aperture of the detector at the normal incidence. The beam at the detector surface has a round shape with a diameter of approximately 5 mm. The alignment is visually verified by using a mask for the clear aperture of the detector with a hole at the centre. The spectral bandwidth is measured to be in the range from 3.5 nm to 4 nm, and the spectral radiant power from $10^{-10}$ W to $10^{-8}$ W, depending on wavelength. The polarisation of the beam is randomised through the use of a fibre bundle in the setup so that the radiation is nearly un-polarised, i.e. the S and P polarisation components of the beam are of the same amount.

## 1.3. Traceability of Measurement

The reference detector used for the spectral responsivity measurement is calibrated traceable to the scale realisation at KRISS based on the absolute cryogenic radiometer at two laser wavelengths and the spectral reflectance of a pyroelectric detector at other wavelengths. The electrical measurements as well as the temperature and humidity measurements are traceable to the up-to-date realisation of the measurement standards at KRISS.

## 1.4. Measurement Uncertainty

The measurement equation of the spectral responsivity at a wavelength $\lambda$ is written as

$$S_{\mathrm{T}}(\lambda) = \frac{y_{\mathrm{T}}}{y_{\mathrm{R}}} S_{\mathrm{R}}(\lambda),$$

where $S_{\mathrm{T}}$ and $S_{\mathrm{R}}$ denote the spectral responsivity of the detector under test (DUT) and of the reference detector (REF), respectively, and $y_{\mathrm{T}}$ and $y_{\mathrm{R}}$ the photo-current reading of DUT and REF, respectively. From the measurement equation above, we can derive the following equation for the relative standard uncertainties:

$$u_r^2(S_{\mathrm{T}}) = u_r^2(y_{\mathrm{T}}) + u_r^2(y_{\mathrm{R}}) + u_r^2(y_{\mathrm{T}} / y_{\mathrm{R}}) + u_r^2(S_{\mathrm{R}}).$$

The uncertainties of the current readings, $u_{\mathrm{r}}(y_{\mathrm{T}})$ and $u_{\mathrm{r}}(y_{\mathrm{R}})$, have two components. The one is a random component evaluated from the standard deviation of the repeated readings. The other is a systematic component propagated from the calibration of the current-reading instruments. The uncertainty due to the ambient stray light is neglected because the dark signal is measured and subtracted at each reading of the DUT as well as the REF.

The uncertainty of the current ratio, $u_{\mathrm{r}}(y_{\mathrm{T}}/ y_{\mathrm{R}})$, consists of multiple components. First, the limited accuracy of the set wavelength of the monochromatic source influences the ratio measurement. The propagation equation of the wavelength error is

$$u_r(y_{\mathrm{T}} / y_{\mathrm{R}}) = \left| \frac{1}{y_{\mathrm{T}}} \frac{\partial y_{\mathrm{T}}}{\partial \lambda} - \frac{1}{y_{\mathrm{R}}} \frac{\partial y_{\mathrm{R}}}{\partial \lambda} \right| \cdot u(\lambda).$$

Here, the uncertainty of setting the centroid wavelength of the monochromatic light source, $u(\lambda)$, is evaluated to be 0.3 nm in the range from 300 nm to 1000 nm.

A change of the radiant power from the monochromatic source is another dominant source of uncertainty for the current ratio measurement. While fast power fluctuations within the duration of each detector reading are considered in the repeatability uncertainty components of each current reading, slow variations in the time scale of a second during subsequent readings of REF and DUT could not be directly monitored in our setup. Therefore, the readings of the current ratio were repeated 6 times and the uncertainty due to power drift of the source was evaluated from its standard deviation as a random component. The uncertainty due to power drift of the source was relatively high for the wavelength range below 400 nm where a Hg(Xe) lamp was used, especially at those wavelengths near the emission peaks.

The uncertainty of the current ratio, $u_{\mathrm{r}}(y_{\mathrm{T}}/ y_{\mathrm{R}})$, include also components due to the spectral bandwidth as well as component due to spectral stray of the light source. Within the spectral bandwidth of less than

4 nm (FWHM), the spectral responsivity of both REF and DUT can be approximated to be linear against the wavelength. Therefore, its dependence on the spectral bandwidth is negligible compared with that on the centroid wavelength error. The spectral stray of the double-stage monochromator in the subtractive configuration as used in the setup is specified to be less than $10^{-8}$ so that its effect is also negligible compared to the uncertainty component due to the lamp instability. For these two minor components, we estimate the standard uncertainty of 0.01 % as the estimated upper-limit.

The uncertainty related to the beam parameters such as beam alignment, beam size and divergence, beam polarisation, etc. contribute to the uncertainty of the current ratio measurement. For single-element detectors, we estimated this uncertainty based on the worst-case assumption: we assume that the beam size can vary from 4 mm to 6 mm, and the beam centring alignment is accurately performed within ±1 mm. Then, we determine the relative variation of the current ratio as the beam parameter varies within the above range. The maximum uncertainty contribution from this representative calculation is used as the uncertainty component due to beam alignment and beam size. The dependence on the beam divergence and beam polarisation is regarded as negligible for the normal incidence condition. However, we had to consider an uncertainty component due to back-reflection of light from a single-element detector at the normal incidence. We found that a noticeable amount of the reflected light from the detector returns to the detector due to reflection at the normal-cut facet of the fibre bundle (see Figure 1-1). This systematic error of the setup was strong in the wavelength range below 400 nm where the reflection from the Si photodiode increases. We estimated the error due to back-reflection by measuring the single-element detectors at another comparator setup where the influence from the back-reflection was confirmed to be negligible. From the relative difference of the results obtained from two different setups, we estimated the uncertainty component due to back-reflection from the single-element detector.

For trap detectors, the error or uncertainty due to back-reflection is neglected. However, the uncertainty components related with the beam parameters were difficult to estimate based on the experimental variation of the beam as the narrow acceptance angle and small input aperture of the transfer detector did not allow a variation of the beam alignment or beam size. Instead, we measured the trap detectors at another comparator setup with a different beam divergence (f/8) and a smaller beam size at the focus (2 mm × 2 mm). From the relative difference of the results obtained from two different setups, we estimated the uncertainty component due to beam alignment, beam size, and beam divergence for trap detectors.

The uncertainty of the REF responsivity, $u_r(S_R)$, is referred to the calibration result of the REF used. The trap detector used as the REF in the setup of Figure 1-1 was calibrated by comparison with another transfer-standard Si trap detector whose spectral responsivity is calibrated in two steps: absolute calibration at two laser wavelengths against the cryogenic radiometer and extrapolation to other wavelengths against a pyroelectric detector[1].

The non-linearity of the responsivity of the same type photodiode of the DUT, Hamamatsu S1337-1010BQ, is measured at a separate linearity tester[2]. Although there exists a wavelength-dependence, we estimated from this representative test results that the maximum variation of responsivity due to non-linearity of responsivity in a photo-current range from 100 nA down to 100 pA is 0.1 %, which corresponds to a relative standard uncertainty component of 0.06 %.

**Table 1-1. Uncertainty budget of spectral responsivity at 300 nm for a trap detector (typical).**

| Uncertainty Component | Standard uncertainty (%) | Type | Probability distribution | Sensitivity coefficient | Contribution (%) | Deg. of freedom | Correlated? |
|---|---|---|---|---|---|---|---|

[1] Seongchong Park *et al.*, Measurement-based extrapolation of spectral responsivity by using a low-NEP pyroelectric detector, *Measurement Science and Technology*, **33**, 015013 (2022)
[2] Dong-Joo Shin *et al.*, High-accuracy measurement of linearity of optical detectors based on flux addition of LEDs in an integrating sphere, *Metrologia*, 51, 25-32 (2014)

| | | | | | | | |
|---|---|---|---|---|---|---|---|
| Reading repeatability of DUT | 0.04 | A | t | 1 | 0.04 | 10 | X |
| Reading repeatability of REF | 0.05 | A | t | 1 | 0.05 | 10 | X |
| Calibration uncertainty of current-reading instrument | 0.002 | B | normal | 1 | 0.002 | ∞ | O |
| Uncertainty from ambient stray light | N.A. | | | | | | |
| Uncertainty from wavelength error of light source | <0.01 | B | rectangular | 1 | <0.01 | ∞ | O |
| Uncertainty from power drift of light source | 0.07 | A | t | 1 | 0.07 | 6 | X |
| Uncertainty from spectral bandwidth of light source | <0.01 | B | rectangular | 1 | <0.01 | ∞ | O |
| Uncertainty from spectral stray of light source | <0.01 | B | rectangular | 1 | <0.01 | ∞ | O |
| Uncertainty related to beam alignment, size, and divergence | 0.06 | B | rectangular | 1 | 0.03 | ∞ | O |
| Uncertainty related to beam polarization | N.A. | | | | | | |
| Uncertainty from calibration of REF | 0.2 | B | normal | 1 | 0.2 | ∞ | O |
| Uncertainty from detector non-linearity of DUT | 0.06 | B | rectangular | 1 | 0.06 | ∞ | O |
| **Combined standard uncertainty (%)** | **--** | **--** | **normal** | **--** | **0.23** | >100 | **--** |

**Table 1-2. Uncertainty budget of spectral responsivity at 500 nm for a trap detector (typical).**

| Uncertainty Component | Standard uncertainty (%) | Type | Probability distribution | Sensitivity coefficient | Contribution (%) | Deg. of freedom | Correlated? |
|---|---|---|---|---|---|---|---|
| Reading repeatability of DUT | 0.02 | A | t | 1 | 0.02 | 10 | X |
| Reading repeatability of REF | 0.02 | A | t | 1 | 0.02 | 10 | X |
| Calibration uncertainty of current-reading instrument | 0.002 | B | normal | 1 | 0.002 | ∞ | O |
| Uncertainty from ambient stray light | N.A. | | | | | | |
| Uncertainty from wavelength error of light source | <0.01 | B | rectangular | 1 | <0.01 | ∞ | O |
| Uncertainty from power drift of light source | 0.005 | A | t | 1 | 0.005 | 6 | X |

| | | | | | | | |
|---|---|---|---|---|---|---|---|
| Uncertainty from spectral bandwidth of light source | <0.01 | B | rectangular | 1 | <0.01 | ∞ | O |
| Uncertainty from spectral stray of light source | <0.01 | B | rectangular | 1 | <0.01 | ∞ | O |
| Uncertainty related to beam alignment, size, and divergence | 0.07 | B | rectangular | 1 | 0.04 | ∞ | O |
| Uncertainty related to beam polarization | N.A. | | | | | | |
| Uncertainty from calibration of REF | 0.2 | B | normal | 1 | 0.2 | ∞ | O |
| Uncertainty from detector non-linearity of DUT | 0.06 | B | rectangular | 1 | 0.06 | ∞ | O |
| **Combined standard uncertainty (%)** | **--** | **--** | **normal** | **--** | **0.22** | >100 | **--** |

**Table 1-3. Uncertainty budget of spectral responsivity at 300 nm for a single-element detector (typical).**

| **Uncertainty Component** | **Standard uncertainty (%)** | **Type** | **Probability distribution** | **Sensitivity coefficient** | **Contribution (%)** | **Deg. of freedom** | **Correlated?** |
|---|---|---|---|---|---|---|---|
| Reading repeatability of DUT | 0.04 | A | t | 1 | 0.04 | 10 | X |
| Reading repeatability of REF | 0.04 | A | t | 1 | 0.04 | 10 | X |
| Calibration uncertainty of current-reading instrument | 0.002 | B | normal | 1 | 0.002 | ∞ | O |
| Uncertainty from ambient stray light | N.A. | | | | | | |
| Uncertainty from wavelength error of light source | 0.06 | B | rectangular | 1 | 0.06 | ∞ | O |
| Uncertainty from power drift of light source | 0.15 | A | t | 1 | 0.15 | 6 | X |
| Uncertainty from spectral bandwidth of light source | <0.01 | B | rectangular | 1 | <0.01 | ∞ | O |
| Uncertainty from spectral stray of light source | <0.01 | B | rectangular | 1 | <0.01 | ∞ | O |
| Uncertainty related to beam alignment and beam size | 0.12 | B | rectangular | 1 | 0.12 | ∞ | O |
| Uncertainty related to beam divergence and polarization | N.A. | | | | | | |
| Uncertainty from calibration of REF | 0.2 | B | normal | 1 | 0.2 | ∞ | O |
| Uncertainty from detector non-linearity of DUT | 0.06 | B | rectangular | 1 | 0.06 | ∞ | O |
| Uncertainty due to back-reflection | 0.18 | B | rectangular | 1 | 0.18 | ∞ | O |

| | | | | | | | |
|---|---|---|---|---|---|---|---|
| **Combined standard uncertainty (%)** | **--** | **--** | **normal** | **--** | **0.35** | >100 | **--** |

**Table 1-4. Uncertainty budget of spectral responsivity at 500 nm for a single-element detector (typical).**

| Uncertainty Component | Standard uncertainty (%) | Type | Probability distribution | Sensitivity coefficient | Contribution (%) | Deg. of freedom | Correlated? |
|---|---|---|---|---|---|---|---|
| Reading repeatability of DUT | 0.02 | A | t | 1 | 0.02 | 10 | X |
| Reading repeatability of REF | 0.03 | A | t | 1 | 0.03 | 10 | X |
| Calibration uncertainty of current-reading instrument | 0.002 | B | normal | 1 | 0.002 | ∞ | O |
| Uncertainty from ambient stray light | N.A. | | | | | | |
| Uncertainty from wavelength error of light source | 0.01 | B | rectangular | 1 | 0.01 | ∞ | O |
| Uncertainty from power drift of light source | 0.04 | A | t | 1 | 0.04 | 6 | X |
| Uncertainty from spectral bandwidth of light source | <0.01 | B | rectangular | 1 | <0.01 | ∞ | O |
| Uncertainty from spectral stray of light source | <0.01 | B | rectangular | 1 | <0.01 | ∞ | O |
| Uncertainty related to beam alignment and beam size | 0.02 | B | rectangular | 1 | 0.02 | ∞ | O |
| Uncertainty related to beam divergence and polarization | N.A. | | | | | | |
| Uncertainty from calibration of REF | 0.2 | B | normal | 1 | 0.2 | ∞ | O |
| Uncertainty from detector non-linearity of DUT | 0.06 | B | rectangular | 1 | 0.06 | ∞ | O |
| Uncertainty due to back-reflection | 0.04 | B | rectangular | 1 | 0.04 | ∞ | O |
| **Combined standard uncertainty (%)** | **--** | **--** | **normal** | **--** | **0.22** | >100 | **--** |

Figure 1-2 and 1-3 show the combined relative standard uncertainties (blue symbols with connecting lines) and the combined relative standard uncertainties of the uncorrelated random components (red symbols with connecting lines) for a trap detector and a single-element detector, respectively, as a function of wavelength. The grey symbols with connecting lines in the figures show the calibration uncertainties of the REF.

For both types of detectors, the random, uncorrelated uncertainty components are increased in the wavelength range below 400 nm mainly due to the poor power stability of the used Hg(Xe) lamp. For trap detectors, an additional increase of the uncertainty compared to the REF uncertainty is dominated by the uncertainty related to beam alignment, size, and divergence. The results from two different setups with different beam parameters showed noticeable differences, which were considered as uncertainty components for trap detectors. For single-element detectors, the combined uncertainties are close to the those of the REF in the visible and near-infrared ranges, while an significant increase in the wavelength below 450 nm is noticeable due to the large uncorrelated uncertainties as well as the uncertainties due to back-reflection from the detector at the normal incidence.

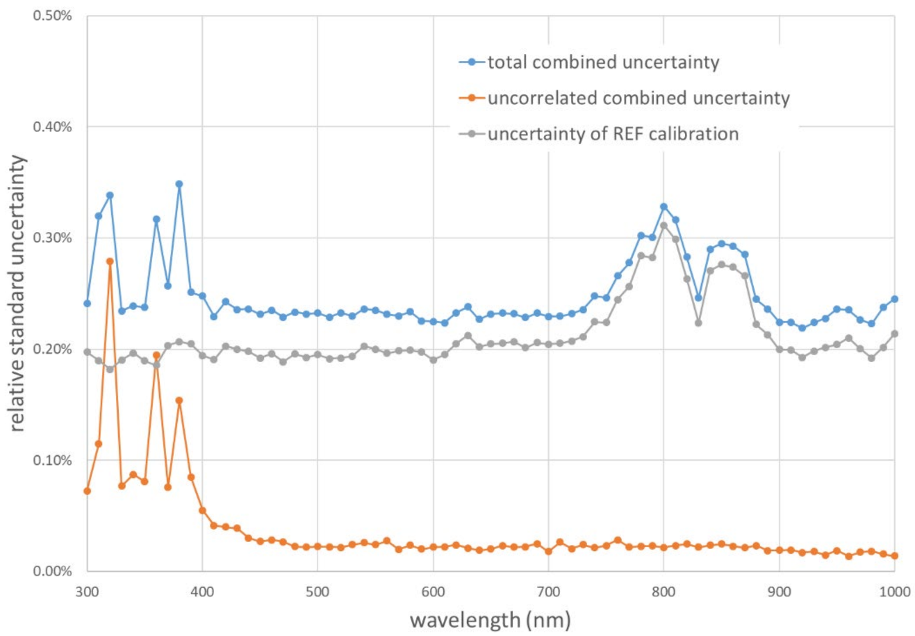


**Figure 1-2. Uncertainty of spectral responsivity for a trap detector at KRISS (typical).**

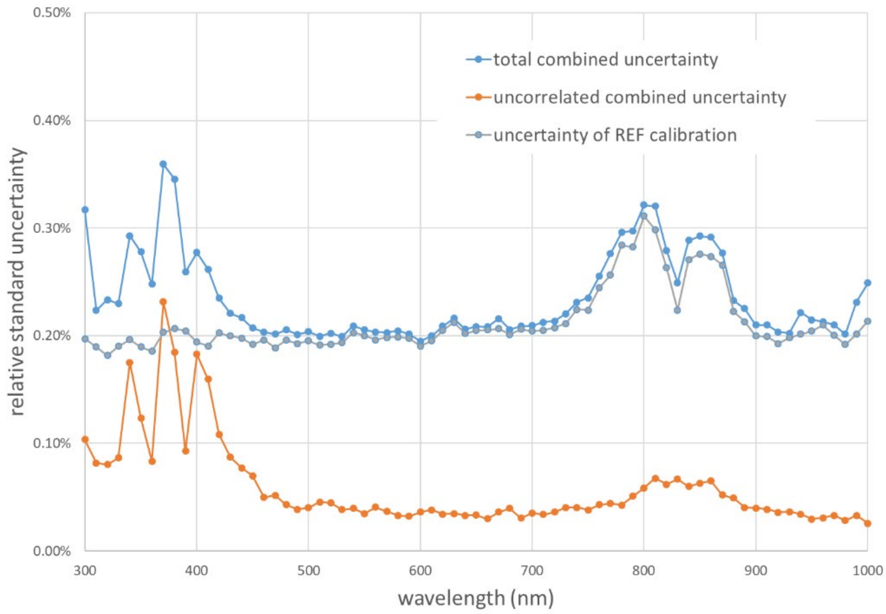


**Figure 1-3. Uncertainty of spectral responsivity for a single-element detector at KRISS (typical).**

### 1.5. Long-term reproducibility

In order to evaluate the long-term reproducibility of the pilot setup during the whole period of the comparison, the relative change of responsivity for the MON mounted at the fixed position and operated at a fixed temperature was recorded from May 2016 to February 2021. The results are shown in Figure 1-4. From the maximum changes at each wavelength, relative uncertainties of long-term reproducibility $u_{PR}$ are calculated assuming a rectangular distribution, as shown in Table 1-5. Figure 1-5 shows the reproducibility uncertainties together with the uncertainties of a single-element detector from Figure 1-3 for comparison.

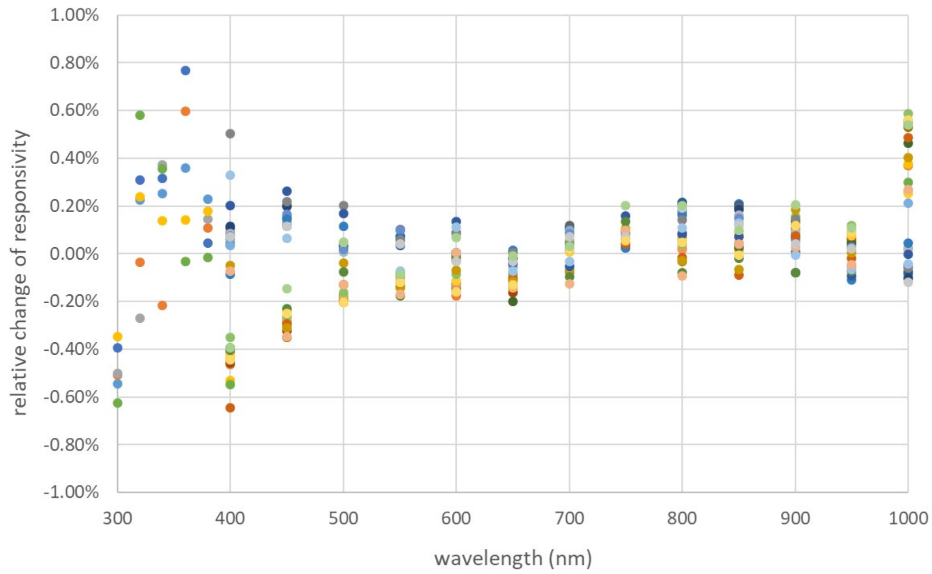


**Figure 1-4. Relative change of the MON responsivity in a period from May 2016 to February 2021 for evaluation of the long-term reproducibility of the KRISS setup.**

**Table 1-5. Long-term reproducibility uncertainty $u_{PR}$ of the pilot lab KRISS.**

| Wavelength (nm) | Relative Standard Uncertainty (%) |
|---|---|
| 300 | 0.36% |
| 320 | 0.34% |
| 340 | 0.21% |
| 360 | 0.72% |
| 380 | 0.13% |
| 400 | 0.37% |
| 450 | 0.20% |
| 500 | 0.12% |
| 550 | 0.10% |
| 600 | 0.10% |
| 650 | 0.11% |
| 700 | 0.07% |
| 750 | 0.12% |

| | |
|---|---|
| 800 | 0.12% |
| 850 | 0.12% |
| 900 | 0.12% |
| 950 | 0.07% |
| 1000 | 0.34% |

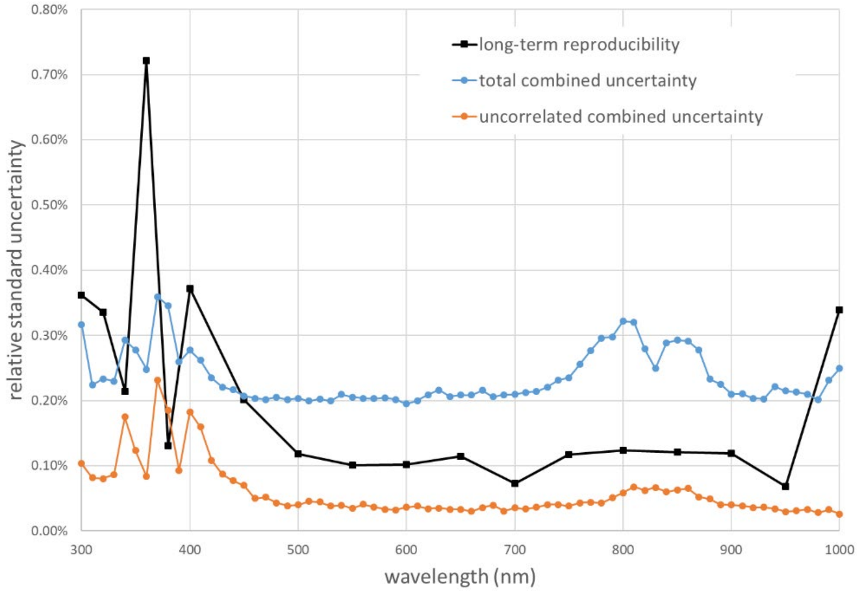


**Figure 1-5. Long-term reproducibility uncertainty of KRISS evaluated from Figure 1-4, compared with typical uncertainty of a single-element detector copied from Figure 1-3.**

The results of Figure 1-4 and 1-5 show that the reproducibility of the setup is at least twice of the uncorrelated uncertainties evaluated for a short-term measurement of a detector. Moreover, at the wavelength range below 450 nm, the reproducibility of the setup was larger than the total uncertainty of the spectral responsivity measurement. At a wavelength of 1000 nm, the large reproducibility can be explained by the temperature-dependence of the REF trap detector, which was not temperature-controlled. The large peak near 350 nm could be related with the emission peak of the Hg(Xe) lamp, at which the stability was generally poor and the error due to back reflection from the detector could be significant due to large radiant power. We conclude from these results that the environmental and operation conditions of the setup was not sufficiently controlled for the whole period of comparison. Note that this reproducibility is not related with any properties of the detectors to be measured.

The long-term reproducibility uncertainties of Figure 1-5 are representatively used as the reproducibility of pilot measurements $u_{\mathrm{r}}\left(s_{i,j}^{PR}\right)$ of each detector *j* of participant *i* in the comparison data analysis.

# 2. NMC-A*STAR

## 2.1. *Measurement Setup and Instruments*

**Description of primary standard, including beam parameters**:

1) Primary standard: Oxford Instruments Ltd. mechanically cooled cryogenic radiometer.
2) Three laser sources were used in the measurement which are:

   a) He-Ne laser: wavelength = 632.8 nm, stabilized power = 0.25 mW
   b) Diode laser: wavelength = 532.0 nm, stabilized power = 0.31 mW
   c) Ti: sapphire laser : wavelength = 799.3 nm, stabilized power = 0.14 mW
3) The laser beams were collimated to about 3 mm to 4 mm in diameter.

**Laboratory transfer standards used:**

1) Absolute transfer standard - a silicon reflection trap detector (NPL customized, s/n: NPL-06), wavelength range : (400 nm – 900 nm)
2) Relative transfer standard - a cavity pyroelectric detector (NPL customized, s/n: CP-09), wavelength range : (200 nm – 2000 nm)
3) Secondary standard - a silicon photodiode (Hamamatsu S2281, s/n: E460), wavelength range: (300 nm – 1000 nm)

**Monochromator used, including beam parameters:**

1) Double-grating monochromator (CVI DK242, f/4) with three types of gratings (UV, Vis and NIR). Second-order filters at the entrance;
2) Additional monitor detector at the output;
3) Sources: a 200 W XENOPHOT HLX halogen lamp for spectral range (300 nm – 450 nm) and a 200 W tungsten strip lamp for spectral range (400 nm – 1000 nm)
4) The beam sizes on detector head are: (f/7.5 for single photodiode detector, f/8.7 for trap detector)
   a) 2 mm by 2 mm (300 nm – 400 nm), bandwidth = 3 nm
   b) 1.333 mm by 2 mm (400 nm – 900 nm), bandwidth = 4 nm
   c) 1.667 mm by 2 mm (900 nm – 1000 nm), bandwidth = 10 nm

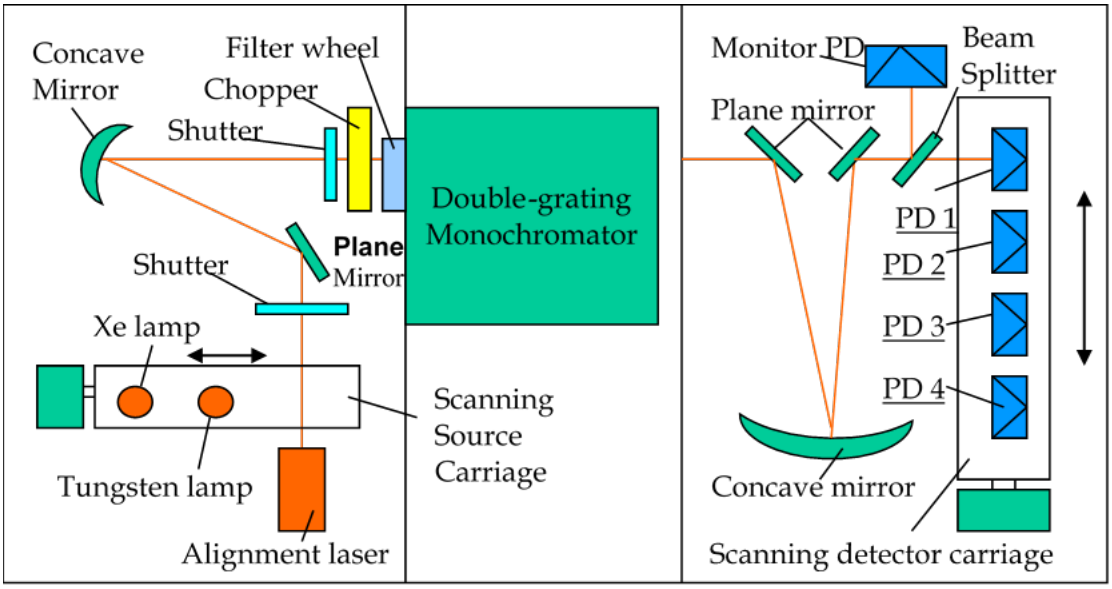


**Figure 2-1. Spectral responsivity calibration facility in NMC, ASTAR Singapore.**

## *2.2. Measurement Conditions and Parameters*

Two KC transfer standard - silicon trap detectors were calibrated by a primary standard – cryogenic radiometer at three laser wavelengths (799.3 nm, 632.8 nm, and 532.0 nm) then their spectral responsivity values were interpolated and extrapolated in the spectral range of 400 nm – 900 nm through linear fitting. Three KC transfer standard – single silicon photodiodes were calibrated by a calibrated KC trap detector in a spectral responsivity calibration facility (SRCF as in Fig. 1) in the spectral range of 400 nm – 900 nm. The calibration was extended into UV range of 300 nm – 400 nm and IR range of 900 nm – 1000 nm through a NMC relative transfer standard - cavity pyroelectric detector (CPD) which is spectrally flat in the range of 200 nm – 2000 nm. All KC transfer detectors were then calibrated by the CPD in the spectral range of 950 nm - 1000 nm, but had to be calibrated against a NMC reference standard – Si photodiode in the spectral range of 300 nm – 380 nm which was calibrated by the CPD before.

The KC transfer detectors and the NMC standard detector were mounted on a scanning carriage with their plane vertical and centre aligned with the direction of measurement. The radiation from 300 nm to 380 nm (20 nm increment) was obtained from a 200 W XENOPHOT HLX halogen lamp and a double grating monochromator (3 nm bandwidth). The radiation from 400 nm to 1000 nm (50 nm increment) was obtained from a 200 W tungsten strip lamp and a double grating monochromator (bandwidth: 4 nm in range of 400 nm - 900 nm and 10 nm in range of 950 nm -1000 nm). Detectors were under filled by the light beam with beam size of 2 x 2 mm$^2$ in the range of 300 nm - 380 nm, 1.3 x 2 mm$^2$ in the range of 400 nm - 900 nm, and 1.67 x 2 mm$^2$ in the range of 950 nm -1000 nm. The short-circuit photocurrents from detectors were measured using calibrated current-to-voltage converter and digital volt meter. The output signal of the cavity pyroelectric detector was measured by a current-to-voltage converter and a lock-in amplifier. The spectral responsivity values of the KC transfer detectors were calculated by the following equation (2-1).

$$s_t(\lambda) = s_r(\lambda)\frac{i_t(\lambda)}{i_r(\lambda)} \qquad (2-1)$$

where $s_t(\lambda)$ and $s_r(\lambda)$ are spectral responsivity values of the KC transfer and NMC standard detectors respectively, and $i_t(\lambda)$ and $i_r(\lambda)$ are photocurrent values of the KC transfer and NMC standard detectors at wavelength $\lambda$ respectively.

**Calibration laboratory conditions:**

1) Laboratory Temperature: (24 ± 2) °C
2) Relative Humidity: (60 ± 10) %

## *2.3. Traceability of Measurement*

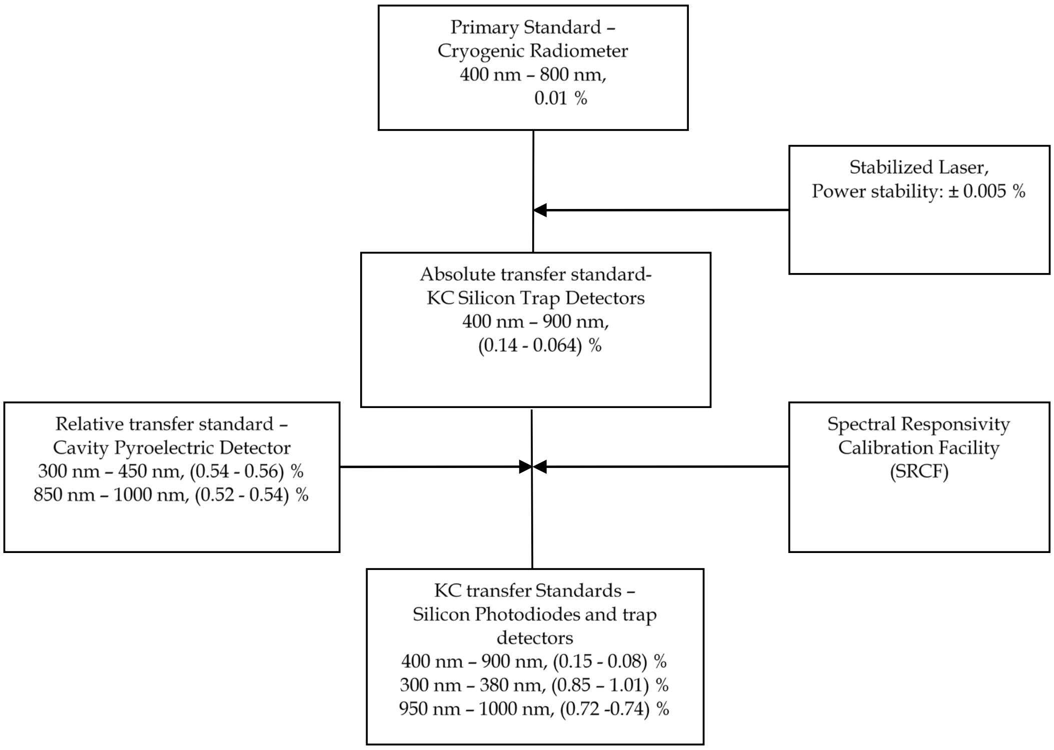


**Figure 2-2. Traceability chart of spectral responsivity scale at NMC (all measurement uncertainty values in the chart are relative standard uncertainty, *k* = 1).**

## *2.4. Measurement Uncertainty*

### 2.4.1. Calibration uncertainty of laser power using cryogenic radiometer (CR)

**Table 2-1. Uncertainty budget for laser power measurement by CR at 632.8 nm**

| s/n | Source of uncertainty | Type | Value ($10^{-4}$) | Sensitivity coefficient (c ) | Probability distribution | Coverage factor (k) | Relative standard uncertainty ($10^{-4}$) | Degree of Freedom |
|---|---|---|---|---|---|---|---|---|
| 1 | Cavity absorption | B | 0.1 | 1 | Rectangular | 1.732 | 0.058 | ∞ |
| 2 | Brewster window transmittance | A | 0.32 | 1 | Normal | 1 | 0.32 | 4 |
| 3 | Brewster window scatter (c=Ps/P=0.00002mW/0.248808 mW=0.00008 ) | B | 125 | 0.00008 | Normal | 1 | 0.01 | ∞ |
| 4 | Electrical power measurement | B | 0.34 | 1 | Normal | 2 | 0.17 | ∞ |
| 5 | Non-equivalence of optical and electrical power | B | 0.02 | 1 | Rectangular | 1.732 | 0.01 | ∞ |
| 6 | Measurement repeatability | A | 0.59 | 1 | | | 0.59 | 4 |
| | Combined standard uncertainty (*k* = *1*) | | | | | | 0.69 | |

**Table 2-2. Uncertainty budget for laser power measurement by CR.**

| s/n | Source of uncertainty | Wavelength / nm | | |
|---|---|---|---|---|
| | | 532.0 | 632.8 | 799.3 |
| | | relative standard uncertainty ($10^{-4}$) | | |
| 1 | Cavity absorption | 0.058 | 0.058 | 0.058 |
| 2 | Brewster window transmittance | 0.31 | 0.32 | 0.35 |
| 3 | Brewster window scatter | 0.01 | 0.01 | 0.03 |
| 4 | Electrical power measurement | 0.17 | 0.17 | 0.17 |
| 5 | Non-equivalence of optical and electrical power | 0.01 | 0.01 | 0.01 |
| 6 | Measurement repeatability | 0.87 | 0.59 | 0.80 |
| | | | | |
| | combined standard uncertainty ($k = 1$) | 0.94 | 0.69 | 0.89 |

## 2.4.2. Calibration uncertainty of KC trap detector by using CR

**Table 2-3. Uncertainty budget for calibration of KC trap detector by CR at 632.8 nm.**

| s/n | Source of uncertainty | Type | Value ($10^{-4}$) | Sensitivity coefficient (c ) | Probability distribution | Coverage factor (k) | Relative standard uncertainty ($10^{-4}$) | Degree of Freedom |
|---|---|---|---|---|---|---|---|---|
| 1 | Optical power measurement by CR | B | 1.38 | 1 | Normal | 2 | 0.69 | ∞ |
| 2 | Detector DVM accuracy | B | 0.47 | 1 | Rectangular | 1.732 | 0.27 | ∞ |
| 3 | Amplifier calibration | B | 0.60 | 1 | Normal | 2 | 0.30 | ∞ |
| 4 | Positional reproducibility | B | 0.43 | 1 | Rectangular | 1.732 | 0.25 | ∞ |
| 5 | Measurement repeatability | A | 0.86 | 1 | | | 0.86 | 4 |
| | | | | | | | | |
| | Combined standard uncertainty ($k = 1$) | | | | | | 1.20 | |

**Table 2-4. Uncertainty budget for calibration of KC trap detector by CR.**

| s/n | Source of uncertainty | Wavelength / nm | | |
|---|---|---|---|---|
| | | 532.0 | 632.8 | 799.3 |
| | | relative standard uncertainty($10^{-4}$) | | |
| 1 | Optical power measurement by CR | 0.94 | 0.69 | 0.89 |
| 2 | Detector DVM accuracy | 0.45 | 0.27 | 0.19 |
| 3 | Amplifier calibration | 0.30 | 0.30 | 0.30 |
| 4 | Positional reproducibility | 0.25 | 0.25 | 0.25 |
| 5 | Measurement repeatability | 0.81 | 0.86 | 0.87 |
| | | | | |
| | Combined standard uncertainty ($k = 1$) | 1.38 | 1.20 | 1.32 |

### 2.4.3. Calibration uncertainty of KC trap detector (400 – 900) nm by linear fitting

The calibration uncertainty of KC trap detector, $u_c(\lambda)$, is combination of uncertainties in the measurement using CR at laser wavelengths, $u_{CR}(\lambda)$, and that of linear fitting, $u_{linearFitting}(\lambda)$, in wavelength range (400 – 900) nm, as shown in equation (2-2):

$$u^2_c(\lambda) = u^2_{CR}(\lambda) + u^2_{linearFitting}(\lambda) \qquad (2\text{-}2)$$

The relative standard uncertainty ($k$ =1) are (0.141% - 0.064%) in wavelength range (400 – 900) nm as shown in Table 2-5 below.

**Table 2-5. Standard uncertainty of KC trap detector calibration (400 – 900) nm**

| Wavelength (nm) | Standard uncertainty ($k$ = 1) % |
|---|---|
| 400 | 0.141 |
| 450 | 0.126 |
| 500 | 0.113 |
| 550 | 0.103 |
| 600 | 0.094 |
| 650 | 0.087 |
| 700 | 0.081 |
| 750 | 0.076 |
| 800 | 0.071 |
| 850 | 0.067 |
| 900 | 0.064 |

### 2.4.4. Calibration uncertainty of KC Si photodiode (PD) by using KC trap detector (TD) (400 – 900) nm

**Table 2-6. Calibration uncertainty of Si photodiode (A#1) using calibrated trap detector (s/n: A#4) at 400 nm**

| s/n | Source of uncertainty | Type | Value (%) | Sensitivity coefficient (c ) | Probability distribution | Coverage factor (k) | Relative standard uncertainty (%) | Degree of Freedom |
|---|---|---|---|---|---|---|---|---|
| 1 | Signal repeatability of Si PD | A | 0.0035 | 1 | | | 0.0035 | 6 |
| 2 | accuracy of DVM (signal channel) | B | 0.0026 | 1 | Normal | 2 | 0.0013 | ∞ |
| 3 | Alignment of Si PD | B | 0.018 | 1 | Rectangular | 1.732 | 0.0104 | ∞ |
| 4 | Signal repeatability of std trap detector (TD) | A | 0.0027 | 1 | | | 0.0027 | 6 |
| 5 | Accuracy of DVM (TD channel) | B | 0.0020 | 1 | Normal | 2 | 0.0010 | ∞ |
| 6 | Alignment of Std TD | B | 0.04 | 1 | Rectangular | 1.732 | 0.0231 | ∞ |
| 7 | Unc. of amplifier gain of Si PD | B | 0.06 | 1 | Normal | 2 | 0.03 | ∞ |
| 8 | Unc. of amplifier gain of Std TD | B | 0.06 | 1 | Normal | 2 | 0.03 | ∞ |
| 9 | Cal unc. of std TD | B | 0.28 | 1 | Normal | 2 | 0.14 | ∞ |

| | | | | | | | | |
|---|---|---|---|---|---|---|---|---|
| 10 | Unc. due to wavelength error (0.1 nm) of monochromator | B | 0.03696 | 1 | Rectangular | 1.732 | 0.0213 | ∞ |
| 11 | Effect of polarisation of beam | B | 0.058 | 1 | Rectangular | 1.732 | 0.0335 | ∞ |
| | Combined standard uncertainty (*k = 1*) | | | | | | 0.15 | |

The combined relative standard uncertainty (k = 1) values for calibration of Si photodiode are 0.15 % – 0.08 % in the spectral range of 400 nm - 900 nm as shown in Table 2-7 below.

**Table 2-7. Combined standard uncertainty of KC single photodiode calibration (400 – 900) nm**

| Wavelength (nm) | Combined uncertainty (k = 1) % |
|---|---|
| 400 | 0.150 |
| 450 | 0.135 |
| 500 | 0.123 |
| 550 | 0.114 |
| 600 | 0.112 |
| 650 | 0.100 |
| 700 | 0.094 |
| 750 | 0.090 |
| 800 | 0.087 |
| 850 | 0.083 |
| 900 | 0.083 |

### 2.4.5. Calibration uncertainty of KC Si photodiode and trap detector by using NMC reference standard – Si detector (300 – 380) nm

**Table 2-8. Uncertainty budget for calibration of Si photodiode (s/n: A#3) using NMC ref. std. (s/n: E460) at 300 nm.**

| s/n | Source of uncertainty | Type | Value (%) | Sensitivity coefficient (c ) | Probability distribution | Coverage factor (k) | Relative standard uncertainty (%) | Degree of Freedom |
|---|---|---|---|---|---|---|---|---|
| 1 | Signal repeatability of Si PD | A | 0.008385 | 1 | | | 0.0084 | 6 |
| 2 | Accuracy of DVM (signal channel) for Si PD | B | 0.010374 | 1 | Normal | 2 | 0.0052 | ∞ |
| 3 | Alignment of Si PD | B | 0.018 | 1 | Rectangular | 1.732 | 0.0104 | ∞ |
| 4 | Signal repeatability of std PD | A | 0.0077 | 1 | | | 0.0077 | 6 |
| 5 | Accuracy of DVM (Std PD channel) | B | 0.0103 | 1 | Normal | 2 | 0.0052 | ∞ |
| 6 | Alignment of Std PD | B | 0.04 | 1 | Rectangular | 1.732 | 0.0231 | ∞ |
| 7 | Unc. of amplifier gain of Si PD | B | 0.06 | 1 | Normal | 2 | 0.03 | ∞ |
| 8 | Unc. of amplifier gain of Std PD | B | 0.06 | 1 | Normal | 2 | 0.03 | ∞ |

| | | | | | | | | |
|---|---|---|---|---|---|---|---|---|
| 9 | Cal unc. of std PD | B | 1.8 | 1 | Normal | 2 | 0.9 | ∞ |
| 10 | Unc. due to wavelength error (0.1 nm) of monochromator | B | 0.055 | 1 | Rectangular | 1.732 | 0.0318 | ∞ |
| 11 | Effect of polarisation of beam | B | 0.058 | 1 | Rectangular | 1.732 | 0.0335 | ∞ |
| | Combined standard uncertainty ($k = 1$) | | | | | | 0.90 | |

The combined relative standard uncertainty (k = 1) values for calibration of KC Si photodiode are 0.85 % – 0.90 % and for KC trap detector are 0.96 % – 1.01 % in the spectral range of 300 nm - 380 nm as shown in Table 2-9 below.

**Table 2-9. Combined standard uncertainty of KC Si photodiode (PD) and trap detector (300 – 380) nm.**

| Wavelength (nm) | Combined uncertainty (PD) (%) (k = 1) | Combined uncertainty (Trap) (%) (k = 1) |
|---|---|---|
| 300 | 0.90 | 0.99 |
| 320 | 0.85 | 1.01 |
| 340 | 0.90 | 0.98 |
| 360 | 0.90 | 0.98 |
| 380 | 0.85 | 0.96 |

### 2.4.6. Calibration uncertainty of cavity pyroelectric detector (CPD) by using KC Si trap photodiode (850 – 900) nm

**Table 2-10. Uncertainty budget for calibration of CPD (s/n: CP-09) using KC trap detector (s/n: A#5) at 900 nm.**

| s/n | Source of uncertainty | Type | Value (%) | Sensitivity coefficient (c ) | Probability distribution | Coverage factor (k) | Relative standard uncertainty (%) | DOF |
|---|---|---|---|---|---|---|---|---|
| 1 | Signal repeatability of test CPD | A | 0.0709 | 1 | | | 0.0709 | 18 |
| 2 | Accuracy of DVM (signal channel) for test CPD | B | 0.0033 | 1 | Normal | 2 | 0.0017 | ∞ |
| 3 | Alignment of test CPD | B | 0.08 | 1 | rectangular | 1.732 | 0.0462 | ∞ |
| 4 | Unc. of amplifier gain of test CPD | B | 0.06 | 1 | Normal | 2 | 0.03 | ∞ |
| 5 | Unc. of Lock-in amplifier gain of test CPD | B | 1.0 | 1 | Normal | 2 | 0.5 | ∞ |
| 6 | Signal repeatability of std Si PD | A | 0.0046 | 1 | | | 0.0046 | 6 |
| 7 | Accuracy of DVM(signal channel) for std Si PD | B | 0.0023 | 1 | Normal | 2 | 0.0012 | ∞ |
| 8 | Alignment of std Si PD | B | 0.08 | 1 | rectangular | 1.732 | 0.046 | ∞ |

| | | | | | | | | |
|---|---|---|---|---|---|---|---|---|
| 9 | Unc. of amplifier gain of std Si PD | B | 0.06 | 1 | Normal | 2 | 0.03 | ∞ |
| 10 | Cal unc. of std Si PD | B | 0.134 | 1 | Normal | 2 | 0.067 | ∞ |
| 11 | Unc due to wavelength error (0.1 nm) of monochromator | B | 0.0119 | 1 | rectangular | 1.732 | 0.0069 | ∞ |
| | Combined relative standard uncertainty (*k = 1*) | | | | | | 0.52 | |

The combined relative uncertainty value for calibration of relative transfer standard – cavity pyroelectric detector is 0.52 % in the spectral range of 850 nm - 900 nm.

### 2.4.7. Calibration uncertainty of KC trap detector by using a cavity pyroelectric detector (CPD) (950 – 1000) nm

**Table 2-11. Uncertainty budget for calibration of KC trap detector (s/n: A#5) using CPD (s/n: CP-09) at 950 nm.**

| s/n | Source of uncertainty | Type | Value (%) | Sensitivity coefficient (c ) | Probability distribution | Coverage factor (k) | Relative standard uncertainty (%) | DoF |
|---|---|---|---|---|---|---|---|---|
| 1 | Signal repeatability of test Si Trap | A | 0.0070 | 1 | | | 0.0070 | 6 |
| 2 | Accuracy of DVM(signal channel) for Si Trap | B | 0.0022 | 1 | Normal | 2 | 0.0011 | ∞ |
| 3 | Alignment of test Si Trap | B | 0.04 | 1 | Rectangular | 1.732 | 0.046 | ∞ |
| 4 | Unc. of amplifier gain of test Si Trap | B | 0.06 | 1 | Normal | 2 | 0.03 | ∞ |
| 5 | Signal repeatability of std CPD | A | 0.0236 | 1 | | | 0.0236 | 18 |
| 6 | Accuracy of DVM(signal channel) for std CPD | B | 0.0030 | 1 | Normal | 2 | 0.0015 | ∞ |
| 7 | Alignment of std CPD | B | 0.08 | 1 | Rectangular | 1.732 | 0.046 | ∞ |
| 8 | Unc. of amplifier gain of std CPD | B | 0.06 | 1 | Normal | 2 | 0.03 | ∞ |
| 9 | Accuracy of lock-in amplifier of std CPD | B | 1.0 | 1 | Normal | 2 | 0.5 | ∞ |
| 10 | Cal unc. of std CPD | B | 1.0 | 1 | Normal | 2 | 0.5 | ∞ |
| 11 | Spectral flatness of CPD | B | 0.2 | 1 | Rectangular | 1.732 | 0.1155 | ∞ |
| | Combined relative standard uncertainty (*k = 1*) | | | | | | 0.72 | |

The combined relative uncertainty value for calibration of KC Trap detector is 0.72 % in the spectral range of 950 nm - 1000 nm.

### 2.4.8. Calibration uncertainty of KC Si photodiode by using CPD (950 – 1000) nm

**Table 2-12. Uncertainty budget for calibration of KC Si single photodiode (s/n: A#3) using reference standard – CPD (s/n: CP-09) at 1000 nm.**

| s/n | Source of uncertainty | Type | Value (%) | Sensitivity coefficient (c ) | Probability distribution | Coverage factor (k) | Relative standard uncertainty (%) | DoF |
|---|---|---|---|---|---|---|---|---|
| 1 | Signal repeatability of Si PD | A | 0.0053 | 1 | | | 0.0053 | 6 |
| 2 | Accuracy of DVM(signal channel) for Si PD | B | 0.0021 | 1 | Normal | 2 | 0.0011 | ∞ |
| 3 | Alignment of Si PD | B | 0.08 | 1 | Rectangular | 1.732 | 0.046 | ∞ |
| 4 | Unc. of amplifier gain of Si PD | B | 0.06 | 1 | Normal | 2 | 0.03 | ∞ |
| 5 | Signal repeatability of CPD | A | 0.0103 | 1 | | | 0.0103 | 18 |
| 6 | Accuracy of DVM(signal channel) for CPD | B | 0.0023 | 1 | Normal | 2 | 0.0012 | ∞ |
| 7 | Alignment of CPD | B | 0.08 | 1 | Rectangular | 1.732 | 0.046 | ∞ |
| 8 | Unc. of amplifier gain of CPD | B | 0.06 | 1 | Normal | 2 | 0.03 | ∞ |
| 9 | Accuracy of lock-in amplifier of CPD | B | 1.0 | 1 | Normal | 2 | 0.5 | ∞ |
| 10 | Cal unc. of CPD | B | 1.05 | 1 | Normal | 2 | 0.525 | ∞ |
| 11 | Spectral flatness of CPD | B | 0.2 | 1 | Rectangular | 1.732 | 0.1155 | ∞ |
| | Combined relative standard uncertainty ($k = 1$) | | | | | | 0.74 | |

The combined relative uncertainty values for calibration of KC Si single photodiodes are 0.74 % in the spectral range of 950 nm - 1000 nm.

# 3. IO-CSIC

## *3.1. Measurement Setup and Instruments*

Detectors' responsivity has been determined by comparing the detector response to that of a standard radiometer under the same irradiation conditions. This is usually known as the direct comparison method. A scheme of the experimental arrangement is shown in Figure 3-1.

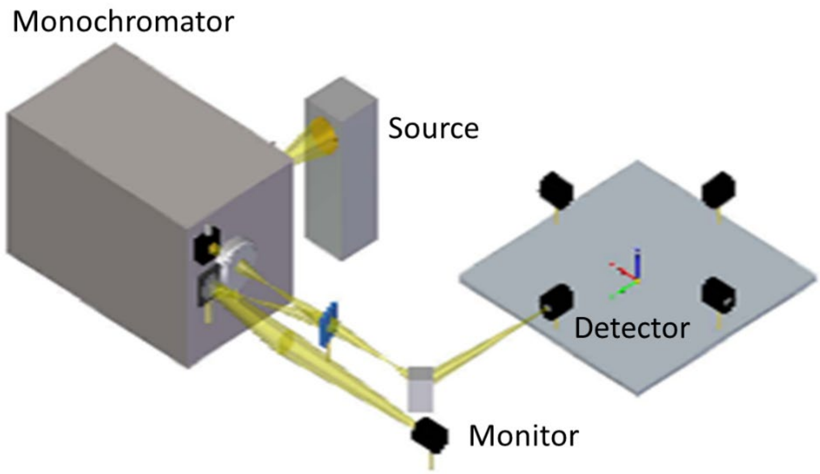


**Figure 3-1. Experimental arrangement for the calibration of spectral responsivity at IO-CSIC.**

The calibration procedure consists in recording the detector's response to the calibration beam at every wavelength and then recording the standard detector's response to the same beam, wavelength by wavelength. The spectral responsivity is determined as the ratio between the detector's short-circuit photocurrent and the radiant flux measured by the standard detector. Another photodiode is used to monitor the power temporal drift of the calibration beam.

Measurements have been done in three different stages corresponding to the different sources of illumination and spectral intervals: The first one corresponds to the UV range (300 nm to 400 nm), the second one to the visible spectral interval (450 nm to 800 nm) and the third one to the near IR spectral interval (800 nm to 1000 nm). The radiant source for the first part was a Hg-Xe lamp (XBO), while a halogen incandescence lamp, current stabilized, was used in the second and third parts. For the UV part, a "Spex 500" monochromator with a 2400 g/mm grating was used to spectrally filter the radiation, while for the VIS and NIR parts an "ARC 500" monochromator was used with a 1200 g/mm grating in the VIS and a 600 g/mm in the NIR. The output slit of the monochromator was imaged onto the detectors. A shutter was introduced in the beam path to register the dark current response. Blocking filters for higher orders wavelength were present in the systems as needed.

Short-circuit photocurrent was measured with Keithley 485 auto-ranging pico-ammeters.

A multimeter HP 3457A was used to measure the resistance of the PT100 thermistor of the detectors to be calibrated.

## *3.2. Measurement Conditions and Parameters*

### 3.2.1. Numerical aperture, incidence angle, and alignment procedure

The numerical aperture of the calibration beam was under 3º (half-angle value).

The angle of incidence was normal to the photodiode's surface for single element detectors and normal to the housing entrance plane for the trap detectors, as recommended. Alignment was done by looking at the beam reflected by the single photodiodes or by a flat mirror placed on the entrance plane of the trap detectors.

### 3.2.2. Radiant spot: form and size

The radiant spot on the calibration plane was square, since it was an image of the exit slit of the monochromator, and its extension was 3 mm by 3 mm in the UV range and 4 mm by 4 mm in the VIS and NIR ranges. Detectors were placed so that the calibration plane was at the sensitive surface of the last detector in the case of trap devices, or at the sensitive surface of the photodiode in the case of single element detectors.

### 3.2.3. Spectral bandwidth and stray light

Spectral intervals were isolated by means of a single grating monochromator with a set of convenient long-wave pass filters to eliminate higher orders wavelength radiation.

Stray light has been determined by measuring the spectral transmittance of different blocking filters in both set-ups. Its value is always lower than 100 ppm in terms of the detector signal in each system.

The spectral bandwidth has been 3.2 nm in the UV range and 5 nm in the VIS and NIR ranges.

### 3.2.4. Radiant flux

Radiant flux incident on the detectors during the calibration process is shown in Figure 3-2. Detectors were kept in darkness except for the calibration exposure time, which was around 15 seconds.

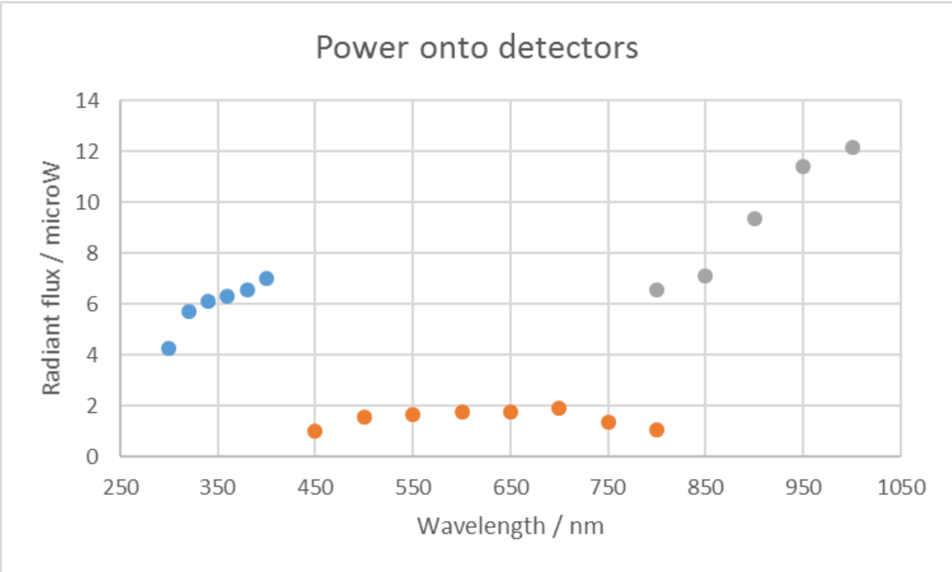


**Figure 3-2. Radiant flux incident on the detectors at IO-CSIC.**

### 3.2.5. Temperature and humidity

Detector's temperature has not been calculated from the PT100 thermistor, although the resistance was measured. The room temperature in the calibration enclosure was 23.0 ºC ± 0.5 ºC.

### 3.2.6. Optical polarization

The degree and state of optical polarization has not been determined in the monochromator used in the UV range, although it is known that it is not negligible. For the Visible and NIR ranges, the ration between both polarizations is approximately 2.

## *3.3. Traceability of Measurement*

Comparison detectors have been calibrated against a single element, silicon photodiode traceable to IO-CSIC spectral responsivity scale. This photodiode is a Hamamatsu S 1337 diode without window, identified as DSS-01.

The responsivity scale is traceable to an ESCR via a two silicon trap radiometers made with windowless silicon photodiodes from Hamamatsu (18 mm x 18 mm). Their responsivity is measured against the ESCR at the laser wavelengths of 465.0 nm, 476.0 nm, 488.0 nm, 496.0 nm, 502.0 nm, 514.0 nm, 632.8 nm, 647.1 nm and 676.4 nm. From those spectral values, responsivity values at any other wavelength between 450 nm and 850 nm are calculated using models for the reflectance and internal quantum efficiency. Outside that spectral interval the spectral responsivity scale is based on an ECPR whose relative responsivity is spectrally neutral and whose absolute responsivity is determined against the previous traps at the 632.8 nm wavelength.

## *3.4. Measurement Uncertainty*

Spectral responsivity of transfer detectors is calculated according to the equation:

$$R_X\,(\lambda) = \frac{(S_X(\lambda) + \Delta S_X(\lambda))\cdot K_{EX}}{(S_S(\lambda) + \Delta S_S(\lambda))\cdot K_{ES}} \cdot K_{SL}(P,\lambda)\cdot K_{ST}(\lambda)\,?\,\frac{S_{MS}(\lambda)}{S_{MX}(\lambda)}\cdot R_S(\lambda)$$

Here, $S$ is the photocurrent, $\Delta S(\lambda)$ is the photocurrent correction due to wavelength error, $K_E$ is the calibration constant of pico-ammeter, $K_{SL}(P,\lambda)$ is the linearity correction of the standard radiometer, $K_{ST}(\lambda)$ is the temperature correction of the standard radiometer, $S_M(\lambda)$ is the monitor's detector signal, and $R_S(\lambda)$ is the spectral responsivity of the standard radiometer. Subscript $S$ stands for the standard radiometer, while $X$ stands for the detector under calibration.

Total uncertainty is calculated form that equation following the uncertainty propagation procedure given in the GUM. Main components are shown in the following tables as requested in the technical protocol of the comparison.

**Table 3-1. Uncertainty budget of spectral responsivity at 300 nm for the trap detector (example).**

| Uncertainty Component | Standard uncertainty (%) | Type | Probability distribution | Sensitivity coefficient | Contrib ution (%) | Deg. of freedo m | Correl ated? |
|---|---|---|---|---|---|---|---|
| Reading repeatability | 0.03 | A | t | 2 | 0.06 | 14 | U |
| Calibration uncertainty of ammeter | 0.05 | B | rectangular | 1 | 0.05 | ∞ | C |
| Calibration uncertainty of reference detector | 0.61 | B | rectangular | 1 | 0.61 | ∞ | U |

| | | | | | | | |
|---|---|---|---|---|---|---|---|
| Uncertainty from wavelength error of light source | 0.1 nm | B | rectangular | Slope of the signal | 0.16 | ∞ | U |
| Uncertainty from spectral stray of light source | < 0.01 | B | rectangular | 1 | < 0.01 | ∞ | C |
| Uncertainty from spectral bandwidth of light source | < 0.01 | B | rectangular | 1 | < 0.01 | ∞ | C |
| Uncertainty related to beam alignment | 0.1 | B | rectangular | 1 | 0.1 | ∞ | C |
| Uncertainty related to beam size and divergence | Not estimated | | | | | | |
| Uncertainty from power instability of light source | 0.05 | A | t | 1 | 0.05 | 14 | C |
| Uncertainty related to polarization of light source | Not estimated | | | | | | |
| Uncertainty from ambient stray light | Negligible | | | | | | |
| Uncertainty from standard detector non-linearity | 0.05 | B | rectangular | 1 | 0.05 | ∞ | C |
| **Combined standard uncertainty (%)** | **--** | **--** | **normal** | **--** | **0.65** | | **U** |

**Table 3-2. Uncertainty budget of spectral responsivity at 500 nm for the trap detector (example).**

| Uncertainty Component | Standard uncertainty (%) | Type | Probability distribution | Sensitivity coefficient | Contribution (%) | Deg. of freedom | Correlated? |
|---|---|---|---|---|---|---|---|
| Reading repeatability | 0.02 | A | t | 2 | 0.04 | 14 | U |
| Calibration uncertainty of ammeter | 0.05 | B | rectangular | 1 | 0.05 | ∞ | C |
| Calibration uncertainty of reference detector | 0.22 | B | rectangular | 1 | 0.22 | ∞ | U |
| Uncertainty from wavelength error of light source | 0.1 nm | B | rectangular | Slope of the signal | 0.03 | ∞ | U |
| Uncertainty from spectral stray of light source | < 0.01 | B | rectangular | 1 | < 0.01 | ∞ | C |
| Uncertainty from spectral bandwidth of light source | < 0.01 | B | rectangular | 1 | < 0.01 | ∞ | C |
| Uncertainty related to beam alignment | 0.01 | B | rectangular | 1 | 0.01 | ∞ | C |
| Uncertainty related to beam size and divergence | Not estimated | | | | | | |
| Uncertainty from power instability of light source | 0.01 | A | t | 1 | 0.01 | 14 | C |
| Uncertainty related to polarization of light source | Not estimated | | | | | | |
| Uncertainty from ambient stray light | Negligible | | | | | | |

| | | | | | | | |
|---|---|---|---|---|---|---|---|
| Uncertainty from standard detector non-linearity | 0.05 | B | rectangular | 1 | 0.05 | ∞ | C |
| **Combined standard uncertainty (%)** | **--** | **--** | **normal** | **--** | **0.24** | | **U** |

**Table 3-3. Uncertainty budget of spectral responsivity at 1000 nm for the trap detector (example).**

| **Uncertainty Component** | **Standard uncertainty (%)** | **Type** | **Probability distribution** | **Sensitivity coefficient** | **Contribution (%)** | **Deg. of freedom** | **Correlated?** |
|---|---|---|---|---|---|---|---|
| Reading repeatability | 0.01 | A | t | 2 | 0.02 | 14 | U |
| Calibration uncertainty of ammeter | 0.05 | B | rectangular | 1 | 0.05 | ∞ | C |
| Calibration uncertainty of reference detector | 0.36 | B | rectangular | 1 | 0.36 | ∞ | U |
| Uncertainty from wavelength error of light source | 0.1 nm | B | rectangular | Slope of the signal | 0.02 | ∞ | U |
| Uncertainty from spectral stray of light source | < 0.01 | B | rectangular | 1 | < 0.01 | ∞ | C |
| Uncertainty from spectral bandwidth of light source | < 0.01 | B | rectangular | 1 | < 0.01 | ∞ | C |
| Uncertainty related to beam alignment | 0.02 | B | rectangular | 1 | 0.02 | ∞ | C |
| Uncertainty related to beam size and divergence | Not estimated | | | | | | |
| Uncertainty from power instability of light source | 0.01 | A | t | 1 | 0.01 | 14 | C |
| Uncertainty related to polarization of light source | Not estimated | | | | | | |
| Uncertainty from ambient stray light | Negligible | | | | | | |
| Uncertainty from standard detector non-linearity | 0.05 | B | rectangular | 1 | 0.05 | ∞ | C |
| **Combined standard uncertainty (%)** | **--** | **--** | **normal** | **--** | **0.37** | ∞ | **--** |

**Table 3-4. Uncertainty budget of spectral responsivity at 300 nm for the single-element detector (example).**

| **Uncertainty Component** | **Standard uncertainty (%)** | **Type** | **Probability distribution** | **Sensitivity coefficient** | **Contribution (%)** | **Deg. of freedom** | **Correlated?** |
|---|---|---|---|---|---|---|---|
| Reading repeatability | 0.03 | A | t | 2 | 0.06 | 14 | U |
| Calibration uncertainty of ammeter | 0.05 | B | rectangular | 1 | 0.05 | ∞ | C |

| | | | | | | | |
|---|---|---|---|---|---|---|---|
| Calibration uncertainty of reference detector | 0.61 | B | rectangular | 1 | 0.61 | ∞ | U |
| Uncertainty from wavelength error of light source | 0.1 nm | B | rectangular | Slope of the signal | 0.16 | ∞ | U |
| Uncertainty from spectral stray of light source | < 0.01 | B | rectangular | 1 | < 0.01 | ∞ | C |
| Uncertainty from spectral bandwidth of light source | < 0.01 | B | rectangular | 1 | < 0.01 | ∞ | C |
| Uncertainty related to beam alignment | 0.07 | B | rectangular | 1 | 0.07 | ∞ | C |
| Uncertainty related to beam size and divergence | Not estimated | | | | | | |
| Uncertainty from power instability of light source | 0.02 | A | t | 1 | 0.02 | 14 | C |
| Uncertainty related to polarization of light source | Not estimated | | | | | | |
| Uncertainty from ambient stray light | Negligible | | | | | | |
| Uncertainty from standard detector non-linearity | 0.05 | B | rectangular | 1 | 0.05 | ∞ | C |
| **Combined standard uncertainty (%)** | **--** | **--** | **normal** | **--** | **0.64** | ∞ | **U** |

**Table 3-5. Uncertainty budget of spectral responsivity at 500 nm for the single-element detector (example).**

| Uncertainty Component | Standard uncertainty (%) | Type | Probability distribution | Sensitivity coefficient | Contribution (%) | Deg. of freedom | Correlated? |
|---|---|---|---|---|---|---|---|
| Reading repeatability | 0.01 | A | t | 2 | 0.02 | 14 | U |
| Calibration uncertainty of ammeter | 0.05 | B | rectangular | 1 | 0.05 | ∞ | C |
| Calibration uncertainty of reference detector | 0.22 | B | rectangular | 1 | 0.22 | ∞ | U |
| Uncertainty from wavelength error of light source | 0.1 nm | B | rectangular | Slope of the signal | 0.03 | ∞ | U |
| Uncertainty from spectral stray of light source | < 0.01 | B | rectangular | 1 | < 0.01 | ∞ | C |
| Uncertainty from spectral bandwidth of light source | < 0.01 | B | rectangular | 1 | < 0.01 | ∞ | C |
| Uncertainty related to beam alignment | 0.02 | B | rectangular | 1 | 0.02 | ∞ | C |
| Uncertainty related to beam size and divergence | Not estimated | | | | | | |
| Uncertainty from power instability of light source | 0.01 | A | t | 1 | 0.01 | 14 | C |
| Uncertainty related to polarization of light source | Not estimated | | | | | | |

| | | | | | | | |
|---|---|---|---|---|---|---|---|
| Uncertainty from ambient stray light | Negligible | | | | | | |
| Uncertainty from standard detector non-linearity | 0.05 | B | rectangular | 1 | 0.05 | ∞ | C |
| **Combined standard uncertainty (%)** | **--** | **--** | **normal** | **--** | **0.24** | ∞ | **U** |

**Table 3-6. Uncertainty budget of spectral responsivity at 1000 nm for the single-element detector (example).**

| Uncertainty Component | Standard uncertainty (%) | Type | Probability distribution | Sensitivity coefficient | Contribution (%) | Deg. of freedom | Correlated? |
|---|---|---|---|---|---|---|---|
| Reading repeatability | 0.01 | A | t | 2 | 0.02 | 14 | U |
| Calibration uncertainty of ammeter | 0.05 | B | rectangular | 1 | 0.05 | ∞ | C |
| Calibration uncertainty of reference detector | 0.36 | B | rectangular | 1 | 0.36 | ∞ | U |
| Uncertainty from wavelength error of light source | 0.1 nm | B | rectangular | Slope of the signal | 0.02 | ∞ | U |
| Uncertainty from spectral stray of light source | < 0.01 | B | rectangular | 1 | < 0.01 | ∞ | C |
| Uncertainty from spectral bandwidth of light source | < 0.01 | B | rectangular | 1 | < 0.01 | ∞ | C |
| Uncertainty related to beam alignment | 0.01 | B | rectangular | 1 | 0.01 | ∞ | C |
| Uncertainty related to beam size and divergence | Not estimated | | | | | | |
| Uncertainty from power instability of light source | 0.01 | A | t | 1 | 0.01 | 14 | C |
| Uncertainty related to polarization of light source | Not estimated | | | | | | |
| Uncertainty from ambient stray light | Negligible | | | | | | |
| Uncertainty from standard detector non-linearity | 0.05 | B | rectangular | 1 | 0.05 | ∞ | C |
| **Combined standard uncertainty (%)** | **--** | **--** | **normal** | **--** | **0.37** | | **U** |

# 4. NMIJ

## *4.1. Measurement Setup and Instruments*

Schematic diagram of the measuring instruments employed for spectral responsivity calibration is illustrated in Figure 4-1. Tungsten-halogen, xenon and deuterium lamps are equipped in the light source section. In the light source section, radiation from a light source selected according to the wavelength setting is focused onto an entrance slit of a double-grating monochromator with the focal length of 25 cm by a concave mirror. In the wavelength range of this international comparison, only the tungsten-halogen lamp was used as the light source. A mechanical shutter is equipped behind the entrance slit to be used when a dark signal is measured. In the monitor/beam focusing section, a filter wheel is placed behind an exit slit of the monochromator to remove higher orders of the monochromated light as well as the stray light inside the monochromator. Both a grating placed on the grating turret and a glass filter attached onto the filter wheel are selected automatically according to the wavelength of the monochromated light. A beam splitting optics on the optical path is used to split the monochromated beam so as to monitor its stability by a monitor photodetector. The monochromated beam is focused onto a photodetector under test or a standard photodetector by one of three concave mirrors of different focal lengths placed onto the mirror turret. The photodetector under test or the standard photodetector is attached to an optics mount and placed onto a 4-axis motorized stage, so as to align the photodetector onto the optical path against the incident monochromated beam. Each output photocurrent of the photodetector under test and the monitor photodetector is converted into voltage by a transimpedance amplifier and measured by a digital voltmeter, respectively. A control software for spectral responsivity calibration is used to scan the monochromator, switch the shutter, select the light source, the glass filter, the grating and the concave mirror, to read the output voltages of digital voltmeters via GP-IB interfaces and to store the data.

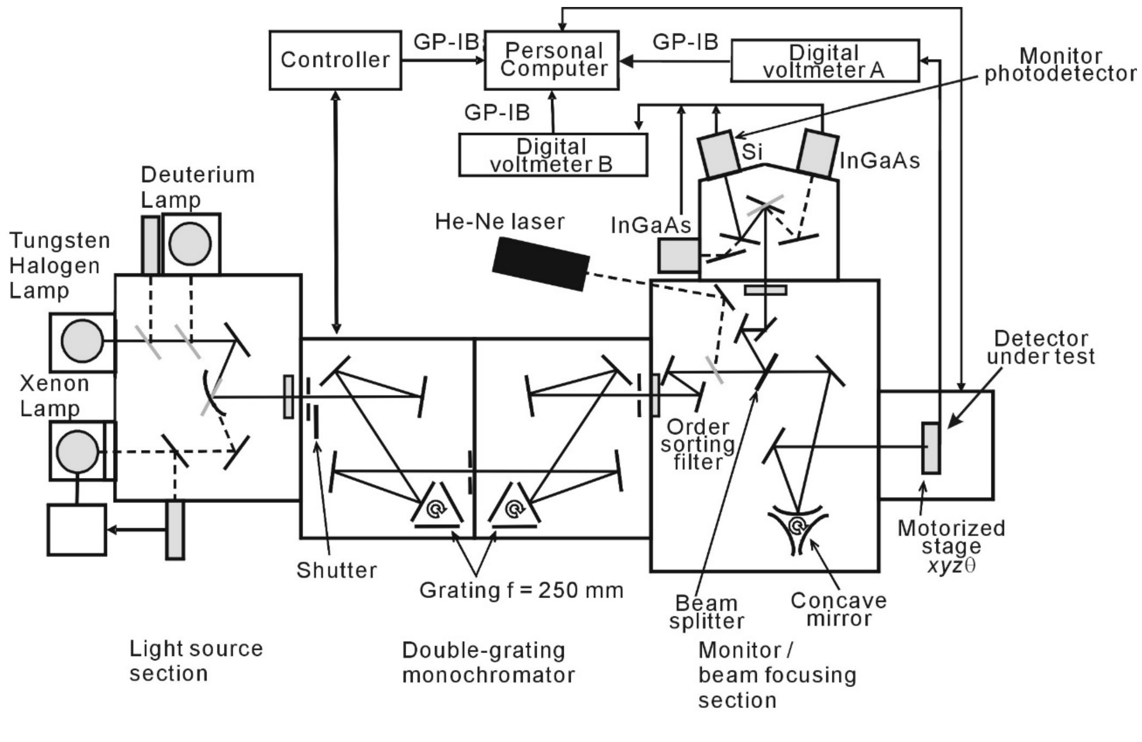


**Figure 4-1. Schematic diagram of the spectral responsivity calibration system at NMIJ.**

## *4.2. Measurement Conditions and Parameters*

In order to confirm the normal incidence, the reflected beam from the detector was monitored so that it should be collinear with the incident beam. The detector was scanned to find the centre of the effective sensitive area.

The room temperature and the relative humidity were controlled to be 23 ºC ± 1 ºC and 40 % ± 20 %, respectively. Actual values were recorded at the time of the measurement.

After alignment waiting time of 10 min was inserted before starting the measurements.

The resistance of the Pt100 of a transfer detector was measured just before the measurement of its responsivity.

The spot size at the detector surface and the f-number of the beam are listed in Table 4-1.

**Table 4-1. The spot size at the detector surface and the f-number for the comparison at NMIJ.**

| type of detector | spot size | f-number |
|---|---|---|
| single | 2.5 mm x 2.0 mm | 5 |
| trap | 2.0 mm x 1.0 mm | 12.5 |

## 4.3. Traceability of Measurement

Traceability of spectral responsivity calibration to SI units is totally guaranteed by calibrating all of the instruments that significantly affect calibration results to be traceable to the national standards and SI as shown in Figure 4-2.

The realization of the unit [A/W] on the absolute power responsivity calibration of the reference trap detector against the electrical substitution cryogenic radiometer is traceable to SI units as shown in Figure 4-3.

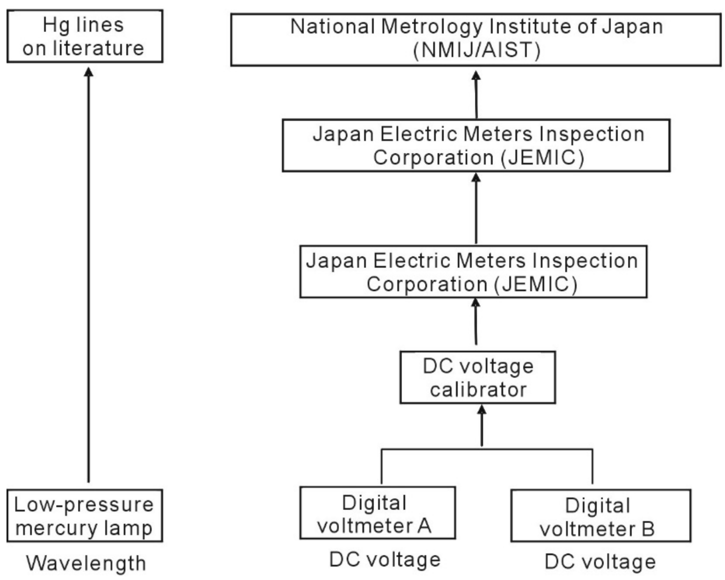


**Figure 4-2. Traceability diagram (1) of NMIJ.**

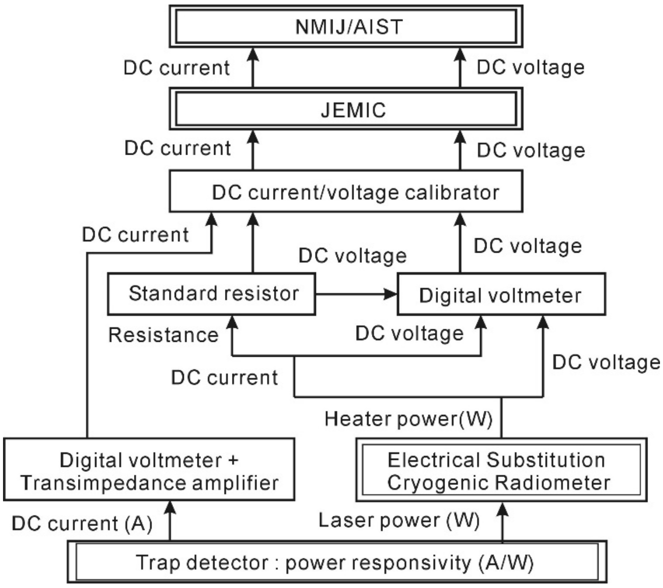


**Figure 4-3. Traceability diagram (2) of NMIJ.**

## *4.4. Measurement Uncertainty*

**Table 4-2. Uncertainty budget of spectral responsivity at 300 nm for the trap detector.**

| Uncertainty Component | Standard uncertainty (%) | Type | Probability distribution | Sensitivity coefficient | Contribution (%) | Deg. of freedom | Correlated? |
|---|---|---|---|---|---|---|---|
| Reading repeatability | 0.008 | A | t | 1 | 0.008 | 9 | X |
| Calibration uncertainty of ammeter | 0.000 | B | normal | 1 | 0.000 | ∞ | O |
| Calibration uncertainty of reference detector | 0.793 | B | normal | 1 | 0.793 | ∞ | O |
| Uncertainty from wavelength error of light source | 0.069 | B | rectangular | 1 | 0.069 | ∞ | X |
| Uncertainty from spectral stray of light source | 0.098 | B | rectangular | 1 | 0.098 | ∞ | O |
| Uncertainty from spectral bandwidth of light source | 0.179 | B | rectangular | 1 | 0.179 | ∞ | O |
| Uncertainty related to beam alignment | 0.121 | B | rectangular | 1 | 0.121 | ∞ | X |
| Uncertainty related to beam size and divergence /polarization of light source | 0.09 | B | rectangular | 1 | 0.09 | ∞ | O |
| Uncertainty from ambient stray light | 0.000 | B | rectangular | 1 | 0.000 | ∞ | O |
| Uncertainty from detector non-linearity | 0.058 | B | rectangular | 1 | 0.058 | ∞ | O |
| Temperature dependence | 0.052 | B | rectangular | 1 | 0.052 | ∞ | X |

| | | | | | | | |
|---|---|---|---|---|---|---|---|
| Stability | 0.087 | B | rectangular | 1 | 0.087 | ∞ | X |
| **Combined standard uncertainty (%)** | **--** | **--** | **normal** | **--** | **0.84** | ∞ | **--** |

**Table 4-3. Uncertainty budget of spectral responsivity at 500 nm for the trap detector.**

| Uncertainty Component | Standard uncertainty (%) | Type | Probability distribution | Sensitivity coefficient | Contribution (%) | Deg. of freedom | Correlated? |
|---|---|---|---|---|---|---|---|
| Reading repeatability | 0.003 | A | t | 1 | 0.003 | 9 | X |
| Calibration uncertainty of ammeter | 0.000 | B | normal | 1 | 0.000 | ∞ | O |
| Calibration uncertainty of reference detector | 0.369 | B | normal | 1 | 0.369 | ∞ | O |
| Uncertainty from wavelength error of light source | 0.004 | B | rectangular | 1 | 0.004 | ∞ | X |
| Uncertainty from spectral stray of light source | 0.009 | B | rectangular | 1 | 0.009 | ∞ | O |
| Uncertainty from spectral bandwidth of light source | 0.011 | B | rectangular | 1 | 0.011 | ∞ | O |
| Uncertainty related to beam alignment | 0.071 | B | rectangular | 1 | 0.071 | ∞ | X |
| Uncertainty related to beam size and divergence /polarization of light source | 0.047 | B | rectangular | 1 | 0.047 | ∞ | O |
| Uncertainty from ambient stray light | 0.000 | B | normal | 1 | 0.000 | ∞ | O |
| Uncertainty from detector non-linearity | 0.060 | B | rectangular | 1 | 0.060 | ∞ | O |
| Temperature dependence | 0.041 | B | rectangular | 1 | 0.041 | ∞ | X |
| Stability | 0.094 | B | rectangular | 1 | 0.094 | ∞ | X |
| **Combined standard uncertainty (%)** | **--** | **--** | **normal** | **--** | **0.40** | ∞ | **--** |

**Table 4-4. Uncertainty budget of spectral responsivity at 1000 nm for the trap detector.**

| Uncertainty Component | Standard uncertainty (%) | Type | Probability distribution | Sensitivity coefficient | Contribution (%) | Deg. of freedom | Correlated? |
|---|---|---|---|---|---|---|---|
| Reading repeatability | 0.004 | A | t | 1 | 0.004 | 9 | X |
| Calibration uncertainty of ammeter | 0.000 | B | normal | 1 | 0.000 | ∞ | O |

| | | | | | | | |
|---|---|---|---|---|---|---|---|
| Calibration uncertainty of reference detector | 0.647 | B | normal | 1 | 0.647 | ∞ | O |
| Uncertainty from wavelength error of light source | 0.026 | B | rectangular | 1 | 0.026 | ∞ | X |
| Uncertainty from spectral stray of light source | 0.001 | B | rectangular | 1 | 0.001 | ∞ | O |
| Uncertainty from spectral bandwidth of light source | 0.016 | B | rectangular | 1 | 0.016 | ∞ | O |
| Uncertainty related to beam alignment | 0.145 | B | rectangular | 1 | 0.145 | ∞ | X |
| Uncertainty related to beam size and divergence /polarization of light source | 0.01 | B | rectangular | 1 | 0.01 | ∞ | O |
| Uncertainty from ambient stray light | 0.000 | B | normal | 1 | 0.000 | ∞ | O |
| Uncertainty from detector non-linearity | 0.193 | B | rectangular | 1 | 0.193 | ∞ | O |
| Temperature dependence | 0.280 | B | rectangular | 1 | 0.280 | ∞ | X |
| Stability | 0.074 | B | rectangular | 1 | 0.074 | ∞ | X |
| **Combined standard uncertainty (%)** | **--** | **--** | **normal** | **--** | **0.75** | ∞ | **--** |

**Table 4-5. Uncertainty budget of spectral responsivity at 300 nm for the single-element detector.**

| Uncertainty Component | Standard uncertainty (%) | Type | Probability distribution | Sensitivity coefficient | Contrib ution (%) | Deg. of freedo m | Correl ated? |
|---|---|---|---|---|---|---|---|
| Reading repeatability | 0.008 | A | t | 1 | 0.008 | 9 | X |
| Calibration uncertainty of ammeter | 0.000 | B | normal | 1 | 0.000 | ∞ | O |
| Calibration uncertainty of reference detector | 0.793 | B | normal | 1 | 0.793 | ∞ | O |
| Uncertainty from wavelength error of light source | 0.069 | B | rectangular | 1 | 0.069 | ∞ | X |
| Uncertainty from spectral stray of light source | 0.098 | B | rectangular | 1 | 0.098 | ∞ | O |
| Uncertainty from spectral bandwidth of light source | 0.179 | B | rectangular | 1 | 0.179 | ∞ | O |
| Uncertainty related to beam alignment | 0.121 | B | rectangular | 1 | 0.121 | ∞ | X |
| Uncertainty related to beam size and divergence /polarization of light source | 0.09 | B | rectangular | 1 | 0.09 | ∞ | O |
| Uncertainty from ambient stray light | 0.000 | B | normal | 1 | 0.000 | ∞ | O |

| | | | | | | | |
|---|---|---|---|---|---|---|---|
| Uncertainty from detector non-linearity | 0.058 | B | rectangular | 1 | 0.058 | ∞ | O |
| Temperature dependence | 0.052 | B | rectangular | 1 | 0.052 | ∞ | X |
| Stability | 0.087 | B | rectangular | 1 | 0.087 | ∞ | X |
| **Combined standard uncertainty (%)** | **--** | **--** | **normal** | **--** | **0.84** | ∞ | **--** |

**Table 4-6. Uncertainty budget of spectral responsivity at 500 nm for the single-element detector.**

| Uncertainty Component | Standard uncertainty (%) | Type | Probability distribution | Sensitivity coefficient | Contribution (%) | Deg. of freedom | Correlated? |
|---|---|---|---|---|---|---|---|
| Reading repeatability | 0.003 | A | t | 1 | 0.003 | 9 | X |
| Calibration uncertainty of ammeter | 0.000 | B | normal | 1 | 0.000 | ∞ | O |
| Calibration uncertainty of reference detector | 0.369 | B | normal | 1 | 0.369 | ∞ | O |
| Uncertainty from wavelength error of light source | 0.004 | B | rectangular | 1 | 0.004 | ∞ | X |
| Uncertainty from spectral stray of light source | 0.009 | B | rectangular | 1 | 0.009 | ∞ | O |
| Uncertainty from spectral bandwidth of light source | 0.011 | B | rectangular | 1 | 0.011 | ∞ | O |
| Uncertainty related to beam alignment | 0.071 | B | rectangular | 1 | 0.071 | ∞ | X |
| Uncertainty related to beam size and divergence /polarization of light source | 0.047 | B | rectangular | 1 | 0.047 | ∞ | O |
| Uncertainty from ambient stray light | 0.000 | B | normal | 1 | 0.000 | ∞ | O |
| Uncertainty from detector non-linearity | 0.060 | B | rectangular | 1 | 0.060 | ∞ | O |
| Temperature dependence | 0.041 | B | rectangular | 1 | 0.041 | ∞ | X |
| Stability | 0.094 | B | rectangular | 1 | 0.094 | ∞ | X |
| **Combined standard uncertainty (%)** | **--** | **--** | **normal** | **--** | **0.40** | ∞ | **--** |

**Table 4-7. Uncertainty budget of spectral responsivity at 1000 nm for the single-element detector.**

| Uncertainty Component | Standard uncertainty (%) | Type | Probability distribution | Sensitivity coefficient | Contribution (%) | Deg. of freedom | Correlated? |
|---|---|---|---|---|---|---|---|

| | | | | | | | |
|---|---|---|---|---|---|---|---|
| Reading repeatability | 0.004 | A | t | 1 | 0.004 | 9 | X |
| Calibration uncertainty of ammeter | 0.000 | B | normal | 1 | 0.000 | ∞ | O |
| Calibration uncertainty of reference detector | 0.647 | B | normal | 1 | 0.647 | ∞ | O |
| Uncertainty from wavelength error of light source | 0.026 | B | rectangular | 1 | 0.026 | ∞ | X |
| Uncertainty from spectral stray of light source | 0.001 | B | rectangular | 1 | 0.001 | ∞ | O |
| Uncertainty from spectral bandwidth of light source | 0.016 | B | rectangular | 1 | 0.016 | ∞ | O |
| Uncertainty related to beam alignment | 0.145 | B | rectangular | 1 | 0.145 | ∞ | X |
| Uncertainty related to beam size and divergence /polarization of light source | 0.01 | B | rectangular | 1 | 0.01 | ∞ | O |
| Uncertainty from ambient stray light | 0.000 | B | normal | 1 | 0.000 | ∞ | O |
| Uncertainty from detector non-linearity | 0.193 | B | rectangular | 1 | 0.193 | ∞ | O |
| Temperature dependence | 0.280 | B | rectangular | 1 | 0.280 | ∞ | X |
| Stability | 0.074 | B | rectangular | 1 | 0.074 | ∞ | X |
| **Combined standard uncertainty (%)** | **--** | **--** | **normal** | **--** | **0.75** | ∞ | **--** |

# 5. LNE-CNAM

## *5.1. Measurement Setup and Instruments*

The measurement of the absolute spectral responsivity has been carried out by comparing, for each wavelength between 300 nm and 1000 nm, the response of the transfer detector to the response of a reference detector, when both detectors receive the same monochromatic radiation.

The experimental set-up used to measure the spectral responsivity of the detectors over a large spectral range is shown schematically in Figure 5-1. It is built up around a double prism-grating monochromator to select a narrow waveband of a few nanometers, from the spectrum of a source, between 200 nm and 2000 nm. Beyond the usual stray light reduction of a double monochromator such a grating/prism monochromator, it can select a wavelength using different orders of the grating without bandpass or long pass additional filters. Two similar but separated devices are used respectively on the following spectral ranges: 200 nm to 400 nm and 300 nm to 1000 nm. The grating and the prism of each monochromator are adapted to the wavelength range. Both devices have been used for the comparison with common wavelengths from 300 nm to 380 nm.

A computer controlled translation stage puts alternatively the detectors into the monochromatic beam. The optical arrangement at the exit of the monochromator allows to have a radiant beam with a small numerical aperture. It has been studied so as to obtain the image of the entrance pupil on the surface of the detectors to be measured, with the suitable size. This method provides a good uniformity of illumination on the surface of the detectors, while having a sufficient level of flux.

The monochromator is used with several sources: a Xenon Arc, a LDLS source (Laser-Driven Light Source) EQ-99 and a Quartz-Halogen lamp.

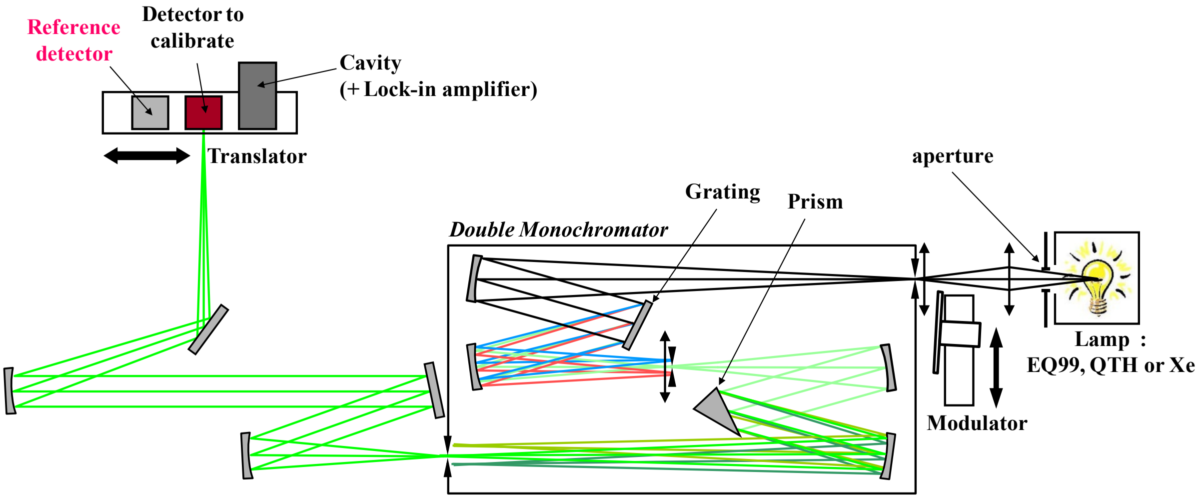


**Figure 5-1. Experimental set-up for the spectral responsivity measurements at the LNE-CNAM.**

## *5.2. Measurement Conditions and Parameters*

For the measurements reported in this document, two reference detectors were used. They are large-area trap detectors:

- one is a three-element reflection trap detector constructed using HAMAMATSU S3204-09 photodiodes. It is used in the wavelength range between 300 nm and 1000 nm.
- the other is a three-element reflection trap detector constructed using Hamamatsu S8553 windowless photodiodes. This detector is used between 200 nm to 400 nm.

The maximum diameter of the active area of these detectors is 14 mm and the full field of view is 11°.

The light sources used for these measurements was the Xenon arc lamp and the EQ99 lamp for the spectral range 300 nm - 380 nm, and the Quartz-Halogen lamp for 400 nm to 1000 nm.

The spot size was about 2x3 $mm^2$ on the effective active area of the detectors. The position of the trap detectors has been adjusted in the beam so that the 2x3 $mm^2$ spot size was situated on the third photodiode in the trap in order to avoid vignetting effects. Depending on the wavelength, the level of the flux was in the range of 0.2 µW to 10 µW.

The spectral bandwidth of the monochromator, defined as the full width at half the maximum, was set at 3 nm.

The detectors were mounted and aligned so that the optical beam is centered to the entrance aperture at normal incidence. This alignment is done by using a laser beam passing through the same path as the beam one. A white screen with a small hole is placed in the laser beam, and the position of the detector is adjusted until the reflected beam passes too by the hole.

The photo-current of the detectors was measured with a current to voltage converter, the input impedance of which was lower than 10 Ω.

Each detector of the comparison was compared 6 times to the reference detector for each wavelength requested. Between each individual measurement, the detector was reinstalled and realigned on the measurement facility. Each individual measure was composed of at least 3 sets of measures. The final value for the spectral responsivity was calculated by the mean of these 6 independent measurements.

The reading of the temperature attached to each transfer detector was recorded as described in the Technical Protocol (§ 3.2).

The temperature in the room was around 24 °C.

### 5.3. Traceability of Measurement

The LNE-CNAM uses an electrically calibrated cryogenic radiometer as the primary standard for its optical radiation measurement scales. The cryogenic radiometer allows direct calibration of trap detectors in absolute spectral responsivity with a relative standard uncertainty in the range of 2 part in $10^4$, but only for a few laser wavelengths between 454 nm to 825 nm.

The measurement of the spectral responsivity of the reference detectors (the large-area trap detectors) over all their spectral range is carried out in two steps:

- in a first step, the detectors are calibrated in absolute spectral responsivity with laser beams at some laser wavelengths, against a secondary standard (trap detector), with a relative standard uncertainty of the order of 5 part in $10^4$.
- in a second step, the determination of the responsivity of the detectors at other wavelengths is based on an interpolation and extrapolation method between the calibration laser wavelengths and the required wavelengths. The interpolation and extrapolation are carried out by comparing the detectors to a non-selective detector on the spectral responsivity measurements set-up. This detector is a non-selective cavity shape pyroelectric detector. The resulting uncertainty of these measurements is between 1 and 3 parts in $10^3$, depending on the wavelength.

### 5.4. Measurement Uncertainty

The measurement model equation for the evaluation of the uncertainties on the measurement of the absolute spectral sensitivity S(λ) is :

$$S(\lambda) = S_{Ref}(\lambda).\bar{R}(\lambda).C_{Volt}.C_{CAV}.C_{\lambda}.C_{stray}.C_{BP}.C_{align.}.C_{polar}.C_{lin}.C_{Temp}$$

with $S_{Ref}(\lambda)$ : the spectral responsivity of the reference detector

$\bar{R}(\lambda)$ : the mean of the N values of the ratio between the response of the transfer detector and the response of the reference detector,

$C_{xxx}$ : the corrections to the spectral responsivity. Each correction has a mean equal to 1, with an associated uncertainty $u_{Cxxx}$.

The different corrections that have been taken into account are:

$C_{Volt}$ for the photo-current measurements with the voltmeter,

$C_{CAV}$ for the gain of the current to voltage converter,

$C_{\lambda}$ for the wavelength error of light source,

$C_{Stray}$ for the spectral stray of light source,

$C_{BP}$ for the spectral bandwidth of light source,

$C_{align}$ for the beam alignment,

$C_{polar}$ for the polarization of light source,

$C_{lin}$ for the detector non-linearity,

$C_{Temp}$ for he effect of ambient temperature (only for wavelength above 900 nm).

The detailed measurement uncertainty budgets for spectral responsivity of the transfer detectors are reported in the following tables for each type of transfer detectors (trap and single-element), and at the selected wavelengths of 300 nm, 500 nm, and 1000 nm. The values given in this table are for relative standard uncertainty ($k = 1$).

The values for the components $R(\lambda)$, $S_{Ref}(\lambda)$, $C_{\lambda}$, and $C_{BP}$ are wavelength dependent and are calculated for each wavelength.

The final standard uncertainty is the combined standard uncertainty $u(\lambda)$, and is calculated also for each wavelength of the comparison.

**Table 5-1. Uncertainty budget of spectral responsivity at 300 nm for the trap detector.**

| Uncertainty Component | Standard uncertainty (%) | Type | Probability distribution | Sensitivity coefficient | Contrib ution (%) | Deg. of freedo m | Correl ated? |
|---|---|---|---|---|---|---|---|
| Ration R(λ) | 0.29 | A | t | 1 | 0.29 | 6 | X |
| Calibration uncertainty of voltmeter | 0.005 | B | normal | 1 | 0.005 | ∞ | O |
| Calibration uncertainty of current-to-voltage convertor | 0.005 | B | normal | 1 | 0.005 | ∞ | O |
| Calibration uncertainty of reference detector | 0.19 | B | normal | 1 | 0.2 | ∞ | O |
| Uncertainty from wavelength error of light source | 0.006 | B | rectangular | 1 | 0.006 | ∞ | X |
| Uncertainty from spectral stray of light source | 0.01 | B | rectangular | 1 | 0.01 | ∞ | O |
| Uncertainty from spectral bandwidth of light source | 0.01 | B | rectangular | 1 | 0.01 | ∞ | X |
| Uncertainty related to beam alignment | 0.01 | B | rectangular | 1 | 0.01 | ∞ | X |
| Uncertainty related to polarization of light source | 0.005 | B | rectangular | 1 | 0.005 | ∞ | O |
| Uncertainty from detector non-linearity | 0.02 | B | rectangular | 1 | 0.02 | ∞ | O |
| **Combined standard uncertainty (%)** | **--** | **--** | **normal** | **--** | **0.35** | ∞ | **--** |

**Table 5-2. Uncertainty budget of spectral responsivity at 500 nm for the trap detector.**

| Uncertainty Component | Standard uncertainty (%) | Type | Probability distribution | Sensitivity coefficient | Contrib ution (%) | Deg. of freedo m | Correl ated? |
|---|---|---|---|---|---|---|---|
| Ration R(λ) | 0.03 | A | t | 1 | 0.03 | 6 | X |
| Calibration uncertainty of voltmeter | 0.005 | B | normal | 1 | 0.005 | ∞ | O |
| Calibration uncertainty of current-to-voltage convertor | 0.005 | B | normal | 1 | 0.005 | ∞ | O |

| | | | | | | | |
|---|---|---|---|---|---|---|---|
| Calibration uncertainty of reference detector | 0.16 | B | normal | 1 | 0.16 | ∞ | O |
| Uncertainty from wavelength error of light source | 0.001 | B | rectangular | 1 | 0.001 | ∞ | X |
| Uncertainty from spectral stray of light source | 0.01 | B | rectangular | 1 | 0.01 | ∞ | O |
| Uncertainty from spectral bandwidth of light source | 0.01 | B | rectangular | 1 | 0.01 | ∞ | X |
| Uncertainty related to beam alignment | 0.01 | B | rectangular | 1 | 0.01 | ∞ | X |
| Uncertainty related to polarization of light source | 0.005 | B | rectangular | 1 | 0.005 | ∞ | O |
| Uncertainty from detector non-linearity | 0.02 | B | rectangular | 1 | 0.02 | ∞ | O |
| **Combined standard uncertainty (%)** | **--** | **--** | **normal** | **--** | **0.17** | ∞ | **--** |

**Table 5-3. Uncertainty budget of spectral responsivity at 1000 nm for the trap detector.**

| **Uncertainty Component** | **Standard uncertainty (%)** | **Type** | **Probability distribution** | **Sensitivity coefficient** | **Contrib ution (%)** | **Deg. of freedo m** | **Correl ated?** |
|---|---|---|---|---|---|---|---|
| Ration R(λ) | 0.29 | A | t | 1 | 0.29 | 6 | X |
| Calibration uncertainty of voltmeter | 0.005 | B | normal | 1 | 0.005 | ∞ | O |
| Calibration uncertainty of current-to-voltage convertor | 0.005 | B | normal | 1 | 0.005 | ∞ | O |
| Calibration uncertainty of reference detector | 0.28 | B | normal | 1 | 0.28 | ∞ | O |
| Uncertainty from wavelength error of light source | 0.02 | B | rectangular | 1 | 0.02 | ∞ | X |
| Uncertainty from spectral stray of light source | 0.01 | B | rectangular | 1 | 0.01 | ∞ | O |
| Uncertainty from spectral bandwidth of light source | 0.01 | B | rectangular | 1 | 0.01 | ∞ | X |
| Uncertainty related to beam alignment | 0.01 | B | rectangular | 1 | 0.01 | ∞ | X |
| Uncertainty related to polarization of light source | 0.005 | B | rectangular | 1 | 0.005 | ∞ | O |
| Uncertainty from detector non-linearity | 0.02 | B | rectangular | 1 | 0.02 | ∞ | O |
| Uncertainty on the temperature effect | 0.06 | B | rectangular | 1 | 0.06 | ∞ | O |
| **Combined standard uncertainty (%)** | **--** | **--** | **normal** | **--** | **0.41** | ∞ | **--** |

**Table 5-4. Uncertainty budget of spectral responsivity at 300 nm for the single-element detector.**

| Uncertainty Component | Standard uncertainty (%) | Type | Probability distribution | Sensitivity coefficient | Contribution (%) | Deg. of freedom | Correlated? |
|---|---|---|---|---|---|---|---|
| Ration R(λ) | 0.15 | A | t | 1 | 0.15 | 6 | X |
| Calibration uncertainty of voltmeter | 0.005 | B | normal | 1 | 0.005 | ∞ | O |
| Calibration uncertainty of current-to-voltage convertor | 0.005 | B | normal | 1 | 0.005 | ∞ | O |
| Calibration uncertainty of reference detector | 0.2 | B | normal | 1 | 0.2 | ∞ | O |
| Uncertainty from wavelength error of light source | 0.006 | B | rectangular | 1 | 0.006 | ∞ | X |
| Uncertainty from spectral stray of light source | 0.01 | B | rectangular | 1 | 0.01 | ∞ | O |
| Uncertainty from spectral bandwidth of light source | 0.01 | B | rectangular | 1 | 0.01 | ∞ | X |
| Uncertainty related to beam alignment | 0.01 | B | rectangular | 1 | 0.01 | ∞ | X |
| Uncertainty related to polarization of light source | 0.005 | B | rectangular | 1 | 0.005 | ∞ | O |
| Uncertainty from detector non-linearity | 0.02 | B | rectangular | 1 | 0.02 | ∞ | O |
| **Combined standard uncertainty (%)** | **--** | **--** | **normal** | **--** | **0.25** | ∞ | **--** |

**Table 5-5. Uncertainty budget of spectral responsivity at 500 nm for the single-element detector.**

| Uncertainty Component | Standard uncertainty (%) | Type | Probability distribution | Sensitivity coefficient | Contribution (%) | Deg. of freedom | Correlated? |
|---|---|---|---|---|---|---|---|
| Ration R(λ) | 0.01 | A | t | 1 | 0.05 | 6 | X |
| Calibration uncertainty of voltmeter | 0.005 | B | normal | 1 | 0.005 | ∞ | O |
| Calibration uncertainty of current-to-voltage convertor | 0.005 | B | normal | 1 | 0.005 | ∞ | O |
| Calibration uncertainty of reference detector | 0.16 | B | normal | 1 | 0.16 | ∞ | O |
| Uncertainty from wavelength error of light source | 0.004 | B | rectangular | 1 | 0.004 | ∞ | X |
| Uncertainty from spectral stray of light source | 0.01 | B | rectangular | 1 | 0.01 | ∞ | O |
| Uncertainty from spectral bandwidth of light source | 0.01 | B | rectangular | 1 | 0.01 | ∞ | X |

| | | | | | | | |
|---|---|---|---|---|---|---|---|
| Uncertainty related to beam alignment | 0.01 | B | rectangular | 1 | 0.01 | ∞ | X |
| Uncertainty related to polarization of light source | 0.005 | B | rectangular | 1 | 0.005 | ∞ | O |
| Uncertainty from detector non-linearity | 0.02 | B | rectangular | 1 | 0.02 | ∞ | O |
| **Combined standard uncertainty (%)** | -- | -- | **normal** | -- | **0.16** | ∞ | -- |

**Table 5-6. Uncertainty budget of spectral responsivity at 1000 nm for the single-element detector.**

| **Uncertainty Component** | **Standard uncertainty (%)** | **Type** | **Probability distribution** | **Sensitivity coefficient** | **Contrib ution (%)** | **Deg. of freedo m** | **Correl ated?** |
|---|---|---|---|---|---|---|---|
| Ration R(λ) | 0.09 | A | t | 1 | 0.09 | 6 | X |
| Calibration uncertainty of voltmeter | 0.005 | B | normal | 1 | 0.005 | ∞ | O |
| Calibration uncertainty of current-to-voltage convertor | 0.005 | B | normal | 1 | 0.005 | ∞ | O |
| Calibration uncertainty of reference detector | 0.28 | B | normal | 1 | 0.28 | ∞ | O |
| Uncertainty from wavelength error of light source | 0.03 | B | rectangular | 1 | 0.03 | ∞ | X |
| Uncertainty from spectral stray of light source | 0.01 | B | rectangular | 1 | 0.01 | ∞ | O |
| Uncertainty from spectral bandwidth of light source | 0.01 | B | rectangular | 1 | 0.01 | ∞ | X |
| Uncertainty related to beam alignment | 0.01 | B | rectangular | 1 | 0.01 | ∞ | X |
| Uncertainty related to polarization of light source | 0.005 | B | rectangular | 1 | 0.005 | ∞ | O |
| Uncertainty from detector non-linearity | 0.02 | B | rectangular | 1 | 0.02 | ∞ | O |
| Uncertainty on the temperature effect | 0.06 | B | rectangular | 1 | 0.06 | ∞ | O |
| **Combined standard uncertainty (%)** | -- | -- | **normal** | -- | **0.30** | ∞ | -- |

# 6. NRC

## *6.1. Measurement Setup and Instruments*

The experiment apparatus used for the CCPR-K2.b.2016 measurements at NRC is shown in Figure 6-1. The wavelength of the optical radiation was controlled by a double subtractive monochromator system with two diffraction gratings blazed at 500 nm and groove spacing of 600 g/mm. Helium and mercury spectral lamps were used to calibrate the wavelength of the monochromator system, and two broad-band light sources were implemented for the spectral responsivity measurements. A laser driven light source (LDLS), a xenon plasma-based source, was used for measurements in the 300 nm to 380 nm range. The LDLS had a longpass 280 nm filter mounted directly onto the focusing optics at the source output to limit the exposure of the optical components inside of the monochromator to UV radiation. A 100 W tungsten lamp was utilized for measurements from 400 nm to 1000 nm. The four light sources were mounted on a motorized linear stage to ensure repeatable alignment to the monochromator entrance slit. A wavelength order-sorting filter wheel was placed at the monochromator output, followed by a beam blocker mounted to a computer-controlled flip mount for dark measurements. Two concave spherical mirrors focused the output beam down to a focus spot of approximately 1.5 mm in diameter, with an f-number of f/7.4. The NRC transfer standard radiometers (labelled TR1, TR2, TR3, and TR7) and the comparison detectors under test (DUTs) were each positioned at the focus of the output beam using a computer controlled linear translation stage. A substitution technique was implemented for the measurements, where the spectral responsivity of the DUT was determined by measuring the signal from the DUT and comparing it to the signal from the NRC transfer standard radiometer, which has a known spectral responsivity, at a given wavelength. The NRC transfer standard radiometers each have a limiting aperture of 6 mm. To limit errors due to scattered light, specialized cylindrical holders with an end face of a 6 mm aperture were fabricated at NRC and mounted on the DUTs for spectral responsivity measurements. Two different holders with 6mm apertures, one positioned for the single element detectors, and one for the trap detectors, were implemented. To ensure an under-filled geometry, an additional limiting aperture was placed in the optical path (Figure 6-1) for measurements of the trap detectors. The photodetectors were each connected with a BNC cable to a transimpedance amplifier and the voltage was read by a digital multimeter (DMM) and switch unit. The same DMM and switch unit were used to read the PT100 temperature sensor from each DUT using the provided cable with LEMO connector. A custom LabVIEW program was used to control the apparatus and collect data for the spectral responsivity measurements.

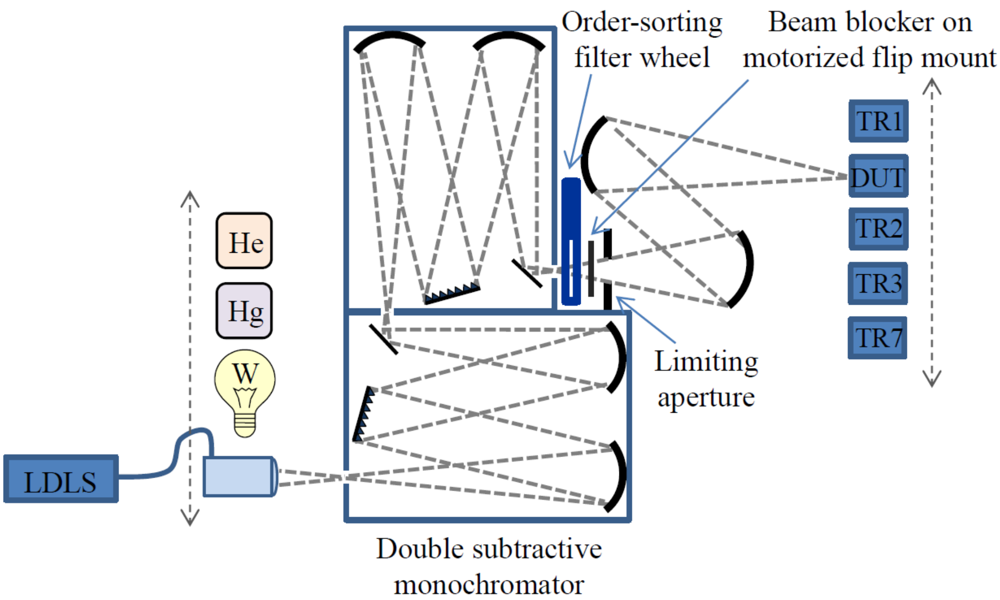


**Figure 6-1. Diagram of apparatus used for spectral responsivity measurements at NRC.**

## 6.2. Measurement Conditions and Parameters

The alignment of photodetectors was carried out using a 550 nm output beam from the monochromator. Each DUT was calibrated against four NRC transfer standard radiometers with all radiometers re-aligned for each measurement. The radiometers were mounted on a linear translation stage allowing for each detector to be positioned at the focus of the monochromator output beam. For fine adjustment of their initial positions, the radiometers had individual three-dimensional translations stages equipped with a rotation stage. For the single element DUTs, the LDLS or the tungsten lamp was used for beam alignment as the beam reflection from the detector active area could be observed with either light source. Only the LDLS was used for alignment of the trap detectors as the reflection of the tungsten lamp was too faint to be observed. A pellicle beam splitter was placed in the beam path for alignment purposes (Figure 6-2). The image of the detector active area and 6 mm aperture was seen visually on the pellicle, allowing for the focused beam to be centred on the detector using the translation stages. After removing the pellicle, the reflected beam from the detector active area was visually verified to be collinear with the incident beam using lens tissue in the optical path.

The temperature in the laboratory itself was controlled to approximately ±2 °C, while the relative humidity in the laboratory was relatively poorly controlled. These conditions were measured using a calibrated temperature and humidity sensor mounted inside the light-tight enclosure which surrounds the measurement apparatus (Figure 6-2). Inside the enclosure, a temperature of approximately 23.3 °C was maintained throughout the measurements. However, the relative humidity showed relatively greater variability i.e., between 13 % and 37 %.

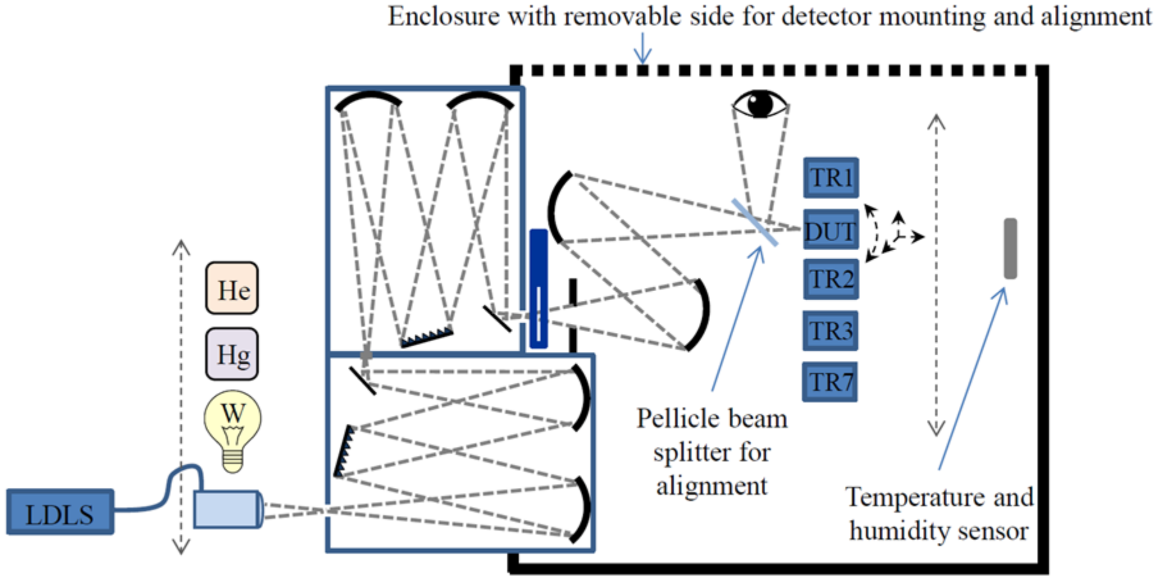


**Figure 6-2. Diagram of spectral responsivity apparatus at NRC showing the light-tight enclosure, pellicle beam splitter used to align the centre of the reference and test photodetectors with the monochromator output, and the location of the temperature and humidity sensor.**

### *6.3. Traceability of Measurement*

The NRC primary standard for spectral responsivity is a monochromator-based cryogenic radiometer system (Figure 6-3). The cryogenic radiometer facility implements the same model of double subtractive monochromator used for the CCPR-K2.b.2016 measurements. Using a flexible vacuum bellows on a rotation platform, the cryogenic radiometer and NRC transfer standard radiometers are alternatively in alignment with the monochromator output beam. The NRC transfer standard radiometers incorporate a single silicon photodiode (Hamamatsu 1337) and quartz window. These transfer radiometers were calibrated directly using the cryogenic radiometer apparatus shown in Figure 6-3. Further details on the NRC transfer standard radiometers and the cryogenic radiometer facility are given in references 1 and 2 below. The uncertainty budget for the NRC transfer standard radiometers implemented in the CCPR-K2.b.2016 measurements is given in Table 6-1.

[1] Boivin L. P. and Gibb K. 1995 Metrologia **32** 565
[2] A. Gamouras *et. al.* 2018 J. Phys.: Conf. Ser. **972** 012014.

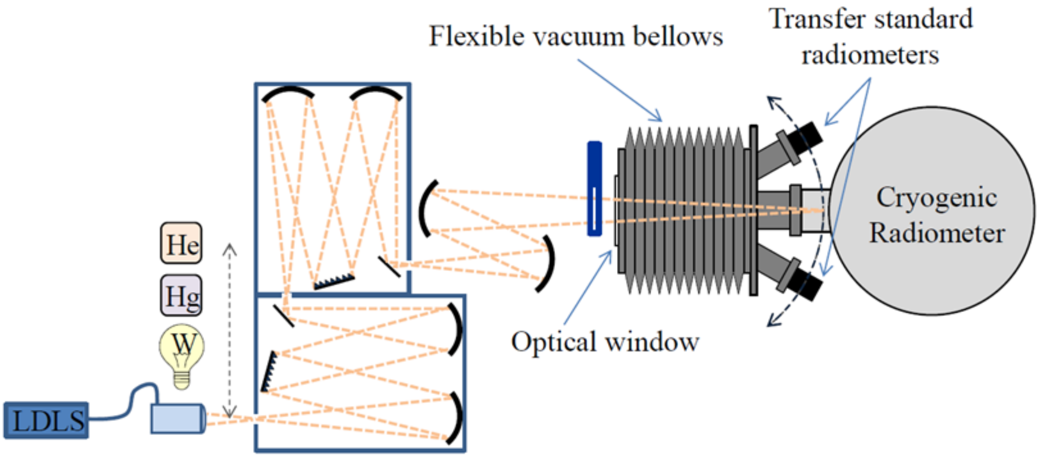


**Figure 6-3. Diagram of monochromator-based cryogenic radiometer facility at NRC.**

## 6.4. Measurement Uncertainty

The uncertainty budgets for the measured CCPR-K2.b transfer detectors are listed in Tables 2 to 6. The spectral responsivity of the DUT at a given wavelength is given by:

$$S_t = S_r \frac{V_t}{V_r}\frac{G_t}{G_r}$$

where $S_r$ is the spectral responsivity of the reference detector, $V_t$, $G_t$, $V_r$, and $G_r$ are the voltage signals and transimpedance amplifier gain factors of the test and reference detector respectively. The standard uncertainty component for the detector photocurrent measurement was calculated from the manufacturers specifications for the DMM used for the voltage measurements using a rectangular distribution, as well as the calibration results of the gain factors for the transimpedance amplifiers using a normal distribution.

The uncertainty due to the monochromator wavelength calibration is proportional to the derivative of the ratio of the test and reference spectral responsivity curves:

$$u_{rel}(S(\lambda)) = \frac{d\left(\frac{S_t}{S_r}\right)}{d\lambda} \times \mathrm{u}(\lambda)$$

where $\mathrm{u}(\lambda)$ is the normal distribution residual wavelength uncertainty obtained after wavelength correction curves have been applied to the monochromator system (±0.06 nm).

The monochromator bandwidth error is calculated by:

$$\delta_{bw}(\lambda_0) = [S_t^m(\lambda_0) - S_t(\lambda_0)]/S_t(\lambda_0)$$

where

$$S_t^m(\lambda_0) = S_r(\lambda_0)\frac{\int_{\lambda_0-\Delta}^{\lambda_0+\Delta} S_t(\lambda)I(\lambda)P(\lambda)}{\int_{\lambda_0-\Delta}^{\lambda_0+\Delta} S_r(\lambda)I(\lambda)P(\lambda)}$$

and where $S_t(\lambda)$ and $S_t^m(\lambda)$ are the true and measured spectral responsivity of the detector under test, $P(\lambda)$ is the spectral distribution of the monochromator output, $I(\lambda)$ is the monochromator slit function, and $\Delta$ is the FWHM spectral bandwidth of the monochromator. From 300 nm to 380 nm, $P(\lambda)$ is the spectral distribution of the output of the monochromator system using the LDLS. Similarly, from 400 nm to 1000 nm, $P(\lambda)$ is the spectral distribution of the output of the monochromator system using the tungsten lamp. The slit function $I(\lambda)$ describes the lineshape of the output of the monochromator. In this case, the monochromator system has a rectangular slit input and a round output which has a slit function described in Appl. Opt. **41** 1929-1935 (2002). A rectangular distribution is used to convert this relative bandwidth error to a standard uncertainty: $u_{rel,bw}$=$\delta_{bw}(\lambda_0)/\sqrt{3}$.

The temperature of the radiometers varied by ±0.1 °C during the spectral responsivity measurements. Wavelength dependent temperature coefficient data for the NRC transfer standard detectors was used to calculate the uncertainty in detector temperature using a rectangular distribution.

Each test detector was calibrated against four NRC transfer standard radiometers. The uncertainty in measurement repeatability was calculated by taking the average of the four uncertainties in measurement repeatability of the four calibrations. The repeatability uncertainty for each calibration was calculated using a normal distribution with six individual measurements. The repeatability component is attributed to the light source instability and detector alignment. Detector non-uniformity was taken into account indirectly in the measurement repeatability as each DUT was rotated by 90° during re-alignment for each measurement. This resulted in measurements being performed for two orthogonal orientations of the detector with respect to the incident beam. As the NRC transfer standard radiometers and the DUTs had equal diameter limiting apertures, the effect of scattered radiation was assumed to be negligible.

**Table 6-1. Uncertainty budget for the calibration of the four NRC single-element reference detectors using the cryogenic radiometer (%).**

| | Cryogenic Radiometer Effects | Detector temperature variation | Detector photocurrent measurement | Mono. wavelength calibration* | Mono. bandwidth effects* | Measurement repeatability* | |
|---|---|---|---|---|---|---|---|
| | Correlated | Correlated | Correlated | Correlated | Correlated | Uncorrelated | |
| Wavelength (nm) | Type B | Type A | Type B | Type B | Type B | Type A | Total |
| 300 | 0.011 | 0.007 | 0.004 | 0.025 | 0.070 | 0.091 | 0.118 |
| 320 | 0.011 | 0.003 | 0.004 | 0.019 | 0.021 | 0.034 | 0.046 |
| 340 | 0.011 | 0.001 | 0.004 | 0.001 | 0.022 | 0.035 | 0.043 |
| 360 | 0.011 | 0.013 | 0.004 | 0.003 | 0.028 | 0.124 | 0.128 |
| 380 | 0.011 | 0.013 | 0.004 | 0.033 | 0.043 | 0.055 | 0.079 |
| 400 | 0.011 | 0.011 | 0.004 | 0.034 | 0.004 | 0.018 | 0.042 |
| 450 | 0.011 | 0.008 | 0.004 | 0.015 | 0.008 | 0.127 | 0.129 |
| 500 | 0.011 | 0.005 | 0.004 | 0.013 | 0.003 | 0.052 | 0.055 |
| 550 | 0.011 | 0.003 | 0.004 | 0.010 | 0.001 | 0.057 | 0.059 |
| 600 | 0.011 | 0.003 | 0.004 | 0.009 | 0.000 | 0.043 | 0.046 |
| 650 | 0.011 | 0.003 | 0.004 | 0.008 | 0.001 | 0.041 | 0.044 |
| 700 | 0.011 | 0.002 | 0.004 | 0.008 | 0.001 | 0.048 | 0.050 |
| 750 | 0.011 | 0.003 | 0.004 | 0.007 | 0.002 | 0.079 | 0.080 |
| 800 | 0.011 | 0.002 | 0.004 | 0.007 | 0.002 | 0.098 | 0.099 |
| 850 | 0.011 | 0.001 | 0.004 | 0.006 | 0.000 | 0.134 | 0.134 |
| 900 | 0.011 | 0.002 | 0.004 | 0.006 | 0.002 | 0.083 | 0.084 |
| 950 | 0.011 | 0.008 | 0.004 | 0.002 | 0.002 | 0.055 | 0.057 |
| 1000 | 0.011 | 0.104 | 0.004 | 0.010 | 0.005 | 0.049 | 0.116 |

*Average of uncertainty components from the four NRC reference detectors

**Table 6-2. Uncertainty budget for spectral responsivity of single-element detector E01 (%).**

| | Reference detector calibration | Detector temperature variation | Detector photocurrent measurement | Mono. wavelength calibration | Mono. bandwidth effects | Measurement repeatability | |
|---|---|---|---|---|---|---|---|
| | Correlated | Correlated | Correlated | Correlated | Correlated | Uncorrelated | |
| Wavelength (nm) | Type B | Type A | Type B | Type B | Type B | Type A | Total |

| | | | | | | | |
|---|---|---|---|---|---|---|---|
| 300 | 0.118 | 0.001 | 0.006 | 0.000 | 0.001 | 0.039 | 0.125 |
| 320 | 0.046 | 0.000 | 0.006 | 0.000 | 0.001 | 0.023 | 0.052 |
| 340 | 0.043 | 0.000 | 0.006 | 0.000 | 0.000 | 0.029 | 0.052 |
| 360 | 0.128 | 0.001 | 0.006 | 0.000 | 0.001 | 0.028 | 0.131 |
| 380 | 0.079 | 0.001 | 0.006 | 0.001 | 0.001 | 0.024 | 0.083 |
| 400 | 0.042 | 0.001 | 0.006 | 0.001 | 0.000 | 0.013 | 0.044 |
| 450 | 0.129 | 0.001 | 0.006 | 0.000 | 0.000 | 0.011 | 0.130 |
| 500 | 0.055 | 0.001 | 0.006 | 0.000 | 0.000 | 0.011 | 0.056 |
| 550 | 0.059 | 0.000 | 0.006 | 0.000 | 0.000 | 0.010 | 0.060 |
| 600 | 0.046 | 0.000 | 0.006 | 0.000 | 0.000 | 0.010 | 0.047 |
| 650 | 0.044 | 0.000 | 0.006 | 0.000 | 0.000 | 0.009 | 0.045 |
| 700 | 0.050 | 0.000 | 0.006 | 0.000 | 0.000 | 0.008 | 0.051 |
| 750 | 0.080 | 0.000 | 0.006 | 0.000 | 0.000 | 0.007 | 0.081 |
| 800 | 0.099 | 0.000 | 0.006 | 0.000 | 0.000 | 0.006 | 0.099 |
| 850 | 0.134 | 0.000 | 0.006 | 0.000 | 0.000 | 0.006 | 0.134 |
| 900 | 0.084 | 0.000 | 0.006 | 0.000 | 0.000 | 0.006 | 0.084 |
| 950 | 0.057 | 0.001 | 0.006 | 0.001 | 0.001 | 0.006 | 0.058 |
| 1000 | 0.116 | 0.010 | 0.006 | 0.006 | 0.002 | 0.008 | 0.117 |

**Table 6-3. Uncertainty budget for spectral responsivity of single-element detector E02 (%).**

| | Reference detector calibration | Detector temperature variation | Detector photocurrent measurement | Mono. wavelength calibration | Mono. bandwidth effects | Measurement repeatability | |
|---|---|---|---|---|---|---|---|
| | Correlated | Correlated | Correlated | Correlated | Correlated | Uncorrelated | |
| Wavelength (nm) | Type B | Type A | Type B | Type B | Type B | Type A | Total |
| 300 | 0.118 | 0.001 | 0.006 | 0.001 | 0.002 | 0.043 | 0.126 |
| 320 | 0.046 | 0.000 | 0.006 | 0.000 | 0.000 | 0.043 | 0.064 |
| 340 | 0.043 | 0.000 | 0.006 | 0.000 | 0.000 | 0.047 | 0.064 |
| 360 | 0.128 | 0.001 | 0.006 | 0.000 | 0.011 | 0.041 | 0.135 |
| 380 | 0.079 | 0.001 | 0.006 | 0.001 | 0.014 | 0.032 | 0.087 |
| 400 | 0.042 | 0.001 | 0.006 | 0.001 | 0.000 | 0.017 | 0.046 |
| 450 | 0.129 | 0.001 | 0.006 | 0.000 | 0.000 | 0.013 | 0.130 |
| 500 | 0.055 | 0.001 | 0.006 | 0.000 | 0.000 | 0.012 | 0.056 |
| 550 | 0.059 | 0.000 | 0.006 | 0.000 | 0.000 | 0.012 | 0.061 |
| 600 | 0.046 | 0.000 | 0.006 | 0.000 | 0.000 | 0.011 | 0.048 |
| 650 | 0.044 | 0.000 | 0.006 | 0.000 | 0.000 | 0.011 | 0.046 |
| 700 | 0.050 | 0.000 | 0.006 | 0.000 | 0.000 | 0.010 | 0.051 |
| 750 | 0.080 | 0.000 | 0.006 | 0.000 | 0.000 | 0.009 | 0.081 |
| 800 | 0.099 | 0.000 | 0.006 | 0.000 | 0.000 | 0.007 | 0.099 |
| 850 | 0.134 | 0.000 | 0.006 | 0.000 | 0.000 | 0.008 | 0.135 |
| 900 | 0.084 | 0.000 | 0.006 | 0.000 | 0.000 | 0.008 | 0.085 |
| 950 | 0.057 | 0.001 | 0.006 | 0.001 | 0.001 | 0.009 | 0.058 |
| 1000 | 0.116 | 0.010 | 0.006 | 0.007 | 0.002 | 0.007 | 0.117 |

**Table 6-4. Uncertainty budget for spectral responsivity of single-element detector E03 (%).**

| Wavelength (nm) | Reference detector calibration | Detector temperature variation | Detector photocurrent measurement | Mono. wavelength calibration | Mono. bandwidth effects | Measurement repeatability | Total |
|---|---|---|---|---|---|---|---|
| | Correlated | Correlated | Correlated | Correlated | Correlated | Uncorrelated | |
| | Type B | Type A | Type B | Type B | Type B | Type A | Total |
| 300 | 0.118 | 0.001 | 0.006 | 0.001 | 0.001 | 0.047 | 0.127 |
| 320 | 0.046 | 0.000 | 0.006 | 0.000 | 0.000 | 0.030 | 0.055 |
| 340 | 0.043 | 0.000 | 0.006 | 0.000 | 0.000 | 0.040 | 0.059 |
| 360 | 0.128 | 0.001 | 0.006 | 0.000 | 0.000 | 0.020 | 0.130 |
| 380 | 0.079 | 0.001 | 0.006 | 0.001 | 0.001 | 0.022 | 0.082 |
| 400 | 0.042 | 0.001 | 0.006 | 0.001 | 0.001 | 0.009 | 0.043 |
| 450 | 0.129 | 0.001 | 0.006 | 0.000 | 0.000 | 0.006 | 0.129 |
| 500 | 0.055 | 0.001 | 0.006 | 0.000 | 0.000 | 0.005 | 0.055 |
| 550 | 0.059 | 0.000 | 0.006 | 0.000 | 0.000 | 0.005 | 0.060 |
| 600 | 0.046 | 0.000 | 0.006 | 0.000 | 0.000 | 0.004 | 0.047 |
| 650 | 0.044 | 0.000 | 0.006 | 0.000 | 0.000 | 0.004 | 0.044 |
| 700 | 0.050 | 0.000 | 0.006 | 0.000 | 0.000 | 0.004 | 0.050 |
| 750 | 0.080 | 0.000 | 0.006 | 0.000 | 0.000 | 0.004 | 0.081 |
| 800 | 0.099 | 0.000 | 0.006 | 0.000 | 0.000 | 0.002 | 0.099 |
| 850 | 0.134 | 0.000 | 0.006 | 0.000 | 0.000 | 0.002 | 0.134 |
| 900 | 0.084 | 0.000 | 0.006 | 0.000 | 0.000 | 0.002 | 0.084 |
| 950 | 0.057 | 0.001 | 0.006 | 0.001 | 0.001 | 0.003 | 0.058 |
| 1000 | 0.116 | 0.010 | 0.006 | 0.006 | 0.001 | 0.007 | 0.117 |

**Table 6-5. Uncertainty budget for spectral responsivity of single-element detector E04 (%).**

| Wavelength (nm) | Reference detector calibration | Detector temperature variation | Detector photocurrent measurement | Mono. wavelength calibration | Mono. bandwidth effects | Measurement repeatability | Total |
|---|---|---|---|---|---|---|---|
| | Correlated | Correlated | Correlated | Correlated | Correlated | Uncorrelated | |
| | Type B | Type A | Type B | Type B | Type B | Type A | Total |
| 300 | 0.118 | 0.001 | 0.006 | 0.048 | 0.048 | 0.035 | 0.141 |
| 320 | 0.046 | 0.000 | 0.006 | 0.016 | 0.002 | 0.029 | 0.057 |
| 340 | 0.043 | 0.000 | 0.006 | 0.028 | 0.034 | 0.028 | 0.068 |
| 360 | 0.128 | 0.001 | 0.006 | 0.024 | 0.015 | 0.033 | 0.135 |
| 380 | 0.079 | 0.001 | 0.006 | 0.037 | 0.031 | 0.021 | 0.095 |
| 400 | 0.042 | 0.001 | 0.006 | 0.038 | 0.007 | 0.007 | 0.058 |
| 450 | 0.129 | 0.001 | 0.006 | 0.006 | 0.002 | 0.007 | 0.130 |
| 500 | 0.055 | 0.001 | 0.006 | 0.004 | 0.000 | 0.004 | 0.056 |
| 550 | 0.059 | 0.000 | 0.006 | 0.002 | 0.000 | 0.004 | 0.060 |
| 600 | 0.046 | 0.000 | 0.006 | 0.001 | 0.000 | 0.005 | 0.047 |
| 650 | 0.044 | 0.000 | 0.006 | 0.001 | 0.000 | 0.004 | 0.045 |
| 700 | 0.050 | 0.000 | 0.006 | 0.001 | 0.000 | 0.005 | 0.050 |
| 750 | 0.080 | 0.000 | 0.006 | 0.001 | 0.000 | 0.031 | 0.086 |
| 800 | 0.099 | 0.000 | 0.006 | 0.000 | 0.000 | 0.030 | 0.103 |
| 850 | 0.134 | 0.000 | 0.006 | 0.000 | 0.000 | 0.031 | 0.138 |
| 900 | 0.084 | 0.000 | 0.006 | 0.000 | 0.000 | 0.034 | 0.091 |

| | | | | | | | |
|---|---|---|---|---|---|---|---|
| 950 | 0.057 | 0.001 | 0.006 | 0.002 | 0.001 | 0.039 | 0.069 |
| 1000 | 0.116 | 0.010 | 0.006 | 0.009 | 0.001 | 0.042 | 0.125 |

**Table 6-6. Uncertainty budget for spectral responsivity of single-element detector E05 (%).**

| | Reference detector calibration | Detector temperature variation | Detector photocurrent measurement | Mono. wavelength calibration | Mono. bandwidth effects | Measurement repeatability | |
|---|---|---|---|---|---|---|---|
| | Correlated | Correlated | Correlated | Correlated | Correlated | Uncorrelated | |
| Wavelength (nm) | Type B | Type A | Type B | Type B | Type B | Type A | Total |
| 300 | 0.118 | 0.001 | 0.006 | 0.047 | 0.047 | 0.033 | 0.139 |
| 320 | 0.046 | 0.000 | 0.006 | 0.016 | 0.002 | 0.035 | 0.060 |
| 340 | 0.043 | 0.000 | 0.006 | 0.028 | 0.034 | 0.034 | 0.071 |
| 360 | 0.128 | 0.001 | 0.006 | 0.024 | 0.015 | 0.058 | 0.144 |
| 380 | 0.079 | 0.001 | 0.006 | 0.037 | 0.031 | 0.043 | 0.102 |
| 400 | 0.042 | 0.001 | 0.006 | 0.038 | 0.007 | 0.018 | 0.060 |
| 450 | 0.129 | 0.001 | 0.006 | 0.006 | 0.002 | 0.021 | 0.131 |
| 500 | 0.055 | 0.001 | 0.006 | 0.004 | 0.000 | 0.021 | 0.059 |
| 550 | 0.059 | 0.000 | 0.006 | 0.002 | 0.000 | 0.023 | 0.064 |
| 600 | 0.046 | 0.000 | 0.006 | 0.001 | 0.000 | 0.023 | 0.052 |
| 650 | 0.044 | 0.000 | 0.006 | 0.001 | 0.000 | 0.022 | 0.050 |
| 700 | 0.050 | 0.000 | 0.006 | 0.001 | 0.000 | 0.017 | 0.053 |
| 750 | 0.080 | 0.000 | 0.006 | 0.001 | 0.000 | 0.019 | 0.083 |
| 800 | 0.099 | 0.000 | 0.006 | 0.000 | 0.000 | 0.018 | 0.100 |
| 850 | 0.134 | 0.000 | 0.006 | 0.000 | 0.000 | 0.018 | 0.135 |
| 900 | 0.084 | 0.000 | 0.006 | 0.000 | 0.000 | 0.020 | 0.087 |
| 950 | 0.057 | 0.001 | 0.006 | 0.002 | 0.001 | 0.019 | 0.061 |
| 1000 | 0.116 | 0.010 | 0.006 | 0.010 | 0.001 | 0.029 | 0.121 |

# 7. UME

## 7.1. *Measurement Setup and Instruments*

The measurement set up used for the responsivity measurements of detectors is shown in the Figure 7-1. This system consist of Deuterium and Tungsten light sources, Bentham double grating monochromator (DTMc 300), output optics, detector holders and electronic system. Bentham double grating monochromator in its each turret has triple gratings with 2400 g/mm blazed at 250 nm, 1200 g/mm blazed at 500 nm and 600 g/mm blazed at 1600 nm. Double monochromator has also 2 x 300mm focal length and order sorting filters at 400 nm, 700 nm, 1250 nm, 2000 nm, 3600 nm and 6000 nm. The output optics consists of off axis mirror and apertures and is used to to collimate the beam and adjust its diameter. The test detectors (TD) and the reference detectors (RD) are placed on the translation stage and the whole system was enclosed in a light tight box. This light box has fan cooling so as to keep temperature inside it to be same as the temperature of laboratory.

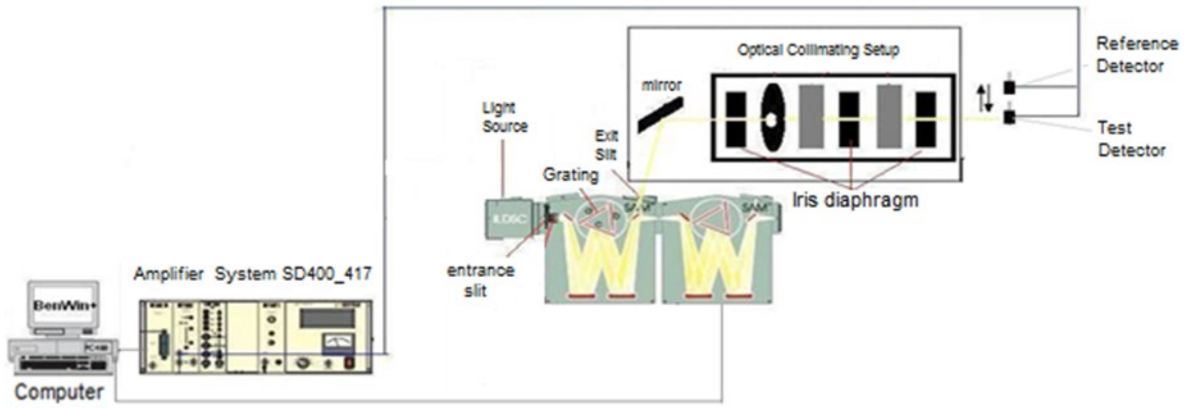


**Figure 7-1. Bentham Monochromator Based Spectral Responsivity Measurement Setup at UME.**

## 7.2. Measurement Conditions and Parameters

The conditions at which the measurements were carried out can be summarised as follows. Light sources, gratings, the wavelengths at which measurements need to be done were programmed and automatically controlled by software. The Deuterium and Tungsten light sources were adjusted to be used for the measurements from 300 nm to 360 nm and from 380 nm to 1000 nm respectively; the 2400 g/mm and 1200 g/mm gratings were used for the measurements from 300 nm to 360 nm and from 380 nm to 1000 nm respectively. The beam diameters manually were adjusted approximately to 4 mm for the single photodiode detectors and approximately to 4 mm at the third photodiode of trap detector.

The temperature and humidity of the laboratory in which the measurements were performed are set to 23 ºC ± 2 ºC and 45 % ± 10 % RH. Moreover, during the measurements the temperature of inside the light tight enclosure was also recorded.

For the measurements the wavelengths at which detectors to be calibrated were defined in to the software and both test and reference detectors were respectively moved to in front of light beam and measurements were performed at the defined wavelengths. At the same time to record the resistance of test detectors their resistance output was connected to a digital multimeter and the resistances at each wavelength were recorded.

## 7.3. Traceability of Measurement

The reference detector was used for these measurements is UME made reflection type trap detector. The photodiodes used in this trap detector are Hamamatsu S1337-11 photodiodes. This trap detector was calibrated against liquid helium cooled cryogenic radiometer at 488 nm, 515 nm and 632 nm laser wavelengths. Then using internal quantum efficiency and reflectance models the responsivity was extrapolated to 350 nm – 850 nm interval. The responsivity from 300 nm to 350 nm and from 850 nm to 1100 nm was obtained by calibrating the trap detector against Electrically Calibrated Pyroelectric Radiometer (ECPR).

## 7.4. Measurement Uncertainty

**Table 7-1. Uncertainty budget of spectral responsivity at 300 nm for the transfer detector with the serial number F1.**

| Uncertainty Component | Standard uncertainty (%) | Type | Probability distribution | Sensitivity coefficient | Contribution (%) | Deg. of freedom | Correlated? |
|---|---|---|---|---|---|---|---|
| Reading repeatability | 0.060 | A | Normal | 1 | 0.060 | 12 | C |
| Calibration uncertainty of ammeter | 0.200 | A | Normal | 1 | 0.200 | ∞ | C |
| Calibration uncertainty of reference detector | 0.515 | A | Normal | 1 | 0.515 | ∞ | C |
| Uncertainty from wavelength error of light source | 0.020 | B | Rectangular | 1 | 0.020 | ∞ | UC |
| Uncertainty from spectral bandwidth of light source | 0.030 | B | Rectangular | 1 | 0.030 | ∞ | UC |
| Uncertainty related to beam alignment | 0.020 | B | Rectangular | 1 | 0.020 | ∞ | UC |
| Uncertainty related to beam size and divergence | 0.010 | B | Rectangular | 1 | 0.010 | ∞ | UC |
| Uncertainty from power instability of light source | 0.010 | B | Rectangular | 1 | 0.010 | ∞ | UC |
| Uncertainty related to polarization of light source | 0.004 | B | Rectangular | 1 | 0.004 | ∞ | UC |
| Uncertainty from spectral stray of light source | 0.001 | B | Rectangular | 1 | 0.001 | ∞ | UC |
| Uncertainty from detector non-linearity | 0.010 | B | Rectangular | 1 | 0.010 | ∞ | UC |
| Uncertainty from ambient stray light | 0.100 | B | Rectangular | 1 | 0.100 | ∞ | UC |
| **Combined standard uncertainty (%)** | **--** | **--** | **Normal** | **--** | **0.57** | **∞** | **--** |

**Table 7-2. Uncertainty budget of spectral responsivity at 300 nm for the transfer detector with the serial number F2.**

| Uncertainty Component | Standard uncertainty (%) | Type | Probability distribution | Sensitivity coefficient | Contribution (%) | Deg. of freedom | Correlated? |
|---|---|---|---|---|---|---|---|
| Reading repeatability | 0.052 | A | Normal | 1 | 0.052 | 12 | C |
| Calibration uncertainty of ammeter | 0.200 | A | Normal | 1 | 0.200 | ∞ | C |
| Calibration uncertainty of reference detector | 0.515 | A | Normal | 1 | 0.515 | ∞ | C |
| Uncertainty from wavelength error of light source | 0.020 | B | Rectangular | 1 | 0.020 | ∞ | UC |
| Uncertainty from spectral bandwidth of light source | 0.030 | B | Rectangular | 1 | 0.030 | ∞ | UC |

| | | | | | | | |
|---|---|---|---|---|---|---|---|
| Uncertainty related to beam alignment | 0.020 | B | Rectangular | 1 | 0.020 | ∞ | UC |
| Uncertainty related to beam size and divergence | 0.010 | B | Rectangular | 1 | 0.010 | ∞ | UC |
| Uncertainty from power instability of light source | 0.010 | B | Rectangular | 1 | 0.010 | ∞ | UC |
| Uncertainty related to polarization of light source | 0.004 | B | Rectangular | 1 | 0.004 | ∞ | UC |
| Uncertainty from spectral stray of light source | 0.001 | B | Rectangular | 1 | 0.001 | ∞ | UC |
| Uncertainty from detector non-linearity | 0.010 | B | Rectangular | 1 | 0.010 | ∞ | UC |
| Uncertainty from ambient stray light | 0.100 | B | Rectangular | 1 | 0.100 | ∞ | UC |
| **Combined standard uncertainty (%)** | **--** | **--** | **Normal** | **--** | **0.57** | **∞** | **--** |

**Table 7-3. Uncertainty budget of spectral responsivity at 300 nm for the transfer detector with the serial number F3.**

| Uncertainty Component | Standard uncertainty (%) | Type | Probability distribution | Sensitivity coefficient | Contribution (%) | Deg. of freedom | Correlated? |
|---|---|---|---|---|---|---|---|
| Reading repeatability | 0.380 | A | Normal | 1 | 0.380 | 12 | C |
| Calibration uncertainty of ammeter | 0.200 | A | Normal | 1 | 0.200 | ∞ | C |
| Calibration uncertainty of reference detector | 0.515 | A | Normal | 1 | 0.515 | ∞ | C |
| Uncertainty from wavelength error of light source | 0.020 | B | Rectangular | 1 | 0.020 | ∞ | UC |
| Uncertainty from spectral bandwidth of light source | 0.030 | B | Rectangular | 1 | 0.030 | ∞ | UC |
| Uncertainty related to beam alignment | 0.020 | B | Rectangular | 1 | 0.020 | ∞ | UC |
| Uncertainty related to beam size and divergence | 0.010 | B | Rectangular | 1 | 0.010 | ∞ | UC |
| Uncertainty from power instability of light source | 0.010 | B | Rectangular | 1 | 0.010 | ∞ | UC |
| Uncertainty related to polarization of light source | 0.004 | B | Rectangular | 1 | 0.004 | ∞ | UC |
| Uncertainty from spectral stray of light source | 0.001 | B | Rectangular | 1 | 0.001 | ∞ | UC |
| Uncertainty from detector non-linearity | 0.010 | B | Rectangular | 1 | 0.010 | ∞ | UC |
| Uncertainty from ambient stray light | 0.100 | B | Rectangular | 1 | 0.100 | ∞ | UC |
| **Combined standard uncertainty (%)** | **--** | **--** | **Normal** | **--** | **0.68** | **∞** | **--** |

**Table 7-4. Uncertainty budget of spectral responsivity at 300 nm for the transfer detector with the serial number F4.**

| Uncertainty Component | Standard uncertainty (%) | Type | Probability distribution | Sensitivity coefficient | Contribution (%) | Deg. of freedom | Correlated? |
|---|---|---|---|---|---|---|---|
| Reading repeatability | 0.048 | A | Normal | 1 | 0.048 | 12 | C |
| Calibration uncertainty of ammeter | 0.200 | A | Normal | 1 | 0.200 | ∞ | C |
| Calibration uncertainty of reference detector | 0.515 | A | Normal | 1 | 0.515 | ∞ | C |
| Uncertainty from wavelength error of light source | 0.020 | B | Rectangular | 1 | 0.020 | ∞ | UC |
| Uncertainty from spectral bandwidth of light source | 0.030 | B | Rectangular | 1 | 0.030 | ∞ | UC |
| Uncertainty related to beam alignment | 0.020 | B | Rectangular | 1 | 0.020 | ∞ | UC |
| Uncertainty related to beam size and divergence | 0.010 | B | Rectangular | 1 | 0.010 | ∞ | UC |
| Uncertainty from power instability of light source | 0.010 | B | Rectangular | 1 | 0.010 | ∞ | UC |
| Uncertainty related to polarization of light source | 0.004 | B | Rectangular | 1 | 0.004 | ∞ | UC |
| Uncertainty from spectral stray of light source | 0.001 | B | Rectangular | 1 | 0.001 | ∞ | UC |
| Uncertainty from detector non-linearity | 0.010 | B | Rectangular | 1 | 0.010 | ∞ | UC |
| Uncertainty from ambient stray light | 0.040 | B | Rectangular | 1 | 0.040 | ∞ | UC |
| **Combined standard uncertainty (%)** | **--** | **--** | **Normal** | **--** | **0.56** | **∞** | **--** |

**Table 7-5. Uncertainty budget of spectral responsivity at 300 nm for the transfer detector with the serial number F5.**

| Uncertainty Component | Standard uncertainty (%) | Type | Probability distribution | Sensitivity coefficient | Contribution (%) | Deg. of freedom | Correlated? |
|---|---|---|---|---|---|---|---|
| Reading repeatability | 0.060 | A | Normal | 1 | 0.060 | 12 | C |
| Calibration uncertainty of ammeter | 0.200 | A | Normal | 1 | 0.200 | ∞ | C |
| Calibration uncertainty of reference detector | 0.515 | A | Normal | 1 | 0.515 | ∞ | C |

| | | | | | | | |
|---|---|---|---|---|---|---|---|
| Uncertainty from wavelength error of light source | 0.020 | B | Rectangular | 1 | 0.020 | ∞ | UC |
| Uncertainty from spectral bandwidth of light source | 0.030 | B | Rectangular | 1 | 0.030 | ∞ | UC |
| Uncertainty related to beam alignment | 0.020 | B | Rectangular | 1 | 0.020 | ∞ | UC |
| Uncertainty related to beam size and divergence | 0.010 | B | Rectangular | 1 | 0.010 | ∞ | UC |
| Uncertainty from power instability of light source | 0.010 | B | Rectangular | 1 | 0.010 | ∞ | UC |
| Uncertainty related to polarization of light source | 0.004 | B | Rectangular | 1 | 0.004 | ∞ | UC |
| Uncertainty from spectral stray of light source | 0.001 | B | Rectangular | 1 | 0.001 | ∞ | UC |
| Uncertainty from detector non-linearity | 0.010 | B | Rectangular | 1 | 0.010 | ∞ | UC |
| Uncertainty from ambient stray light | 0.040 | B | Rectangular | 1 | 0.040 | ∞ | UC |
| **Combined standard uncertainty (%)** | **--** | **--** | **Normal** | **--** | **0.56** | **∞** | **--** |

**Table 7-6. Uncertainty budget of spectral responsivity at 500 nm for the transfer detector with the serial number F1.**

| Uncertainty Component | Standard uncertainty (%) | Type | Probability distribution | Sensitivity coefficient | Contribution (%) | Deg. of freedom | Correlated? |
|---|---|---|---|---|---|---|---|
| Reading repeatability | 0.024 | A | Normal | 1 | 0.02 | 12 | C |
| Calibration uncertainty of ammeter | 0.200 | A | Normal | 1 | 0.20 | ∞ | C |
| Calibration uncertainty of reference detector | 0.130 | A | Normal | 1 | 0.13 | ∞ | C |
| Uncertainty from wavelength error of light source | 0.020 | B | Rectangular | 1 | 0.02 | ∞ | UC |
| Uncertainty from spectral bandwidth of light source | 0.030 | B | Rectangular | 1 | 0.03 | ∞ | UC |
| Uncertainty related to beam alignment | 0.020 | B | Rectangular | 1 | 0.02 | ∞ | UC |
| Uncertainty related to beam size and divergence | 0.010 | B | Rectangular | 1 | 0.01 | ∞ | UC |
| Uncertainty from power instability of light source | 0.010 | B | Rectangular | 1 | 0.01 | ∞ | UC |
| Uncertainty related to polarization of light source | 0.004 | B | Rectangular | 1 | 0.00 | ∞ | UC |
| Uncertainty from spectral stray of light source | 0.001 | B | Rectangular | 1 | 0.00 | ∞ | UC |

| | | | | | | | |
|---|---|---|---|---|---|---|---|
| Uncertainty from detector non-linearity | 0.010 | B | Rectangular | 1 | 0.01 | ∞ | UC |
| Uncertainty from ambient stray light | 0.100 | B | Rectangular | 1 | 0.10 | ∞ | UC |
| **Combined standard uncertainty (%)** | **--** | **--** | **Normal** | **--** | **0.26** | **∞** | **--** |

**Table 7-7. Uncertainty budget of spectral responsivity at 500 nm for the transfer detector with the serial number F2.**

| Uncertainty Component | Standard uncertainty (%) | Type | Probability distribution | Sensitivity coefficient | Contribution (%) | Deg. of freedom | Correlated? |
|---|---|---|---|---|---|---|---|
| Reading repeatability | 0.016 | A | Normal | 1 | 0.02 | 12 | C |
| Calibration uncertainty of ammeter | 0.200 | A | Normal | 1 | 0.20 | ∞ | C |
| Calibration uncertainty of reference detector | 0.130 | A | Normal | 1 | 0.13 | ∞ | C |
| Uncertainty from wavelength error of light source | 0.020 | B | Rectangular | 1 | 0.02 | ∞ | UC |
| Uncertainty from spectral bandwidth of light source | 0.030 | B | Rectangular | 1 | 0.03 | ∞ | UC |
| Uncertainty related to beam alignment | 0.020 | B | Rectangular | 1 | 0.02 | ∞ | UC |
| Uncertainty related to beam size and divergence | 0.010 | B | Rectangular | 1 | 0.01 | ∞ | UC |
| Uncertainty from power instability of light source | 0.010 | B | Rectangular | 1 | 0.01 | ∞ | UC |
| Uncertainty related to polarization of light source | 0.004 | B | Rectangular | 1 | 0.00 | ∞ | UC |
| Uncertainty from spectral stray of light source | 0.001 | B | Rectangular | 1 | 0.00 | ∞ | UC |
| Uncertainty from detector non-linearity | 0.010 | B | Rectangular | 1 | 0.01 | ∞ | UC |
| Uncertainty from ambient stray light | 0.100 | B | Rectangular | 1 | 0.10 | ∞ | UC |
| **Combined standard uncertainty (%)** | **--** | **--** | **Normal** | **--** | **0.26** | **∞** | **--** |

**Table 7-8. Uncertainty budget of spectral responsivity at 500 nm for the transfer detector with the serial number F3.**

| Uncertainty Component | Standard uncertainty (%) | Type | Probability distribution | Sensitivity coefficient | Contribution (%) | Deg. of freedom | Correlated? |
|---|---|---|---|---|---|---|---|

| | | | | | | | |
|---|---|---|---|---|---|---|---|
| Reading repeatability | 0.036 | A | Normal | 1 | 0.04 | 12 | C |
| Calibration uncertainty of ammeter | 0.200 | A | Normal | 1 | 0.20 | ∞ | C |
| Calibration uncertainty of reference detector | 0.130 | A | Normal | 1 | 0.13 | ∞ | C |
| Uncertainty from wavelength error of light source | 0.020 | B | Rectangular | 1 | 0.02 | ∞ | UC |
| Uncertainty from spectral bandwidth of light source | 0.030 | B | Rectangular | 1 | 0.03 | ∞ | UC |
| Uncertainty related to beam alignment | 0.020 | B | Rectangular | 1 | 0.02 | ∞ | UC |
| Uncertainty related to beam size and divergence | 0.010 | B | Rectangular | 1 | 0.01 | ∞ | UC |
| Uncertainty from power instability of light source | 0.010 | B | Rectangular | 1 | 0.01 | ∞ | UC |
| Uncertainty related to polarization of light source | 0.004 | B | Rectangular | 1 | 0.00 | ∞ | UC |
| Uncertainty from spectral stray of light source | 0.001 | B | Rectangular | 1 | 0.00 | ∞ | UC |
| Uncertainty from detector non-linearity | 0.010 | B | Rectangular | 1 | 0.01 | ∞ | UC |
| Uncertainty from ambient stray light | 0.100 | B | Rectangular | 1 | 0.10 | ∞ | UC |
| **Combined standard uncertainty (%)** | **--** | **--** | **Normal** | **--** | **0.26** | **∞** | **--** |

**Table 7-9. Uncertainty budget of spectral responsivity at 500 nm for the transfer detector with the serial number F4.**

| Uncertainty Component | Standard uncertainty (%) | Type | Probability distribution | Sensitivity coefficient | Contribution (%) | Deg. of freedom | Correlated? |
|---|---|---|---|---|---|---|---|
| Reading repeatability | 0.034 | A | Normal | 1 | 0.03 | 12 | C |
| Calibration uncertainty of ammeter | 0.200 | A | Normal | 1 | 0.20 | ∞ | C |
| Calibration uncertainty of reference detector | 0.130 | A | Normal | 1 | 0.13 | ∞ | C |
| Uncertainty from wavelength error of light source | 0.020 | B | Rectangular | 1 | 0.02 | ∞ | UC |
| Uncertainty from spectral bandwidth of light source | 0.030 | B | Rectangular | 1 | 0.03 | ∞ | UC |
| Uncertainty related to beam alignment | 0.020 | B | Rectangular | 1 | 0.02 | ∞ | UC |
| Uncertainty related to beam size and divergence | 0.010 | B | Rectangular | 1 | 0.01 | ∞ | UC |

| | | | | | | | |
|---|---|---|---|---|---|---|---|
| Uncertainty from power instability of light source | 0.010 | B | Rectangular | 1 | 0.01 | ∞ | UC |
| Uncertainty related to polarization of light source | 0.004 | B | Rectangular | 1 | 0.00 | ∞ | UC |
| Uncertainty from spectral stray of light source | 0.001 | B | Rectangular | 1 | 0.00 | ∞ | UC |
| Uncertainty from detector non-linearity | 0.010 | B | Rectangular | 1 | 0.01 | ∞ | UC |
| Uncertainty from ambient stray light | 0.040 | B | Rectangular | 1 | 0.04 | ∞ | UC |
| Combined standard uncertainty (%) | -- | -- | **Normal** | -- | **0.25** | ∞ | -- |

**Table 7-10. Uncertainty budget of spectral responsivity at 500 nm for the transfer detector with the serial number F5.**

| Uncertainty Component | Standard uncertainty (%) | Type | Probability distribution | Sensitivity coefficient | Contribution (%) | Deg. of freedom | Correlated? |
|---|---|---|---|---|---|---|---|
| Reading repeatability | 0.011 | A | Normal | 1 | 0.01 | 12 | C |
| Calibration uncertainty of ammeter | 0.200 | A | Normal | 1 | 0.20 | ∞ | C |
| Calibration uncertainty of reference detector | 0.130 | A | Normal | 1 | 0.13 | ∞ | C |
| Uncertainty from wavelength error of light source | 0.020 | B | Rectangular | 1 | 0.02 | ∞ | UC |
| Uncertainty from spectral bandwidth of light source | 0.030 | B | Rectangular | 1 | 0.03 | ∞ | UC |
| Uncertainty related to beam alignment | 0.020 | B | Rectangular | 1 | 0.02 | ∞ | UC |
| Uncertainty related to beam size and divergence | 0.010 | B | Rectangular | 1 | 0.01 | ∞ | UC |
| Uncertainty from power instability of light source | 0.010 | B | Rectangular | 1 | 0.01 | ∞ | UC |
| Uncertainty related to polarization of light source | 0.004 | B | Rectangular | 1 | 0.00 | ∞ | UC |
| Uncertainty from spectral stray of light source | 0.001 | B | Rectangular | 1 | 0.00 | ∞ | UC |
| Uncertainty from detector non-linearity | 0.010 | B | Rectangular | 1 | 0.01 | ∞ | UC |
| Uncertainty from ambient stray light | 0.040 | B | Rectangular | 1 | 0.04 | ∞ | UC |
| Combined standard uncertainty (%) | -- | -- | **Normal** | -- | **0.25** | ∞ | -- |

**Table 7-11. Uncertainty budget of spectral responsivity at 1000 nm for the transfer detector with the serial number F1.**

| Uncertainty Component | Standard uncertainty (%) | Type | Probability distribution | Sensitivity coefficient | Contribution (%) | Deg. of freedom | Correlated? |
|---|---|---|---|---|---|---|---|
| Reading repeatability | 0.032 | A | Normal | 1 | 0.032 | 12 | C |
| Calibration uncertainty of ammeter | 0.200 | A | Normal | 1 | 0.200 | ∞ | C |
| Calibration uncertainty of reference detector | 0.515 | A | Normal | 1 | 0.515 | ∞ | C |
| Uncertainty from wavelength error of light source | 0.020 | B | Rectangular | 1 | 0.020 | ∞ | UC |
| Uncertainty from spectral bandwidth of light source | 0.030 | B | Rectangular | 1 | 0.030 | ∞ | UC |
| Uncertainty related to beam alignment | 0.020 | B | Rectangular | 1 | 0.020 | ∞ | UC |
| Uncertainty related to beam size and divergence | 0.010 | B | Rectangular | 1 | 0.010 | ∞ | UC |
| Uncertainty from power instability of light source | 0.010 | B | Rectangular | 1 | 0.010 | ∞ | UC |
| Uncertainty related to polarization of light source | 0.004 | B | Rectangular | 1 | 0.004 | ∞ | UC |
| Uncertainty from spectral stray of light source | 0.001 | B | Rectangular | 1 | 0.001 | ∞ | UC |
| Uncertainty from detector non-linearity | 0.010 | B | Rectangular | 1 | 0.010 | ∞ | UC |
| Uncertainty from ambient stray light | 0.100 | B | Rectangular | 1 | 0.100 | ∞ | UC |
| Combined standard uncertainty (%) | **--** | **--** | **Normal** | **--** | **0.56** | **∞** | **--** |

**Table 7-12. Uncertainty budget of spectral responsivity at 1000 nm for the transfer detector with the serial number F2.**

| Uncertainty Component | Standard uncertainty (%) | Type | Probability distribution | Sensitivity coefficient | Contribution (%) | Deg. of freedom | Correlated? |
|---|---|---|---|---|---|---|---|
| Reading repeatability | 0.052 | A | Normal | 1 | 0.052 | 12 | C |
| Calibration uncertainty of ammeter | 0.200 | A | Normal | 1 | 0.200 | ∞ | C |
| Calibration uncertainty of reference detector | 0.515 | A | Normal | 1 | 0.515 | ∞ | C |
| Uncertainty from wavelength error of light source | 0.020 | B | Rectangular | 1 | 0.020 | ∞ | UC |
| Uncertainty from spectral bandwidth of light source | 0.030 | B | Rectangular | 1 | 0.030 | ∞ | UC |

| | | | | | | | |
|---|---|---|---|---|---|---|---|
| Uncertainty related to beam alignment | 0.020 | B | Rectangular | 1 | 0.020 | ∞ | UC |
| Uncertainty related to beam size and divergence | 0.010 | B | Rectangular | 1 | 0.010 | ∞ | UC |
| Uncertainty from power instability of light source | 0.010 | B | Rectangular | 1 | 0.010 | ∞ | UC |
| Uncertainty related to polarization of light source | 0.004 | B | Rectangular | 1 | 0.004 | ∞ | UC |
| Uncertainty from spectral stray of light source | 0.001 | B | Rectangular | 1 | 0.001 | ∞ | UC |
| Uncertainty from detector non-linearity | 0.010 | B | Rectangular | 1 | 0.010 | ∞ | UC |
| Uncertainty from ambient stray light | 0.100 | B | Rectangular | 1 | 0.100 | ∞ | UC |
| Combined standard uncertainty (%) | -- | -- | **Normal** | -- | **0.57** | **∞** | -- |

**Table 7-13. Uncertainty budget of spectral responsivity at 1000 nm for the transfer detector with the serial number F3.**

| **Uncertainty Component** | **Standard uncertainty (%)** | **Type** | **Probability distribution** | **Sensitivity coefficient** | **Contribution (%)** | **Deg. of freedom** | **Correlated?** |
|---|---|---|---|---|---|---|---|
| Reading repeatability | 0.085 | A | Normal | 1 | 0.085 | 12 | C |
| Calibration uncertainty of ammeter | 0.200 | A | Normal | 1 | 0.200 | ∞ | C |
| Calibration uncertainty of reference detector | 0.515 | A | Normal | 1 | 0.515 | ∞ | C |
| Uncertainty from wavelength error of light source | 0.020 | B | Rectangular | 1 | 0.020 | ∞ | UC |
| Uncertainty from spectral bandwidth of light source | 0.030 | B | Rectangular | 1 | 0.030 | ∞ | UC |
| Uncertainty related to beam alignment | 0.020 | B | Rectangular | 1 | 0.020 | ∞ | UC |
| Uncertainty related to beam size and divergence | 0.010 | B | Rectangular | 1 | 0.010 | ∞ | UC |
| Uncertainty from power instability of light source | 0.010 | B | Rectangular | 1 | 0.010 | ∞ | UC |
| Uncertainty related to polarization of light source | 0.004 | B | Rectangular | 1 | 0.004 | ∞ | UC |
| Uncertainty from spectral stray of light source | 0.001 | B | Rectangular | 1 | 0.001 | ∞ | UC |
| Uncertainty from detector non-linearity | 0.010 | B | Rectangular | 1 | 0.010 | ∞ | UC |
| Uncertainty from ambient stray light | 0.100 | B | Rectangular | 1 | 0.100 | ∞ | UC |

| | | | | | | | |
|---|---|---|---|---|---|---|---|
| Combined standard uncertainty (%) | **--** | **--** | **Normal** | **--** | **0.57** | **∞** | **--** |

**Table 7-14. Uncertainty budget of spectral responsivity at 1000 nm for the transfer detector with the serial number F4.**

| **Uncertainty Component** | **Standard uncertainty (%)** | **Type** | **Probability distribution** | **Sensitivity coefficient** | **Contribu tion (%)** | **Deg. of freedo m** | **Correl ated?** |
|---|---|---|---|---|---|---|---|
| Reading repeatability | 0.044 | A | Normal | 1 | 0.044 | 12 | C |
| Calibration uncertainty of ammeter | 0.200 | A | Normal | 1 | 0.200 | ∞ | C |
| Calibration uncertainty of reference detector | 0.515 | A | Normal | 1 | 0.515 | ∞ | C |
| Uncertainty from wavelength error of light source | 0.020 | B | Rectangular | 1 | 0.020 | ∞ | UC |
| Uncertainty from spectral bandwidth of light source | 0.030 | B | Rectangular | 1 | 0.030 | ∞ | UC |
| Uncertainty related to beam alignment | 0.020 | B | Rectangular | 1 | 0.020 | ∞ | UC |
| Uncertainty related to beam size and divergence | 0.010 | B | Rectangular | 1 | 0.010 | ∞ | UC |
| Uncertainty from power instability of light source | 0.010 | B | Rectangular | 1 | 0.010 | ∞ | UC |
| Uncertainty related to polarization of light source | 0.004 | B | Rectangular | 1 | 0.004 | ∞ | UC |
| Uncertainty from spectral stray of light source | 0.001 | B | Rectangular | 1 | 0.001 | ∞ | UC |
| Uncertainty from detector non-linearity | 0.010 | B | Rectangular | 1 | 0.010 | ∞ | UC |
| Uncertainty from ambient stray light | 0.040 | B | Rectangular | 1 | 0.040 | ∞ | UC |
| Combined standard uncertainty (%) | **--** | **--** | **Normal** | **--** | **0.56** | **∞** | **--** |

**Table 7-15. Uncertainty budget of spectral responsivity at 1000 nm for the transfer detector with the serial number F5.**

| **Uncertainty Component** | **Standard uncertainty (%)** | **Type** | **Probability distribution** | **Sensitivity coefficient** | **Contribu tion (%)** | **Deg. of freedo m** | **Correl ated?** |
|---|---|---|---|---|---|---|---|
| Reading repeatability | 0.043 | A | Normal | 1 | 0.043 | 12 | C |
| Calibration uncertainty of ammeter | 0.200 | A | Normal | 1 | 0.200 | ∞ | C |

| | | | | | | | |
|---|---|---|---|---|---|---|---|
| Calibration uncertainty of reference detector | 0.515 | A | Normal | 1 | 0.515 | ∞ | C |
| Uncertainty from wavelength error of light source | 0.020 | B | Rectangular | 1 | 0.020 | ∞ | UC |
| Uncertainty from spectral bandwidth of light source | 0.030 | B | Rectangular | 1 | 0.030 | ∞ | UC |
| Uncertainty related to beam alignment | 0.020 | B | Rectangular | 1 | 0.020 | ∞ | UC |
| Uncertainty related to beam size and divergence | 0.010 | B | Rectangular | 1 | 0.010 | ∞ | UC |
| Uncertainty from power instability of light source | 0.010 | B | Rectangular | 1 | 0.010 | ∞ | UC |
| Uncertainty related to polarization of light source | 0.004 | B | Rectangular | 1 | 0.004 | ∞ | UC |
| Uncertainty from spectral stray of light source | 0.001 | B | Rectangular | 1 | 0.001 | ∞ | UC |
| Uncertainty from detector non-linearity | 0.010 | B | Rectangular | 1 | 0.010 | ∞ | UC |
| Uncertainty from ambient stray light | 0.040 | B | Rectangular | 1 | 0.040 | ∞ | UC |
| Combined standard uncertainty (%) | **--** | **--** | **Normal** | **--** | **0.56** | **∞** | **--** |

# 8. NIST

## *8.1. Measurement Setup and Instruments*

The CCPR K2.b intercomparison measurements were performed on the NIST Visible/NIR Spectral Comparator Facility, VisSCF. The VisSCF is a monochromator-based facility in which the detector-substitution method is used for all calibrations.

The main instrument in the VisSCF is a Cary 14 double monochromator[3], which consists of a prism predisperser and grating. A 100 W quartz tungsten halogen (QTH) lamp is used as the broad-band source for the monochromator. The lamp is focused onto the entrance slit of the monochromator using a flat turning mirror and a fixed spherical mirror. The schematic of the setup is shown in Figure 8-1 and the photo shown in Figure 8-2. The flat turning mirror, M1, is used so that different sources of radiation can be selected without changing the source optical axis which would be introduced by turning the spherical mirror, M2. The focusing optics at the exit of the monochromator create a one-to-one image of the intermediate stop, A2, at the detector. A spectrally flat, metal-reflective beamsplitter is placed near the end of the optical path which allows for the use of the two-beam method where one of the beams is measured by the detector being tested and the second beam is directed towards the monitor detector. The ratio of the two detectors' signals, which are measured simultaneously, compensates for possible source instabilities.

[3] Certain commercial equipment, instruments, or materials are identified in this paper to foster understanding. Such identification does not imply recommendation or endorsement by the National Institute of Standards and Technology, nor does it imply that the material or equipment are necessarily the best available for the purpose.

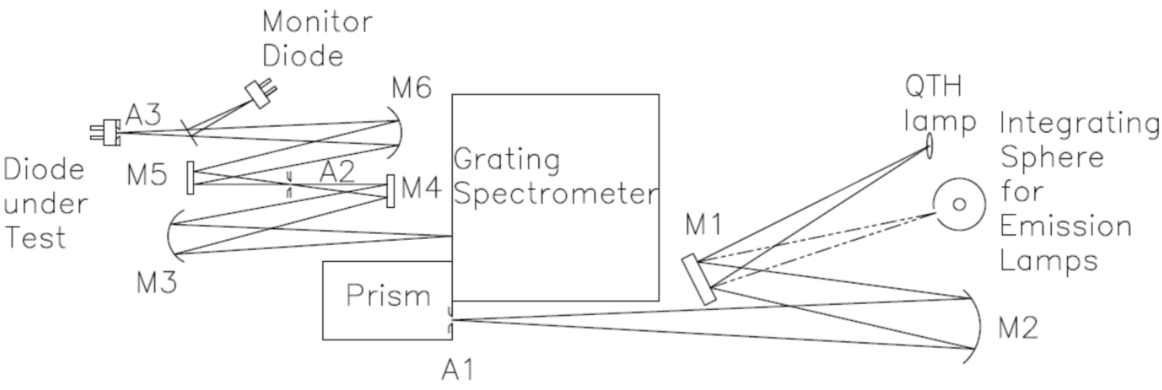


**Figure 8-1. VisSCF at NIST: Schematic diagram of the optical layout.**

The size of the optical beam incident on the detector can be changed by adjusting the width of the entrance slits on the monochromator, A1, and the vertical height adjustment on the intermediate aperture, A2. These adjustments allow changes to the beam sizes which were critical for the trap detector measurements. The rear of the monochromator, its exit slit, and the imaging optics are contained within a light tight box with an internal dust cover which is closed during all measurements. The radiation imaged at the detector plane was a 2 mm by 2 mm square optical beam converging with an F/9 geometry. The light tight box prevents contamination by ambient stray light. A measurement cycle consists of a full signal and a dark signal to correct for scattered radiation in the beam.

The complete measurement setup, measurement equation, and all relevant details are found in our calibration document, the SP250-41a located at https://www.nist.gov/calibrations/sp-250-publications.

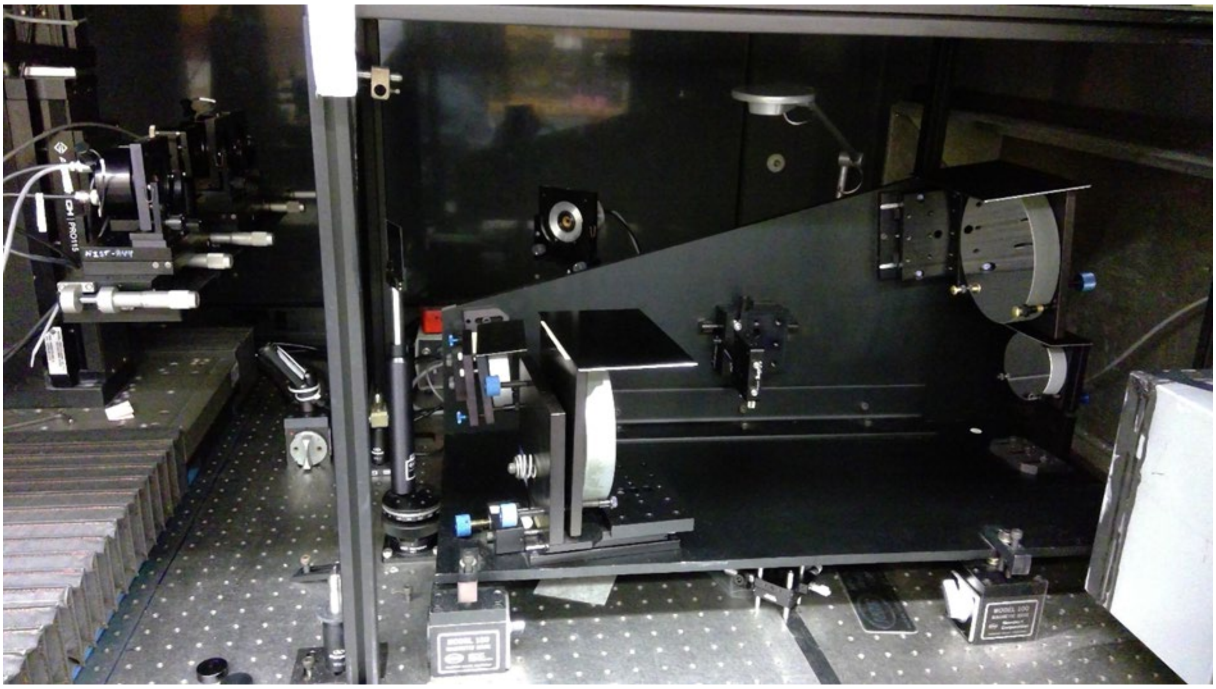

**Figure 8-2. VisSCF at NIST: The interior of the light tight box with the imaging optics and the automated translation stages is shown above.**

## *8.2. Measurement Conditions and Parameters*

The calibration of the intercomparison artefacts were carried out in a restricted-access lab. The lab is maintained at a temperature of 23 °C, +/- 1 °C. If the room temperature went outside those bounds, then the calibrations were suspended until the room temperature met the intercomparison conditions. The humidity was monitored but not controlled.

Initially the room temperatures and the resistances of the detector Platinum resistance thermometers were measured at the beginning and the end of each measurement run. The runs lasted less than 10 minutes, and the temperatures of the detectors and environment were stable over the short term. Since the measurements were of such a short duration and the temperatures did not change, a decision was made to only use the initial temperatures in the reporting of the average temperatures. The fluctuations of the temperatures on a day-to-day basis or in between measurements runs resulted in a larger temperature spread of +/- 0.3 ° C during the measurements of single element diodes and +/- 0.75° C during the measurements of the trap detectors.

The intercomparison artefacts were measured with two different alignment methods. The initial alignments with the artefacts were performed using the supplied target. The artefacts were then mounted and also aligned using the normal, automated center-finding method that we use to align devices for calibration. Comparisons of the obtained spectral responsivities show no differences between the alignments.

For the NIST, or the automated alignment method, the intercomparison detectors were mounted on an automated X-Y stage and set in gimbal mounts. The detector was first manually aligned in the focal plane, and then further aligned to find the X- and Y-center positions. Micrometer controls on the gimbal mounts were used to align the detector to be orthogonal to the incident radiation by examining the retro-reflected beam at a 1 m distance such that the reflected laser beam overlaps with the incident laser beam. Initial alignments with the artefacts used the supplied target. Once the detectors were manually aligned, an automated program was used to find the position of the center by locating the average between the 80% signal points. The single element detectors were placed to have their active areas at the focal plane of the monochromator output.

The traps were aligned with the target in the focal plane and then translated forward along the optical axis by 2.5 cm to position the focus on the trap's third detector. Checks of the alignment for any possible vignetting were performed before fully aligning the trap detectors. Once we determined that the incident beam was not internally clipped in the trap detectors, then the traps were also autoaligned.

Additional tests were made as per the intercomparison protocols. Since the single-element detectors arrived from the pilot lab with visible contaminants on their active areas, a decision was made to measure spatial uniformities of the single element detectors at 300 nm, 400 nm, 500 nm, and 1000 nm. The two traps' uniformities were measured at 300 nm, 350 nm, 400 nm, 500 nm, 600 nm, 800 nm, 900 nm, 950 nm and 1000 nm. The single element devices showed about a 0.5% graduated nonuniformity across the active area at 300 nm but were more uniform at longer wavelengths. The spatial uniformities of the power responsivities for most diodes at other wavelengths were about 0.3% or smaller. Artefact A1 showed the greatest nonuniformities of up to 0.7% at 300 nm. The traps were uniform to better then 0.2% across the active area. Dust causing significant anomalies was seen on the edges of detectors A1, A2, and A5.

The polarization of the monochromator system was tested using a ½ waveplate polarizer and found to be in agreement with previously measured dependencies[4] with increasing polarization of the output beam in the near-infrared wavelength region. Since all the measurements were performed with the face of the detectors perpendicular to the incident optical beam, any polarization sensitivities are minimized. All detector measurements were performed at optical output power which were below several µW, with decreasing power towards the shorter wavelengths due to the decreasing output of the 100 W QTH lamp.

[4] Marian E. Hills, Allen L. Olsen, and Lawrence W. Nichols, "Polarization in Cary Model 14 Spectrophotometers and Its Effect on Transmittance Measurements of Anisotropic Materials," Appl. Opt. 7, 1437-1441 (1968).

### 8.3. Traceability of Measurement

The spectral power responsivity scales for the NIST VisSCF are derived from the NIST cryogenic radiometer, POWR[5]. Trap detectors were calibrated by POWR from 365 nm to 1000 in 5 nm steps while nitride-Si detectors were used to transfer the ASR scale from POWR to the VisSCF from 300 nm to 360 nm. In the POWR facility, laser sources were used for the calibrations from 300 nm to 480 nm and a laser-line tunable filter source was used for wavelengths from 485 nm to 1000 nm. The laser-line tunable filter consists of a supercontinuum source with a volume holographic grating which results in quasi-monochromatic, about 1 nm bandwidth collimated output. The scale was in-turn transferred from the transfer detectors onto the VisSCF working standards, which are Hamamatsu S2281s.

### 8.4. Measurement Uncertainty

The NIST uncertainty budgets for this intercomparison shown below are similar to the uncertainty tables that are included with regular NIST calibration reports. The attached requested format for the uncertainties is described below.

Reading Repeatability: Each measurement consisted of 10 ratio voltage measurements. The statistics for those measurements are listed.

Calibration uncertainty of ammeter of working standard: NIST uses current-to-voltage transimpedance amplifiers for measurements of photocurrents from our working and calibration standards. The preamplifiers have been calibrated using the NIST current-to-voltage conversion calibration facility[6].

Calibration uncertainty of the reference detector: These uncertainties are generated from the absolute detector calibrations in the NIST POWR or cryogenic radiometer facility.

Wavelength Error of light source: The monochromator and lamp were calibrated prior to the intercomparison measurements using He/Ne laser, Hg-, Kr-, Ar-, and Ne-elemental line sources using the configuration shown in Fig. 1. These measurements were analysed for the centroid wavelengths and spectral bandwidths.

Uncertainty from spectral stray of light source: Cary 14 double monochromator has been measured for spectral stray light using laser sources[7]. Since the reference standards and devices-under test have the same spectral responsivity shapes, any effects due to the stray light from the double monochromator are expected to be negligible.

Uncertainty from spectral bandwidth of light source: The spectral bandwidth dependence was calculated from the differences of the bandwidth-convolved spectral responsivities compared to the cryogenic radiometer calibrations using lasers and the laser line tunable filter.

Uncertainty from beam alignment: Each device was mounted and aligned at least 3 times to determine the reproducibility of the measurements. NIST uses an automated alignment procedure using dual axis motorized stages. The average of the readings has been submitted for the intercomparison. The percent standard deviation for the reproducibility has been listed in the uncertainty budget.

Uncertainty from beam size and divergence: The effects of these uncertainties are minimized for the single-element detectors since the NIST calibration standard detectors have the same detector area dimensions as the comparison artefacts. For the trap detector calibrations, the focus position of the trap detector was translated along the optical axis by 2.5 cm to ensure that the beam was not internally clipped.

---

[5] J. M. Houston and J. P. Rice, "NIST reference cryogenic radiometer designed for versatile performance," Metrologia 43, S31-S35 (2006).

[6] Thomas Larason and C. Cameron Miller, "Gain calibration of current-to-voltage converters," *J. Res. NIST* 123, 123019 (2018).

[7] R. D. Saunders and J. B. Shumaker, "Apparatus function of a prism-grating double monochromator," *Applied Optics*, vol. 25, no. 20, pp. 3710–3714, 1986.

Uncertainty from power instability of the light source: The VisSCF uses a two-beam method for measurements. A final beamsplitter in the optical path directs the beams to both a test detector and a monitor detector where the signal measurements are performed simultaneously. The ratio of the test/monitor signals to the standard/monitor signals compensates for and reduces any source instability.

Uncertainty from polarization: The output of the monochromator is circularly to elliptically polarized. Detectors are all measured with their surfaces perpendicular to the incident radiation, and thus measurements of spectral power responsivities are expected to be insensitive to the polarization state of the incident radiation. For the intercomparison the polarization sensitivity was tested using a ½ wave plate beamsplitter mounted in the 0 degree and 90 degree position. The ratio of these two positions show that these measurements are not sensitive to the polarization state of the radiation.

Uncertainty from ambient stray light: The SCF measurements are performed in a light-tight box. The net signal ratios are measured by using an automated shutter to subtract the dark signals and any ambient signals inside the light-tight enclosure.

Uncertainty from detector non-linearity: The detector non-linearity was not tested since the output signal from the VisSCF is in the range of μW or lower and in the range where Si diodes are linear[8]. The detectors were only exposed to these output power levels.

Uncertainty from ammeter calibration used with comparison detectors: NIST uses current-to-voltage transimpedance amplifiers for measurements of photocurrents from the comparison artifacts. The preamplifiers have been calibrated using the NIST current-to-voltage conversion calibration facility[9].

**Table 8-1. Uncertainty budget of spectral responsivity at 300 nm for the trap detector.**

| Uncertainty Component | Standard uncertainty (%) | Type | Probability distribution | Sensitivity coefficient | Contribution (%) | Deg. of freedom | Correlated? |
|---|---|---|---|---|---|---|---|
| Reading repeatability | 0.037 | A | t | 1 | 0.037 | 9 | X |
| Calibration uncertainty of ammeter | 0.0035 | B | normal | 1 | 0.004 | ∞ | O |
| Calibration uncertainty of reference detector | 0.101 | B | normal | 1 | 0.101 | ∞ | O |
| Uncertainty from wavelength error of light source | 0.004 | B | rectangular | 1 | 0.004 | ∞ | X |
| Uncertainty from spectral stray of light source | --- | B | rectangular | 0 | --- | ∞ | O |
| Uncertainty from spectral bandwidth of light source | 0.018 | B | rectangular | 1 | 0.018 | ∞ | X |
| Uncertainty related to beam alignment | 0.176 | B | rectangular | 1 | 0.176 | ∞ | X |
| Uncertainty related to beam size and divergence | --- | B | rectangular | 0 | --- | ∞ | X |
| Uncertainty from power instability of light source | --- | B | rectangular | 0 | --- | ∞ | X |

[8] A. Thompson, H. M. Chen, "Beamcon III: a linearity measurement instrument for optical detectors," J. Res. Natl. Inst. Stand. Technol. 99, 751–755 (1994).

[9] Thomas Larason and C. Cameron Miller, "Gain calibration of current-to-voltage converters," *J. Res. NIST* 123, 123019 (2018).

| | | | | | | | |
|---|---|---|---|---|---|---|---|
| Uncertainty related to polarization of light source | --- | B | rectangular | 0 | --- | ∞ | O |
| Uncertainty from ambient stray light | --- | B | rectangular | 0 | --- | ∞ | O |
| Uncertainty from detector non-linearity | --- | B | rectangular | 0 | --- | ∞ | O |
| amplifier calibration | 0.005 | B | normal | 1 | 0.005 | ∞ | O |
| **Combined standard uncertainty (%)** | -- | -- | **normal** | -- | 0.208 | ∞ | -- |

**Table 8-2. Uncertainty budget of spectral responsivity at 500 nm for the trap detector.**

| Uncertainty Component | Standard uncertainty (%) | Type | Probability distribution | Sensitivity coefficient | Contribution (%) | Deg. of freedom | Correlated? |
|---|---|---|---|---|---|---|---|
| Reading repeatability | 0.001 | A | t | 1 | 0.001 | 9 | X |
| Calibration uncertainty of ammeter | 0.0035 | B | normal | 1 | 0.004 | ∞ | O |
| Calibration uncertainty of reference detector | 0.037 | B | normal | 1 | 0.037 | ∞ | O |
| Uncertainty from wavelength error of light source | 0.000 | B | rectangular | 1 | 0.000 | ∞ | X |
| Uncertainty from spectral stray of light source | --- | B | rectangular | 0 | --- | ∞ | O |
| Uncertainty from spectral bandwidth of light source | 0.000 | B | rectangular | 1 | 0.000 | ∞ | X |
| Uncertainty related to beam alignment | 0.034 | B | rectangular | 1 | 0.034 | ∞ | X |
| Uncertainty related to beam size and divergence | --- | B | rectangular | 0 | --- | ∞ | X |
| Uncertainty from power instability of light source | --- | B | rectangular | 0 | --- | ∞ | X |
| Uncertainty related to polarization of light source | --- | B | rectangular | 0 | --- | ∞ | O |
| Uncertainty from ambient stray light | --- | B | rectangular | 0 | --- | ∞ | O |
| Uncertainty from detector non-linearity | --- | B | rectangular | 0 | --- | ∞ | O |
| amplifier calibration | 0.005 | B | normal | 1 | 0.005 | ∞ | O |
| **Combined standard uncertainty (%)** | -- | -- | **normal** | -- | 0.051 | ∞ | -- |

**Table 8-3. Uncertainty budget of spectral responsivity at 1000 nm for the trap detector.**

| Uncertainty Component | Standard uncertainty (%) | Type | Probability distribution | Sensitivity coefficient | Contribution (%) | Deg. of freedom | Correlated? |
|---|---|---|---|---|---|---|---|
| Reading repeatability | 0.001 | A | t | 1 | 0.001 | 9 | X |
| Calibration uncertainty of ammeter | 0.0035 | B | normal | 1 | 0.004 | ∞ | O |
| Calibration uncertainty of reference detector | 0.167 | B | normal | 1 | 0.167 | ∞ | O |
| Uncertainty from wavelength error of light source | 0.009 | B | rectangular | 1 | 0.009 | ∞ | X |
| Uncertainty from spectral stray of light source | --- | B | rectangular | 0 | --- | ∞ | O |
| Uncertainty from spectral bandwidth of light source | 0.012 | B | rectangular | 1 | 0.012 | ∞ | X |
| Uncertainty related to beam alignment | 0.062 | B | rectangular | 1 | 0.062 | ∞ | X |
| Uncertainty related to beam size and divergence | --- | B | rectangular | 0 | --- | ∞ | X |
| Uncertainty from power instability of light source | --- | B | rectangular | 0 | --- | ∞ | X |
| Uncertainty related to polarization of light source | --- | B | rectangular | 0 | --- | ∞ | O |
| Uncertainty from ambient stray light | --- | B | rectangular | 0 | --- | ∞ | O |
| Uncertainty from detector non-linearity | --- | B | rectangular | 0 | --- | ∞ | O |
| amplifier calibration | 0.005 | B | normal | 1 | 0.005 | ∞ | O |
| **Combined standard uncertainty (%)** | -- | -- | **normal** | -- | 0.179 | ∞ | -- |

**Table 8-4. Uncertainty budget of spectral responsivity at 300 nm for the single-element detector.**

| Uncertainty Component | Standard uncertainty (%) | Type | Probability distribution | Sensitivity coefficient | Contribution (%) | Deg. of freedom | Correlated? |
|---|---|---|---|---|---|---|---|
| Reading repeatability | 0.037 | A | t | 1 | 0.037 | 9 | X |
| Calibration uncertainty of ammeter | 0.0035 | B | normal | 1 | 0.004 | ∞ | O |
| Calibration uncertainty of reference detector | 0.101 | B | normal | 1 | 0.101 | ∞ | O |
| Uncertainty from wavelength error of light source | 0.004 | B | rectangular | 1 | 0.004 | ∞ | X |

| | | | | | | | |
|---|---|---|---|---|---|---|---|
| Uncertainty from spectral stray of light source | --- | B | rectangular | 0 | --- | ∞ | O |
| Uncertainty from spectral bandwidth of light source | 0.018 | B | rectangular | 1 | 0.018 | ∞ | X |
| Uncertainty related to beam alignment | 0.031 | B | rectangular | 1 | 0.031 | ∞ | X |
| Uncertainty related to beam size and divergence | --- | B | rectangular | 0 | --- | ∞ | X |
| Uncertainty from power instability of light source | --- | B | rectangular | 0 | --- | ∞ | X |
| Uncertainty related to polarization of light source | --- | B | rectangular | 0 | --- | ∞ | O |
| Uncertainty from ambient stray light | --- | B | rectangular | 0 | --- | ∞ | O |
| Uncertainty from detector non-linearity | --- | B | rectangular | 0 | --- | ∞ | O |
| amplifier calibration | 0.005 | B | normal | 1 | 0.005 | ∞ | O |
| **Combined standard uncertainty (%)** | **--** | **--** | **normal** | **--** | 0.114 | ∞ | **--** |

**Table 8-5. Uncertainty budget of spectral responsivity at 500 nm for the single-element detector.**

| Uncertainty Component | Standard uncertainty (%) | Type | Probability distribution | Sensitivity coefficient | Contribution (%) | Deg. of freedom | Correlated? |
|---|---|---|---|---|---|---|---|
| Reading repeatability | 0.001427606 | A | t | 1 | 0.001 | 9 | X |
| Calibration uncertainty of ammeter | 0.004 | B | normal | 1 | 0.004 | ∞ | O |
| Calibration uncertainty of reference detector | 0.037 | B | normal | 1 | 0.037 | ∞ | O |
| Uncertainty from wavelength error of light source | 0.000 | B | rectangular | 1 | 0.000 | ∞ | X |
| Uncertainty from spectral stray of light source | --- | B | rectangular | 0 | --- | ∞ | O |
| Uncertainty from spectral bandwidth of light source | 0.000 | B | rectangular | 1 | 0.000 | ∞ | X |
| Uncertainty related to beam alignment | 0.010 | B | rectangular | 1 | 0.010 | ∞ | X |
| Uncertainty related to beam size and divergence | --- | B | rectangular | 0 | --- | ∞ | X |
| Uncertainty from power instability of light source | --- | B | rectangular | 0 | --- | ∞ | X |
| Uncertainty related to polarization of light source | --- | B | rectangular | 0 | --- | ∞ | O |
| Uncertainty from ambient stray light | --- | B | rectangular | 0 | --- | ∞ | O |

| | | | | | | | |
|---|---|---|---|---|---|---|---|
| Uncertainty from detector non-linearity | --- | B | rectangular | 0 | --- | ∞ | O |
| amplifier calibration | 0.005 | B | normal | 1 | 0.005 | ∞ | O |
| **Combined standard uncertainty (%)** | **--** | **--** | **normal** | **--** | 0.038 | ∞ | **--** |

**Table 8-6. Uncertainty budget of spectral responsivity at 1000 nm for the single-element detector.**

| **Uncertainty Component** | **Standard uncertainty (%)** | **Type** | **Probability distribution** | **Sensitivity coefficient** | **Contribution (%)** | **Deg. of freedom** | **Correlated?** |
|---|---|---|---|---|---|---|---|
| Reading repeatability | 0.001 | A | t | 1 | 0.001 | 9 | X |
| Calibration uncertainty of ammeter | 0.0035 | B | normal | 1 | 0.004 | ∞ | O |
| Calibration uncertainty of reference detector | 0.167 | B | normal | 1 | 0.167 | ∞ | O |
| Uncertainty from wavelength error of light source | 0.009 | B | rectangular | 1 | 0.009 | ∞ | X |
| Uncertainty from spectral stray of light source | --- | B | rectangular | 0 | --- | ∞ | O |
| Uncertainty from spectral bandwidth of light source | 0.012 | B | rectangular | 1 | 0.012 | ∞ | X |
| Uncertainty related to beam alignment | 0.041 | B | rectangular | 1 | 0.041 | ∞ | X |
| Uncertainty related to beam size and divergence | --- | B | rectangular | 0 | --- | ∞ | X |
| Uncertainty from power instability of light source | --- | B | rectangular | 0 | --- | ∞ | X |
| Uncertainty related to polarization of light source | --- | B | rectangular | 0 | --- | ∞ | O |
| Uncertainty from ambient stray light | --- | B | rectangular | 0 | --- | ∞ | O |
| Uncertainty from detector non-linearity | --- | B | rectangular | 0 | --- | ∞ | O |
| amplifier calibration | 0.005 | B | normal | 1 | 0.005 | ∞ | O |
| **Combined standard uncertainty (%)** | **--** | **--** | **normal** | **--** | 0.172 | ∞ | **--** |

# 9. VNIIOFI

## 9.1. Measurement Setup and Instruments

VNIIOFI standard trap-detector was calibrated in terms of spectral power responsivity against an absolute cryogenic radiometer (ACR) of the L-1 type using a monochromatic source based on double grating monochromator. The diagram of the setup is shown in Figure 9-1.

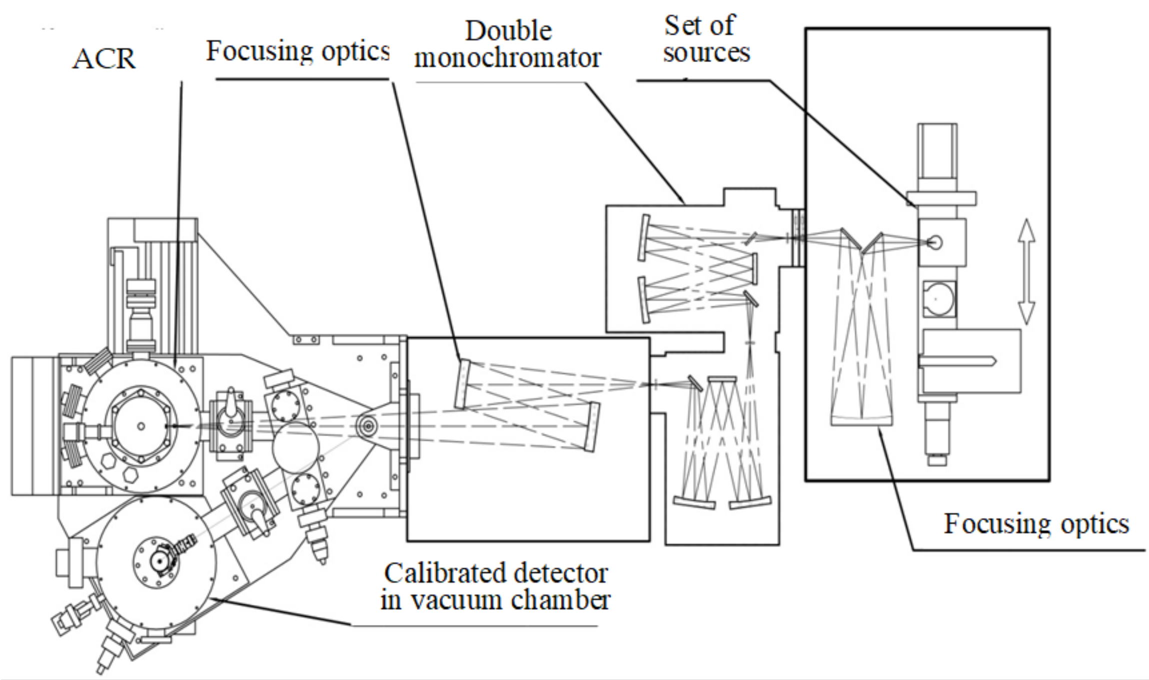


**Figure 9-1. Setup for calibrating standard trap-detector against absolute cryogenic radiometer (ACR) at VNIIOFI.**

The CCPR-K2b detectors spectral responsivity was measured by means of comparing with the VNIIOFI standard trap-detector using a spectral comparator shown in Figure 9-2.

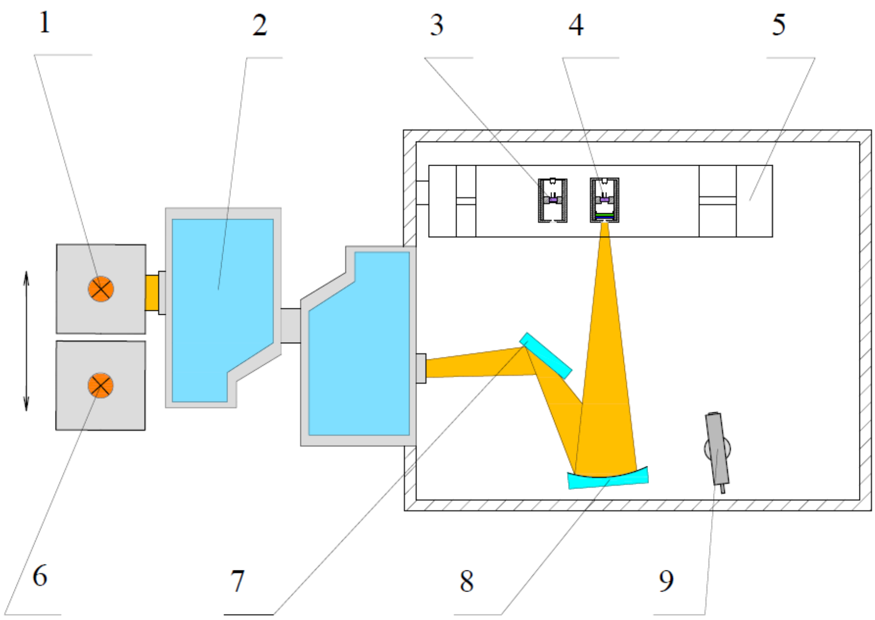


**Figure 9-2. Spectral power responsivity measurement facility at VNIIOFI. (1 – quartz halogen lamp, 2 – double grating monochromator, 3 – standard trap, 4 – calibrated detector, 5 – translation stage, 6 – spectral lamp, 7 – flat mirror, 8 - focusing mirror, 9 – alignment laser)**

### *9.2. Measurement Conditions and Parameters*

The minimal size of the beam spot was 1x1 mm. The single-photodiode detectors were placed in the plane of the minimum spot size. The trap-detectors were placed in such a way that the minimal spot was located in the plane of the third photodiode. The beam incident normally to the sensitive element of the photodiodes or to the front surface of the traps.

Spectral bandwidth of the monochromator was 1 nm in the range 300 nm to 600 nm and 2 nm in the range 650 nm to 1000 nm.

Temperature in the room was controlled by means of air conditioning. The temperature of defectors was monitored using the built-in PT100 temperature sensor. The temperature of the comparison detectors was maintained at the level of (23 ± 0.5) °C.

### *9.3. Traceability of Measurement*

Spectral power responsivity measurement at VNIIOFI is traceable to ACR working with a tuneable monochromatic source based on a double grating monochromator. The calibrated trap-detector is placed in the single vacuum volume with ACR, and the same window is used for both detectors.

### *9.4. Measurement Uncertainty*

**Table 9-1. Uncertainty budget of spectral responsivity at 300 nm for the trap detector.**

| Uncertainty Component | Standard uncertainty (%) | Type | Probability distribution | Sensitivity coefficient | Contribution (%) | Deg. of freedom | Correlated? |
|---|---|---|---|---|---|---|---|
| Measurement repeatability (with independent alignment) | 0.13 | A | t | 1 | 0.13 | 5 | No |
| Calibration uncertainty of ammeter | 0.02 | B | normal | 1 | 0.02 | ∞ | Yes |
| Calibration uncertainty of reference detector | 0.35 | B | normal | 1 | 0.35 | ∞ | Yes |
| Uncertainty from wavelength error of light source | 0.008 | B | rectangular | 1 | 0.008 | ∞ | Yes |
| Uncertainty from spectral stray of light source | 0.01 | B | rectangular | 1 | 0.01 | ∞ | Yes |
| Uncertainty from spectral bandwidth of light source | 0.001 | B | rectangular | 1 | 0.001 | ∞ | Yes |
| Uncertainty related to beam alignment, beam size and divergence | 0.03 | B | rectangular | 1 | 0.03 | ∞ | Yes |
| Uncertainty from power instability of light source | | | | | | | |
| Uncertainty related to polarization of light source | 0.01 | B | rectangular | 1 | 0.01 | ∞ | Yes |
| Uncertainty from ambient stray light | 0.05 | B | rectangular | 1 | 0.05 | ∞ | Yes |
| Uncertainty from detector non-linearity | 0.005 | B | rectangular | 1 | 0.005 | ∞ | Yes |
| **Combined standard uncertainty (%)** | **--** | **--** | **normal** | **--** | **0.38** | ∞ | **--** |

**Table 9-2. Uncertainty budget of spectral responsivity at 500 nm for the trap detector.**

| Uncertainty Component | Standard uncertainty (%) | Type | Probability distribution | Sensitivity coefficient | Contribution (%) | Deg. of freedom | Correlated? |
|---|---|---|---|---|---|---|---|
| Measurement repeatability (with independent alignment) | 0.02 | A | t | 1 | 0.02 | 5 | No |
| Calibration uncertainty of ammeter | 0.02 | B | normal | 1 | 0.02 | ∞ | Yes |
| Calibration uncertainty of reference detector | 0.15 | B | normal | 1 | 0.15 | ∞ | Yes |
| Uncertainty from wavelength error of light source | 0.004 | B | rectangular | 1 | 0.004 | ∞ | Yes |
| Uncertainty from spectral stray of light source | 0.005 | B | rectangular | 1 | 0.005 | ∞ | Yes |

| | | | | | | | |
|---|---|---|---|---|---|---|---|
| Uncertainty from spectral bandwidth of light source | 0.001 | B | rectangular | 1 | 0.001 | ∞ | Yes |
| Uncertainty related to beam alignment, beam size and divergence | 0.03 | B | rectangular | 1 | 0.03 | ∞ | Yes |
| Uncertainty from power instability of light source | | | | | | | |
| Uncertainty related to polarization of light source | 0.01 | B | rectangular | 1 | 0.01 | ∞ | Yes |
| Uncertainty from ambient stray light | 0.01 | B | rectangular | 1 | 0.01 | ∞ | Yes |
| Uncertainty from detector non-linearity | 0.003 | B | rectangular | 1 | 0.003 | ∞ | Yes |
| **Combined standard uncertainty (%)** | **--** | **--** | **normal** | **--** | **0.16** | ∞ | **--** |

**Table 9-3. Uncertainty budget of spectral responsivity at 1000 nm for the trap detector.**

| Uncertainty Component | Standard uncertainty (%) | Type | Probability distribution | Sensitivity coefficient | Contrib ution (%) | Deg. of freedo m | Correl ated? |
|---|---|---|---|---|---|---|---|
| Measurement repeatability (with independent alignment) | 0.03 | A | t | 1 | 0.03 | 5 | No |
| Calibration uncertainty of ammeter | 0.02 | B | normal | 1 | 0.02 | ∞ | Yes |
| Calibration uncertainty of reference detector | 0.25 | B | normal | 1 | 0.25 | ∞ | Yes |
| Uncertainty from wavelength error of light source | 0.015 | B | rectangular | 1 | 0.015 | ∞ | Yes |
| Uncertainty from spectral stray of light source | 0.002 | B | rectangular | 1 | 0.002 | ∞ | Yes |
| Uncertainty from spectral bandwidth of light source | 0.003 | B | rectangular | 1 | 0.003 | ∞ | Yes |
| Uncertainty related to beam alignment, beam size and divergence | 0.03 | B | rectangular | 1 | 0.03 | ∞ | Yes |
| Uncertainty from power instability of light source | | | | | | | |
| Uncertainty related to polarization of light source | 0.01 | B | rectangular | 1 | 0.01 | ∞ | Yes |
| Uncertainty from ambient stray light | 0.01 | B | rectangular | 1 | 0.01 | ∞ | Yes |
| Uncertainty from detector non-linearity | 0.005 | B | rectangular | 1 | 0.005 | ∞ | Yes |
| **Combined standard uncertainty (%)** | **--** | **--** | **normal** | **--** | **0.26** | ∞ | **--** |

**Table 9-4. Uncertainty budget of spectral responsivity at 300 nm for the single-element detector.**

| Uncertainty Component | Standard uncertainty (%) | Type | Probability distribution | Sensitivity coefficient | Contribution (%) | Deg. of freedom | Correlated? |
|---|---|---|---|---|---|---|---|
| Measurement repeatability (with independent alignment) | 0.15 | A | t | 1 | 0.15 | 7 | No |
| Calibration uncertainty of ammeter | 0.02 | B | normal | 1 | 0.02 | ∞ | Yes |
| Calibration uncertainty of reference detector | 0.35 | B | normal | 1 | 0.35 | ∞ | Yes |
| Uncertainty from wavelength error of light source | 0.07 | B | rectangular | 1 | 0.07 | ∞ | Yes |
| Uncertainty from spectral stray of light source | 0.01 | B | rectangular | 1 | 0.01 | ∞ | Yes |
| Uncertainty from spectral bandwidth of light source | 0.005 | B | rectangular | 1 | 0.005 | ∞ | Yes |
| Uncertainty related to beam alignment, beam size and divergence | 0.015 | B | rectangular | 1 | 0.015 | ∞ | Yes |
| Uncertainty from power instability of light source | | | | | | | |
| Uncertainty related to polarization of light source | 0.015 | B | rectangular | 1 | 0.015 | ∞ | Yes |
| Uncertainty from ambient stray light | 0.05 | B | rectangular | 1 | 0.05 | ∞ | Yes |
| Uncertainty from detector non-linearity | 0.005 | B | rectangular | 1 | 0.005 | ∞ | Yes |
| **Combined standard uncertainty (%)** | **--** | **--** | **normal** | **--** | **0.38** | ∞ | **--** |

**Table 9-5. Uncertainty budget of spectral responsivity at 500 nm for the single-element detector.**

| Uncertainty Component | Standard uncertainty (%) | Type | Probability distribution | Sensitivity coefficient | Contribution (%) | Deg. of freedom | Correlated? |
|---|---|---|---|---|---|---|---|
| Measurement repeatability (with independent alignment) | 0.02 | A | t | 1 | 0.02 | 7 | No |
| Calibration uncertainty of ammeter | 0.02 | B | normal | 1 | 0.02 | ∞ | Yes |
| Calibration uncertainty of reference detector | 0.15 | B | normal | 1 | 0.15 | ∞ | Yes |
| Uncertainty from wavelength error of light source | 0.001 | B | rectangular | 1 | 0.01 | ∞ | Yes |
| Uncertainty from spectral stray of light source | 0.005 | B | rectangular | 1 | 0.005 | ∞ | Yes |

| | | | | | | | |
|---|---|---|---|---|---|---|---|
| Uncertainty from spectral bandwidth of light source | 0.003 | B | rectangular | 1 | 0.003 | ∞ | Yes |
| Uncertainty related to beam alignment, beam size and divergence | 0.015 | B | rectangular | 1 | 0.015 | ∞ | Yes |
| Uncertainty from power instability of light source | | | | | | | |
| Uncertainty related to polarization of light source | 0.015 | B | rectangular | 1 | 0.015 | ∞ | Yes |
| Uncertainty from ambient stray light | 0.01 | B | rectangular | 1 | 0.01 | ∞ | Yes |
| Uncertainty from detector non-linearity | 0.003 | B | rectangular | 1 | 0.003 | ∞ | Yes |
| **Combined standard uncertainty (%)** | **--** | **--** | **normal** | **--** | **0.16** | ∞ | **--** |

**Table 9-6. Uncertainty budget of spectral responsivity at 1000 nm for the single-element detector.**

| **Uncertainty Component** | **Standard uncertainty (%)** | **Type** | **Probability distribution** | **Sensitivity coefficient** | **Contribution (%)** | **Deg. of freedom** | **Correlated?** |
|---|---|---|---|---|---|---|---|
| Measurement repeatability (with independent alignment) | 0.04 | A | t | 1 | 0.04 | 7 | No |
| Calibration uncertainty of ammeter | 0.02 | B | normal | 1 | 0.02 | ∞ | Yes |
| Calibration uncertainty of reference detector | 0.25 | B | normal | 1 | 0.25 | ∞ | Yes |
| Uncertainty from wavelength error of light source | 0.002 | B | rectangular | 1 | 0.002 | ∞ | Yes |
| Uncertainty from spectral stray of light source | 0.002 | B | rectangular | 1 | 0.002 | ∞ | Yes |
| Uncertainty from spectral bandwidth of light source | 0.005 | B | rectangular | 1 | 0.005 | ∞ | Yes |
| Uncertainty related to beam alignment, beam size and divergence | 0.015 | B | rectangular | 1 | 0.015 | ∞ | Yes |
| Uncertainty from power instability of light source | | | | | | | |
| Uncertainty related to polarization of light source | 0.015 | B | rectangular | 1 | 0.015 | ∞ | Yes |
| Uncertainty from ambient stray light | 0.01 | B | rectangular | 1 | 0.01 | ∞ | Yes |
| Uncertainty from detector non-linearity | 0.005 | B | rectangular | 1 | 0.005 | ∞ | Yes |
| **Combined standard uncertainty (%)** | **--** | **--** | **normal** | **--** | **0.26** | ∞ | **--** |

# 10. PTB

## *10.1. Measurement Setup and Instruments*

The transfer standards were calibrated against the reference detectors at a facility based on a double monochromator, consisting of two 0.25 m Czerny-Turner type instruments operated in additive-dispersion mode. The monochromators were equipped with grating turrets that allowed four gratings of different groove density to be used. A circular aperture stop was installed in the vicinity of the exit slit of the second monochromator in order to define the beam size in the direction perpendicular to the dispersion plane. In front of the first monochromator entrance slit, a shutter and a filter wheel containing bulk filters for order sorting were installed. A xenon arc lamp and a tungsten halogen lamp were used as radiation sources in the wavelength ranges below 400 nm and from 400 nm to 1000 nm, respectively. The bulb of the tungsten halogen lamp had been subjected to sand-blast treatment to assure a uniform radiance distribution. The radiation of this lamp was collected by a spherical mirror such that an image of the radiating area, demagnified by a factor of 2, was formed in the plane of the first monochromator entrance slit. The radiation of the xenon arc lamp was collected by a lens such that a magnified image of the radiating area was formed in the plane of the first monochromator entrance slit. The entrance slit was overfilled in horizontal direction by the images of both lamps. The spectrally dispersed radiation emerging from the exit slit was refocused by another spherical mirror. The measurement position of the detectors in the direction of the optical axis was in the plane in which the beam cross section was almost circular with a diameter of (3.1 ± 0.2) mm and had an almost rectangular intensity profile. The radiation thereby had a full cone angle of 2.4 degrees. A beam splitter after the spherical mirror directed a small part of the spectrally dispersed radiation into a silicon trap detector serving as a monitor detector.

The investigated detectors and the reference detector standards were mounted inside a light-tight enclosure (called detector box, see Figure 10-1) containing a horizontal motorized translation stage on which the detectors were mounted on individual motorized translation stages for vertical positioning. Each detector mount allowed for skew and tilt alignment of the detectors. For the measurements, the detectors were aligned for normal incidence of the spectrally dispersed radiation by passing a pilot laser beam along the optical axis through the double monochromator assembly and adjusting the detector orientation such that the laser beam was reflected back into itself. Prior to each measurement run, i.e. after changing detectors or detector orientation, the center position of each detector was determined by scanning the detector through the beam of the spectrally dispersed radiation for a fixed monochromator setting in order to determine the detector positions for which the measured signal was reduced to half the maximum signal. Each time several iterations were used scanning alternately in the vertical or the horizontal direction, and the arithmetic mean of the two positions of half-maximum signal was used as the respective center position.

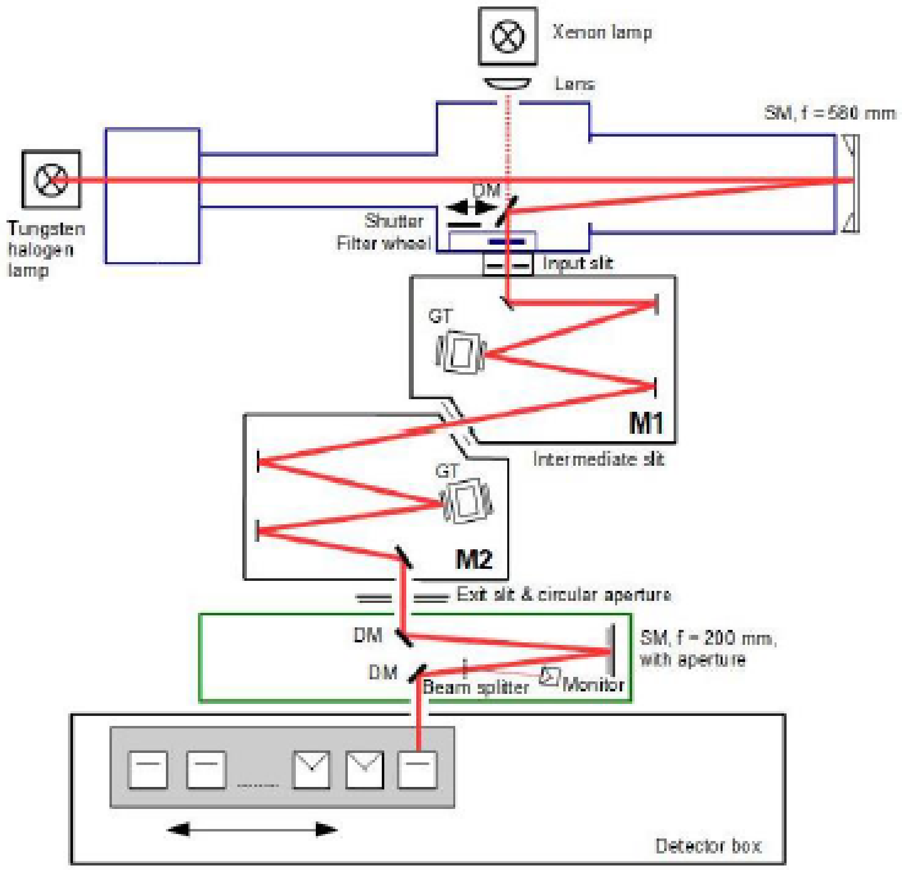


**Figure 10-1. Scheme of the calibration facility at PTB. (DM – deflecting mirror, SM – spherical mirror, GT – grating turret, M1 and M2 – first and second monochromator of the additive double monochromator system)**

The measurements to determine the spectral responsivity were performed such that the double monochromator was set to the desired wavelength $\lambda$ and the reference detectors and the detectors under test were moved in turn to their respective center positions to measure their output signal. The output signal is the output voltage, measured by a digital voltmeter, of a current-to-voltage converter. The input of the current-to-voltage converter is connected to the terminals of the detectors via a multiplexer switching system. The dark signals of all detectors were measured before the measurement of the first wavelength and after the measurement of the last wavelength of each wavelength range that could be covered by the same grating and order-sorting filter. The signal of the monitor detector was recorded simultaneously to the recording of the signal of each detector under test and reference detector. The signal of each detectors under test and reference detectors was divided by the corresponding signal of the monitor detector, giving the so-called signal-to-monitor ratio $R$, to correct for fluctuations of the radiation sources.

In order to eliminate the effect of beam polarization on the detector response, each measurement run was conducted as two series of repeated measurements. From one series of each measurement run to the next, the detector standards under test and the reference detector standards were rotated by 90° about the optical axis of the incident beam and subsequently realigned for normal incidence of the radiation. The ratio of the signal-to-monitor ratios of the detectors under test and of the reference detectors was determined for each series of measurement, and the results were averaged as geometric mean and then multiplied by the known responsivity of the reference detectors and corrections to derive the responsivity of the detector under test to unpolarized radiation.

## 10.2. Measurement Conditions and Parameters

The positioning and tilt alignment of the detectors is described in Section 10.1.

The ambient temperature in the detector box was about 25 °C. Each reference detector was equipped with a Pt100 temperature sensor. The resistance of the Pt100 temperature sensors of reference and transfer detectors was recorded during the duration of the measurements using a demultiplexer and a resistance meter performing 4-wire measurements. The detector housings were wrapped round with flexible tube containing water which is pumped by a thermostat. Two thermostats were used to control and set temperature of the reference detectors to 25 °C and that of the transfer detectors to 23 °C.

The humidity was measured with a calibrated datalogger.

## 10.3. Traceability of Measurement

The transfer detectors were calibrated against two sets of reference detectors, each consisting of two silicon trap detectors. The first set, called set A, was used at wavelengths smaller than 400 nm and was calibrated against a monochromator-based cryogenic radiometer calibration facility (see Meindl, P., Klinkmüller, A. E., Werner, L., Johannsen, U., & Grützmacher, K. New UV spectral responsivity scale of the PTB based on a cryogenic radiometer and an argon plasma arc radiation source. Metrologia, 43 (2006) S72–S77). The second set, called set B, was used in the wavelength range from 400 nm to 1000 nm and was calibrated against a laser-based cryogenic radiometer calibration facility. The principle of this calibration is described in Werner, L., Fischer, J., Johannsen, U., & Hartmann, J. Accurate determination of the spectral responsivity of silicon trap detectors between 238 nm and 1015 nm using a laser-based cryogenic radiometer. Metrologia, 37 (2000) 279-284. One reference detector of the second set was used only in the wavelength range from 400 nm to 700 nm. Thus, only one reference detector was used from 750 nm to 1000 nm.

## 10.4. Measurement Uncertainty

The spectral responsivity $s$DUT($\lambda$) of the detector under test (DUT), i.e. transfer detector, at wavelength $\lambda$ is determined according to the following equation:

$$s_{\mathrm{DUT}}\left(\lambda\right)=R\left(I_{\mathrm{DUT}},I_{\mathrm{Ref}}\right)\cdot s_{\mathrm{Ref}}\left(\lambda\right)\cdot C \qquad (10\text{-}1)$$

with

- $s_{\mathrm{DUT}}\left(\lambda\right)$: known spectral responsivity of the reference detector at wavelength $\lambda$,,
- $C$ : product of correction factors described below,
- $R\left(I_{\mathrm{DUT}},I_{\mathrm{Ref}}\right)$: ratio of the photocurrent of the DUT $I_{\mathrm{DUT}}$ and the photocurrent of the reference detector $I_{\mathrm{Ref}}$ for unpolarised radiation.

The photocurrent ratio $R(I_{\mathrm{DUT}}, I_{\mathrm{Ref}})$ is determined as the geometric mean of two ratios $R^{\leftrightarrow\leftrightarrow}$ and $R^{\updownarrow\updownarrow}$ whereas the orientation of the detectors during the measurement of both ratios differs by 90° with respect to the rotation around the axis of the incoming radiation:

$$R\left(I_{\mathrm{DUT}},I_{\mathrm{Ref}}\right)=\sqrt{R^{\leftrightarrow\leftrightarrow}\left(I_{\mathrm{DUT}},I_{\mathrm{Ref}}\right)\cdot R^{\updownarrow\updownarrow}\left(I_{\mathrm{DUT}},I_{\mathrm{Ref}}\right)} \qquad (10\text{-}2)$$

The photocurrent ratio $R^{\pi}(I_{\mathrm{DUT}}, I_{\mathrm{Ref}})$ for one orientation $\pi \in \{\leftrightarrow\leftrightarrow, \updownarrow\updownarrow\}$ is corrected for an instable incident radiant power by using the ratio of detector signal to monitor signal and furthermore for a non-zero dark signal:

$$R^{\pi}\left(I_{\text{DUT}}, I_{\text{Ref}}\right) = \frac{1}{N}\sum_{i=1}^{N}\left[\frac{\dfrac{\left(U_{\text{DUT,irr}} - U_{\text{DUT,dark}}\right)/R_{\text{f}}}{\left(U_{\text{Mon(DUT),irr}} - U_{\text{Mon(DUT),dark}}\right)/R_{\text{f,Mon}}}}{\dfrac{\left(U_{\text{Ref,irr}} - U_{\text{Ref,dark}}\right)/R_{\text{f}}}{\left(U_{\text{Mon(Ref),irr}} - U_{\text{Mon(Ref),dark}}\right)/R_{\text{f,Mon}}}}\right]_{\pi,i} = \frac{1}{N}\sum_{i=1}^{N}\left[\frac{\dfrac{\left(U_{\text{DUT,irr}} - U_{\text{DUT,dark}}\right)}{\left(U_{\text{Mon(DUT),irr}} - U_{\text{Mon(DUT),dark}}\right)}}{\dfrac{\left(U_{\text{Ref,irr}} - U_{\text{Ref,dark}}\right)}{\left(U_{\text{Mon(Ref),irr}} - U_{\text{Mon(Ref),dark}}\right)}}\right]_{\pi,i} \quad (10\text{-}3)$$

with

- $U_{\text{X,y}}$ : the voltage at the output of the current-to-voltage converter with feedback resistance $R_{\text{f}}$ measuring the photocurrent of the DUT or the reference detector (X = DUT or X = Ref, respectively) when irradiated or not irradiated (y = irr or y = dark, respectively),
- $U_{\text{Mon(X),y}}$ : the voltage at the output of the current-to-voltage converter with feedback resistance $R_{\text{f,Mon}}$ measuring the photocurrent of the monitor detector simultaneously to the measurement of $U_{X,y}$,
- $R_{\text{f}}$ : the resistance of the feedback resistor of the current-to-voltage converter connected to the photocurrent terminal of the DUT or the reference detector,
- $R_{\text{f,Mon}}$ : the resistance of the feedback resistor of the current-to-voltage converter connected to the photocurrent terminal of the monitor detector,
- $N$ : number of measurements of $R_{\pi}(I_{\text{DUT}}, I_{\text{Ref}})$.

Since the photocurrent of DUT and reference detector are measured with the same current-to-voltage converter and the same $R_{\text{f}}$ and because the photocurrent of the monitor detector is measured with unchanged $R_{\text{f,Mon}}$, the fraction in equation (10-3) can be reduced so that $R_{\text{f}}$ and $R_{\text{f,Mon}}$ do not occur.

The quantity $C$ in equation (10-1) is the product of correction factors:

$$C = \prod_{z} C_z \quad (10\text{-}4)$$

The sources of uncertainty including the correction factors $C_z$ for the determination of the spectral responsivity of a DUT against one reference detector according to equations (10-1) to (10-4) are listed in the following tables. The sensitivity coefficient $c_i$ for quantity $X_i$ is $c_i = \partial s_{\text{DUT}}(\lambda)/\partial Xi$ evaluated at the estimates $x_i$ ($Xi = xi$, $i = 1 \ldots N$). $u_{\text{rel},i}(s_{\text{DUT}})$ is the contribution to the relative combined standard uncertainty $u(s_{\text{DUT}})/|s_{\text{DUT}}|$ resulting from the standard uncertainty $u(x_i)$ associated with the input estimate $x_i$, and is calculated according to $u_{\text{rel},i}(s_{\text{DUT}}) = |c_i|u(x_i)/|s_{\text{DUT}}|$. We also added the column "Correlated?". "Yes" in this column means that the component is systematic and artefact-independent. The statement "No" means that the component is random and/or artefact-dependent.

Two reference detectors were used in the wavelength range from 300 nm to 700 nm. Thus, two results $s_{\text{DUT,Ref1}}(\lambda)$ and $s_{\text{DUT,Ref2}}(\lambda)$ were obtained by the calibrations according to equation (10-1) against the reference detectors Ref1 and Ref2, respectively. Both results are highly correlated. The final result $s_{\text{DUT,Ref2\&Ref2}}(\lambda)$ and its relative standard uncertainty are calculated according to

$$s_{\text{DUT,Ref1\&Ref2}}\left(\lambda\right) = \left(s_{\text{DUT,Ref1}}\left(\lambda\right) + s_{\text{DUT,Ref2}}\left(\lambda\right)\right)/2 \quad (10\text{-}5)$$

$$u_{\text{rel}}\left(s_{\text{DUT,Ref1\&Ref2}}\left(\lambda\right)\right) = \sqrt{\left(\frac{u_{\text{rel}}\left(s_{\text{DUT,Ref1}}\left(\lambda\right)\right) + u_{\text{rel}}\left(s_{\text{DUT,Ref2}}\left(\lambda\right)\right)}{2}\right)^2 + u_{\text{rel}}^2\left(C_{\text{diff}}\right)} \quad (10\text{-}6)$$

with $C_{\text{diff}}$ : the correction for the difference between the calibration results obtained with the two reference detectors.

The tables in the following sections state the uncertainty budgets of the spectral responsivity at the wavelengths 300 nm, 500 nm, and 1000 nm for the single-element detector D#1 and the trap detector D#4.

A separate document with the title "Comments of PTB on the uniformity of the spectral responsivity of the transfer detectors" describes the considerable non-uniformity of the spectral responsivity of the transfer detectors (see "PTB_comments_on_uniformity_of_CCPR-K2.b_transfer_detectors.pdf"). Because the associated uncertainty contribution to the uncertainty of the spectral responsivity depends on the difference in beam size and beam profile between the participants (and the pilot), it hasn't been estimated by PTB and hasn't been included in the uncertainty budgets of PTB. One option is to include this uncertainty (for some or all transfer detectors) in the uncertainty budget of the transfer uncertainty.

### 10.4.1. Uncertainty of single element detector D#1 at wavelength 300 nm

The uncertainty budgets of the spectral responsivity of detector D#1 at the wavelength $\lambda$ = 300 nm determined against the reference detectors Ref1 and Ref2 of set A are shown in Table 10-1 and Table 10-2, respectively. The uncertainty of the final result $u_{\mathrm{rel}}(s_{\mathrm{D\#1,Ref1\&Ref2}}(\lambda))$ = 0.12% was calculated according to equation (10-6) with $u_{\mathrm{rel}}(C_{\mathrm{diff}})$ = 0.0028%.

**Table 10-1. Uncertainty budget of spectral responsivity at 300 nm for the single-element detector D#1 calibrated against reference detector Ref1 of set A. Relative standard uncertainties are stated.**

| Source of uncertainty | Quantity $X_i$ | Relative standard uncertainty $u(x_i)/x_i$ | Type | Probability distribution | Sensitivity coefficient $c_i$ | Contribution to the relative standard uncertainty $u_{\mathrm{rel},i}(s_{\mathrm{DUT}})$ | Deg. of freedom | Correlated? |
|---|---|---|---|---|---|---|---|---|
| Spectral responsivity of reference detector | $s_{\mathrm{Ref}}(\lambda)$ | 0.0963% | B | normal | $s_{\mathrm{DUT}}(\lambda)/s_{\mathrm{Ref}}(\lambda)$ | 0.0963% | 400 | Yes |
| Correction for drift of spectral responsivity of reference detector | $C_{\mathrm{drift}}$ | 0.0026% | B | normal | $s_{\mathrm{DUT}}(\lambda)/C_{\mathrm{drift}}$ | 0.0026% | ∞ | Yes |
| Photocurrent ratio | $R(I_{\mathrm{DUT}}, I_{\mathrm{Ref}})$ | 0.0012% | A | normal | $s_{\mathrm{DUT}}(\lambda)/R(I_{\mathrm{DUT}}, I_{\mathrm{Ref}})$ | 0.0012% | 30 | No |
| Correction for polarisation dependence of reference detector | $C_{\mathrm{pol,ref}}$ | 0.0010% | B | rectangular | $s_{\mathrm{DUT}}(\lambda)/C_{\mathrm{pol,ref}}$ | 0.0010% | ∞ | Yes |
| Correction for polarisation dependence of photocurrent ratio $R$ | $C_{\mathrm{pol,ratio}}$ | 0.0003% | A | normal | $s_{\mathrm{DUT}}(\lambda)/C_{\mathrm{pol,ratio}}$ | 0.0003% | 1 | No |
| Correction for non-uniformity | $C_{\mathrm{non-unif}}$ | 0.0113% | B | rectangular | $s_{\mathrm{DUT}}(\lambda)/C_{\mathrm{non-unif}}$ | 0.0113% | ∞ | No |
| Correction for temperature of reference detector | $C_{\mathrm{temp}}$ | 0.0007% | B | rectangular | $s_{\mathrm{DUT}}(\lambda)/C_{\mathrm{temp}}$ | 0.0007% | ∞ | Yes |
| Correction for wavelength | $C_{\mathrm{wl}}$ | 0.0682% | B | rectangular | $s_{\mathrm{DUT}}(\lambda)/C_{\mathrm{wl}}$ | 0.0682% | ∞ | Yes |
| Correction for bandwidth effect | $C_{\mathrm{band}}$ | 0.0026% | B | rectangular | $s_{\mathrm{DUT}}(\lambda)/C_{\mathrm{band}}$ | 0.0026% | ∞ | Yes |
| Correction for stray radiation | $C_{\mathrm{stray}}$ | 0.0072% | B | rectangular | $s_{\mathrm{DUT}}(\lambda)/C_{\mathrm{stray}}$ | 0.0072% | 8 | Yes |
| Correction for nonlinearity of detectors | $C_{\mathrm{NL}}$ | 0.0020% | B | rectangular | $s_{\mathrm{DUT}}(\lambda)/C_{\mathrm{NL}}$ | 0.0020% | ∞ | Yes |
| Correction spectral impurity | $C_{\mathrm{imp}}$ | 0.0014% | B | rectangular | $s_{\mathrm{DUT}}(\lambda)/C_{\mathrm{imp}}$ | 0.0014% | ∞ | Yes |
| Correction for angle of incidence | $C_{\mathrm{inc}}$ | 0.0014% | B | rectangular | $s_{\mathrm{DUT}}(\lambda)/C_{\mathrm{inc}}$ | 0.0014% | ∞ | Yes |
| Correction for divergence of radiation beam | $C_{\mathrm{div}}$ | 0.0014% | B | rectangular | $s_{\mathrm{DUT}}(\lambda)/C_{\mathrm{div}}$ | 0.0014% | ∞ | Yes |
| Correction for power instability of radiation source | $C_{\mathrm{inst}}$ | 0.0018% | B | rectangular | $s_{\mathrm{DUT}}(\lambda)/C_{\mathrm{inst}}$ | 0.0018% | ∞ | Yes |
| Correction for voltage measurement (calibration of voltmeters) | $C_{\mathrm{el}}$ | 0.0018% | B | rectangular | $s_{\mathrm{DUT}}(\lambda)/C_{\mathrm{el}}$ | 0.0018% | ∞ | Yes |
| Correction for nonlinearity of current-to-voltage converters | $C_{\mathrm{CVC}}$ | 0.0051% | B | rectangular | $s_{\mathrm{DUT}}(\lambda)/C_{\mathrm{CVC}}$ | 0.0051% | ∞ | Yes |
| | | | | | | | | |
| Spectral responsivity of DUT | $s_{\mathrm{DUT}}(\lambda)$ | | | normal | | 0.12% | 930 | |

**Table 10-2. Uncertainty budget of spectral responsivity at 300 nm for the single-element detector D#1 calibrated against reference detector Ref2 of set A. Relative standard uncertainties are stated.**

| Source of uncertainty | Quantity $X_i$ | Relative standard uncertainty $u(x_i)/x_i$ | Type | Probability distribution | Sensitivity coefficient $c_i$ | Contribution to the relative standard uncertainty $u_{\mathrm{rel},i}(s_{\mathrm{DUT}})$ | Deg. of freedom | Correlated? |
|---|---|---|---|---|---|---|---|---|
| Spectral responsivity of reference detector | $s_{\mathrm{Ref}}(\lambda)$ | 0.0902% | B | normal | $s_{\mathrm{DUT}}(\lambda)/s_{\mathrm{Ref}}(\lambda)$ | 0.0902% | 300 | Yes |
| Correction for drift of spectral responsivity of reference detector | $C_{\mathrm{drift}}$ | 0.0026% | B | normal | $s_{\mathrm{DUT}}(\lambda)/C_{\mathrm{drift}}$ | 0.0026% | ∞ | Yes |
| Photocurrent ratio | $R(I_{\mathrm{DUT}}, I_{\mathrm{Ref}})$ | 0.0013% | A | normal | $s_{\mathrm{DUT}}(\lambda)/R(I_{\mathrm{DUT}}, I_{\mathrm{Ref}})$ | 0.0013% | 30 | No |
| Correction for polarisation dependence of reference detector | $C_{\mathrm{pol,ref}}$ | 0.0032% | B | rectangular | $s_{\mathrm{DUT}}(\lambda)/C_{\mathrm{pol,ref}}$ | 0.0032% | ∞ | Yes |
| Correction for polarisation dependence of photocurrent ratio $R$ | $C_{\mathrm{pol,ratio}}$ | 0.0184% | A | normal | $s_{\mathrm{DUT}}(\lambda)/C_{\mathrm{pol,ratio}}$ | 0.0184% | 1 | No |
| Correction for non-uniformity | $C_{\mathrm{non-unif}}$ | 0.0113% | B | rectangular | $s_{\mathrm{DUT}}(\lambda)/C_{\mathrm{non-unif}}$ | 0.0113% | ∞ | No |
| Correction for temperature of reference detector | $C_{\mathrm{temp}}$ | 0.0007% | B | rectangular | $s_{\mathrm{DUT}}(\lambda)/C_{\mathrm{temp}}$ | 0.0007% | ∞ | Yes |
| Correction for wavelength | $C_{\mathrm{wl}}$ | 0.0681% | B | rectangular | $s_{\mathrm{DUT}}(\lambda)/C_{\mathrm{wl}}$ | 0.0681% | ∞ | Yes |
| Correction for bandwidth effect | $C_{\mathrm{band}}$ | 0.0027% | B | rectangular | $s_{\mathrm{DUT}}(\lambda)/C_{\mathrm{band}}$ | 0.0027% | ∞ | Yes |
| Correction for stray radiation | $C_{\mathrm{stray}}$ | 0.0072% | B | rectangular | $s_{\mathrm{DUT}}(\lambda)/C_{\mathrm{stray}}$ | 0.0072% | 8 | Yes |
| Correction for nonlinearity of detectors | $C_{\mathrm{NL}}$ | 0.0020% | B | rectangular | $s_{\mathrm{DUT}}(\lambda)/C_{\mathrm{NL}}$ | 0.0020% | ∞ | Yes |
| Correction spectral impurity | $C_{\mathrm{imp}}$ | 0.0014% | B | rectangular | $s_{\mathrm{DUT}}(\lambda)/C_{\mathrm{imp}}$ | 0.0014% | ∞ | Yes |
| Correction for angle of incidence | $C_{\mathrm{inc}}$ | 0.0014% | B | rectangular | $s_{\mathrm{DUT}}(\lambda)/C_{\mathrm{inc}}$ | 0.0014% | ∞ | Yes |
| Correction for divergence of radiation beam | $C_{\mathrm{div}}$ | 0.0014% | B | rectangular | $s_{\mathrm{DUT}}(\lambda)/C_{\mathrm{div}}$ | 0.0014% | ∞ | Yes |
| Correction for power instability of radiation source | $C_{\mathrm{inst}}$ | 0.0018% | B | rectangular | $s_{\mathrm{DUT}}(\lambda)/C_{\mathrm{inst}}$ | 0.0018% | ∞ | Yes |
| Correction for voltage measurement (calibration of voltmeters) | $C_{\mathrm{el}}$ | 0.0018% | B | rectangular | $s_{\mathrm{DUT}}(\lambda)/C_{\mathrm{el}}$ | 0.0018% | ∞ | Yes |
| Correction for nonlinearity of current-to-voltage converters | $C_{\mathrm{CVC}}$ | 0.0051% | B | rectangular | $s_{\mathrm{DUT}}(\lambda)/C_{\mathrm{CVC}}$ | 0.0051% | ∞ | Yes |
| | | | | | | | | |
| Spectral responsivity of DUT | $s_{\mathrm{DUT}}(\lambda)$ | | | normal | | 0.12% | 530 | |

## 10.4.2. Uncertainty of single element detector D#1 at wavelength 500 nm

The uncertainty budgets of the spectral responsivity of detector D#1 at the wavelength $\lambda$ = 500 nm determined against the reference detectors Ref1 and Ref2 of set B are shown in Table 10-3 and Table 10-4, respectively. The uncertainty of the final result $u_{\mathrm{rel}}(s_{\mathrm{D\#1,Ref1\&Ref2}}(\lambda))$ = 0.024% was calculated according to equation (10-6) with $u_{\mathrm{rel}}(C_{\mathrm{diff}})$ = 0.0031%.

**Table 10-3. Uncertainty budget of spectral responsivity at 500 nm for the single-element detector D#1 calibrated against reference detector Ref1 of set B. Relative standard uncertainties are stated.**

| Source of uncertainty | Quantity $X_i$ | Relative standard uncertainty $u(x_i)/x_i$ | Type | Probability distribution | Sensitivity coefficient $c_i$ | Contribution to the relative standard uncertainty $u_{\mathrm{rel},i}(s_{\mathrm{DUT}})$ | Deg. of freedom | Correlated? |
|---|---|---|---|---|---|---|---|---|
| Spectral responsivity of reference detector | $s_{\mathrm{Ref}}(\lambda)$ | 0.0178% | B | normal | $s_{\mathrm{DUT}}(\lambda)/s_{\mathrm{Ref}}(\lambda)$ | 0.0178% | 60 | Yes |
| Correction for drift of spectral responsivity of reference detector | $C_{\mathrm{drift}}$ | 0.0009% | B | normal | $s_{\mathrm{DUT}}(\lambda)/C_{\mathrm{drift}}$ | 0.0009% | ∞ | Yes |
| Photocurrent ratio | $R(I_{\mathrm{DUT}}, I_{\mathrm{Ref}})$ | 0.0009% | A | normal | $s_{\mathrm{DUT}}(\lambda)/R(I_{\mathrm{DUT}}, I_{\mathrm{Ref}})$ | 0.0009% | 30 | No |
| Correction for polarisation dependence of reference detector | $C_{\mathrm{pol,ref}}$ | 0.0010% | B | rectangular | $s_{\mathrm{DUT}}(\lambda)/C_{\mathrm{pol,ref}}$ | 0.0010% | ∞ | Yes |
| Correction for polarisation dependence of photocurrent ratio $R$ | $C_{\mathrm{pol,ratio}}$ | 0.0025% | A | normal | $s_{\mathrm{DUT}}(\lambda)/C_{\mathrm{pol,ratio}}$ | 0.0025% | 1 | No |
| Correction for non-uniformity | $C_{\mathrm{non-unif}}$ | 0.0057% | B | rectangular | $s_{\mathrm{DUT}}(\lambda)/C_{\mathrm{non-unif}}$ | 0.0057% | ∞ | No |
| Correction for temperature of reference detector | $C_{\mathrm{temp}}$ | 0.0011% | B | rectangular | $s_{\mathrm{DUT}}(\lambda)/C_{\mathrm{temp}}$ | 0.0011% | ∞ | Yes |
| Correction for wavelength | $C_{\mathrm{wl}}$ | 0.0029% | B | rectangular | $s_{\mathrm{DUT}}(\lambda)/C_{\mathrm{wl}}$ | 0.0029% | ∞ | Yes |
| Correction for bandwidth effect | $C_{\mathrm{band}}$ | 0.0000% | B | rectangular | $s_{\mathrm{DUT}}(\lambda)/C_{\mathrm{band}}$ | 0.0000% | ∞ | Yes |
| Correction for stray radiation | $C_{\mathrm{stray}}$ | 0.0096% | B | rectangular | $s_{\mathrm{DUT}}(\lambda)/C_{\mathrm{stray}}$ | 0.0096% | 8 | Yes |
| Correction for nonlinearity of detectors | $C_{\mathrm{NL}}$ | 0.0020% | B | rectangular | $s_{\mathrm{DUT}}(\lambda)/C_{\mathrm{NL}}$ | 0.0020% | ∞ | Yes |
| Correction spectral impurity | $C_{\mathrm{imp}}$ | 0.0014% | B | rectangular | $s_{\mathrm{DUT}}(\lambda)/C_{\mathrm{imp}}$ | 0.0014% | ∞ | Yes |
| Correction for angle of incidence | $C_{\mathrm{inc}}$ | 0.0014% | B | rectangular | $s_{\mathrm{DUT}}(\lambda)/C_{\mathrm{inc}}$ | 0.0014% | ∞ | Yes |
| Correction for divergence of radiation beam | $C_{\mathrm{div}}$ | 0.0014% | B | rectangular | $s_{\mathrm{DUT}}(\lambda)/C_{\mathrm{div}}$ | 0.0014% | ∞ | Yes |
| Correction for power instability of radiation source | $C_{\mathrm{inst}}$ | 0.0018% | B | rectangular | $s_{\mathrm{DUT}}(\lambda)/C_{\mathrm{inst}}$ | 0.0018% | ∞ | Yes |
| Correction for voltage measurement (calibration of voltmeters) | $C_{\mathrm{el}}$ | 0.0018% | B | rectangular | $s_{\mathrm{DUT}}(\lambda)/C_{\mathrm{el}}$ | 0.0018% | ∞ | Yes |
| Correction for nonlinearity of current-to-voltage converters | $C_{\mathrm{CVC}}$ | 0.0051% | B | rectangular | $s_{\mathrm{DUT}}(\lambda)/C_{\mathrm{CVC}}$ | 0.0051% | ∞ | Yes |
| | | | | | | | | |
| Spectral responsivity of DUT | $s_{\mathrm{DUT}}(\lambda)$ | | | normal | | 0.022% | 91 | |

**Table 10-4. Uncertainty budget of spectral responsivity at 500 nm for the single-element detector D#1 calibrated against reference detector Ref2 of set B. Relative standard uncertainties are stated.**

| Source of uncertainty | Quantity $X_i$ | Relative standard uncertainty $u(x_i)/x_i$ | Type | Probability distribution | Sensitivity coefficient $c_i$ | Contribution to the relative standard uncertainty $u_{\mathrm{rel},i}(s_{\mathrm{DUT}})$ | Deg. of freedom | Correlated? |
|---|---|---|---|---|---|---|---|---|
| Spectral responsivity of reference detector | $s_{\mathrm{Ref}}(\lambda)$ | 0.0177% | B | normal | $s_{\mathrm{DUT}}(\lambda)/s_{\mathrm{Ref}}(\lambda)$ | 0.0177% | 55 | Yes |
| Correction for drift of spectral responsivity of reference detector | $C_{\mathrm{drift}}$ | 0.0009% | B | normal | $s_{\mathrm{DUT}}(\lambda)/C_{\mathrm{drift}}$ | 0.0009% | ∞ | Yes |
| Photocurrent ratio | $R(I_{\mathrm{DUT}}, I_{\mathrm{Ref}})$ | 0.0009% | A | normal | $s_{\mathrm{DUT}}(\lambda)/R(I_{\mathrm{DUT}}, I_{\mathrm{Ref}})$ | 0.0009% | 30 | No |
| Correction for polarisation dependence of reference detector | $C_{\mathrm{pol,ref}}$ | 0.0010% | B | rectangular | $s_{\mathrm{DUT}}(\lambda)/C_{\mathrm{pol,ref}}$ | 0.0010% | ∞ | Yes |
| Correction for polarisation dependence of photocurrent ratio $R$ | $C_{\mathrm{pol,ratio}}$ | 0.0042% | A | normal | $s_{\mathrm{DUT}}(\lambda)/C_{\mathrm{pol,ratio}}$ | 0.0042% | 1 | No |
| Correction for non-uniformity | $C_{\mathrm{non-unif}}$ | 0.0057% | B | rectangular | $s_{\mathrm{DUT}}(\lambda)/C_{\mathrm{non-unif}}$ | 0.0057% | ∞ | No |
| Correction for temperature of reference detector | $C_{\mathrm{temp}}$ | 0.0002% | B | rectangular | $s_{\mathrm{DUT}}(\lambda)/C_{\mathrm{temp}}$ | 0.0002% | ∞ | Yes |
| Correction for wavelength | $C_{\mathrm{wl}}$ | 0.0041% | B | rectangular | $s_{\mathrm{DUT}}(\lambda)/C_{\mathrm{wl}}$ | 0.0041% | ∞ | Yes |
| Correction for bandwidth effect | $C_{\mathrm{band}}$ | 0.0000% | B | rectangular | $s_{\mathrm{DUT}}(\lambda)/C_{\mathrm{band}}$ | 0.0000% | ∞ | Yes |
| Correction for stray radiation | $C_{\mathrm{stray}}$ | 0.0128% | B | rectangular | $s_{\mathrm{DUT}}(\lambda)/C_{\mathrm{stray}}$ | 0.0128% | 8 | Yes |
| Correction for nonlinearity of detectors | $C_{\mathrm{NL}}$ | 0.0020% | B | rectangular | $s_{\mathrm{DUT}}(\lambda)/C_{\mathrm{NL}}$ | 0.0020% | ∞ | Yes |
| Correction spectral impurity | $C_{\mathrm{imp}}$ | 0.0014% | B | rectangular | $s_{\mathrm{DUT}}(\lambda)/C_{\mathrm{imp}}$ | 0.0014% | ∞ | Yes |
| Correction for angle of incidence | $C_{\mathrm{inc}}$ | 0.0014% | B | rectangular | $s_{\mathrm{DUT}}(\lambda)/C_{\mathrm{inc}}$ | 0.0014% | ∞ | Yes |
| Correction for divergence of radiation beam | $C_{\mathrm{div}}$ | 0.0014% | B | rectangular | $s_{\mathrm{DUT}}(\lambda)/C_{\mathrm{div}}$ | 0.0014% | ∞ | Yes |
| Correction for power instability of radiation source | $C_{\mathrm{inst}}$ | 0.0018% | B | rectangular | $s_{\mathrm{DUT}}(\lambda)/C_{\mathrm{inst}}$ | 0.0018% | ∞ | Yes |
| Correction for voltage measurement (calibration of voltmeters) | $C_{\mathrm{el}}$ | 0.0018% | B | rectangular | $s_{\mathrm{DUT}}(\lambda)/C_{\mathrm{el}}$ | 0.0018% | ∞ | Yes |
| Correction for nonlinearity of current-to-voltage converters | $C_{\mathrm{CVC}}$ | 0.0051% | B | rectangular | $s_{\mathrm{DUT}}(\lambda)/C_{\mathrm{CVC}}$ | 0.0051% | ∞ | Yes |
| | | | | | | | | |
| Spectral responsivity of DUT | $s_{\mathrm{DUT}}(\lambda)$ | | | normal | | 0.024% | 64 | |

## 10.4.3. Uncertainty of single element detector D#1 at wavelength 1000 nm

The uncertainty budget of the spectral responsivity of detector D#1 at the wavelength $\lambda$ = 1000 nm determined against the reference detectors Ref1 of set B is shown in Table 10-5.

**Table 10-5. Uncertainty budget of spectral responsivity at 1000 nm for the single-element detector D#1 calibrated against reference detector Ref1 of set B. Relative standard uncertainties are stated.**

| Source of uncertainty | Quantity $X_i$ | Relative standard uncertainty $u(x_i)/x_i$ | Type | Probability distribution | Sensitivity coefficient $c_i$ | Contribution to the relative standard uncertainty $u_{\mathrm{rel},i}(s_{\mathrm{DUT}})$ | Deg. of freedom | Correlated? |
|---|---|---|---|---|---|---|---|---|
| Spectral responsivity of reference detector | $s_{\mathrm{Ref}}(\lambda)$ | 0.0424% | B | normal | $s_{\mathrm{DUT}}(\lambda)/s_{\mathrm{Ref}}(\lambda)$ | 0.0424% | 60 | Yes |
| Correction for drift of spectral responsivity of reference detector | $C_{\mathrm{drift}}$ | 0.0011% | B | normal | $s_{\mathrm{DUT}}(\lambda)/C_{\mathrm{drift}}$ | 0.0011% | ∞ | Yes |
| Photocurrent ratio | $R(I_{\mathrm{DUT}}, I_{\mathrm{Ref}})$ | 0.0006% | A | normal | $s_{\mathrm{DUT}}(\lambda)/R(I_{\mathrm{DUT}}, I_{\mathrm{Ref}})$ | 0.0006% | 30 | No |
| Correction for polarisation dependence of reference detector | $C_{\mathrm{pol,ref}}$ | 0.0022% | B | rectangular | $s_{\mathrm{DUT}}(\lambda)/C_{\mathrm{pol,ref}}$ | 0.0022% | ∞ | Yes |
| Correction for polarisation dependence of photocurrent ratio $R$ | $C_{\mathrm{pol,ratio}}$ | 0.0011% | A | normal | $s_{\mathrm{DUT}}(\lambda)/C_{\mathrm{pol,ratio}}$ | 0.0011% | 1 | No |
| Correction for non-uniformity | $C_{\mathrm{non-unif}}$ | 0.0071% | B | rectangular | $s_{\mathrm{DUT}}(\lambda)/C_{\mathrm{non-unif}}$ | 0.0071% | ∞ | No |
| Correction for temperature of reference detector | $C_{\mathrm{temp}}$ | 0.0365% | B | rectangular | $s_{\mathrm{DUT}}(\lambda)/C_{\mathrm{temp}}$ | 0.0365% | ∞ | Yes |
| Correction for wavelength | $C_{\mathrm{wl}}$ | 0.0379% | B | rectangular | $s_{\mathrm{DUT}}(\lambda)/C_{\mathrm{wl}}$ | 0.0379% | ∞ | Yes |
| Correction for bandwidth effect | $C_{\mathrm{band}}$ | 0.0069% | B | rectangular | $s_{\mathrm{DUT}}(\lambda)/C_{\mathrm{band}}$ | 0.0069% | ∞ | Yes |
| Correction for stray radiation | $C_{\mathrm{stray}}$ | 0.0116% | B | rectangular | $s_{\mathrm{DUT}}(\lambda)/C_{\mathrm{stray}}$ | 0.0116% | 8 | Yes |
| Correction for nonlinearity of detectors | $C_{\mathrm{NL}}$ | 0.0020% | B | rectangular | $s_{\mathrm{DUT}}(\lambda)/C_{\mathrm{NL}}$ | 0.0020% | ∞ | Yes |
| Correction spectral impurity | $C_{\mathrm{imp}}$ | 0.0014% | B | rectangular | $s_{\mathrm{DUT}}(\lambda)/C_{\mathrm{imp}}$ | 0.0014% | ∞ | Yes |
| Correction for angle of incidence | $C_{\mathrm{inc}}$ | 0.0014% | B | rectangular | $s_{\mathrm{DUT}}(\lambda)/C_{\mathrm{inc}}$ | 0.0014% | ∞ | Yes |
| Correction for divergence of radiation beam | $C_{\mathrm{div}}$ | 0.0014% | B | rectangular | $s_{\mathrm{DUT}}(\lambda)/C_{\mathrm{div}}$ | 0.0014% | ∞ | Yes |
| Correction for power instability of radiation source | $C_{\mathrm{inst}}$ | 0.0018% | B | rectangular | $s_{\mathrm{DUT}}(\lambda)/C_{\mathrm{inst}}$ | 0.0018% | ∞ | Yes |
| Correction for voltage measurement (calibration of voltmeters) | $C_{\mathrm{el}}$ | 0.0018% | B | rectangular | $s_{\mathrm{DUT}}(\lambda)/C_{\mathrm{el}}$ | 0.0018% | ∞ | Yes |
| Correction for nonlinearity of current-to-voltage converters | $C_{\mathrm{CVC}}$ | 0.0051% | B | rectangular | $s_{\mathrm{DUT}}(\lambda)/C_{\mathrm{CVC}}$ | 0.0051% | ∞ | Yes |
| | | | | | | | | |
| Spectral responsivity of DUT | $s_{\mathrm{DUT}}(\lambda)$ | | | normal | | 0.070% | 419 | |

## 10.4.4. Uncertainty of trap detector D#4 at wavelength 300 nm

The uncertainty budgets of the spectral responsivity of detector D#4 at the wavelength $\lambda$ = 300 nm determined against the reference detectors Ref1 and Ref2 of set A are shown in Table 10-6 and Table 10-7, respectively. The uncertainty of the final result $u_{\mathrm{rel}}(s_{\mathrm{D\#4,Ref1\&Ref2}}(\lambda))$ = 0.095% was calculated according to equation (10-6) with $u_{\mathrm{rel}}(C_{\mathrm{diff}})$ = 0.0027%.

**Table 10-6. Uncertainty budget of spectral responsivity at 300 nm for the trap detector D#4 calibrated against reference detector Ref1 of set A. Relative standard uncertainties are stated.**

| Source of uncertainty | Quantity $X_i$ | Relative standard uncertainty $u(x_i)/x_i$ | Type | Probability distribution | Sensitivity coefficient $c_i$ | Contribution to the relative standard uncertainty $u_{\mathrm{rel},i}(s_{\mathrm{DUT}})$ | Deg. of freedom | Correlated? |
|---|---|---|---|---|---|---|---|---|
| Spectral responsivity of reference detector | $s_{\mathrm{Ref}}(\lambda)$ | 0.0963% | B | normal | $s_{\mathrm{DUT}}(\lambda)/s_{\mathrm{Ref}}(\lambda)$ | 0.0963% | 400 | Yes |
| Correction for drift of spectral responsivity of reference detector | $C_{\mathrm{drift}}$ | 0.0026% | B | normal | $s_{\mathrm{DUT}}(\lambda)/C_{\mathrm{drift}}$ | 0.0026% | ∞ | Yes |
| Photocurrent ratio | $R(I_{\mathrm{DUT}}, I_{\mathrm{Ref}})$ | 0.0006% | A | normal | $s_{\mathrm{DUT}}(\lambda)/R(I_{\mathrm{DUT}}, I_{\mathrm{Ref}})$ | 0.0006% | 30 | No |
| Correction for polarisation dependence of reference detector | $C_{\mathrm{pol,ref}}$ | 0.0010% | B | rectangular | $s_{\mathrm{DUT}}(\lambda)/C_{\mathrm{pol,ref}}$ | 0.0010% | ∞ | Yes |
| Correction for polarisation dependence of photocurrent ratio $R$ | $C_{\mathrm{pol,ratio}}$ | 0.0102% | A | normal | $s_{\mathrm{DUT}}(\lambda)/C_{\mathrm{pol,ratio}}$ | 0.0102% | 1 | No |
| Correction for non-uniformity | $C_{\mathrm{non-unif}}$ | 0.0113% | B | rectangular | $s_{\mathrm{DUT}}(\lambda)/C_{\mathrm{non-unif}}$ | 0.0113% | ∞ | No |
| Correction for temperature of reference detector | $C_{\mathrm{temp}}$ | 0.0007% | B | rectangular | $s_{\mathrm{DUT}}(\lambda)/C_{\mathrm{temp}}$ | 0.0007% | ∞ | Yes |
| Correction for wavelength | $C_{\mathrm{wl}}$ | 0.0031% | B | rectangular | $s_{\mathrm{DUT}}(\lambda)/C_{\mathrm{wl}}$ | 0.0031% | ∞ | Yes |
| Correction for bandwidth effect | $C_{\mathrm{band}}$ | 0.0003% | B | rectangular | $s_{\mathrm{DUT}}(\lambda)/C_{\mathrm{band}}$ | 0.0003% | ∞ | Yes |
| Correction for stray radiation | $C_{\mathrm{stray}}$ | 0.0060% | B | rectangular | $s_{\mathrm{DUT}}(\lambda)/C_{\mathrm{stray}}$ | 0.0060% | 8 | Yes |
| Correction for nonlinearity of detectors | $C_{\mathrm{NL}}$ | 0.0020% | B | rectangular | $s_{\mathrm{DUT}}(\lambda)/C_{\mathrm{NL}}$ | 0.0020% | ∞ | Yes |
| Correction spectral impurity | $C_{\mathrm{imp}}$ | 0.0014% | B | rectangular | $s_{\mathrm{DUT}}(\lambda)/C_{\mathrm{imp}}$ | 0.0014% | ∞ | Yes |
| Correction for angle of incidence | $C_{\mathrm{inc}}$ | 0.0014% | B | rectangular | $s_{\mathrm{DUT}}(\lambda)/C_{\mathrm{inc}}$ | 0.0014% | ∞ | Yes |
| Correction for divergence of radiation beam | $C_{\mathrm{div}}$ | 0.0014% | B | rectangular | $s_{\mathrm{DUT}}(\lambda)/C_{\mathrm{div}}$ | 0.0014% | ∞ | Yes |
| Correction for power instability of radiation source | $C_{\mathrm{inst}}$ | 0.0018% | B | rectangular | $s_{\mathrm{DUT}}(\lambda)/C_{\mathrm{inst}}$ | 0.0018% | ∞ | Yes |
| Correction for voltage measurement (calibration of voltmeters) | $C_{\mathrm{el}}$ | 0.0018% | B | rectangular | $s_{\mathrm{DUT}}(\lambda)/C_{\mathrm{el}}$ | 0.0018% | ∞ | Yes |
| Correction for nonlinearity of current-to-voltage converters | $C_{\mathrm{CVC}}$ | 0.0051% | B | rectangular | $s_{\mathrm{DUT}}(\lambda)/C_{\mathrm{CVC}}$ | 0.0051% | ∞ | Yes |
| | | | | | | | | |
| Spectral responsivity of DUT | $s_{\mathrm{DUT}}(\lambda)$ | | | normal | | 0.098% | 408 | |

**Table 10-7. Uncertainty budget of spectral responsivity at 300 nm for the trap detector D#4 calibrated against reference detector Ref2 of set A. Relative standard uncertainties are stated.**

| Source of uncertainty | Quantity $X_i$ | Relative standard uncertainty $u(x_i)/x_i$ | Type | Probability distribution | Sensitivity coefficient $c_i$ | Contribution to the relative standard uncertainty $u_{\mathrm{rel},i}(s_{\mathrm{DUT}})$ | Deg. of freedom | Correlated? |
|---|---|---|---|---|---|---|---|---|
| Spectral responsivity of reference detector | $s_{\mathrm{Ref}}(\lambda)$ | 0.0902% | B | normal | $s_{\mathrm{DUT}}(\lambda)/s_{\mathrm{Ref}}(\lambda)$ | 0.0902% | 300 | Yes |
| Correction for drift of spectral responsivity of reference detector | $C_{\mathrm{drift}}$ | 0.0026% | B | normal | $s_{\mathrm{DUT}}(\lambda)/C_{\mathrm{drift}}$ | 0.0026% | ∞ | Yes |
| Photocurrent ratio | $R(I_{\mathrm{DUT}}, I_{\mathrm{Ref}})$ | 0.0005% | A | normal | $s_{\mathrm{DUT}}(\lambda)/R(I_{\mathrm{DUT}}, I_{\mathrm{Ref}})$ | 0.0005% | 30 | No |
| Correction for polarisation dependence of reference detector | $C_{\mathrm{pol,ref}}$ | 0.0032% | B | rectangular | $s_{\mathrm{DUT}}(\lambda)/C_{\mathrm{pol,ref}}$ | 0.0032% | ∞ | Yes |
| Correction for polarisation dependence of photocurrent ratio $R$ | $C_{\mathrm{pol,ratio}}$ | 0.0085% | A | normal | $s_{\mathrm{DUT}}(\lambda)/C_{\mathrm{pol,ratio}}$ | 0.0085% | 1 | No |
| Correction for non-uniformity | $C_{\mathrm{non-unif}}$ | 0.0113% | B | rectangular | $s_{\mathrm{DUT}}(\lambda)/C_{\mathrm{non-unif}}$ | 0.0113% | ∞ | No |
| Correction for temperature of reference detector | $C_{\mathrm{temp}}$ | 0.0007% | B | rectangular | $s_{\mathrm{DUT}}(\lambda)/C_{\mathrm{temp}}$ | 0.0007% | ∞ | Yes |
| Correction for wavelength | $C_{\mathrm{wl}}$ | 0.0032% | B | rectangular | $s_{\mathrm{DUT}}(\lambda)/C_{\mathrm{wl}}$ | 0.0032% | ∞ | Yes |
| Correction for bandwidth effect | $C_{\mathrm{band}}$ | 0.0001% | B | rectangular | $s_{\mathrm{DUT}}(\lambda)/C_{\mathrm{band}}$ | 0.0001% | ∞ | Yes |
| Correction for stray radiation | $C_{\mathrm{stray}}$ | 0.0060% | B | rectangular | $s_{\mathrm{DUT}}(\lambda)/C_{\mathrm{stray}}$ | 0.0060% | 8 | Yes |
| Correction for nonlinearity of detectors | $C_{\mathrm{NL}}$ | 0.0020% | B | rectangular | $s_{\mathrm{DUT}}(\lambda)/C_{\mathrm{NL}}$ | 0.0020% | ∞ | Yes |
| Correction spectral impurity | $C_{\mathrm{imp}}$ | 0.0014% | B | rectangular | $s_{\mathrm{DUT}}(\lambda)/C_{\mathrm{imp}}$ | 0.0014% | ∞ | Yes |
| Correction for angle of incidence | $C_{\mathrm{inc}}$ | 0.0014% | B | rectangular | $s_{\mathrm{DUT}}(\lambda)/C_{\mathrm{inc}}$ | 0.0014% | ∞ | Yes |
| Correction for divergence of radiation beam | $C_{\mathrm{div}}$ | 0.0014% | B | rectangular | $s_{\mathrm{DUT}}(\lambda)/C_{\mathrm{div}}$ | 0.0014% | ∞ | Yes |
| Correction for power instability of radiation source | $C_{\mathrm{inst}}$ | 0.0018% | B | rectangular | $s_{\mathrm{DUT}}(\lambda)/C_{\mathrm{inst}}$ | 0.0018% | ∞ | Yes |
| Correction for voltage measurement (calibration of voltmeters) | $C_{\mathrm{el}}$ | 0.0018% | B | rectangular | $s_{\mathrm{DUT}}(\lambda)/C_{\mathrm{el}}$ | 0.0018% | ∞ | Yes |
| Correction for nonlinearity of current-to-voltage converters | $C_{\mathrm{CVC}}$ | 0.0051% | B | rectangular | $s_{\mathrm{DUT}}(\lambda)/C_{\mathrm{CVC}}$ | 0.0051% | ∞ | Yes |
| | | | | | | | | |
| Spectral responsivity of DUT | $s_{\mathrm{DUT}}(\lambda)$ | | | normal | | 0.092% | 315 | |

### 10.4.5. Uncertainty of trap detector D#4 at wavelength 500 nm

The uncertainty budgets of the spectral responsivity of detector D#4 at the wavelength $\lambda$ = 500 nm determined against the reference detectors Ref1 and Ref2 of set B are shown in Table 10-8 and Table 10-9, respectively. The uncertainty of the final result $u_{\text{rel}}(s_{\text{D\#4,Ref1\&Ref2}}(\lambda))$ = 0.022% was calculated according to equation (10-6) with $u_{\text{rel}}(C_{\text{diff}})$ = 0.0031%.

**Table 10-8. Uncertainty budget of spectral responsivity at 500 nm for the trap detector D#4 calibrated against reference detector Ref1 of set B. Relative standard uncertainties are stated.**

| Source of uncertainty | Quantity $X_i$ | Relative standard uncertainty $u(x_i)/x_i$ | Type | Probability distribution | Sensitivity coefficient $c_i$ | Contribution to the relative standard uncertainty $u_{\text{rel},i}(s_{\text{DUT}})$ | Deg. of freedom | Correlated? |
|---|---|---|---|---|---|---|---|---|
| Spectral responsivity of reference detector | $s_{\text{Ref}}(\lambda)$ | 0.0178% | B | normal | $s_{\text{DUT}}(\lambda)/s_{\text{Ref}}(\lambda)$ | 0.0178% | 60 | Yes |
| Correction for drift of spectral responsivity of reference detector | $C_{\text{drift}}$ | 0.0009% | B | normal | $s_{\text{DUT}}(\lambda)/C_{\text{drift}}$ | 0.0009% | ∞ | Yes |
| Photocurrent ratio | $R(I_{\text{DUT}}, I_{\text{Ref}})$ | 0.0006% | A | normal | $s_{\text{DUT}}(\lambda)/R(I_{\text{DUT}}, I_{\text{Ref}})$ | 0.0006% | 30 | No |
| Correction for polarisation dependence of reference detector | $C_{\text{pol,ref}}$ | 0.0010% | B | rectangular | $s_{\text{DUT}}(\lambda)/C_{\text{pol,ref}}$ | 0.0010% | ∞ | Yes |
| Correction for polarisation dependence of photocurrent ratio $R$ | $C_{\text{pol,ratio}}$ | 0.0003% | A | normal | $s_{\text{DUT}}(\lambda)/C_{\text{pol,ratio}}$ | 0.0003% | 1 | No |
| Correction for non-uniformity | $C_{\text{non-unif}}$ | 0.0057% | B | rectangular | $s_{\text{DUT}}(\lambda)/C_{\text{non-unif}}$ | 0.0057% | ∞ | No |
| Correction for temperature of reference detector | $C_{\text{temp}}$ | 0.0011% | B | rectangular | $s_{\text{DUT}}(\lambda)/C_{\text{temp}}$ | 0.0011% | ∞ | Yes |
| Correction for wavelength | $C_{\text{wl}}$ | 0.0010% | B | rectangular | $s_{\text{DUT}}(\lambda)/C_{\text{wl}}$ | 0.0010% | ∞ | Yes |
| Correction for bandwidth effect | $C_{\text{band}}$ | 0.0000% | B | rectangular | $s_{\text{DUT}}(\lambda)/C_{\text{band}}$ | 0.0000% | ∞ | Yes |
| Correction for stray radiation | $C_{\text{stray}}$ | 0.0080% | B | rectangular | $s_{\text{DUT}}(\lambda)/C_{\text{stray}}$ | 0.0080% | 8 | Yes |
| Correction for nonlinearity of detectors | $C_{\text{NL}}$ | 0.0020% | B | rectangular | $s_{\text{DUT}}(\lambda)/C_{\text{NL}}$ | 0.0020% | ∞ | Yes |
| Correction spectral impurity | $C_{\text{imp}}$ | 0.0014% | B | rectangular | $s_{\text{DUT}}(\lambda)/C_{\text{imp}}$ | 0.0014% | ∞ | Yes |
| Correction for angle of incidence | $C_{\text{inc}}$ | 0.0014% | B | rectangular | $s_{\text{DUT}}(\lambda)/C_{\text{inc}}$ | 0.0014% | ∞ | Yes |
| Correction for divergence of radiation beam | $C_{\text{div}}$ | 0.0014% | B | rectangular | $s_{\text{DUT}}(\lambda)/C_{\text{div}}$ | 0.0014% | ∞ | Yes |
| Correction for power instability of radiation source | $C_{\text{inst}}$ | 0.0018% | B | rectangular | $s_{\text{DUT}}(\lambda)/C_{\text{inst}}$ | 0.0018% | ∞ | Yes |
| Correction for voltage measurement (calibration of voltmeters) | $C_{\text{el}}$ | 0.0018% | B | rectangular | $s_{\text{DUT}}(\lambda)/C_{\text{el}}$ | 0.0018% | ∞ | Yes |
| Correction for nonlinearity of current-to-voltage converters | $C_{\text{CVC}}$ | 0.0051% | B | rectangular | $s_{\text{DUT}}(\lambda)/C_{\text{CVC}}$ | 0.0051% | ∞ | Yes |
| | | | | | | | | |
| Spectral responsivity of DUT | $s_{\text{DUT}}(\lambda)$ | | | normal | | 0.021% | 97 | |

**Table 10-9. Uncertainty budget of spectral responsivity at 500 nm for the trap detector D#4 calibrated against reference detector Ref2 of set B. Relative standard uncertainties are stated.**

| Source of uncertainty | Quantity $X_i$ | Relative standard uncertainty $u(x_i)/x_i$ | Type | Probability distribution | Sensitivity coefficient $c_i$ | Contribution to the relative standard uncertainty $u_{\text{rel},i}(s_{\text{DUT}})$ | Deg. of freedom | Correlated? |
|---|---|---|---|---|---|---|---|---|
| Spectral responsivity of reference detector | $s_{\text{Ref}}(\lambda)$ | 0.0177% | B | normal | $s_{\text{DUT}}(\lambda)/s_{\text{Ref}}(\lambda)$ | 0.0177% | 55 | Yes |
| Correction for drift of spectral responsivity of reference detector | $C_{\text{drift}}$ | 0.0009% | B | normal | $s_{\text{DUT}}(\lambda)/C_{\text{drift}}$ | 0.0009% | ∞ | Yes |
| Photocurrent ratio | $R(I_{\text{DUT}}, I_{\text{Ref}})$ | 0.0006% | A | normal | $s_{\text{DUT}}(\lambda)/R(I_{\text{DUT}}, I_{\text{Ref}})$ | 0.0006% | 30 | No |
| Correction for polarisation dependence of reference detector | $C_{\text{pol,ref}}$ | 0.0010% | B | rectangular | $s_{\text{DUT}}(\lambda)/C_{\text{pol,ref}}$ | 0.0010% | ∞ | Yes |
| Correction for polarisation dependence of photocurrent ratio $R$ | $C_{\text{pol,ratio}}$ | 0.0020% | A | normal | $s_{\text{DUT}}(\lambda)/C_{\text{pol,ratio}}$ | 0.0020% | 1 | No |
| Correction for non-uniformity | $C_{\text{non-unif}}$ | 0.0057% | B | rectangular | $s_{\text{DUT}}(\lambda)/C_{\text{non-unif}}$ | 0.0057% | ∞ | No |
| Correction for temperature of reference detector | $C_{\text{temp}}$ | 0.0002% | B | rectangular | $s_{\text{DUT}}(\lambda)/C_{\text{temp}}$ | 0.0002% | ∞ | Yes |
| Correction for wavelength | $C_{\text{wl}}$ | 0.0002% | B | rectangular | $s_{\text{DUT}}(\lambda)/C_{\text{wl}}$ | 0.0002% | ∞ | Yes |
| Correction for bandwidth effect | $C_{\text{band}}$ | 0.0000% | B | rectangular | $s_{\text{DUT}}(\lambda)/C_{\text{band}}$ | 0.0000% | ∞ | Yes |
| Correction for stray radiation | $C_{\text{stray}}$ | 0.0105% | B | rectangular | $s_{\text{DUT}}(\lambda)/C_{\text{stray}}$ | 0.0105% | 8 | Yes |
| Correction for nonlinearity of detectors | $C_{\text{NL}}$ | 0.0020% | B | rectangular | $s_{\text{DUT}}(\lambda)/C_{\text{NL}}$ | 0.0020% | ∞ | Yes |
| Correction spectral impurity | $C_{\text{imp}}$ | 0.0014% | B | rectangular | $s_{\text{DUT}}(\lambda)/C_{\text{imp}}$ | 0.0014% | ∞ | Yes |
| Correction for angle of incidence | $C_{\text{inc}}$ | 0.0014% | B | rectangular | $s_{\text{DUT}}(\lambda)/C_{\text{inc}}$ | 0.0014% | ∞ | Yes |
| Correction for divergence of radiation beam | $C_{\text{div}}$ | 0.0014% | B | rectangular | $s_{\text{DUT}}(\lambda)/C_{\text{div}}$ | 0.0014% | ∞ | Yes |
| Correction for power instability of radiation source | $C_{\text{inst}}$ | 0.0018% | B | rectangular | $s_{\text{DUT}}(\lambda)/C_{\text{inst}}$ | 0.0018% | ∞ | Yes |
| Correction for voltage measurement (calibration of voltmeters) | $C_{\text{el}}$ | 0.0018% | B | rectangular | $s_{\text{DUT}}(\lambda)/C_{\text{el}}$ | 0.0018% | ∞ | Yes |
| Correction for nonlinearity of current-to-voltage converters | $C_{\text{CVC}}$ | 0.0051% | B | rectangular | $s_{\text{DUT}}(\lambda)/C_{\text{CVC}}$ | 0.0051% | ∞ | Yes |
| | | | | | | | | |
| Spectral responsivity of DUT | $s_{\text{DUT}}(\lambda)$ | | | normal | | 0.022% | 77 | |

### 10.4.6. Uncertainty of trap detector D#4 at wavelength 1000 nm

The uncertainty budget of the spectral responsivity of detector D#4 at the wavelength $\lambda$ = 1000 nm determined against the reference detectors Ref1 of set B is shown in Table 10-10.

**Table 10-10. Uncertainty budget of spectral responsivity at 1000 nm for the trap detector D#4 calibrated against reference detector Ref1 of set B. Relative standard uncertainties are stated.**

| Source of uncertainty | Quantity $X_i$ | Relative standard uncertainty $u(x_i)/x_i$ | Type | Probability distribution | Sensitivity coefficient $c_i$ | Contribution to the relative standard uncertainty $u_{\mathrm{rel},i}(s_{\mathrm{DUT}})$ | Deg. of freedom | Correlated? |
|---|---|---|---|---|---|---|---|---|
| Spectral responsivity of reference detector | $s_{\mathrm{Ref}}(\lambda)$ | 0.0424% | B | normal | $s_{\mathrm{DUT}}(\lambda)/s_{\mathrm{Ref}}(\lambda)$ | 0.0424% | 60 | Yes |
| Correction for drift of spectral responsivity of reference detector | $C_{\mathrm{drift}}$ | 0.0011% | B | normal | $s_{\mathrm{DUT}}(\lambda)/C_{\mathrm{drift}}$ | 0.0011% | ∞ | Yes |
| Photocurrent ratio | $R(I_{\mathrm{DUT}}, I_{\mathrm{Ref}})$ | 0.0003% | A | normal | $s_{\mathrm{DUT}}(\lambda)/R(I_{\mathrm{DUT}}, I_{\mathrm{Ref}})$ | 0.0003% | 30 | No |
| Correction for polarisation dependence of reference detector | $C_{\mathrm{pol,ref}}$ | 0.0022% | B | rectangular | $s_{\mathrm{DUT}}(\lambda)/C_{\mathrm{pol,ref}}$ | 0.0022% | ∞ | Yes |
| Correction for polarisation dependence of photocurrent ratio $R$ | $C_{\mathrm{pol,ratio}}$ | 0.0138% | A | normal | $s_{\mathrm{DUT}}(\lambda)/C_{\mathrm{pol,ratio}}$ | 0.0138% | 1 | No |
| Correction for non-uniformity | $C_{\mathrm{non-unif}}$ | 0.0071% | B | rectangular | $s_{\mathrm{DUT}}(\lambda)/C_{\mathrm{non-unif}}$ | 0.0071% | ∞ | No |
| Correction for temperature of reference detector | $C_{\mathrm{temp}}$ | 0.0365% | B | rectangular | $s_{\mathrm{DUT}}(\lambda)/C_{\mathrm{temp}}$ | 0.0365% | ∞ | Yes |
| Correction for wavelength | $C_{\mathrm{wl}}$ | 0.0056% | B | rectangular | $s_{\mathrm{DUT}}(\lambda)/C_{\mathrm{wl}}$ | 0.0056% | ∞ | Yes |
| Correction for bandwidth effect | $C_{\mathrm{band}}$ | 0.0013% | B | rectangular | $s_{\mathrm{DUT}}(\lambda)/C_{\mathrm{band}}$ | 0.0013% | ∞ | Yes |
| Correction for stray radiation | $C_{\mathrm{stray}}$ | 0.0097% | B | rectangular | $s_{\mathrm{DUT}}(\lambda)/C_{\mathrm{stray}}$ | 0.0097% | 8 | Yes |
| Correction for nonlinearity of detectors | $C_{\mathrm{NL}}$ | 0.0020% | B | rectangular | $s_{\mathrm{DUT}}(\lambda)/C_{\mathrm{NL}}$ | 0.0020% | ∞ | Yes |
| Correction spectral impurity | $C_{\mathrm{imp}}$ | 0.0014% | B | rectangular | $s_{\mathrm{DUT}}(\lambda)/C_{\mathrm{imp}}$ | 0.0014% | ∞ | Yes |
| Correction for angle of incidence | $C_{\mathrm{inc}}$ | 0.0014% | B | rectangular | $s_{\mathrm{DUT}}(\lambda)/C_{\mathrm{inc}}$ | 0.0014% | ∞ | Yes |
| Correction for divergence of radiation beam | $C_{\mathrm{div}}$ | 0.0014% | B | rectangular | $s_{\mathrm{DUT}}(\lambda)/C_{\mathrm{div}}$ | 0.0014% | ∞ | Yes |
| Correction for power instability of radiation source | $C_{\mathrm{inst}}$ | 0.0018% | B | rectangular | $s_{\mathrm{DUT}}(\lambda)/C_{\mathrm{inst}}$ | 0.0018% | ∞ | Yes |
| Correction for voltage measurement (calibration of voltmeters) | $C_{\mathrm{el}}$ | 0.0018% | B | rectangular | $s_{\mathrm{DUT}}(\lambda)/C_{\mathrm{el}}$ | 0.0018% | ∞ | Yes |
| Correction for nonlinearity of current-to-voltage converters | $C_{\mathrm{CVC}}$ | 0.0051% | B | rectangular | $s_{\mathrm{DUT}}(\lambda)/C_{\mathrm{CVC}}$ | 0.0051% | ∞ | Yes |
| | | | | | | | | |
| Spectral responsivity of DUT | $s_{\mathrm{DUT}}(\lambda)$ | | | normal | | 0.060% | 138 | |

# 11. MSL

## 11.1. Measurement Setup and Instruments

The measurement facility, Figure 11-1, is built around a McPherson 2051, 1 m, f/8.7, single monochromator with a prism pre-disperser.

The output beam from the monochromator is collimated and then focused through an iris then collimated again using 350 mm focal length, 9 ° off-axis parabolic mirrors. The last off-axis mirror can be rotated to direct the focused light beam onto four different detectors. The beam has a diameter of 3 mm on the single element diode detector and at the entrance port of the trap detectors.

Over the wavelength range 300 nm to 1000 nm a tungsten lamp is used as the light source. The incident power at the detector is between 0.5 nW to 20 nW.

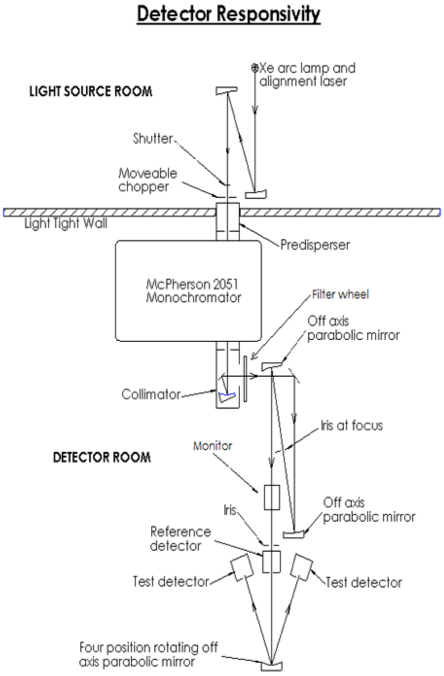


**Figure 11-1. Optical layout of the detector spectral responsivity measurement facility at MSL.**

## *11.2. Measurement Conditions and Parameters*

Each detector under test (DUT) was compared against an MSL reference trap detector using the MSL high accuracy spectrophotometer as a comparator. The DUTs and the MSL reference trap were aligned in the beam so that the reflected beam of the detector is collinear with the incident beam. The beam is centred onto the centre of the sensitive surface of each detector and a control scan in the horizontal and vertical axis was performed (see Figures 11-2, 3 4, 5 and 6) to assess effect of this alignment and the non-uniformity of each DUT. The light beam spot has a diameter size of about 3 mm on the single element based DUTs. MSL 5-element trap detectors and 3-elements trap DUTs are positioned such that the converging light beam enters the trap detector with a size of 3 mm and focusses to a diameter of 2 mm on the last diode of the trap (3$^{rd}$ and 5$^{th}$ diode respectively for MSL traps and DUTs). The measurements were made over the wavelength range 300 nm to 1000 nm with a spectral bandwidth of 1.6 nm. The DUT currents were converted to voltages using calibrated current to voltage converters traceable to MSL. The spectrophotometer room was maintained at (23.3 ± 0.6) °C during the measurements; humidity was not controlled. Using MSL heat-pipe temperature stabilisation systems the MSL reference trap detector were stabilised at 20 °C.

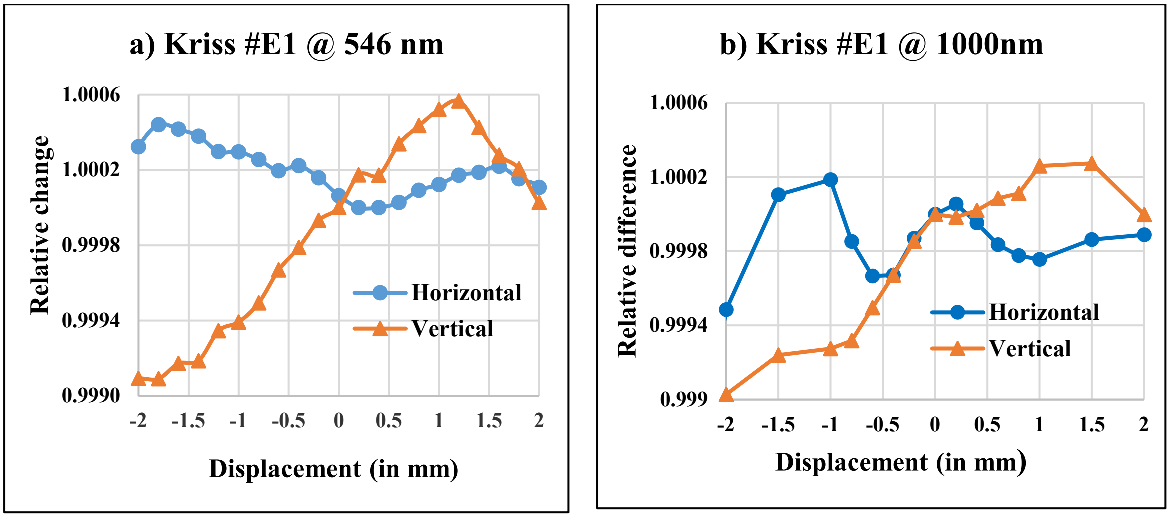


**Figure 11-2. Spatial Uniformity of DUT Kriss #E1 with 3 mm beam along vertical and horizontal axis at a) 546 nm and b) 1000 nm.**

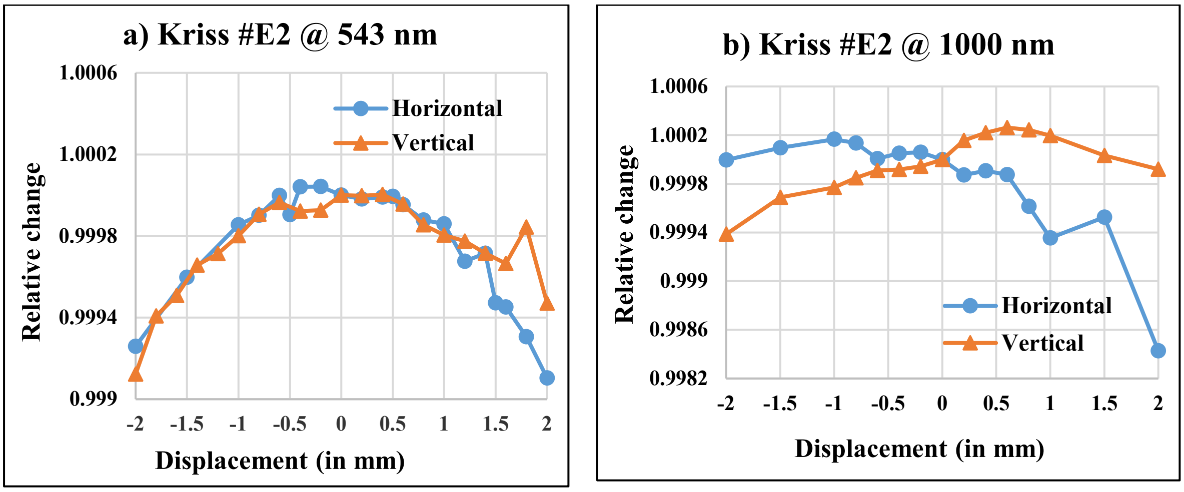


**Figure 11-3. Spatial Uniformity of DUT Kriss #E2 with 3 mm beam along vertical and horizontal axis at a) 543 nm and b) 1000 nm.**

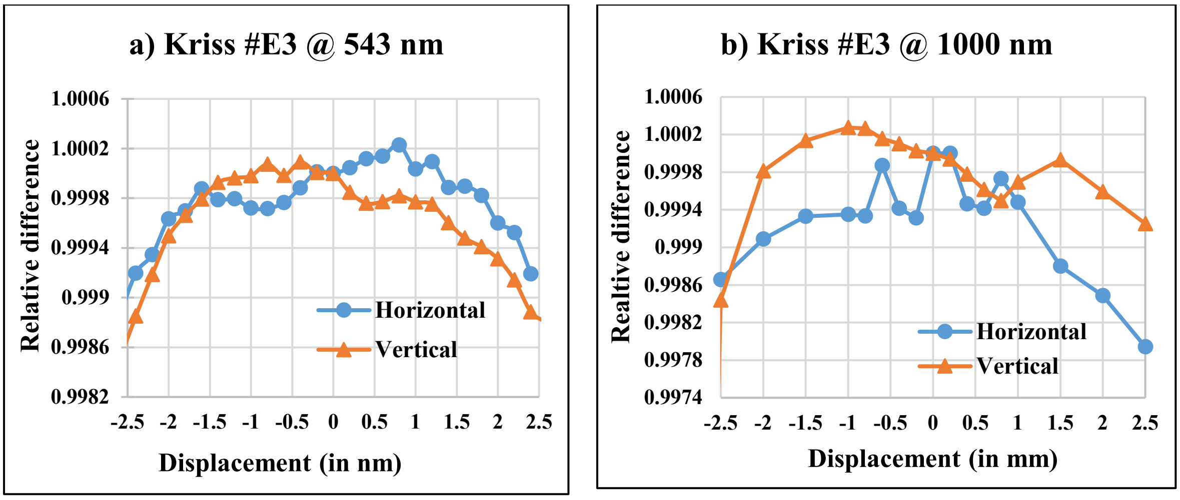

**Figure 11-4. Spatial Uniformity of DUT Kriss #E3 with 3 mm beam along vertical and horizontal axis at a) 543 nm and b) 1000 nm.**

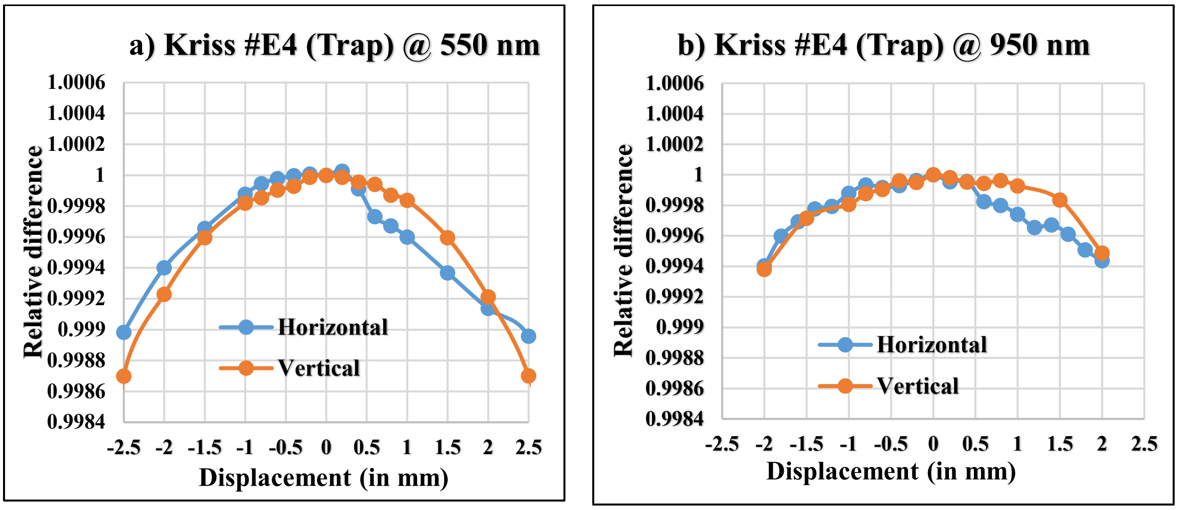


**Figure 11-5. Spatial Uniformity of DUT Kriss #E4 (Trap) with 3 mm beam along vertical and horizontal axis at a) 550 nm and b) 950 nm.**

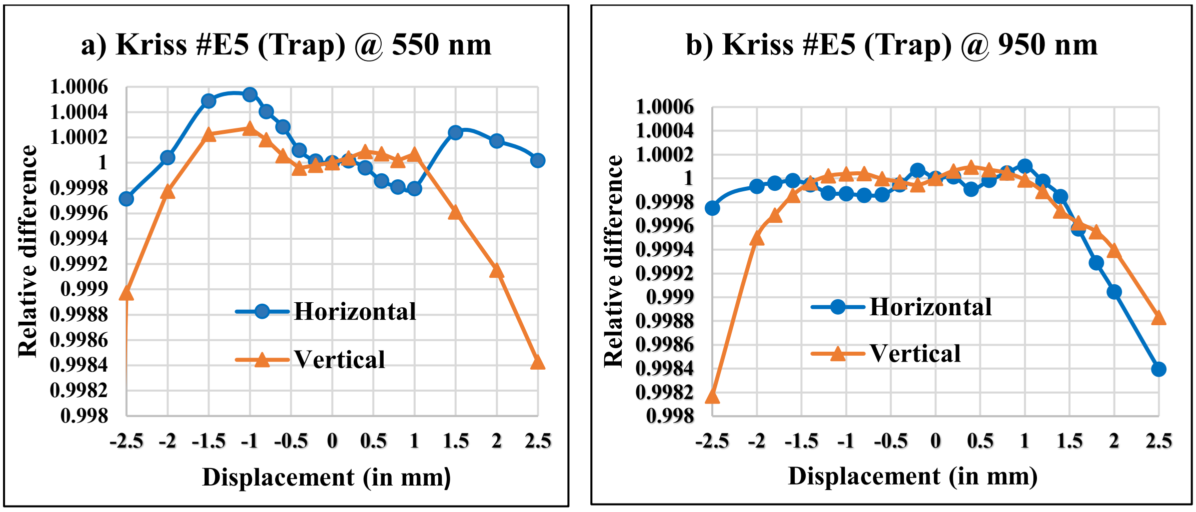


**Figure 11-6. Spatial Uniformity of DUT Kriss #E5 (Trap) with 3 mm beam along vertical and horizontal axis at a) 550 nm and b) 950 nm.**

### *11.3. Traceability of Measurement*

1. The primary optical radiation standard at MSL is an Oxford Instruments cryogenic radiometer.
2. Sets of trap configured silicon photodiode detectors calibrated for spectral responsivity, R(λ), against the cryogenic radiometer at five laser lines between 406.733 nm and 647.1 nm.
3. The residual spectral reflectance, ρ(λ), of these detectors was measured at the same laser lines.
4. Using R(λ) and ρ(λ), values of internal quantum efficiency, IQE(λ), were calculated at each wavelength for each detector.

5. To interpolate between these laser lines, and to extrapolate to wavelengths above and below, a model similar to that in reference[10] was fitted to the known values of IQE(λ).
6. From the above a scale of spectral responsivity from 400 nm to 950 nm was derived, using modelled values of the spectral reflectance of the detectors. Relative response measurements of the MSL trap detectors were made using a pyroelectric detector to determine the wavelength at which the responsivity of trap detectors is no longer linear in variation with wavelength (approximately 950 nm). These relative measurements were used to inform the extrapolation of the model of IQE(λ).
7. From 240 nm to 400 nm the scale was derived from measurements of the traps against a pyroelectric detector. These measurements have been scaled by the known responsivities of the traps at the laser lines.
8. From 950 nm to 1050 nm the scale was derived from a combination of relative response measurements of the detectors against a pyroelectric detector and the model for internal quantum efficiency.
9. Due to ongoing technical issues with MSL cryogenic radiometer that occurred sometime before the reception of artefacts at MSL (October-November 2017), the responsivity scale used at the end is the one realized in 2014. Monitoring measurements carried out post comparison measurements have given indication of changes in MSL scale that are included as an uncertainty in the scale.

**Table 11-1. Main sources of uncertainty in the MSL Cryogenic Radiometer and MSL detector spectral responsivity scale.**

| **Sources of uncertainty in MSL scale.** | Relative Uncertainty ($k$=1) ($\times10^{-4}$) |
|---|---|
| **Calibration of trap against the cryogenic radiometer (typical)** | |
| Window transmittance and scattered light | 0.2 |
| Cavity absorptance | 0.07 |
| Optical power measurement | 0.1 – 0.2 |
| Electrical power measurements | 0.06 |
| Non-equivalence | 0.1 |
| Detector measurements | 0.05 |
| I/V convertors | 0.1 – 0.3 |
| DVM | 0.1 |
| Detector uniformity | 0.5 – 1.0 |
| Polarization sensitivity | 0.2 |
| Laser stability | 0.05 |
| (1 – ρ(λ)) | 0 |
| **Mathematical model (underpinned with laser lines 407 nm - 647.1 nm)** | |
| Interpolation | 1.5 – 3 |
| Extrapolation (650 nm – 900 nm) | 1.6 – 10 |
| Extrapolation (900 nm – 1000 nm) informed with relative data via pyroelectric detector | 10 – 16 |

[10] Gentile T. R., Houston J. M., Cromer C. L., Applied Optics 1996, 35, 4392-4403.

| | |
|---|---|
| **Spectrally flat detector (240 nm – 400 nm)**<br>Includes residual non-spectral flatness, stability, wavelength, bandwidth effects, lock-in linearity, scaling factor) | 20 – 8 |
| **Reference change 2014-2017** | |
| 300 nm – 380 nm | 47 |
| 380 nm – 500 nm | 47 – 11 |
| 500 nm – 550 nm | 11 – 7.3 |
| 550 – 900 nm | 7.3 |
| 900 nm – 1000 nm | 7.3 – 14.2 |

## 11.4. Measurement Uncertainty

The responsivity of the DUT, $R_{\mathrm{DUT}}$, at a given wavelength, λ, can be found from:

$$R_{\mathrm{DUT}} = R_{\mathrm{rel}} \times \frac{G_{\mathrm{ref}}}{G_{\mathrm{DUT}}} \times R_{\mathrm{ref}} \times C_{\lambda} \times C_{\mathrm{unif\,DUT}} \times C_{\mathrm{unif\,ref}} \times C_{\mathrm{temp\,DUT}} \times C_{\mathrm{temp\,ref}} \times C_{\mathrm{BW}} \times C_{\mathrm{scatter}} \times C_{\mathrm{pol}}$$

where:

- $R_{\mathrm{rel}}$ is the ratio of the voltage reading of the DUT relative to that of the MSL reference detector.
- $G_{\mathrm{ref}}$ and $G_{\mathrm{DUT}}$ are the gains of the current to voltage convertors used to amplify the signals from the MSL reference and the DUT respectively,
- $C_{\lambda}$ is the correction due to offset in the wavelength scale of the monochromator,
- $C_{\mathrm{unif\,DUT}}$ and $C_{\mathrm{unif\,ref}}$ are corrections due to the spatial uniformity of response of the DUT and MSL reference respectively,
- $C_{\mathrm{temp\,DUT}}$ and $C_{\mathrm{temp\,ref}}$ are corrections due to the offset in the required operating temperature of the DUT and MSL reference respectively,
- $C_{\mathrm{drift}}$ is the correction in the scale due to drift since the time the scale was realized,
- $C_{\mathrm{BW}}$ is the correction due to the measurement bandwidth.
- $C_{\mathrm{scatter}}$ is the correction due to the light scattered around the light beam.
- $C_{\mathrm{pol}}$ is the correction due to the polarization sensitivity of the detectors.

There are other corrections that can be considered, including corrections due to the linearity of response of the DUT and the MSL reference. However, the size of these corrections and their uncertainties are small and they have not been included in this report.

The uncertainty budget of the spectral responsivities are given at 300 nm, 500 nm and 1000nm for the artefact Kriss E#1 (in Tables 11-2, 3 and 4), for the artefact Kriss E#2 (in Tables 11-5, 6 and 7), for the artefact Kriss E#3 (in Table 11-8, 9 and 10), for the artefact Kriss E#4 (in Tables 11-11, 12 and 13) and for the artefact Kriss E#5 (in Tables 11-14, 15 and 16).

**Table 11-2. Uncertainty budget of spectral responsivity at 300 nm for the single-element detector Kriss E#1.**

| Uncertainty Component | Standard uncertainty (%) | Type | Probability distribution | Sensitivity coefficient | Contribution (%) | Deg. of freedom | Correlated? |
|---|---|---|---|---|---|---|---|
| Reading repeatability | 0.010 | A | normal | 1 | 0.010 | 13 | X |
| Calibration uncertainty of reference detector | 0.49 | B | normal | 1 | 0.49 | 82 | X |

| | | | | | | | |
|---|---|---|---|---|---|---|---|
| Uncertainty from wavelength error of light source | 0.056 | B | normal | 1 | 0.056 | 50 | X |
| Uncertainty from spectral bandwidth of light source | < 0.001 | B | rectangular | 1 | < 0.001 | 50 | X |
| Uncertainty related to beam alignment on artefact | 0.019 | B | rectangular | 1 | 0.019 | 50 | X |
| Uncertainty related to beam alignment on reference | 0.041 | B | rectangular | 1 | 0.041 | 50 | X |
| Uncertainty from current- to voltage amplifier of artefact | 0.001 | B | normal | 1 | 0.001 | 18 | X |
| Uncertainty from current- to voltage amplifier of reference | 0.001 | B | normal | 1 | 0.001 | 11 | X |
| Uncertainty in artefact response from temperature | 0.003 | B | rectangular | 1 | 0.003 | 50 | X |
| Uncertainty in reference response from temperature | 0.001 | B | rectangular | 1 | 0.001 | 50 | X |
| Uncertainty in artefact due to scattered light | 0.025 | B | rectangular | 1 | 0.025 | 50 | X |
| Uncertainty from polarization | 0.016 | B | rectangular | 1 | 0.016 | 50 | X |
| **Combined standard uncertainty (%)** | **--** | **--** | **normal** | **--** | **0.50** | **86** | **--** |

**Table 11-3. Uncertainty budget of spectral responsivity at 500 nm for the single-element detector Kriss E#1.**

| Uncertainty Component | Standard uncertainty (%) | Type | Probability distribution | Sensitivity coefficient | Contribution (%) | Deg. of freedom | Correlated? |
|---|---|---|---|---|---|---|---|
| Reading repeatability | 0.001 | A | normal | 1 | 0.001 | 13 | X |
| Calibration uncertainty of reference detector | 0.12 | B | normal | 1 | 0.12 | 72 | X |
| Uncertainty from wavelength error of light source | 0.002 | B | normal | 1 | 0.002 | 50 | X |
| Uncertainty from spectral bandwidth of light source | < 0.001 | B | rectangular | 1 | < 0.001 | 50 | X |
| Uncertainty related to beam alignment on artefact | 0.019 | B | rectangular | 1 | 0.019 | 50 | X |
| Uncertainty related to beam alignment on reference | 0.041 | B | rectangular | 1 | 0.041 | 50 | X |
| Uncertainty from current- to voltage amplifier of artefact | 0.001 | B | normal | 1 | 0.001 | 18 | X |
| Uncertainty from current- to voltage amplifier of reference | 0.001 | B | normal | 1 | 0.001 | 11 | X |
| Uncertainty in artefact response from temperature | 0.002 | B | rectangular | 1 | 0.002 | 50 | X |

| | | | | | | | |
|---|---|---|---|---|---|---|---|
| Uncertainty in reference response from temperature | < 0.001 | B | rectangular | 1 | < 0.001 | 50 | X |
| Uncertainty in artefact due to scattered light | 0.053 | B | rectangular | 1 | 0.053 | 50 | X |
| Uncertainty from polarization | 0.016 | B | rectangular | 1 | 0.016 | 50 | X |
| **Combined standard uncertainty (%)** | **--** | **--** | **normal** | **--** | **0.14** | **127** | **--** |

**Table 11-4. Uncertainty budget of spectral responsivity at 1000 nm for the single-element detector Kriss E#1.**

| Uncertainty Component | Standard uncertainty (%) | Type | Probability distribution | Sensitivity coefficient | Contribution (%) | Deg. of freedom | Correlated? |
|---|---|---|---|---|---|---|---|
| Reading repeatability | 0.009 | A | normal | 1 | 0.009 | 13 | X |
| Calibration uncertainty of reference detector | 0.21 | B | normal | 1 | 0.21 | 112 | X |
| Uncertainty from wavelength error of light source | 0.002 | B | normal | 1 | 0.002 | 50 | X |
| Uncertainty from spectral bandwidth of light source | 0.005 | B | rectangular | 1 | 0.005 | 50 | X |
| Uncertainty related to beam alignment on artefact | 0.019 | B | rectangular | 1 | 0.019 | 50 | X |
| Uncertainty related to beam alignment on reference | 0.041 | B | rectangular | 1 | 0.041 | 50 | X |
| Uncertainty from current- to voltage amplifier of artefact | 0.001 | B | normal | 1 | 0.001 | 18 | X |
| Uncertainty from current- to voltage amplifier of reference | 0.001 | B | normal | 1 | 0.001 | 11 | X |
| Uncertainty in artefact response from temperature | 0.042 | B | rectangular | 1 | 0.042 | 50 | X |
| Uncertainty in reference response from temperature | 0.011 | B | rectangular | 1 | 0.011 | 50 | X |
| Uncertainty in artefact due to scattered light | 0.054 | B | rectangular | 1 | 0.054 | 50 | X |
| Uncertainty from polarization | 0.016 | B | rectangular | 1 | 0.016 | 50 | X |
| **Combined standard uncertainty (%)** | **--** | **--** | **normal** | **--** | **0.23** | **148** | **--** |

**Table 11-5. Uncertainty budget of spectral responsivity at 300 nm for the single-element detector Kriss E#2.**

| Uncertainty Component | Standard uncertainty (%) | Type | Probability distribution | Sensitivity coefficient | Contribution (%) | Deg. of freedom | Correlated? |
|---|---|---|---|---|---|---|---|
| Reading repeatability | 0.013 | A | normal | 1 | 0.013 | 13 | X |
| Calibration uncertainty of reference detector | 0.49 | B | normal | 1 | 0.49 | 82 | X |
| Uncertainty from wavelength error of light source | 0.054 | B | normal | 1 | 0.054 | 50 | X |
| Uncertainty from spectral bandwidth of light source | < 0.001 | B | rectangular | 1 | < 0.001 | 50 | X |
| Uncertainty related to beam alignment on artefact | 0.013 | B | rectangular | 1 | 0.013 | 50 | X |
| Uncertainty related to beam alignment on reference | 0.041 | B | rectangular | 1 | 0.041 | 50 | X |
| Uncertainty from current- to voltage amplifier of artefact | 0.001 | B | normal | 1 | 0.001 | 18 | X |
| Uncertainty from current- to voltage amplifier of reference | 0.001 | B | normal | 1 | 0.001 | 11 | X |
| Uncertainty in artefact response from temperature | 0.003 | B | rectangular | 1 | 0.003 | 50 | X |
| Uncertainty in reference response from temperature | 0.001 | B | rectangular | 1 | 0.001 | 50 | X |
| Uncertainty in artefact due to scattered light | 0.025 | B | rectangular | 1 | 0.025 | 50 | X |
| Uncertainty from polarization | 0.016 | B | rectangular | 1 | 0.016 | 50 | X |
| **Combined standard uncertainty (%)** | **--** | **--** | **normal** | **--** | **0.50** | **86** | **--** |

**Table 11-6. Uncertainty budget of spectral responsivity at 500 nm for the single-element detector Kriss E#2.**

| Uncertainty Component | Standard uncertainty (%) | Type | Probability distribution | Sensitivity coefficient | Contribution (%) | Deg. of freedom | Correlated? |
|---|---|---|---|---|---|---|---|
| Reading repeatability | 0.001 | A | normal | 1 | 0.001 | 13 | X |
| Calibration uncertainty of reference detector | 0.12 | B | normal | 1 | 0.12 | 72 | X |
| Uncertainty from wavelength error of light source | 0.002 | B | normal | 1 | 0.002 | 50 | X |
| Uncertainty from spectral bandwidth of light source | < 0.001 | B | rectangular | 1 | < 0.001 | 50 | X |

| | | | | | | | |
|---|---|---|---|---|---|---|---|
| Uncertainty related to beam alignment on artefact | 0.013 | B | rectangular | 1 | 0.013 | 50 | X |
| Uncertainty related to beam alignment on reference | 0.041 | B | rectangular | 1 | 0.041 | 50 | X |
| Uncertainty from current- to voltage amplifier of artefact | 0.001 | B | normal | 1 | 0.001 | 18 | X |
| Uncertainty from current- to voltage amplifier of reference | 0.001 | B | normal | 1 | 0.001 | 11 | X |
| Uncertainty in artefact response from temperature | 0.002 | B | rectangular | 1 | 0.002 | 50 | X |
| Uncertainty in reference response from temperature | < 0.001 | B | rectangular | 1 | < 0.001 | 50 | X |
| Uncertainty in artefact due to scattered light | 0.053 | B | rectangular | 1 | 0.053 | 50 | X |
| Uncertainty from polarization | 0.016 | B | rectangular | 1 | 0.016 | 50 | X |
| **Combined standard uncertainty (%)** | **--** | **--** | **normal** | **--** | **0.14** | **124** | **--** |

**Table 11-7. Uncertainty budget of spectral responsivity at 1000 nm for the single-element detector Kriss E#2.**

| Uncertainty Component | Standard uncertainty (%) | Type | Probability distribution | Sensitivity coefficient | Contribution (%) | Deg. of freedom | Correlated? |
|---|---|---|---|---|---|---|---|
| Reading repeatability | 0.007 | A | normal | 1 | 0.007 | 13 | X |
| Calibration uncertainty of reference detector | 0.21 | B | normal | 1 | 0.21 | 112 | X |
| Uncertainty from wavelength error of light source | 0.005 | B | normal | 1 | 0.005 | 50 | X |
| Uncertainty from spectral bandwidth of light source | < 0.001 | B | rectangular | 1 | < 0.001 | 50 | X |
| Uncertainty related to beam alignment on artefact | 0.013 | B | rectangular | 1 | 0.013 | 50 | X |
| Uncertainty related to beam alignment on reference | 0.041 | B | rectangular | 1 | 0.041 | 50 | X |
| Uncertainty from current- to voltage amplifier of artefact | 0.001 | B | normal | 1 | 0.001 | 18 | X |
| Uncertainty from current- to voltage amplifier of reference | 0.001 | B | normal | 1 | 0.001 | 11 | X |
| Uncertainty in artefact response from temperature | 0.042 | B | rectangular | 1 | 0.042 | 50 | X |
| Uncertainty in reference response from temperature | 0.011 | B | rectangular | 1 | 0.011 | 50 | X |
| Uncertainty in artefact due to scattered light | 0.054 | B | rectangular | 1 | 0.054 | 50 | X |

| | | | | | | | |
|---|---|---|---|---|---|---|---|
| Uncertainty from polarization | 0.016 | B | rectangular | 1 | 0.016 | 50 | X |
| **Combined standard uncertainty (%)** | **--** | **--** | **normal** | **--** | **0.23** | **147** | **--** |

**Table 11-8. Uncertainty budget of spectral responsivity at 300 nm for the single-element detector Kriss E#3.**

| Uncertainty Component | Standard uncertainty (%) | Type | Probability distribution | Sensitivity coefficient | Contribution (%) | Deg. of freedom | Correlated? |
|---|---|---|---|---|---|---|---|
| Reading repeatability | 0.013 | A | normal | 1 | 0.013 | 13 | X |
| Calibration uncertainty of reference detector | 0.49 | B | normal | 1 | 0.49 | 82 | X |
| Uncertainty from wavelength error of light source | 0.056 | B | normal | 1 | 0.056 | 50 | X |
| Uncertainty from spectral bandwidth of light source | < 0.001 | B | rectangular | 1 | < 0.001 | 50 | X |
| Uncertainty related to beam alignment on artefact | 0.034 | B | rectangular | 1 | 0.0134 | 50 | X |
| Uncertainty related to beam alignment on reference | 0.041 | B | rectangular | 1 | 0.041 | 50 | X |
| Uncertainty from current- to voltage amplifier of artefact | 0.001 | B | normal | 1 | 0.001 | 7 | X |
| Uncertainty from current- to voltage amplifier of reference | 0.001 | B | normal | 1 | 0.001 | 11 | X |
| Uncertainty in artefact response from temperature | 0.003 | B | rectangular | 1 | 0.003 | 50 | X |
| Uncertainty in reference response from temperature | 0.001 | B | rectangular | 1 | 0.001 | 50 | X |
| Uncertainty in artefact due to scattered light | 0.025 | B | rectangular | 1 | 0.025 | 50 | X |
| Uncertainty from polarization | 0.016 | B | rectangular | 1 | 0.016 | 50 | X |
| **Combined standard uncertainty (%)** | **--** | **--** | **normal** | **--** | **0.50** | **86** | **--** |

**Table 11-9. Uncertainty budget of spectral responsivity at 500 nm for the single-element detector Kriss E#3.**

| Uncertainty Component | Standard uncertainty (%) | Type | Probability distribution | Sensitivity coefficient | Contribution (%) | Deg. of freedom | Correlated? |
|---|---|---|---|---|---|---|---|
| Reading repeatability | 0.001 | A | normal | 1 | 0.001 | 13 | X |

| | | | | | | | |
|---|---|---|---|---|---|---|---|
| Calibration uncertainty of reference detector | 0.12 | B | normal | 1 | 0.12 | 72 | X |
| Uncertainty from wavelength error of light source | 0.002 | B | normal | 1 | 0.002 | 50 | X |
| Uncertainty from spectral bandwidth of light source | < 0.001 | B | rectangular | 1 | < 0.001 | 50 | X |
| Uncertainty related to beam alignment on artefact | 0.034 | B | rectangular | 1 | 0.0134 | 50 | X |
| Uncertainty related to beam alignment on reference | 0.041 | B | rectangular | 1 | 0.041 | 50 | X |
| Uncertainty from current- to voltage amplifier of artefact | 0.001 | B | normal | 1 | 0.001 | 7 | X |
| Uncertainty from current- to voltage amplifier of reference | 0.001 | B | normal | 1 | 0.001 | 11 | X |
| Uncertainty in artefact response from temperature | 0.002 | B | rectangular | 1 | 0.002 | 50 | X |
| Uncertainty in reference response from temperature | < 0.001 | B | rectangular | 1 | < 0.001 | 50 | X |
| Uncertainty in artefact due to scattered light | 0.053 | B | rectangular | 1 | 0.053 | 50 | X |
| Uncertainty from polarization | 0.016 | B | rectangular | 1 | 0.016 | 50 | X |
| **Combined standard uncertainty (%)** | **--** | **--** | **normal** | **--** | **0.14** | **137** | **--** |

**Table 11-10. Uncertainty budget of spectral responsivity at 1000 nm for the single-element detector Kriss E#3.**

| Uncertainty Component | Standard uncertainty (%) | Type | Probability distribution | Sensitivity coefficient | Contribution (%) | Deg. of freedom | Correlated? |
|---|---|---|---|---|---|---|---|
| Reading repeatability | 0.008 | A | normal | 1 | 0.008 | 1 | X |
| Calibration uncertainty of reference detector | 0.21 | B | normal | 1 | 0.21 | 112 | X |
| Uncertainty from wavelength error of light source | 0.004 | B | normal | 1 | 0.004 | 20 | X |
| Uncertainty from spectral bandwidth of light source | < 0.001 | B | rectangular | 1 | < 0.001 | 50 | X |
| Uncertainty related to beam alignment on artefact | 0.034 | B | rectangular | 1 | 0.034 | 50 | X |
| Uncertainty related to beam alignment on reference | 0.041 | B | rectangular | 1 | 0.041 | 50 | X |
| Uncertainty from current- to voltage amplifier of artefact | 0.001 | B | normal | 1 | 0.001 | 7 | X |
| Uncertainty from current- to voltage amplifier of reference | 0.001 | B | normal | 1 | 0.001 | 11 | X |

| | | | | | | | |
|---|---|---|---|---|---|---|---|
| Uncertainty in artefact response from temperature | 0.042 | B | rectangular | 1 | 0.042 | 50 | X |
| Uncertainty in reference response from temperature | 0.011 | B | rectangular | 1 | 0.011 | 50 | X |
| Uncertainty in artefact due to scattered light | 0.054 | B | rectangular | 1 | 0.054 | 50 | X |
| Uncertainty from polarization | 0.016 | B | rectangular | 1 | 0.016 | 50 | X |
| **Combined standard uncertainty (%)** | **--** | **--** | **normal** | **--** | **0.23** | **152** | **--** |

**Table 11-11. Uncertainty budget of spectral responsivity at 300 nm for the single-element detector Kriss E#4.**

| Uncertainty Component | Standard uncertainty (%) | Type | Probability distribution | Sensitivity coefficient | Contrib ution (%) | Deg. of freedo m | Correl ated? |
|---|---|---|---|---|---|---|---|
| Reading repeatability | 0.021 | A | normal | 1 | 0.021 | 1 | X |
| Calibration uncertainty of reference detector | 0.49 | B | normal | 1 | 0.49 | 82 | X |
| Uncertainty from wavelength error of light source | 0.009 | B | normal | 1 | 0.009 | 50 | X |
| Uncertainty from spectral bandwidth of light source | < 0.001 | B | rectangular | 1 | < 0.001 | 50 | X |
| Uncertainty related to beam alignment on artefact | 0.041 | B | rectangular | 1 | 0.041 | 50 | X |
| Uncertainty related to beam alignment on reference | 0.041 | B | rectangular | 1 | 0.041 | 50 | X |
| Uncertainty from current- to voltage amplifier of artefact | 0.001 | B | normal | 1 | 0.001 | 7 | X |
| Uncertainty from current- to voltage amplifier of reference | 0.001 | B | normal | 1 | 0.001 | 11 | X |
| Uncertainty in artefact response from temperature | 0.003 | B | rectangular | 1 | 0.003 | 50 | X |
| Uncertainty in reference response from temperature | < 0.001 | B | rectangular | 1 | < 0.001 | 50 | X |
| Uncertainty in artefact due to scattered light | 0.005 | B | rectangular | 1 | 0.005 | 50 | X |
| Uncertainty from polarization | 0.016 | B | rectangular | 1 | 0.016 | 50 | X |
| **Combined standard uncertainty (%)** | **--** | **--** | **normal** | **--** | **0.50** | **84** | **--** |

**Table 11-12. Uncertainty budget of spectral responsivity at 500 nm for the single-element detector Kriss E#4.**

| Uncertainty Component | Standard uncertainty (%) | Type | Probability distribution | Sensitivity coefficient | Contribution (%) | Deg. of freedom | Correlated? |
|---|---|---|---|---|---|---|---|
| Reading repeatability | 0.001 | A | normal | 1 | 0.001 | 1 | X |
| Calibration uncertainty of reference detector | 0.12 | B | normal | 1 | 0.12 | 72 | X |
| Uncertainty from wavelength error of light source | 0.009 | B | normal | 1 | 0.009 | 50 | X |
| Uncertainty from spectral bandwidth of light source | < 0.001 | B | rectangular | 1 | < 0.001 | 50 | X |
| Uncertainty related to beam alignment on artefact | 0.041 | B | rectangular | 1 | 0.041 | 50 | X |
| Uncertainty related to beam alignment on reference | 0.041 | B | rectangular | 1 | 0.041 | 50 | X |
| Uncertainty from current- to voltage amplifier of artefact | 0.001 | B | normal | 1 | 0.001 | 7 | X |
| Uncertainty from current- to voltage amplifier of reference | 0.001 | B | normal | 1 | 0.001 | 11 | X |
| Uncertainty in artefact response from temperature | 0.001 | B | rectangular | 1 | 0.001 | 50 | X |
| Uncertainty in reference response from temperature | < 0.001 | B | rectangular | 1 | < 0.001 | 50 | X |
| Uncertainty in artefact due to scattered light | 0.035 | B | rectangular | 1 | 0.035 | 50 | X |
| Uncertainty from polarization | 0.016 | B | rectangular | 1 | 0.016 | 50 | X |
| **Combined standard uncertainty (%)** | **--** | **--** | **normal** | **--** | **0.13** | **127** | **--** |

**Table 11-13. Uncertainty budget of spectral responsivity at 1000 nm for the single-element detector Kriss E#4.**

| Uncertainty Component | Standard uncertainty (%) | Type | Probability distribution | Sensitivity coefficient | Contribution (%) | Deg. of freedom | Correlated? |
|---|---|---|---|---|---|---|---|
| Reading repeatability | 0.004 | A | normal | 1 | 0.004 | 1 | X |
| Calibration uncertainty of reference detector | 0.21 | B | normal | 1 | 0.21 | 112 | X |
| Uncertainty from wavelength error of light source | 0.006 | B | normal | 1 | 0.006 | 50 | X |
| Uncertainty from spectral bandwidth of light source | < 0.001 | B | rectangular | 1 | < 0.001 | 50 | X |

| | | | | | | | |
|---|---|---|---|---|---|---|---|
| Uncertainty related to beam alignment on artefact | 0.041 | B | rectangular | 1 | 0.041 | 50 | X |
| Uncertainty related to beam alignment on reference | 0.041 | B | rectangular | 1 | 0.041 | 50 | X |
| Uncertainty from current- to voltage amplifier of artefact | 0.001 | B | normal | 1 | 0.001 | 7 | X |
| Uncertainty from current- to voltage amplifier of reference | 0.001 | B | normal | 1 | 0.001 | 11 | X |
| Uncertainty in artefact response from temperature | 0.049 | B | rectangular | 1 | 0.049 | 50 | X |
| Uncertainty in reference response from temperature | 0.009 | B | rectangular | 1 | 0.009 | 50 | X |
| Uncertainty in artefact due to scattered light | 0.010 | B | rectangular | 1 | 0.010 | 50 | X |
| Uncertainty from polarization | 0.016 | B | rectangular | 1 | 0.016 | 50 | X |
| **Combined standard uncertainty (%)** | **--** | **--** | **normal** | **--** | **0.23** | **144** | **--** |

**Table 11-14. Uncertainty budget of spectral responsivity at 300 nm for the single-element detector Kriss E#5.**

| Uncertainty Component | Standard uncertainty (%) | Type | Probability distribution | Sensitivity coefficient | Contribution (%) | Deg. of freedom | Correlated? |
|---|---|---|---|---|---|---|---|
| Reading repeatability | 0.018 | A | normal | 1 | 0.018 | 13 | X |
| Calibration uncertainty of reference detector | 0.49 | B | normal | 1 | 0.49 | 82 | X |
| Uncertainty from wavelength error of light source | 0.009 | B | normal | 1 | 0.009 | 50 | X |
| Uncertainty from spectral bandwidth of light source | < 0.001 | B | rectangular | 1 | < 0.001 | 50 | X |
| Uncertainty related to beam alignment on artefact | 0.041 | B | rectangular | 1 | 0.041 | 50 | X |
| Uncertainty related to beam alignment on reference | 0.041 | B | rectangular | 1 | 0.041 | 50 | X |
| Uncertainty from current- to voltage amplifier of artefact | 0.001 | B | normal | 1 | 0.001 | 18 | X |
| Uncertainty from current- to voltage amplifier of reference | 0.001 | B | normal | 1 | 0.001 | 11 | X |
| Uncertainty in artefact response from temperature | 0.003 | B | rectangular | 1 | 0.003 | 50 | X |
| Uncertainty in reference response from temperature | < 0.001 | B | rectangular | 1 | < 0.001 | 50 | X |
| Uncertainty in artefact due to scattered light | 0.005 | B | rectangular | 1 | 0.005 | 50 | X |

| | | | | | | | |
|---|---|---|---|---|---|---|---|
| Uncertainty from polarization | 0.016 | B | rectangular | 1 | 0.016 | 50 | X |
| **Combined standard uncertainty (%)** | **--** | **--** | **normal** | **--** | **0.50** | **84** | **--** |

**Table 11-15. Uncertainty budget of spectral responsivity at 500 nm for the single-element detector Kriss E#5.**

| Uncertainty Component | Standard uncertainty (%) | Type | Probability distribution | Sensitivity coefficient | Contribution (%) | Deg. of freedom | Correlated? |
|---|---|---|---|---|---|---|---|
| Reading repeatability | 0.002 | A | normal | 1 | 0.002 | 13 | X |
| Calibration uncertainty of reference detector | 0.12 | B | normal | 1 | 0.12 | 72 | X |
| Uncertainty from wavelength error of light source | < 0.001 | B | normal | 1 | < 0.001 | 50 | X |
| Uncertainty from spectral bandwidth of light source | < 0.001 | B | rectangular | 1 | < 0.001 | 50 | X |
| Uncertainty related to beam alignment on artefact | 0.041 | B | rectangular | 1 | 0.041 | 50 | X |
| Uncertainty related to beam alignment on reference | 0.041 | B | rectangular | 1 | 0.041 | 50 | X |
| Uncertainty from current- to voltage amplifier of artefact | 0.001 | B | normal | 1 | 0.001 | 18 | X |
| Uncertainty from current- to voltage amplifier of reference | 0.001 | B | normal | 1 | 0.001 | 11 | X |
| Uncertainty in artefact response from temperature | 0.001 | B | rectangular | 1 | 0.001 | 50 | X |
| Uncertainty in reference response from temperature | < 0.001 | B | rectangular | 1 | < 0.001 | 50 | X |
| Uncertainty in artefact due to scattered light | 0.035 | B | rectangular | 1 | 0.035 | 50 | X |
| Uncertainty from polarization | 0.016 | B | rectangular | 1 | 0.016 | 50 | X |
| **Combined standard uncertainty (%)** | **--** | **--** | **normal** | **--** | **0.13** | **127** | **--** |

**Table 11-16. Uncertainty budget of spectral responsivity at 1000 nm for the single-element detector Kriss E#5.**

| Uncertainty Component | Standard uncertainty (%) | Type | Probability distribution | Sensitivity coefficient | Contribution (%) | Deg. of freedom | Correlated? |
|---|---|---|---|---|---|---|---|
| Reading repeatability | 0.004 | A | normal | 1 | 0.004 | 13 | X |

| | | | | | | | |
|---|---|---|---|---|---|---|---|
| Calibration uncertainty of reference detector | 0.21 | B | normal | 1 | 0.21 | 112 | X |
| Uncertainty from wavelength error of light source | 0.007 | B | normal | 1 | 0.007 | 50 | X |
| Uncertainty from spectral bandwidth of light source | < 0.001 | B | rectangular | 1 | < 0.001 | 50 | X |
| Uncertainty related to beam alignment on artefact | 0.041 | B | rectangular | 1 | 0.041 | 50 | X |
| Uncertainty related to beam alignment on reference | 0.041 | B | rectangular | 1 | 0.041 | 50 | X |
| Uncertainty from current- to voltage amplifier of artefact | 0.001 | B | normal | 1 | 0.001 | 18 | X |
| Uncertainty from current- to voltage amplifier of reference | 0.001 | B | normal | 1 | 0.001 | 11 | X |
| Uncertainty in artefact response from temperature | 0.049 | B | rectangular | 1 | 0.049 | 50 | X |
| Uncertainty in reference response from temperature | 0.009 | B | rectangular | 1 | 0.009 | 50 | X |
| Uncertainty in artefact due to scattered light | 0.010 | B | rectangular | 1 | 0.010 | 50 | X |
| Uncertainty from polarization | 0.016 | B | rectangular | 1 | 0.016 | 50 | X |
| **Combined standard uncertainty (%)** | **--** | **--** | **normal** | **--** | **0.23** | **144** | **--** |

# 12. NPL

## *12.1. Measurement Setup and Instruments*

### 12.1.1.Measurement facility

The measurement facility used to measure the spectral responsivity of the CCPR-K2.b.2015 detectors is shown in Figure 12-1 below.

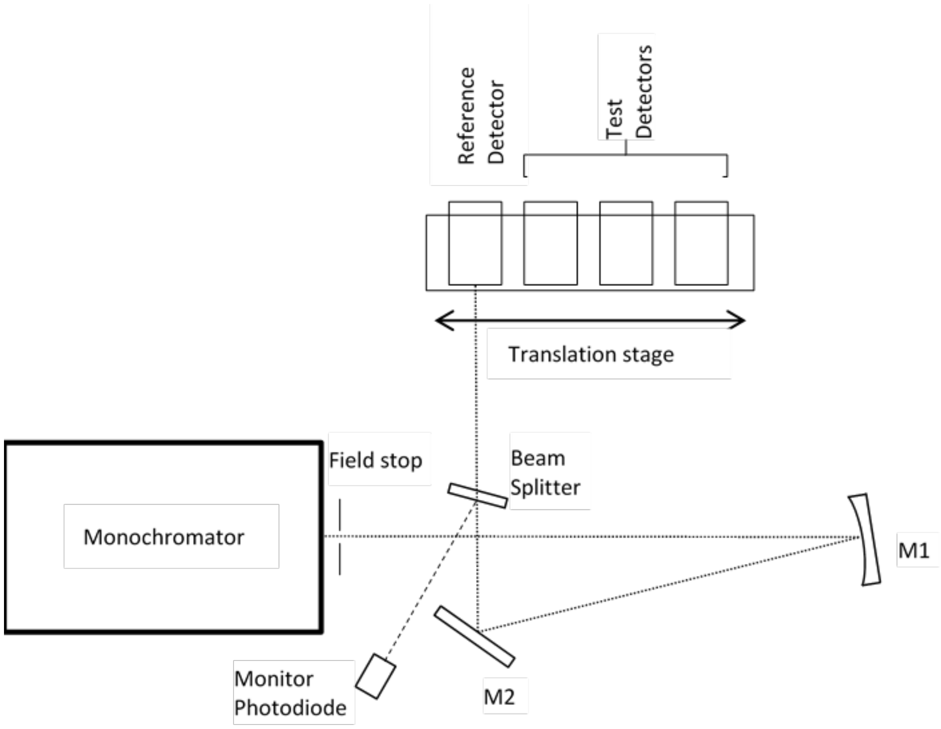


**Figure 12-1. NPL Spectral Responsivity Facility. M1 is a spherical mirror. M2 is a plane mirror. Not shown: source and optics located before the monochromator (source, mirrors, shutter and chopper), the monitor screen, the detector enclosure, and the electrical system.**

A quartz tungsten halogen source was imaged into the monochromator using mirrors. A shutter and a chopper (used for relative measurements against the pyroelectric reference detector for some wavelengths) were positioned before the entrance port of the monochromator. The chopping frequency (when measuring with the pyroelectric detector) was 71 Hz.

A McPherson model 2035 double subtractive Czerny-Turner monochromator was used, which had an f/number of f/4.8. The entrance and exit slits of each half of the monochromator were variable in both width and height. The width was set to 1.25 mm to give a bandwidth of approximately 5 nm (triangular), and the height was set to 2 mm. Built-in order sorting filters were located immediately before the entrance slit. The gratings installed in the monochromator for these measurements were blazed at 240 nm for measurements in the range 300 nm to 400 nm, 500 nm for measurements in the range 380 nm to 920 nm and 1.25 µm for measurements in the range 800 nm to 1000 nm. All gratings had a groove density of 600 g/mm.

A variable aperture, placed after the monochromator, was used as a field stop. It was used to control the f/number of the beam. A spherical mirror (M1) was used to form a one-to-one image of the exit port of the monochromator and a turning mirror (M2) was used to steer the image to the reference and test detectors. A beam splitter was used to reflect a small percentage of the power in the beam to a monitor detector, which was used to monitor any change in power of the beam during the measurements. The monitor detector was screened from the other detectors as much as possible. The detectors were mounted on a computer-controlled translation stage in order to ensure reproducible positioning of each detector with respect to the beam.

The distance between the detector surface and mirror M2 was adjusted according to the size of irradiated area required i.e.:

- The reference trap detectors were positioned such that they were underfilled, and so that an image of the exit port of the monochromator was formed on the last (third) detector.
- The reference pyroelectric detector was positioned such that the beam passed through the port of the hemisphere (fixed to the front of the detector) without clipping.

- The comparison single element detectors were positioned such that the beam falling on the detector surface was approximately circular, and approximately 7 mm in diameter.
- The comparison trap detectors were positioned such that they were underfilled and so that an image of the exit port of the monochromator was formed on the last (third) detector.

The detector side of the system (i.e. from the monochromator exit port onwards) was enclosed within a light tight enclosure.

Each detector was connected to a transimpedance amplifier. The output from the amplifier was then measured by a voltmeter (directly for d.c. measurements and via a lock-in amplifier for a.c. measurements).

The temperature within the enclosure was monitored using a platinum resistance thermometer (PRT).

### 12.1.2. Measurement methodology

To achieve the best possible measurement uncertainty for the measurement of the single element comparison detectors, absolute measurements were made directly against NPL's reference silicon trap detectors at wavelengths from 380 nm to 920 nm and these were combined with relative measurements against NPL's reference cavity pyroelectric detector from 300 nm to 400 nm and from 890 to 1000 nm. The overlap points, defined as the wavelengths at which both absolute and relative measurements were made, were used to determine a normalisation constant (one for the UV region and another for the IR region). The relevant normalisation constant was applied to each of the associated relative data points to calculate the absolute spectral responsivity at these wavelengths. This allowed the absolute spectral responsivity of the comparison detectors to be determined at each wavelength required for the comparison (see Section 12.1.5 for more details).

In the case of the comparison trap detectors the differing geometry requirements meant that it was not possible to measure against the pyroelectric reference detector. Measurements were instead made against NPL's reference silicon trap detectors from 380 nm to 920 nm (as for the single element comparison detectors) and against the single element comparison detectors from 300 nm to 400 nm and 890 nm to 1000 nm. The single element detectors were used to provide information on the relative spectral responsivity only; these data were used to determine a normalisation constant from which absolute responsivity values were calculated, as detailed in Section 12.1.5.

Measurements were automated using the control program. The sequence for each measurement scan was as follows:

1. Set the monochromator to the first (lowest) wavelength required.
2. Record the light and dark readings (made with the shutter open and closed respectively) from the reference detector.
3. Repeat step 2 for each individual test detector in turn.
4. Set the monochromator to the next wavelength required.
5. Repeat steps 2 and 3.
6. Repeat steps 4 and 5 until all required wavelengths have been measured.

The monitor detector was measured simultaneously and was used to correct for any change in the output of the source during the course of the measurements.

Up to eight repeated scans were carried out, depending on the signal-to-noise, to form one 'independent measurement'. The mean and standard deviation of the scans forming each independent measurement were calculated. Several independent measurements were carried out (three in the case of the absolute measurements, each using a different reference trap detector, and two in the case of the relative measurements) and these were averaged to obtain the final measurement result. All the detectors (reference and test) were realigned between each independent measurement.

### 12.1.3. Absolute measurements

Absolute measurements were made by reference to NPL's three-element reference silicon trap detectors over the wavelength range 380 nm to 920 nm. The spectral responsivity of the trap detectors was calibrated against the NPL Primary Standard Cryogenic Radiometer at several Krypton ion lines in the UV, visible and NIR. The responsivity of the trap detectors at wavelengths longer than 799.3 nm was extrapolated from the responsivity at 799.3 nm by assuming constant quantum efficiency; this defines the NPL responsivity scale over the range 800 nm to 920 nm.

The absolute spectral responsivity of the comparison detectors was calibrated directly against the trap detectors at 5 nm intervals from 380 nm to 400 nm, 50 nm intervals from 400 nm to 850 nm, and at 5 nm intervals from 900 nm to 920 nm. The absolute results at 380 nm, 400 nm to 850 nm and 900 nm were used directly for the comparison. The other wavelengths were only used to determine a normalisation constant (see Section 12.1.5) and are not reported as part of this comparison.

Measurement parameters:

| | |
|---|---|
| Modulation frequency | d.c. |
| f/number | At least f/21 |

### 12.1.4. Relative measurements

In the case of the single element comparison detectors, relative measurements were made by reference to the NPL reference cavity pyroelectric detector, which incorporates an aluminium hemisphere for measurements from 300 nm to 400 nm and a gold hemisphere for measurements from 800 nm to 1000 nm[11]. For the trap comparison detectors, the single element detectors were used as the reference for the relative measurements. In both cases data were collected at 20 nm intervals from 300 nm to 380 nm, at 5 nm intervals from 380 nm to 400 nm and from 890 nm to 920 nm, and at 950 nm and 1000 nm. The absolute and relative overlap points were then used to determine a normalisation constant, as described in Section 12.1.5.

Measurement parameters:

| | |
|---|---|
| Modulation frequency | a.c. |
| f/number | Approximately f/4.8 |

### 12.1.5. Normalisation constant

As outlined above, the absolute responsivity values were obtained by applying a normalisation constant, $C_{\text{norm,avg}}$, to the relative spectral responsivity values determined from the measurements against the pyroelectric reference detector or (in the case of the comparison trap detectors) the single element silicon photodiode comparison detectors. In other words, the absolute responsivity $R(\lambda_i)$ at wavelength $\lambda_i$ was calculated from the corresponding relative spectral responsivity value, $R_{\text{rel}}(\lambda_i)$, using:

$$R(\lambda_i) = C_{\text{norm,avg}} * R_{\text{rel}}(\lambda_i). \qquad (12\text{-}1)$$

The normalisation constant at each overlap point $\lambda_j$ (i.e. 380 nm, 385 nm, 390 nm, 395 nm, 400 nm, 890 nm, 895 nm, 900 nm, 905 nm, 910 nm, 915 nm and 920 nm, where measurements were made against the traps and the pyroelectric or single element comparison detector) was calculated as the ratio of absolute response at that wavelength, $R_{\text{abs}}(\lambda_j)$ (obtained from the measurements against the trap detectors)

[11] Theocharous, E., *The establishment of the NPL Infrared relative spectral responsivity scale using cavity pyroelectric detectors*. Metrologia, 2006, **43**: S115-S119.

to the relative response at that wavelength, $R_{rel}(\lambda_j)$ (obtained from measurements against the pyroelectric or single element comparison detector):

$$C_{\text{norm}}(\lambda_j) = \frac{R_{\text{abs}}(\lambda_j)}{R_{\text{rel}}(\lambda_j)} \quad (12\text{-}2)$$

The average normalisation constants $C_{norm,avg,UV}$ (for the 380 nm to 400 nm region) and $C_{norm,avg,IR}$ (for the 895 nm to 920 nm region) were then calculated using the weighted mean of the results from the relevant overlap wavelengths using:

$$C_{\text{norm,avg}} = \sum_1^n C_{\text{norm}}(\lambda_j)\omega(\lambda_j) \quad (12\text{-}3)$$

where $n$ is the number of overlap wavelengths for the wavelength region considered and the weights $\omega(\lambda_j)$ are given by:

$$\omega(\lambda_j) = \frac{1/u_{\text{abs,c}}^2(\lambda_j)}{\sum_1^n (1/u_{\text{abs,c}}^2(\lambda_j))} \quad (12\text{-}4)$$

Here $u_{\text{abs,c}}(\lambda_j)$ is the combined standard uncertainty associated with the absolute responsivity at each of the overlap wavelengths $\lambda_j$ (see Section 12.4.2).

The reproducibility of the $n$ individual normalisation constants used to calculate the mean (each corresponding to a different 'overlap' wavelength) was allowed for as an additional component in the uncertainty budget (see Tables 12-3 and 12-4). The mean of the uncertainties of the absolute responsivities at the normalisation wavelengths was also included.

## 12.2. Measurement Conditions and Parameters

Each comparison detector was set perpendicular to the incident radiation using the beam reflected from its active area as a guide and was centred on the incident radiation by scanning the detector while monitoring the detector signal. The f-number for the measurements was f/4.8 for measurements in the 300 nm to 400 nm range and 800 nm to 1000 nm range for the comparison single-element detectors, and f/21 for all other measurements. The width of the monochromator slits was set to give a bandwidth of approximately 5 nm (triangular).

The temperature in the laboratory was maintained in the range 22.9 °C to 23.6 °C during the course of the measurements. The temperature of each detector was monitored via the in-built platinum resistance thermometer and the mean resistance values are reported in the tables of results. Humidity was not monitored but the air conditioning system is designed to maintain this within the range 30 % RH to 60 % RH.

## 12.3. Traceability of Measurement

The measurements made by NPL were traceable to the NPL Primary Standard Cryogenic Radiometer. NPL-designed three-element silicon trap detectors were used as reference transfer standards to provide measurements of the absolute spectral response and a cavity pyroelectric detector was used to provide the relative spectral responsivity for wavelengths below 380 nm and above 900 nm. Further details are given in Sections 12.1.3 and 12.1.4 above. The traceability route is shown in Figure 12-2.

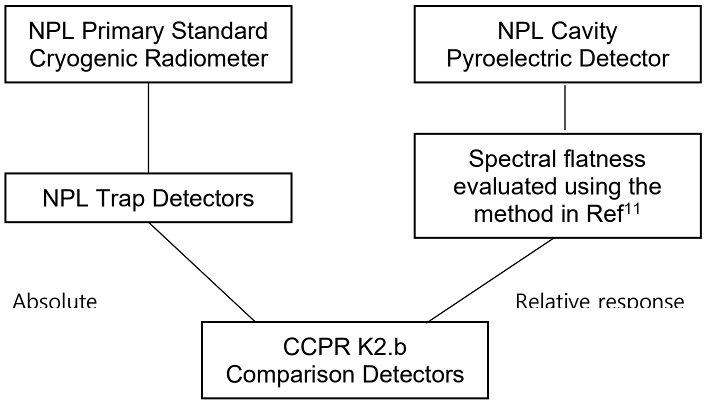


**Figure 12-2. Traceability chain for the NPL measurements for the CCPR-K2.b.2015 comparison.**

## *12.4. Measurement Uncertainty*

### 12.4.1. Uncertainty in the calibration of the reference trap detectors

The expanded uncertainty associated with the calibration of the reference trap detectors against the NPL cryogenic radiometer was 0.02 % at the laser wavelengths of calibration. Table 1 shows the breakdown of these uncertainties; further details are available in Ref[12]. The spectral responsivity of the reference trap detectors at intermediate wavelengths was obtained by interpolation, using a model of the form described in Ref[13] and with the model parameters optimised to minimise the differences between the modelled and measured responsivity at the laser wavelengths. Linear extrapolation of the model parameters was used to extend the spectral responsivity of the traps to 350 nm (the lowest wavelength at which they were calibrated against the NPL cryogenic radiometer was 356.4 nm). At wavelengths above 799.3 nm (the highest wavelength at which a direct measurement of the trap detectors against the NPL cryogenic radiometer was carried out) the responsivity was obtained by extrapolation using a constant quantum efficiency model (note this assumption defines the NPL spectral responsivity scale over this wavelength range).

An additional uncertainty of 0.05 % (rectangular uncertainty distribution) was included at all wavelengths to allow for field of view (FOV) effects for the reference trap detectors, due to the different beam geometries of the cryogenic radiometer and the spectral responsivity facility[12]. Allowing for this and for the uncertainties associated with interpolation/extrapolation increased the expanded uncertainty associated with the calibration of the reference trap detectors to about 1.6 % at 350 nm, 1.1 % at 360 nm, 0.35 % at 380 nm, 0.07 % between 400 nm and 890 nm, 0.08 % at 900 nm and 0.21 % at 920 nm.

**Table 12-1. Uncertainty budget for calibration of the NPL reference trap detectors against the NPL cryogenic radiometer (at laser wavelengths).**

| Uncertainty Component | Standard uncertainty (%) | Type | Probability distribution | Sensitivity coefficient | Contribution (%) | Deg. of freedom | Correlated? |
|---|---|---|---|---|---|---|---|
| cavity absorptance | 0.0012 | B | rectangular | 1 | 0.0012 | ∞ | Y |
| window transmittance | 0.0050 | A | normal | 1 | 0.0050 | ∞ | Y |

[12] Fox, N.P., *Trap Detectors and their Properties* Metrologia, 1991, **28**: 197-202.
[13] Werner, L., Fischer, J., Johannsen, U. and Hartmann, J., *Accurate determination of the spectral responsivity of silicon trap detectors between 238 nm and 1015 nm using a laser-based cryogenic radiometer.* Metrologia, 2000, **37**: 279-284.

| | | | | | | | |
|---|---|---|---|---|---|---|---|
| window scatter | 5.0000 | B | normal | 1/10000 | 0.0005 | ∞ | Y |
| sensitivity of radiometer | 0.0006 | B | rectangular | 1 | 0.0006 | ∞ | Y |
| electrical power measurement | 0.0020 | B | normal | 1 | 0.0020 | ∞ | Y |
| changes in scattered & thermal radiation | 0.0006 | B | rectangular | 1 | 0.0006 | ∞ | N |
| detector dvm calibration | 0.0009 | B | rectangular | 1 | 0.0009 | ∞ | Y |
| detector dvm drift | 0.0003 | B | rectangular | 1 | 0.0003 | ∞ | Y |
| amplifier calibration | 0.0058 | B | rectangular | 1 | 0.0058 | ∞ | Y |
| amplifier drift | 0.0006 | B | rectangular | 1 | 0.0006 | ∞ | Y |
| beam size | 0.0029 | B | rectangular | 1 | 0.0029 | ∞ | Y |
| laser stability | 0.0029 | B | rectangular | 1 | 0.0029 | ∞ | N |
| positional reproducibility | 0.0025 | A | normal | 1 | 0.0025 | ∞ | N |
| measurement repeatability | 0.0040 | A | normal | 1 | 0.0040 | 2 | N |
| | | | | | | | |
| **Combined standard uncertainty (%)** | **--** | **--** | **normal** | **--** | **0.010** | ∞ | **--** |

## 12.4.2. Uncertainty in the calibration of the comparison detectors against the NPL reference trap detectors (wavelength range 380 nm to 900 nm)

The comparison detectors were calibrated in terms of their absolute spectral responsivity directly against the NPL reference trap detectors from 380 nm to 920 nm. The results at the comparison wavelengths in this range are reported and the associated uncertainties are given in Table 12-2. Details of the uncertainty contributions are given in Sections 12.4.2.1 to 12.4.2.10.

**Table 12-2. Uncertainty budget for calibration of comparison detectors against NPL reference trap detectors.**

| **Uncertainty Component** | **Standard uncertainty (%)** | | | **Type** | **Probability distribution** | **Sensitivity coefficient** | **Contribution (%)** | | | **Deg. of freedom** | **Correlated?** |
|---|---|---|---|---|---|---|---|---|---|---|---|
| | **380 nm** | **400 nm – 850 nm** | **900 nm** | | | | **380 nm** | **400 nm – 850 nm** | **900 nm** | | |
| trap detector calibration | 0.010 | 0.010 | 0.010 | B | normal | 1 | 0.010 | 0.010 | 0.010 | ∞ | Y |
| FOV effects | 0.029 | 0.029 | 0.029 | B | rectangular | 1 | 0.029 | 0.029 | 0.029 | ∞ | Y |

| | | | | | | | | | | |
|---|---|---|---|---|---|---|---|---|---|---|
| interpolation* | 0.173 | 0.020 | 0.026 | B | normal | 1 | 0.173 | 0.020 | 0.026 | ∞ | Y |
| ageing since calibration* | 0.116 | 0.018 | 0.011 | B | rectangular | 1 | 0.116 | 0.018 | 0.011 | ∞ | Y |
| monochromator wavelength* | 0.028 | 0.001 | 0.000 | B | rectangular | 1 | 0.028 | 0.001 | 0.000 | ∞ | Y |
| monochromator bandwidth | 0.000 | 0.000 | 0.000 | B | rectangular | 1 | 0.000 | 0.000 | 0.000 | ∞ | Y |
| temperature | 0.000 | 0.000 | 0.000 | B | rectangular | 1 | 0.000 | 0.000 | 0.000 | ∞ | N |
| non-uniformity | 0.012 | 0.012 | 0.012 | B | rectangular | 1 | 0.012 | 0.012 | 0.012 | ∞ | N |
| stray light | 0.000 | 0.000 | 0.000 | B | rectangular | 1 | 0.000 | 0.000 | 0.000 | ∞ | Y |
| electronics | 0.014 | 0.014 | 0.014 | B | rectangular | 1 | 0.014 | 0.014 | 0.014 | ∞ | Y |
| scan repeatability# | 0.013 | 0.001 | 0.001 | A | normal | 1 | 0.013 | 0.001 | 0.001 | 7 | N |
| independent meas. repeatability# | 0.044 | 0.023 | 0.020 | A | normal | 1 | 0.044 | 0.023 | 0.020 | 2 | N |
| polarisation | 0.000 | 0.000 | 0.000 | B | rectangular | 1 | 0.000 | 0.000 | 0.000 | ∞ | Y |
| beam geometry | 0.000 | 0.000 | 0.000 | B | rectangular | 1 | 0.000 | 0.000 | 0.000 | ∞ | Y |
| | | | | | | | | | | | |
| **Combined standard uncertainty (%)** | **--** | **--** | **--** | **--** | **normal** | **--** | **0.218** | **0.050** | **0.050** | ∞ | **--** |

*Varies with wavelength - representative value given

# Typical value; actual value calculated individually for each set of results

### 12.4.2.1. Uncertainty due to trap detector calibration

The expanded uncertainty associated with the calibration of the NPL reference trap detectors against the NPL cryogenic radiometer is given in Table 12-1. The additional uncertainty due to interpolation of the reference trap responsivity is included in Table 12-2.

### 12.4.2.2. Uncertainty due to ageing of the traps

No correction was made for potential ageing of the NPL reference trap detectors since the time of last calibration, but an allowance for this effect was included in the uncertainty budget, based on historical data obtained over a number of years.

### 12.4.2.3. Uncertainty due to wavelength

The standard uncertainty associated with the measured spectral responsivity of the comparison detectors due to uncertainty in the wavelength scale of the monochromator was estimated to be[14]:

[14] Woolliams, E.R., Baribeau, R., Bialek, A., and Cox, M. G., *Spectrometer bandwidth correction for generalized bandpass functions.* Metrologia, 2011, **48**: 164–172.

$$\frac{S_\mathrm{R}(\lambda)}{S_\mathrm{T}(\lambda)}\frac{\partial}{\partial\lambda}\left\{\frac{S_\mathrm{T}(\lambda)}{S_\mathrm{R}(\lambda)}\right\}\frac{u(\lambda)}{\sqrt{3}} \tag{12-5}$$

where $S_\mathrm{R}(\lambda)$ and $S_\mathrm{T}(\lambda)$ are the signals from the reference and test detector respectively, and $u(\lambda)$ is the semi-range for the wavelength scale uncertainty, estimated to be 0.1 nm. The differential term was estimated by:

$$\frac{\phi(\lambda_{i+1})-\phi(\lambda_i)}{\lambda_{i+1}-\lambda_i}+\frac{\phi(\lambda_{i-1})-\phi(\lambda_i)}{\lambda_{i-1}-\lambda_i} \tag{12-6}$$

where $\phi(\lambda) = S_\mathrm{T}(\lambda)/S_\mathrm{R}(\lambda)$.

### 12.4.2.4. Uncertainty due to bandwidth

Measurements were made using a bandwidth of 5 nm, in accordance with the protocol, and therefore it was not necessary to apply any bandwidth correction to the results. Nevertheless, the difference between the spectral responsivity profiles of the reference and comparison detectors meant that the influence of bandwidth on the results had to be considered in the evaluation of the measurement uncertainty. The uncertainty due to bandwidth was estimated by calculating the size of the bandwidth correction (the correction to be applied to obtain the 'true' value for infinitely narrow bandwidth), using a 3-point correction method and assuming a triangular bandpass function[14] i.e. using:

$$C_0=\left[-\frac{\Delta^2}{12\delta^2}\right]M_{-1}+\left[1+\frac{\Delta^2}{6\delta^2}\right]M_0+\left[-\frac{\Delta^2}{12\delta^2}\right]M_{+1} \tag{12-7}$$

where $C_0$ is the corrected value for the wavelength being considered, $\Delta$ is the bandwidth, $\delta$ is the measurement step interval and $M_0$, $M_{-1}$ and $M_{+1}$ are, respectively, the measured values at the wavelength being considered, the wavelength point one below this and the wavelength point one above this. The difference between $C_0$ and $M_0$ was found to be very small in all cases, meaning that even if the uncertainty due to bandwidth was taken as being equal to the size of the resultant bandwidth correction (a gross over-estimate of the likely uncertainty), it had negligible impact on the final measurement uncertainty.

### 12.4.2.5. Uncertainty due to temperature

The temperature coefficient of response of trap detectors was determined in the CCPR-K2.b comparison and was taken to be representative of the NPL three element reference trap detectors as these are made from the same type of diodes (i.e. Hamamatsu S1337)[15]. The temperature of the reference trap detectors was highly stable during the course of the measurements and therefore this temperature coefficient was estimated to have a negligible impact on the measurement uncertainty.

The temperature of the comparison detectors was measured and is reported as part of the results (in the form of the measured resistance of the associated PRT). The variations in the temperature of the comparison detectors during measurement were small and therefore the associated uncertainty was assumed to be negligible.

[15] R. Goebel and M. Stock., *Report on the key comparison CCPR-K2.b of spectral responsivity measurements in the wavelength range 300 nm to 1000 nm. Metrologia,* 2004, **41**: 02004.

### 12.4.2.6. Uncertainty due to detector non-uniformity

The uncertainty due to non-uniformity of the reference trap detectors was based on previous research[12]. The test detectors were realigned several times during the course of the measurements, with the orientation being changed as part of each realignment. As a result, the uncertainties due to non-uniformities in the test detectors and/or beam were included as part of the 'independent measurement repeatability' component of the uncertainty budget.

### 12.4.2.7. Uncertainty due to stray light

The stray light performance of the monochromator has been estimated in the past using combinations of filters. As expected for a well-designed double monochromator, the stray light performance was found to be good, and to have negligible impact on the measurement uncertainty.

### 12.4.2.8. Uncertainty due to electronics

The uncertainty associated with the electronics (amplifier and DVM, including linearity and gain effects) was estimated based on the associated electrical calibration uncertainties, historical data relating to drift in the calibration values over time, and manufacturer's data. The range of signal levels used during the measurements was small, meaning that uncertainties due to linearity in particular were also small.

### 12.4.2.9. Uncertainty due to random effects ('scan repeatability' and 'independent measurement repeatability')

The standard uncertainties due to random effects for an individual determination of detector responsivity was estimated as the standard error associated with the mean (SEOM) for a series of spectral scans, given by:

$$\sigma_{\text{scan}}=\sigma/\sqrt{N} \qquad (12\text{-}8)$$

where $N$ is the number of spectral scans (usually 8) and $\sigma$ is the standard deviation of these scans. By its nature, the random error varied for each independent determination of detector responsivity. However, it was observed that for a given detector at a given wavelength, the SEOM was similar for each determination, and it was therefore reasonable to take the average value of SEOM from the 3 independent measurements for the uncertainty budget. This is included in the uncertainty budget under the heading 'scan repeatability'.

The detectors were realigned for each independent measurement, as described in Section 12.1.2, and this would be expected to result in some additional random variation in the results, beyond that determined from the SEOM of the repeated scans. This additional uncertainty, $u_{\text{repro}}(\lambda)$, was calculated using:

$$\text{If } \sigma_{\text{repeat}}(\lambda) \leq u_{\text{scan}}(\lambda) \text{ then } u_{\text{repro}}(\lambda) = 0,$$
$$\text{otherwise } u_{\text{repro}}(\lambda) = \sqrt{\sigma_{\text{repeat}}^2(\lambda) - u_{\text{scan}}^2(\lambda)} \qquad (12\text{-}9)$$

where $\sigma_{\text{repeat}}(\lambda)$ is the standard error associated with the mean (SEOM) for the series of independent measurements. This is included in the uncertainty budget under the heading 'independent measurement repeatability'. As indicated in 12.4.2.6, this also included the uncertainty due to detector non-uniformity since the detector was realigned (and re-orientated) for each independent measurement.

#### 12.4.2.10. Uncertainties due to polarisation and beam geometry

The uncertainties associated with polarisation and beam geometry (vignetting of the trap and beam divergence effects) were all considered to be negligible, based on the results of previous investigations.

### 12.4.3. Uncertainty in the measurement of the single element comparison detectors against the cavity pyroelectric detector

As discussed previously, the single element comparison detectors were calibrated in terms of their relative spectral responsivity against the NPL reference cavity pyroelectric detector at 20 nm intervals from 300 nm to 380 nm, at 5 nm intervals from 380 nm to 400 nm and from 890 nm to 920 nm, and at 950 nm and 1000 nm. The results from 380 nm to 400 nm and 890 nm to 920 nm were combined with those from measurements against the reference trap detectors to determine a normalisation constant for each single element comparison detector, which was used to transform the relative measurements at 300 nm, 320 nm, 340 nm, 360 nm, 950 nm and 1000 nm to absolute values, as described in Section 12.1.5.

The uncertainty budget for the absolute calibration at these wavelengths is given in Table 12-3; details of the uncertainty contributions are given in Sections 12.4.3.1 to 12.4.3.11.

**Table 12-3. Uncertainty budget for calibration of single element comparison detectors against NPL reference pyroelectric detector (note uncertainties vary slowly with wavelength – results at selected wavelengths only are quoted).**

| Uncertainty Component | Standard uncertainty (%) | | | | Type | Probability distribution | Sensitivity coefficient | Contribution (%) | | | | Deg. of free dom | Correlated? |
|---|---|---|---|---|---|---|---|---|---|---|---|---|---|
| | 300 nm | 340 nm | 950 nm | 1000 nm | | | | 300 nm | 340 nm | 950 nm | 1000 nm | | |
| pyroelectric spectral flatness | 0.058 | 0.058 | 0.058 | 0.058 | B | rectangular | 1 | 0.058 | 0.058 | 0.058 | 0.058 | ∞ | Y |
| monochromator wavelength* | 0.030 | 0.003 | 0.001 | 0.006 | B | rectangular | 1 | 0.030 | 0.003 | 0.001 | 0.006 | ∞ | Y |
| monochromator bandwidth | 0.000 | 0.000 | 0.000 | 0.000 | B | rectangular | 1 | 0.000 | 0.000 | 0.000 | 0.000 | ∞ | Y |
| temperature | 0.087 | 0.087 | 0.087 | 0.087 | B | rectangular | 1 | 0.087 | 0.087 | 0.087 | 0.087 | ∞ | Y |
| non-uniformity | 0.046 | 0.046 | 0.046 | 0.046 | B | rectangular | 1 | 0.046 | 0.046 | 0.046 | 0.046 | ∞ | Y |
| stray light | 0.000 | 0.000 | 0.000 | 0.000 | B | rectangular | 1 | 0.000 | 0.000 | 0.000 | 0.000 | ∞ | Y |
| electronics | 0.014 | 0.014 | 0.014 | 0.014 | B | rectangular | 1 | 0.014 | 0.014 | 0.014 | 0.014 | ∞ | Y |
| non-linearity | 0.058 | 0.058 | 0.058 | 0.058 | B | rectangular | 1 | 0.058 | 0.058 | 0.058 | 0.058 | ∞ | Y |
| scan repeatability # | 0.039 | 0.032 | 0.045 | 0.025 | A | normal | 1 | 0.039 | 0.032 | 0.045 | 0.025 | 7 | N |
| independent meas. repeatability # | 0.104 | 0.067 | 0.065 | 0.019 | A | normal | 1 | 0.104 | 0.067 | 0.065 | 0.019 | 1 | N |

| | | | | | | | | | | | | | |
|---|---|---|---|---|---|---|---|---|---|---|---|---|---|
| polarisation/ beam geometry | 0.000 | 0.000 | 0.000 | 0.000 | B | rectangular | 1 | 0.000 | 0.000 | 0.000 | 0.000 | ∞ | Y |
| normalisation (systematic) * | 0.290 | 0.290 | 0.000 | 0.000 | B | rectangular | 1 | 0.290 | 0.290 | 0.000 | 0.000 | ∞ | Y |
| normalisation (random)# | 0.064 | 0.064 | 0.028 | 0.028 | A | normal | 1 | 0.064 | 0.064 | 0.028 | 0.028 | 2 | N |
| absolute responsivity from traps# | 0.168 | 0.168 | 0.068 | 0.068 | B | normal | 1 | 0.168 | 0.168 | 0.068 | 0.068 | ∞ | Y |
| | | | | | | | | | | | | | |
| **Combined standard uncertainty (%)** | **--** | | **--** | **--** | **--** | **normal** | **--** | **0.383** | **0.372** | **0.168** | **0.152** | ∞ | **--** |

* Varies with wavelength - representative value given

\# Typical value; actual value calculated individually for each set of results

### 12.4.3.1. Uncertainty due to spectral flatness of cavity pyroelectric detector

The spectral flatness of the cavity pyroelectric reference detector has been estimated by measuring the change in response of the pyroelectric detector with and without the cavity in place, following the method of Theocharous[11]; the associated uncertainty is included in the uncertainty budget. Since the pyroelectric detector was used only to determine the relative spectral responsivity, and not to assign absolute values, there was no need to include any additional uncertainty for its absolute calibration. Furthermore, there was no allowance made for ageing of the cavity pyroelectric reference detector, since measurements have shown this type of detector to be highly stable with time[11].

### 12.4.3.2. Uncertainty due to wavelength and bandwidth

These uncertainties were analysed as described in Sections 12.4.2.3 and 12.4.2.4 above. As in the case of the calibration of the comparison detectors against the trap detectors, the uncertainty due to bandwidth effects was found to be negligibly small for the calibration of the comparison detectors against the pyroelectric detector.

### 12.4.3.3. Uncertainty due to temperature

The temperature coefficient of response of the cavity pyroelectric reference detector was taken to be approximately 0.15 % $°C^{-1}$ based on previous measurements[11]. The temperature of the pyroelectric detector was controlled to well within ±1 °C during the course of the measurements and therefore the uncertainty due to temperature drifts for the pyroelectric was taken to be 0.15 % (rectangular).

The temperature of the comparison detectors was measured and is reported as part of the results (in the form of the measured resistance of the associated PRT). The variations in the temperature of the comparison detectors during measurement were small and therefore the associated uncertainty was assumed to be negligible.

### 12.4.3.4. Uncertainty due to detector uniformity

The uncertainty due to non-uniformity of the cavity pyroelectric reference detector was based on previous research[11]. The test detectors were realigned between each independent measurement, with the orientation being changed as part of each realignment. As a result, the uncertainties due to non-uniformities in the test detectors and/or beam were included as part of the 'independent measurement repeatability' component of the uncertainty budget.

#### 12.4.3.5. Uncertainty due to stray light

As described in 12.4.2.7, the expected stray light performance of the double monochromator used for these measurements was found to be good, and to have negligible impact on the measurement uncertainty.

#### 12.4.3.6. Uncertainty due to electronics

The uncertainty associated with the electronics (DVM, preamplifier and chopper) was estimated based on the associated electrical calibration uncertainties, historical data relating to drift in the calibration values over time, and manufacturer's data.

#### 12.4.3.7. Uncertainty due to lock-in-non-linearity

The uncertainty associated with the non-linearity of the lock-in amplifier was estimated based on manufacturer's data.

#### 12.4.3.8. Uncertainty due to random effects ('scan repeatability' and 'independent measurement repeatability')

The standard uncertainties due random effects were evaluated as described in Section 12.4.2.9.

#### 12.4.3.9. Uncertainties due to polarisation and beam geometry effects

The uncertainties associated with polarisation and beam geometry were considered to be negligible, based on the results of previous investigations.

#### 12.4.3.10. Uncertainty due to normalisation

The reproducibility of the individual normalisation constants (each corresponding to a different 'overlap point') was allowed for as an additional component in the uncertainty budget. In the case of the IR measurements the normalisation constant showed entirely random behaviour as a function of wavelength. However, for the UV wavelengths a significant systematic shift with wavelength was seen, which was allowed for through the inclusion of the 'normalisation (systematic) uncertainty' term in Table 12-3.

#### 12.4.3.11. Uncertainty due to absolute responsivity against traps

The mean of the combined standard uncertainties associated with the absolute responsivity at each of the overlap wavelengths, $u_{\mathrm{abs,c}}(\lambda_j)$, obtained from calibration against the trap detectors (see Section 12.4.2), was allowed for as an additional component in the uncertainty budget. Only Type B effects were considered, since the Type A (random) effects were included in the normalisation uncertainties.

### 12.4.4. Uncertainty in the measurement of the trap comparison detectors against the single element comparison detectors

As discussed previously, the trap comparison detectors could not be calibrated in terms of their relative spectral responsivity against the NPL reference cavity pyroelectric detector outside of the NPL trap region (i.e. for wavelengths below 380 nm and above 920 nm); instead the single element comparison detectors were used as a reference for the UV and IR regions. In all other respects the calibration was as described in 12.4.3. Measurements were made at 20 nm intervals from 300 nm to 380 nm, at 5 nm intervals from 380 nm to 400 nm and from 890 nm to 920 nm, and at 950 nm and 1000 nm. The results at the overlap wavelengths (380 nm to 400 nm and 890 nm to 920 nm) were combined with those from measurements against the reference trap detectors to determine a normalisation constant for each trap comparison detector, which was used to transform the relative measurements at 300 nm, 320 nm, 340 nm, 360 nm, 950 nm and 1000 nm to absolute values, as described in Section 12.1.5. The uncertainty budget for the absolute calibration at these wavelengths is given in Table 12-4; details of the uncertainty contributions are given in Sections 12.4.4.1 to 12.4.4.10.

**Table 12-4. Uncertainty budget for calibration of trap comparison detectors against single element comparison detectors (note uncertainties vary slowly with wavelength – results at selected wavelengths only are quoted).**

| Uncertainty Component | Standard uncertainty (%) | | | | Type | Probability distribution | Sensitivity coefficient | Contribution (%) | | | | Deg. of freedom | Correlated? |
|---|---|---|---|---|---|---|---|---|---|---|---|---|---|
| | 300 nm | 340 nm | 950 nm | 1000 nm | | | | 300 nm | 340 nm | 950 nm | 1000 nm | | |
| single element comparison detector* | 0.383 | 0.372 | 0.168 | 0.151 | B | normal | 1 | 0.383 | 0.372 | 0.168 | 0.151 | ∞ | Y |
| monochromator wavelength* | 0.017 | 0.011 | 0.004 | 0.007 | B | rectangular | 1 | 0.017 | 0.011 | 0.004 | 0.007 | ∞ | Y |
| monochromator bandwidth | 0.000 | 0.000 | 0.000 | 0.000 | B | rectangular | 1 | 0.000 | 0.000 | 0.000 | 0.000 | ∞ | Y |
| temperature | 0.000 | 0.000 | 0.000 | 0.000 | B | rectangular | 1 | 0.000 | 0.000 | 0.000 | 0.000 | ∞ | Y |
| non-uniformity | 0.000 | 0.000 | 0.000 | 0.000 | B | rectangular | 1 | 0.000 | 0.000 | 0.000 | 0.000 | ∞ | Y |
| stray light | 0.000 | 0.000 | 0.000 | 0.000 | B | rectangular | 1 | 0.000 | 0.000 | 0.000 | 0.000 | ∞ | Y |
| electronics and non-linearity | 0.014 | 0.014 | 0.014 | 0.014 | B | rectangular | 1 | 0.014 | 0.014 | 0.014 | 0.014 | ∞ | Y |
| scan repeatability # | 0.006 | 0.006 | 0.002 | 0.002 | A | normal | 1 | 0.006 | 0.006 | 0.002 | 0.002 | 7 | N |
| independent meas. repeatability # | 0.079 | 0.077 | 0.025 | 0.034 | A | normal | 1 | 0.079 | 0.077 | 0.025 | 0.034 | 2 | N |
| polarisation/ beam geometry | 0.000 | 0.000 | 0.000 | 0.000 | B | rectangular | 1 | 0.000 | 0.000 | 0.000 | 0.000 | ∞ | Y |
| normalisation (random)# | 0.069 | 0.069 | 0.018 | 0.018 | A | normal | 1 | 0.069 | 0.069 | 0.018 | 0.018 | 2 | N |
| | | | | | | | | | | | | | |
| **Combined standard uncertainty (%)** | -- | | -- | -- | -- | **normal** | -- | **0.397** | **0.387** | **0.172** | **0.157** | ∞ | -- |

* Varies with wavelength - representative value given

# Typical value; actual value calculated individually for each set of results

#### 12.4.4.1.Uncertainty due to calibration of single element comparison detector

This was taken directly from the calibration results for the single element comparison detectors.

#### 12.4.4.2. Uncertainty due to wavelength and bandwidth

These uncertainties were analysed as described in Sections 12.4.2.3 and 12.4.2.4 above.

#### 12.4.4.3. Uncertainty due to temperature

The temperature of the comparison detectors was measured and is reported as part of the results (in the form of the measured resistance of the associated PRT). The variations in the temperature of the comparison detectors during measurement were small and therefore the associated uncertainty was assumed to be negligible.

#### 12.4.4.4. Uncertainty due to detector uniformity

The detectors were realigned between each independent measurement, with the orientation being changed as part of each realignment. As a result, the uncertainties due to due to non-uniformities in the detectors and/or beam were included as part of the ‘independent measurement repeatability’ component of the uncertainty budget.

#### 12.4.4.5. Uncertainty due to stray light

As described in 12.4.2.7, the expected stray light performance of the double monochromator used for these measurements was found to be good, and to have negligible impact on the measurement uncertainty.

#### 12.4.4.6. Uncertainty due to electronics and non-linearity

The uncertainty associated with the electronics (amplifier and DVM, including linearity and gain effects) was estimated based on the associated electrical calibration uncertainties, historical data relating to drift in the calibration values over time, and manufacturer’s data. The range of signal levels used during the measurements was small, meaning that uncertainties due to linearity in particular were also small.

#### 12.4.4.7. Uncertainty due to random effects (‘scan repeatability’ and ‘independent measurement repeatability’)

The standard uncertainties due random effects were evaluated as described in Section 12.4.2.9.

#### 12.4.4.8. Uncertainties due to polarisation and beam geometry effects

The uncertainties associated with polarisation and beam geometry were considered to be negligible, based on the results of previous investigations.

#### 12.4.4.9. Uncertainty due to normalisation

The reproducibility of the individual normalisation constants (each corresponding to a different ‘overlap point’) was allowed for as an additional component in the uncertainty budget. The normalisation constant showed entirely random behaviour as a function of wavelength in both the UV and IR regions and no ‘normalisation (systematic) uncertainty’ was required in this case.

### 12.4.4.10. Uncertainty due to absolute responsivity against traps

The combined standard uncertainties associated with the absolute responsivity at each of the overlap wavelengths, $u_{\mathrm{abs,c}}(\lambda_j)$, obtained from calibration against the trap detectors (see Section 12.4.2), had already been included in the absolute calibration of the single element comparison detectors and therefore did not need to be included again.

# CCPR-K2.b.2016

# Spectral Responsivity 300 nm to 1000 nm

# Final Report

# Appendix C

# Report on Stability Test of Transfer Detectors

## CCPR k2.b.2016 Detector Stability results as measured at NIST, 2021-11

Introduction:

The CCPR-K2.b.2016 is a star patterned intercomparison of the spectral power responsivity (ASR) with KRISS as the pilot laboratory and measurements conducted from 2015 through to 2018. Preliminary results from the intercomparison showed a +/- 0.4% change in the Si photodiodes as measured before round 3 and then after round 3 (Figure 1).

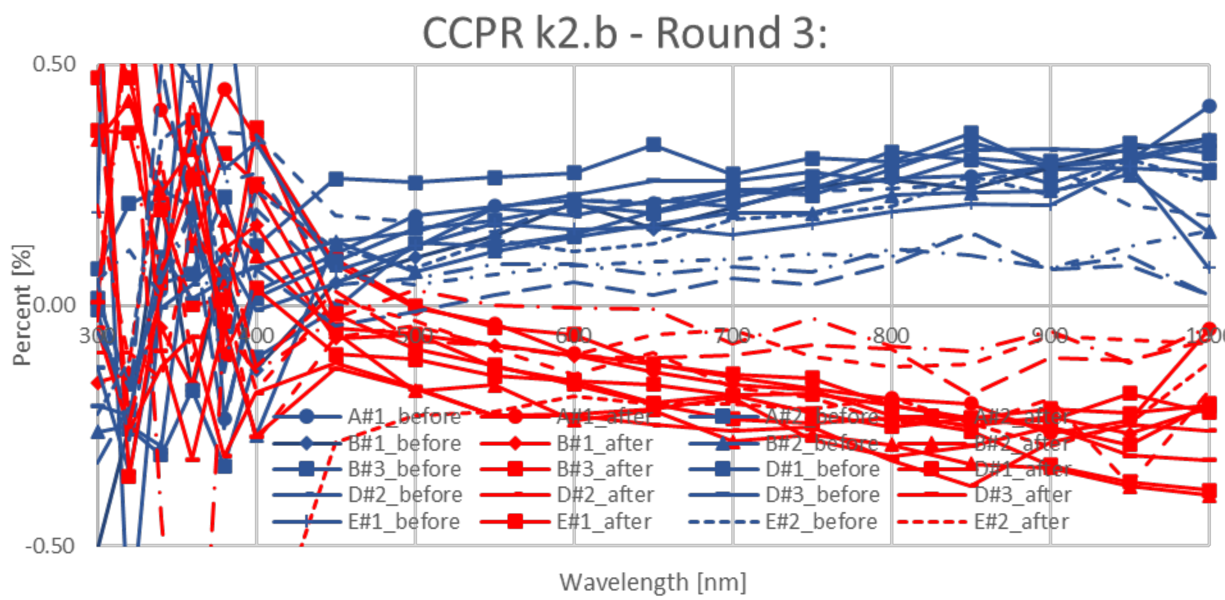


Figure 1: The changes shown by the KRISS measurements in the different intercomparison artifacts before and after the 3rd round.

One suggested cause to the large ASR changes was the photodiode's stability. In a meeting of the intercomparison participants it was agreed that the detector stability, for both single element and trap devices, needed to be determined before a decision was made as to the next step in the intercomparison.

NIST agreed to work with KRISS in the detector stability determinations.

**<u>Detector Stability Measurements: The chosen devices and protocol</u>**

KRISS and NIST agreed to the protocol listed below for the detector stability measurements. We agreed for both KRISS and NIST to measure the same set of detectors, Set A. Set A consists of 3 single element devices, A#1, A#2, A#3, and 2 trap devices, A#4, and A#5. Initially it was agreed that Set A would be measured in a star pattern with KRISS measuring the devices 3 times while NIST measured twice. The Set A detectors were measured by KRISS in August-September2021 and then by NIST in October-November 2021. The Set A detectors were measured by NIST in 2017 for round 3 of the CCPR k2.b intercomparison.

The protocols for the detector stability measurement include:

1. KRISS would perform initial cleaning of the single element devices before the stability tests started.
2. The devices were not to be cleaned during the measurement process.
3. The ASR measurement range was from 300 nm to 1000 nm.
4. The temperature on the detectors were not measured during these stability measurements.
5. Measurements of each device's uniformities were to be performed, 3 single element and 2 trap detectors, at 400 nm, 550 nm, 800 nm.

The alignments of all 5 devices were to use the CCPR k2.b intercomparison protocols.

**NIST's measurements of the Set A artifacts**

In 2017 NIST followed the stated CCPR k2.b protocols for the intercomparison but also included additional, more extensive measurements to characterize the Set A artifacts. NIST measured the ASR from 300 nm to 1000 nm in 5 nm steps, as well as the spatial power responsivity uniformity of the devices at multiple wavelengths, 300 nm, 350 nm, 400 nm, 500 nm, 800 nm, 900 nm, 950 nm, and 1000 nm. The spatial power responsivity uniformities were measured to better understand the reproducibility contributions to the measurements. The additional uniformity measurements below 400 nm and above 800 nm were to understand the artifacts where the silicon diode's performance was not optimal.

In 2021 NIST measured Set A using the same parameters for the 2021 detector stability tests, both uniformity and ASR.

**Alignment of the Artifacts:**

At NIST the artifacts were aligned using the CCPR k2.b protocols. The single element devices were first positioned in the focal plane of the beam. Using a laser that defines the beam path, the Si photodiode was angularly aligned for the beam to reflect back onto the optical path. Finally, the alignment jig was positioned in the detector housing and the 1 mm by 1 mm beam focused QTH beam was located its center.

The trap detectors were measured by first moving the capped artifact to the detector plane with the focus at the cap. The traps' angular alignment was found using the same method as the single element devices. The beam was positioned to the alignment jig's center then moved forward along the optical path 25 mm to locate the focus on the 3$^{rd}$ diode's reflective surface. The distance from the cap to the 3$^{rd}$ surface was determined by both a calculation from the drawings in the protocol and by the measured ASR with the trap positioned along the range of +/- 37 mm from that calculated distance. The largest value ASR occurred over a few mm distance along the optical path and indicated that the beam was not clipped. The center distance of the plateaued ASR signals was the position for the measurements.

**The Measurements:**

The single photodiode devices A1, A2, and A3 were measured from 300 nm to 1000 nm every 5 nm. Each photodiode was aligned with the ASR measured three times per alignment. The spatial spectral power responsivities were measured at 300 nm, 350 nm, 400 nm, 550 nm, 800 nm, 900 nm, 950 nm, and 1000 nm to compare to the 2017 uniformity mappings. The detectors were realigned two more times to determine the reproducibility uncertainty

The spectral power responsivities for the traps, A4 and A5, were also measured using 3 alignments, each alignment included the three repeatability measurements. The same wavelengths were used for the initial uniformity mappings, but in the subsequent alignments the uniformities were measured at 300 nm, 400 nm, 550 nm, 800 nm, and 1000nm.

An evaluation of the measured trap uniformities at the different alignments showed that there was a large difference in the "center" location as defined by the different jig alignments. The spectral power uniformity mappings showed that active areas were not centered nor repeatable in position when the alignment jig was positioned in the trap cap. The best center alignment occurred when the jig was positioned in the detector housing directly. Additional measurements were made to determine the effect of the jig placement on the trap center positioning and resulting ASRs.

**The 2021 Detector Stability Results – Repeatability, and Reproducibility:**

Both single element and trap detectors were measured using three separate alignments to determine reproducibility uncertainty. For most all the devices the repeatability in each set of measurements as well as the reproducibility of the three alignments were determined. Alignment 3 for A3 had only one ASR measurement. The repeatability of the single element detectors was about 0.002% and the reproducibility was 0.004% in the visible range. The trap's repeatability was similar to the single element devices but reproducibility was by a factor of 10 larger than the single element devices.

The repeatabilities and reproducibilities are shown in the figures below.

A1 Repeatability

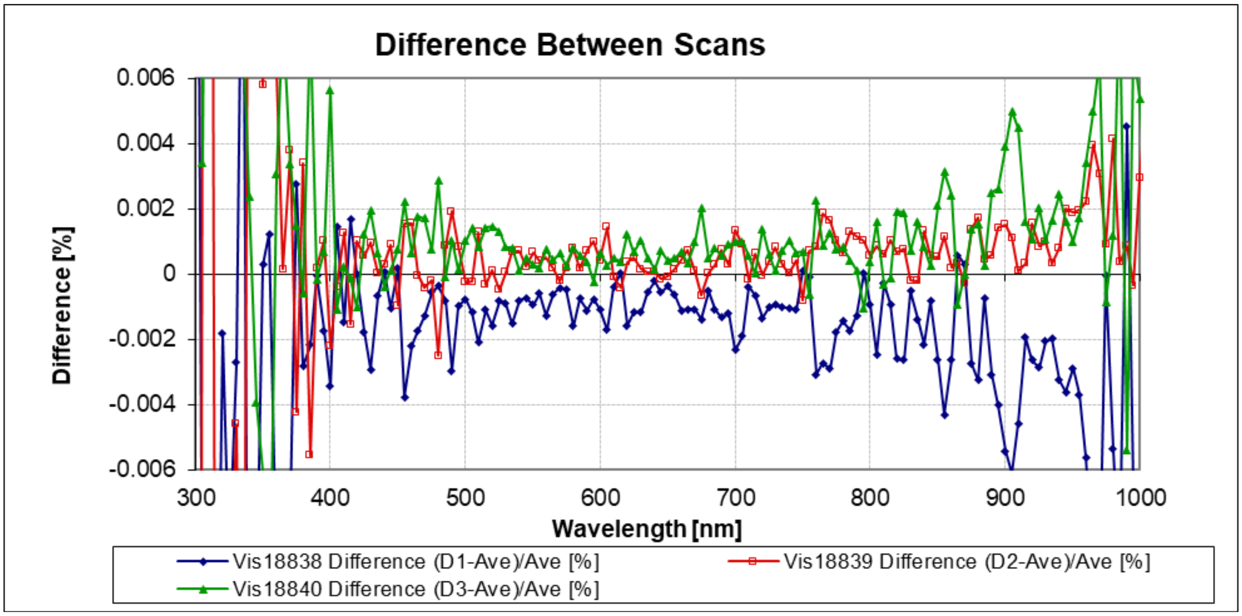


Figure 1a: Repeatability of A1 1st alignment

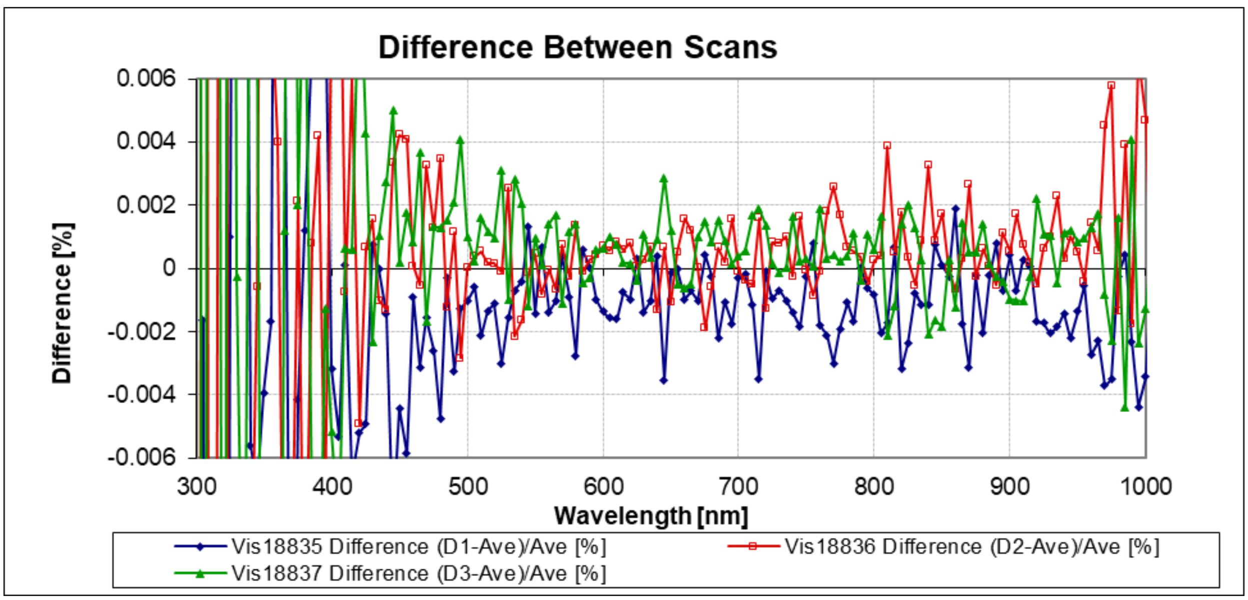


Figure 1b: Repeatability of A1 2nd alignment

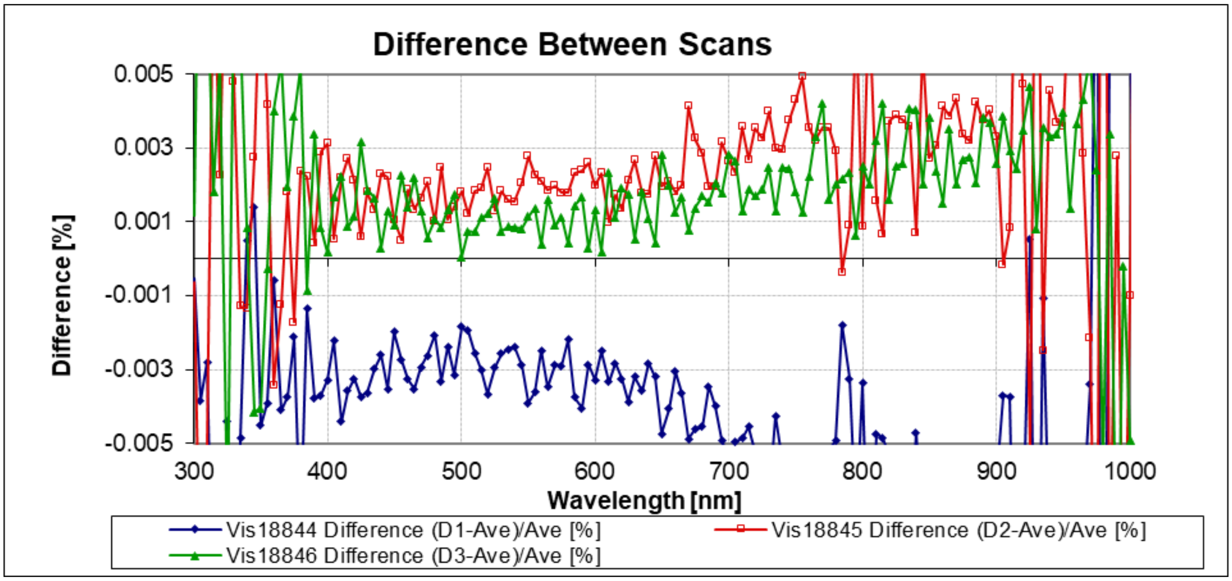


Figure 1c: Repeatability of A1 3rd alignment

<u>A1 Reproducibility</u>

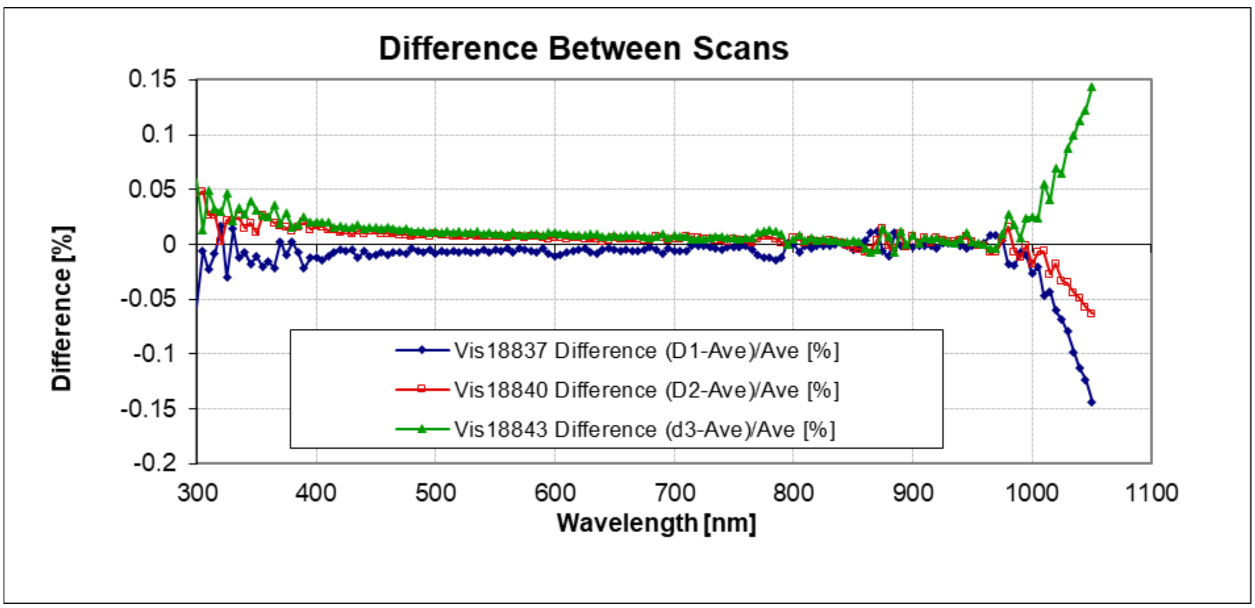


Figure 2: Reproducibility of A1 measurements

A2 Repeatability

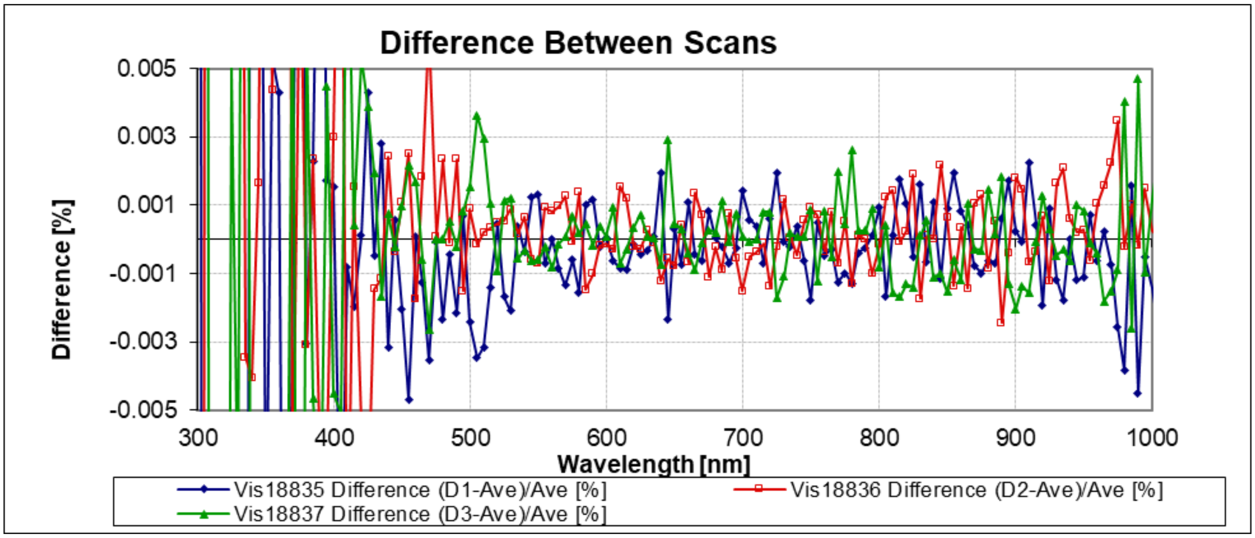


Figure 3a: Repeatability of A2 1st alignment

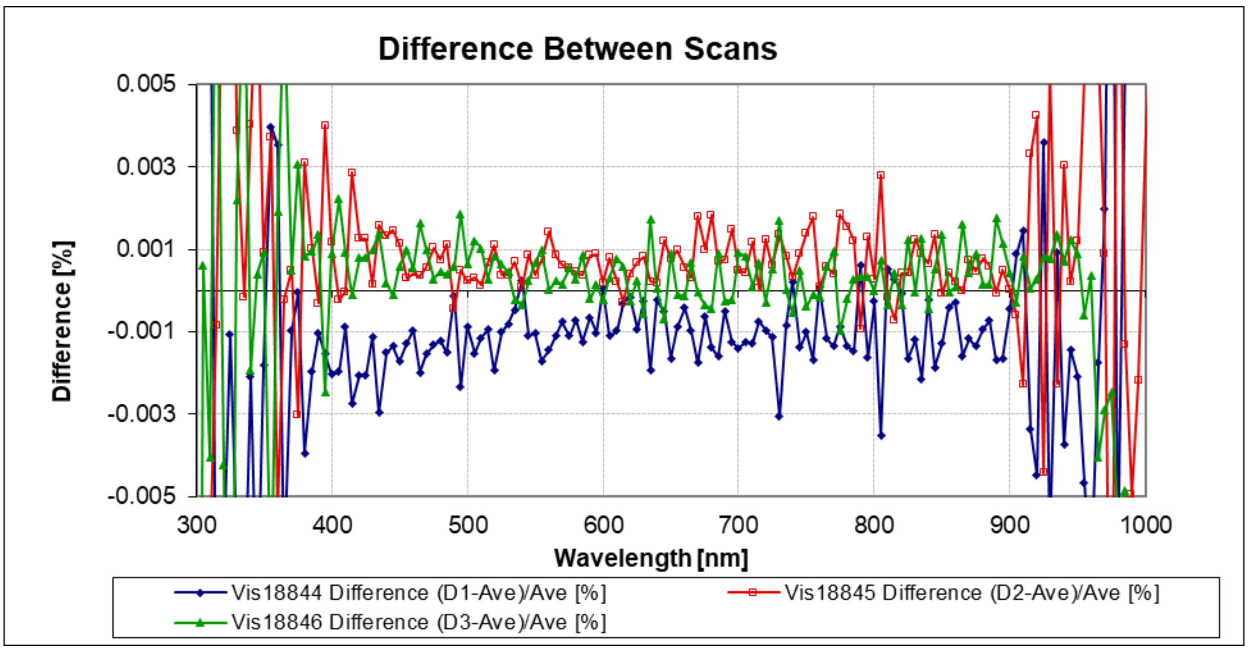


Figure 3b: Repeatability of A2 2nd alignment

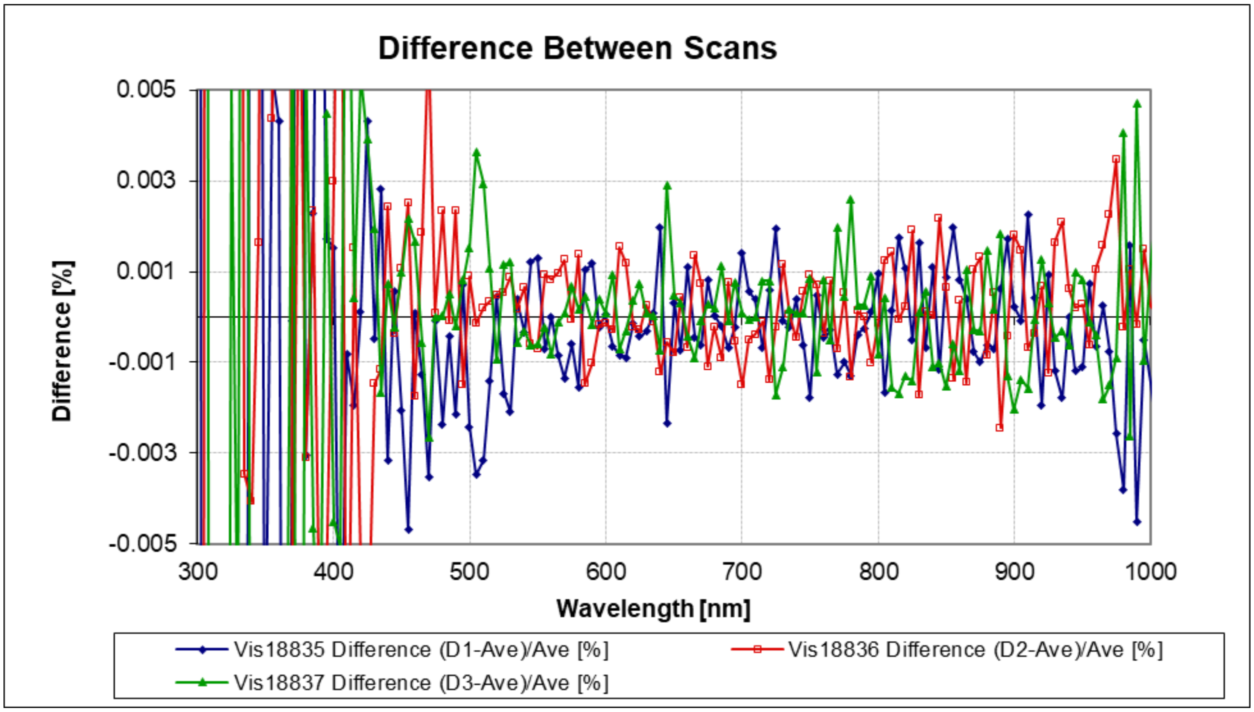


Figure 3c: Repeatability of A2 3rd alignment

A2 Reproducibility

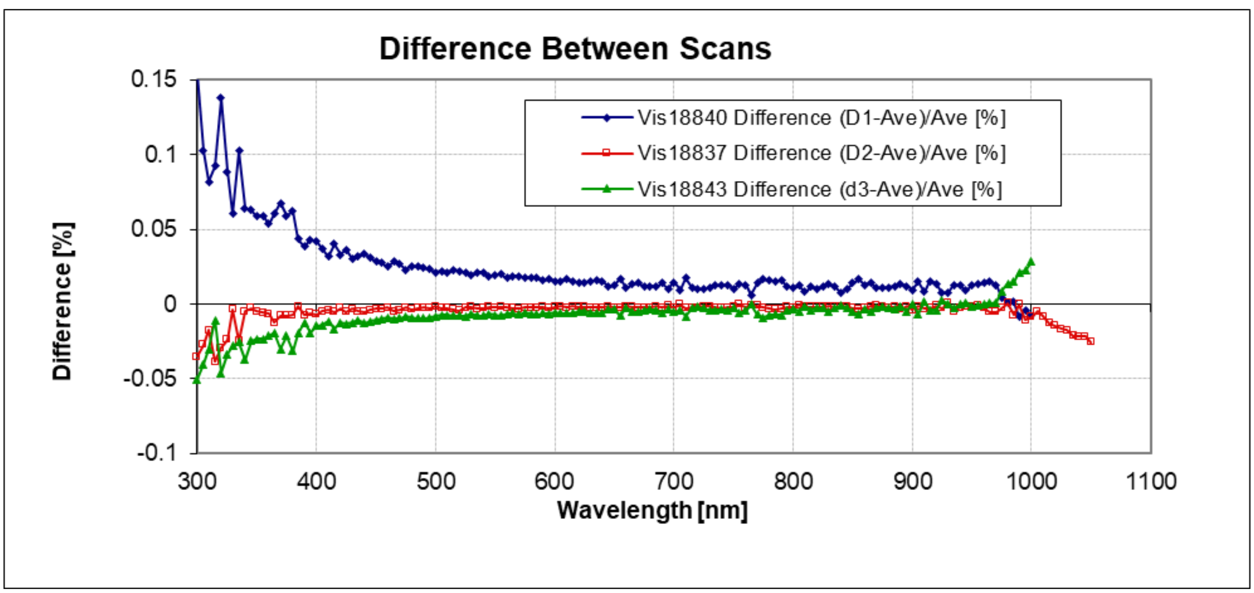


Figure 4: Reproducibility of A2 measurements

A3 Repeatability

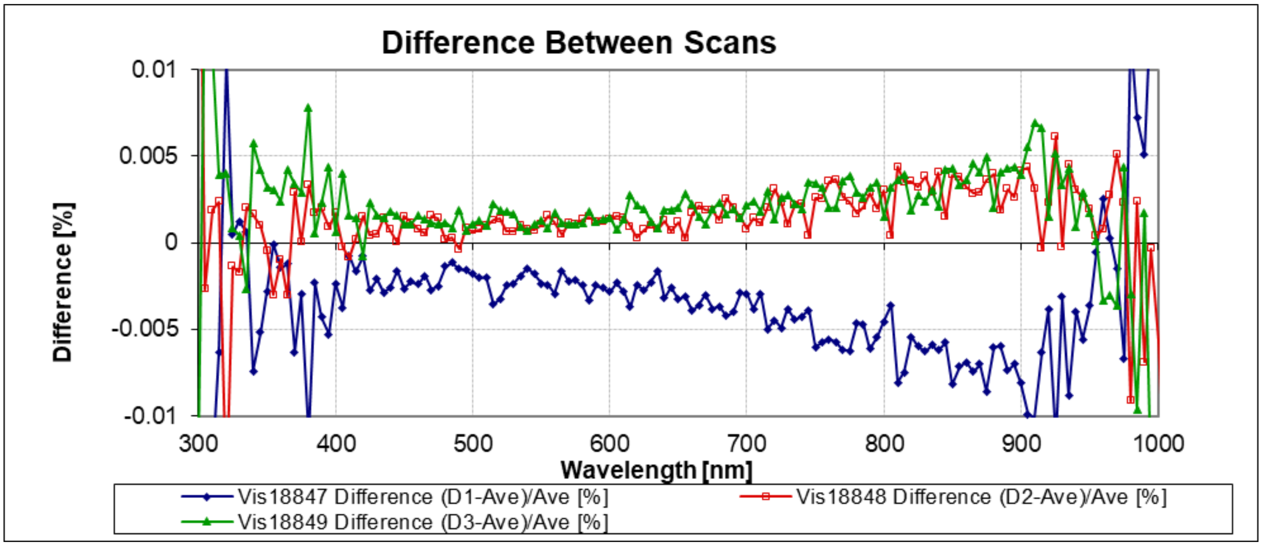


Figure 5a: Repeatability of A3 1st alignment

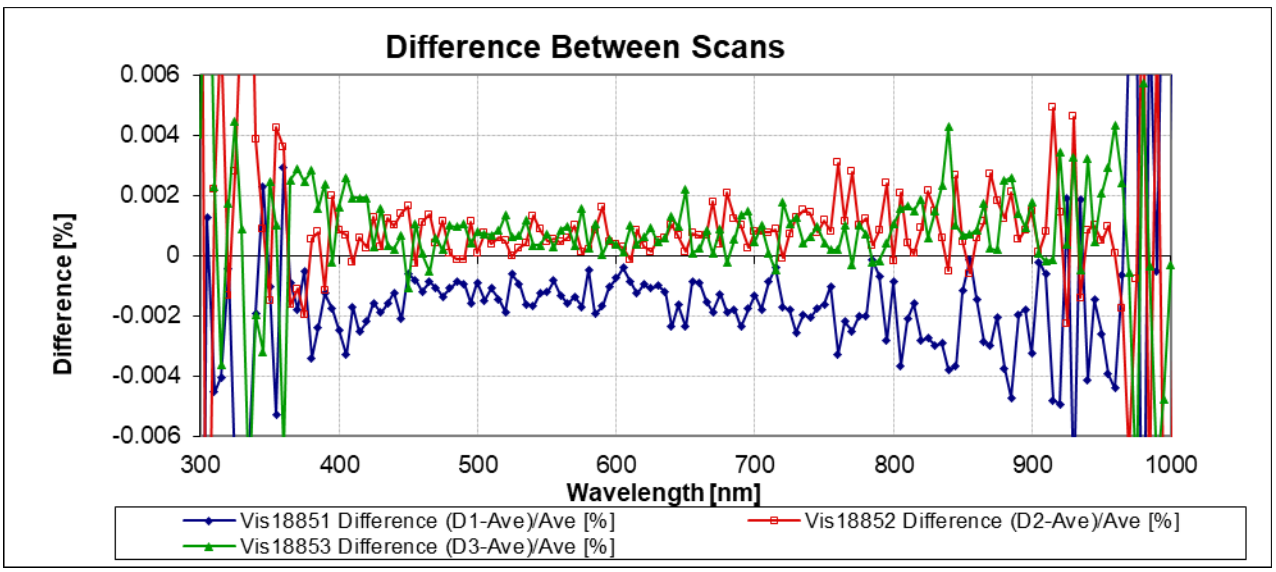


Figure 5b: Repeatability of A3 2nd alignment

A3 Reproducibility

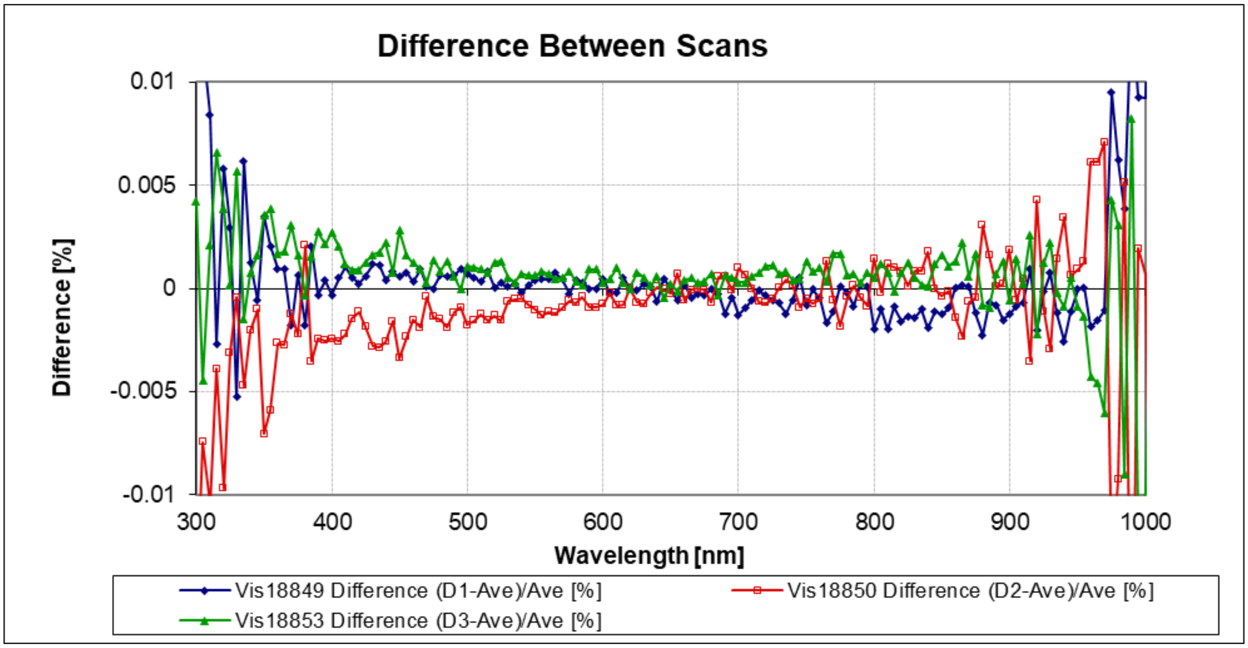


Figure 6: Reproducibility of A3 measurements

A4 Repeatability

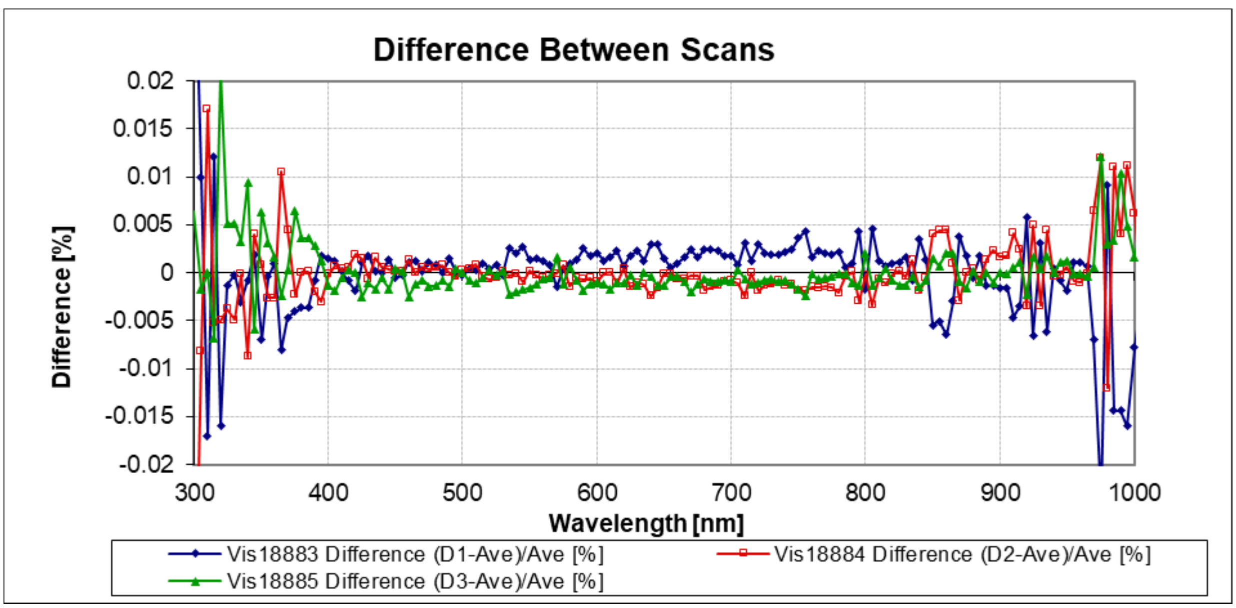


Figure 7a: Repeatability of A4 1st alignment

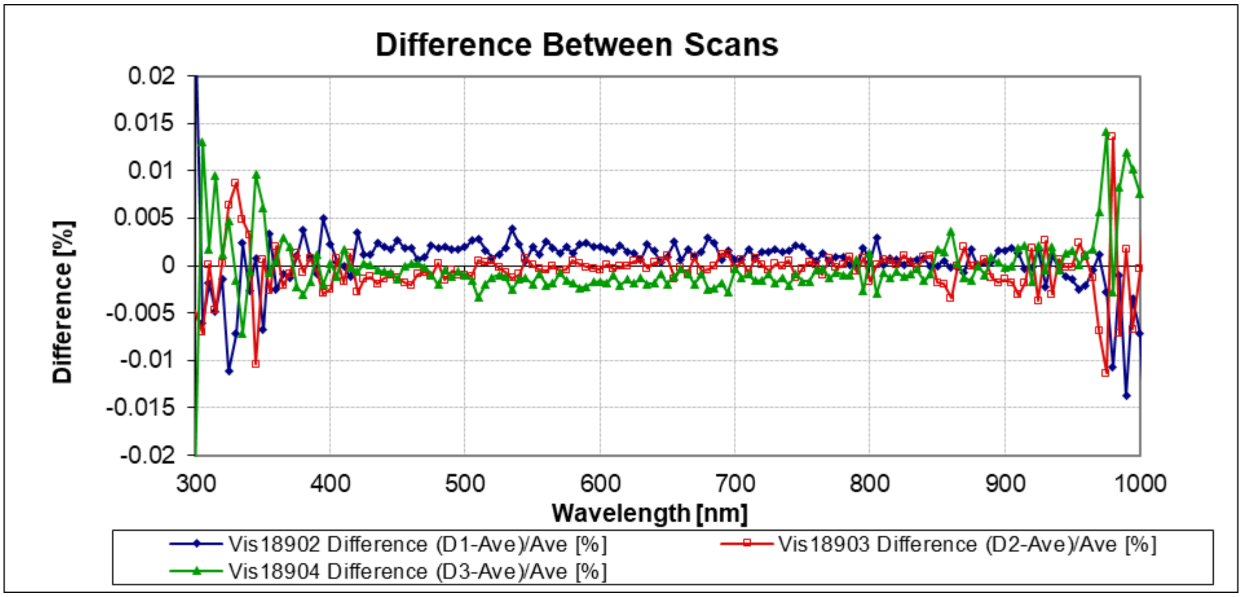


Figure 7b: Repeatability of A4 2nd alignment

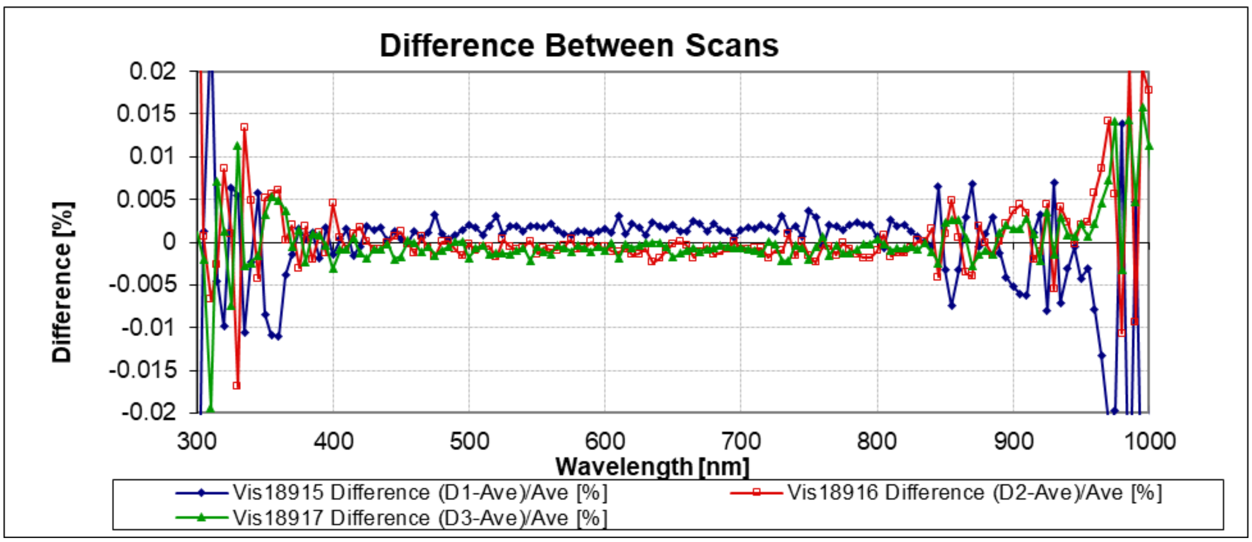


Figure 7c: Repeatability of A4 3rd alignment

A4 Reproducibility

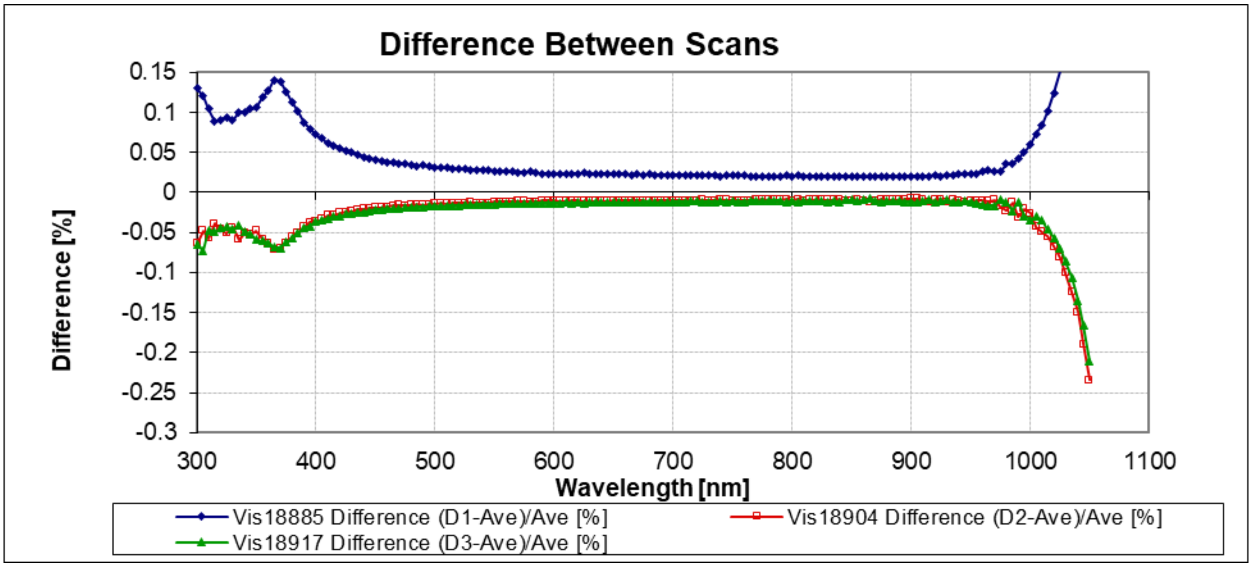


Figure 8: Reproducibility of A4 measurements

A5 Repeatability

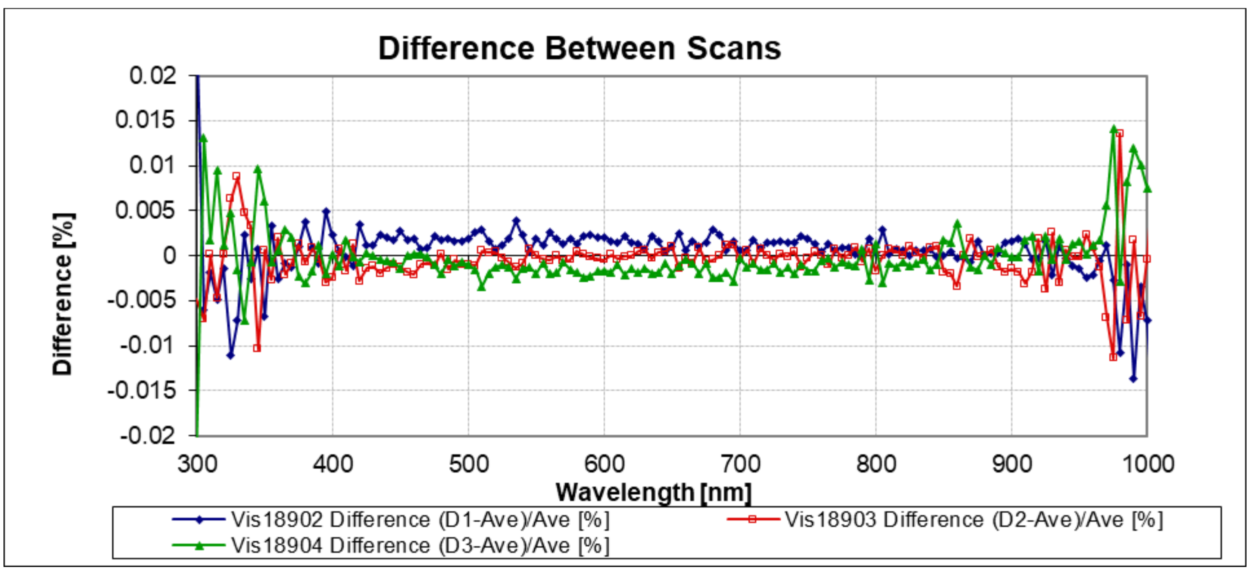


Figure 9a: Repeatability of A5 1st alignment

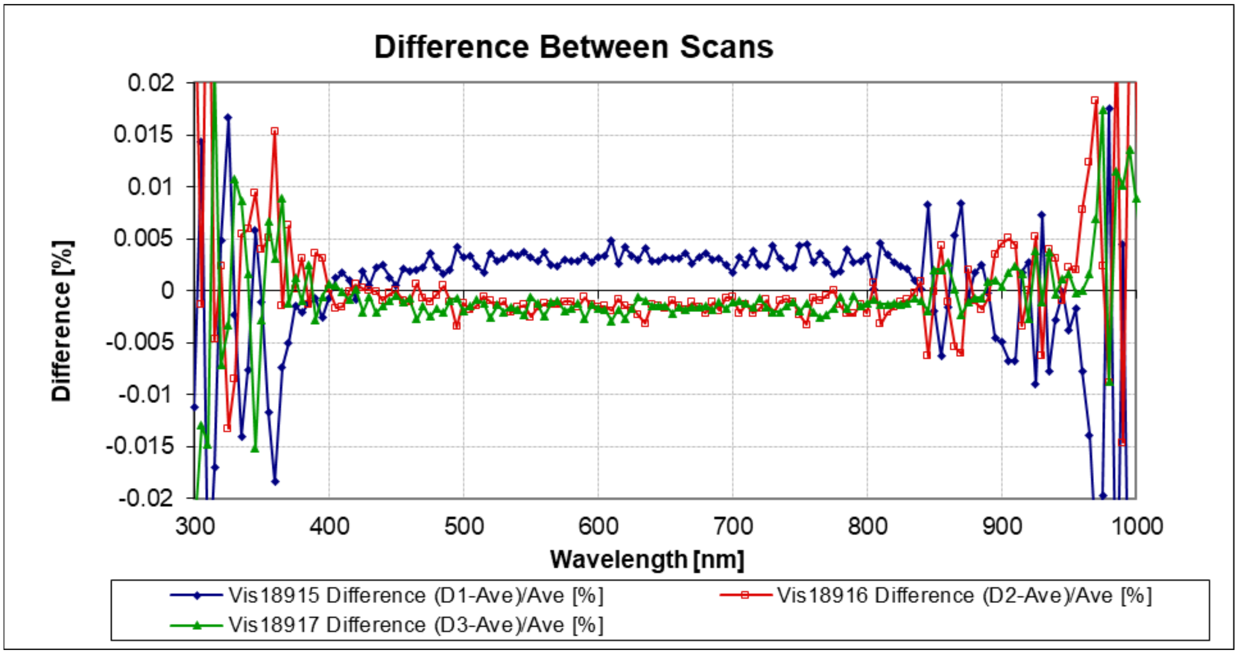


Figure 9b: Repeatability of A5 2nd alignment

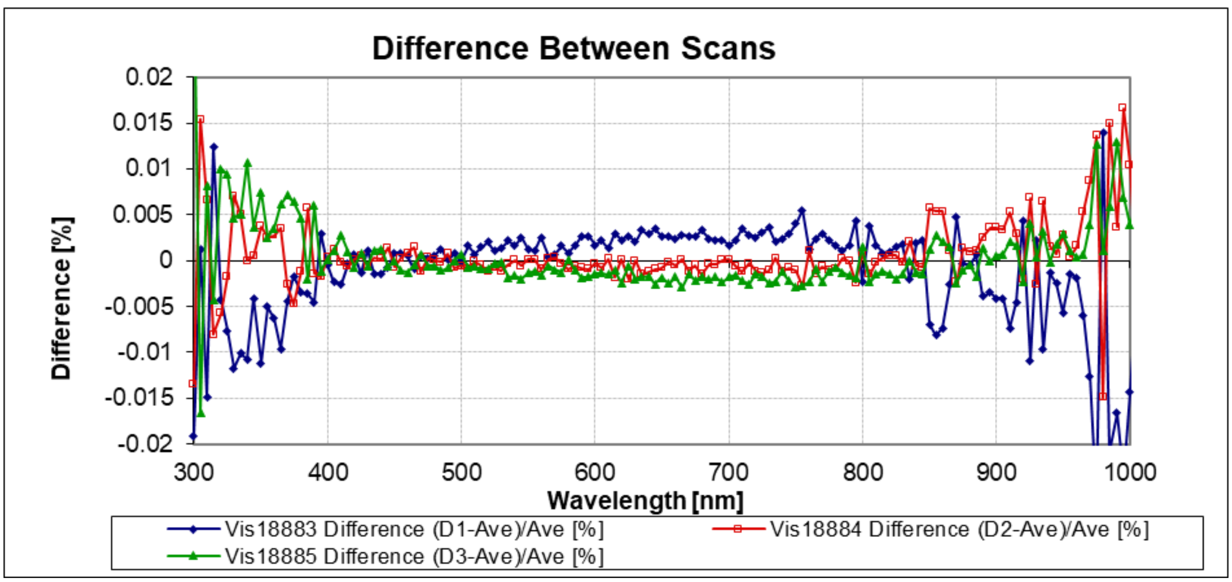


Figure 9c: Repeatability of A5 3rd alignment

A5 Reproducibility

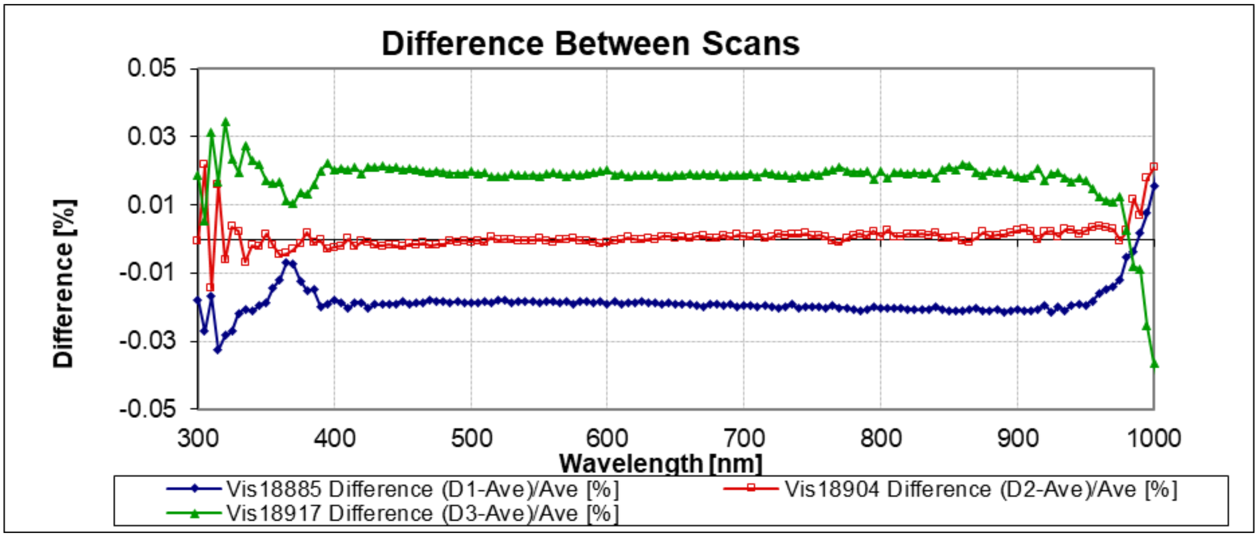


Figure 10: Reproducibility of A5 measurements

**The Results – A 2021 to 2017 comparison of the NIST Measurements:**

CCPR k2.b Set A detectors were measured by NIST in 2017 for the intercomparison and in 2021 for the detector stability measurements. The only deliberate change between these measurements was the cleaning of the single element devices, A1, A2, and A3 before the detector stability tests in 2021. The NIST ASR and uniformity results for Set A from 2021 were compared to the those from 2017.

The overall difference seen in the uniformities were in the single element devices. In 2017 the artifacts were not cleaned throughout the entire intercomparison so there was an accumulation of dust, i.e. contamination by the third round. Since the single element Si detectors were cleaned before the 2021 stability tests there was less contamination in A2 and A3. The traps did not show a significant difference.

Uniformities:

A1: Single element device

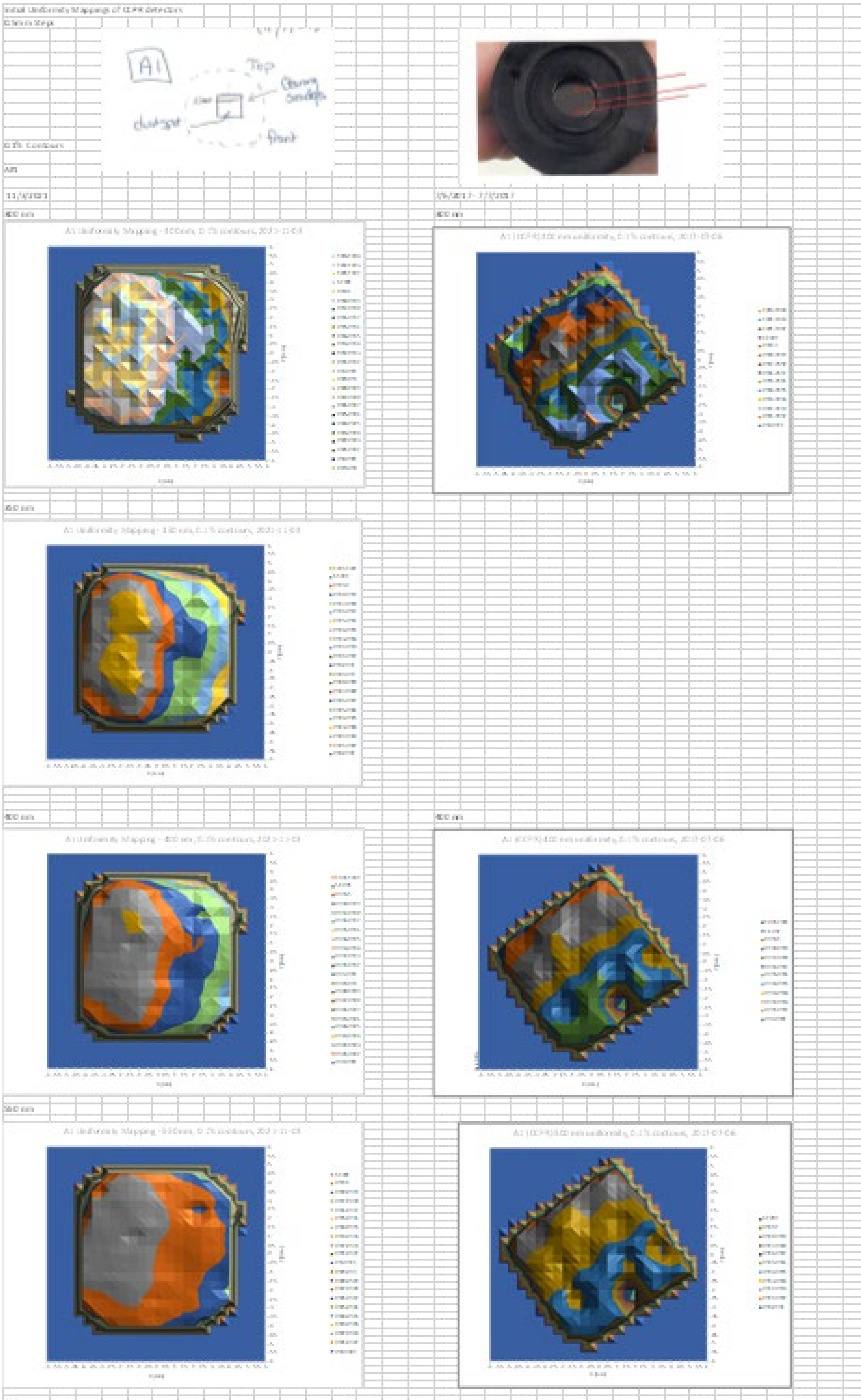

Figure 11a: A1 Uniformity Mappings

A1: Single element device

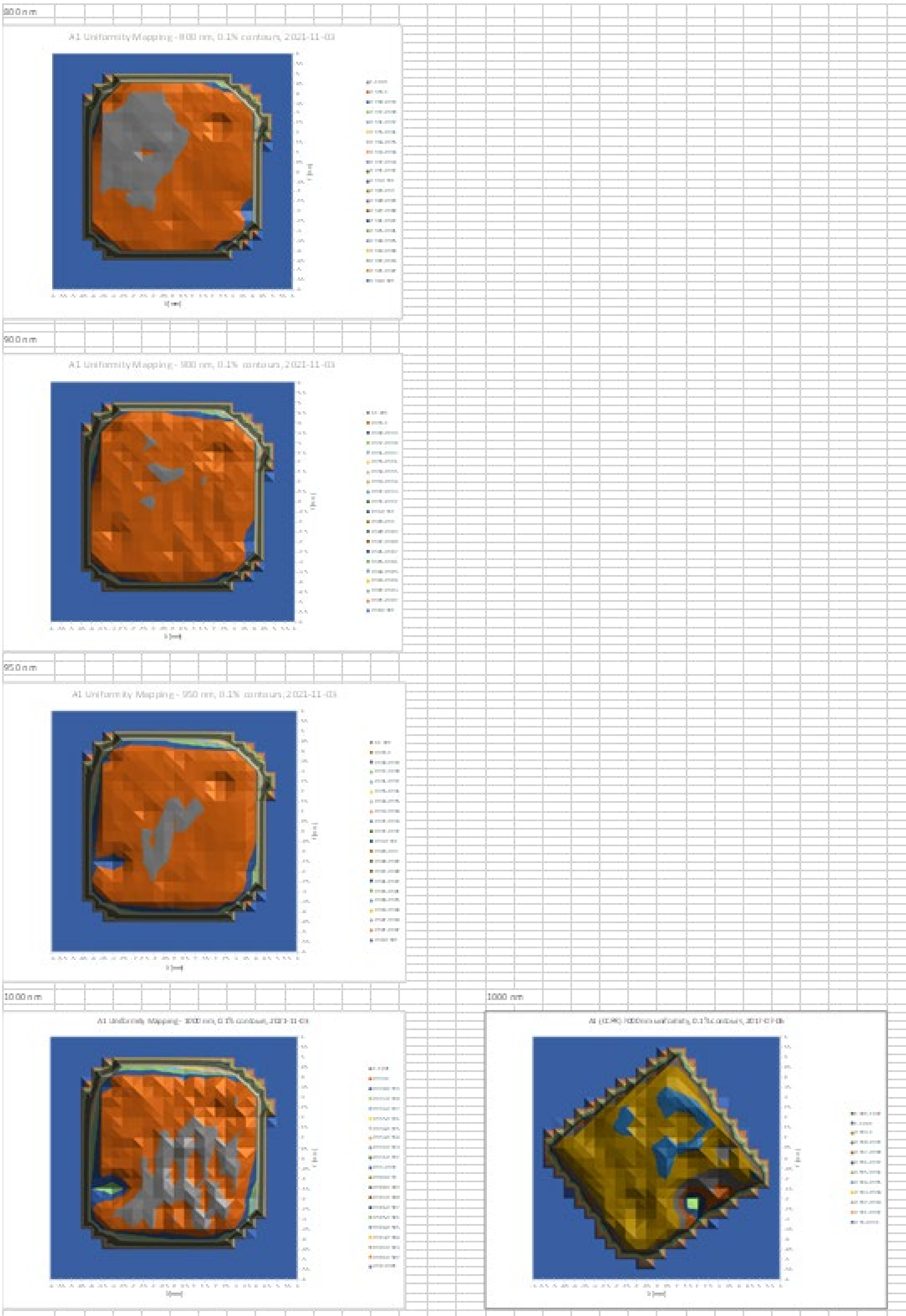


Figure 11b: A1 Uniformity Mappings

A2: single element device

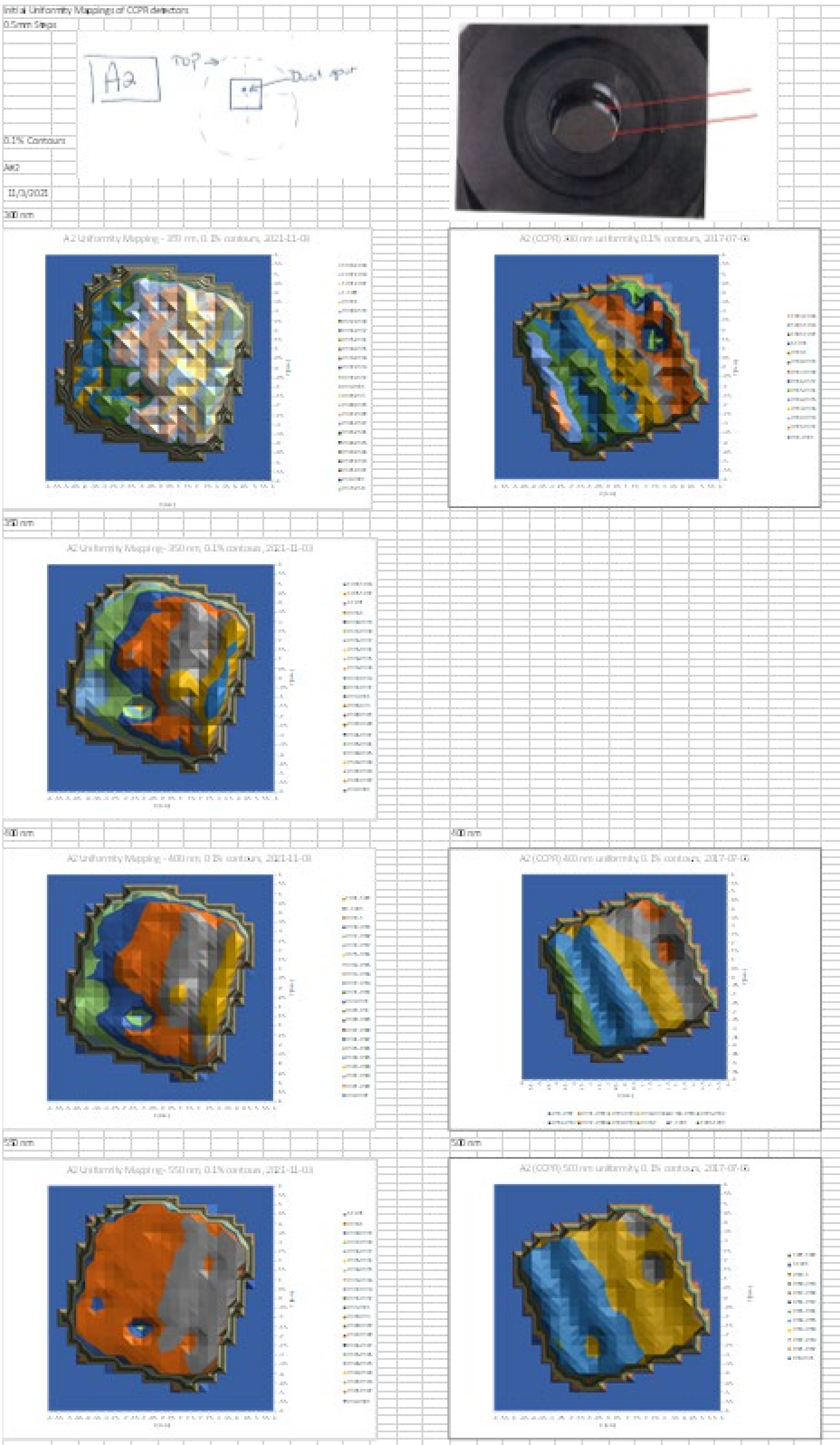


Figure 12a: A2 Uniformity Mappings

A2: Single Element Device

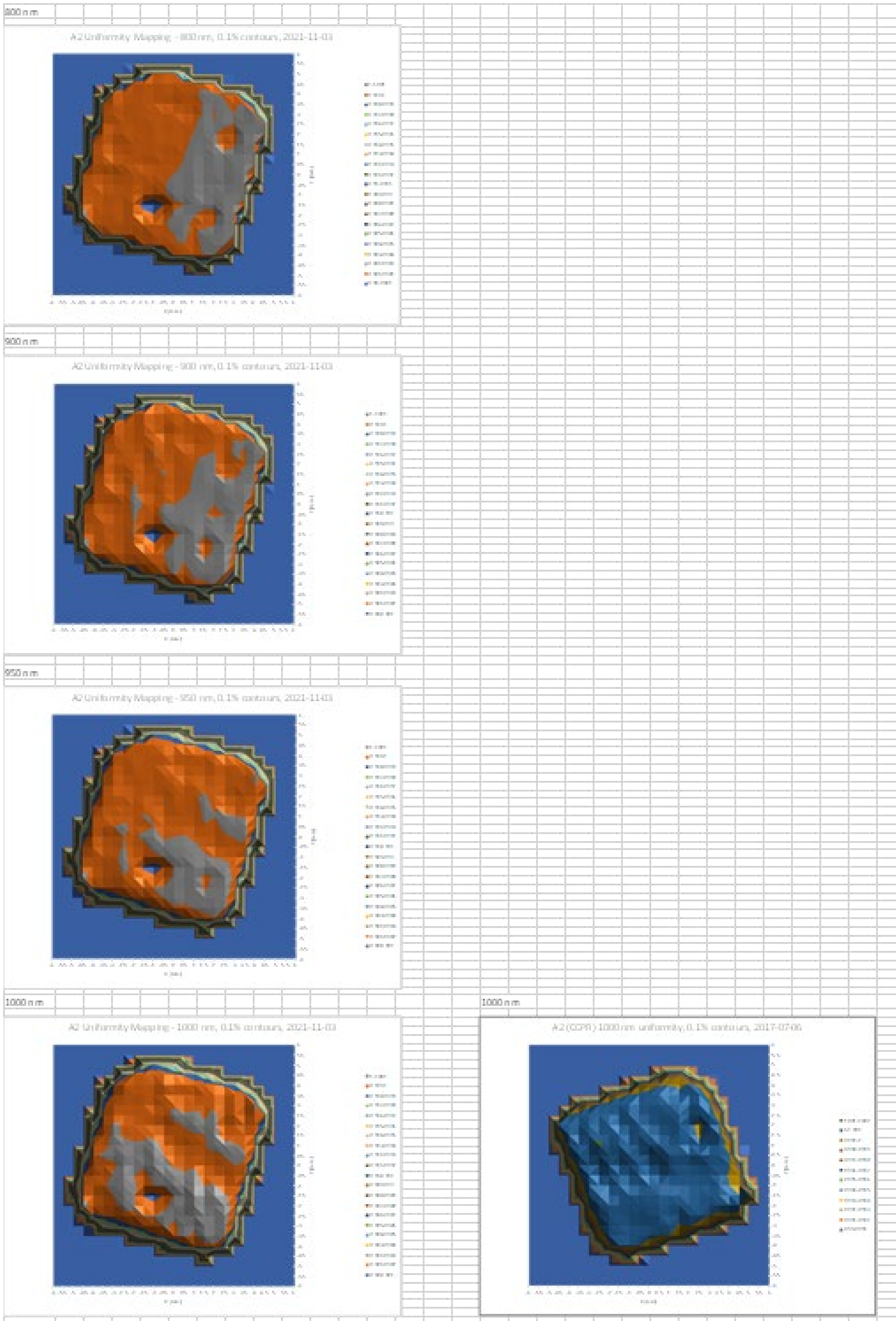


Figure 12b: A2 Uniformity Mappings

A3: single element device


Figure 13a: A3 Uniformity Mappings

A3: single element device

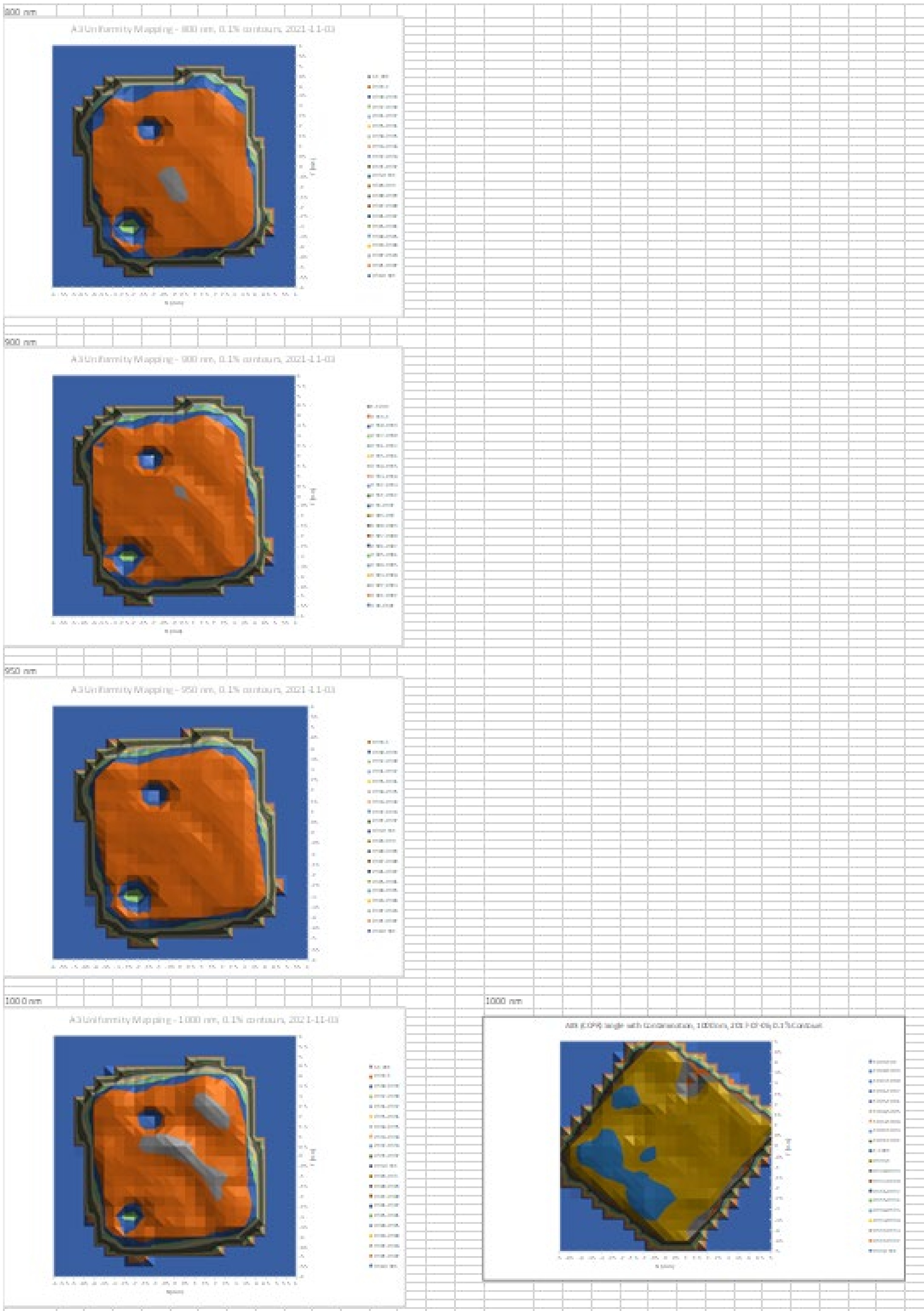


Figure 13b: A3 Uniformity Mappings

A4: Silicon Photodiode trap


Figure 14a: A4 Uniformity Mappings

A4: Silicon Photodiode trap


Figure 14b: A4 Uniformity Mappings

A5: Silicon Photodiode trap

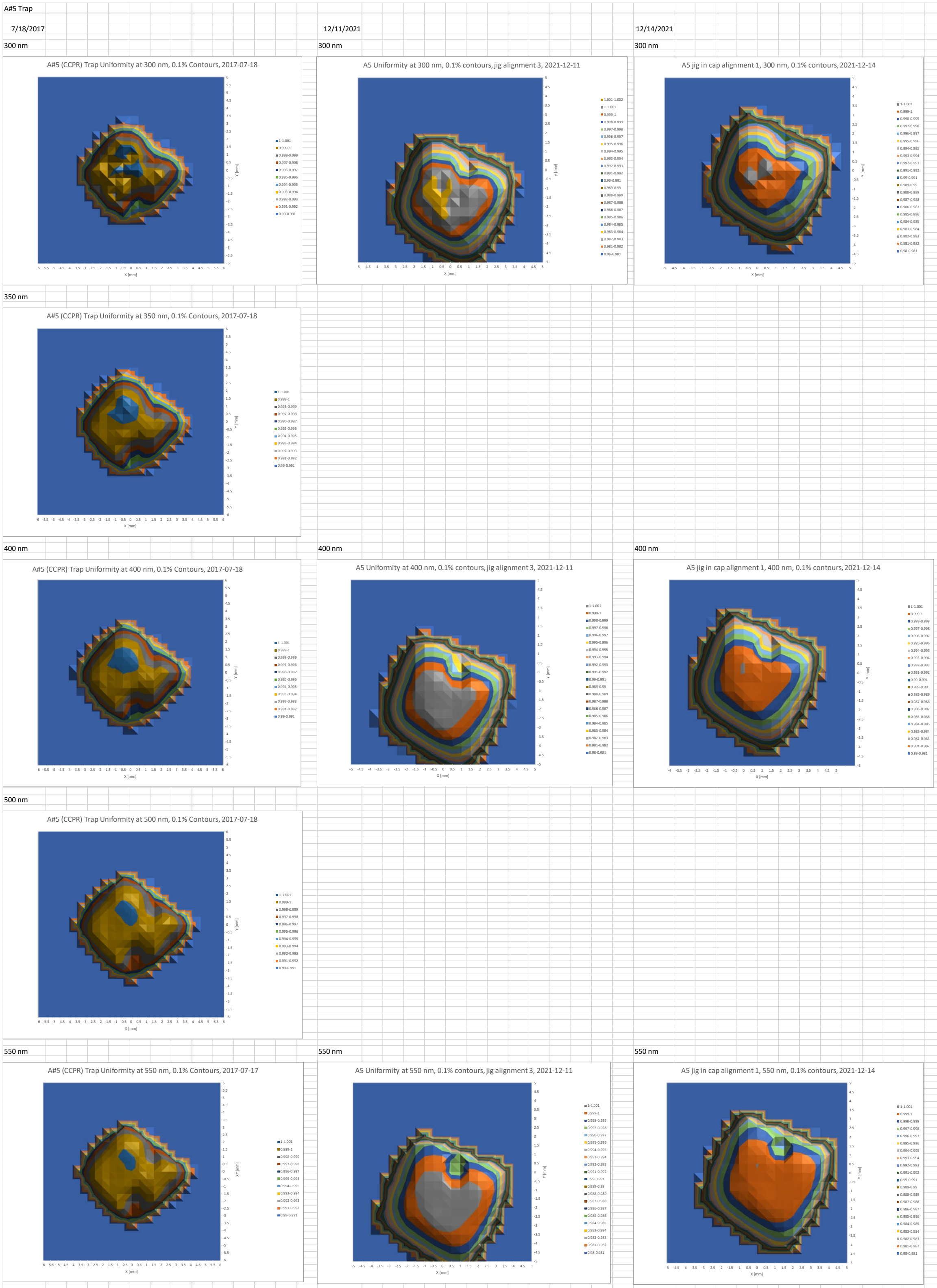


Figure 15a: A5 Uniformity Mappings

A5: Silicon Photodiode trap

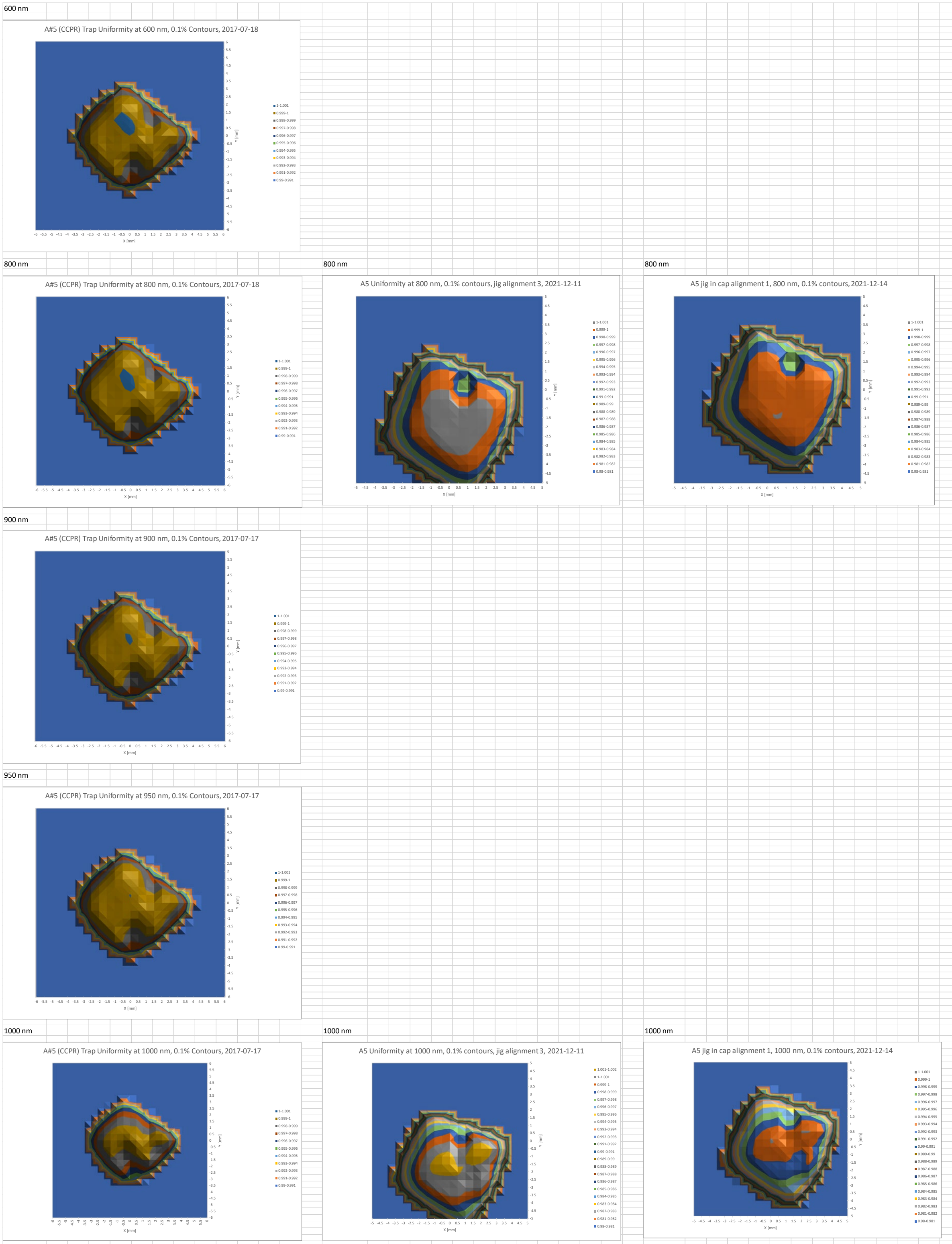


Figure 15b: A5 Uniformity Mappings

The uniformity of the traps remained about the same over the 4 years but the difference seen in the traps center is due to the alignment. A review of the protocol did not specify where the target was to be set, in the cap or in the detector mount itself. The target was loose in the cap and did not repeat in position. The effect was that the trap was not optimally aligned. The alignment jig was also placed directly into the detector mount with the uniformity results more centered.

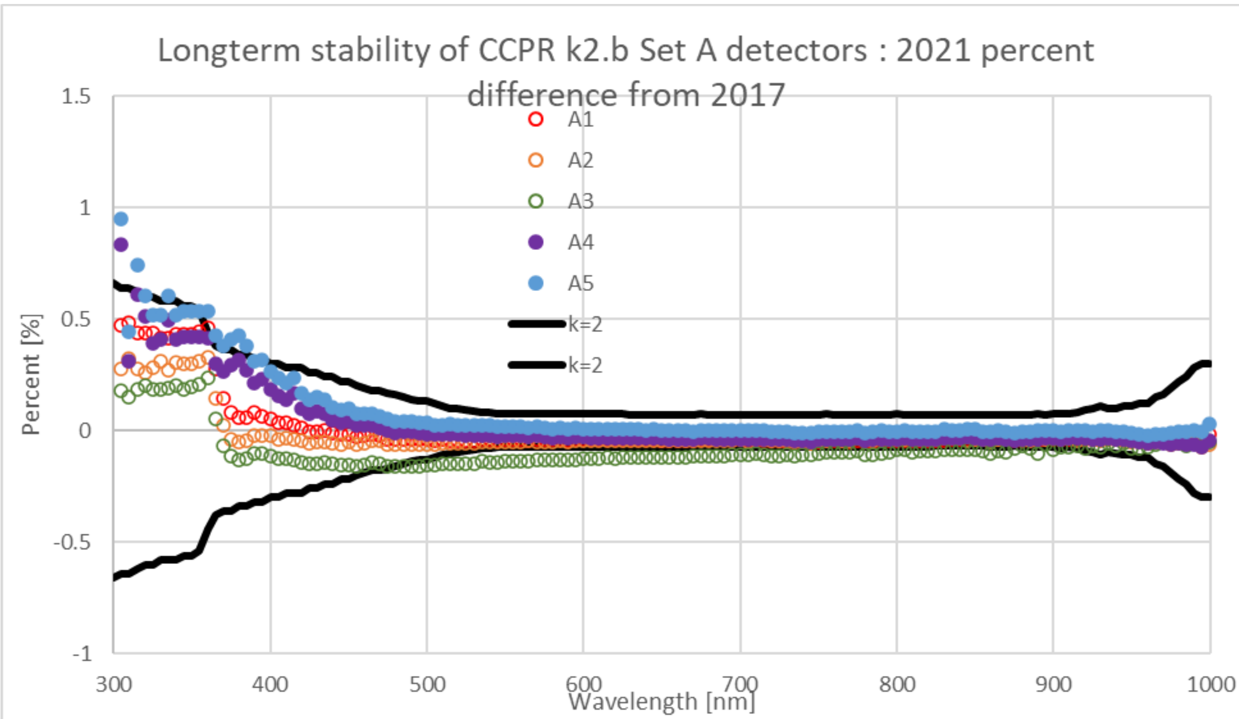


Figure 16a: Percent difference between the ASRs of Set A from 2017 to 2021

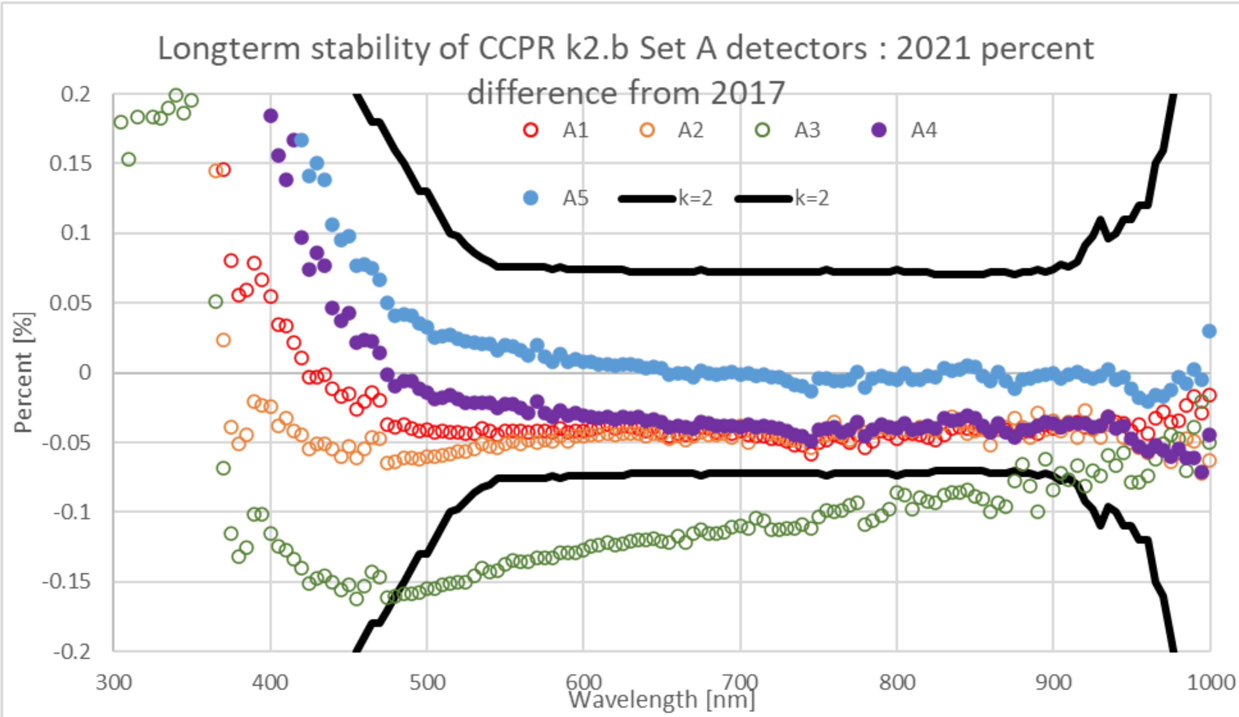


Figure 16 b: Percent difference between the ASRs of Set A from 2017 to 2021 (expanded y-axis scale)

**Summary**

The detector stability study was established to understand long-term behaviors in the single and trap detectors used in the CCPR k2.b intercomparison. The study structure was a star pattern between KRISS and NIST with KRISS starting and ending the measurement sequence using the same Set A devices that NIST previously measured. These presented results represent only measurements made at NIST.

In 2017 NIST performed measurements beyond the required intercomparison protocols that included uniformity studies as well as ASR scans from 300 nm to 1000 nm within 5 nm steps. These measurements were repeated at NIST in 2021 and the results compared.

Almost all the detectors, both the single Si photodiodes and the trap detectors, repeated their ASRs to within 0.05% of the 2017 ASR measurements (Figures 16a and 16b). The differences are within NISTs relative expanded uncertainty (k = 2) [%] for the Hamamatsu S2281 Si photodiodes. The single Si photodiodes' cleaning did not alter the responsivity of the detectors. The Set A detectors were stable in the visible range to 0.05% from 2017 to 2021. There is a shift in the UV from 300 nm to 370 nm that is attributed to the scale derivation using a different transfer standard. The key element to note is that the detectors remained stable in the UV over the 4 years between measurements.

Uniformity mappings from 2017 and 2021 showed that the 2021 detector cleaning removed some of the contaminants but in the 2021 NIST measurements there were other contaminants on the single diode devices. The contamination that existed in 2017 and in 2021 while different, did not impact the ASR measurements as shown by the agreement. The NIST uniformity measurements show that the traps and single element devices are uniform to 0.1% over the central active areas and that the uniformities did not change in the four years between scans.

The intercomparison protocol for the traps' alignment did not specify how the alignment jig was to be implemented, mounted in the cap or in the detector housing. Knowledge of how the traps were aligned by each participant is critical to understanding any differences seen. If the intercomparison is rerun, then a more specific trap alignment protocol is highly recommended.

The initial plan for the detector stability study was to have a star pattern intercomparison between KRISS and NIST where there would be 2 sets of measurements at NIST. The agreement of the Set A ASRs to be better than NIST's relative expanded uncertainty for a Hamamatsu S2281, 0.05% in the visible, over a 4-year time frame demonstrates that additional measurements at NIST are not needed.

The Set A CCPR k2.b artifacts are stable and not the cause of the ASR responses seen between Set 2 and Set 3. Using this Set as a sample for the other 5 artifact sets, it is projected that they too are stable and not the cause for changes seen.